

An analytical and experimental evaluation of concrete cross tie and fastener loads / Robert H. Prause ... [et al.].

Washington : Dept. of Transportation, Federal Highway Administration, Office of Research and Development ; Springfield, Va. : 1977.

<http://hdl.handle.net/2027/mdp.39015040727094>

HathiTrust



www.hathitrust.org

Public Domain, Google-digitized

http://www.hathitrust.org/access_use#pd-google

We have determined this work to be in the public domain, meaning that it is not subject to copyright. Users are free to copy, use, and redistribute the work in part or in whole. It is possible that current copyright holders, heirs or the estate of the authors of individual portions of the work, such as illustrations or photographs, assert copyrights over these portions. Depending on the nature of subsequent use that is made, additional rights may need to be obtained independently of anything we can address. The digital images and OCR of this work were produced by Google, Inc. (indicated by a watermark on each page in the PageTurner). Google requests that the images and OCR not be re-hosted, redistributed or used commercially. The images are provided for educational, scholarly, non-commercial purposes.

701-C

REPORT NO. FRA/ORD-77/71

PB

UMMU
TF
256
.C66
A52
1977

AN ANALYTICAL AND EXPERIMENTAL EVALUATION OF CONCRETE CROSSTIE AND FASTENER LOADS



December 1977
Interim Report

THE UNIVERSITY
OF MICHIGAN

ENGINEERING
LIBRARY

Document is available to the public through the
National Technical Information Service,
Springfield, Virginia 22161.

UNIVERSITY OF MICHIGAN
LIBRARIES

APR 14 1978

DEPOSITED BY THE
UNITED STATES OF AMERICA

Prepared for
U.S. DEPARTMENT OF TRANSPORTATION
FEDERAL RAILROAD ADMINISTRATION
Office of Research and Development

Digitized by Google

Original from
UNIVERSITY OF MICHIGAN

NOTICE

This document is disseminated under the sponsorship of the Department of Transportation in the interest of information exchange. The United States Government assumes no liability for its contents or use thereof.

NOTICE

The United States Government does not endorse products or manufacturers. Trade or manufacturers' names appear herein solely because they are considered essential to the object of this report.



Technical Report Documentation Page

1. Report No. FRA/ORD-77/71		2. Government Accession No.		3. Recipient's Catalog No.	
4. Title and Subtitle AN ANALYTICAL AND EXPERIMENTAL EVALUATION OF CONCRETE CROSS TIE AND FASTENER LOADS				5. Report Date December 1977	
				6. Performing Organization Code TSC-744	
7. Author(s) Robert H. Prause*, Harold D. Harrison** James C. Kennedy*, and Robert C. Arnlund				8. Performing Organization Report No.	
9. Performing Organization Name and Address * Battelle-Columbus Laboratories Bechtel, Incorporated 505 King Avenue. 15740 Shady Grove Rd. Columbus, Ohio 43201 Gaithersburg, MD 20750 (Subcontractor)				10. Work Unit No. (TRAIS) RR719/R7327	
				11. Contract or Grant No. DOT-TSC-1044	
12. Sponsoring Agency Name and Address U.S. Department of Transportation Federal Railroad Administration Office of Research and Development Washington DC 20590				13. Type of Report and Period Covered Interim Report July 1975-December 1976	
				14. Sponsoring Agency Code RRD-32	
15. Supplementary Notes * Under Contract U.S. Department of Transportation to: Transportation Systems Center Kendall Square Cambridge MA 02142					
16. Abstract This report has been prepared as part of the Improved Track Structures Research Program sponsored by the Office of Rail Safety Research of the Federal Railroad Administration. The report covers a review and evaluation of track analysis models for predicting tie and fastener loads. The principal track analysis model selected includes the effects of tie bending, ballast depth, and ballast and subgrade elastic properties in a unified manner. The report also includes a statistical description of track loads measured for revenue traffic operating on three sections of concrete tie track on the Florida East Coast Railway. Measured tie loads are compared to maximum design loads used in current specifications for concrete ties and fasteners.					
17. Key Words Track Loading, Track Instrumentation Track Design, Concrete Cross Ties, Track Components			18. Distribution Statement Document is available to the U.S. public through the National Technical Informa- tion Service, Springfield, Virginia 22161		
19. Security Classif. (of this report) UNCLASSIFIED		20. Security Classif. (of this page) UNCLASSIFIED		21. No. of Pages 345	22. Price

Form DOT F 1700.7 (8-72)

Reproduction of completed page authorized

UMMU
TF
256
.C66
A52
1977

UMMU
DEPOS.

0 1 107

PREFACE

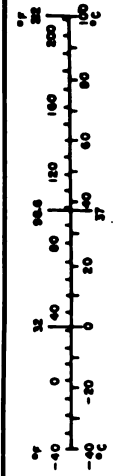
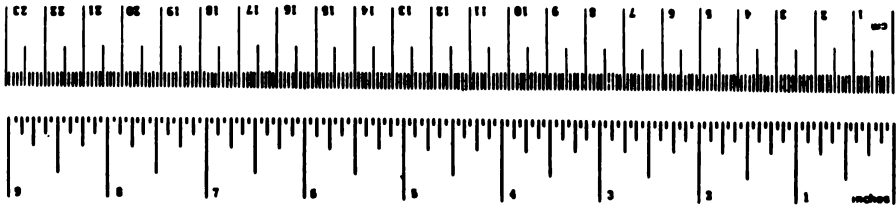
This report was prepared by Battelle's Columbus Laboratories (BCL) and Bechtel, Incorporated under Contract No. DOT-TSC-1044 as part of the Improved Track Structures Research Program managed by the Transportation Systems Center (TSC). This program is sponsored by the Office of Rail Safety Research, Improved Track Structures Research Division, of the Federal Railroad Administration, Washington, D.C.

The overall objective of this contract is to improve the serviceability of cross tie track. This includes an evaluation of the technical and economic feasibility of using synthetic cross ties and rail fastener assemblies to obtain improved component life and long-term performance of railroad track for North American service. This interim technical report covers the review and selection of track analysis models for predicting tie and fastener loads. It also includes a statistical description of track loads measured on three sections of concrete tie track on the Florida East Coast Railway (FEC). This is the second interim report for this contract. The first interim report (FRA/ ORD-77-03) was a planning document for the track measurements.

Dr. Andrew Kish and Mr. Donald McConnell of TSC were the technical monitor and alternate technical monitor, respectively, for the work reported herein. Their cooperation and suggestions are gratefully acknowledged. Steve Noble, Ken Schueller and Robert Gertler of BCL and staff from Bechtel, Incorporated and the Waterways Experiment Station (WES) also deserve recognition for their work on the track measurement program. And finally, the enthusiastic cooperation of a large number of people from the FEC was instrumental for the success of our work and for a memorable personal experience for the authors.

METRIC CONVERSION FACTORS

Approximate Conversions to Metric Measures				Approximate Conversions from Metric Measures			
Symbol	When You Know	Multiply by	To Find	Symbol	When You Know	Multiply by	To Find
LENGTH							
in	inches	2.5	centimeters	mm	millimeters	0.04	inches
ft	feet	30	centimeters	cm	centimeters	0.4	inches
yd	yards	0.9	meters	m	meters	3.3	feet
mi	miles	1.6	kilometers	km	kilometers	1.1	yards
						0.6	miles
AREA							
sq ft	square inches	6.5	square centimeters	sq in	square inches	0.16	square centimeters
sq ft	square feet	0.09	square meters	sq ft	square feet	1.2	square meters
sq yd	square yards	0.8	square meters	sq yd	square yards	0.4	square meters
ac	square miles	2.5	hectares	ac	square miles	2.5	hectares (10,000 m ²)
	acres	0.4	hectares		acres		hectares
MASS (weight)							
oz	ounces	28	grams	g	grams	0.035	ounces
lb	pounds	0.45	kilograms	kg	kilograms	2.2	pounds
	short tons (2000 lb)	0.9	tonnes	t	tonnes (1000 kg)	1.1	short tons
VOLUME							
cup	teaspoons	5	milliliters	ml	milliliters	0.03	fluid ounces
fl oz	tablespoons	15	milliliters	fl oz	fluid ounces	2.1	tablespoons
cup	fluid ounces	24	milliliters	cup	fluid ounces	1.06	quarts
qt	quarts	0.95	liters	qt	quarts	0.95	liters
gal	gallons	3.8	liters	gal	gallons	3.8	liters
cu ft	cubic feet	2.2	cubic meters	cu ft	cubic feet	0.028	cubic meters
cu yd	cubic yards	0.76	cubic meters	cu yd	cubic yards	1.3	cubic meters
TEMPERATURE (exact)							
°F	Fahrenheit temperature	5/9 (after subtracting 32)	Celsius temperature	°C	Celsius temperature	9/5 (then add 32)	Fahrenheit temperature



CONTENTS

<u>Section</u>	<u>Page</u>
1. INTRODUCTION	1
2. SUMMARY OF RESULTS AND CONCLUSIONS	2
2.1 STATISTICAL DESCRIPTION OF TRACK LOADS	2
2.2 SELECTION AND EVALUATION OF TRACK ANALYSIS MODELS	4
3. TRACK ANALYSIS METHODOLOGY	6
3.1 REVIEW OF TRACK FAILURE MODES AND PERFORMANCE INDICES	8
3.1.1 Tie Failure	9
3.1.2 Rail Fastener Failures	12
3.1.3 Track Surface Deterioration	15
3.1.4 Track Alinement Deterioration	19
3.1.5 Rail Rollover	21
3.1.6 Wide Gage	24
3.1.7 Track Analysis Requirements	26
3.2 REVIEW OF TRACK ANALYSIS MODELS	26
3.2.1 Elastic Foundation Track Models	26
3.2.2 Two-Dimensional Finite Element Track Models	30
3.2.3 Three-Dimensional Finite-Element Track Models	32
3.2.4 Ballast/Subgrade Models	33
3.3 TRACK MODEL SELECTION	34
3.3.1 Vertical Track Model	35
3.3.2 Vertical Tie Model	35
3.3.3 Lateral Track Model	38
3.4 RESULTS OF BENCHMARK PROBLEM SOLUTIONS	41
3.5 EVALUATION OF WHEEL/RAIL LOAD DYNAMICS	43
3.6 TRACK DYNAMIC RESPONSE	53
4. MEASUREMENTS OF CROSS TIE AND FASTENER LOADS	59
4.1 TEST SITE DESCRIPTIONS	59
4.1.1 Site 1 - Tangent Track with 24-Inch Tie Spacing	62
4.1.2 Site 2 - Tangent Track with 20-Inch Tie Spacing	62
4.1.3 Site 3 - Curved Track with 24-Inch Tie Spacing	62
4.2 INSTRUMENTATION INSTALLATION AND CALIBRATION	63
4.2.1 Wheel/Rail Load Circuits	65
4.2.2 Rail Seat Loads	67
4.2.3 Tie Moments	70
4.2.4 Tie/Ballast Pressures	73
4.2.5 Track Deflection	73
4.2.6 Rail Fastener Bolt Loads	75
4.2.7 Rail Bending Strain	75
4.2.8 Rail and Tie Acceleration	78
4.3 BALLAST AND SUBGRADE PROPERTIES	78
4.3.1 Plate Bearing Tests	79
4.3.2 Subgrade Property Measurements	83
4.4 DATA ACQUISITION AND RECORDING	87
4.5 DATA ANALYSIS	92
4.6 FORMATS FOR STATISTICAL DATA	96
4.7 RESULTS FROM STATISTICAL ANALYSIS	98

CONTENTS (Continued)

<u>Section</u>	<u>Page</u>
4.7.1 Track Component Loads from Revenue Traffic	101
4.7.2 Effect of Tie Spacing	126
4.7.3 Effect of Car Type	129
4.7.4 Effect of Train Speed	132
4.7.5 Comparison with Test Data from Kansas Test Track	140
4.7.6 Summary of Results	145
4.8 TRACK DYNAMIC RESPONSE	149
4.8.1 Frequency Analysis of Tie Vibration	152
4.8.2 Rail and Tie Acceleration	156
4.8.3 Rail Corrugation	159
4.8.4 Track Vertical Natural Frequency	159
5. EVALUATION OF TRACK ANALYSIS MODEL	159
5.1 COMPARISON OF MEASURED AND PREDICTED LOADS	162
5.1.1 Effect of Track Modulus on Rail Seat Loads	162
5.1.2 Tie/Ballast Pressure Distribution	166
5.1.3 Track Displacement Predictions	177
5.1.4 Track Modulus Measurements	180
5.1.5 Track Response for Light and Heavy Cars	183
5.2 SUMMARY OF RESULTS AND CONCLUSIONS	186
APPENDIX A - REVIEW OF TRACK ANALYSIS MODELS	189
APPENDIX B - TRACK ANALYSIS BENCHMARK PROBLEMS	220
APPENDIX C - CALIBRATION OF INSTRUMENTED TIE PLATES	246
APPENDIX D - CALIBRATION OF FRA/PCA LOAD CELL TIES	256
APPENDIX E - CALIBRATION OF STRAIN GAGED CONCRETE TIES	273
APPENDIX F - SUBGRADE SIEVE ANALYSIS AND MOISTURE DENSITY DATA	286
APPENDIX G - VIBROSEISMIC SURVEY DATA OBTAINED BY THE USAE WATERWAYS EXPERIMENT STATION (WES)	289
APPENDIX H - STATISTICAL ANALYSIS OF TRACK LOAD DATA	305
APPENDIX I - REPORT OF INVENTIONS	340
REFERENCES	341

ILLUSTRATIONS

Figure

3-1. GENERAL FORMAT FOR TRACK ANALYSIS METHODOLOGY	7
3-2. TRACK DEFLECTION CRITERIA FOR DURABILITY [3-8]	17
3-3. TRACK MODEL FOR MULTA PROGRAM	36

ILLUSTRATIONS (Continued)

<u>Figure</u>	<u>Page</u>
3-4. VERTICAL TIE MODEL	37
3-5. LATERAL TRACK MODEL	39
3-6. COMPARISON OF SEVERAL FORMULAS USED TO PREDICT WHEEL DYNAMIC LOAD FACTORS	45
3-7. DYNAMIC WHEEL LOAD FACTORS USED BY DB (GERMANY) FOR 99.7 PERCENT CONFIDENCE LEVEL (n=3)	47
3-8. TYPICAL DATA ON WHEEL DYNAMIC LOAD FACTORS FOR LOCOMOTIVES	48
3-9. MAXIMUM WHEEL DYNAMIC LOAD FACTOR FOR FREIGHT CAR IMPACT AT BOLTED RAIL JOINTS	51
3-10. EQUIVALENT WHEEL DYNAMIC LOAD FACTOR FOR THE EFFECT OF FLAT WHEELS ON RAIL BENDING STRESS	52
3-11. WHEEL PASS EXCITATION FREQUENCIES	55
3-12. ESTIMATE OF MAXIMUM TIE ACCELERATION	57
4-1. RCCC TIE INSTALLED ON FLORIDA EAST COAST RAILROAD	61
4-2. LAYOUT OF TRACK TEST SITES	64
4-3. MAIN ARRAY INSTRUMENTATION	66
4-4. FIELD CALIBRATION OF LATERAL W/R LOAD CIRCUITS	68
4-5. TYPICAL CALIBRATION DATA FOR LATERAL W/R LOAD CIRCUITS	69
4-6. THREE STRAIN-GAGED TIES IN MAIN ARRAY	71
4-7. LOAD-CELL TIE	74
4-8. RAIL FASTENER BOLT LOAD MEASUREMENT	76
4-9. LOCATION OF STRAIN GAGES FOR RAIL STRESS MEASUREMENTS	77
4-10. BALLAST PLATE BEARING MEASUREMENTS	80
4-11. FORCE-DISPLACEMENT CURVE FOR SUBGRADE PLATE BEARING TEST @ 6.5 IN. FROM RAIL SEAT - SITE 1	81
4-12. CONDUCTING VIBROSEISMIC MEASUREMENTS AT SITE 2	86
4-12A. BASIC DATA ACQUISITION AND RECORDING SYSTEM COMPONENTS	89
4-13. DATA ACQUISITION AND RECORDING SYSTEM INSTALLATION	90
4-13A. DATA ANALYSIS PROCEDURES	94

ILLUSTRATIONS (Continued)

<u>Figure</u>	<u>Page</u>
4-14. TYPICAL PROBABILITY DISTRIBUTION AND DENSITY HISTOGRAMS FOR VERTICAL W/R LOAD FOR ALL CARS AND ALL SPEEDS	97
4-15. PEAK VERTICAL WHEEL/RAIL LOAD STATISTICS FOR ALL TRAFFIC AT SITE 1 (1.2 kip load interval)	105
4-16. PEAK LATERAL W/R LOAD STATISTICS FOR ALL TRAFFIC AT SITE 1 (0.6 kip load interval)	106
4-17. PEAK LATERAL W/R LOAD STATISTICS FOR ALL TRAFFIC AT SITE 3 (0.6 kip load interval)	107
4-18. PEAK VERTICAL RAIL SEAT LOAD STATISTICS FOR ALL TRAFFIC AT SITE 1 (0.6 kip load interval)	109
4-19. PEAK VERTICAL RAIL SEAT LOAD STATISTICS FOR ALL TRAFFIC AT SITE 3 (0.6 kip load interval)	110
4-20. PEAK RAIL SEAT MOMENT STATISTICS FOR ALL TRAFFIC AT SITE 1 (2.4 kip-in. load interval)	111
4-21. PEAK RAIL SEAT MOMENT STATISTICS FOR ALL TRAFFIC AT SITE 3 (2.4 kip-in. load interval)	112
4-22. PEAK TIE RAIL SEAT BENDING MOMENT STATISTICS FOR ALL TRAFFIC AT SITE 1 (2.4 in.-kips load interval)	114
4-23. PEAK TIE RAIL SEAT BENDING MOMENT STATISTICS FOR ALL TRAFFIC AT SITE 3 (2.4 in.-kips load interval)	115
4-24. PEAK RAIL SEAT BENDING MOMENT STATISTICS FOR TIE LOCATION 85E (35) AT SITE 1 (2.4 in.-kips load interval)	117
4-25. PEAK TIE CENTER BENDING MOMENT STATISTICS FOR ALL TRAFFIC AT SITE 3 (2.4 in.-kips load interval)	120
4-26. PEAK TIE TORSION MOMENT STATISTICS FOR ALL TRAFFIC	122
4-27. PEAK DYNAMIC RAIL FASTENER BOLT FORCE STATISTICS FOR ALL TRAFFIC AT SITE 3 (0.24 kips load interval)	124
4-28. PEAK RAIL AND TIE LATERAL DISPLACEMENTS FOR ALL TRAFFIC AT SITE 1	125
4-29. EFFECT OF CAR TYPE ON WHEEL/RAIL LOADS (SITE 1, 50-60 MPH SPEED RANGE)	130
4-30. EFFECT OF CAR WEIGHT ON RAIL SEAT LOAD AND TIE BENDING MOMENTS (SITE 1, 50-60 MPH SPEED RANGE)	131
4-31. EFFECT OF TRAIN SPEED ON AVERAGE VERTICAL AND LATERAL WHEEL/RAIL LOADS FOR ALL TRAFFIC ON TANGENT TRACK (SITE 1)	133

ILLUSTRATIONS (Continued)

<u>Figure</u>	<u>Page</u>
4-32. EFFECT OF TRAIN SPEED ON AVERAGE VERTICAL WHEEL/RAIL LOADS ON HIGH RAIL IN CURVE (SITE 3) FOR ALL CARS (1.2 kips load interval)	135
4-33. EFFECT OF CAR WEIGHT AND TRAIN SPEED ON LATERAL WHEEL/RAIL LOADS ON HIGH RAIL IN CURVE (SITE 3), LOCATION 18E (17)	136
4-34. EFFECT OF TIE SPACING ON MEAN RAIL SEAT LOADS FOR LOCOMOTIVES .	141
4-35. EFFECT OF TIE SPACING ON MEAN TIE RAIL SEAT BENDING MOMENTS . .	143
4-36. EFFECT OF TIE SPACING ON MEAN TIE CENTER BENDING MOMENTS . . .	144
4-37. TYPICAL RECORDING OF TIE LOADS FOR SEVERAL CARS	150
4-38a. TIME HISTORY OF TIE RESPONSE TO LOCOMOTIVE	151
4-38b. TIME HISTORY OF TIE RESPONSE TO LIGHT CAR WITH WHEEL FLATS. . .	151
4-39. TIE CENTER BENDING SPECTRAL RESPONSE FOR LIGHT CAR WITH WHEEL FLATS	153
4-40. TIE RAIL SEAT BENDING MOMENT SPECTRAL RESPONSE FOR LIGHT CAR WITH WHEEL FLATS	154
4-41. TIE RAIL SEAT BENDING MOMENT SPECTRAL RESPONSE FOR HEAVY CAR WITH SMOOTH WHEELS	155
4-42. TYPICAL TIE ACCELERATION RESPONSE	157
4-43. TYPICAL TIE ACCELERATION SPECTRAL RESPONSE UNDER LIGHT FLAT WHEELS	158
4-44. RAIL CORRUGATIONS AT CURVE	160
4-45. RAIL SEAT LOAD DYNAMIC RESPONSE AT SITE 1	161
5-1a. MAXIMUM VERTICAL RAIL-SEAT LOAD AT SITE 1	163
5-1b. MAXIMUM VERTICAL RAIL-SEAT LOAD AT SITE 2	163
5-2. COMPARISON OF EXPERIMENTAL AND ANALYTICAL RAIL SEAT LOADS FOR SITE 2 (Tangent track with 20-inch tie spacing)	165
5-3. COMPARISON OF MEASURED AND PREDICTED VERTICAL RAIL SEAT LOADS AT SITE 1	167
5-4. COMPARISON OF MEASURED AND PREDICTED VERTICAL RAIL SEAT LOADS AT SITE 2	168

ILLUSTRATIONS (Continued)

<u>Figure</u>	<u>Page</u>
5-5. TIE/BALLAST PRESSURE DATA FROM LCT-18 AT SITE 1	170
5-6. BALLAST/TIE VERTICAL PRESSURE NORMALIZED TO RESPECTIVE RAIL SEAT REACTION, LCT-18 AT SITE 1	172
5-7. TIE/BALLAST PRESSURE DATA FROM LCT-100 AT SITE 1	173
5-8. BALLAST/TIE VERTICAL PRESSURE NORMALIZED TO RESPECTIVE RAIL SEAT REACTION, LCT=100 AT SITE 1	174
5-9. TIE/BALLAST VERTICAL PRESSURE, LCT - 0 DATA AT SITE 3	175
5-10. BALLAST/TIE VERTICAL PRESSURE NORMALIZED TO RESPECTIVE RAIL SEAT REACTION, LCT-0 DATA AT SITE 3	176
5-11. TIE SHEAR FORCE, LCT-0 DATA (SITE 3)	178
5-12. TIE BENDING MOMENT, LCT-0 DATA (SITE 3)	178
5-13. PREDICTED TIE LOAD AND DISPLACEMENT DISTRIBUTION (SITE 1)	179
5-14. PREDICTED TIE LOAD AND DISPLACEMENT DISTRIBUTIONS (SITE 2)	179
5-15. TRACK RESPONSE FOR SLOW ROLL BY OF WORK TRAIN AT SITE 1	185
5-16. INFLUENCE OF ADJACENT AXLE ON TIE PLATE REACTIONS AT SITE 1	187

TABLES

<u>Table</u>	
3-1. PRIORITY RANKING OF RAIL FASTENER DATA REQUIREMENTS [3-3]	13
3-2. SUMMARY OF TRACK DEGRADATION MODE ANALYSIS REQUIREMENTS	27
3-3. SUMMARY OF AVAILABLE TRACK ANALYSIS MODELS	28
3-4. STANDARD DEVIATION OF WHEEL DYNAMIC LOAD FACTOR USED BY DB [6]	46
4-1. MODEL PARAMETERS FROM PLATE BEARING TESTS	83
4-2. SUMMARY OF TRACK SUBGRADE PROPERTY DATA	84
4-3. SUMMARY OF SOIL ELASTIC PROPERTIES FROM VIBROSEISMIC SURVEY ADJACENT TO TRACK ROADBED	88
4-4. SUMMARY OF TRANSDUCER SPECIFICATIONS	91
4-5. COMPONENT SPECIFICATIONS FOR DATA ACQUISITION SYSTEM	93

TABLES (Continued)

<u>Table</u>	<u>Page</u>
4-6. SUMMARY OF AXLE COUNT AND MEAN VALUES FOR PEAK VERTICAL WHEEL/ RAIL LOADS AT ALL SITES	99
4-7. SUMMARY OF TRACK COMPONENT LOAD STATISTICS FOR ALL CARS, ALL SPEEDS, AT MAXIMUM LOAD LOCATION	102
4-8. SUMMARY OF TIE LOAD REQUIREMENTS FROM AREA SPECIFICATIONS FOR CONCRETE TIES AND FASTENINGS	103
4-9. EXTRAPOLATED STATISTICS FOR RAIL SEAT BENDING MOMENTS BASED ON MOST SEVERE TIE LOADING	118
4-10. SUMMARY OF RAIL AND TIE LATERAL DISPLACEMENT STATISTICS AT SITE 1 FOR ALL TRAFFIC	126
4-11. EFFECT OF TIE SPACING ON AVERAGE TRACK COMPONENT LOAD STATISTICS FOR ALL SPEEDS	127
4-12. EFFECT OF TRAIN SPEEDS ON VERTICAL WHEEL/RAIL LOADS AT SITE 3 (3° 52' CURVE)	134
4-13. COMPARISON OF AVERAGE TRACK COMPONENT LOADS FOR ALL TRAFFIC ON TANGENT AND CURVE TRACK WITH 24-IN TIE SPACING	138
4-14. COMPARISON OF EXTRAPOLATED STATISTICS FOR AVERAGE TIE BENDING MOMENTS IN TANGENT AND CURVED TRACK	139
5-1. MAXIMUM MEASURED RAIL-SEAT TO WHEEL-LOAD RATIO (Q/P) IN PERCENT (%)	164
5-2. COMPARISON OF MEASURED AND PREDICTED TRACK DISPLACEMENTS	181
5-3. MEASURED VALUES OF TRACK MODULUS	182
5-4. SUMMARY OF TRACK MODULUS VALUES	184

1. INTRODUCTION

The improvement of the safety and serviceability of cross tie track is an important factor in maintaining the viability of rail transportation. The use of concrete ties and compatible rail fasteners seemingly offers considerable potential for extending tie life and reducing track maintenance, but there have been considerable problems in developing concrete ties which are suitable for main-line service in North America. Tie center binding and end binding are familiar conditions for wood tie track, but the inherent resilience of wood minimizes damage from these undesirable loading conditions. Concrete, however, is a very brittle material and is considerably more susceptible to failure when stressed beyond its design limits.

The development of concrete ties in the U.S. has followed closely the development of the AREA Specifications for Concrete Ties (and Fastenings). These specifications have evolved through several modifications whereby tie strength requirements were gradually increased as a result of premature cracking in various concrete tie test installations. Minimum bending strength at the rail seat and tie center and corresponding static acceptance tests are the major considerations. However, the lack of accurate descriptions of tie service loads has been a major deterrent to the development of these specifications.

The principal objectives of the research discussed in this report were to select and evaluate analytical procedures for predicting the distribution of loads and stresses within the track and to obtain some typical statistical data on the service loads for concrete tie/fastener assemblies used for main-line track. The analytical procedures were selected based on requirements for predicting loads which cause tie and fastener failures, track surface and alignment deterioration, rail rollover and wide gage. A measurement program was conducted on tangent and curved track sections of concrete ties on the Florida East Coast Railway to obtain statistical descriptions of wheel/rail loads, tie loads, tie bending and torsional moments, ballast pressures and rail deflections. These statistical descriptions of track loads have been used to validate the track analysis models. They will also be used in later phases of the project to develop tie and fastener performance specifications and to develop track design guidelines which include the effects of various tie/fastener characteristics, tie spacing and ballast depth. This project also includes an evaluation of life cycle costs which includes the maintenance frequency, rail life and tie life for wood and concrete tie track.

2. SUMMARY OF RESULTS AND CONCLUSIONS

2.1 STATISTICAL DESCRIPTION OF TRACK LOADS

Three different sections of concrete tie track on the Florida East Coast Railway (FEC) were instrumented extensively to record wheel/rail loads, tie loads, tie bending moments and tie/ballast pressures for several days of revenue traffic. The instrumented track sites included two sections of tangent track with ties spaced at 20 and 24 inches to evaluate the effect of tie spacing. The third test site, at a $3^{\circ} 52'$ curve, was selected to provide a comparison of loads from tangent and curved track sections. The tangent track sites had been in service for about one year and the curve site had been in service for about five years. However, the curve had been surfaced and lined at the same time the tangent track was constructed. Track geometry measurements made prior to the field tests showed that track geometry was excellent throughout.

Vertical wheel/rail load measurements showed little variation over a speed range of 30 to 60 mph except for an increase in load on the high rail in the curve at speeds above the 45 mph balance speed. The vertical loads also showed negligible variation at different locations within each test site indicating that vehicle dynamic response from track geometry irregularities was minimal on this smooth track.

Overall lateral wheel/rail loads were nearly identical for the tangent and curved track sites and mean lateral loads for all traffic were quite low, less than 2 kips. Locomotives and heavily loaded cars caused occasional lateral forces up to 15 kips at the curve site. Tangent track lateral forces from light cars increased considerably at speeds above 50 mph, indicating possible car hunting. Lateral forces from light and empty cars operating at 50-60 mph were lower on the curve than on tangent track. These data indicate that hunting was probably reduced by flanging on the curve.

Measurements of tie bending moments and the distribution of tie/ballast pressures under ties showed large tie-to-tie variations and a load dependent support condition whereby many ties were center bound for light wheel loads. However, the ballast reactions became more uniform with heavy wheel loads, indicating that possible voids or depressions may have developed in the ballast near the tie ends and the rail seat region.

A comparison of rail seat load and tie bending moment data from the FEC with similar data from other sections of concrete tie track in the U.S. showed good agreement. Tie loads from revenue traffic were considerably lower than current flexural strength requirements for concrete ties even for a probabilistic prediction of maximum loads for a 50 year life. It is conjectured that small cracks may be initiated in prestressed concrete ties at relatively low loads, and that once initiated, the cracks propagate from the repeated cycling of normal traffic until they reach a sufficient size to be detected. It is not known if the initiation mechanism is due to fatigue from cyclic compressive stress where the total stress at the tie surface remains in compression due to the prestress, or whether it is caused by the total stress at the tie surface exceeding the tensile strength of concrete.

It is very difficult to determine at what load a small crack is initiated in a prestressed tie, and this has not been included in any previous tie tests. This report recommends an experiment in which the surface of a new tie is instrumented to determine the static bending moment for initial cracking. Fatigue tests using service load spectra reported herein are also recommended to determine the critical loading for tie cracking under cyclic loads. Also, the long-term performance of ties which have structural cracks has not been sufficiently verified by service experience to determine if this represents a true failure condition. Data from the Facility for Accelerated Service Testing (FAST) track installation of cracked RT-7 ties from the Kansas Test Track should provide a valuable measure of cracked tie performance under accelerated loading. Answers to these questions about the failure mode of concrete ties are needed in order to develop appropriate performance specifications for future design and acceptance tests.

The effect of reducing tie spacing from 24 to 20 inches, a 16% reduction, resulted in reducing mean rail seat vertical loads on the average tie by about 9%. Mean and maximum (0.1% probability) tie bending moments at the rail seat were reduced by 36% and 12%, respectively. However, large tie-to-tie variations resulted in the maximum tie loads for 20 inch spacing equalling the maximum tie loads for 24 inch spacing, although fewer highly stressed ties would be expected with the reduced spacing.

Maximum tie bending moments were 25% higher at the rail seat and 50% higher at the tie center at the curve site due to the increased vertical loads on the high rail. The importance of this increase in the low-probability maximum loads depends on the failure mode for concrete ties. This increase on curves is very important if failures result from infrequent occurrences of very high loads; but fatigue failures are more sensitive to the mean cyclic load, and this should be the same as tangent track for a properly designed curve. In either case, differential vertical loads on curved track can be minimized by operating close to the balance speed.

Track vibration excited by flat wheel impacts, particularly with empty cars, appeared to be greater on the concrete tie track than has been observed from previous experience with wood tie track. A fundamental track resonant frequency of about 50 Hz and tie bending frequencies at 90 Hz and 140 Hz were evident from spectral analysis. Lightly loaded cars with wheel flats caused tie bending moments which exceeded those for heavy cars with wheels in good condition. The increase in dynamic loads from wheel flats on heavy cars is not nearly as severe as that for light cars due to the load-dependent ballast support distribution. The effects of wheel flats on track loads require additional investigation. Longer test durations and higher sampling rates for data analysis are needed to accurately include the effects of flat wheel impacts in the statistical data base.

Some minor corrugations with a wavelength equal to the 24 inch tie spacing were observed on the high rail at the curve site. These appeared to excite vibrations in the 30-40 Hz frequency range for speeds of 40 to 50 mph. Rail corrugations with a tie-spacing wavelength might be caused by the variation in track stiffness between ties on track having a very stiff roadbed. No corrugations were observed on tangent track.

2.2 SELECTION AND EVALUATION OF TRACK ANALYSIS MODELS

A computer program called MULTA (Multi-Layer Track Analysis), which combines a multi-layer elastic continuum representation for the ballast and subgrade with a finite element representation of the rails and ties, was developed to predict track vertical response. Experimental data from the FEC track indicated that track modulus based on rail seat load measurements ranged from 47 to 58 ksi for track with 24-inch and 20-inch tie spacing,

respectively. This unusually high track stiffness is attributed to a track construction consisting of granite ballast on a well compacted subgrade of sand and limestone ballast that was used for a previous wood tie track roadbed. However, when the model input data were adjusted to match the measured track modulus data, good agreement was obtained between measured and predicted values of tie/ballast pressure and rail seat loads.

This evaluation showed that the MULTA track analysis program would be adequate for track design parametric studies planned for future project work where it is important to evaluate the effects of ballast depth, tie size, tie bending stiffness and tie spacing on track response. These predictions of track response will be presented in a format which is suitable for track design trade-off studies. Wood and concrete tie track configurations expected to have equal maintenance intervals will be determined as a basis for subsequent life cycle cost comparisons.

3. TRACK ANALYSIS METHODOLOGY

The development of a predictive methodology for cross-tie track was directed toward three basic objectives. These objectives were:

- (1) To determine the effect of synthetic cross-ties on track response and service performance
- (2) To develop guidelines for track design using synthetic ties
- (3) To evaluate current industry specifications for synthetic tie/fastener assemblies.

Figure 3-1 shows the general format for a predictive methodology to meet these objectives. A statistical description of wheel/rail load represents the track loading for revenue traffic. This description of wheel/rail loads would be obtained from field measurement programs and/or analytical models of vehicle/track dynamic response.

Track analysis models, which will be discussed in this report, are needed to predict the load distribution through the track structure and to predict those response parameters, such as rail deflections, ballast and subgrade pressures, and tie bending moments which govern track design and performance. Failure criteria are needed for specific modes of track degradation to relate the response parameters to a measure of track performance which is meaningful to current U.S. railroad operations. For example, while the ballast and subgrade pressures may be the track response parameters which determine track settlement, appropriate failure criteria and performance measures are needed to predict how a change in these pressures will affect maintenance intervals for track surfacing in order to have a practical impact on railroad operations.

This section of the report includes a review of the principal modes of track component failure and long-term degradation to identify the formats for performance measures. These formats have only been identified in sufficient detail to evaluate and select appropriate track analysis models that predict the governing response parameters. Additional work on the development of quantitative criteria for describing track performance is planned for subsequent phases of this project and will undoubtedly continue to be a major topic for research.

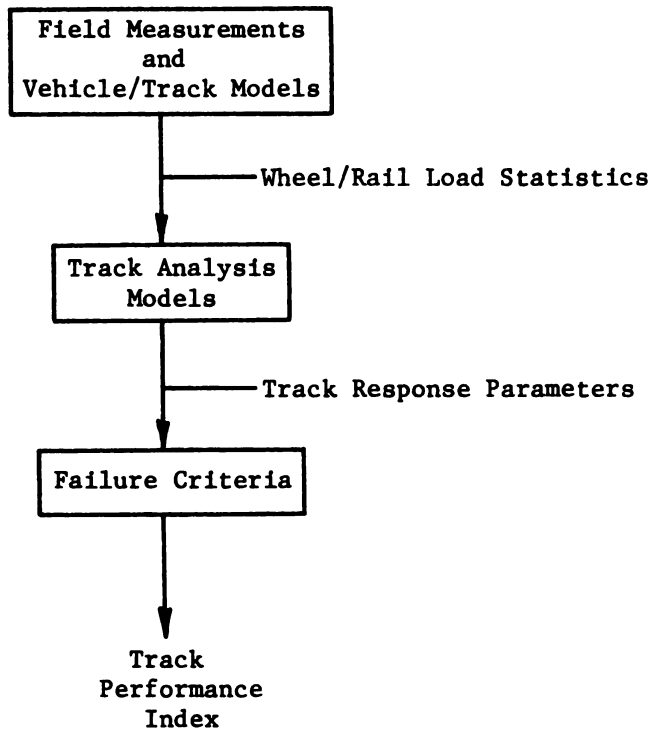


FIGURE 3-1. GENERAL FORMAT FOR TRACK ANALYSIS METHODOLOGY

3.1 REVIEW OF TRACK FAILURE MODES AND PERFORMANCE INDICES

Available information on the service performance of concrete tie track has been reviewed to determine the principal modes of component failure and long-term degradation expected for synthetic cross tie track. Despite considerable favorable experience with concrete ties in Europe and Japan, the U.S. experience with concrete track for mainline railroads has been relatively limited and disappointing. This can be partially attributed to the initial use of foreign ties which were designed for lighter axle loads and less severe operating conditions. Incorrect manufacturing procedures and poor ballast conditions were also responsible for a large percentage of the initial tie failures, resulting in a poor image for concrete ties in this country.

The major modes of track degradation which have been identified are:

- A. Failure Due to Non-Retention of Track Geometry
 - a. Track surface (profile and cross-level) deterioration
 - b. Track alinement deterioration
 - c. Wide gage
 - d. Rail rollover
 - e. Track buckling and lateral shift
- B. Component Failure
 - a. Rail failure
 - b. Tie failure due to bending and torsion
 - c. Rail fastener and pad failure
 - d. Ballast and subgrade failure.

The long-term deterioration of track geometry (surface, cross level, alinement, gage and track twist) and abrupt failures such as rail rollover and track lateral shift are of particular interest. Track buckling induced by high thermal loads is also an important track failure mode, but investigations of track buckling are being done concurrently on other research projects and will not be addressed herein. Rail failure, a very important failure mode, is also being investigated in other concurrent research projects.

The long-term deterioration of track geometry is responsible for a major portion of track maintenance costs and the increased loads on the track

and rolling stock which result from geometry deterioration cause increased vehicle maintenance and a reduction in safety. Also, the Track Safety Standards (TSS)[3-4]* published by the Federal Railroad Administration establish maximum permitted track geometry errors for different speed limits. This required reduction in train speeds over poorly maintained track is to improve safety and reduce derailment costs. However, it also increases operating costs for train crews, increases delivery schedules with a potential loss in business to competing transporting modes, and reduces the load capacity of the railroad unless capital funds are used to purchase additional cars.

The major track degradation modes and performance criteria are reviewed briefly in the following sections.

3.1.1 Tie Failure

Concrete cross ties were developed originally as a substitute for wood ties in areas of Europe where wood was scarce. Basic economies stimulated the initial development, and this continues to be a dominant factor as the cost and demand for wood increases and the supply diminishes. However, several other potential advantages frequently cited for concrete ties are:

- a. Their larger effective bearing areas usually permits wider tie spacings; therefore, the number of ties and fasteners which must be purchased, installed, and maintained is reduced.
- b. Their increased weight contributes to greater lateral track stability.
- c. They provide an opportunity to use a rail fastener that has been designed to provide resilience, adjustability, and improved rail restraint with minimum maintenance. The rail fastener also permits frequent rail replacement or swapping. The minimum maintenance aspect has been difficult to achieve, and fastener development work is still being done.
- d. The resistance of concrete ties to chemicals, weather, and abrasion is the basis for claims of long life, but there has been insufficient service time to demonstrate the advantage in durability that concrete ties have over the wood tie.

* Numbers in brackets denote references listed in the Reference Section.

Concrete ties also have some disadvantages which, in some cases, result from the same characteristic included as an advantage. The principal disadvantages which are frequently cited for concrete ties are:

- a. Their increased weight makes them difficult to handle and install, particularly for spot renewals.
- b. Attaching rail fasteners to the ties is a critical design problem.
- c. Their lack of structural resilience makes them more susceptible to major damage by the wheels of derailed cars or from non-uniform ballast support.

The many different designs of concrete ties are usually divided into separate categories for monoblock and two-block configurations. Monoblock ties are emphasized in this report because they have received the greatest interest for railroad service in the U.S. However, there are many similarities in the load environment and failure modes for monoblock and two-block ties.

The principal failure modes for monoblock concrete ties have been cracking in the rail seat area due to positive bending and cracking in the tie center due to negative bending and torsion. Cracking in the rail seat region is frequently attributed to the formation of a gap under the rail seat caused by crushing and flow of the ballast in the rail seat region (end bound tie). Negative bending in the tie center increases when the tie loses support in the end region (center bound tie). Torsional cracks have occurred most frequently with ties having a wedge-shaped center section which reduces torsional strength.

Current designs of monoblock concrete ties use prestress to utilize the compressive strength of concrete in resisting the tensile strains imposed by bending. The prestress is transmitted from the stretched tendons, or strands, to the concrete through the bonding of the concrete to the tendons which takes place prior to release of the preload. This bond strength, and hence, the effective transfer length depends on the diameter and surface condition of the wire and the detailed configuration of the prestress strands. The retention of adequate bond strength throughout the tie's life is a major factor for concrete tie performance.

Concrete tie failures can result from cumulative fatigue damage or an abrupt fracture caused by a single high load. The critical loading parameter for fracture is the probability of occurrence of maximum bending moments. When this is compared to a similar probability description of allowable tie bending

moment based on the strength of a particular tie design, a performance index can be developed in the form of the number of expected tie failures per mile for a specified service traffic.

The development of a performance index for tie fatigue damage is more complex. Fatigue statistics of the loading history can be used with a cumulative damage law to predict the cumulative damage for a specified service traffic. Miner's criterion (linear damage law) is a popular choice for estimating fatigue damage, assuming that data for the fatigue characteristics (S-N curves) for a particular tie are available. Typical concrete endurance strengths for 1 to 2 million cycles of compression from zero to a maximum are 50 to 55 percent of the ultimate compressive strength. The endurance strength for either one-way or reversed bending of plain beams is about 50% of the static flexural strength. These results indicate that failure due to cyclic loading can occur with compressive loading of the type expected for a prestressed concrete tie subjected to bending moments below the design strength.

At the present time, the question of whether concrete ties typically fail due to an abrupt fracture from a single high load or from cumulative fatigue damage has not been answered. This topic is discussed in greater detail in Section 4.7 of this report.

The current industry specifications for concrete ties are published in the American Railway Engineering Association (AREA) Bulletin 655 [3-1], with minor revisions given in Bulletin 660 [3-2]. Flexural strength requirements for monoblock ties include positive and negative maximum bending moments at the rail seat and tie center. The specified maximum required bending moments depend on tie spacing and tie length, and these maximum moments are used as static test specifications for no cracking within 30 days of casting. A repeated load test of 3×10^6 cycles of positive bending at the rail seat is also required for a precracked tie using a load range from 4 kips to 1.1 P, where P is the load required for the maximum static bending moment. It is not clear what service life the repeated load tests on the cracked tie are intended to represent, but the high loading used must be intended to represent only locomotives and very heavy cars rather than a more normal traffic mix. Also, the statistical aspects of the static load requirements are neglected. However, the specified loads are

certainly intended to represent a low probability of occurrence in service, because a crack-free tie has been a stated objective. None of the load tests on an uncracked tie are related to the initiation of a crack under repeated (fatigue) loading.

3.1.2 Rail Fastener Failures

The service history of rail fasteners used with concrete ties indicates the type of problems which can be expected for fasteners used with synthetic ties of any type. Typical problems include fracture and wear of rail clips, loose fasteners (particularly threaded), deterioration and dislocation of rail pads, failure of electrical insulation components and inadequate longitudinal restraint. The pull-out of fastener inserts and surface spalling where fasteners contact the tie have also been major design problems for particular concrete tie/fastener assemblies.

It is important to realize that many fastener failures result from the details of particular design configurations. The intent of this review is to determine the critical parameters and criteria governing fastener performance in general that are independent of design details.

Performance Criteria

The parameters which govern rail fastener performance were reviewed in a previous report [3-3]. Table 3-1 from this report summarizes the priority ranking of data needed to describe fastener performance. The priorities listed in Table 3-1 are ranked from I to IV in order of descending priority with regard to their application to laboratory life tests, fastener design criteria and the validation of analytical models.

The results in Table 3-1 indicate that the highest priority fastener loads are the vertical (V) and lateral (L) forces and the L/V force ratio. The rollover moment and moment ratio (M_r/V) at the rail base are equally important for defining fastener loading pertinent to fastener fracture and overall track performance.

TABLE 3-1. PRIORITY RANKING OF RAIL FASTENER DATA REQUIREMENTS [3-3]

	Laboratory Life Test	Fastener Design Criteria	Analytical Model Validation
I. Wheel/Rail Loads			
a. Vertical (V)	III	II	I
b. Lateral (L)	III	II	I
c. L/V	III	II	I
d. Longitudinal (L_o)	III	III	II
e. L_o/V	IV	III	IV
II. Fastener Loads			
a. Vertical (V)	I	I	I
b. Lateral (L)	I	I	I
c. L/V	I	I	I
d. Longitudinal (L_o)			
1. Thermal	II	I	II
2. Dynamic	II	II	II
e. L_o/V	II	II	II
f. Rollover Moment (M_r)	I	I	I
g. M_r/V	I	I	I
h. Long. Pitch Moment	III	III	III
i. M_r/V	IV	IV	IV
j. Yaw Moment (M_y)	III	III	III
k. M_y/V	IV	IV	II
III. Fastener Motion			
a. Vertical Disp.	II	I	I
b. Vertical Rail & Tie Accel.	III	III	II
c. Lateral Rail Head Disp.	I	I	I
d. Lateral Rail Base Disp.	III	II	I
e. Lateral Rail & Tie Accel.	IV	IV	II
f. Rail Roll Angle	II	II	II
g. Rail Long. Disp.			
1. Thermal	II	II	II
2. Dynamic	I	I	III
h. Rail Pitch Angle	III	III	III
i. Rail Yaw Angle	III	III	II
j. Track Gage	NA*	I	I
IV. Fastener Component Loads			
a. Hold-Down Loads	I	I	I
b. Rail Clip Stress	IV	IV	IV

(*) NA - Not Applicable.

The fastener response in terms of deflection under service loading is also important because rail deflection is more directly related to safety aspects such as wide gage and rail rollover. For these reasons, lateral displacement of the rail head and track gage are identified as high priority items. However, the criteria for wide gage and rail rollover will be discussed as separate topics.

The category of fastener component loads includes only the hold-down forces in the fastener attachment bolts and stresses in the rail clip. Both of these parameters depend on the particular fastener design configuration, but the frequent occurrence of failures and loosening of attachment bolts (on those fasteners which use bolts), and the need for realistic pull-out load specifications for the fastener inserts in the tie make the evaluation of hold-down load a high priority parameter.

As discussed previously for tie failure, the critical data requirement for evaluating abrupt fracture of rail fastener components is the probability of occurrence of maximum vertical loads V (both compressive and up-lift), and the lateral force L and rollover moment M_r load ratios L/V and M_r/V at the rail base. Statistical data on these parameters will depend on the fastener stiffnesses in the vertical, lateral and rollover directions for any fasteners which have stiffnesses of the same order as, or lower than, the corresponding stiffness from the track structure. The loads transmitted through fasteners which are rigid relative to the track are governed by the track stiffness and will be relatively insensitive to variations in fastener stiffness.

A comparison of the probability of occurrence statistics for peak loads with similar data for fastener strength can be used to evaluate performance in terms of the number of expected fastener failures per mile for a specified service traffic.

Current industry specifications [3-1, 3-2] have been developed for concrete tie fasteners. The lateral load requirements in this specification are based on a lateral load of 14,000 lbs per foot (35,000 lb for 30-inch tie spacing) with an equal vertical load applied simultaneously. Longitudinal load requirements of 1480 lbs per foot are based on having the fastener restraint equal or exceed the estimated longitudinal tie/ballast resistance for

unloaded track. A 12-kip pullout load test and a 250 ft-lb torque test are required for all fastener inserts.

Current fastener tests include an uplift static load of 1.5 times the initial fastener preload (not to exceed 10 kips) with no failure of the inserts or fastener components or release of the rail. Repeated load tests of 3×10^6 cycles include a 30 kip compressive load and an uplift load of 60 percent of the fastener preload applied at a 20° angle to the vertical. No structural failures are permitted.

Longitudinal restraint tests following the repeated load tests limit the maximum rail movement to 1/4 inch with a longitudinal load based on tie spacing. Lateral load restraint tests are made with a 30° load angle. A maximum lateral displacement of 1/8 inch is permitted at the rail base with a 41 kip load and a fixed loading ram. A maximum lateral rail head displacement due to rail rotation of 1/4 inch is permitted with a 20.5 kip load and a roller-bearing ram. These criteria are presumably related to maximum allowable gage change and potential rail rollover failures under traffic, but this relation is not documented in current specifications or other literature. The criteria for wide gage and rail rollover are discussed in a later section.

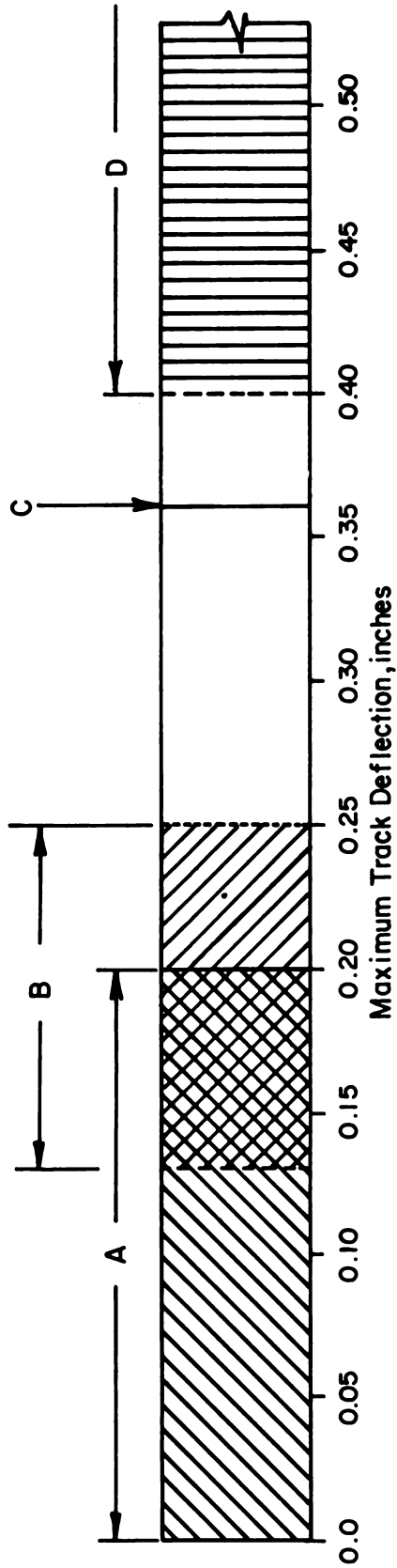
3.1.3 Track Surface Deterioration

The deterioration of track surface is determined by the differential vertical settlement of each rail (rail profile) and the differential settlement between rails at the same location (cross level). Surface maintenance is particularly prevalent on bolted-joint track. However, only continuous welded-rail (CWR) track is being considered in this program, because CWR will usually be used for new track construction having synthetic ties. Track settlement in the vicinity of structures, such as bridges or highway grade crossings is also a perpetual problem. Some settlement relative to a fixed structure is inevitable, and this causes an abrupt change in track surface and stiffness. However, the general deterioration of the surface of CWR track that is constructed on what would normally be considered a uniform roadbed is of principal concern for this project.

A recent report [3-5] reviewing current track design procedures indicated that although track geometry is a key parameter in track performance, there are no design criteria directly related to the degradation of track surface from differential settlement along the track route. What is done in track design is to prepare the roadbed to a minimum acceptable soil-bearing capacity and then to use a track construction which is uniform in terms of ballast depth, tie spacing and rail size. The track design parameters are selected using past experience and analytical predictions of track deflection and average ballast and subgrade pressures. This results in a track which can have considerable variation in stiffness and strength from one location to another; hence, differential settlement can be expected.

The AREA recommendation [3-6] of a maximum track deflection of 0.25 inches based on the beam on elastic foundation analysis procedure has been used for recent design evaluations [3-7] of new track construction for the Northeast Corridor (NEC). Figure 3-2 from Reference [3-8] shows similar track deflection criteria based on Talbot's studies for the AREA Special Committee on Stresses in Railroad Track.

A review of the literature indicates that there are no quantitative performance measures to relate a description of the railroad traffic with the track design parameters and track surface deterioration rate. Some laboratory investigations [3-21 thru 3-23] using triaxial repeated load tests with granular and cohesive soils give an indication of the way typical ballast and subgrade materials will behave under uniform loading conditions. Settlement rate appears to be proportional to some power n of deviatoric stress σ_d^n , and the settlement increases proportional to N or $\log N$, where N is the number of cycles at a specified loading. A cumulative settlement law for combining the various stress amplitudes and number of cycles representing typical traffic has not been established for utilizing results from these laboratory material tests.



Range	Track Behavior
A	Deflection range for track which will last indefinitely.
B	Normal maximum desirable deflection for heavy track to give requisite combination of flexibility and stiffness.
C	Limit of desirable deflection for track of light construction (≤ 100 lb rail).
D	Weak or poorly maintained track which will deteriorate quickly.

Values of deflection are exclusive of any looseness or play between rail and plate or tie and represent deflections under load.

FIGURE 3-2. TRACK DEFLECTION CRITERIA FOR DURABILITY [3-8]

The Japanese National Railway (JNR) has done some track settlement tests to develop empirical relations for settlement due to ballast flow and long term degradation. These results indicate a settlement rate that is related to the product of average tie/ballast pressure and ballast acceleration. A linear dependence on number of loading cycles is proposed following an initial high rate of settlement before consolidation has been established. The linear relation is particularly attractive for combining traffic conditions with different axle loads and train speeds. The JNR made no attempt to separate ballast settlement from subgrade settlement except to determine the effect of different ballast depths on overall settlement rates.

The current state-of-the-art regarding track settlement indicates that only a relatively simplified performance index is justified. However, this index should include the fundamental ballast and subgrade parameters needed for evaluating the effects of variations in track design parameters. This requires identifying the relative contributions from the ballast and subgrade to the total settlement.

The critical parameters which are needed as output from a track analysis model are the average deviatoric stress in a layered representation of the roadbed for the statistical loading description of the railroad traffic. Other operating parameters, such as train speed which affect dynamic wheel loads, track roughness, etc. would be included by using a probability density description for wheel/rail loads to calculate the resulting roadbed stresses.

The FRA track safety standards [3-4] are the only current U.S. specifications on track geometry except for those standards which individual railroads may use. The transit industry has a similar set of geometry standards which are somewhat more restrictive for the same operating speeds because of the emphasis on passenger comfort rather than safety. The FRA track safety standards specify maximum deviations in the profile of each rail under a 62-ft chord, so the geometry characteristics as a function of wavelength are important for a performance index using these criteria. Similar limits are given for the deviations in cross level on tangent and spirals and the difference in cross level (twist) in intervals less than 62 ft on tangent and spirals. Specific

dimensional limits are specified for each track class, which also designates different maximum operating speed for freight and passenger traffic.

3.1.4 Track Alinement Deterioration

The deterioration of track alinement is determined by the differential lateral displacement of the track centerline. This can arise from relative displacement between the rails and ties and from a lateral shifting of the ties in the ballast. However, the displacement of the rails relative to the ties usually increases the track gage, and this mode of deterioration will be discussed as a separate section entitled "wide gage". The primary emphasis in this section is on the degradation in track alinement which is caused by lateral motion of the ties in the ballast from a combination of wheel/rail forces and thermal forces. The potential for increased lateral resistance for a synthetic tie is an important factor in comparing the performance of synthetic ties with standard wood ties.

Conventional track design procedures result in selecting tie size, the spacing and rail size to meet vertical load requirements. Therefore, ballast type or the width of the ballast shoulder at the tie ends are about the only independent design parameters which can be varied to change the lateral resistance of wood tie track. For synthetic tie/fastener systems, however, the tie shape and weight and the ability of the fastener to prevent the rail from rotating in a horizontal plane (rotation about a vertical axis) can also increase the track's lateral resistance.

When the track is occupied by a train, the lateral strength must be sufficient to resist both the thermal forces and the lateral component of the wheel/rail loads. The presence of the vertical wheel loads is an important factor in increasing track lateral strength. However, it is believed that some occurrences of track buckling have been initiated where the track lateral resistance is reduced substantially in the uplift region between the front and rear trucks of a car or immediately in front of the locomotive or behind the last car in a train. The mechanics of track buckling are quite complex, and the limited discussion in this section is intended only to illustrate the type of information available for evaluating track design and performance. Considerable research on track buckling and track lateral resistance is being done

currently in the United States and Europe, so additional information on this topic should be available soon. At this time, there is much less known about lateral track characteristics than vertical because of the emphasis on vertical track response criteria for track design.

The current United States design procedure related to the lateral strength of track is based on the lateral resistance required to resist thermal loads on unloaded track in curves [3-6]. The equation used to determine the lateral force produced by thermal loads with CWR is:

$$P_f = 0.441D_c (\Delta T) \quad , \quad (3-1)$$

where P_f is the lateral track force (pounds per foot of track length), D_c is the degree of curve (degrees), and the ΔT is the temperature change ($^{\circ}F$) from the initial rail laying temperature (zero longitudinal load).

The lateral resistance of unloaded track is based on available data for the lateral resistance R (pounds per tie) for a specified ballast type and shoulder width, so the maximum tie spacing given by

$$l_t \leq \frac{R}{P_f} \quad (3-2)$$

can be compared to the tie spacing determined by vertical load requirements. If increased lateral resistance is needed, it can be obtained by reducing the spacing, by increasing the ballast shoulder width, by "humping" the ballast above the tie at its ends, or by increasing tie size or weight. However, any of these approaches requires quantitative data on the effect of these parameter variations.

Current design values for 7-in. x 9-in. wood ties are based on an estimated lateral resistance of 300 lbs. [3-6] for a tie buried to a 4-in. depth of ballast with a 6-in. shoulder width. Tie resistance is assumed to be totally dependent on shoulder width, W , according to:

$$R = R_o \left(\frac{W}{W_o} \right) \quad , \quad (3-3)$$

where R_o and W_o are the tie resistance and shoulder width for a known reference. A sample calculation for an 8-degree curve and $\Delta t = 65^{\circ}F$ gives $P_f = 229$ lb per foot. A ballast shoulder width of 7-1/2 in. would be required for a 19-1/2-in. tie spacing using the current track design procedure.

Typical measurements show that lateral tie resistance does not increase significantly for shoulder widths greater than 14-16 in., so a linear relation must be used with caution. Also, the shear forces on the sides and bottom of the tie contribute some resistance which is not identified by the simplified approach given by Equation (3-3). The tie sides and ends typically provide 20-30 percent of the total resistance each, and the tie bottom provides about 50 percent of the total resistance.

The FRA track safety standards [3-4] give alinement standards in terms of maximum deviations of the mid-offset (tangent track) or mid-ordinate (curve track) of the line rail from a 62-ft chord. These range from 1/2-in. for Class 6 track to 5 in. for Class 1 track. A performance index suitable for this type of long-term degradation criterion would be similar to that for vertical settlement in that the differential settlement as a function of wavelength is required. Very little research has been done on the mechanisms governing this type of cumulative degradation in the lateral direction.

As discussed previously, the major emphasis has been on determining an effective elastic limit or critical force as a safeguard against the relatively large lateral track deflections which can occur when this limit is exceeded. For this failure mode, the ratio of critical lateral load to the actual lateral load from individual axles indicates an operating safety factor. Statistical data in the form of probability densities for the total lateral force from individual axles and the corresponding vertical axle force are needed to evaluate the probability of exceeding the critical load for track lateral shift. Similar statistical data for track lateral resistance limits are needed to predict the number of expected exceedances per mile for a specified track section and traffic.

3.1.5 Rail Rollover

The track failure mode known as rail rollover could be classified as a rail fastener failure, a wide gage problem or a lateral alinement problem.

The failure is characterized by the sudden occurrence of sufficient lateral motion of the rail head so that one rail collapses completely or the track gage becomes sufficiently wide that the wheel drops off the opposite rail. Rail rollover is sufficiently distinct from other failure modes and represents such a severe condition that it has been classified separately by the railroad industry.

The resistance of the rail to lateral forces depends on a complex combination of lateral bending and torsion of the rail combined with restoring moment from vertical forces and the resistance from rail fasteners. The contribution from the rail fasteners used for wood and concrete ties is considerably different. The cut spikes used for U.S. wood ties are installed with a nominal 1/8-in. gap between the spike head and the rail base, and this gap is frequently increased to 1/2 to 1 in. during service. Therefore, the spike resistance does not restrain rail rollover until the inside edge of the rail base has lifted off the tie a sufficient distance to contact the spike head. In comparison, the type of fasteners normally used with synthetic ties grip the rail base with an established preload and provide a relatively well-defined elastic restraint for loads less than the fastener load. Consequently, the rail rollover problem is expected to be of much less importance for synthetic ties and fasteners than it is for wood tie track with cut spikes.

The ratio of lateral (L) to vertical (V) wheel loads, L/V , has been used by the railroad industry as the governing parameter for rail rollover. A conservative evaluation of this limiting condition can be estimated using a simplified model consisting of one truck on a 39-ft rail section that has loose joint bars at each end. Therefore, the rail torsional restraint can be neglected. If the rail fastener restraint is also assumed negligible, the overturning stability depends only on the rail geometry. For typical rail geometries, this ratio ranges from 0.5 to 0.66. Therefore, a conservative limit of $(L/V)_{\max} = 0.5$ for the wheels on one side of a truck has been retained as the industry criteria for rail rollover.

This critical ratio can be increased by the restraint from sound spikes or a good fastener. The Association of American Railroads (AAR) Research Center conducted tests [3-9] to determine the resistance for cut spikes with a wood tie and for a rail clip with a concrete tie. These results showed an additional lateral force capability at the rail head of:

new cut spikes on wood tie	5500 lb/tie
rail clip on concrete tie	10,000 lb/tie.

These restraint limits were determined by the load which caused a rapid increase in deflection for a small increase in load. The limit for the wood tie with cut spikes occurred at a maximum deflection of about 1/4 in., whereas the concrete tie fastener permitted a 3/4-in. deflection. This fastener restraint, assuming the fasteners on only two ties are effective, gives:

$$(L/V)_{\max} = 0.5 + \frac{11,000}{V} \quad \text{Wood tie}$$

$$(L/V)_{\max} = 0.5 + \frac{20,000}{V} \quad \text{Concrete tie.}$$

A vertical load of 72,000 lbs for 2 wheels on one side of a truck gives an L/V of 0.65 for wood ties and 0.78 for concrete ties. However, this additional restraint from cut spikes should probably be ignored considering the frequently poor condition of wood ties in service.

A more detailed evaluation of rail deflections from the lateral and vertical loads from several wheels with the distributed effects of rail torsion included is relatively complex. The AAR is currently measuring this resistance for wood tie track loaded by an actual car as part of an investigation to determine if longitudinal forces are a major factor in producing rail rollover. It has been hypothesized that the presence of longitudinal loads in conjunction with simultaneous vertical and lateral loads might be the most adverse condition for causing rail rollover.

As discussed previously, the criterion for rail rollover which is generally accepted by industry is a minimum L/V ratio of 0.5 for all wheels on one side of a truck. This is a somewhat conservative criterion for wood tie track, depending on its condition. Test results show that rail rollover failures are initiated when the rail head lateral deflection relative to the tie exceeds about 1/4 in. for wood tie track.

Elastic rail fasteners of the type used on synthetic ties provide increased restraint for rail rollover, but they do permit larger deflections at loads below the critical load. Railhead deflections on the order of 3/4 to 1 in. can be endured without failure.

The current AREA test specifications for concrete tie fasteners [3-1,3-2] restrict the lateral deflection of a rail section held by one fastener to 1/8 in. at the base under a 35 kip vertical load and 20.5- kip lateral load ($L/V = 0.5$). A second requirement is for a maximum rail head deflection of 1/4 in. with a lateral load of 17.5 kips and vertical load of 10.25 kips ($L/V = 0.5$) using a loading ram which allows free lateral head motion.

For reference purposes, normal freight car axles are sized to operate with a ± 0.350 -in. clearance from the nominal centered position to flange contact. Once flange contact is made, an additional rail deflection of about 2 inches would be required before the wheel edge moves on top of the rail head with the possibility of suddenly dropping down between the rails. Consequently, rail rollover should occur before wheel drop-off.

3.1.6 Wide Gage

A gradual increase in the track gage under traffic is generally classified as a wide gage problem. It is a type of track geometry deterioration which can become a safety problem if the gage widens excessively. The problem of wide gage has become increasingly important during the past decade with the increasing use of six-axle diesel locomotives and 100-ton freight cars. This problem is most frequently associated with tight curves where the lateral forces are high. However, some railroads operating freight trains up to 70 mph have observed rapid gage widening on tangent track, particularly with frozen ballast conditions. The gage on tangent track has been observed to increase as much as 3/4 in. in four months during the winter. High lateral forces on tangent track can be attributed to freight car hunting.

The failure mode causing wide gage includes tie plate cutting, severe indentation of the tie surface on the field side of the tie plates and lateral deflection of the cut spikes from bending and from deformation of the tie/spike interface. This deterioration permits the rail and tie plate to move laterally and rotate outward under high lateral loads, and the resulting permanent deformation increases track gage.

Permanent deformations of wood ties and spikes are the main contributors to wide gage. The governing load parameters are the vertical and lateral forces and the rollover moment applied to the tie plate. The L/V ratio governs tie plate motion which causes tie cutting and transmits lateral loads to the spikes. The combined vertical load and rollover moment determine the maximum compressive load on the field side of the tie plate that causes tie crushing when the compressive strength is exceeded. The important consideration for reducing wide gage is to prevent lateral motion of the tie plates relative to the tie and to keep compressive loads on the tie plate ends below the tie crushing strength. Larger tie plates, higher cant tie plates and more spikes have been used by industry to combat this problem. It is also recognized that heavy cars and locomotives and hunting cars are producing the loading which causes wide gage. Reduced operating speed will alleviate wide gage problems, but this is often undesirable.

A major advantage of using synthetic ties and fasteners is that wide gage can be eliminated. Current fasteners used with concrete ties are capable of maintaining close gage tolerances under high tonnage with very little long-term deterioration. The elimination of the spike-killing problem which results from frequent re-gaging in curved territory has been cited as a major reason for replacing wood ties with concrete ties.

The FRA track safety standards [3-4] specify maximum limits for track gage for each track class. Nominal track gage is 4' 8-1/2", and a minimum gage of 4'8" (1/2-in. tight) is permitted for all track. The maximum gage for tangent track varies from 1/4-in. wide for Class 6 track to 1 1/4 in. wide for Class 1 track. The maximum gage for curved track varies from 1/2 to 1 1/4-in. wide for the same track classes. This allows for a 1/4-in. increase in nominal gage that is used by some railroads for curved track.

Current AREA specifications for concrete tie fasteners [3-1,3-2] include a repeated load test of 3×10^6 cycles to represent the vertical and lateral loading from traffic. No structural failure of the fastener is permitted, and a subsequent lateral load restraint test, discussed in the rail rollover section, insures that wear of the fastener components is not excessive for maintaining track gage. The wide gage problem is mainly associated with wood tie track using cut spikes. It should not be a significant factor in the performance of synthetic ties and fasteners. The virtual elimination of premature gage maintenance (normal gage change is required by rail wear) is a major advantage for synthetic cross tie track.

3.1.7 Track Analysis Requirements

Table 3-2 summarizes the performance indices and critical track parameters which govern each of the major modes of track degradation. These factors were used to determine the types of track models and the formats for track loads which are needed to analytically evaluate track performance. Also listed in the table are the approximate frequency ranges of interest for each degradation mode.

3.2 REVIEW OF TRACK ANALYSIS MODELS

Existing track analysis models were reviewed during the first phase of this research project. Many of the available track models were developed or assembled by the AAR under contract to the FRA. The role of BCL was to select those models which were most suitable for meeting the requirements listed in Table 3-2 for the specific objectives of this project.

Table 3-3 summarizes the capabilities of available track analysis models and additional details are given in Appendix A. The discussion in this section of the report will be limited to a description of the major differences and limitations of the different types of models.

3.2.1 Elastic Foundation Track Models

Several track models for vertical or lateral loading of rails or single ties are based on the well known solutions for a continuous beam supported by an elastic foundation. These models are used to predict rail and tie deflections and bending moments for specified track stiffnesses representing different values of tie spacing and track modulus. The principal advantages of these models are that reasonably accurate predictions of rail deflections and rail bending stresses can be obtained if the support stiffness is selected carefully, and the computational efficiency from closed form solutions makes this an attractive choice for parametric studies.

TABLE 3-2 SUMMARY OF TRACK DEGRADATION MODE ANALYSIS REQUIREMENTS

Degradation Mode	Performance Index	Critical Parameters	Analysis Model Requirements	Load Requirements	Frequency Range, Hz
1. Tie failure from bending and torsion	Number of expected tie failures per mile per MGT based on probability of fracture or exceeding fatigue life	Tie bending and torsion moment probability density for specified traffic. Tie strength probability density for static load failure. Fatigue statistics for tie bending and torsion moments and statistical description of tie fatigue strength in torsion and bending	Single vertical tie finite element model with rail seat loads and moments and variable stiffness ballast support to predict tie bending moments. Estimate of maximum torsional moment based on predicted statistical tie plate loads	Probability distributions of peak vertical rail seat loads and rollover moment for the specified traffic, speeds, and track condition	0-50
2. Rail fastener failure a) Pull-out of tie inserts b) Failure of rail clips	Number of expected fastener component failures per mile per MGT based on probability of fracture or exceeding fatigue life	Probability density of maximum rail seat loads L/V & M_r/V at rail base. Probability density of fastener component strength for static load failure. Statistical description of fastener component fatigue strength	3-D finite element track model which includes non-symmetrical vertical and lateral W/R loads, fastener stiffness, rail torsion and non-linear stiffnesses for fastener and ballast	Probability density of peak vertical, lateral and L/V W/R loads and peak rail seat loads and moments	0-2000
3. Track surface deterioration (vertical profile and cross level) a) Ballast failure and flow b) Subgrade failure and settlement.	Rate of rail profile and cross level deterioration versus wavelength	Probability density of maximum and average tie ballast pressure, maximum subgrade deviator stress (G_1-G_2), cumulative settlement data for ballast and subgrade materials	Vertical track model using Ruster's multi-layer roadbed model and load distribution program to predict ballast and subgrade pressures and tie deflections	Probability density of peak vertical W/R and rail seat loads for specified traffic	0-50
4. Track alignment deterioration	Number of occurrences per mile where critical load for track lateral shift is exceeded	Probability density of maximum lateral force ratio H/P for individual axes. Probability density of track critical lateral force ratio H_c/P	Vertical track model using Ruster's multi-layer roadbed model and load distribution program to predict vertical tie loads. 2-D finite element lateral track model with thermal loads, rail fastener torsional resistance and nonlinear ballast resistance which is dependent on vertical tie loads	Joint probability density of peak vertical and H/P axle load ratio for specified traffic	0-10
5. Rail rollover	Probability of exceeding critical rail loading condition (L/V)	Probability density of maximum lateral force ratio (L/V) for one rail. Probability density of rail critical L/V for rollover	3-D finite element track model which includes non-symmetrical vertical and lateral W/R loads, fastener stiffness, rail torsion and non-linear stiffnesses for fastener and ballast	Probability density of lateral/vertical load ratio for all wheels on one side of one truck	0-10
6. Wide gage	Probability of exceeding critical ratio for tie plate loading on wood ties. Probability of exceeding tie compressive strength on field side of tie plate. Rate of gage change per MGT.	Probability density of maximum L/V load ratio and maximum M_r/V moment ratio for tie plates. Probability density of allowable L/V and M_r/V for tie plate slip and tie crushing on wood ties	3-D finite element track model which includes non-symmetrical vertical and lateral W/R loads, fastener stiffness, rail torsion and non-linear stiffnesses for fastener and ballast	Probability density of L/V load ratio for individual wheels	0-50

H = Lateral axle force
 L = Lateral wheel force
 P = Vertical axle force
 V = Vertical wheel force
 M_r = Rail rollover moment

TABLE 3-3. SUMMARY OF AVAILABLE TRACK ANALYSIS MODELS

Model Description	Stresses	Deflections	Missing Ties	Off Loading	Multi-layers	Vertical Load	Lateral Load	Weak Spot in Ballast	Static	Dynamic	Linear	Linear	Joists
I. Elastic Foundation													
a. Rail on Elastic Found., Vertical BCL	Rail bending	Vert.	No	No	No	4	No	No	Yes	No	Yes	No	No
b. Rail on Elastic Found. with Axial Load, Vertical	Rail bending	Vert.	No	No	No	4	No	No	Yes	No	Yes	No	No
c. Tie on Elastic Found., Vertical BCL	Tie bending	Vert.	No	No	No	2	No	No	Yes	No	Yes	No	No
d. Rail on Elastic Found., Vertical, AAR	Rail bending	Vert.	No	No	No	Yes	No	No	Yes	No	Yes	No	Yes
e. Rail on Elastic Found., Lateral, AAR	Rail bending	Lat.	No	No	No	No	Yes	No	Yes	No	Yes	No	Yes
II. 2-D Finite Element													
a. Finite Element Lundgren	2-Dimen.	2-Dimen.	Yes	Yes	Yes	Yes	No	Yes	Yes	No	No	Yes	Yes
b. ILLITRAK Univ. of Illinois	Vert., Hor.	Vert., Hor.	Yes	No	Yes	Yes	No	Yes	Yes	No	No	Yes	Yes
c. Finite Element Lateral Rail AAR	Yes	Lat., Rot.	Yes	Yes	Yes	Multiple	No	Yes	Yes	No	No	Yes	Yes
d. Finite Element Rail, BCL	Yes	Vert., Rot.	Yes	Yes	No	Multiple	No	No	Yes	No	Yes	No	Yes
e. Finite Element Vertical Rail, AAR	Yes	Vert., Long. Rot.	Yes	No	Yes	Multiple	No	Yes	Yes	No	No	Yes	No
III. 3-D Finite Element													
a. Finite Element Rail-tie, Kilmartin	No	Vert., Lat. + 3 rot.	Yes	Yes	No	Multiple	Multiple	No	Yes	No	No	Yes	Yes
b. Finite Element 3-D Track AAR	Yes	Vert., Lat. 3 rot.	Yes	Yes	Yes	Multiple	Multiple	Yes	Yes	No	No	Yes	Yes
c. Finite Element Rail-Fastener AAR	Yes	3 rot.	Yes	Yes	Yes	Yes	Yes	Yes	Yes	No	No	Yes	Yes
d. Finite Element 3-D Herrmann	3 normal components	Vert., Lat., Long.	Yes	Yes	Yes	Yes	Yes	No	Yes	No	Yes	No	Yes
e. 3-D Finite Element Queen's University	3-D	3-D in Ballast Vert. in Rail	Yes	Yes	Yes	Yes	No	Yes	Yes	No	No	Yes	Yes

TABLE 3-3. (Continued)

Model Description	Stresses	Deflections	Missing Ties	Off Loading	Multi-layers	Vertical Load	Lateral Load	Weak Spot in Ballast	Static	Dynamic	Linear	Non-linear	Joints
IV. Ballast/Subgrade													
a. Talbot's Eq.	Vert.	No	No	No	No	Yes	No	No	Yes	No	No	Yes	Yes
b. Pyramid Model	Vert.	Yes	No	Yes	Yes	Yes	No	No	Yes	No	No	Yes	No
c. Boussineq's Eq.	Vert., Rad., Ang., Shear	Vert., and Radial	No	Yes	No	Yes	No	No	Yes	No	No	Yes	No
d. Westergaard's Sol.	Vert.	No	No	Yes	No	Yes	No	No	Yes	No	No	Yes	No
e. Cerruti's Sol.	No	Vert., Lat. Long.	No	Yes	No	No	Yes	No	Yes	No	No	Yes	No
f. Burmister's	Vert., Rad., Shear	Vert. and Horiz.	No	Yes	Yes	Yes	No	No	Yes	No	No	Yes	No
g. JNR Model	Subgrade Vert.	No	No	No	No	Yes	No	No	Yes	No	No	Yes	No
h. Love Equation	Subgrade Vert.	No	No	No	No	Yes	No	No	Yes	No	No	Yes	No
i. Salem and Hay	Vert.	No	No	No	No	Yes	No	No	Yes	No	No	Yes	No
j. Weissmann	Vert. at Top of Soil	Vert. at Top of Soil	No	No	No	Yes	No	No	Yes	Yes	Yes	No	No

The principal limitations of these models are:

a. The Winkler elastic foundation model neglects shear coupling in the roadbed which may distort the effect of variations in tie spacing -- a major design parameter.

b. Variations in ballast depth and subgrade properties cannot be evaluated directly.

c. Estimates of ballast and subgrade pressures require approximations which do not include the effect of tie size and tie bending.

d. Non-uniform tie spacing or track support conditions or off loading (different wheel loads on a common axle) cannot be included.

3.2.2 Two-Dimensional Finite Element Track Models

Two-dimensional finite element track models can be used to analyze the ballast and subgrade and to predict loads and displacements of the tie, pad, fastener and rail. A distinct advantage in using finite elements is the ability to vary the properties of each element, so that the analysis is no longer that of an ideal system. The main disadvantage of any finite-element analysis is the increased cost of the computer runs.

Finite Element Model - Lundgren

This finite-element model utilizes a computer solution based on matrix structural analysis methods to evaluate a track structure under static vertical loads. The main advantages of this model are that it includes:

- a. Different soil properties at each element, if needed.
- b. The effect of missing ties or variable tie spacing.
- c. Predictions of soil shear and tensile failure using maximum stress criteria.
- d. Non-linear behavior of soil.

The main disadvantages with this model are that:

- a. No longitudinal or lateral loads are incorporated

b. Rail fasteners are not included in the model.

This model experiences numerical instability problems in cases of very light loads applied to stiff systems, but this would probably not be an important limitation for track design analysis.

Finite Element Model - Robnett

This model uses a two stage solution procedure. The model first considers vertical loading in a vertical longitudinal plane. The output from the longitudinal analysis in the form of either maximum reaction or maximum deflection at the tie is then used as input to the transverse model. The advantages and disadvantages associated with this model are practically the same as those listed previously for the Lundgren model. All ballast and subgrade pressure predictions utilize and assumed effective length for the tie bearing area, so tie bending effects are not included.

Finite Element Vertical or Lateral Rail Model - AAR

This model consists of a two-dimensional finite element representation of a track structure. The analysis program used is "FRAM 2", a standard program for frame analysis. The roadbed tie stiffness is represented by beam members of finite length and cross section. These springs may have linear or non-linear characteristics. The model could be modified to incorporate off loading and staggered joints in the rails. Validations show reasonable agreement with listed data and a comparison with results from a beam-on-an-elastic-foundation model shows good agreement. The principal disadvantage of these finite element models is the difficulty in evaluating the effect of changing ballast depth or the material properties of the ballast and subgrade.

Finite Element Vertical Track Model - BCL

A single rail is divided into a large number of grid points. Variable distance between grid points is allowed. The support from individual

ties and fasteners is included in the model by discrete springs. Therefore, ineffective ties or fasteners, rail joints, and multiple wheel loads can be investigated. This vertical-only model does not include off-loading.

3.2.3. Three-Dimensional Finite-Element Track Models

Three-dimensional finite-element models permit variable element properties and loads. However, three-dimensional models require increased input data, and the computer costs are usually greater than for the simplified models.

Rail Tie Model - Kilmartin

This finite element model has a good representation of the rail-tie structure, but the ballast is not modeled in detail. The advantages of this model are:

- a. Variable tie spacing and rail joint stiffness can be included.
- b. Vertical and lateral deflections and three rotations are calculated at each connection point.

Two disadvantages are:

- a. The analysis does not include rail pad stiffness, rail fasteners, or variable ballast modulus.
- b. No lateral or longitudinal loads are included.

Track Structure and Rail Fastener Models - AAR

These are three-dimensional track models representing the rails, fasteners, ties, and roadbed by structural members and springs. Rails and ties are represented by beams and the roadbed is represented by springs. Some of the disadvantages of this model are the ability to include

- a. Variable tie spacing or missing ties
- b. Multiple wheel loads
- c. Irregularities in the rail and rail joints
- d. Off loading and staggered joints.

Hermann Prismatic Solid Analysis (PSA) Model

This is a three-dimensional finite-element roadbed model that analyzes a periodically loaded prismatic solid. The PSA model assumes the prismatic body is infinite in length with constant cross sectional and material properties in the longitudinal direction.

Some advantages of the model are:

- a. Material properties can vary from point to point in the cross section and the geometry of the ballast section can be represented accurately.
- b. Off-loading can be included.
- c. Temperature and body forces can be included.
- d. Missing ties and rail joints can be investigated.

The main disadvantages are:

- a. The output from this roadbed model must be combined with a loads combination which includes the rails and ties for a complete track structure analysis.
- b. The loads in the longitudinal direction have to be equally spaced and of equal intensity.
- c. When the spacing between loads becomes too large, a large number of Fourier-series terms have to be computed, resulting in excessive computer time.
- d. The roadbed cross-section must have finite width and depth dimensions, and a large number of elements are required if the boundaries are to be sufficiently far away to represent actual track.
- e. The foundation materials are assumed to be homogeneous and isotropic.

3.2.4 Ballast/Subgrade Models

Most of the models identified under the ballast/subgrade heading are only algebraic equations for predicting pressures in an elastic continuum. These are theory of elasticity solutions for homogeneous materials

having different types of loading and various restrictions on displacements. Some of the solutions predict both stresses and displacements, while others predict only stresses.

Models by Talbot, the Japanese National Railway (JNR), Love, and Salem and Hay have been used to predict the pressures on a track subgrade as a function of ballast depth and to derive correction factors which give a reasonable fit to the particular test conditions selected. The difficulties with all of these models are that the differences in material properties between ballast and subgrade are not included, and that those equations which predict only stresses are not amenable to use with an overall track model where the roadbed displacements and stresses must be compatible.

The stress-pyramid model utilizes a simplified model of the variation in ballast pressure with depth. This gives an estimate of deflections at the ballast and subgrade interfaces so that ballast depth and material properties for ballast and subgrade can be varied independently. The stress-pyramid model has been coupled with the equations for a beam on elastic foundation to give a complete track model. The principal limitation is that the effective bearing area of each tie must be estimated, and equations for this estimate do not include an accurate evaluation of tie-bending effects. The importance of tie-bending effects are discussed in a later section.

The Burmister model can be used to represent a layered elastic half-space having different material properties in up to seven layers. Displacement and stress distributions are predicted for any number of circular areas loaded by uniform vertical pressure. The infinite horizontal dimensions of this half-space model preclude representing the actual ballast cross-section geometry. However, the Burmister model does provide for the evaluation of ballast depth and variations in ballast and subgrade properties without the additional complexity and cost of using a complete finite element model.

3.3 TRACK MODEL SELECTION

Data requirements for the different modes of track degradation (Section 3.1) and the results of the model review (Section 3.2) were evaluated in order to select a specific set of track models for use during this project.

3.3.1 Vertical Track Model

The evaluation of track performance and track design for vertical loads requires the ability to predict realistic pressure distributions at the tie/ballast interface and at the ballast/subgrade interface. This requires a model which includes the effect of tie bending and changes in ballast depth, roadbed material properties, and tie spacing in a unified manner. In such a model, changes in roadbed configuration that affect track modulus and the resulting redistribution of loads from the rail to individual ties would be readily apparent.

The AAR had developed a loads-combination program to combine load/deflection influence coefficients from the Hermann PSA ballast/subgrade model with similar influence coefficients for a track superstructure of individual rails and ties. However, a comparison of the PSA and the Burmister multi-layer roadbed models indicated the latter would be a more cost-effective approach without sacrificing any significant features provided by the PSA finite element representation. As a result, the multi-layer model was selected to obtain roadbed influence coefficients for the loads-combination program, and this was modified at BCL for use as the principal track model for this project.

Figure 3-3 shows a schematic of this combination model which has been designated MULTA for Multi-Layer Track Aalysis. This provides a linear track analysis which includes single or multiple wheel loads on 2 rails supported by ties of variable size and spacing and having a bending rigidity. The tie area is divided into segments of approximately square dimensions, and these are used to generate influence coefficients for pressures and displacements from the multi-layer roadbed model. This system of equations is solved using matrix analysis techniques to yield numerical values for ballast and subgrade stresses and the displacements of the rails and ties. Rail and tie bending moments are computed from the tie and rail reaction load distributions.

3.3.2 Vertical Tie Model

Figure 3-4 shows a finite-element bending model of a single tie which is recommended as a complement to the MULTA program. This approach would

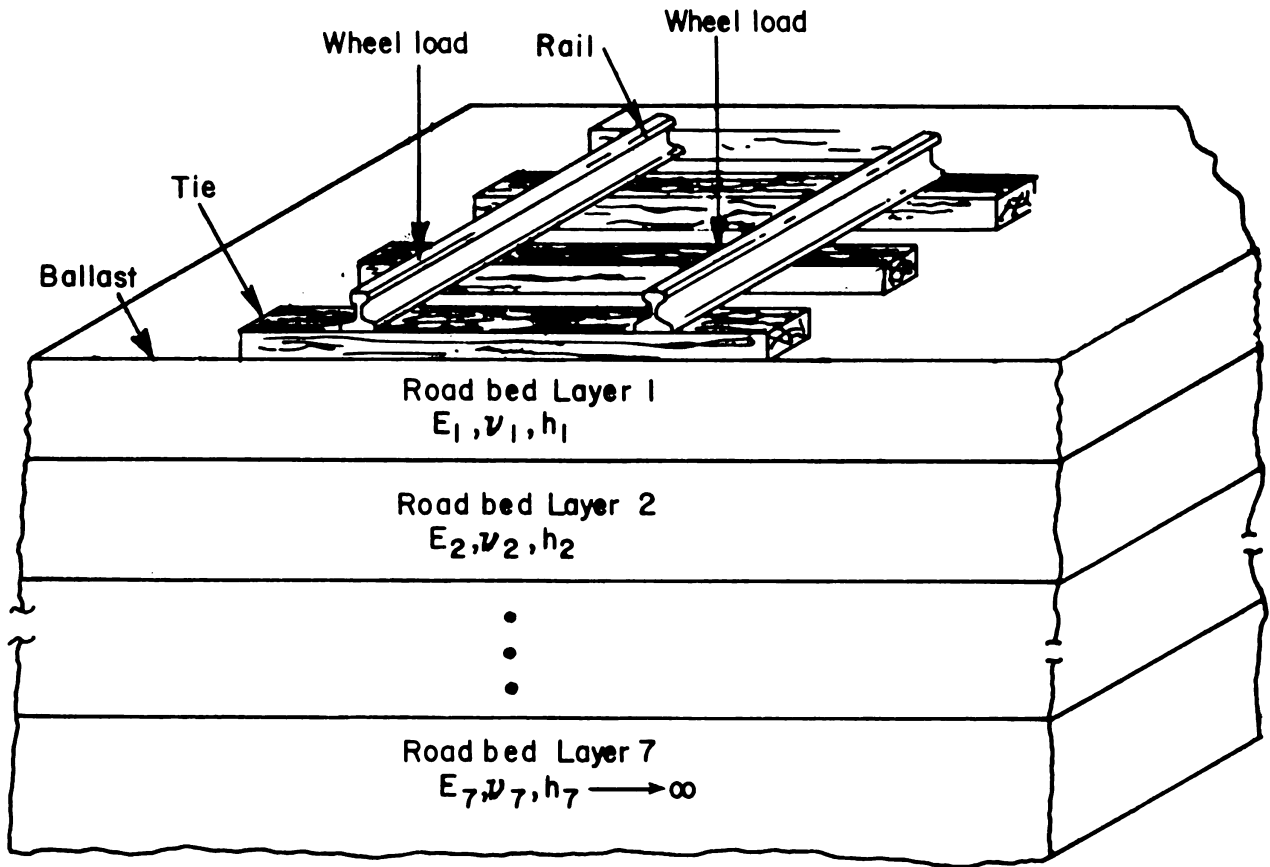


FIGURE 3-3. TRACK MODEL FOR MULTA PROGRAM

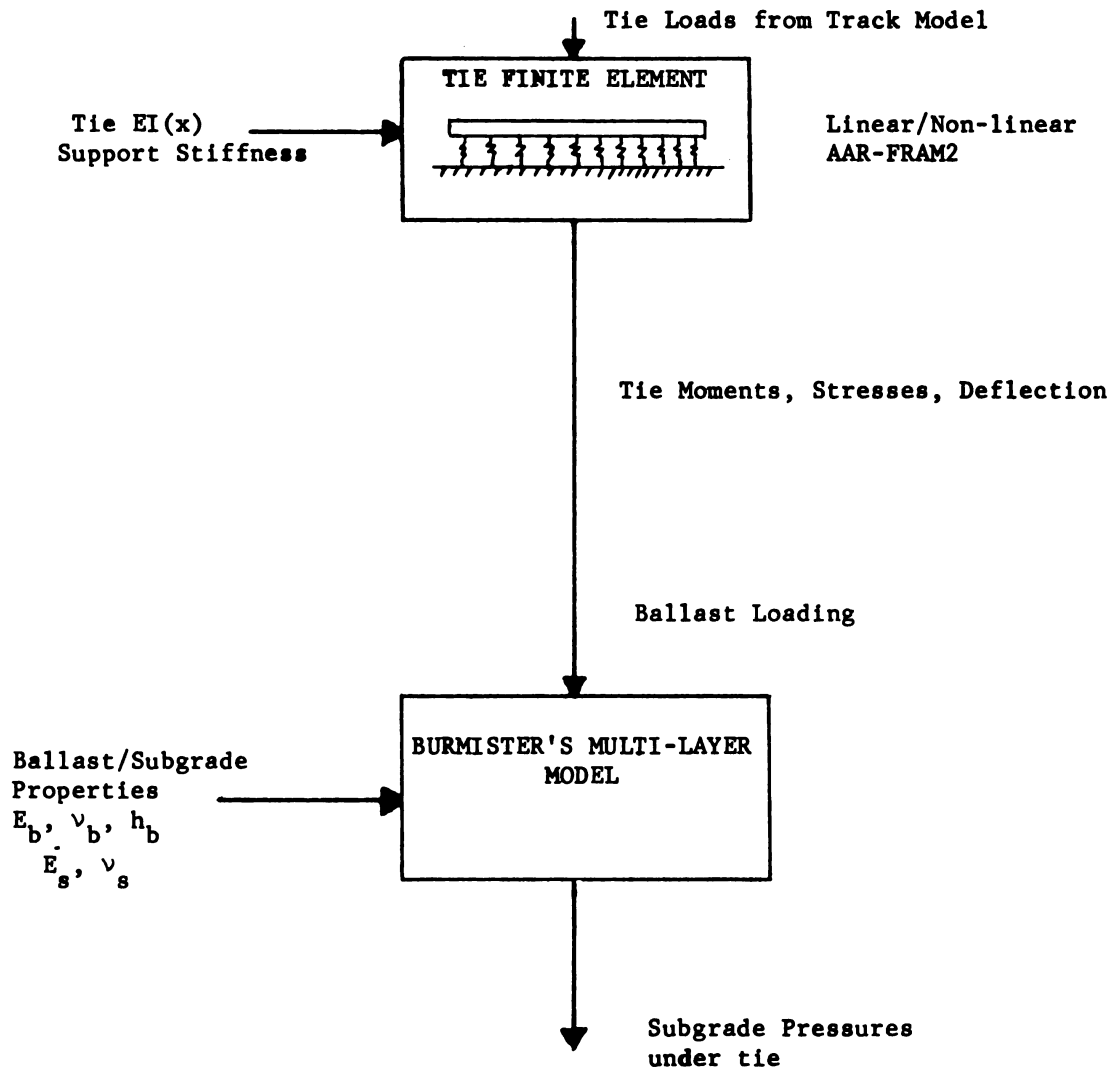


FIGURE 3-4. VERTICAL TIE MODEL

utilize vertical rail seat loads predicted by the MULTA program for a specified roadbed design to provide a more detailed evaluation of tie bending moments and ballast pressures. The AAR FRAM2 code could be used to evaluate length-wise variations in tie bending rigidity (EI) and linear or nonlinear ballast support conditions. The resulting ballast loads could then be input to the Burmister multi-layer roadbed model, or other equations, to predict roadbed stresses.

This single-tie model was not used during the first phase of this project. This, or a similar model, may be used for the more detailed tie stress analysis planned for a later task.

3.3.3 Lateral Track Model

The evaluation of track degradation modes and the review of available track analysis models indicate a need for further development of a 3-D finite element model having a detailed representation of a rail fastener. This model would be used to predict rail deflections, fastener loads, and rail-seat loads related to rail rollover, wide gage, and rail fastener behavior. The same model would also be used to determine the boundary conditions in terms of rail moments and tie reactions needed for detailed rail stress analyses, but this application has lower priority since other techniques may be adequate.

The requirements for a 3-D lateral track model are discussed below and shown schematically in Figure 3-5.

- a. Vertical and lateral wheel loads applied simultaneously
- b. A detailed, nonlinear fastener representation. This is particularly important for the large deflections incurred during rail rollover. This would include the vertical, lateral, rollover, and yaw resistance of the rail fastener.
- c. The rail should be represented by a beam with bending resistance in the vertical and lateral planes and torsional resistance.
- d. Individual ties would include tie bending in the vertical plane because this contributes to deflections at the rail head. Lateral bending of ties could be included also, but this is considered to be of secondary importance for the previously listed failure modes.
- e. The track roadbed would be represented by spring elements supporting each tie in the vertical and lateral directions. The capability for linear or nonlinear vertical springs should be included. Nonlinear lateral

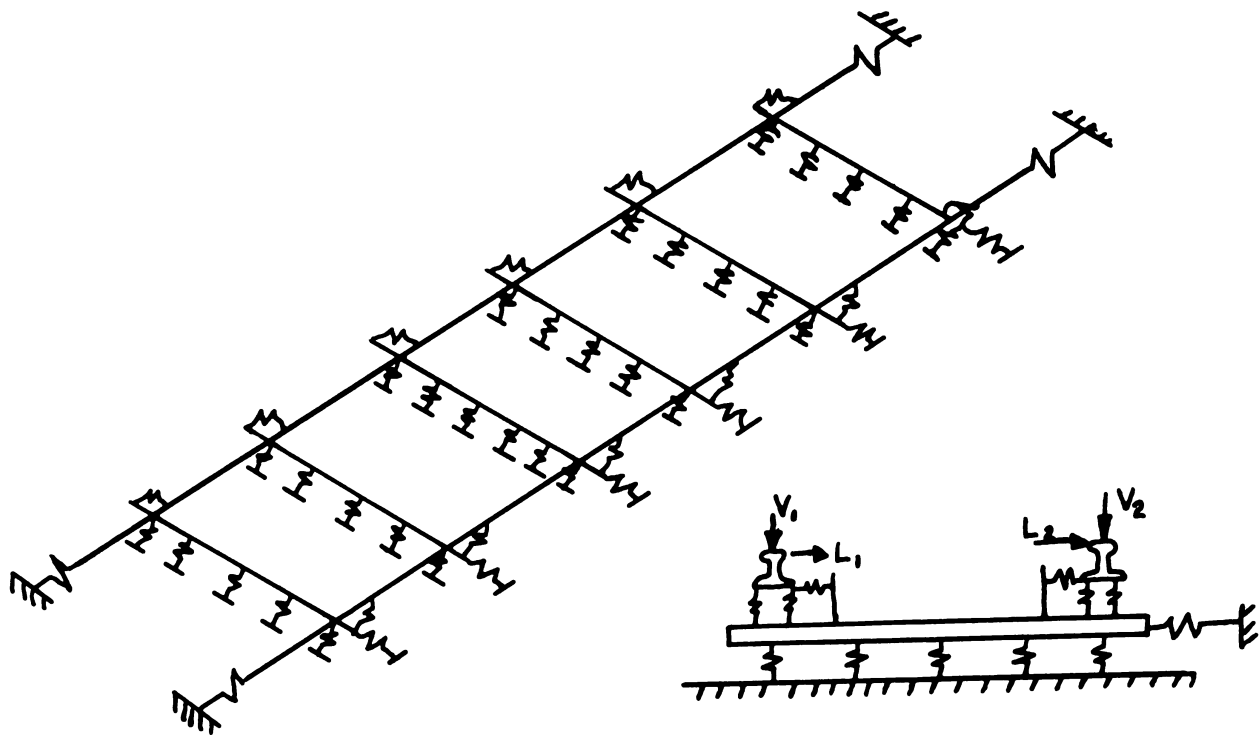


FIGURE 3-5. LATERAL TRACK MODEL

springs having an elastic-plastic characteristic representing realistic ballast behavior are required. The parameters for the lateral springs also depend on the vertical load applied to each tie. This is probably too difficult to model using general-purpose finite-element programs, so the vertical load effect would be included by the input lateral resistance based on other analyses of vertical load distribution.

f. The model should also include the effects of rail longitudinal loads from thermal effects or traction/braking loads from vehicle wheels.

The "Rail-Fastener Model" developed by AAR comes the closest to satisfying the above requirements, but this model has several significant deficiencies for the purposes of this project. The AAR program utilizes SAP4, a general-purpose, linear finite-element computer code for structural analysis. The use of non-linear elements would require the development of an iteration procedure incorporating SAP4 as a subroutine, or the use of another general-purpose finite element code that has non-linear elements. The availability of unidirectional translation and rotation spring elements, rather than modeling springs by judicious selection of the area and moment of inertia properties of beam elements, is an important asset for the recommended 3-D track model. The SAP4 program does not have spring elements, and this causes some difficulty in eliminating the cross-coupling between stiffness elements when beams are used for springs. However, user flexibility and simplicity of generating input data are the major reasons for utilizing spring elements.

An alternative to developing a 3-D track model is to utilize the FRAM2 2-D finite-element code that AAR uses for both vertical and lateral track models. This code can include non-linear ballast resistance in the lateral direction, and a track model having a frame formed by two rails attached to ties by flexible restraints can replace the "single" rail model used now. This would, however, neglect the lateral displacement of the rail due to vertical tie bending and rail torsion, and only a simplified model could be used for the fastener. Lateral deflections due to lateral translation and bending would be included, but the more complicated fastener response contributing to rail rollover and wide gage would not be included accurately. Also, the use of beam elements to represent unidirectional springs by FRAM2 has the same disadvantages for the user that were discussed previously.

In view of these restrictions in available models, the implementation of a 3-D track model using the NASTRAN finite element program is recommended for future use. NASTRAN was selected rather than some other general-purpose programs because it has all of the technical capabilities required and is readily available at many government, industrial, and CDC computer centers for minimal cost. The implementation of a track model using NASTRAN would include preparing and documenting a pre-processor program to generate the input data for selected track parameters in addition to developing a realistic rail fastener and track model suitable for wide-gage and rail-rollover analysis. However, an important advantage of NASTRAN is that its full dynamic analysis capability can be readily applied for future requirements with only the additional effort needed to determine the mass distribution and appropriate dynamic forcing function.

The development and implementation of a 3-D lateral track model was not undertaken under this current contract, and no other lateral response analysis was done during the time period covered by this interim report. Track response to vertical loading represents the highest priority for evaluating concrete or synthetic tie track where problems of rail rollover, wide gage and lateral buckling are minimized by the rigid rail fasteners.

3.4 RESULTS OF BENCHMARK PROBLEM SOLUTIONS

The evaluation of vertical track analysis models included implementing both the Hermann PSA and Burmister multi-layer ballast/subgrade programs (MULTA) on the BCL computer facility to provide a direct comparison. Several benchmark problems were selected to demonstrate how the programs operated, and to evaluate the significance of limitations and assumptions of each model. A detailed comparison of these programs and the solutions to several selected problems are included in Appendix B. The major results and conclusions from this work are summarized in the following paragraphs.

a. For comparable models, the MULTA program had a 3:1 advantage in computation time for a 2-layer roadbed model and a 2:1 advantage for a 3-layer model. Preparation time for input data was also considerably less for the MULTA program.

b. Use of the MULTA program requires subdividing the tie into a number of rectangular segments. A circular region of equal area is used for the pressure loading and the overlap or gaps between these segments produces an unrealistic oscillation in the computed stresses. These variations can be minimized by using nearly square segments for the tie and using data for stresses and displacements directly under the centers of the load segments rather than at their edges.

c. The effect of ballast cross section geometry was evaluated by comparing the PSA results for a typical ballast section with those from MULTA, which assumes infinite horizontal dimensions. These results showed that the finite dimensions of the ballast shoulder had a negligible effect on the ballast and subgrade pressures under the ties.

d. The effect of tie bending on tie/ballast pressures was evaluated for typical wood and concrete ties. The pressure distributions for wood ties show maximum pressures under the rail seats, as expected. However, the increased bending stiffness of the concrete tie shifted the maximum pressure location toward the tie end and produced a more uniform pressure distribution under the tie. However, this comparison does depend on the relative stiffness of the tie compared to the roadbed. A tie which is flexible relative to the roadbed produces high pressures in the rail seat region. A tie which is stiff relative to the roadbed creates a more uniform pressure distribution. A very rigid tie modeled with MULTA will resemble the classical elasticity solution for a punch where the maximum pressures are at the edges (ends) and the minimum pressure is at the tie center. It is questionable if this behavior would even appear in track with the granular ballast materials.

The comparison of solutions for pressures and deflections from the PSA and MULTA programs showed good agreement when the two programs were adjusted to give comparable boundary conditions. The infinite extent of the elastic half-space model used in MULTA is an important advantage for simulating the depth of actual track subgrades, and the effects of the finite width of the ballast section appear negligible. On the other hand, the boundary locations used in the PSA program are critical because a large depth is required to simulate real track. This requires a large number of elements and increases computer costs.

3.5 EVALUATION OF WHEEL/RAIL LOAD DYNAMICS

The dynamic forces exerted by the wheels of rail vehicles have a significant effect on the maintenance and safety of both track and vehicles. Those forces are dependent on vehicle speed, track geometry irregularities, the vehicle suspension system and the dynamic response characteristics of the track. Furthermore, the dynamic forces cover a frequency range which includes the low frequency response of the car body (0 - 10H_z) up to the very high frequency response (500 - 2,000 H_z) caused by wheel impact at rail joints, welds and switch points and from flat wheels.

The transmission of these dynamic forces from the rail head down into the ties and roadbed varies considerably for the different frequency ranges. The high frequency components of the impact force are of greatest concern for rail damage. These high frequency loads are local in nature and are attenuated significantly before they reach the ties and roadbed. However, the lower-frequency components of the wheel/rail loads are transmitted to all components of the track, and it is these loads which are of greater importance for degradation of ties, ballast and subgrade. Conventional procedures for track design utilize an empirically-derived, speed-dependent load factor, or impact factor, applied to the static wheel load to represent design loads for rail bending stresses and for track components below the rail. Very different loads are needed to represent impact forces on the rail head.

This section of the report reviews several of the different approaches used to determine the effect of speed on dynamic wheel loads for track design. The vertical dynamic wheel load, or design load, P_d, is given by

$$P_d = K P_s, \quad (3-4)$$

Where P_s is the vertical static wheel load and K is a dynamic wheel load factor.

The dynamic wheel load factor used most frequently for U.S. track design is given in AREA Bulletin 645 [3-10] as

$$K = 1 + \frac{33V}{100D}, \quad (3-5)$$

where V is train speed in miles per hour and D is wheel diameter in inches. This is usually described as a speed, or impact, factor, and it does not include the effect of variations in track geometry, track stiffness, or vehicle type. However, track design procedures do include additional factors to estimate the effect of track condition (non-bearing ties or soft spots in the roadbed)

on rail bending stress and tie loads. Also, the static wheel load P_g can be adjusted to include the load transfer from torque reactions in locomotives and non-uniform freight loading when these effects can be estimated.

The Indian Railways [3-11] uses a dynamic wheel load factor given by

$$K = 1 + \frac{V}{3\sqrt{U}}, \quad (3-6)$$

where U is the track modulus in units of psi. It is conjectured that the dependence of track modulus in this equation is intended to represent track condition, i.e., stiff track (high U) will have good geometry compared to poor track (low U), and therefore, dynamic loads will be lower. This is in contrast to the case where dynamic loads from a specified track geometry error will be greater on the more rigid track (high U).

Some other equations used for dynamic wheel load factor by European railroads show a V^2 relation [3-12], but most of the available data indicate the V^2 relation predicts excessive wheel loads at high train speeds. Measured data indicate that rail flexural stresses vary with train speed with a proportionality between V and $V^{1.2}$ [3-13]. Of course, most of these empirical speed factors were formulated for train speeds no higher than 100 mph.

Figure 3-6 shows that the results from the AREA and Indian Railways formulas are quite similar. The dynamic load factor recommended [3-14] for the design of Northeast Corridor (NEC) track for 150 mph passenger service is also shown for comparison. The NEC design factor was increased above the AREA formula at low train speeds to include an estimate of the additional forces from track irregularities.

A different approach to the estimation of track design loads recognizes the statistical nature of wheel loads and the effect of different standards of track maintenance. Experience from the German Federal Railroad, Deutsch Bundesbahn (DB), for the effect of train speed on rail bending stress and rail deflection shows that wheel dynamic load factors can be represented by [3-15]

$$K = 1 + n\sigma, \quad (3-7)$$

where

σ = standard deviation of wheel dynamic load factor

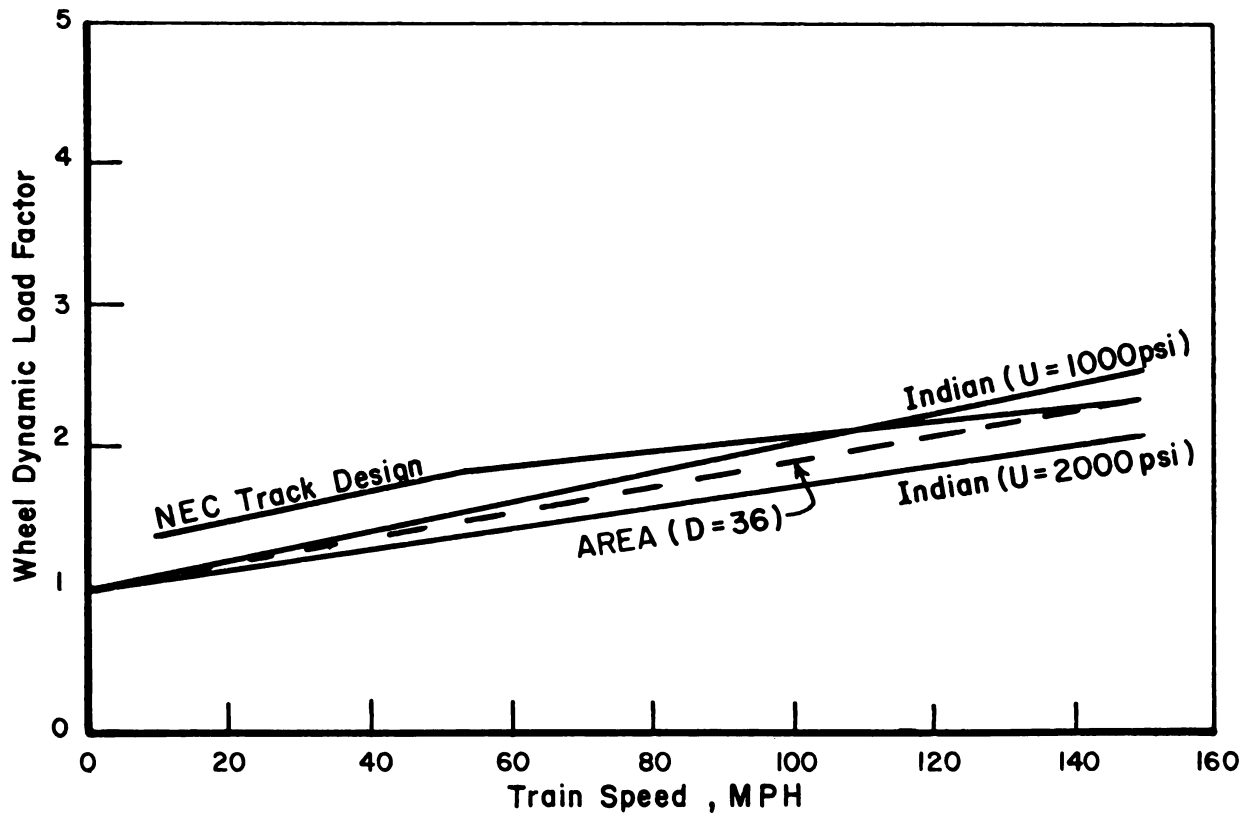


FIGURE 3-6. COMPARISON OF SEVERAL FORMULAS USED TO PREDICT WHEEL DYNAMIC LOAD FACTORS

n = number of standard deviations depending on
 statistical confidence level P that the dynamic
 wheel load will not exceed the value of $\pm n\sigma$.

The relationship between n and P for a Gaussian probability distribution is shown below for reference:

<u>n</u>	<u>P(%)</u>
1	68.8
2	95.4
3	99.7.

The DB uses n = 3 for estimating maximum track loads for predicting rail bending stress and tie loads. They have developed guidelines for track condition as shown in Table 3-4. These relations are also plotted in Figure 3-7, and the AREA dynamic wheel load factor is shown for comparison. It is important to realize that the track design and maintenance standards used by DB are probably the most conservative of any of the European countries, so dynamic wheel loads for their very good track would be expected to be quite low. By comparison, the AREA dynamic load factor agrees closely with the DB criterion for good track in the higher speed range, which suggests that the AREA factor may underestimate wheel loads on typical U.S. track. It is also apparent from Figure 3-7 that the load factor used by DB includes some of the effects of load transfer at low speed in addition to the speed effect shown by the AREA criterion.

TABLE 3-4. STANDARD DEVIATION OF WHEEL DYNAMIC LOAD FACTOR USED BY DB [6].

<u>Track Condition</u>	<u>Speed, mph (km/h)</u>	
	<u>0 - 37 (60)</u>	<u>37 - 124 (200)</u>
Very Good	$\sigma = 0.1$	$\sigma = 0.1 [1 + (V-37)/87]$
Good	$\sigma = 0.2$	$\sigma = 0.2 [1 + (V-37)/87]$
Bad	$\sigma = 0.3$	$\sigma = 0.3 [1 + (V-37)/87]$

Some other results for the DB reported by Birmann [3-16] show variations in wheel dynamic load factor for a range of track condition and for the different maintenance condition of locomotives used for 87 mph (140 km/h) and 124 mph (200 km/h) service. Figure 3-8 shows some measured data in comparison to the AREA

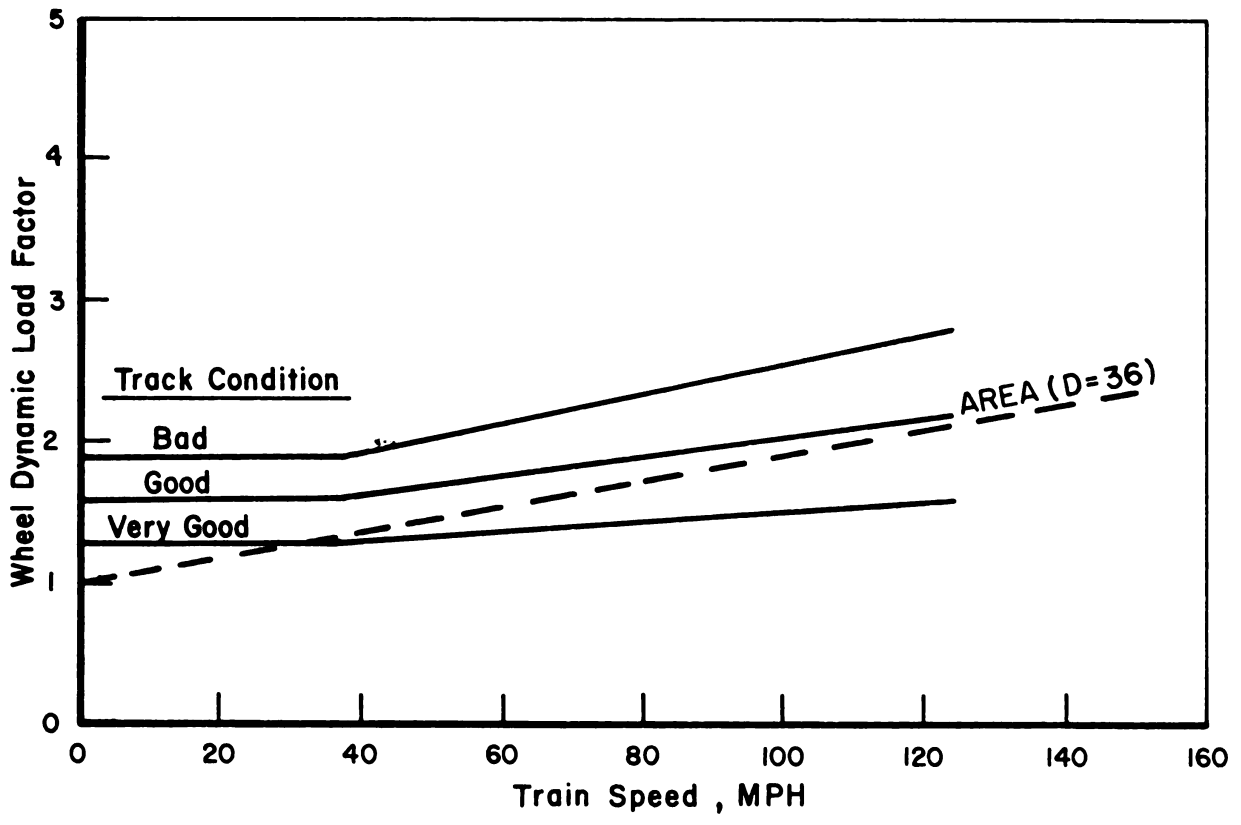


FIGURE 3-7. DYNAMIC WHEEL LOAD FACTORS USED BY DB (GERMANY) FOR 99.7% CONFIDENCE LEVEL (n=3)

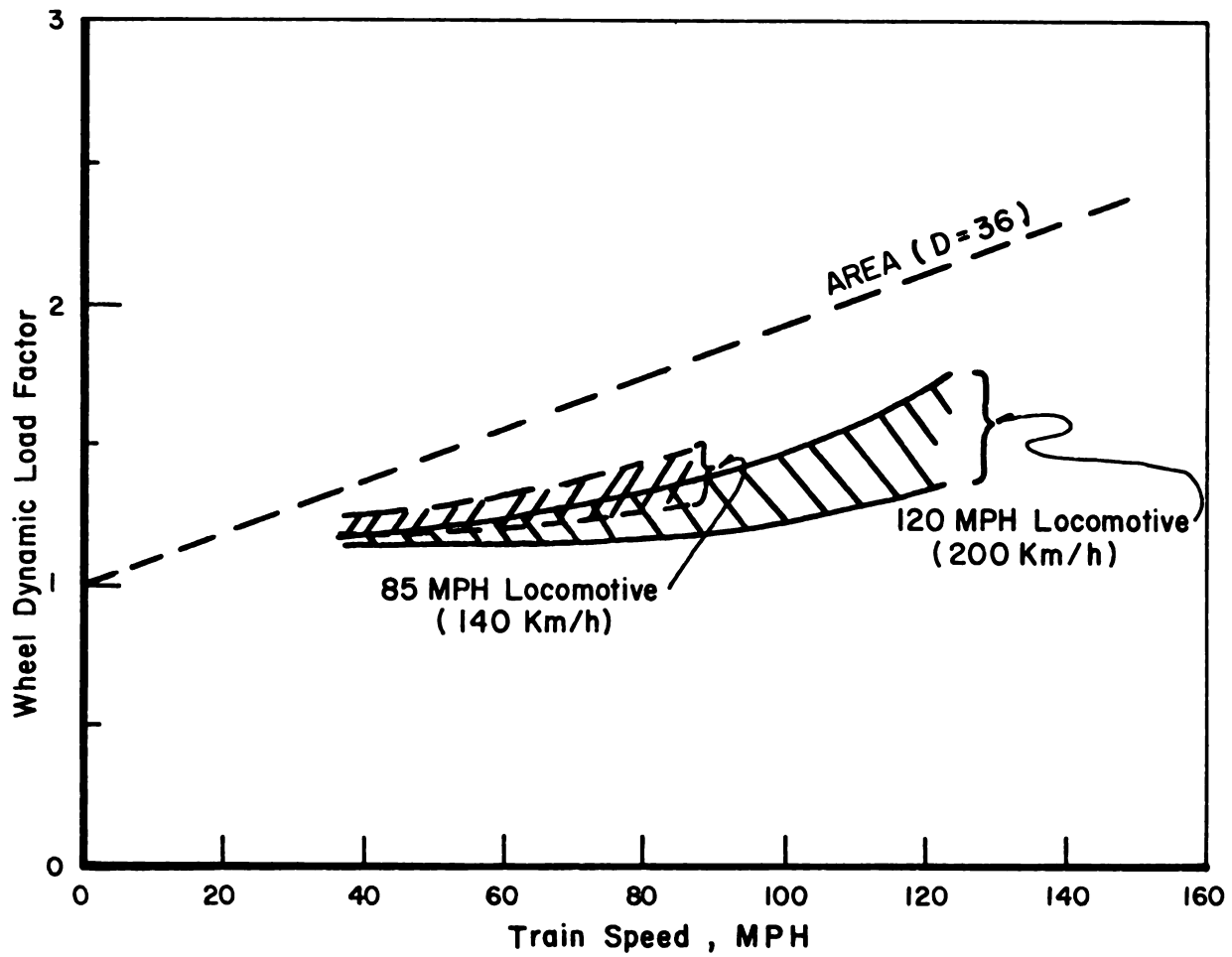


FIGURE 3-8. TYPICAL DATA ON WHEEL DYNAMIC LOAD FACTORS FOR LOCOMOTIVES

dynamic load factor. Similar data for 2-axle and 4-axle European freight cars show comparable dynamic load factors, but total wheel loads will be highest for the locomotives due to their higher static axle loads. The measured data are considerably lower than the criteria shown in Figure 3-7. However, the criteria are intended to cover the statistical nature of infrequently occurring high wheel loads, whereas the measured data may represent an average load condition.

Birmann [3-16] has used typical average load data to develop a dynamic load factor which includes both track and vehicle locomotive condition by

$$K = 1 + \alpha + \beta + \gamma \quad (3-8)$$

where

$$\alpha = 0.04 \left(\frac{V}{100} \right)^3 \quad (3-9)$$

gives the speed effect for new vehicles.

The factor β gives the vertical load transfer in curves using the following typical data for current vehicle suspensions:

$$\beta = 13-17\% \text{ for DB (unbalance} = 100 - 130 \text{ mm)}$$

$$\beta = 20\% \text{ for SNCF (unbalance} = 150 \text{ mm).}$$

The factor γ depends on train speed, track condition, and the type and age (condition) of the locomotive.

$$\gamma = \gamma_0 \cdot a \cdot b \quad (3-10)$$

where

$$\gamma_0 = 0.10 + 0.017 \left(\frac{V}{100} \right)^3 \quad (3-11)$$

<u>Speed Limit (km/h)</u>	<u>Locomotive Factor, a</u>	<u>Track factor, b</u>	<u>a · b</u>
140	2	1.3	2.6
200	1.5	1.2	1.8

Using these values for $V = 140$ km/h gives $K = 1.49$, and $K = 1.75$ for $V = 200$ km/h on tangent track ($\beta = 0$). These values agree with the highest values shown on Figure 3-8 for the respective speed ranges. The lower values represent the condition of $a = b = 1$ for new vehicles and excellent track.

While the development of dynamic wheel load factors, or impact factors, has been directed toward establishing criteria for track design in general, it is generally recognized that specific anomalies such as rail joints, rail welds, flat wheels and switch points can produce much higher impact forces. These impact forces are strongly dependent on vehicle unsprung mass, the track effective mass under dynamic loading, the severity of the track anomaly and speed of the vehicle. Figure 3-9 shows some sample calculations based on results reported in [3-17] where the P1 (high frequency input) and P2 (lower frequency track response) forces for joint impact were estimated for the maximum allowable track geometry deviations for U.S. Class 4 and Class 6 track. The considerable variation in the P2 forces for joint condition (track class) indicate that the current speed limits would probably cause a much higher rate of joint degradation for Class 4 track when the joints approach their respective geometry limits. The P1 forces are much higher than the P2 forces, but inertial effects attenuate these considerably before they reach track components below the rail.

Figure 3-10 shows some data on the effect of wheel flats on rail bending stresses measured by the AREA [3-18] in 1952. The characteristic behavior of wheel flats is that rail deflections and rail bending stresses reach a maximum value in the 15-30 mph range and then decrease as speed increases to about 40 mph. At speeds above 40 mph, the rail bending stresses increase gradually but do not exceed the maximum values recorded at lower speeds.

This behavior in rail bending stress and rail deflection has been confirmed by measurements in Japan [3-19]. British Railways has done some analytical work [3-20] which also confirms this behavior in rail deflection. However, the analytical results for rail bending stress and rail contact stress show a general increase in response with speed, with a minor peak around 20 mph which is exceeded by a considerable margin for speeds above 50 mph. This analytical prediction for rail bending stress is questionable because rail bending response to high frequency impact loads will be attenuated by the rail mass. The increase in contact stress at high speeds is not unexpected.

Wheel flats produce much higher track loads than are accounted for by the AREA impact factor, but the frequency of occurrence of a flat wheel impact

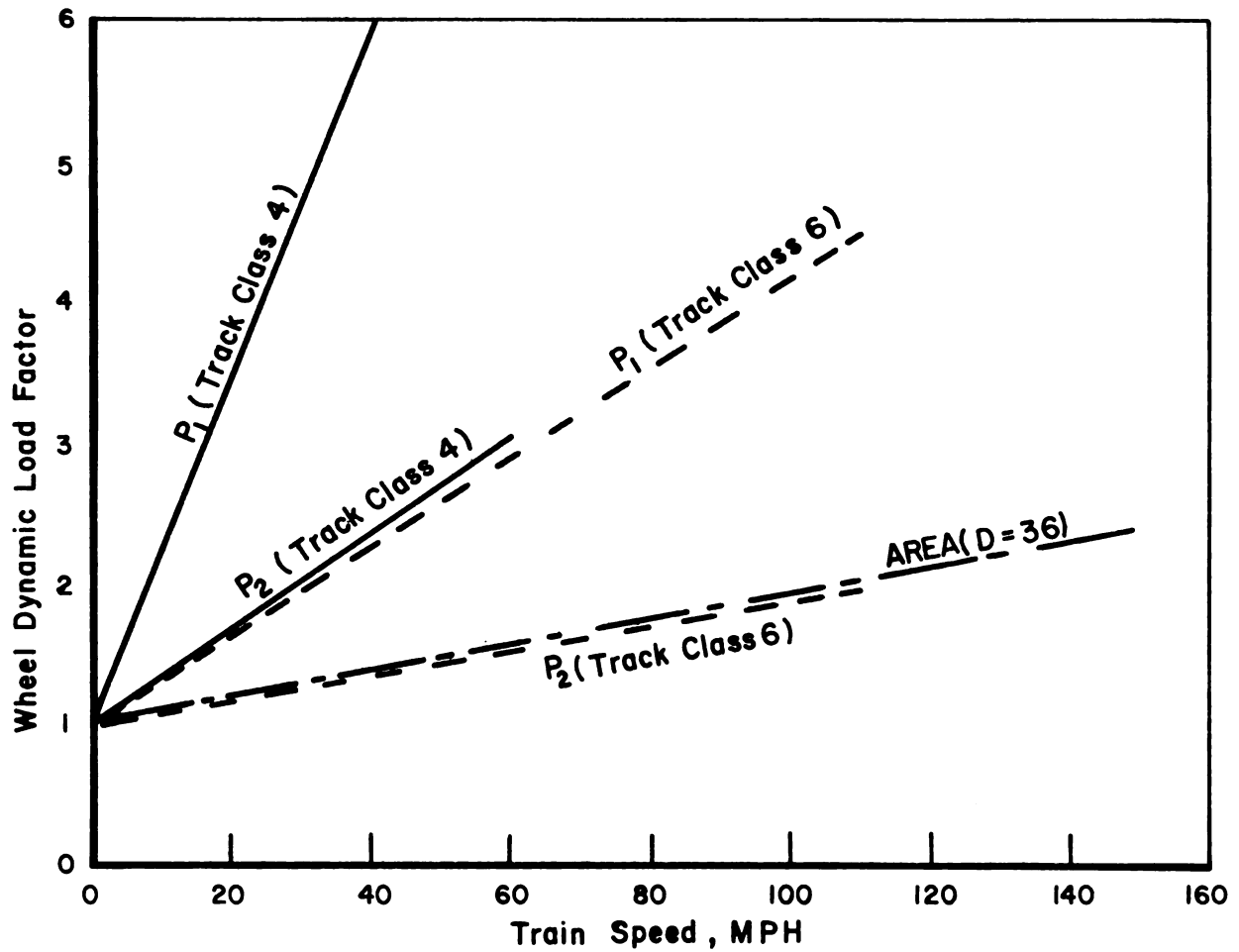


FIGURE 3-9. MAXIMUM WHEEL DYNAMIC LOAD FACTOR FOR FREIGHT CAR IMPACT AT BOLTED RAIL JOINTS

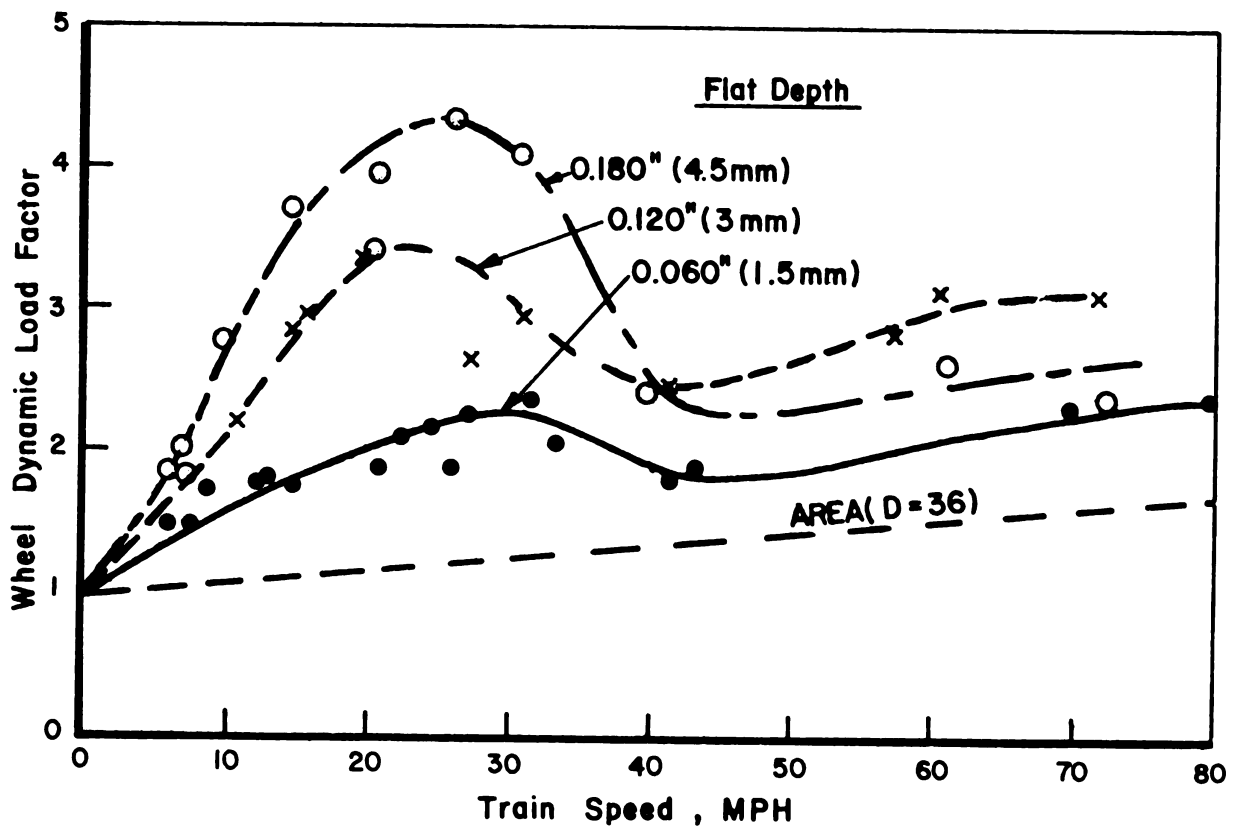


FIGURE 3-10. EQUIVALENT WHEEL DYNAMIC LOAD FACTOR FOR THE EFFECT OF FLAT WHEELS ON RAIL BENDING STRESS

on one particular spot on the track is low compared to the loading from normal wheel passes. The effect of an infrequent occurrence of a high impact force on the different track degradation modes is largely unknown at this time. This will be discussed further in Section 4.

This review of wheel/rail load dynamics presents current world-wide practice for the selection of track loads for track design purposes. Track design loads have been developed historically based on the estimated maximum load condition as a function of train speed. This has been refined to include empirical statistical descriptions for different levels of track condition. The current AREA specification for concrete ties and fasteners [3-1,3-2] includes an assumed impact factor of 150 percent above the static vertical wheel load to estimate the dynamic effect of wheel and track irregularities. This gives a dynamic wheel load factor of $K = 1 + 1.5 + 2.5$ times the static wheel load. A maximum static wheel load of 41 kips is assumed to derive the maximum tie rail seat loads using a distribution factor as a function of tie spacing to include the load shared by several ties. This results in a 52.6 kip rail seat load for 24-in. tie spacing and a 61.5 kip load for ties spaced at 30 in. A 2.5 dynamic wheel load factor is considerably greater than the guideline shown in Figures 3-6 thru 3-8 for normal freight service up to 60 mph.

The major disadvantage of these types of load estimates is that an estimate of the maximum load, even with statistical data for frequency of occurrence, does not describe the load spectrum to which a typical section of track would be subjected in normal service. The evaluation of track degradation due to cumulative fatigue damage requires a load spectrum description for the total load environment in addition to the statistical description of low-probability maximum loads.

3.6 TRACK DYNAMIC RESPONSE

It may have been noted that the extensive list of track analysis models reviewed in Section 3.2 and the models recommended for this project in Section 3.3 were limited to static response predictions in that the effect of acceleration or damping forces in the track were neglected. Conventional track design procedures are based on using track loads which include estimates for dynamic effects, as discussed in Section 3.5, but track-response predictions utilize the

maximum dynamic load as an equivalent static load. Simplified track dynamic models are frequently used in studies of rail vehicle dynamics and vehicle/track interaction to predict wheel/rail loads. However, no detailed track models similar to MULTA have been developed to solve the complete vehicle/track interaction problem and include the effect of inertial (acceleration) and damping forces on the transmission of loads into the ties, ballast, and subgrade. The reasoning behind why these dynamic effects are not included in track analysis models is reviewed briefly in this section.

Any particular section of track is subjected to a series of vertical and lateral load pulses on the rail as each axle of a train passes. The magnitude of the vertical load pulses depends on the vehicle's static weight plus any additional load due to vehicle dynamic response or wheel irregularities. Figure 3-11 shows the calculated excitation frequencies of the track loading from the load pulses due to individual axles and trucks. The excitation frequency from these pulses depends on the pertinent axle and truck spacing and increases linearly with train speed. This repetitive loading on the track can excite a track resonance when the excitation frequency is close to the track's resonant frequency. This would produce a greater response of the track (higher displacements and loads) than would be predicted by a static analysis.

Available data show that the lowest resonant frequencies of track are in the range of 30 to 45 Hz for wood tie track, and the damping ranges from 15-45% of critical. Resonant frequencies for concrete tie track might be somewhat higher, but no substantial increase is expected because the typical increase in track stiffness is usually matched by a corresponding increase in the effective mass from the roadbed. Figure 3-11 shows that the excitation frequency for freight car axles does not exceed 20 Hz for operating speeds below 80 mph. This excitation frequency is sufficiently below expected track resonant frequencies to justify neglecting any dynamic amplification from the basic load pulses due to traffic.

Higher frequency dynamic response can be excited by impacts at joints or from flat wheels. As discussed in Section 3.5, high frequency impact forces are reacted by the mass of the rail in a local region, and this reduces the force transmitted to the ties and ballast. Variations in the elasticity of rail fasteners (pads) for synthetic cross ties have the greatest potential for attenuating impact loads. The prediction of these impact forces requires an

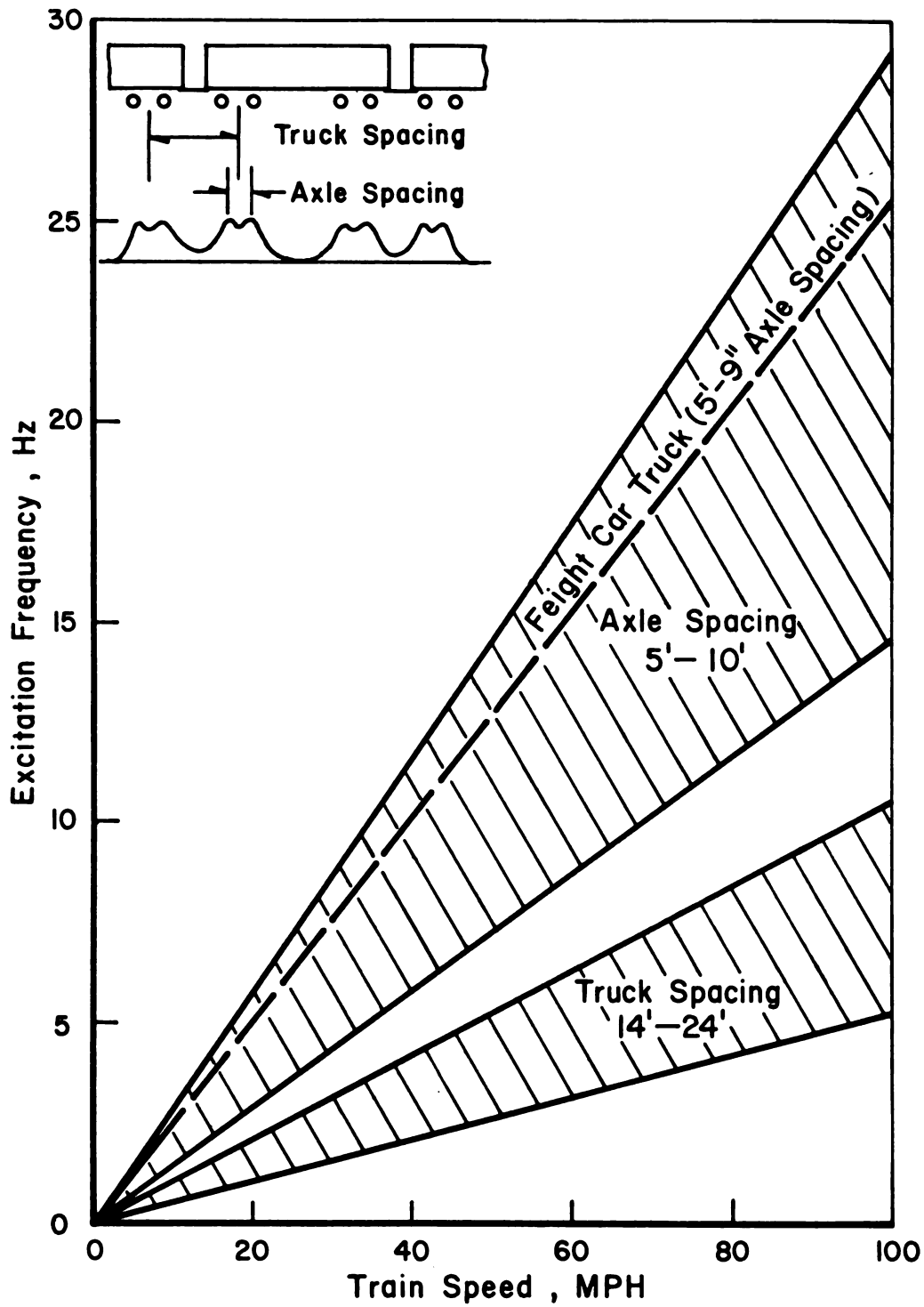


FIGURE 3-11. WHEEL PASS EXCITATION FREQUENCIES

appropriate dynamic model for the vehicle and track. However, the effect of the loads transmitted to the ties and ballast can be evaluated in an approximate manner by using an equivalent static load based on the lower frequency excitation transmitted through the track structure. The transmission of impact forces into the track is an important area for future research on track response, but further information on the contribution of impact forces to overall track degradation relative to the loads from wheel passes is needed to establish their relative importance.

An alternative way to evaluate dynamic effects in track response is to estimate what percentage of tie loads can be attributed to acceleration forces. Figure 3-12 shows some approximate analytical predictions of maximum tie acceleration as a function of train speed for a typical range of track modulus. These predictions were made by differentiating the beam-on-elastic-foundation solution for rail deflection $y(x,t)$ for a point load P moving at speed V to give the equations

$$y(x,t) = \frac{Pe^{-\beta(x-vt)}}{8EI\beta^3} [\text{Sin } \beta(x-vt) + \text{Cos } \beta(x-vt)], \quad (3-12)$$

$$\ddot{y}_{\max} = \frac{PV^2}{4EI\beta} \quad , \quad (3-13)$$

where $\beta^4 = \frac{U}{4EI}$, U = track modulus per rail (lb/in./in.), and EI = rail bending rigidity (lb-in.²).

The results in Figure 3-12 give the maximum acceleration of a fixed point on the track during passage of a wheel load of $P = 35$ kips. The maximum acceleration occurs at the time of maximum deflection when the wheel is directly over the reference location. Maximum accelerations on the order of 1 g correspond to inertial forces on the tie rail seat on the order of 400 lb (1/2 concrete tie weight). This is negligible relative to the rail seat load of 12-20 kips. Therefore, the effect of the tie inertial forces on maximum ballast pressures is negligible for the low frequencies associated with wheel passage. Higher tie accelerations will result from tie bending vibration response to flat wheel impacts. However, the excitation of tie bending will have a negligible effect on rail seat loads.

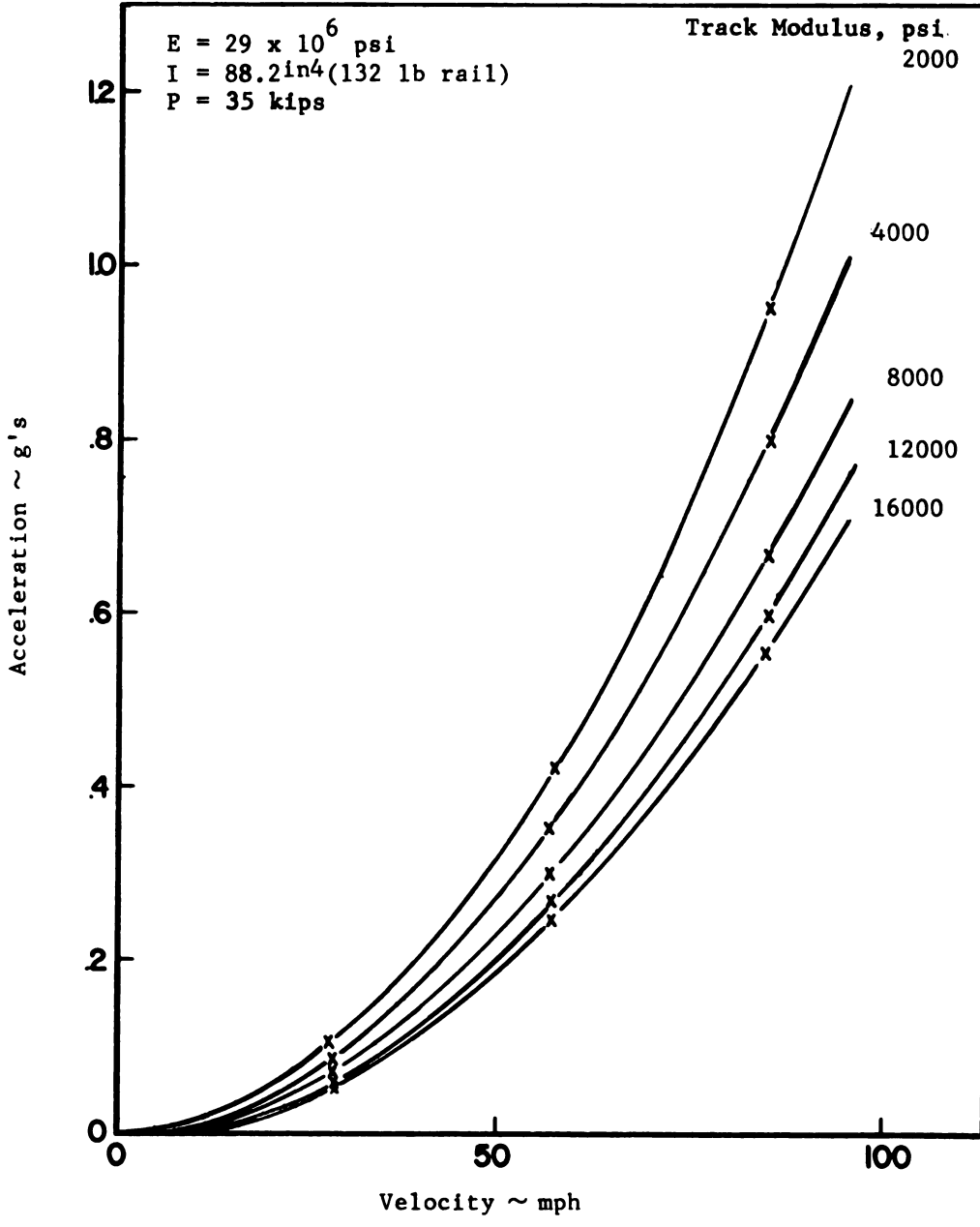


FIGURE 3-12. ESTIMATE OF MAXIMUM TIE ACCELERATION

Generated for Ricardo Jose Quiros Orozco (University of Illinois at Urbana-Champaign) on 2018-07-23 00:57 GMT / http://hdl.handle.net/2027/mdp.39015040727094
 Public Domain, Google-digitized / http://www.hathitrust.org/access_use#pd-google

The relatively brief evaluation of the effect of track dynamic response discussed in this section indicates that static track analytical models which neglect inertial and damping forces should be quite adequate for the major track loading caused by wheel passage. Rail loads caused by flat wheels or short wavelength corrugations where the excitation frequency is above the 30-45 Hz range for the fundamental track resonance require a comprehensive dynamic model. However, static track models should provide useful estimates of tie and ballast loads if the applied loads reflect the attenuation of high frequency components by the rail mass.

4. MEASUREMENTS OF CROSS TIE AND FASTENER LOADS

Analytical models discussed in the previous section have been selected to predict track response to train loads and to evaluate a wide range of track and fastener design parameters. It was originally expected that available instrumented sections of wood and concrete tie track in the Kansas Test Track (KTT) would be used to obtain measured track response data for validating the analysis models before proceeding with parametric design studies. It was also desirable to obtain statistical data on the loading environment of cross ties and fasteners for revenue traffic in order to evaluate performance specifications for ties and fasteners. Unfortunately, the premature failure of the KTT required the selection and complete instrumentation of a new test site location. The details of the instrumentation and site selection and the statistical basis for the data recording requirements are discussed in a separate measurement plan [4-1]. Only those items needed to describe the actual measurement program and results will be repeated in this report.

Several potential test sites having concrete ties were evaluated to select the most suitable site for meeting the specific objectives of this program. These objectives were to obtain data on the service loads and reactions of cross ties and fasteners and on the load transfer between track components that are needed to:

- a. Validate analytical models for predicting track response for a range of track design parameters.
- b. Provide a statistical description of the loading environment for a typical track section to be used as a basis for design evaluation and laboratory testing of improved cross tie and fastener assemblies.

4.1 TEST SITE DESCRIPTIONS

Detailed test site selection criteria for meeting these program objectives are discussed in [4-1]. Two key requirements for the program were to have uniform track sections of concrete ties having variable tie spacing and to have test sections on both curves and tangent track. Variable tie

spacing was recommended to provide a critical validation check for the analytical model because tie spacing is a major track design parameter. A section of curved track was recommended to determine the most severe lateral loading effects on rail fasteners. The combined vertical and lateral loading on the fasteners in curves represents a critical condition for fastener design.

The Florida East Coast (FEC) Railroad was the only property meeting these two major requirements. The fact that the Railroad Concrete Crosstie Corporation (RCCC) ties shown in Figure 4-1, a modification of the original MR-2 design, do not meet current AREA specifications was not considered a detriment for the objectives of this project. Also, the fact that the temperate Florida climate is not a typical North American environment was not considered critical for obtaining load data over a short time period.

The FEC test sites selected for this project included two concrete tie tangent track sections, one having a nominal tie spacing of 24 inches and the other having a nominal tie spacing of 20 inches, and a concrete tie curve site with 24-inch tie spacing. The RCCC tie shown in Figure 4-1 and True Temper Cliploc fasteners with a 1/8-inch thick polyethylene rail pad are the tie/fastener combination used throughout the test sites.

A tie spacing of 24 inches is standard for the FEC; however, a length of tangent track had been constructed with 0.5 mile sections of ties spaced at 24, 22, and 20 inches to evaluate these designs. These sections were located about 6 miles north of Jupiter, Florida on track adjacent to the Jonathan Dickinson State Park on U. S. Route 1. Annual traffic was estimated to be 18-20 million gross tons (MGT) of mixed freight and 100-ton hopper cars with stone and travel. The maximum train speed for the test sites was 60 mph, which is the maximum speed permitted on the FEC railroad.

Specific locations for instrumentation were selected on the tangent track sections to provide uniform subgrade conditions away from any embankments and at locations shown by track geometry charts to be free of any anomalies in profile, alignment or gage. Results from a complete set of measurements from the DOT track geometry car showed that the track was in excellent condition throughout the entire test section. The particular sites selected are discussed in the following sections.

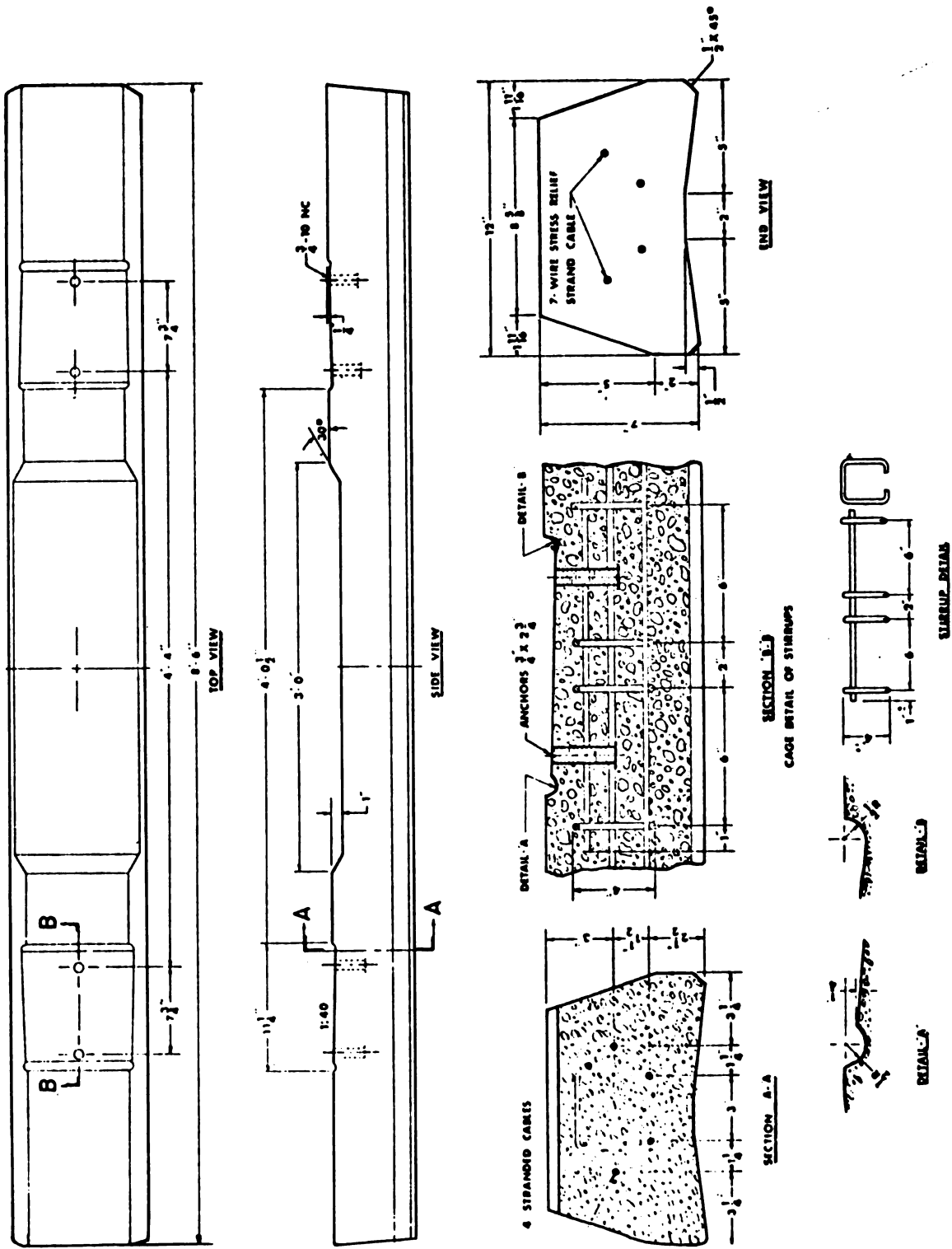


FIGURE 4-1. RCC TIE INSTALLED ON FLORIDA EAST COAST RAILROAD

4.1.1 Site 1 - Tangent Track with 24-Inch Tie Spacing

Site 1 was located at MP 278.1 in the tangent track section having 24-inch tie spacing. This site was about 0.3 miles south of Camp Murphy North crossing. This concrete tie track was constructed in June 1975 (approximately one year before testing) with 132 lb/yd welded rail and 10-12 inches of granite ballast. The track was located on an old roadbed which had been scraped to provide an even surface and to remove the old limestone ballast. Subsequent excavation at one location during the test program showed a ballast depth of about 6-1/2 inches under the tie and a clear demarcation between the new granite ballast and the old roadbed. The old roadbed (subgrade) was a well compacted mixture of soil and limestone ballast. No significant maintenance had been required during the year after the track was constructed.

4.1.2 Site 2 - Tangent Track with 20-Inch Tie Spacing

Site 2 was located at MP 279.0 in the tangent track section having 20-inch tie spacing. This site was located about 1.2 miles south of the Camp Murphy North crossing, and the track was constructed at the same time as Site 1. An excavation at this site also showed a ballast depth of about 6-1/2 inches under the tie and the roadbed appeared identical to that at Site 1. Both Sites 1 and 2 were paralleled by a section of old wood tie track used as a passing siding. No significant maintenance had been required during the year after the track was constructed.

4.1.3 Site 3 - Curved Track with 24-Inch Tie Spacing

Site 3 was located in the middle of a 3° 52' curve at MP 275.5. The curve had a superelevation of 5-1/2 inches with entry and exit spiral lengths of about 350 feet. The balance speed for this curve as given by the AREA formula is

$$V = \frac{E_a}{0.0007d} = \frac{5.5}{(0.0007)(3.87)} = 45 \text{ mph}, \quad (4-1)$$

and the maximum allowable speed for operation at 3 inches of unbalance is

$$V = \frac{E_a + 3}{0.0007d} = \frac{5.5 + 3}{(0.0007)(3.87)} = 56 \text{ mph}, \quad (4-2)$$

where

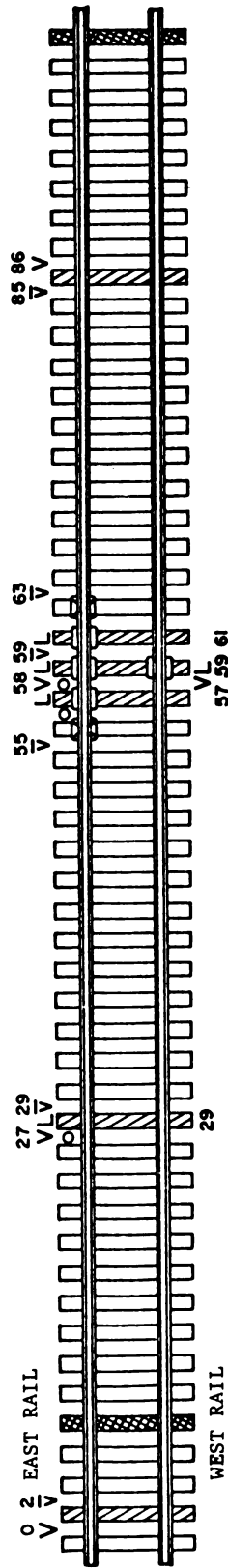
- V = Train speed (mph)
- E_a = Actual elevation of outside rail (inches)
- d = Degree of curvature (degrees).

The concrete tie track was constructed in July, 1970 at Site 3 using the same construction standards used for Sites 1 and 2. It was last surfaced in May, 1975, so it has been subjected to about the same traffic conditions since maintenance even though it was constructed 5 years earlier than the two tangent track sites. The curve test site was in single-track territory.

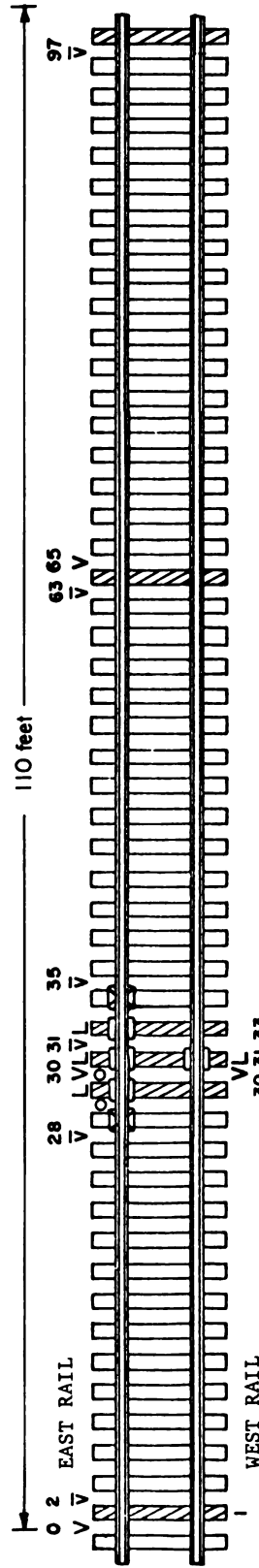
4.2 INSTRUMENTATION INSTALLATION AND CALIBRATION

The selection of measurement parameters, instrumentation, and data requirements for meeting the objectives of this project are discussed in detail in [4-1]. Figure 4-2 shows the locations and identification of the instrumentation that was installed at the test sites. All three sites included a main instrument array which extended over 7 adjacent ties. The purpose of this continuous section was to obtain a complete set of track load and response data over a nominally uniform track section. The section of 7 ties provided a length of about 14 feet so the center tie and two adjacent instrumented ties would be within the wheel influence zone from either end of the main array. This was done to minimize the effect of disturbances to the ballast, because the installation of instrumented tie plates (described in Appendix C) required lowering each tie about one inch in the ballast to provide the required clearance. In this way, all ties within the wheel influence zone were adjusted similarly. The ties were lowered and dummy spacer plates were installed one month before the measurement program started to allow reconsolidation of the ballast under 1-2 MGT of traffic.

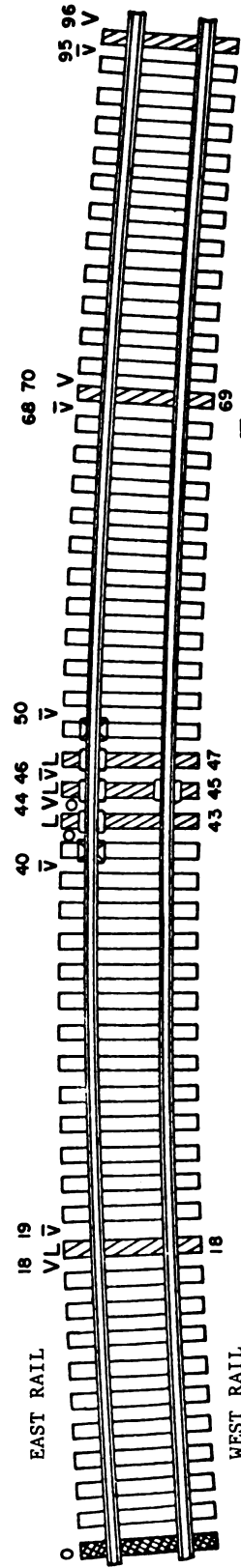
The FRA/PCA load cell ties described in Section 4.2 and shown in Figure 4-2 were also installed in track one month before any measurements were



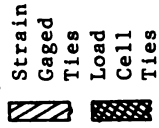
SITE 1. TANGENT TRACK (24" TIE SPACING)



SITE 2. TANGENT TRACK (20" TIE SPACING)



SITE 3. 3°52' CURVE TRACK (24" TIE SPACING)



□ Instrumented Tie Plates

V Vertical Circuits

L Lateral Circuits

VL Axle Detector Circuits

O Deflection Circuits

▣ Tie Plate Spacers

FIGURE 4-2. LAYOUT OF TRACK TEST SITES

made. The load cell ties were installed and the 7 ties in the main array were lowered with minimum disturbance to the ballast. However, it was necessary to hand-tamp the rail seat region under each tie following these adjustments to eliminate free-play. The track in each main array was lifted by track jacks and tamped so it was humped about 1/4 inch above the normal level. This hump had virtually disappeared after one day of traffic, and one month of traffic caused a dip of about 0.06 inches in the main array in each test section. This dip was removed by the addition of an extra 1/8-inch thick tie pad under the instrumented tie plates. It was also necessary to add a tie pad at each rail seat of the load cell ties.

Figure 4-3 is a photograph of the main array instrumentation. Brief descriptions of the instrumentation and calibration procedures are given in the following sections.

4.2.1 Wheel/Rail Load Circuits

The instrumentation in the main array includes strain gages applied to the rail web to measure vertical and lateral wheel/rail loads on the rail near the center tie. The strain gages oriented at 45° on the rail web measure the principal strains from vertical shear force. A total of 8 gages located on a rail section between two ties are wired into a single bridge, and the bridge output is proportional to vertical wheel load with an influence length nearly equal to the space between the chevrons. The vertical wheel/rail load data was added from both rails in the main array to determine axle loads to identify car weight categories. Additional vertical wheel/rail load circuits were installed adjacent to the strain gaged ties outside the main array. The signals from a pair of vertical wheel/rail load circuits spaced about 25 feet apart at either end of the instrumentation section were used to calculate train speed as a train entered the test section from either direction. This speed calculation and accurately measured distances to the different instrumented locations were used to establish time delays for axle identification during the data analysis.

The strain gage circuits used to measure lateral wheel rail loads were applied to the rail web immediately over a tie. The lateral shear force

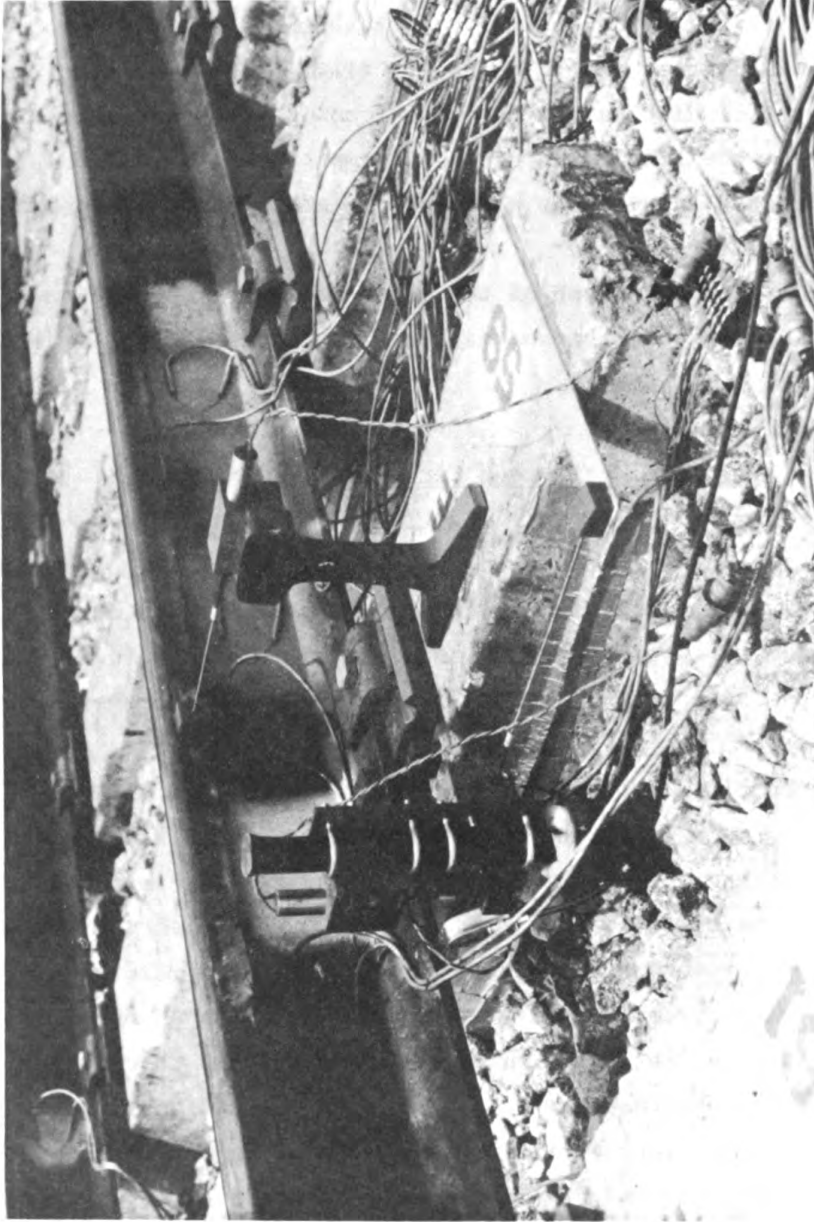


FIGURE 4-3. MAIN ARRAY INSTRUMENTATION

circuit utilizes the principal that shear force in a cantilever beam is proportional to the change in bending moment.

The vertical wheel/rail load circuits were calibrated by observing the output amplitudes during the passage of a work train having an empty and fully loaded hopper car that had been weighed prior to arriving at the test site. The average output sensitivity of the vertical wheel load circuits was 10 micro volts per excitation volt per 1000 lb, and this varied by about ± 10 percent for the different circuits in one track section.

The lateral rail load circuits were calibrated with a hydraulic ram placed between the two rails as shown in Figure 4-4. Figure 4-5 shows typical calibration data for the lateral wheel rail load circuits. Calibrations were nearly identical in both an unloaded condition and with a vertical load from a loaded vehicle positioned adjacent to the lateral load circuits. A high pressure lubricant was applied on the rail at the wheel/rail contact patch for these measurements to reduce the lateral load transmitted into the vehicle axle. Data from previous BCL tests using instrumented wheel sets indicates that the maximum lateral load transmitted to the vehicle wheels is approximately 1200 lb, and this is included in the calibration factor. The average calibration factor for the lateral wheel/rail load circuits on the concrete tie sections was 34 microvolts per volt per 1000 lb. This calibration factor varied by approximately ± 10 percent for the different locations.

4.2.2 Rail Seat Loads

The main array of each test section contained 6 instrumented tie plates, with 5 on one rail. The instrumented tie plates were used to record rail seat loading throughout the influence zone of the center tie for purposes of model validation. The combined statistics from the five tie plates under the primary rail were also used to record statistical load variations. Instrumented tie plates were not used outside the main array because it was believed that disturbing a single tie to install tie plates might produce an anomaly in the track support condition that was greater than any normal spatial variations. Inserting the load cell ties at isolated locations did create some free-play, and a similar problem would have occurred with the instrumented tie plates.

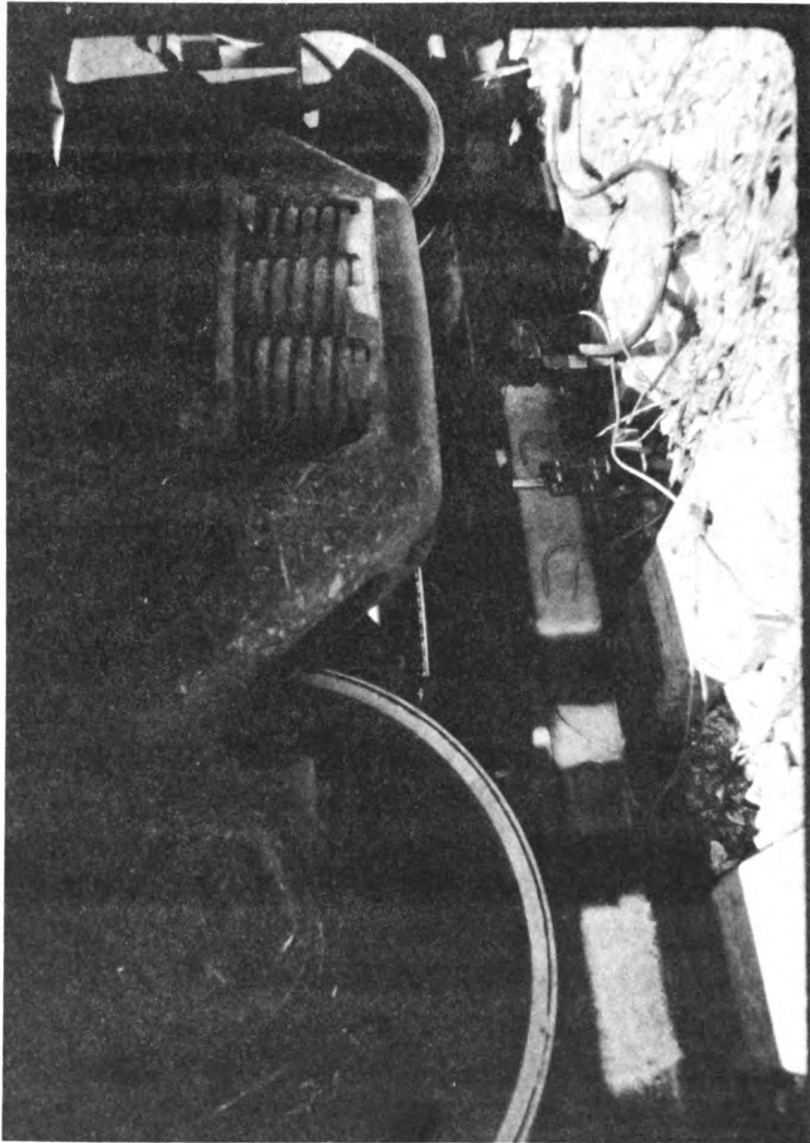


FIGURE 4-4. FIELD CALIBRATION OF LATERAL W/R LOAD CIRCUITS

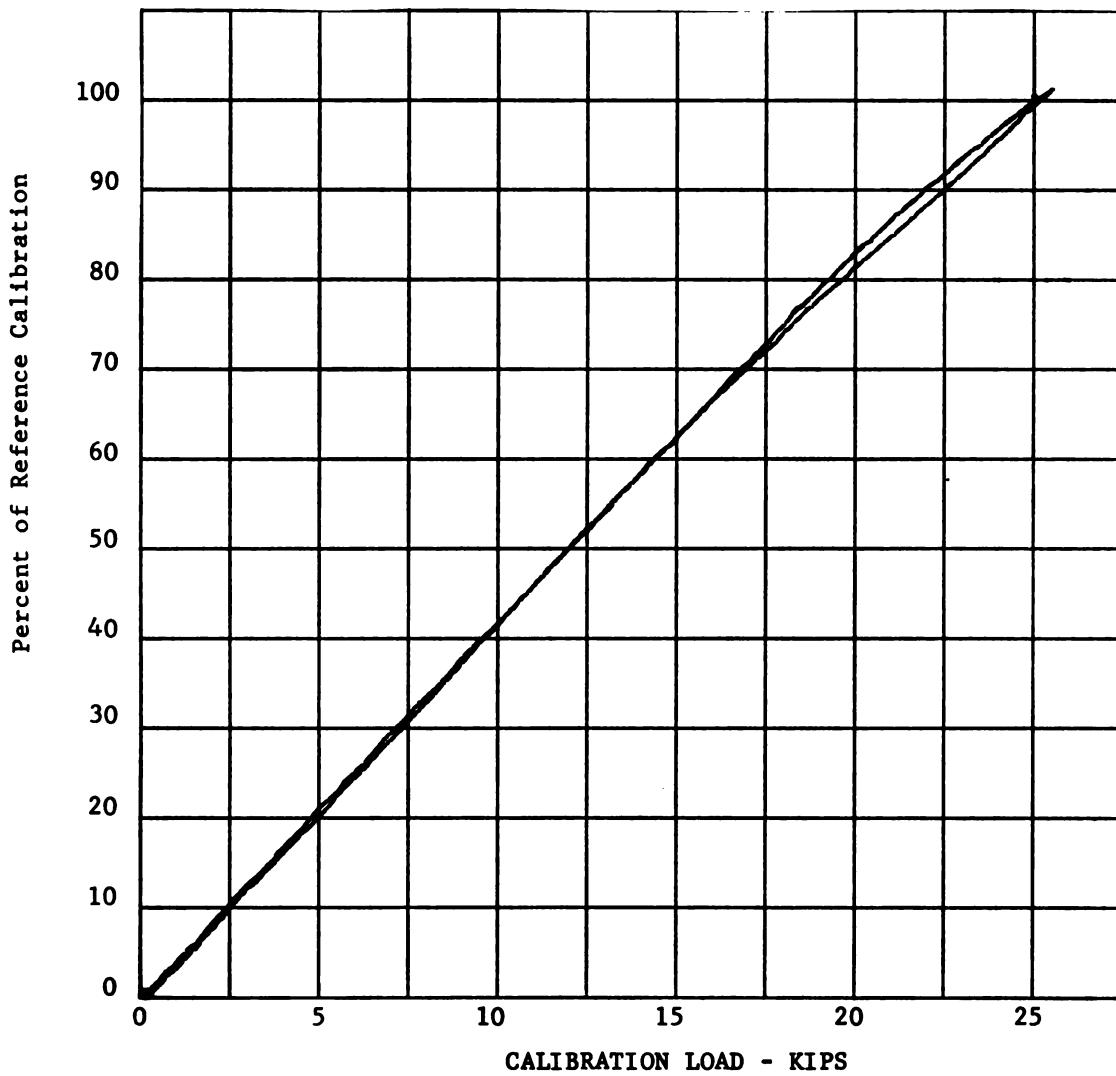


FIGURE 4-5. TYPICAL CALIBRATION DATA FOR LATERAL W/R LOAD CIRCUITS

Each instrumented tie plate had a pair of load cell washers. The signals from the two load cell washers were added to measure total vertical rail seat load and the signals were subtracted to measure the net rail seat moment. Appendix C gives a more detailed description of the instrumented tie plates and their calibration.

4.2.3 Tie Moments

A total of three strain gage ties (see Figure 4-6) were used in the main array to measure the bending moment under the rail seats and the bending and torsion moments at the tie center. Three additional strain gage ties were located randomly within each 110-ft test section. The additional ties were used to record any spatial variations in tie loading which might be caused by vehicle dynamic effects, and also to provide a comparison for data from the main array where it was necessary to disturb the ballast during installation of the instrumented tie plates. Bending and torsional moments within the tie were measured by strain gages installed directly on the ties in service. A full bridge with four active gages wired to measure bending or torsional moment directly was used for this project. The output of the bridge was calibrated directly in inch/lbs of moment using a laboratory calibration of equivalent ties. Detailed descriptions of the strain gage circuits, the gage installation procedures, and the circuit calibrations are included in Appendix D.

The possible presence of tie cracks in or near the gage locations was a major concern for the use of strain gage ties. The presence of a crack running through a gage location will produce a significant increase in strain when the tie is loaded sufficiently to open the crack. A crack adjacent to a gage location will limit the strain on that gage to the preload strain when the crack is open. In either case, the output from the bridge will be nonlinear and considerably different from the calibration data obtained from an uncracked tie. These effects were evaluated during the laboratory calibration procedure and the results are reported in Appendix D.

During an initial trip to the test sites to select the main array locations, the ballast was removed from several cribs so that the ties could be

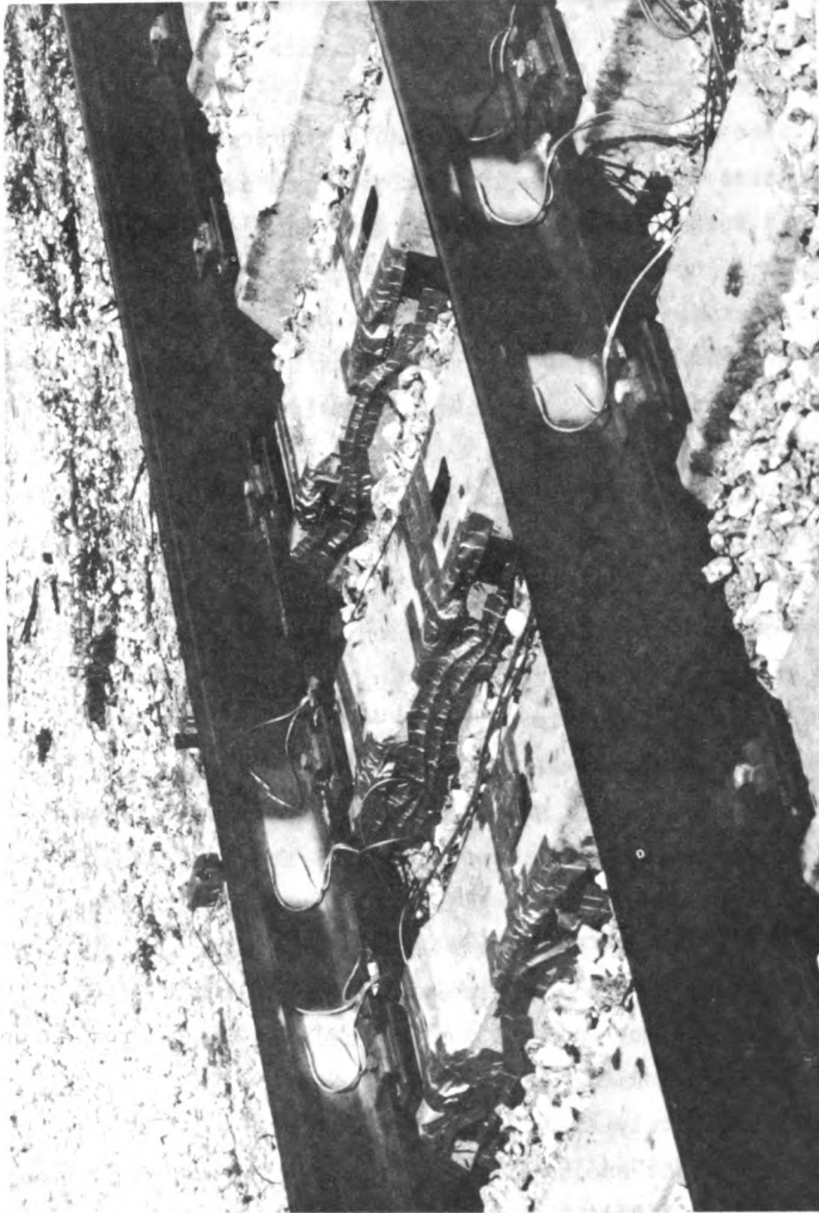


FIGURE 4-6. THREE STRAIN-GAGED TIES IN MAIN ARRAY

inspected for cracks and other defects. The initial intention of this inspection was to avoid picking a location for the main array that might have a cracked tie. All ties were inspected visually with the occasional aid of 3X and 5X magnifying glasses. Specific attention was directed to the rail seat region near the bottom of the ties and to the top of the ties in the center region.

An initial inspection included 6 ties at Site 1, and none of these exhibited any visible cracks. It was necessary to excavate the cribs around a total of 12 ties at Site 2 in order to find 6 ties that did not have any apparent cracks and were therefore judged suitable for strain gaging. The visible cracks were quite small and required close examination for detection. Some of these ties had been chipped and gouged near the tie bottom, apparently from the use of tampers with these closely spaced ties (20-inch nominal spacing). In addition to tamping damage, several ties showed one-half inch to one-inch chunks broken from their bottom edges as a result of high contact stresses between the relatively sharp edge of the tie and individual pieces of ballast. The cracks in the rail seat region of the ties at Site 2 frequently appeared to originate in the vicinity of these damaged locations.

The inspections of ties at Site 3 included a total of 13 ties, and all ties had hairline cracks in the rail seat region under the high rail. One or more cracks were also visible on the top surface in the center section of six of these ties. Consequently, the search for uncracked ties to use for strain gaging was abandoned because it was apparent the locating a sufficient number was highly unlikely. The locations of the cracks were marked, and when the strain gages were applied later, the gages located near the tie bottom under the rail seats were moved approximately one inch from the nominal position to avoid placing gages directly over a crack. The calibration data recorded in Appendix D show that the presence of a crack at or near the gages will not have a substantial effect as long as the tie bending moments are below about 75 inch-kips at the rail seat and 60 inch-kips at the tie center. These levels were rarely exceeded during the measurement program, as will be shown later.

Although the relatively small cracks in the rail seat and tie center regions caused some concern for applying strain gages to measure tie moments, service experience may prove that this type of crack has very little effect on tie life as long as the prestress is retained. It is noteworthy that the greatest number of cracks were found under the high rail at Site 3, which had

been in service for a period of 6 years and was located on a rather sharp curve where the vertical loads on the high rail are considerably higher than on tangent track.

4.2.4 Tie/Ballast Pressures

The Federal Railroad Administration/Portland Cement Association (FRA/PCA) special design load cell ties developed for the Kansas Test Track were used to measure tie support reactions at the tie/ballast interface. These ties have ten separate segments along the bottom to convert bearing pressures to discrete loads. Each rail seat is instrumented to measure vertical rail seat loads. A detailed description of the construction of the FRA/PCA load cell tie and a comparison of the bending stiffness between the load cell tie and the RCCC tie can be found in Appendix E.

Two of the load cell ties were installed at Site 1, and one load cell tie was installed on the curve at Site 3. As discussed previously, these ties were placed in track and hand-tamped approximately one month before beginning the measurement program to allow for reconsolidation of the disturbed ballast. The purpose of using these load cell ties was to simultaneously measure vertical rail seat loads and the resulting distribution of tie/ballast pressure on the 10 instrumented segments along the tie length. It was recognized that inserting a single tie in the track might result in that tie supporting less than the normal percentage of wheel load. Therefore, data from the pressure distribution on the load cell ties have been normalized by the rail seat load to minimize this influence.

Figure 4-7 shows a photograph of the load cell tie installed in track. As discussed in Appendix E, the load cell ties were refurbished at BCL prior to use on the measurement program, and each of the bottom pressure cells and the rail seat load cells were calibrated in a static load machine.

4.2.5 Track Deflection

The main array included displacement transducers to measure absolute vertical rail deflection, lateral deflection of the rail head relative to the tie, and absolute lateral displacement of the tie. The displacement transducers

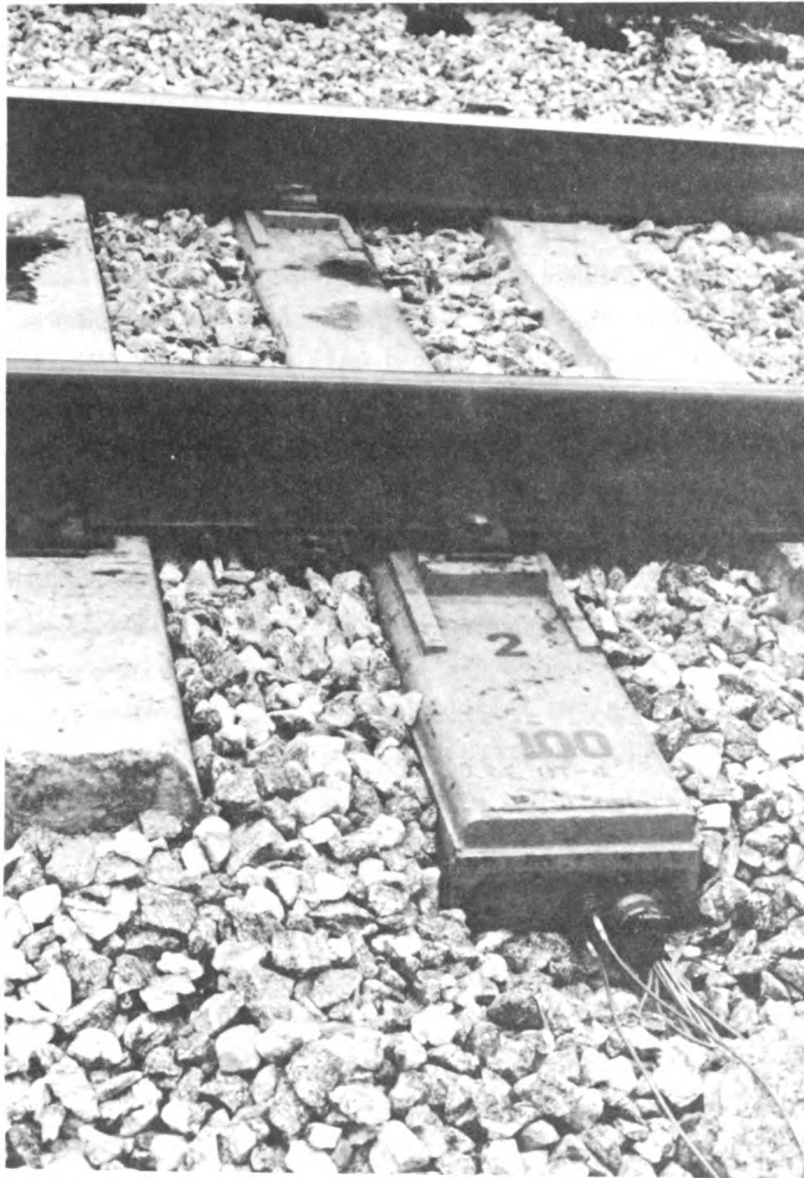


FIGURE 4-7. LOAD-CELL TIE

are shown in Figure 4-3. All measurements were made adjacent to the center tie using Direct Current Differential Transformers (DCDT) having a displacement range of ± 0.5 inches. The absolute vertical and lateral displacement of the rail or tie were referenced to a "ground stake" which consisted of a 1-inch diameter steel rod driven through a concentric hollow casing through the ballast into the subgrade. The casing was about 4 feet long to isolate the rod from ballast movements. The 1-inch diameter steel rod was 8 feet long and it was driven into the roadbed until about only 8 inches projected above the ballast surface.

The lateral displacement of the rail head relative to the tie was measured using a small section of rail epoxyed to the tie surface for purposes of attaching a DCDT. Vertical rail deflections were also measured at one of the strain gaged ties located away from the main array to provide data on vertical track modulus at two independent locations.

An end-to-end calibration of the displacement transducers and signal conditioning amplifiers was made using the in-track installation. The DCDT's were first adjusted to center the rods in the middle of the displacement range. Then a physical calibration was performed over a displacement range of 0.1 inch by rotating the No. 4-40 threaded rod (used to mount the displacement transducer core) by four turns.

4.2.6 Rail Fastener Bolt Loads

Two load washers of the type shown in Figure 4-8 were used to monitor the fastener bolt-load fluctuations on one rail-fastener assembly. These load cell washers were the same type as those used for the instrumented tie plate load cells, and they were calibrated in a laboratory load machine before the measurement program started. Appendix C shows typical data for instrumented tie plate load cell and the fastener bolt load measurements made simultaneously on a single fastener.

4.2.7 Rail Bending Strain

Figure 4-9 shows the strain gage locations used to provide data on rail

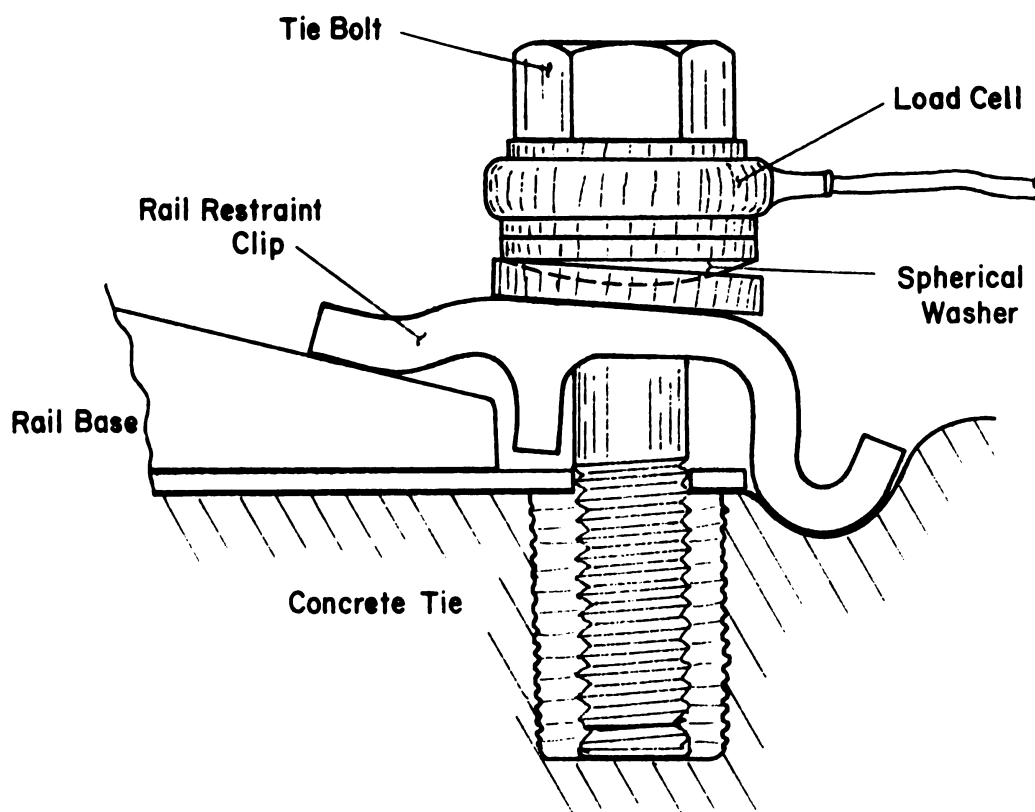
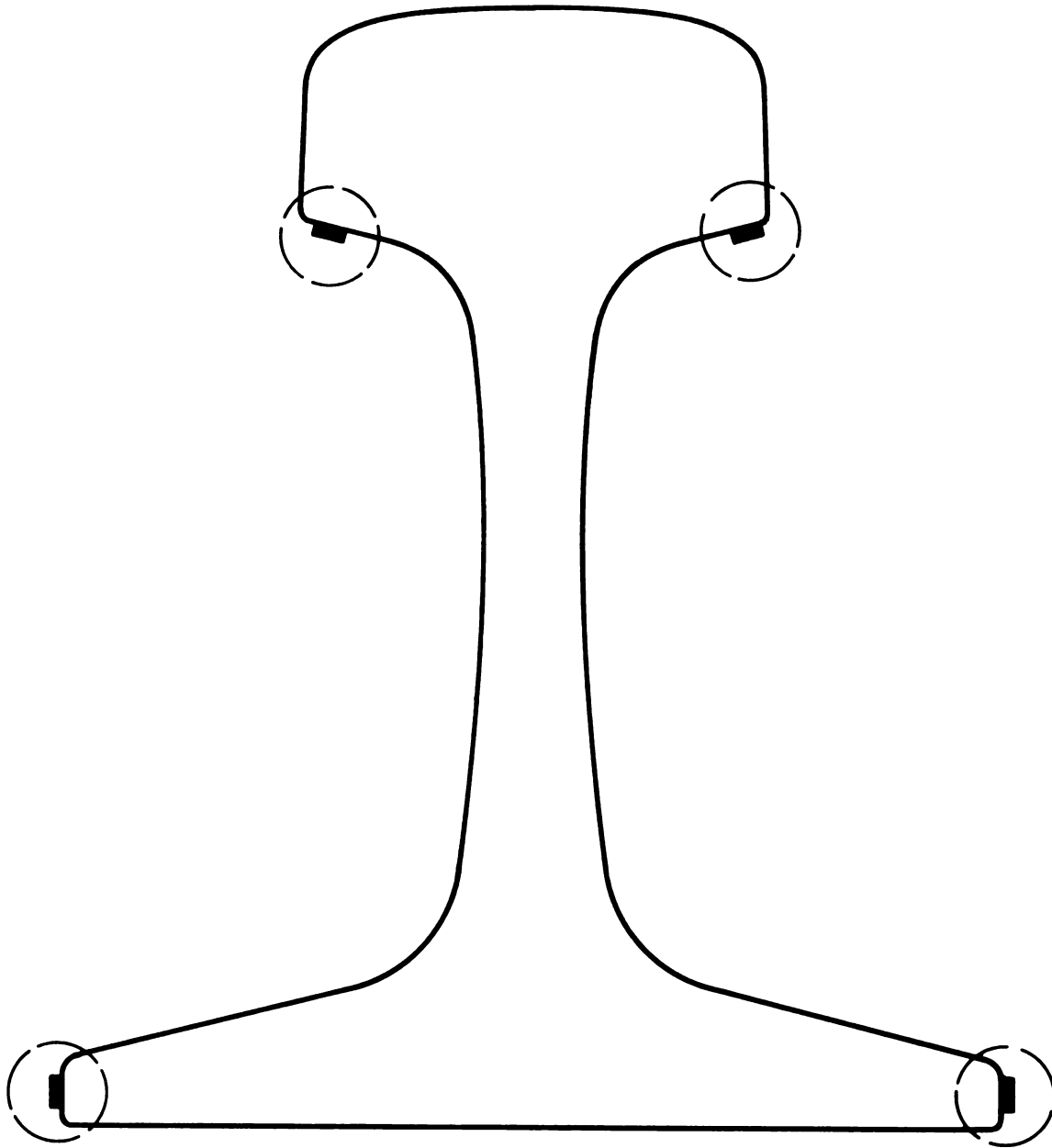


FIGURE 4-8. RAIL FASTENER BOLT LOAD MEASUREMENT



132 LB. RE RAIL SECTION

FIGURE 4-9. LOCATION OF STRAIN GAGES FOR RAIL STRESS MEASUREMENTS

bending strain. These gages were oriented longitudinally and wired in separate bridges to measure strain from lateral and vertical bending. The gages were located adjacent to the center tie in the main array and centered in the crib between the Chevron gage patterns for the vertical wheel rail load circuit. The outputs from the two gages on the rail base were averaged to use as an independent verification of vertical track modulus. Data from the gages in the rail fillet regions have been used to compare with predictions from a rail stress analysis model.

The sensitivities of the individual bridges for the rail bending strain gages were determined by calculating the circuit response with the gage factor provided by the gage manufacturer. This circuit sensitivity was then simulated by a precision strain calibrator to verify overall system sensitivity.

4.2.8 Rail and Tie Acceleration

Accelerometers were placed on the rail and on an immediately adjacent tie to measure the vertical acceleration at these two locations. Data from several revenue trains passing the site were recorded in order to compare the frequency content of the rail and tie accelerations to determine attenuation through the rail fastener and to determine typical tie accelerations caused by rail uplift.

Piezoelectric accelerometers and charge amplifiers having an overall flat frequency response from 1 Hz to 5,000 Hz were used for these measurements. The amplifiers and the recorder were calibrated end-to-end by mounting each accelerometer on a calibration shaker. The amplifier output was then adjusted for a nominal sensitivity.

4.3 BALLAST AND SUBGRADE PROPERTIES

Input data requirements for the MULTA track analysis model include the elastic properties for a layered representation of the ballast and subgrade. The following sections discuss the plate bearing tests which were made on the ballast and subgrade and several soil property measurements which were made to characterize the subgrade material.

4.3.1 Plate Bearing Tests

The following plate bearing test procedure was used to obtain representative data for the elastic properties of the ballast and subgrade:

(1) Two adjacent ties were removed sufficiently far away to avoid any affect on the instrumentation, and load-deflection plate bearing measurements were made on the ballast surface in the footprint of one tie, as shown in Figure 4-10. An 8-inch diameter circular loading plate was used on the ballast surface, and this area was covered with plaster-of-paris (dental cement) so that the loading plate would bear uniformly on the ballast. A fixed wooden reference beam supported outside the track was used as a displacement reference for two displacement transducers (DCDT) attached to the plate. Displacements were recorded for ballast loading up to about 125 psi, which exceeds the ballast pressure encountered in service by a considerable margin. Typical ballast pressures in service rarely exceeded about 50-60 psi.

(2) The ballast crib was excavated at the location of the two removed ties to determine the actual ballast depth. The ballast depth under the bottom of the tie was 6.5 inches at both Site 1 and Site 2. The plate bearing tests were repeated on the subgrade without using the dental cement. Data from Steps (1) and (2) were then used with the multi-layer track analysis model to determine representative values of Young's modulus for the ballast and subgrade layers.

The load bearing tests on the ballast were made at three positions along the tie's length. These positions were (1) at the center of the tie, (2) at 6.5 inches (gage side) from the rail center, and (3) at 18 inches (field side) from the rail center.

Plate bearing tests on the subgrade were made at two positions along the tie length. These positions were at the tie center and 615 inches (gage side) from the rail center.

The loading cycle was repeated three consecutive times at each of the positions along the length of the tie. As shown in Figure 4-11, the initial load cycle has a much lower slope (force versus displacement) value than the second loading cycle. In fact, after the initial load cycle, the subsequent load cycles have almost the same slope. Data shown in Figure 4-11 are for the

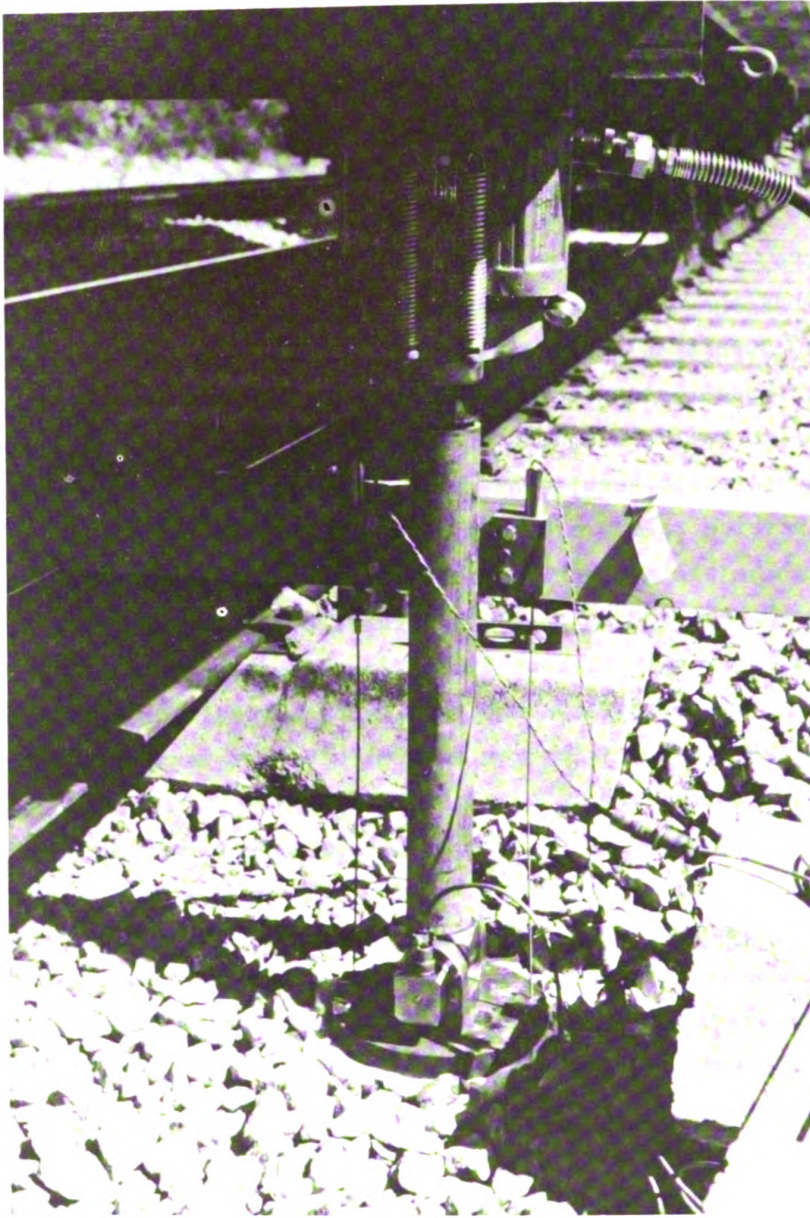


FIGURE 4-10. BALLAST PLATE BEARING MEASUREMENTS

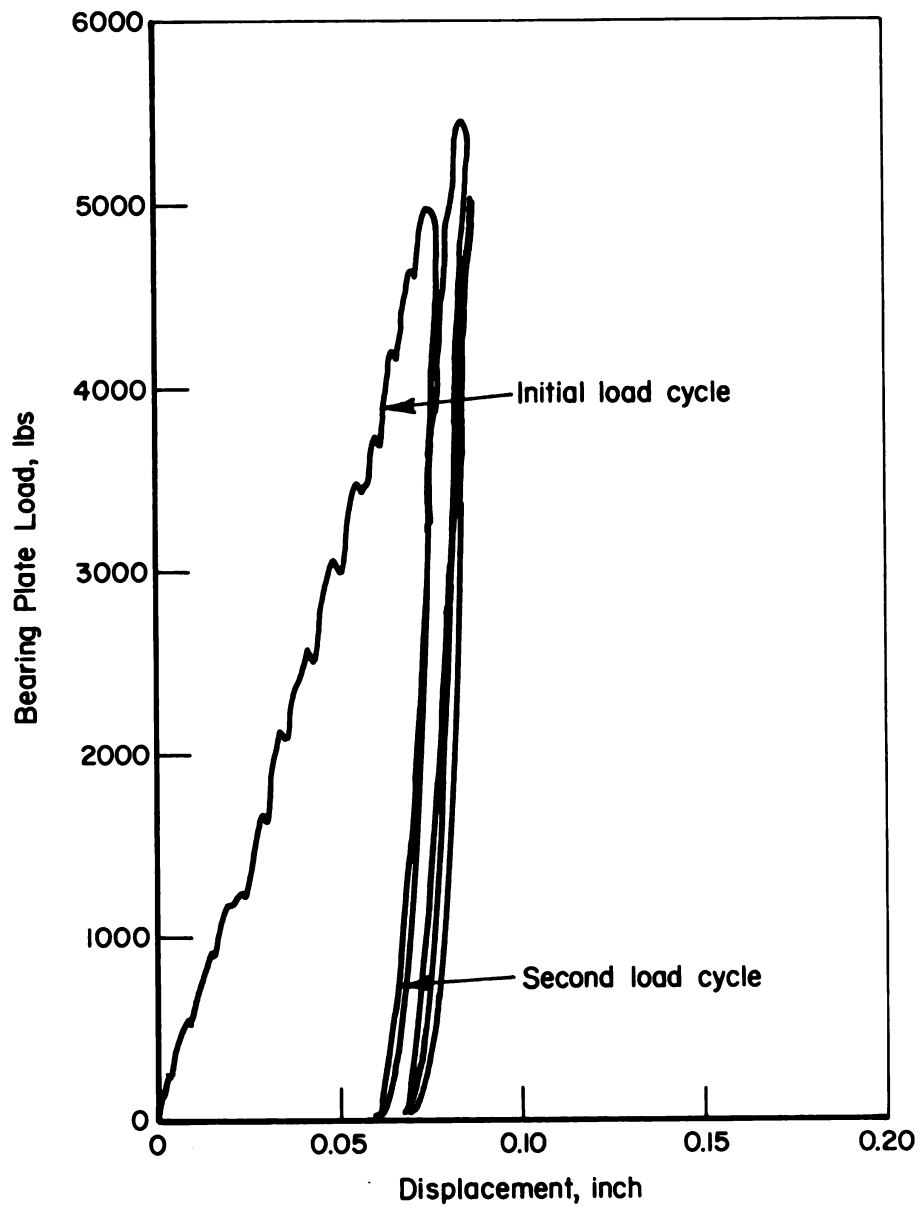


FIGURE 4-11. FORCE-DISPLACEMENT CURVE FOR SUBGRADE
 PLATE BEARING TEST @ 6.5 in. FROM RAIL
 SEAT - SITE 1

Site 1 subgrade at 6.5 inches on the gage side of the rail. Data for the other locations are characteristically similar.

Initial and final slope values from the subgrade tests were used to estimate Young's modulus (E_2) for the subgrade, using theory of elasticity solutions for the deflection of an elastic half-space loaded by a rigid, circular plate. Having determined E_2 , the ballast stiffness data were used to estimate Young's modulus (E_1) for the ballast. This estimate was made using the multi-layer program in an iterative scheme until predicted load-deflection values for the circular plate load were sufficiently close to the experimental values. It was hoped that using initial and final stiffness values would place a bound on the value of E_2 so that the predicted value of track modulus (U) would compare favorably with the measured data for track modulus.

Values of Poisson's ratio for the subgrade and ballast layers are also needed as input to the MULTA program. Typical values of $\nu_1 = 0.4$ for ballast and $\nu_2 = 0.4$ for subgrade Poisson's ratio were picked from the subgrade property data in Appendix F.

Table 4-1 shows the values of ballast modulus (E_1), subgrade modulus (E_2) and track modulus U based on initial and final plate stiffness data in conjunction with the MULTA program. The predicted modulus values U are based on the beam-on-elastic foundation equation involving applied wheel load P and the average maximum tie-plate load Q measured in the main array. A sample of the ballast material was also tested at the University of Illinois to determine the resilient modulus under repeated load. The resilient modulus ranged from 30 to 45 ksi for a bulk stress range of 30 to 65 psi.

TABLE 4-1. MODEL PARAMETERS FROM PLATE BEARING TESTS⁽¹⁾

	Young's Modulus (ksi)		Predicted Track Modulus (ksi) ⁽²⁾
	Initial	Final	
I. Tangent Site, 24 inch tie spacing (Site 1)	$E_1 = 24.$ $E_2 = 8.9$	$E_1 = 30.$ $E_2 = 17.8$	15.2 - 25.5
II. Tangent Site, 20 inch tie spacing (Site 2)	$E_1 = 15.$ $E_2 = 4.8$	$E_1 = 28.$ $E_2 = 17.8$	10.5 - 30.4

Notes:

- (1) E_1 = ballast modulus, E_2 = subgrade modulus, Ballast depth = 6.5 inch., Poisson's ratio = 0.4
- (2) Range for initial to final values for model parameters based on predicted maximum tie plate load.

4.3.2 Subgrade Property Measurements

In addition to the plate bearing measurements discussed in the previous section, several independent measurements were made to document soil types and properties characteristic of the track subgrade. Table 4-2 summarizes data obtained by Pittsburgh Testing Laboratories at Sites 1 and 2. In-situ subgrade density and moisture measurements were made in the track excavations used for the plate bearing tests. A nuclear radiation probe was used at three locations across the track. The subgrade density was higher at Site 1, which may be a result of a higher local content of old limestone ballast as evidenced by the sieve analysis results in Appendix F. The density measurements did not show any tendency for the subgrade at the track center to be either more or less compacted than it was under the rails.

Soil samples were taken from the excavation in the immediate vicinity of the probe sites. These samples were evaluated to determine the moisture/density relationships (Proctor curves), also shown in Appendix F. The soil material was a mixture of sand and limestone gravel, and therefore no plasticity (NP) was measured by the Atterburg limit test. No soil data were obtained for

TABLE 4-2. SUMMARY OF TRACK SUBGRADE PROPERTY DATA

Site No.	Soil Description	Max. Dry Density, lb/cu ft	Optimum Moisture, percent	Atterburg Limit	In-Situ Soil Data				
					Field Moisture, percent	Density, lb/cu ft	Wet	Dry	Compaction, percent
1	Brown sand with lime-rock	129.6	8.6	NP	East rail	9.4	127.1	116.2	89.6
					Track Center	9.5	139.4	127.3	98.2
					West Rail	8.3	135.1	124.8	96.3
2	Tan sand with traces of limerock	111.7	13.8	NP	East Rail	4.9	113.2	107.9	96.6
					Track Center	4.3	112.8	108.1	96.8
					West Rail	3.8	117.3	113.0	101.2
Site 1 - Tangent track with 24-inch tie spacing, MP 278.2									
Site 2 - Tangent track with 20-inch tie spacing, MP 279.0									

Site 3 because there was insufficient time to make an excavation for plate bearing tests without interrupting train traffic at this single track site. Visual inspection of the subgrade indicated the soil was probably similar to that at the other sites.

Additional vibroseismic measurements were made at each test site to determine representative data for Young's modulus, Poisson's ratio and shear modulus as a function of subgrade depth. These measurements included surface refraction seismic tests and vibratory tests conducted by staff from the U. S. Army Engineers Waterways Experiment Station (WES) in Vicksburg, Mississippi. The surface refraction seismic tests were made by placing 12 vertical velocity-type geophones at 2-ft and 5-ft intervals in a straight line parallel to the track. A steel plate placed on the ground at one end of the seismic line was struck with a sledge hammer. The time required for the compression wave to travel along the seismic line was used to determine the compression-wave speed.

A 50-lb electromagnetic vibrator was used to generate variable-frequency vertical excitation to measure the wavelength as a function of frequency. These data were used to compute the shear wave velocity, which can be related to shear modulus G if the soil density is known. The measurements of compression and shear wave velocities were used to calculate Poisson's ratio ν . The compression modulus E (Young's modulus) is then determined from the familiar equation:

$$E = 2 (1 + \nu) G. \quad (4-1)$$

Experience by WES indicates that variations in E and G with frequency correlate best with other exploration methods when it is assumed that the effective depth for the measured properties is equal to one-half the wavelength of the surface wave. Therefore, the computed values for E and G at different frequencies give the elastic moduli as a function of depth.

Figure 4-12 shows the vibroseismic measurements being made at Site 2. It would have been desirable to make these measurements in an excavation on the track roadbed rather than beside it. However, the transverse pits used for the plate-bearing tests were too short, and an excavation on the order of 20 feet down the track center was prohibitive. Consequently, the soil moduli determined from the measurements beside the track are judged to be lower bound



FIGURE 4-12. CONDUCTING VIBROSEISMIC MEASUREMENTS AT SITE 2

estimates because they do not include the effect of traffic-induced compaction or the mixture of soil and limestone ballast that was apparent in the track subgrade.

A more detailed discussion of the vibroseismic measurements and the data reported by WES is included in Appendix G. Representative data for Young's modulus and Poisson's ratio versus depth are summarized in Table 4-3 for the three test sites. The modulus data for the two tangent track sites where the plate bearing tests were made were quite similar. This was expected because of their proximity and similar appearance. The subgrade moduli at the curve (Site 3) were somewhat higher. The curve site was located on a cut into the side of a small hill. The difficulty experienced in driving the vertical displacement reference rods into the roadbed indicates the possibility of rock relatively close to the subgrade surface.

Poisson's ratio data showed relatively small variations with depth or between sites. A uniform value of $\nu = 0.4$ was recommended for the analysis model.

4.4 DATA ACQUISITION AND RECORDING

Figure 4-12A shows a block diagram of the data acquisition and recording system used for this measurement program, and Figure 4-13 shows the system as installed in the test van. Specific transducers and signal conditioning amplifiers are listed in Table 4-4 with their range and frequency response specifications. The effective frequency response for the complete data channel is also listed to show those channels which might be limited by recorder response or input filters.

To accommodate more than 14 channels on one standard IRIG tape recorder, this data system incorporated frequency division multiplexing. Two 14-channel multiplexes utilizing constant-bandwidth (CBW) voltage controlled oscillators (VCO) provided 28 out of the 38-channel system capacity. The remaining 10 channels were recorded on 10 discrete FM tape tracks. Each multiplex was recorded on a direct recording tape track and required a 150 KHz bandwidth. The tape recorder was operated at 30 inches per second (ips) to achieve this.

TABLE 4-3. SUMMARY OF SOIL ELASTIC PROPERTIES FROM VIBROSEISMIC SURVEY ADJACENT TO TRACK ROADBED

Depth Below Subgrade Surface, ft	Young's Modulus, ksi			Poisson's Ratio		
	Site 1 (1)	Site 2 (2)	Site 3 (3)	Site 1	Site 2	Site 3
0-1	5.5	6.5	9.0	0.35	0.38	0.38
1-2	7.0	9.0	11.3	0.43	0.41	0.35
2-4	7.0	10.5	11.8	0.43	0.45	0.43
4-8	7.5	11.2	12.0	0.43	0.45	0.42

- (1) Site 1 - Tangent track with 24-inch tie spacing, MP 278.2
- (2) Site 2 - Tangent track with 20-inch tie spacing, MP 279.0
- (3) Site 3 - Curved track with 24-inch tie spacing, MP 275.5.

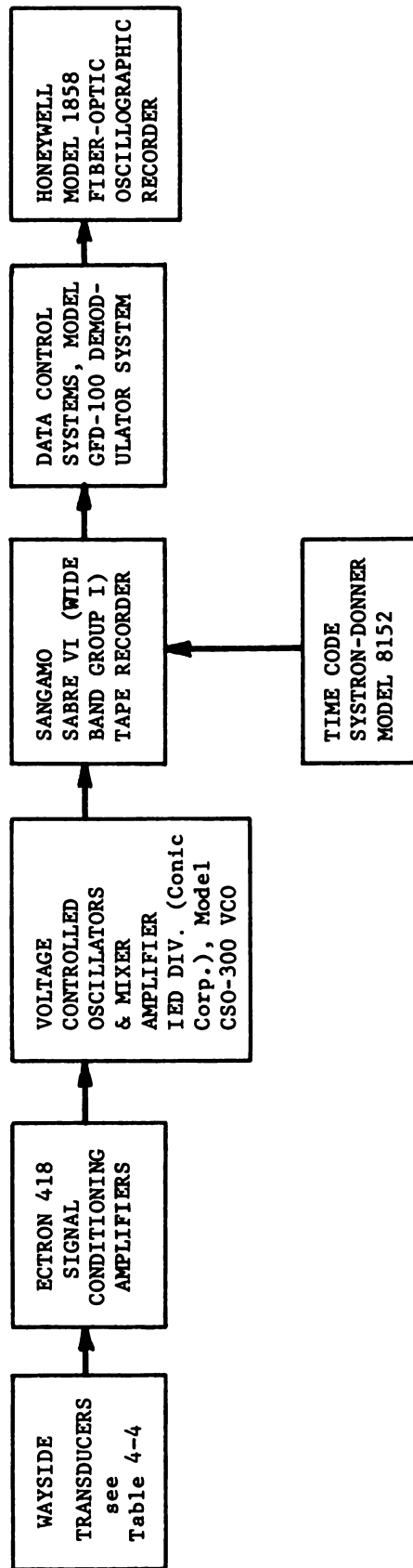


FIGURE 4-12A. BASIC DATA ACQUISITION AND RECORDING SYSTEM COMPONENTS



FIGURE 4-13. DATA ACQUISITION AND RECORDING SYSTEM INSTALLATION

TABLE 4-4. SUMMARY OF TRANSDUCER SPECIFICATIONS

Measurement Parameter	Transducer	Amplifier	Transducer Max. Range	Transducer Freq. Resp., Hz	Channel Freq. Resp., Hz
I. Wheel/Rail loads	Ailtech Weldable Strain Gages, Model SG 129	Ectron	> 2000 μ e	> 2000	2000
a. Vertical					
b. Lateral					
II. Rail Fastener Loads	Lebow 3701-625 load cells Lebow 3701-625 load cells Lebow 3701-750 load cells	Ectron	30,000 lb	500	500
a. Vertical Rail Seat Load					
b. Rail Seat Moment					
c. Bolt Force	Lebow 3701-750 load cells	Ectron	45,000 lb	500	500
III. Tie Loads	Micro Measurements Strain Gages	Ectron	> 2000 μ e	2000	2000
a. Tie Bending Moment					
b. Tie Torsion Moment					
c. Tie/Ballast Pressure					
IV. Track Deflection	Trans.-Tek Model 244-000 DCDT	Ectron	± 500 in.	110	110
a. Vertical Rail Displacement					
b. Lateral Rail/Tie Displacement					
c. Lateral Tie Displacement					
V. Track Acceleration	Kristal 802A Accelerometer	Unholtz Dickie	10,000 g	5000	2000
VI. Rail Bending Strain	Ailtech Weldable Strain Model SG 129	Ectron	> 2000 μ e	> 2000	2000

The two remaining tape tracks were used for recording time code and tape speed compensation signals. Table 4-5 summarizes the component specifications for this data system.

The data demodulator system and a fiber-optic oscillograph were used to monitor data at the test site after they were recorded on magnetic tape. Shunt and voltage insertion calibrations were made on the tape and checked on the oscillograph immediately after each train. The voice edge track and log sheets were used to identify each train by locomotive number, time of day and date, and tape location. Train speed and total axle counts were also identified from the oscillograph records to maintain a record of axle counts versus speed bands for the statistical analysis.

4.5 DATA ANALYSIS

Oscillograph records for the work train and for selected revenue trains were used to provide typical time histories of track response and to check the recorded data prior to statistical analysis. The first step in the statistical data analysis diagrammed in Figure 4-13A requires an analog-to-digital (A/D) conversion of the data. A minicomputer system was used to control the digitized process, calculate peak values within the data "window" for each axle pass, and store the "raw" data in the form of digitized voltages blocked as sequential axles for each train. The computer program for this task used the train speed calculated from the transit time through the speed trap to "track" each axle as it passed through the test site. A time delay was established for each measurement location and the time code was used to initiate a data window equivalent to a length of 38 inches. The operation time for these calculations determines the maximum effective data-sampling rate within each window. This sampling rate was 125 Hz, which provided approximately 5 data points within each data window for calculating a peak value at the highest train speed of about 55 mph. The time code signal was also used to provide a time correlation for the data obtained from the three different passes required to digitize 38 channels with a 16-channel A/D converter.

TABLE 4-5. COMPONENT SPECIFICATIONS FOR DATA ACQUISITION SYSTEM

<p>I. <u>Signal Conditioning Amplifiers</u> Ectron Model 418APWY-5M419 Bandwidth: DC - 3 KHz Gain: 10 - 3000 (fixed or variable steps) Dynamic Range: > 60 dB Common Mode Voltage: 100 v Common Mode Rejection: 140 dB at DC, 120 dB at 60 Hz, balanced input Linearity: 0.05 percent Drift: 0.7 mv/C at gain 1000 Temp. Range: -25 C to +71 C Bridge Excitation: 5 VDC at 50 ma, isolated Bridge Balance: RTI zero suppression (\pm 40 mv)</p>	<p>III. <u>Magnetic Tape Recorder - Sangamo Sabre VI</u> Tracks: 14 + 2 edge tracks Amplifiers: 14 FM + 4 direct (combined as reqd.) Bandwidth: IRIG WIDEBAND Group 1 Tape: 1 in. x 1.5 or 1.0 mil on 14-in. reels Power: 115 VAC or 12 VDC Weight: 85 lb</p>																																																				
<p>II. <u>Voltage Controlled Oscillators</u> Led Division Subcarrier Freq: "OA" 8 KHz \pm 2 KHz</p> <table border="0"> <tbody> <tr> <td>IRIG 1A</td> <td>16</td> <td>"</td> <td>"</td> </tr> <tr> <td>" 2A</td> <td>24</td> <td>"</td> <td>"</td> </tr> <tr> <td>" 3A</td> <td>32</td> <td>"</td> <td>"</td> </tr> <tr> <td>" 4A</td> <td>40</td> <td>"</td> <td>"</td> </tr> <tr> <td>" 5A</td> <td>48</td> <td>"</td> <td>"</td> </tr> <tr> <td>" 6A</td> <td>56</td> <td>"</td> <td>"</td> </tr> <tr> <td>" 7A</td> <td>64</td> <td>"</td> <td>"</td> </tr> <tr> <td>" 8A</td> <td>72</td> <td>"</td> <td>"</td> </tr> <tr> <td>" 9A</td> <td>80</td> <td>"</td> <td>"</td> </tr> <tr> <td>" 11B</td> <td>96</td> <td>"</td> <td>+ 4 KHz</td> </tr> <tr> <td>" 13B</td> <td>112</td> <td>"</td> <td>"</td> </tr> <tr> <td>" 15B</td> <td>128</td> <td>"</td> <td>"</td> </tr> <tr> <td>" 17B</td> <td>144</td> <td>"</td> <td>"</td> </tr> </tbody> </table> <p>Linearity: 0.5 percent</p>	IRIG 1A	16	"	"	" 2A	24	"	"	" 3A	32	"	"	" 4A	40	"	"	" 5A	48	"	"	" 6A	56	"	"	" 7A	64	"	"	" 8A	72	"	"	" 9A	80	"	"	" 11B	96	"	+ 4 KHz	" 13B	112	"	"	" 15B	128	"	"	" 17B	144	"	"	<p>IV. <u>Time Code Generator</u> Systron/Donner 8152 Output format: IRIG B</p> <p>V. <u>Data Demodulators</u> Data Control Systems GFD-100 Subcarrier Frequencies: Same as VCO's Low Pass Filters: 2 KHz max (MI-1 on IRIG CBW-A channels) 5 pole Bessel</p> <p>VI. <u>Quick-Look Oscilloscope</u> Paper: 8-in. rapid access Channels: 18 Bandwidth: DC - 5 KHz at up to 7.2 in. deflection Accuracy: 0.5 percent</p> <p>VII. <u>Overall System Performance</u> Channels - 28 multiplexed 10 discrete (FM recorded) Bandwidth: DC - 2 KHz max - multiplexed DC - 3 KHz max - discrete Linearity: 0.5 percent S/N: 40 dB - multiplexed (depends on playback filter bandwidth) 48 dB - discrete FM channels</p>
IRIG 1A	16	"	"																																																		
" 2A	24	"	"																																																		
" 3A	32	"	"																																																		
" 4A	40	"	"																																																		
" 5A	48	"	"																																																		
" 6A	56	"	"																																																		
" 7A	64	"	"																																																		
" 8A	72	"	"																																																		
" 9A	80	"	"																																																		
" 11B	96	"	+ 4 KHz																																																		
" 13B	112	"	"																																																		
" 15B	128	"	"																																																		
" 17B	144	"	"																																																		

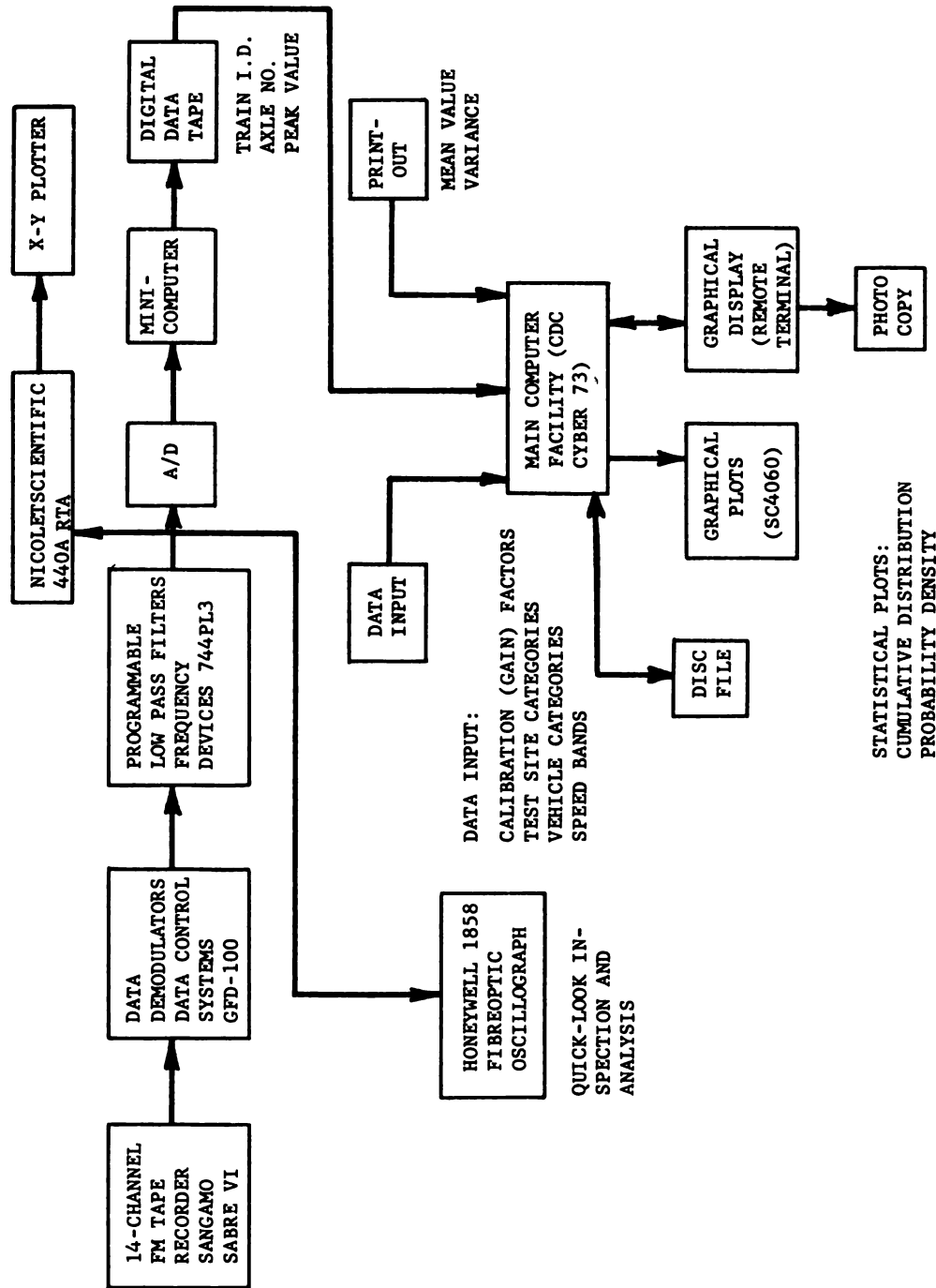


FIGURE 4-13A. DATA ANALYSIS PROCEDURES

The second step in the data processing procedure was to process the digital data tape in the main computer facility. Calibration factors were used to transform the voltage data to physical units (pounds, inches, etc.) and to add an identification for car weight and vehicle speed categories. Car weight was established from the vertical wheel/rail load circuits in the center of the main array. The average axle load from three axles was used to determine car weight. Data from the heaviest axle are disregarded to avoid the effect of flat wheels. Car speed categories of 30-40, 40-50, and 50-60-mph were selected for these test sites. Car weight categories included locomotives as a separate class, and cars were divided into (a) those under 50 gross tons (light and empty cars), and (b) those exceeding 50 gross tons (heavy cars). Data from all trains recorded at a test site were then sorted into the car and speed categories and stored on a disk file for subsequent data analysis.

The final step in the data processing was to perform the statistical calculations needed to obtain mean values, standard deviations, probability densities and probability distributions for the peak value data from each measurement. Data in each of the speed and weight categories were analyzed separately for each measurement (channel), and summations could be made for any category. Data from selected categories at different measurement locations (channels) could also be combined to form a new data set. For example, data from the five wheel/rail load circuits at Site 1 could be combined for heavy cars in the 50-60-mph speed range to include effects of spatial variations.

Statistical calculations were made by dividing the total expected data range into 200 equal intervals and summing the number of peak values (axles) falling in each interval. These data were stored on disk according to subcategory identification number. Graphs of probability density (histogram) and probability distribution were then plotted on an interactive graphics terminal using the identification numbers for single categories and combinations. An option to increase the interval size and reduce the number of intervals for plotting is included in the data processing program. Fifty data intervals were used for all of the probability density calculations and plots for this program.

A limited number of frequency analyses were made of selected acceleration and bending moment measurements using a real time analyzer (RTA).

As shown in Figure 4-13A, the frequency analysis was made directly from the analog output of the data system through a 600-Hz low pass filter and the amplitude spectrum was plotted on an x-y plotter. A section of tape from the passage of one train was selected to provide a record length of up to 20 seconds, which includes approximately 20 cars at 50 mph. The analyzer was set up to give an analysis bandwidth of 0-500 Hz with a frequency resolution of $\Delta f = 1.2$ Hz.

4.6 FORMATS FOR STATISTICAL DATA

The format for statistical analysis results shown in Figure 4-14 has typical plots of the probability distribution function (left-hand graph) and the probability density histogram (right-hand graph) for a measurement of peak vertical wheel/rail loads. These data are the peak loads on one rail for all cars and all speeds (all traffic) at one measurement location. The probability density histogram shows the ratio of the number of peak loads within each of the 50, 1.2-kip load intervals which cover the total range of 60 kips. It is important to note that the quantitative results for the histogram depend on the selected load interval W_N , and are therefore not unique. Increasing the load interval (reducing the number of intervals) will increase the number of occurrences at a particular load level. This improves the averaging used for the estimate but reduces the resolution--a tradeoff decision. Load intervals which are too small for the data base cause irregularities in the density curve at extreme loads because of an insufficient number of data points to provide a reliable average for these low probability events.

The amplitude probability distribution function shown in Figure 4-14 gives the percentage of peak loads that exceed a specified load level. This is calculated from the integral of the density function, and therefore the quantitative results are unique and do not depend on the load interval used to generate the histogram. The vertical axis for the probability distribution function is expanded to provide greater resolution of the extreme values. Insufficient data points to provide a reliable estimate for low probability events appear in the distribution function as horizontal segments, which shows there were no data points at that load level. The accuracy of the low probability estimates at these points is questionable.

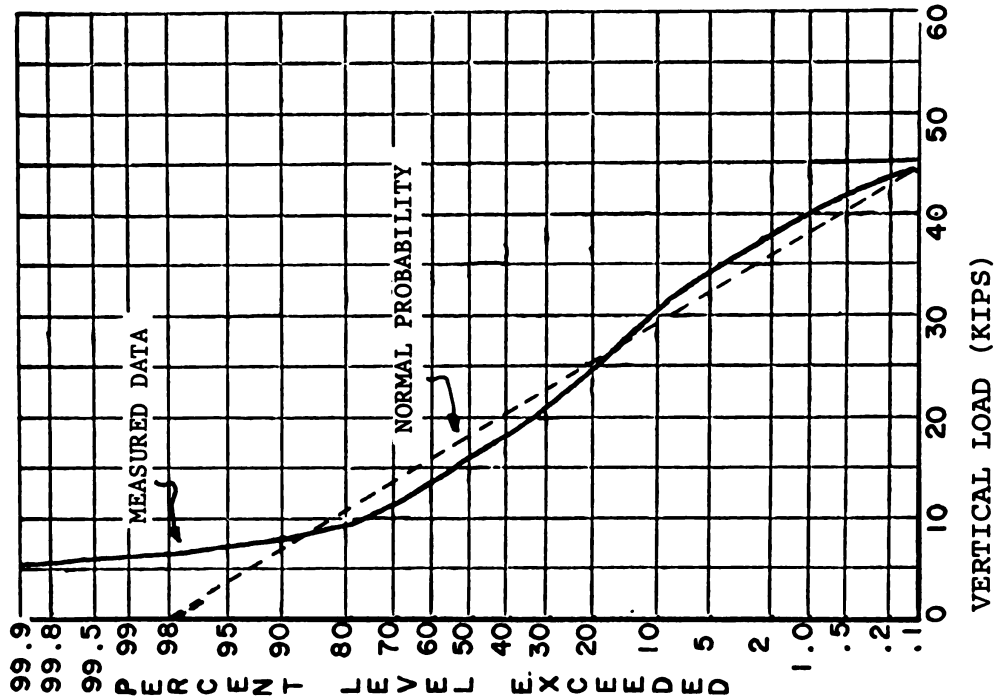
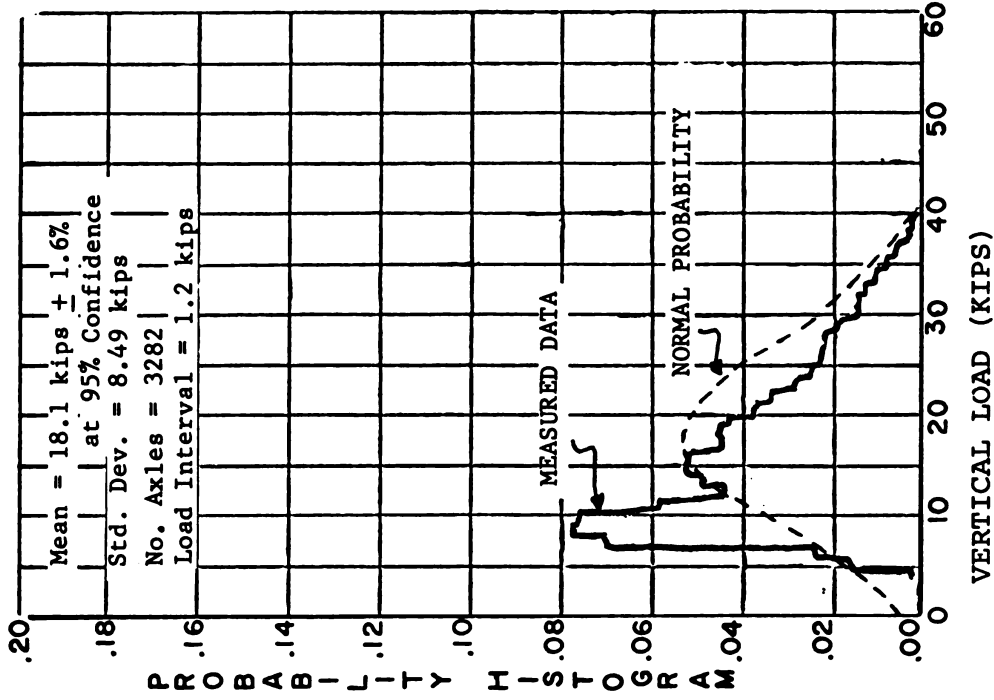


FIGURE 4-14. TYPICAL PROBABILITY DISTRIBUTION AND DENSITY HISTOGRAMS FOR VERTICAL W/R LOAD FOR ALL CARS AND ALL SPEEDS

Statistical data having a normal (Gaussian) distribution will appear as the familiar bell-shaped curve on the density plot and as a straight line on the scale used for the distribution curve. These curves are shown in Figure 4-14 for comparison. The 50 percent probability level gives the median load (50 percent higher and 50 percent lower) for any distribution. If the experimental data had a perfectly normal distribution, the the median peak load would be identical to the mean peak load, 18.1 kips in this example. The theoretical curves for the normal distribution shown in the figure have the same mean value and standard deviation as the measured data. For this particular measurement the normal curve gives a relatively good estimate of data at low probability levels even though it is not a good match elsewhere.

4.7 RESULTS FROM STATISTICAL ANALYSIS

As discussed in Section 4.5, the generation of probability histograms and calculations of mean values and standard deviations for each vehicle and speed category provided the base data for all subsequent data combinations. Appendix H contains a channel number versus track location index and the computer listings of mean value, standard deviations (S.D.) and axle count for each category at all three measurement sites. Also included are accuracy evaluations for the mean value estimates in terms of the confidence levels for ± 10 and ± 20 percent mean value tolerance bands and the estimated tolerance band at the 90 and 95 percent confidence levels.

Table 4-6 summarizes the axle count and mean load data found in Appendix H for the case of vertical wheel/rail loads measured on one rail at the center of the main array at each of the three sites. An inspection of these data reveals several interesting conclusions:

a. Data from the two tangent track sections (Sites 1 and 2) show a definite weight bias in the speed ranges. The mean wheel loads for heavy cars and all cars were highest in the 30-40-mph low-speed range and lowest in the 40-50-mph range. It appears that the distribution of car weights is a greater influence on speed effects (trains with heavy cars go slowly) than any dynamic effects on vertical loads for this smooth track. Mean loads for locomotives, which were all 4-axle of similar design, show no significant vehicle dynamics speed effect on the tangent track sections.

TABLE 4-6. SUMMARY OF AXLE COUNT AND MEAN VALUES FOR PEAK VERTICAL WHEEL/RAIL LOADS AT ALL SITES

Speed Range, mph	Number of Axles-Site 1 (1)			Number of Axles-Site 2 (2)			Number of Axles-Site 3 (3)						
	Locos.	Light Cars	Heavy Cars All Cars	Locos.	Light Cars	Heavy Cars All Cars	Locos.	Light Cars	Heavy Cars All Cars				
30 - 40	12	28	408	448	24	464	448	936	16	408	144	568	
40 - 50	20	724	244	988	12	444	196	652	40	592	432	1064	
50 - 60	72	658	1116	1846	28	404	212	644	52	528	628	1208	
All speeds	104	1410	1768	3282	64	1312	856	2232	108	1528	1204	2840	
	Mean Vertical Wheel/Rail Load(kips) - Site 1 (1)			Mean Vertical Wheel/Rail Load(kips) - Site 2 (2)			Mean Vertical Wheel/Rail Load(kips) - Site 3 (3)						
30 - 40	35.3	11.8	28.4	27.6	32.9	10.3	25.2	18.0	29.8	8.4	21.6	12.4	
40 - 50	37.2	10.3	20.0	13.3	33.2	8.3	18.9	12.0	32.7	8.9	19.5	14.1	
50 - 60	35.4	11.7	21.3	18.4	30.2	9.1	23.5	14.8	35.9	11.6	25.3	19.8	
All speeds	35.7	11.0	22.8	18.1	31.8	9.3	23.3	15.3	33.8	9.7	22.7	16.2	

- (1) Data for Vertical Wheel Load at center of main array. Location 58E (Channel 6)
- (2) Data for Vertical Wheel Load at center of main array. Location 31W (Channel 38)
- (3) Data for Vertical Wheel Load at center of main array. Location 44E (Channel 6) on high rail.

b. Even though Sites 1 and 2 were located within one mile of each other on the same track, the mean vertical W/R loads for all cars in the low-speed range was significantly different. The results indicate that the low-speed data recorded at Site 1 consisted of only one or two trains of very heavy cars, probably 100-ton hopper cars loaded with gravel. It would be expected that the mean loads within each subcategory would be about the same for Sites 1 and 2 if data were recorded over a sufficient time to average the traffic-speed distributions. It is evident that the 3-4 days of recording time at each site were insufficient to remove a weight bias in the low-speed range. Therefore, comparisons of track component loads from the two sites must be restricted to categories having similar mean loads, such as heavy cars at all speeds, or the results must be normalized to remove the differences from variations in average car weight.

c. The mean vertical wheel/rail loads at the curve (Site 3) show a definite speed effect whereby the vertical load on the high rail increases with speed and that on the low rail (not shown in Table 4-6) is reduced as speed increases. The balance speed for the curve was 45 mph.

As shown in Table 4-6, statistical data were collected for a total of 16 different categories for each measurement channel at each of the three measurement sites. Limitations on data collection time precluded obtaining a sufficient data sample to give accurate estimates for low probability events in all categories at all test sites. These data requirements were discussed in detail in the measurement plan [4-1]. However, the basic plan was to obtain a complete data set for Sites 1 and 3, and to use a limited data set for Site 2 for evaluating the effect of tie spacing on the tangent track sections.

The volume of available data and the possible combinations of speed and car categories for the different measurements makes organizing this report difficult. The procedure selected has been to address several specific objectives of major interest for this program rather than attempting a very general review of the data. Briefly, these objectives were:

a. To determine average and maximum load statistics for concrete tie track components subjected to typical revenue traffic. These load statistics will provide a basis for describing the track load environment for future design and testing of track components.

b. To determine the effect of tie spacing on track component loads for track of otherwise identical construction.

c. To determine the variation in track component loads between curved and tangent track. The question of whether lateral wheel/rail loads on curves have an important effect on overall tie and fastener loads is an important issue.

d. To compare loading statistics for locomotive, light freight cars, and heavy freight cars to determine their relative contributions to track degradation.

e. To determine the effect of train operating speed on track component loads.

The following sections of the report present and discuss data selected for these particular objectives.

4.7.1 Track Component Loads from Revenue Traffic

Data in Table 4-7 summarize the load statistics for the most severe load location for each of the three track test sites. For example, the vertical W/R load data for Site 1 are for Location 58E, which had the highest loads of all five W/R load measurement locations. These load parameters are based on the entire data base (all cars, all speeds) for each site. Mean values, standard deviation (S.D.) and the 0.1 percent load level are reported. The 0.1 percent load level was used to pick the maximum load location in cases where the mean and 0.1 percent loads were not a maximum at the same location. The mean and S.D. can be used to predict low probability loads by assuming a normal distribution for the data. The measured 0.1 percent load level is a load which was exceeded by only 1 of every 1000 axles for the actual distribution of the measured data, so no assumptions regarding a statistical distribution are involved. Annual traffic of 20 MGT averages about 4000 axles per day, so the 0.1 percent load level would be exceeded about four times per day for this traffic.

The following sections discuss the loads on individual track components and show the spatial distributions for the different measurement parameters. For reference purposes, Table 4-8 lists the vertical rail seat

TABLE 4-7. SUMMARY OF TRACK COMPONENT LOAD STATISTICS
FOR ALL CARS, ALL SPEEDS, AT MAXIMUM LOAD
LOCATION

	Site 1-Tangent 24-In. Tie Spacing	Site 2-Tangent 20-In. Tie Spacing	Site 3-Curve 24-In. Tie Spacing
1. Vertical W/R Load (P)			
Mean, kips (95% TB)	18.1 (\pm 1.6%)	15.3 (\pm 2.4%)	16.2 (\pm 2%)
S.D., kips (% mean)	8.5 (47%)	8.73 (57%)	8.85 (55%)
0.1% Load, kips (Mean Ratio)	45 (2.5)	46 (3.0)	50 (3.1)
Location (Ch.)	58E (6)	31W (38)	44E (6)
2. Lateral W/R Load			
Mean, kips (95% TB)	0.98 (\pm 11%)	2.0 (\pm 4%)	1.65 (\pm 7.3%)
S.D., kips	3.04	1.91	3.18
0.1% Load, kips (S.D. Ratio)	15.5 (5.1)	16 (8.4)	15 (4.7)
Location (Ch.)	59E (19)	1E (24)	18E (17)
3. Rail Seat Vertical Load (Q)			
Mean, kips (95% TB)	8.75 (\pm 1.9%)	5.90 (\pm 2.7%)	11.3 (\pm 2.3%)
S.D., kips (% mean)	4.76 (54%)	3.89 (66%)	6.62 (58%)
Mean Ratio, Q/P	0.48	0.38	0.70
0.1% Load, kips (Mean Ratio)	24 (2.7)	21 (3.6)	31 (2.7)
Location (Ch.)	55E (36)	35E (33)	49E (39)
4. Rail Seat Moment			
Mean, kip-in. (95% TB)	4.88 (\pm 2.2%)	4.56 (\pm 3%)	6.13 (\pm 4.4%)
S.D., kip-in.	3.09	3.24	7.38
0.1% Load, kip-in.	21, -22	+17, -20	+44, -21
Location (Ch.)	63E (26)	35E (34)	47E (38)
5. Tie Rail Seat Bending Moment			
Mean, kip-in. (95% TB)	31.3 (\pm 1.0%)	7.44 (\pm 4.8%)	38.4 (\pm 1.3%)
S.D., kip-in. (% mean)	9.1 (29%)	8.69 (117%)	13.2 (34%)
0.1% Load, kip-in.	66	77	78
Location (Ch.)	57E (32)	97E (23)	47 (34)
6. Tie Center Bending Moment(Negative)			
Mean, kip-in. (95% TB)	-0.37 (\pm 92%)	-6.48 (\pm 5.8%)	-0.64 (\pm 69%)
S.D., kip-in.	10.0	9.06	12.1
0.1% Load, kip-in.	-30	-56	-42
Location (Ch.)	2 (15)	97 (22)	18 (21)
7. Tie Center Bending Moment(Positive)			
Mean, kip-in. (95% TB)	21.0 (\pm 9%)	13.5 (\pm 1.3%)	10.1 (\pm 5.2%)
S.D., kip-in.	5.6	4.13	14.3
0.1% Load, kip-in.	38	39	67
Location (Ch.)	59 (17)	30 (25)	43 (26)
8. Tie Center Torsion Moment			
Mean, kip-in. (95% TB)	8.45 (\pm 1.9%)	4.19 (\pm 1.9%)	3.37 (\pm 3.6%)
S.D. kip-in.	4.73	1.97	3.26
0.1% Load, kip-in.	25	12.5	16
Location (Ch.)	85 (33)	1 (19)	18 (22)
9. Rail Fastener Bolt Force (Dynamic)			
Mean, kips (95% TB)	0.13 (\pm 14.4%)	0.72 (\pm 2.5%)	0.16 (\pm 14.2%)
S.D., kips	0.17	0.44	0.46
0.1% Load, kips (S.D. Ratio)	0.75 (4.4)	2.3 (5.2)	2.3 (5.0)
Location (Ch.)	29G (42)	1G (28)	18G (28)

Note: Appendix H has an index of channel numbers and a diagram of load locations.

TABLE 4-8. SUMMARY OF TIE LOAD REQUIREMENTS FROM AREA SPECIFICATIONS FOR CONCRETE TIES AND FASTENINGS (1)

Tie Spacing, in.	Vertical Rail Seat Load		Flexural Strength Requirements, in.-kips (2)			
	Percent Wheel Load	kips	Rail Seat +	Rail Seat -	Center -	Center +
21	46.5	48.15	225	115	200	90
24	51	52.6	250	115	200	90
27	55.5	57.05	275	115	200	100
30	60	61.5	300	115	200	110

- (1) AREA Bulletins 655 and 660 [3-1, 3-2].
 (2) Strength requirement for 8'-6" tie length.

loads and tie bending moment requirements from the current AREA specification for concrete ties and fasteners. The RCCC concrete tie used on the FEC has a minimum flexural strength of 150 inch-kips, and one tie out of every 200 is checked to this limit when the ties are removed from the mold after 18 hours of curing. Some additional increase in strength would be expected with time. However, this smaller tie cannot be expected to meet the 250-inch-kip positive bending moment required by the current specifications for 24-inch tie spacing.

4.7.1.1 Vertical Wheel/Rail Load

Figure 4-15 shows that the statistical distributions for all five measurements of vertical W/R load at Site 1 are nearly identical. There is no significant spatial variation at Site 1, and data for the other sites are similar. Data in Table 4-7 show that the maximum 0.1 percent load level was 50 kips, and this was recorded on the high rail at the curve site. The S.D. showed little variation between sites and was about 50 percent of the mean vertical W/R load for this traffic.

4.7.1.2 Lateral Wheel/Rail Load

Figures 4-16 and 4-17 show the statistical distributions for lateral W/R load measurements at the tangent track site (Site 1) and the curve site (Site 3), respectively. High positive lateral loads are caused by flanging forces on the rail head directed toward the field site. Negative lateral forces from friction and creep in the wheel/rail contact zone occur frequently but are limited by the maximum coefficient of friction. The data in Table 4-7 show that the maximum 0.1 percent lateral loads at all sites were nearly identical. However, the graphs show a substantial spatial variation for the two different measurement locations at each site. A greater number of measurement locations would be needed to define these variations within each site.

The recorded data show that the mean lateral loads at all sites are no greater than 2 kips, which is quite low. Also, there is no apparent

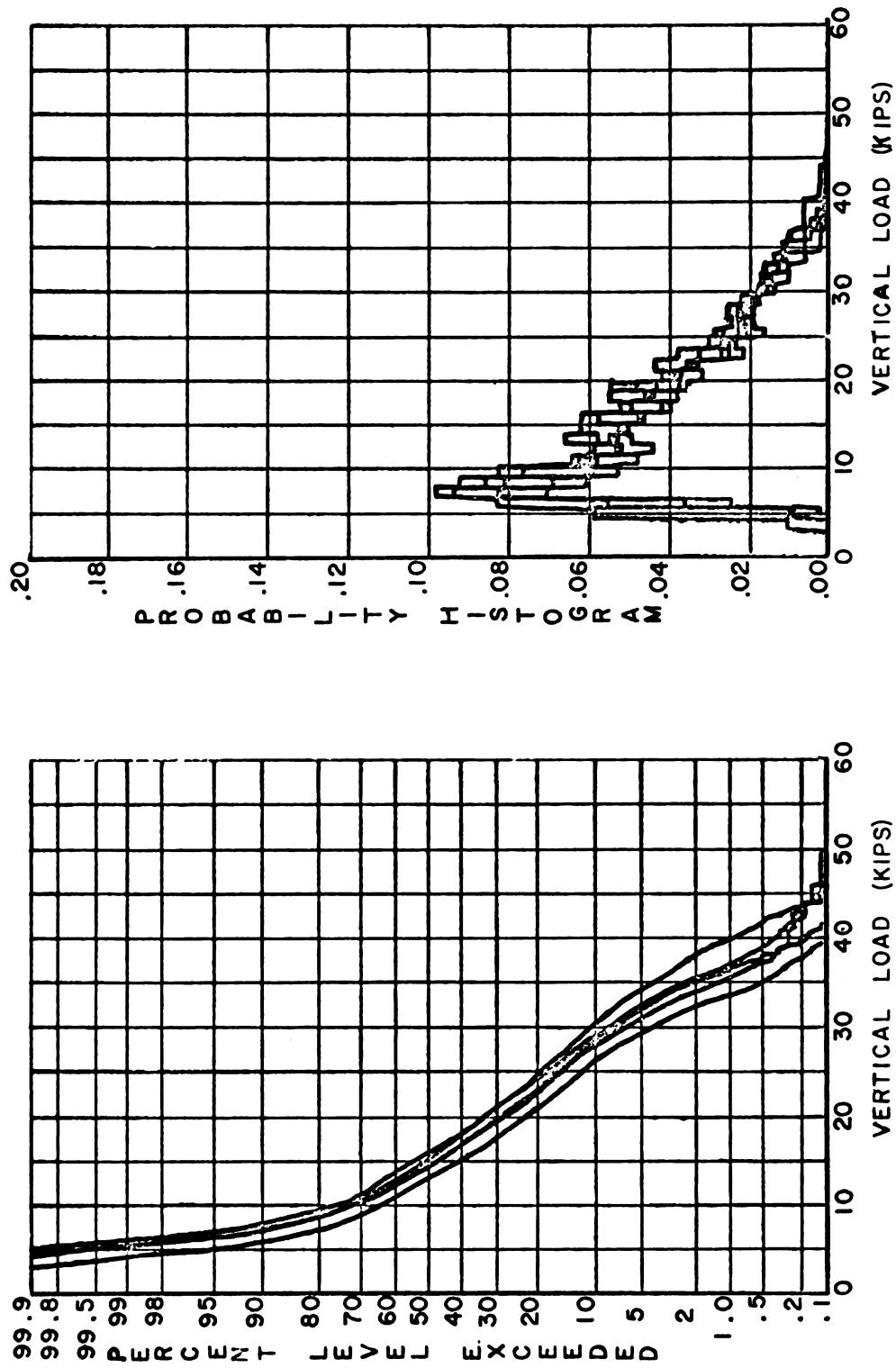


FIGURE 4-15. PEAK VERTICAL WHEEL/RAIL LOAD STATISTICS FOR ALL TRAFFIC AT SITE 1 (1.2 kip load interval)

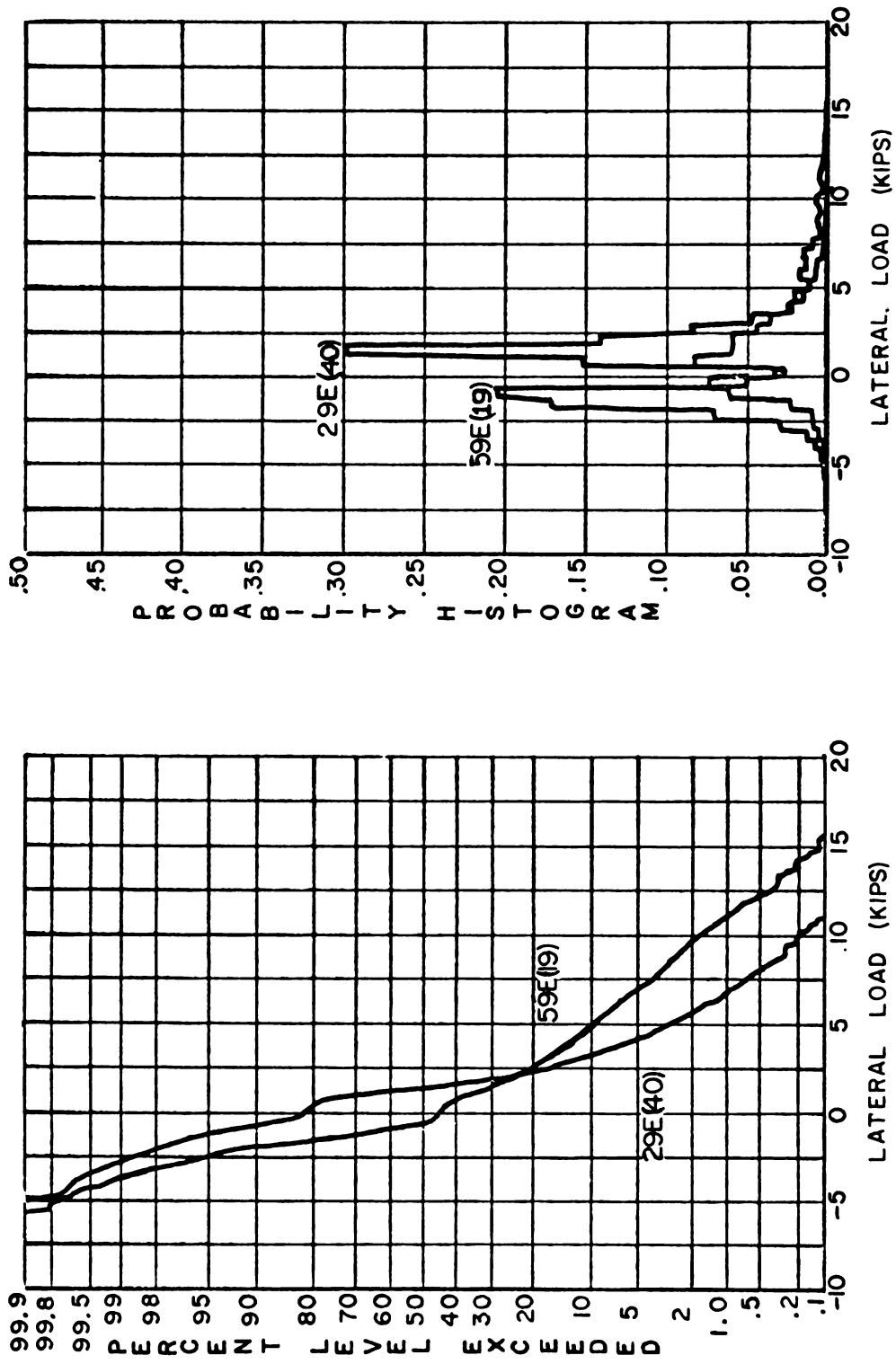


FIGURE 4-16. PEAK LATERAL W/R LOAD STATISTICS FOR ALL TRAFFIC AT SITE 1 (0.6 kip load interval)

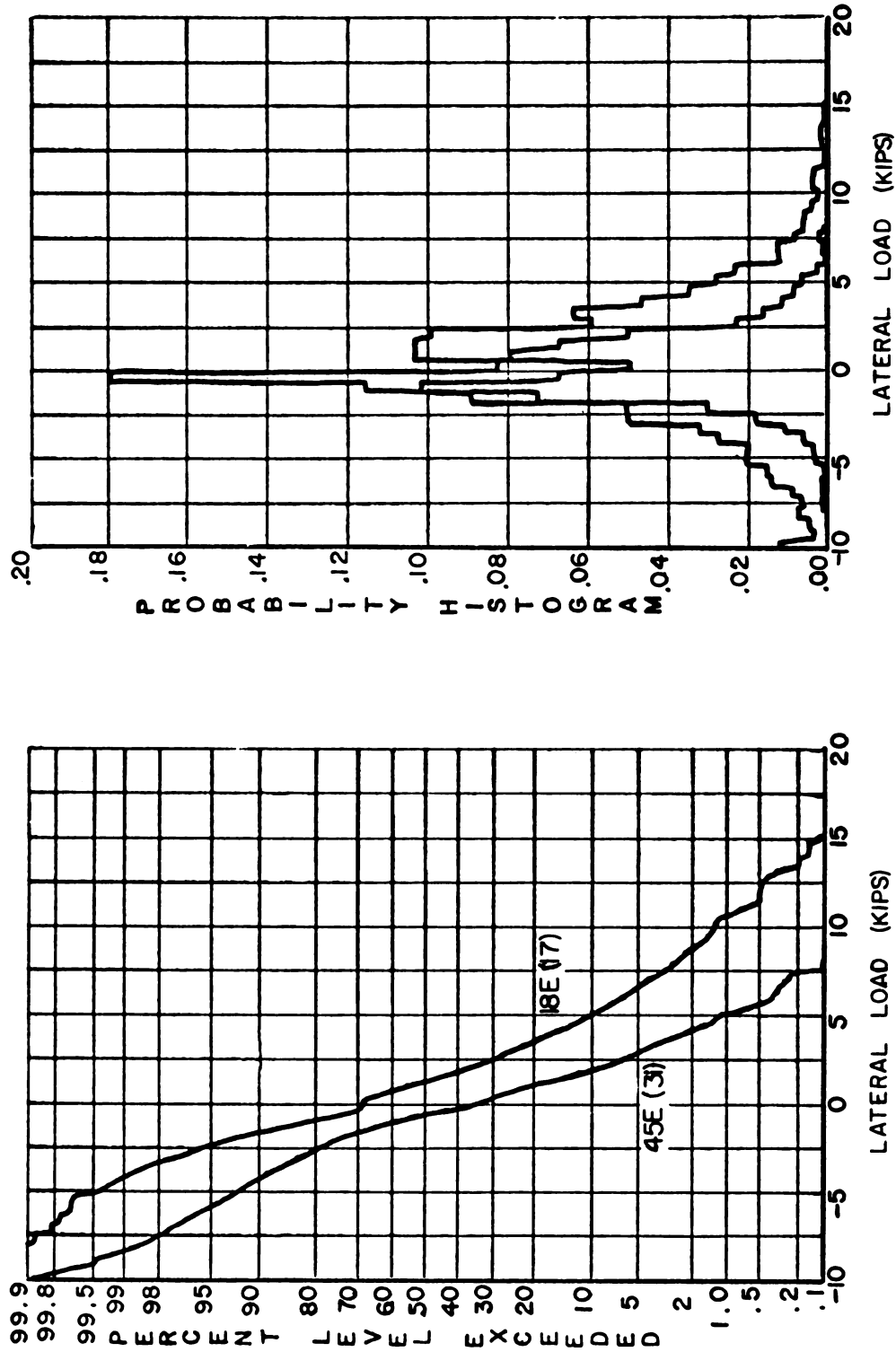


FIGURE 4-17. PEAK LATERAL W/R LOAD STATISTICS FOR ALL TRAFFIC AT SITE 3 (0.6 kip load interval)

increase in the mean lateral load or S.D. on the high rail at the curve. A more detailed evaluation of data from different vehicle weight and speed subcategories shows some differences in the loading mechanisms between curved and tangent track, but the overall load statistics do not show any major differences in lateral W/R loads.

4.7.1.3 Vertical Rail Seat Load

Statistical distributions for vertical rail seat (tie plate) loads are shown in Figure 4-18 for Site 1 (tangent) and in Figure 4-19 for Site 3 (curve). There is considerable tie-to-tie variation in the support reaction, with the median load varying over a 3:1 range at Site 1. It is also apparent that two of the four ties at Site 1 and one tie at Site 3 recorded a considerable number of zero peak vertical rail seat loads -- a surprising occurrence. Zero loads are actually negative values which are collected in the zero load bin by the calculation procedure. A negative load only indicates that the load on the instrumented tie plate is less than the normal compressive pre-load measured with an unloaded track. Further investigation of this showed that the two ties in question at Site 1 were at locations 59E and 61E in the center of the main array. A visual inspection of the time history records at 59E showed an apparent load cell failure for the last three trains recorded, so these data are questionable.

Table 4-7 shows that the mean rail seat load and the 0.1 percent load for the most severely loaded tie were 11.3 and 31 kips, respectively, and these occurred under the high rail in the curve. These loads are considerably below the 52.6 kip rail seat load recommended for tie design, see Table 4-8.

As expected, the rail seat loads at Site 2 were lowest because the average vertical W/R loads were somewhat lower (traffic distribution), and because the reduction in tie spacing to 20 inches distributes load to more ties. The effect of tie spacing will be discussed in a later section.

4.7.1.4 Rail Seat Moment

Figures 4-20 and 4-21 show statistical distributions for rail seat

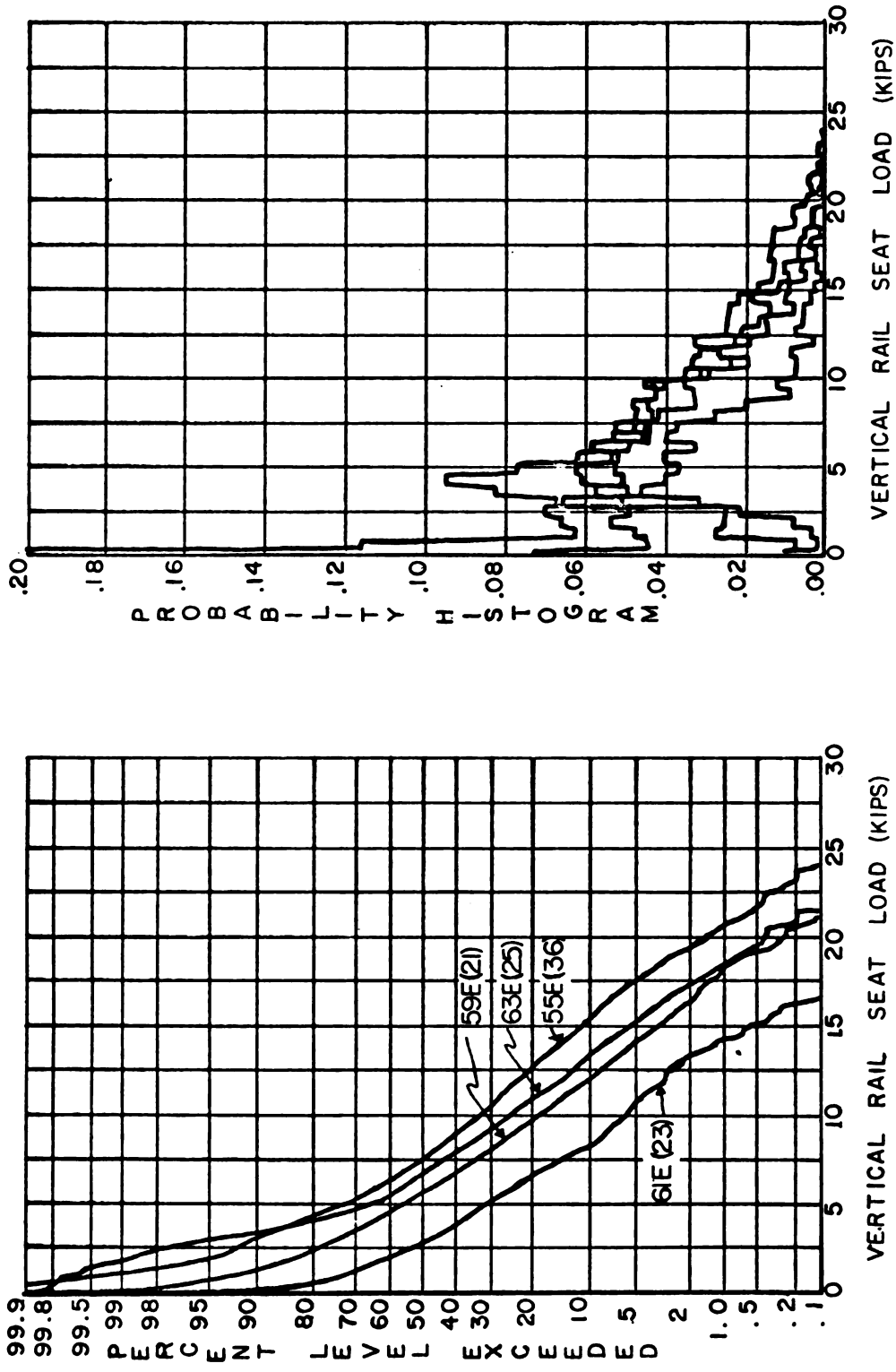


FIGURE 4-18. PEAK VERTICAL RAIL SEAT LOAD STATISTICS FOR ALL TRAFFIC AT SITE 1 (0.6 kip load interval)

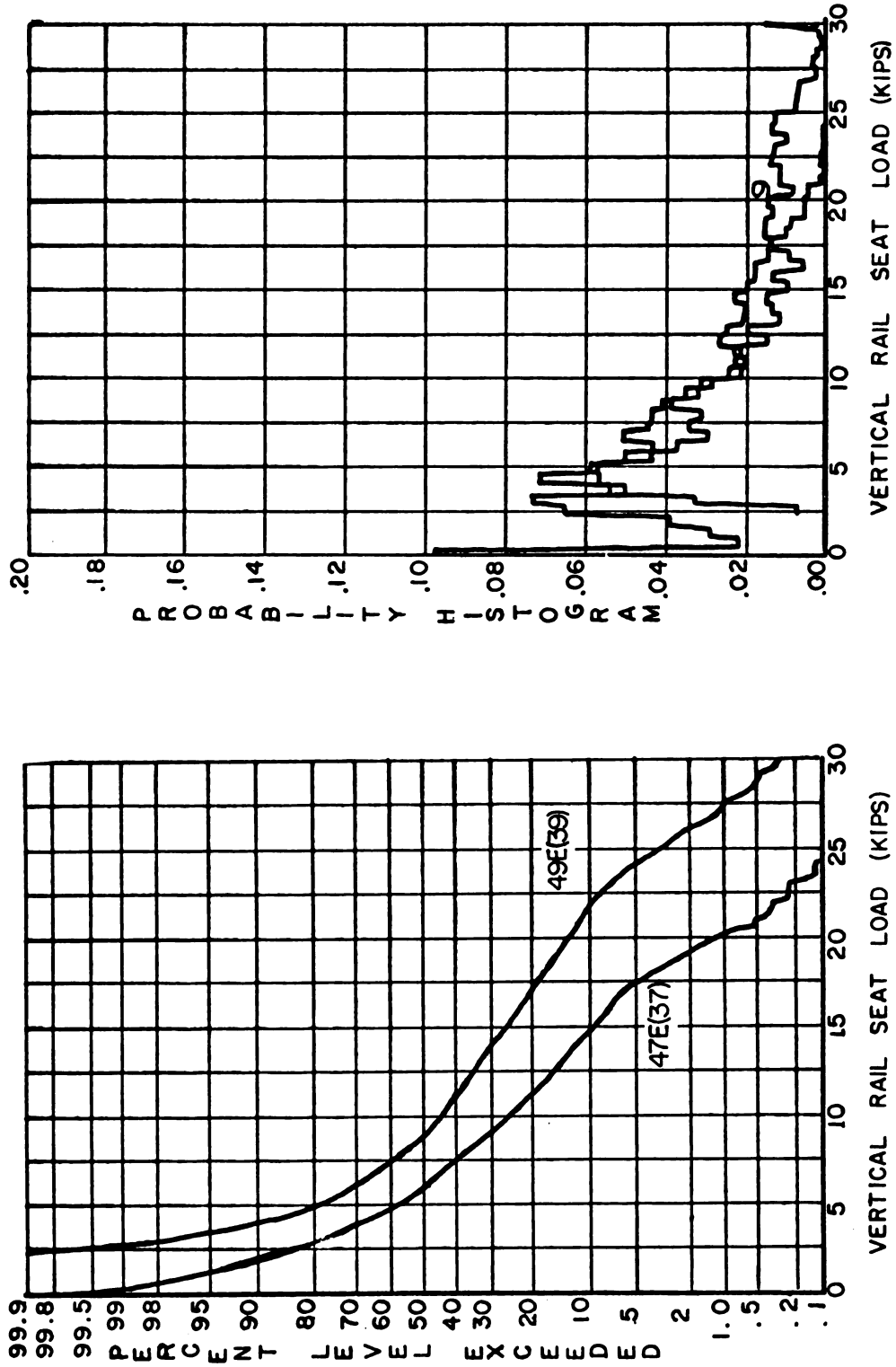


FIGURE 4-19. PEAK VERTICAL RAIL SEAT LOAD STATISTICS FOR ALL TRAFFIC AT SITE 3 (0.6-kip load interval)

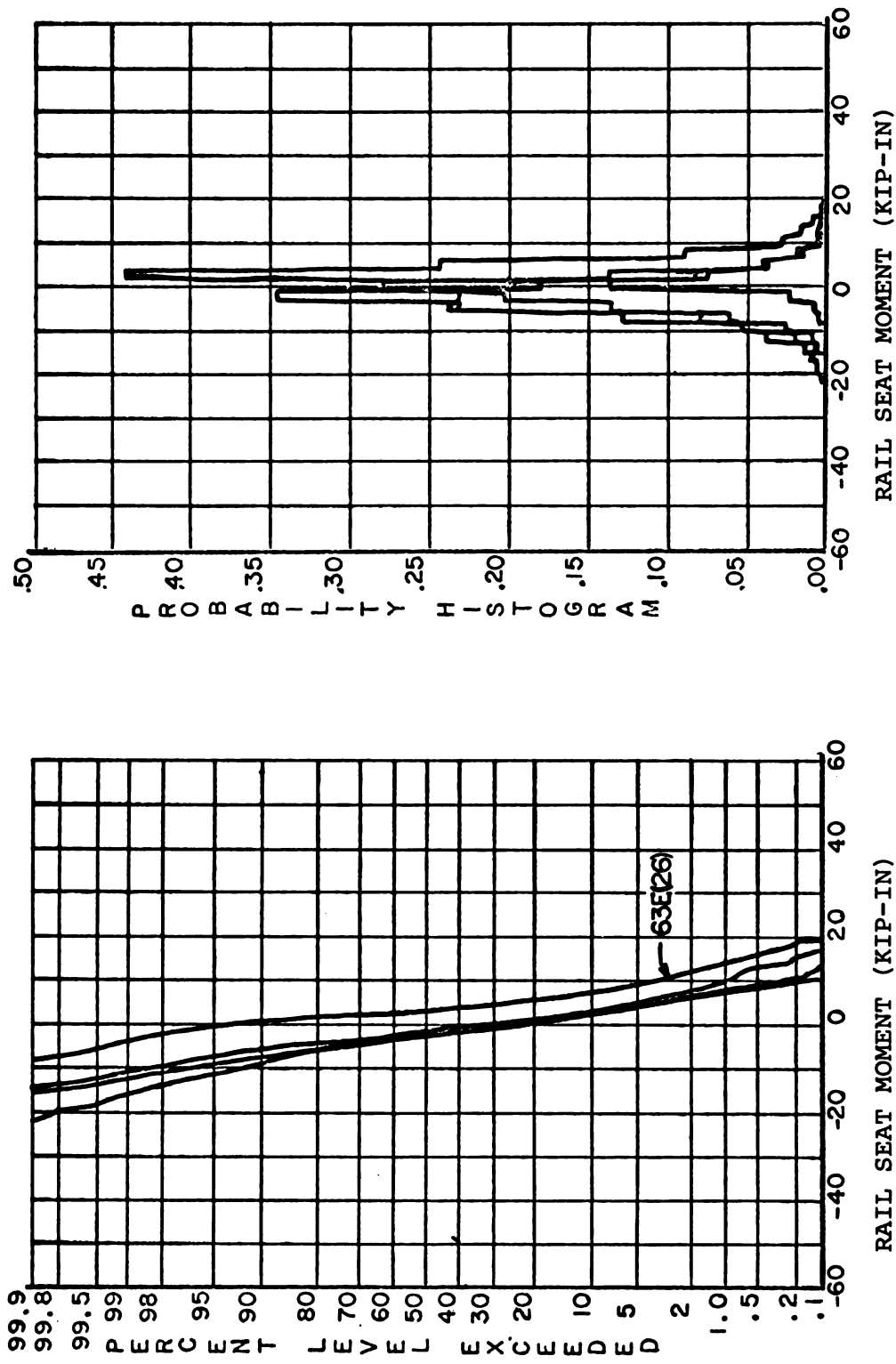


FIGURE 4-20. PEAK RAIL SEAT MOMENT STATISTICS FOR ALL TRAFFIC AT SITE 1 (2.4 kip-in load interval)

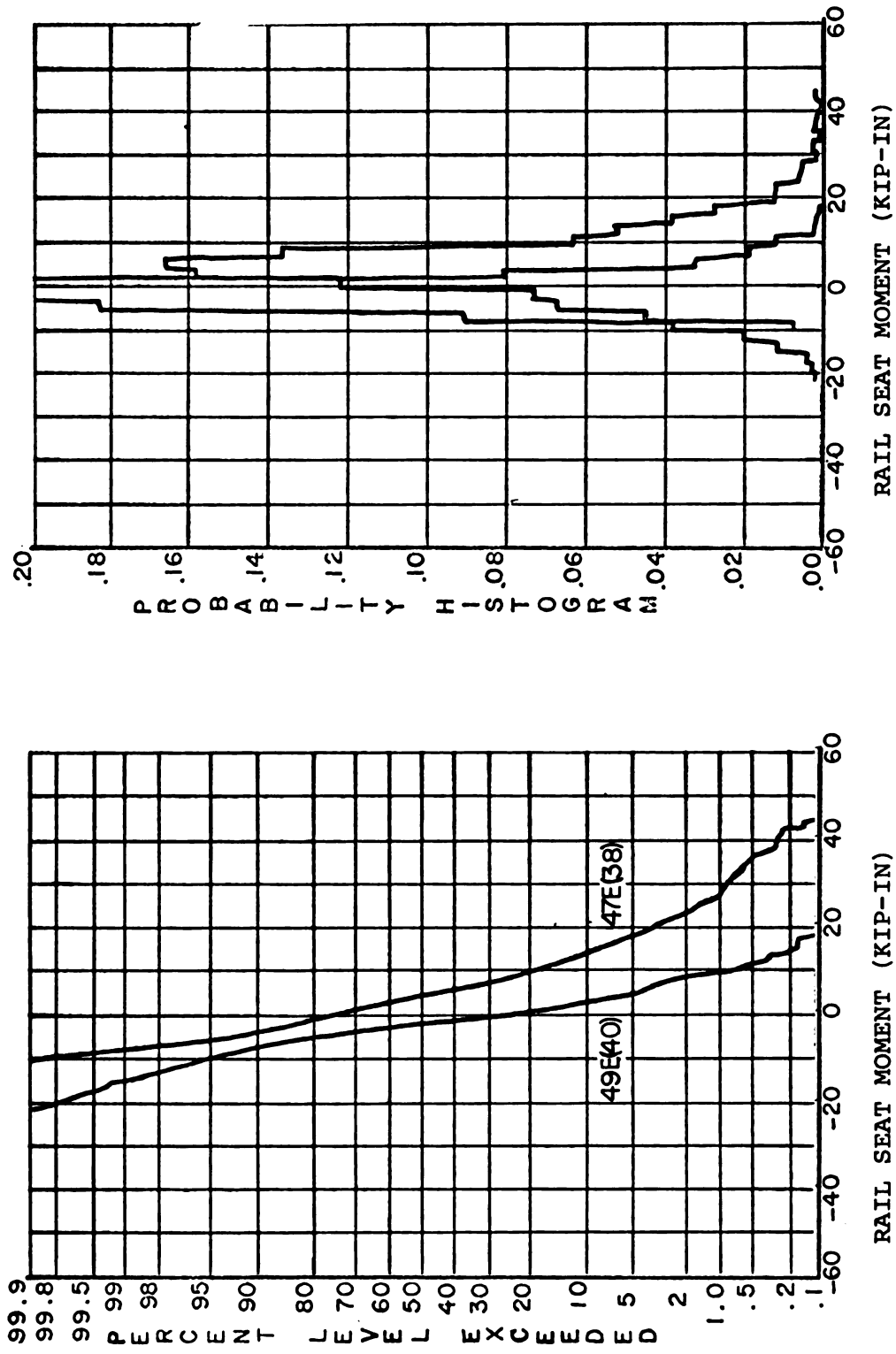


FIGURE 4-21. PEAK RAIL SEAT MOMENT STATISTICS FOR ALL TRAFFIC AT SITE 3 (2.4 kip-in load interval)

moment at Site 1 (tangent) and Site 3 (curve). These moments were measured using the load cell separation distance and the difference in load recorded on the two load cells which supported the rail base in the instrumented tie plate. A positive moment indicates the rail is being rolled toward the field side. The term "rail rollover moment" has frequently been used to designate this parameter.

The figures and data listed in Table 4-7 show that the mean rail seat moment is quite low on both tangent and curve sections and the 0.1 percent maximum loads of about 22 kip-in. are symmetrically distributed on the tangent track sections. This indicates a desirable design condition to minimize rail pad cutting. The data shown in Figure 4-21 for the curve site show a maximum 0.1 percent moment of 44 kip-in. on one of the ties, and the shape of the distribution for the curve site verifies the higher S.D. listed in Table 4-7. More detailed inspection of the curve site data shows that the low-probability high moments increase with speed, whereas these moments are relatively independent of speed on tangent track. Since the measured lateral W/R forces were about the same at all sites, it was conjectured that the increased moment on the curve may have been caused by the combined effect of higher vertical loads on the high rail and a shift in the wheel/rail contact point on the rail head at high speeds to produce a greater rail roll over moment. However, conclusions based on data from only two ties must be viewed with considerable caution when variations in tie support conditions are so great.

4.7.1.5 Tie Rail Seat Bending Moment

Figures 4-22 and 4-23 show the statistical distributions for rail seat bending moments measured on several different ties at Site 1 and Site 3. Data from Site 2 are similar. A characteristic of tie bending moment data is the large tie-to-tie variation in the mean and 0.1 percent moments. Also, all ties except one at both sites show both positive and negative peak bending moments indicative of a ballast support condition that is very load dependent. Negative rail seat bending moments can be caused by a center bound condition. Positive moments are expected for a uniform support condition, an end-bound support condition, or a support condition where a ballast pocket may have formed under the rail seat.

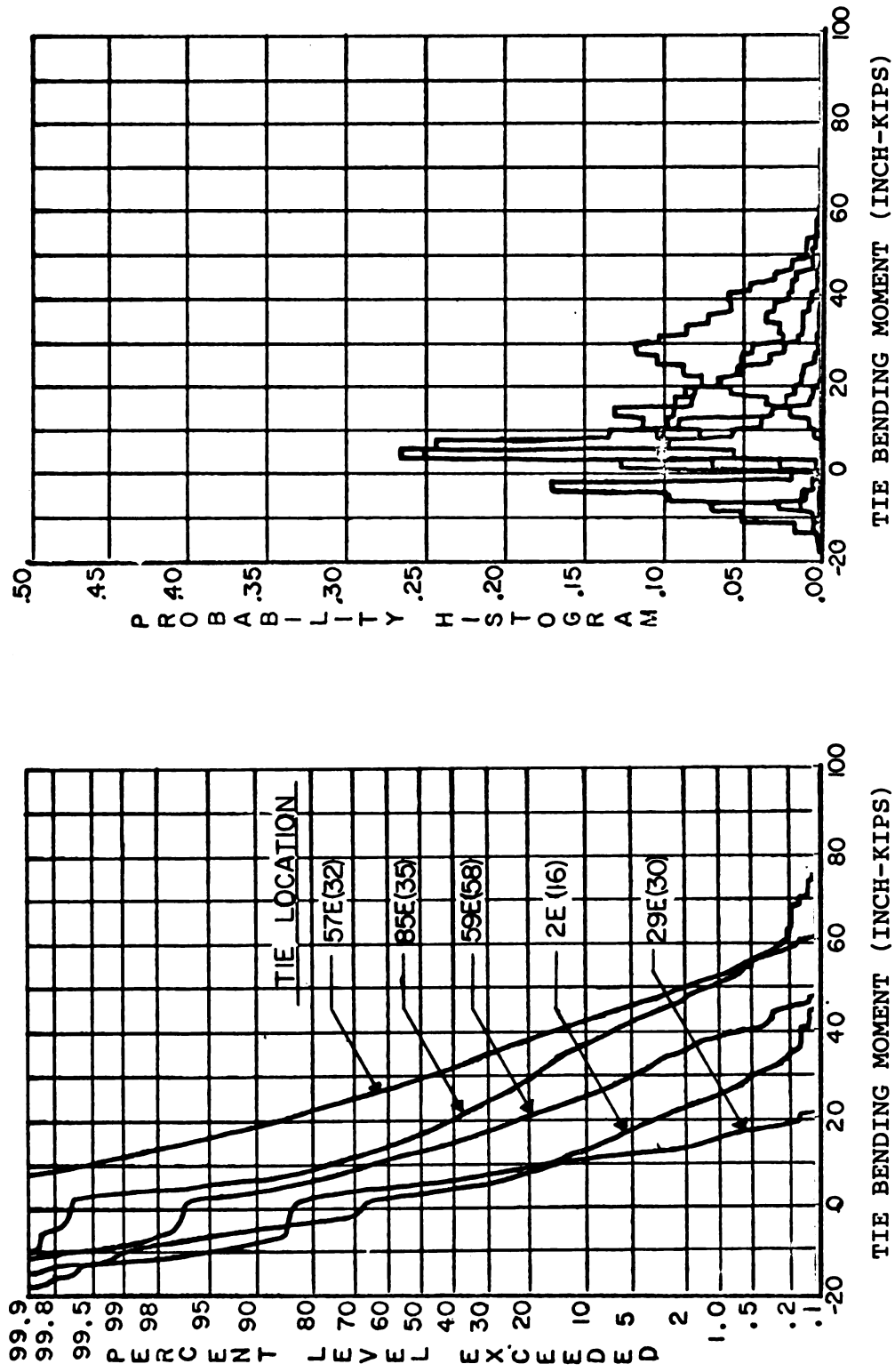


FIGURE 4-22. PEAK TIE RAIL SEAT BENDING MOMENT STATISTICS FOR ALL TRAFFIC AT SITE 1 (2.4 in-kips load interval)

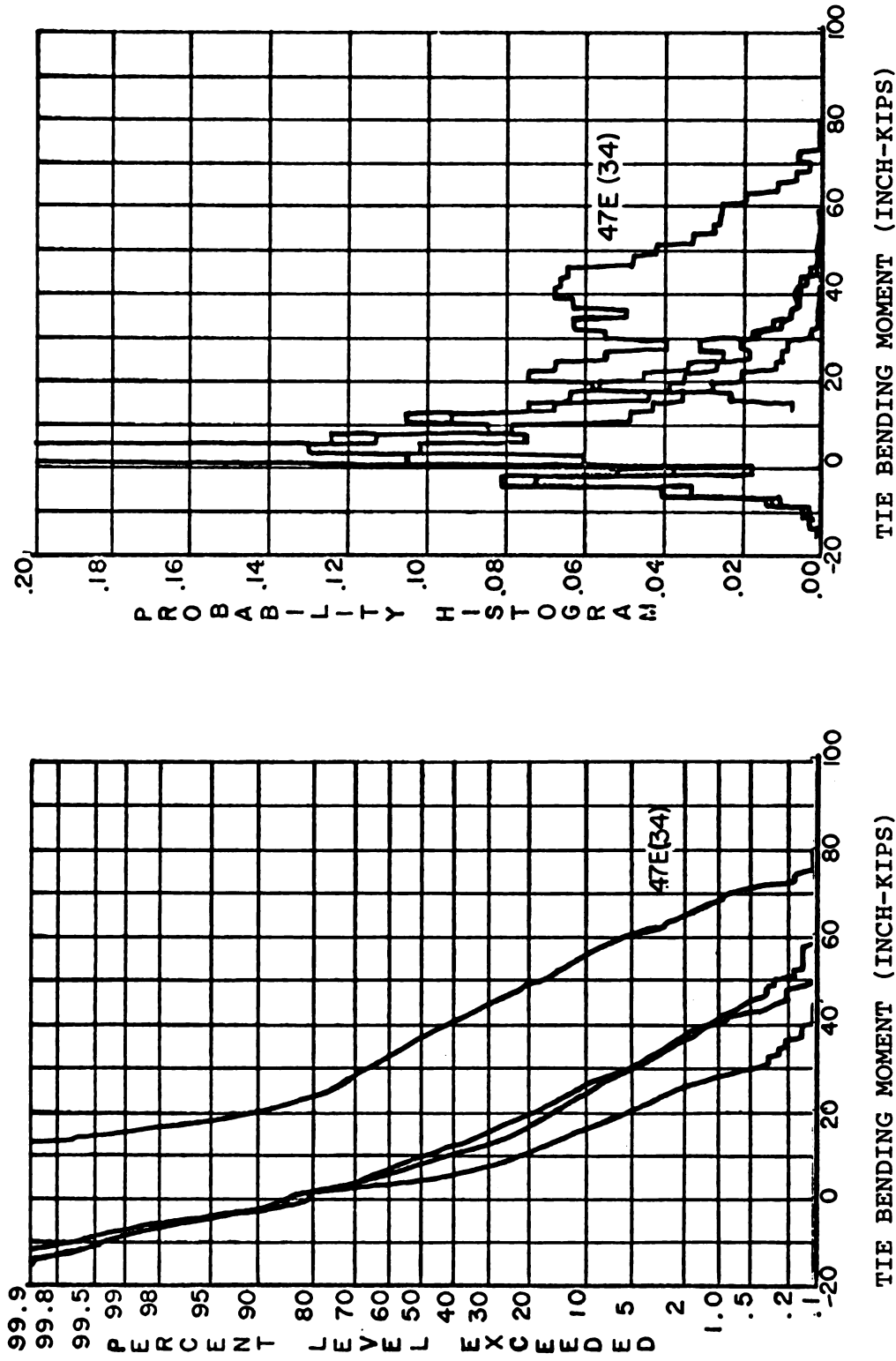


FIGURE 4-23. PEAK TIE-RAIL SEAT BENDING MOMENT STATISTICS FOR ALL TRAFFIC AT SITE 3 (2.4 in-kips load interval)

Figure 4-24 shows a typical load-dependent effect by comparing the bending moment data for a single tie with locomotives, light cars, and heavy cars identified separately. For this particular tie, the peak rail seat bending moment was positive for all of the locomotives and heavy cars, but some negative values were recorded for light cars. It is also evident that the locomotives are responsible for the highest mean loads as a class, but that the heavy freight cars cause as high, or higher, loads at the 0.1 percent probability level. Table 4-6 shows about a 15:1 ratio for total axles in the heavy car versus locomotive category, so the heavy-car class is responsible for by far the greatest number of high tie loads. It also appears that the probability distribution curves for heavy cars and locomotives cross near the 0.1 percent load level so that the loads from heavy cars will dominate the high-load, low-probability tail of the probability distribution curve.

The maximum 0.1 percent rail seat bending moments listed in Table 4-7 are quite similar for all three measurement sites, but the highest loaded tie at the curve site has a higher S.D. than those measured at the other sites. Table 4-9 shows the low-probability statistics that would be predicted using the measured mean and S.D. for the highest loaded tie at Site 3 and assuming a normal probability distribution. The percent probability of exceeding the indicated bending moment is shown along with the corresponding number of axles between occurrences, i.e., a bending moment of 79.3 inch-kips would be exceeded by 0.1 percent of the axle passes, or 1 of every 1000 axles. The comparison between predictions of bending moments using a normal distribution and the actual measured distribution shown in Figure 4-23 shows very good agreement over the limited range of the measurements. However, this extrapolation is based on vehicle load statistics for a specific tie and does not include statistical variations for bending moments at different ties.

For reference purposes, Table 4-9 also lists an estimated number of days between exceedences for different annual traffic densities. These data indicate that bending moments exceeding about 120 inch-kips would not be expected during a 50-year life ($50 \times 300 = 15,000$ days) at any of the listed traffic levels, assuming the predicted distribution is valid for this period of time. This is less than 50 percent of the 250-inch-kip bending moment requirement listed in current specifications, Table 4-8.

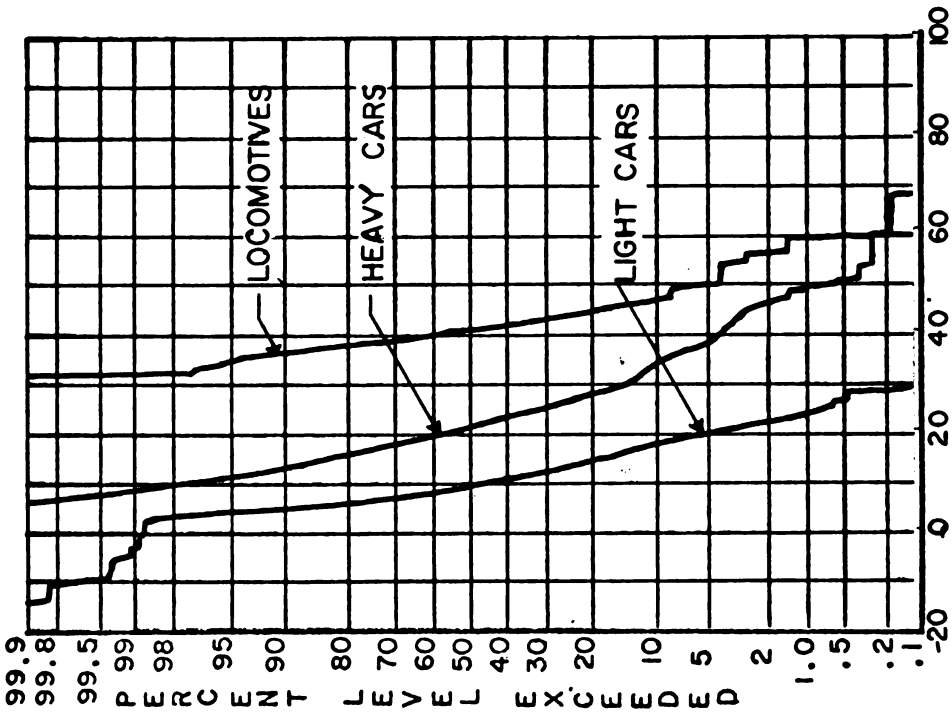
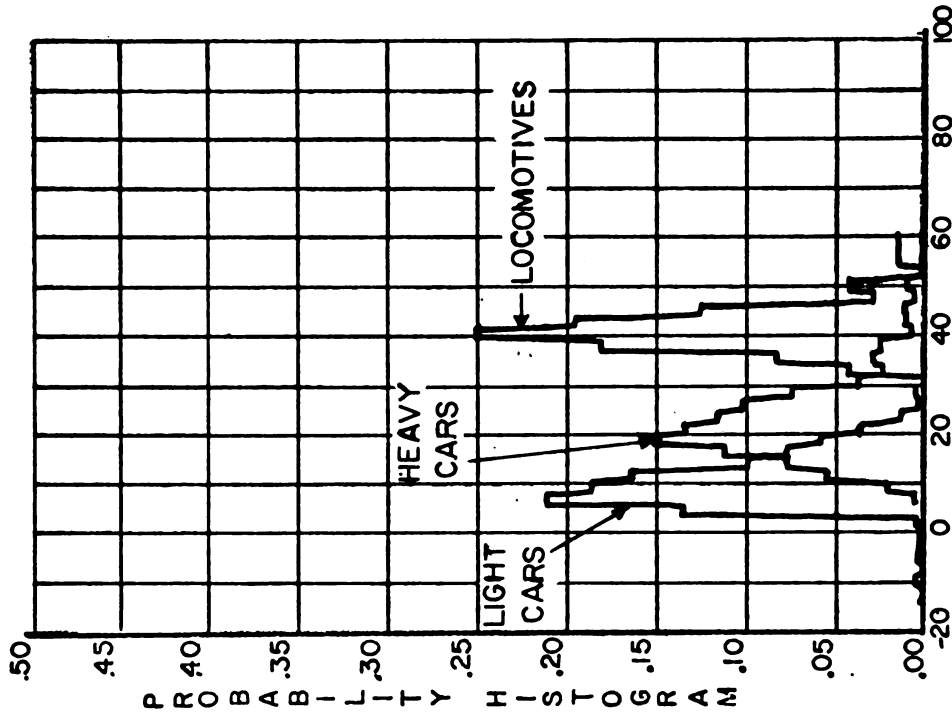


FIGURE 4-24. PEAK RAIL SEAT BENDING MOMENT STATISTICS FOR TIE LOCATION 85E(35) AT SITE 1 (2.4 inch-kips load interval)

TABLE 4-9. EXTRAPOLATED STATISTICS FOR RAIL SEAT BENDING MOMENTS BASED ON MOST SEVERE TIE LOADING(1)

Z Level Exceeded	No. Axles Between Exceedance	Normal Variable, Z (2)	Rail Seat Bending Moment, inch-kips Predicted (Meas.)	Est. Time Between Exceedances (days) (3)		
				20 MGT	40 MGT	60 MGT
50	7	0	38.4 (37)			
1.0	10	2.33	69.1 (68)			
0.1	1000	3.1	79.3 (78)	0.27	0.13	0.09
0.01	10 ⁴	3.75	87.9	2.7	1.3	0.9
0.001	10 ⁵	4.3	95.2	27	13	9.0
10 ⁻⁴	10 ⁶	4.75	101.1	270	130	90
10 ⁻⁵	10 ⁷	5.22	107.3	2700	1300	900
10 ⁻⁶	10 ⁸	5.65	113.0	27,000	13,000	9,000
10 ⁻⁷	10 ⁹	6.00	117.6	270,000	130,000	90,000

Notes:

1. Mean Moment = 38.4 inch-kips, S.D. = 13.2 inch-kips
2. $Z = (X - \bar{X}) / (S.D.)$
3. Time Estimates based on 3700 axles per day for 20 MGT annual traffic

Further study will be given to the question of whether the normal distribution gives a conservative estimate of the very low probability, high moments which might be caused by severe wheel flat impacts.

4.7.1.6 Tie Center Bending Moment

Figure 4-25 shows the statistical distribution for the bending moment measured at the center of five different ties at the curve site (Site 3). Data from Sites 1 and 2 were similar. Considerable tie-to-tie variation is apparent, and all ties except one show both positive and negative peak bending moments. Negative center bending moments represent a center-bound support condition and cause tension in the top surface of the tie. Bending cracks in the middle of concrete ties almost always start at the top surface, so negative bending moments have historically been of major importance. Positive bending moments at the tie center can be caused by an end-bound support condition. If the rail seat loads were distributed symmetrically on a well compacted support region under each rail seat, the bending moments in the tie center would be quite low.

The summary data in Table 4-7 list both the maximum negative and positive bending moments at the tie center for all three sites. A maximum 0.1 percent negative moment of 56 inch-kips occurred at Site 2 (tangent with 20-inch tie spacing), and this was exceeded by a maximum positive moment of 67 inch-kips on one tie at Site 3. These maximum moments at the tie center are only about 15 percent lower than the maximum positive moments in the rail seat region. However, they are considerably lower than the 200 inch-kips negative and 90 to 110 inch-kips positive strength requirements in current AREA specifications.

Data from individual weight categories show that the bending moment at the tie center is practically independent of car weight for many ties. This indicates a nonlinear support condition whereby the distribution of reaction loads along the tie length is changing with load to maintain a relatively constant bending moment. For example, a tie which has voids under each end would develop a large negative bending moment under light loads. However, the tie

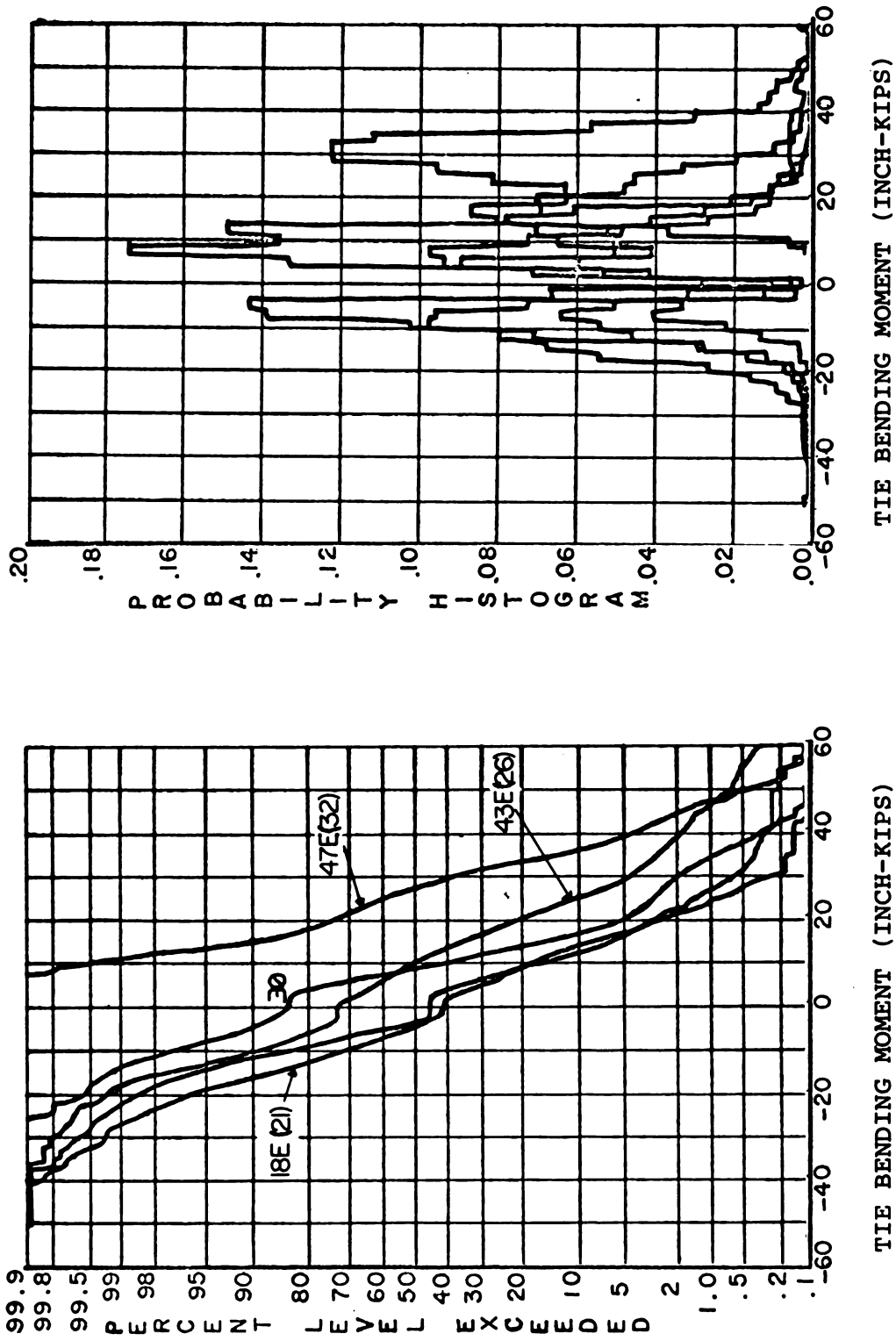


FIGURE 4-25. PEAK TIE CENTER BENDING MOMENT STATISTICS FOR ALL TRAFFIC AT SITE 3 (2.4 inch-kips load interval)

deflection into the ballast plus some tie bending under heavy loads would be sufficient to shift the reaction loads toward the tie ends and maintain a nearly constant center bending moment.

4.7.1.7 Tie Center Torsional Moment

All six of the strain gaged ties at each site were instrumented to measure torsional moments at the tie centers. However, statistical data were only recorded for the one tie at each site which showed the highest moments during passage of the work train. Figure 4-26 shows the statistical distributions for these most severely loaded ties, and Table 4-7 lists the mean values and 0.1 percent load levels.

The highest moments at Sites 1 and 2 were negative, whereas the highest moments at Site 3 were positive. However, there is no significance to the sign of the torsional moment, and only the maximum values are of real importance for describing the load environment. The highest 0.1 percent moment was 25 inch-kips at Site 1 and this tie also had the highest mean value.

Although current specifications for concrete ties do not include any torsional load requirements, the occurrence of torsional cracking was a problem with some early tie designs which had wedge-shaped cross sections at the tie center. Torsional moments are generally attributed to differential tilt of the rail seats in the direction of the rail. The current specifications do include a maximum allowable differential tilt of 1/16 inch (on a width of 6 inches) in an effort to reduce the torsional moment. Reducing the width of the rail pad between the rail and the tie also reduces the torsional moment which can be caused by the edge loading from differential tilt of the rail seats.

4.7.1.8 Rail Fastener Bolt Force

The two rail fastener bolts on one fastener at each site were instrumented with load cell washers to record the dynamic variations in bolt force under traffic. The rail fastener bolts were installed with a torque of 150 ft-lb,

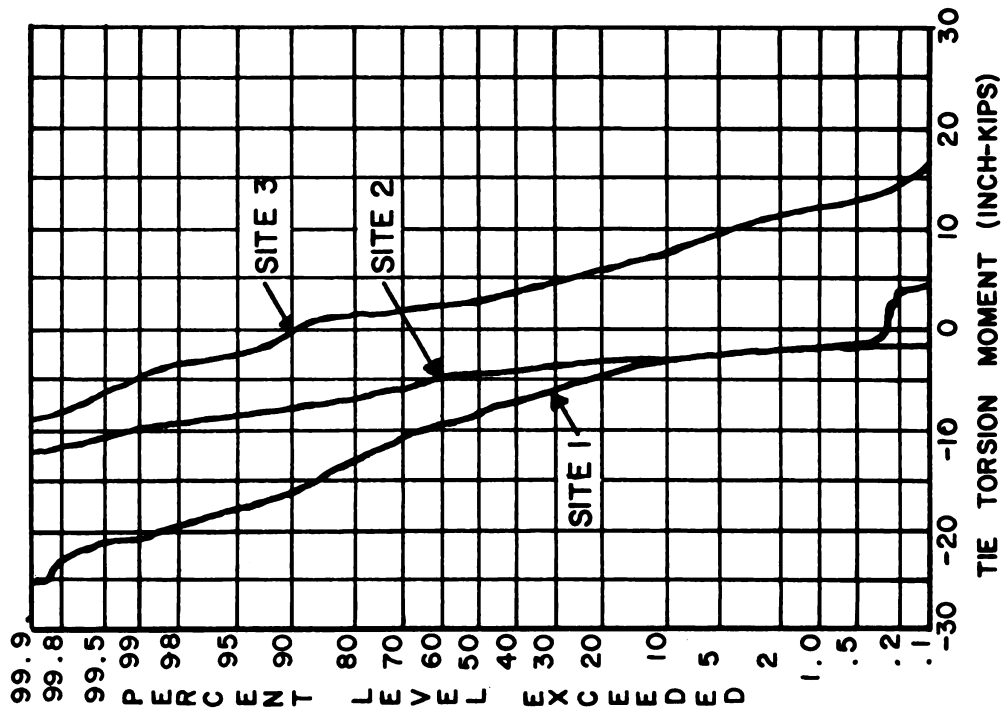


FIGURE 4-26. PEAK TIE TORSION MOMENT STATISTICS FOR ALL TRAFFIC

which produces a preload tensile force of about 12 kips in these 3/4 -10 NC bolts. Table 4-7 lists the load data for the bolt on the gage side at each site because the gage bolt showed the highest dynamic loads under traffic. These dynamic loads would be superimposed on the preload force.

Figure 4-27 shows the bolt force load statistics for the curve (Site 3) where the mean dynamic load was only 160 pounds with a 0.1 percent load of 2.3 kips. Dynamic load variations showed nearly equal positive and negative excursions at the tangent track sites. However, the gage bolt on the high rail of the curve showed somewhat higher tensile forces which can be attributed to the wheel flange loading which tends to rotate the rail toward the field side. Although the maximum dynamic loads represent a load variation of less than 20 percent of the preload force, this can produce fatigue failures or a fractured bolt from exceeding the ultimate strength. Bolts are typically tightened to about 75 percent of their minimum proof load. It is important to remember that these bolt force variations are only characteristic of the particular rail fastener design used on the FEC, which employs a very rigid rail pad to minimize the variation in load transmitted through the rail clips and bolts. A softer rail pad used with the rigid rail clips would produce much larger variations in bolt load.

4.7.1.9 Track Lateral Deflections

Statistical data for revenue traffic were recorded for the lateral deflection of the rail head relative to the tie (rail deflection) and for the lateral deflection of the tie relative to a ground reference (tie deflection). These measurements were made at only one location at each test site to obtain typical values, but data discussed previously show that response from lateral loads varies considerably at different locations along the track. Figure 4-28 shows the displacement statistics for rail and tie deflections at Site 1 (tangent track), and Table 4-10 summarizes the results. As expected for this type of track having quite stiff rail fasteners, the lateral displacements are quite small. Maximum lateral rail displacements two to four times greater than those listed below are not unusual on wood tie track with similar train speeds.

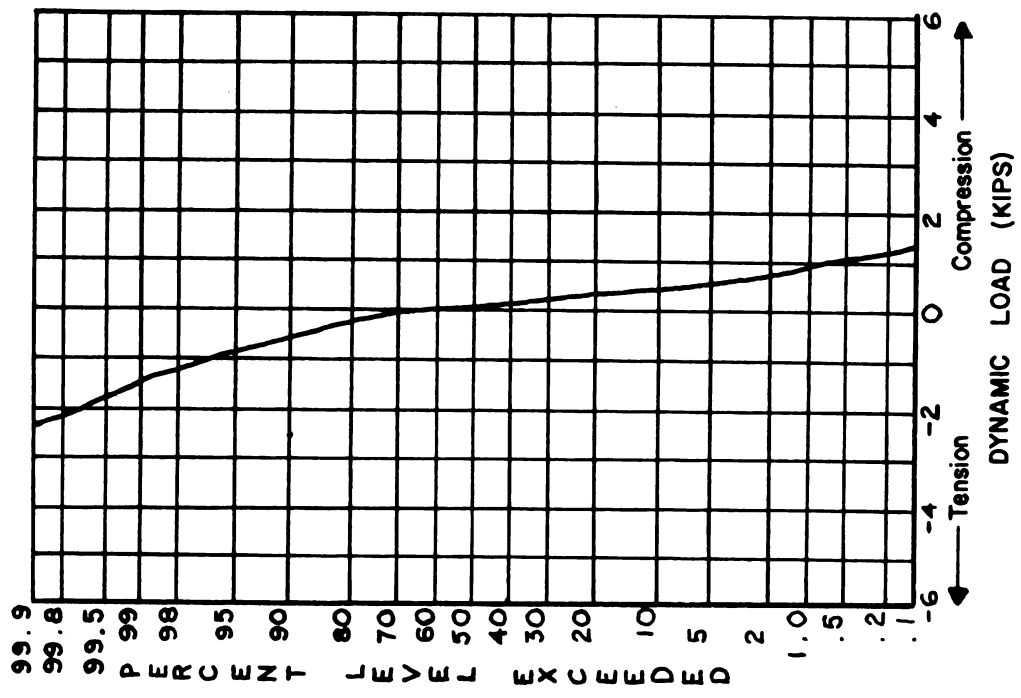


FIGURE 4-27. PEAK DYNAMIC RAIL FASTENER BOLT FORCE STATISTICS FOR ALL TRAFFIC AT SITE 3 (0.24 kips load interval)

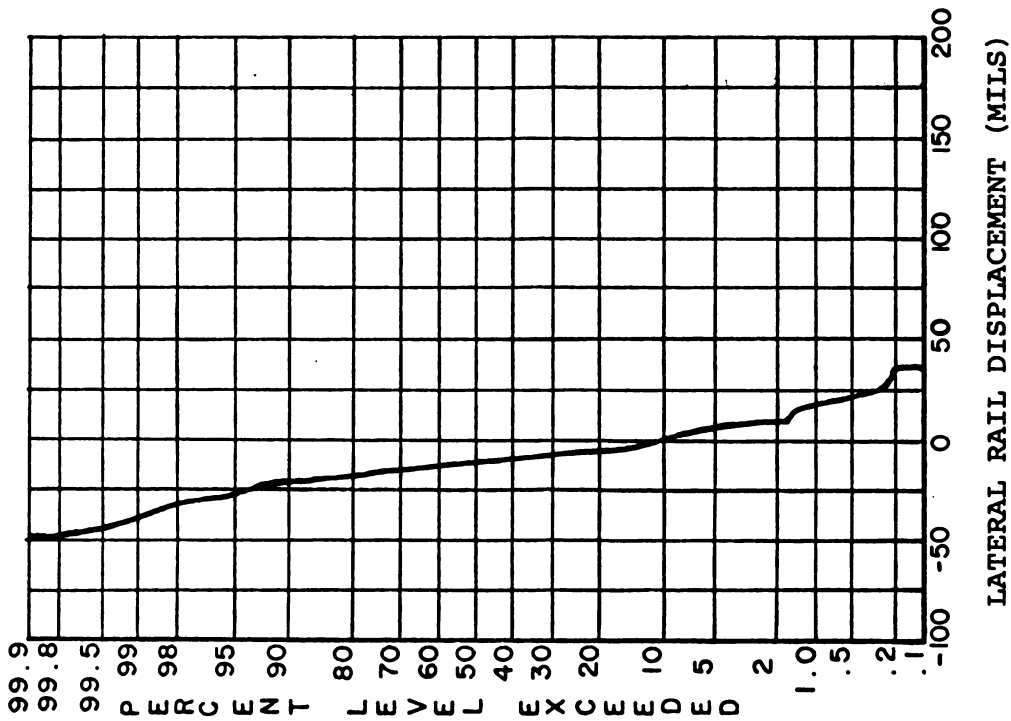
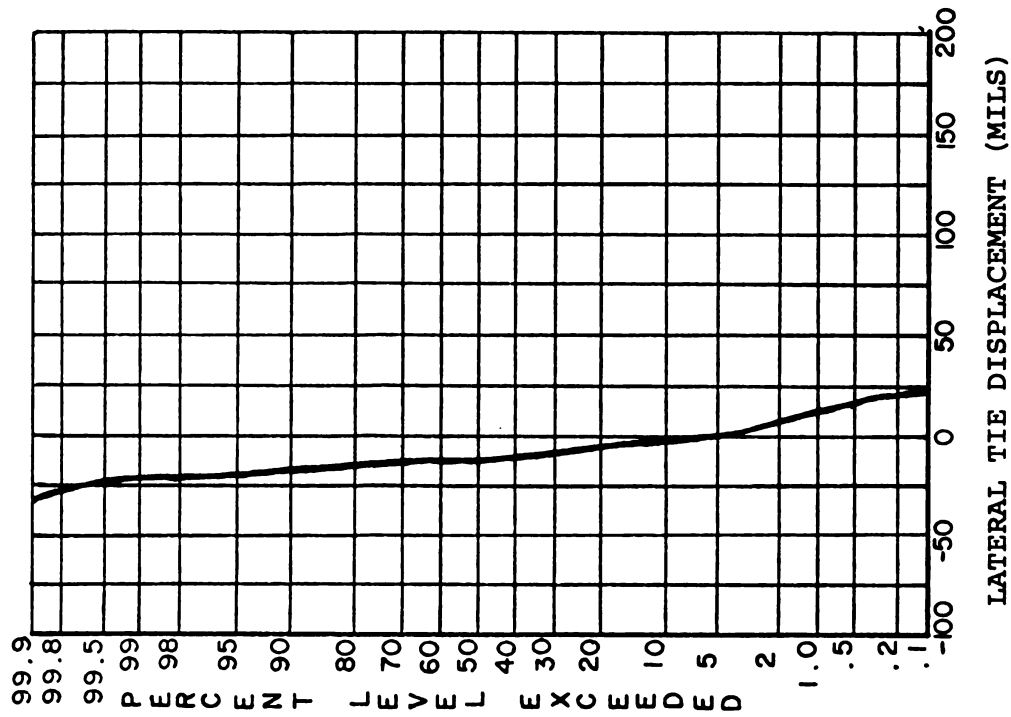


FIGURE 4-28. PEAK RAIL AND TIE LATERAL DISPLACEMENTS FOR ALL TRAFFIC AT SITE 1

TABLE 4-10. SUMMARY OF RAIL AND TIE LATERAL DISPLACEMENT STATISTICS AT SITE 1 FOR ALL TRAFFIC

	Lateral Deflection, mils	
	Rail	Tie
Mean (95 percent TB)	-8.4 (+ 4.4%)	-6.7 (+ 4.3%)
S. D.	9.3	7.1
0.1% Exceedance	-45	-30

4.7.2 Effect of Tie Spacing

Data discussed in the previous sections and listed in Table 4-7 showed the maximum loads measured at each test site. In most cases the maximum (0.1 percent exceedance) tie loads and bending moments measured at Site 2 with 20-inch tie spacing were not significantly lower than those measured at Site 1 having a 24-inch tie spacing. Reducing the tie spacing from 24 to 20 inches is normally expected to reduce vertical rail seat loads and tie bending moments by about 16 percent. However, the large tie-to-tie variation in support conditions makes it difficult to compare results for different track designs using single tie measurements. It is more appropriate to average data for identical measurements at several different locations to include these typical spatial variations.

Table 4-11 summarizes the load data for the two different tie spacings based on averaging the mean values and standard deviations from all of the common measurements at each site. This provided an average for five different locations for vertical wheel/rail loads and tie bending moments and three to four locations for rail seat load and moment. As discussed previously, there was an apparent difference in the car weight distributions at the two sites as evidenced by the fact that the average mean vertical W/R load of 14.8 kips at Site 2 was 12 percent lower than the 16.8 kips average load at Site 1. For this reason, data in the locomotive and heavy car subcategories were also reviewed, but these also show differences of about 8 percent in average mean W/R load. Therefore, the average mean W/R load in each

TABLE 4-11 EFFECT OF TIE SPACING ON AVERAGE TRACK COMPONENT LOAD STATISTICS FOR ALL SPEEDS

	Site 1 - Tangent with 24-inch Tie Spacing			Site 2 - Tangent with 20-inch Tie Spacing		
	All Cars	Locomotives	Heavy Cars	All Cars	Locomotives	Heavy Cars
1. Vertical W/R Load (P)						
Average Mean, kips	16.8	33.3	21.3	14.8	30.9	23.0
Average S.D., kips (% mean)	8.0 (47)	3.5 (10)	6.3 (30)	8.3 (56)	2.7 (9)	6.6 (29)
Average 0.1% Load, kips	41.6	44.1	40.8	40.5	39.3	43.4
2. Rail Seat Vertical Load (Q)						
Average Mean, kips	6.6	15.1	8.7	5.3	11.4	7.8
Average S.D., kips (% mean)	4.1 (61)	2.8 (19)	3.5 (40)	3.3 (62)	1.3 (11)	2.9 (37)
Mean Ratio, Q/P	0.393	0.453	0.408	0.358	0.369	0.339
Average 0-1% Load, kips	19.3	23.8	19.6	15.5	15.4	16.8
3. Rail Seat Moment						
Average Mean, inch-kips	0.5	2.2	0	3.7	1.9	1.9
Average S.D., inch-kips	3.9	6.0	4.01	3.1	4.9	3.7
Average 0.1% Load, inch-kips	12.6, -11.6	21, -16.4	+12.4	13.3, -5.9	17.1, -13.3	13.4, -9.6
4. Tie Rail Seat Bending Moment (M _{rs})						
Average Mean, inch-kips	15.5	31.4	19.1	8.7	21.9	13.1
Average S.D., inch-kips (% mean)	8.8 (57)	6.6 (21)	7.6 (40)	7.2 (83)	5.5 (25)	5.7 (44)
Mean Ratio, M _{rs} /P	0.923	0.943	0.897	0.587	0.709	0.569
Average 0.1% Load, inch-kips	40.0	51.9	42.7	31	39	30.8
5. Tie Center Bending Moment, M _c						
Average Mean, inch-kips	8.9	15.4	9.34	3.3	2.3	-0.4
Average S.D., inch-kips (% mean)	6.4 (72)	5.8 (38)	6.7 (72)	6.6	6.7	5.6
Average 0.1% Load, inch-kips	29, -11	33.4, -2.6	30.1, -11.4	24, -17	23, -18.5	17, -18

Note: Average 0.1% load levels predicted from average mean and S.D. assuming normal probability distribution, i.e. 0.1% Load = Mean ± 3.1 (SD)

subcategory was used to normalize the mean values for rail seat load and for tie rail seat bending moment--the two load parameters most directly affected by tie spacing. The percent change in average mean and 0.1 percent load levels caused by reducing tie spacing from 24 to 20 inches (16 percent reduction) are listed below:

	Percent Reduction in Load due to 16 Percent Reduction in Tie Spacing					
	Average Mean			Average 0.1 Percent Load		
	All Cars	Locos.	Heavy Cars	All Cars	Locos.	Heavy Cars
Rail Seat Vertical Load	8.9	18.5	16.9	8.8	30.2	20.6
Tie Rail Seat Bending Moment	36.4	24.8	36.5	12.0	19.0	33.2

These data demonstrate the difficulties in reaching definitive conclusions using track response measurements. Reducing tie spacing by 16 percent reduces average and maximum vertical rail seat loads by about 9 percent for all traffic. Average tie bending moments at the rail seat were reduced more than rail seat loads. This indicates a nonlinear support condition whereby the reduced tie loading provides a substantially greater reduction in both average mean and average 0.1 percent bending moments, with the maximum bending moments being reduced by 12 percent and the average mean being reduced by 36 percent for all traffic. It should be noted, however, that Table 4-7 shows that there is no difference in the maximum rail seat loads and tie bending moments for the most severely loaded tie at the different tie spacing locations, but there should be fewer ties subjected to these maximum loads in the section with 20-inch spacing.

Many of the measured data indicate that nonlinear support conditions have a very significant effect on track loads. The results suggest that if the population of heavy cars becomes a greater portion of revenue service, i.e., if there were more unit trains of 70- and 100-ton hopper cars, changes in tie spacing might have a much greater effect on tie moments than normally expected from using conventional track design estimates. Therefore, while a reduction in tie spacing might provide a large benefit, an increase in tie spacing may cause an unexpectedly large increase in tie bending moments. This suggestion

requires additional evaluation because the effect of these variations in tie support conditions cannot be predicted for an increase in average wheel load.

4.7.3 Effect of Car Type

Figure 4-29 shows the effect of car type (weight) on vertical and lateral wheel/rail loads. Data recorded in the 50-60-mph speed range at the maximum load location in Site 1 were used to illustrate characteristic behavior. As expected, locomotives generate the highest mean vertical loads, and the variation in vertical load, as measured by the standard deviation, is relatively small compared to the heavy and light car classes. This is shown by the fact that the curve for locomotive vertical loads is closer to a vertical line than are those for the other car classes. For this particular location, the 0.1 percent load levels are about equal for locomotives and heavy cars. The relative frequency of occurrence of these loads can be determined from the number of axles listed in parentheses for this data base. These results show a ratio of $1116/72 = 15$ for the frequency of occurrence of 0.1 percent loads from heavy cars compared to locomotives.

Data for lateral wheel/rail loads in Figure 4-29 show that the median load is relatively independent of car weight. A major difference in maximum vertical and lateral loads is that light cars cause the highest low-probability lateral loads, particularly at speeds above 50 mph. These results have been confirmed by other measurements on wood tie track, and the explanation is that lightly loaded and empty freight cars have a lower critical speed for hunting than heavy cars.

Figure 4-30 shows the effect of car weight on vertical rail seat loads and tie bending moments. The statistical distributions for vertical rail seat load and tie bending moments are similar to those for vertical W/R loads, as expected. Rail seat bending moment data do not show a significant influence from lateral wheel/rail loads at the 0.1 percent load levels.

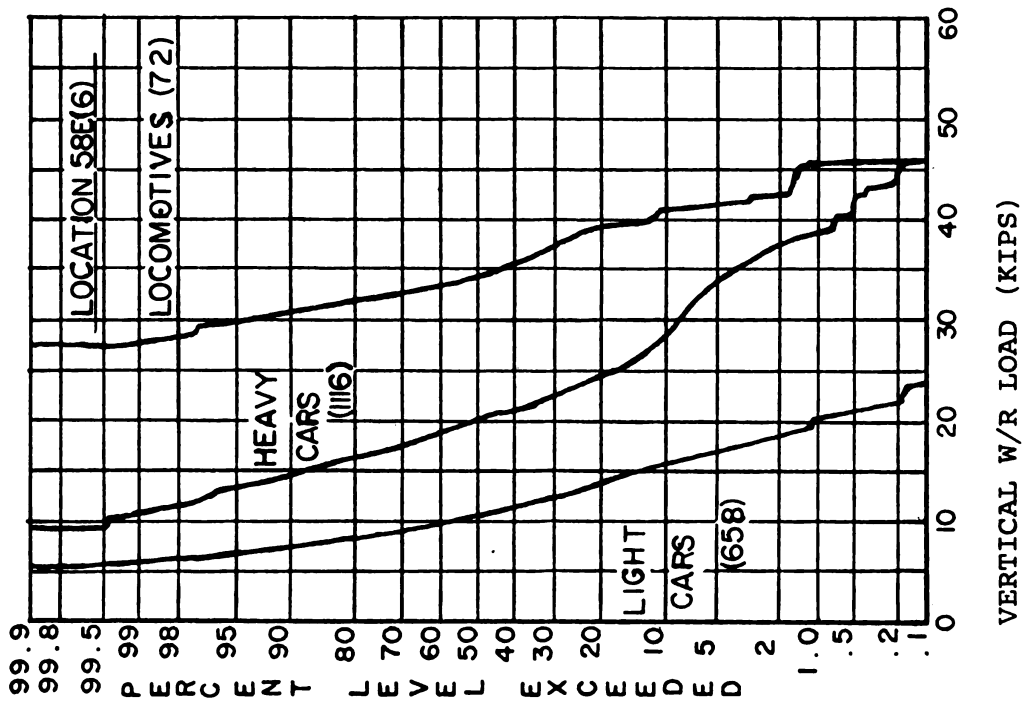
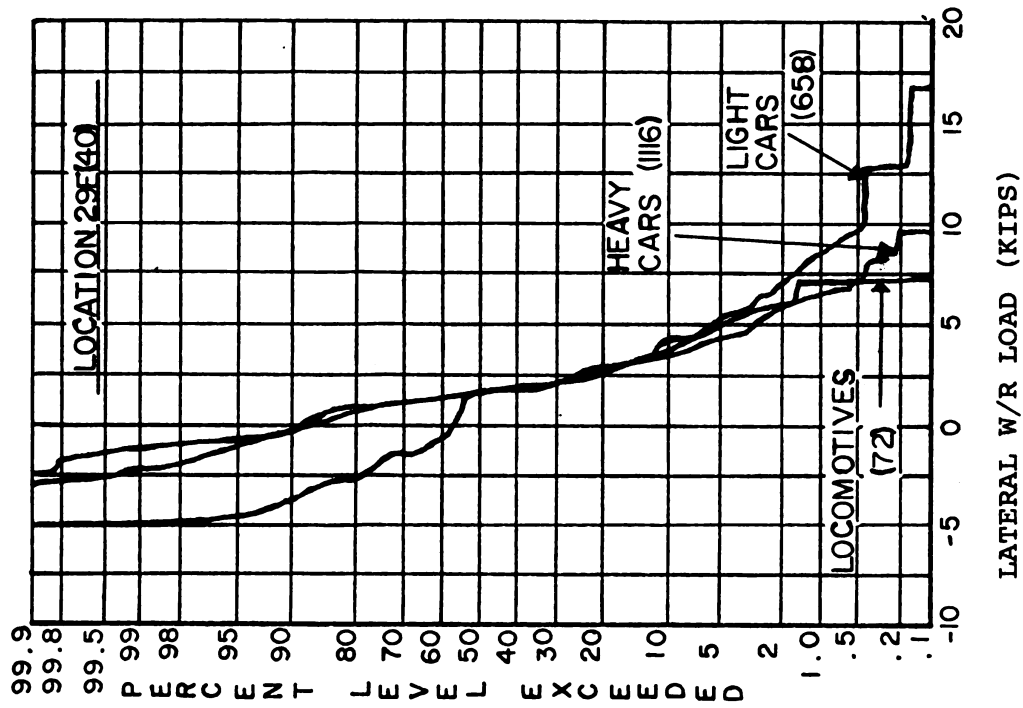


FIGURE 4-29. EFFECT OF CAR TYPE ON WHEEL/RAIL LOADS (SITE 1, 50-60 MPH SPEED RANGE)

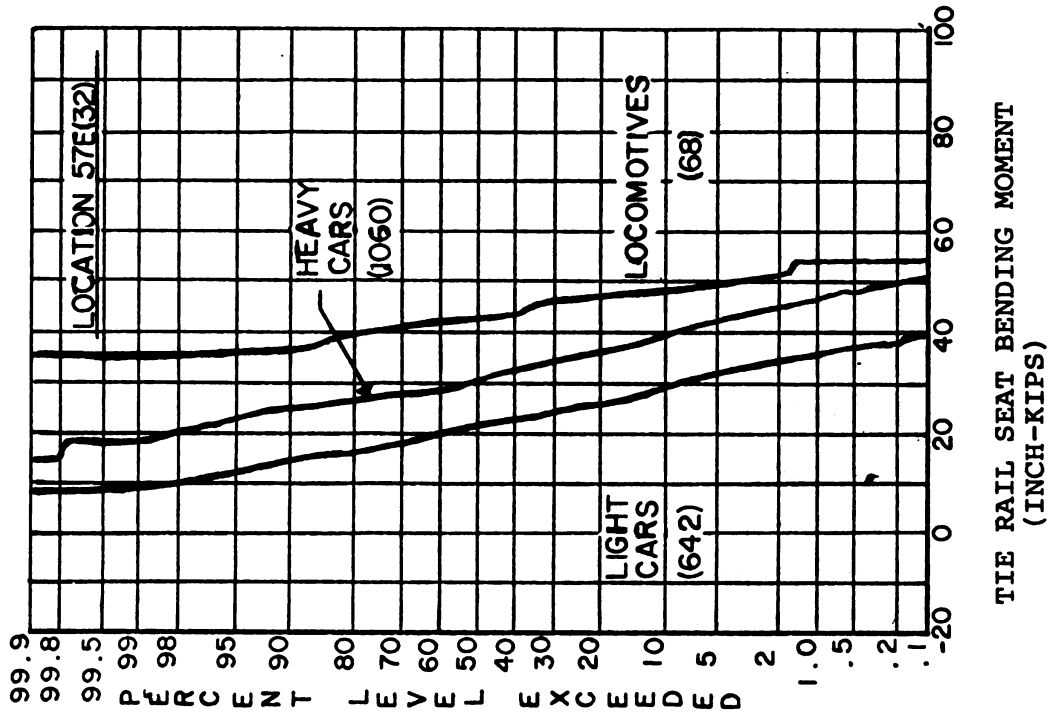
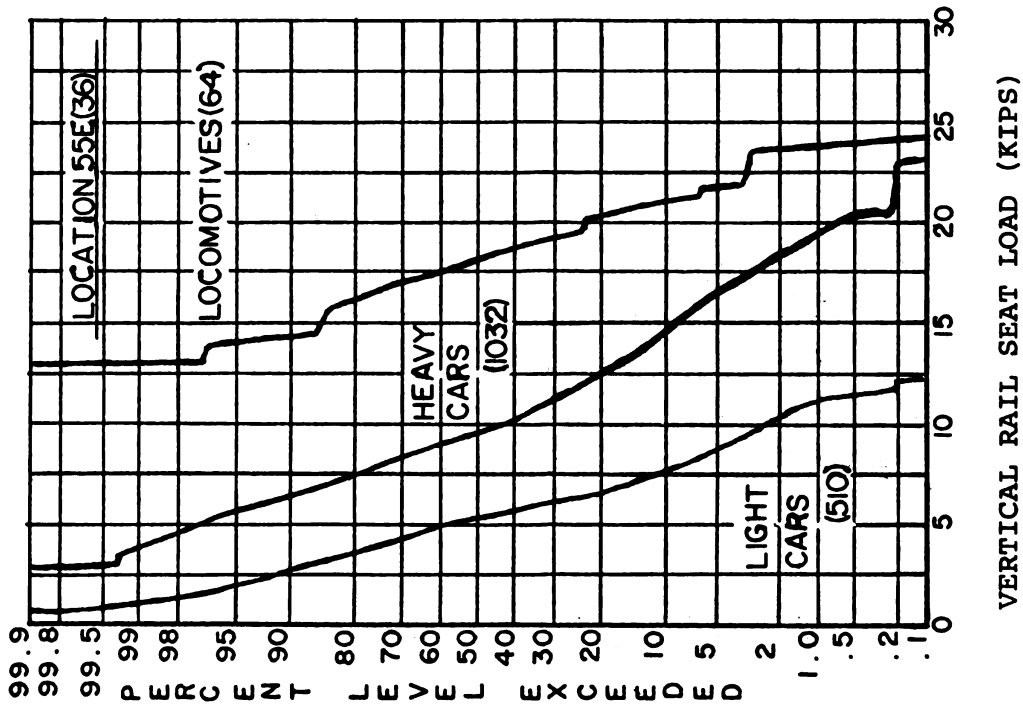


FIGURE 4-30. EFFECT OF CAR WEIGHT ON RAIL SEAT LOAD AND TIE BENDING MOMENTS (SITE 1, 50-60 MPH SPEED RANGE)

4.7.4 Effect of Train Speed

The evaluation of the effect of train speeds on track loads will be discussed separately for the tangent and curved track measurement sites.

4.7.4.1 Tangent Track Loads

Table 4-6 lists typical mean values for vertical wheel/rail loads in the different car weight and speed categories. As discussed previously, these data showed that trains with heavily loaded cars operated at lower speeds past the test sites than trains which had a larger percentage of light or empty cars. Average wheel loads for all cars in the low, 30-40 mph, speed range were as much as 50 percent higher than the average for all traffic. This type of speed effect reflects railroad operations rather than vehicle dynamic effects. Further investigation would be required to determine if this is typical of operations at other track sites or on other railroads.

Speed effects related to vehicle dynamics can only be evaluated using data for a common type vehicle. Data listed in Table 4-6 show that variations in mean vertical loads for locomotives operating at different speeds are less than ± 5 percent from the mean for all speeds. It was concluded from this that the effect of operating speed on vertical track loads from vehicle dynamic effects was negligible on the tangent track test sites.

Figure 4-31 shows the effect of train operating speed on the vertical and lateral W/R loads. It is evident that the vertical weight bias in the 30-40-mph range is responsible for that speed also causing the highest lateral loads for the all-car category. This is true also for the heavy car category alone. However, data for light cars, where the load bias versus speed is small, show that the highest lateral loads occur above 50 mph and the lowest lateral loads occur at 30 mph. This is indicative of hunting cars.

4.7.4.2 Curved Track Loads

The two major effects of train speed on curved track are the differences in vertical loads on the low and high rails and the increase in lateral

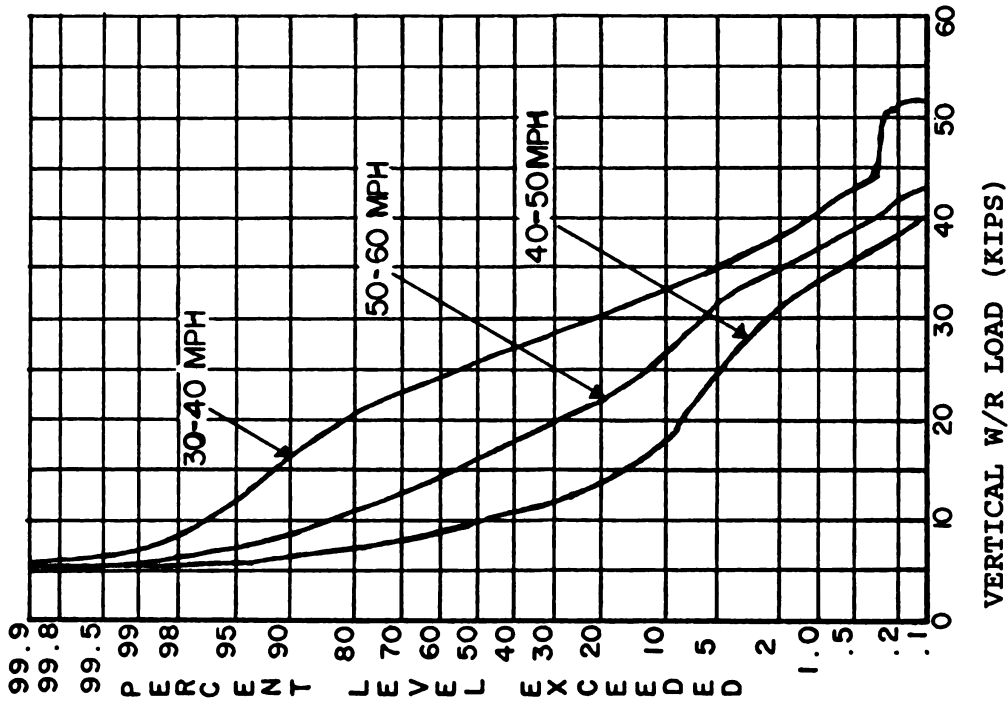
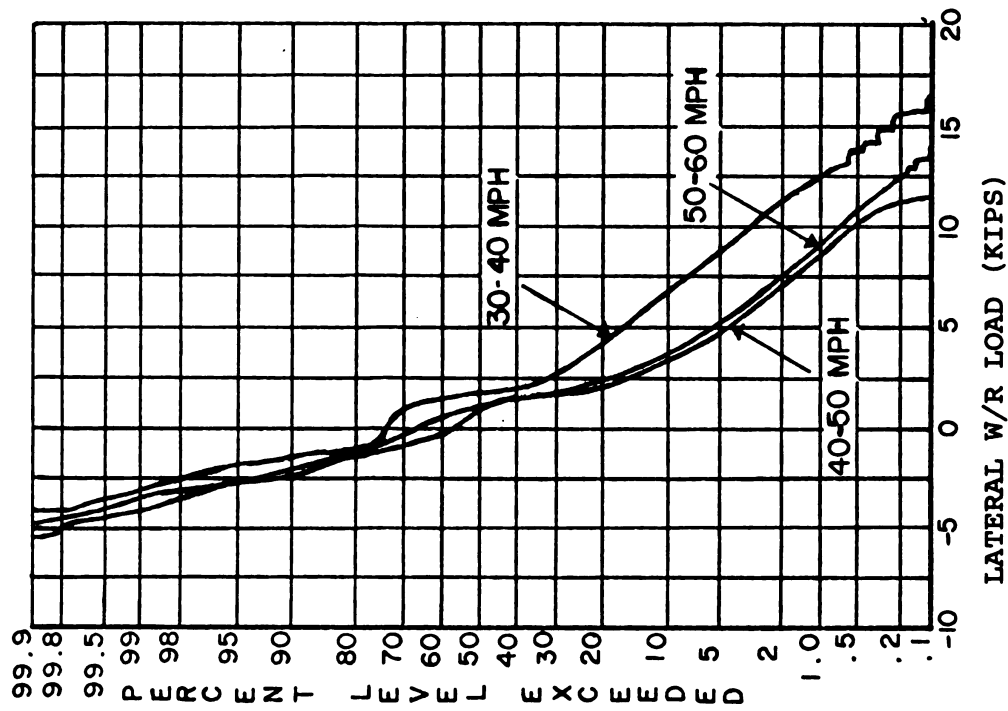


FIGURE 4-31. EFFECT OF TRAIN SPEED ON AVERAGE VERTICAL AND LATERAL WHEEL/RAIL LOADS FOR ALL TRAFFIC ON TANGENT TRACK (Site 1)

loads due to the curving forces from the truck and the unbalanced centrifugal forces on the cars. Table 4-12 shows the variation in vertical wheel/rail loads on the low and high rails. These data confirm that trains running at 30-40 mph were below the theoretical 45-mph balance speed. Trains in the 50-60 mph range were operating above the balance speed, and the mean vertical load was about 10 percent higher than at the balance speed.

TABLE 4-12. EFFECT OF TRAIN SPEEDS ON VERTICAL WHEEL/RAIL LOADS AT SITE 3 (3° 52' CURVE)

Speed Range, mph	Percent Axle Load (Mean) on High and Low Rails					
	Locomotives		Heavy Cars		Light Cars	
	High	Low	High	Low	High	Low
30-40	45	55	43	57	49	51
40-50	48	52	48	52	47	53
50-60	54	46	55	45	57	43

Figure 4-32 shows the statistical distribution for average vertical wheel/rail loads on the high rail. Both the median loads and the maximum loads were increased considerably on the high rail when train speeds exceeded the balance speed for the curve.

Figure 4-33 shows the effect of car weight and train speed on the lateral W/R forces on the high rail. The lateral loads from light cars (left side of Figure 4-33) are much lower than those for the heavy cars and locomotives on the curve, and the lateral loads for the light cars are also lower on the curve than they were on tangent track. It appears that the flanging on curves reduces, or eliminates, car hunting, and forces from light cars due to track curving are much lower than those from hunting.

The effect of car speed on the heavy car category is shown on the right side of Figure 4-33. The increase in both the median and maximum loads with speed was expected. However, the more important question is how do the overall track loads on the curve compare to those on tangent track. Data from the tangent and curved track sites are discussed in the following paragraphs.

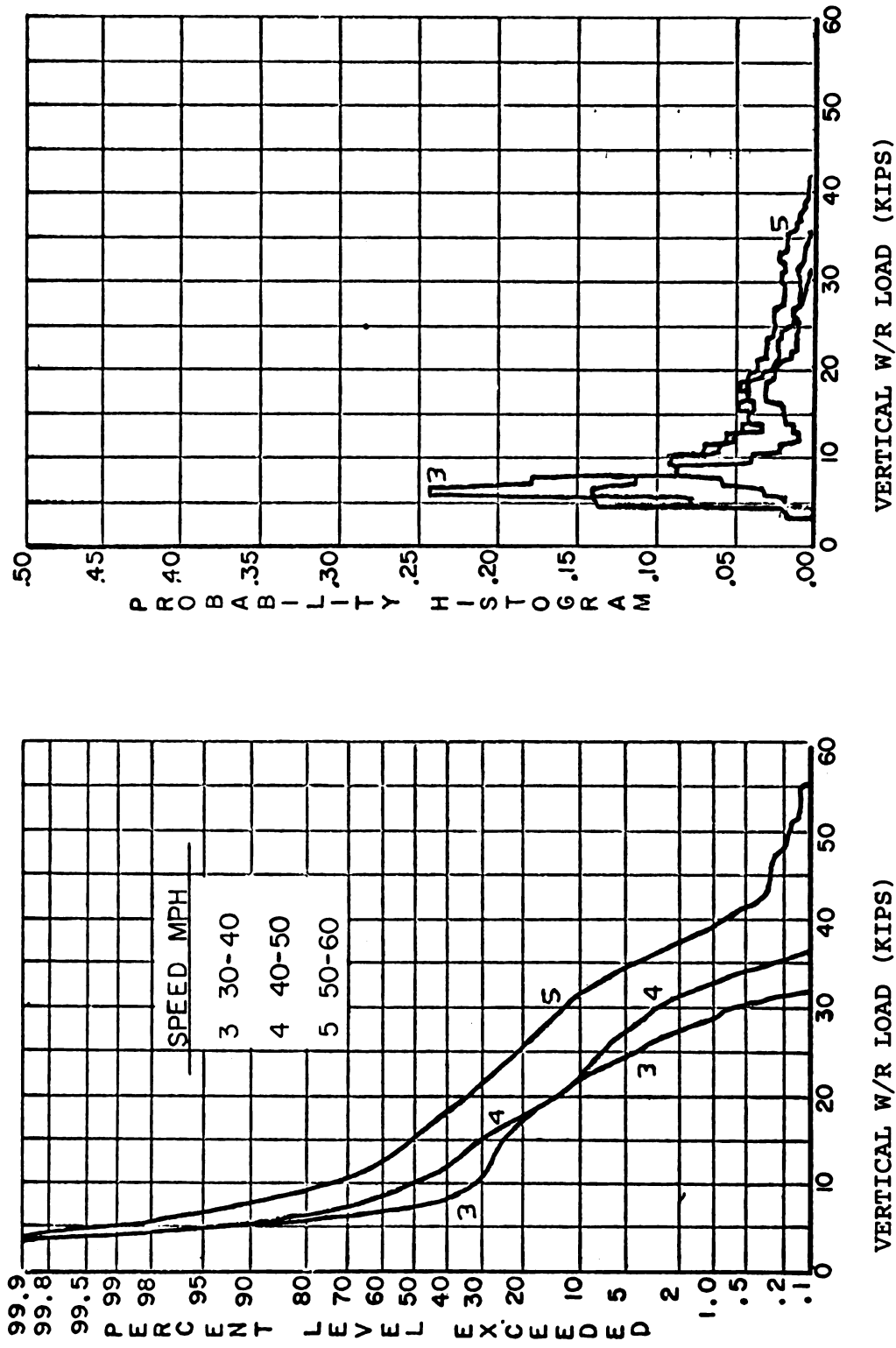


FIGURE 4-32. EFFECT OF TRAIN SPEED ON AVERAGE VERTICAL WHEEL/RAIL LOADS ON HIGH RAIL IN CURVE (Site 3) FOR ALL CARS (1.2 kips load interval)

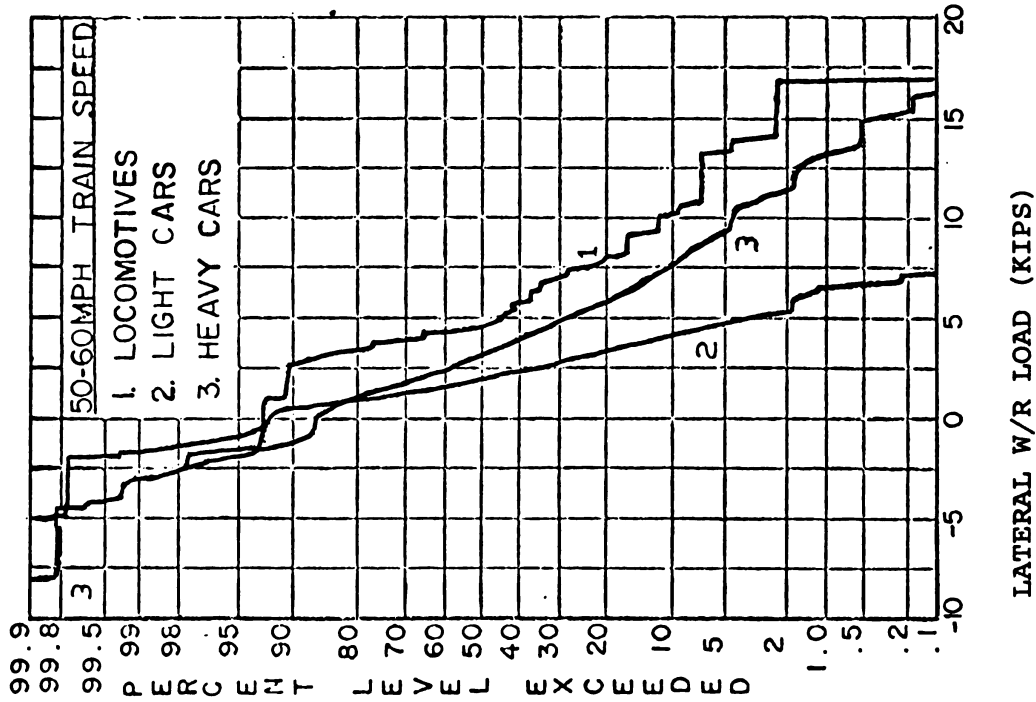
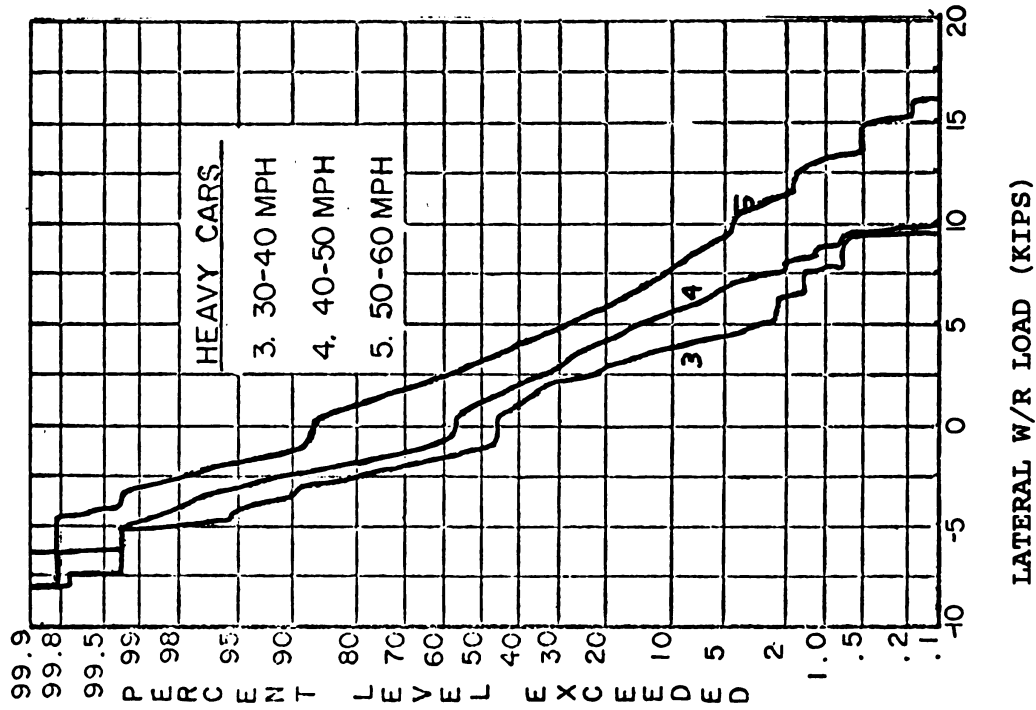


FIGURE 4-33. EFFECT OF CAR WEIGHT AND TRAIN SPEED ON LATERAL WHEEL/RAIL LOADS ON HIGH RAIL IN CURVE (Site 3), LOCATION 18E (17)

Table 4-13 summarizes the overall statistics for all traffic (all cars, all speeds) at the curve site and compares these to the same data for the tangent site (Site 1) having the same 24-inch tie spacing. The major differences between the two sites are that the average tie bending moments at the 0.1 percent exceedance level are 25 percent higher at the rail seat and 50 percent higher at the tie center than they were on tangent track even though the mean bending moments were nearly identical. This is a result of the increase in the load variation (S.D.) which occurs in the curve from trains operating both below and above the balance speed. The significance of the higher variability of loads in the curve is that the low-probability high loads will exceed those on tangent track even though the mean loads will be quite similar.

Table 4-14 shows an estimate of the low probability loads for the average tie. The tie bending moments for curved track at the 10^{-4} percent exceedance level are 16 percent greater at the rail seat, and there is a 56 percent and 90 percent increase in the positive and negative tie center bending moments, respectively. The 10^{-4} percent exceedance level represents approximately one occurrence each year for 20 MGT annual traffic, as shown in Table 4-9.

The importance of this increase in the low-probability high loads on curves depends on what causes particular track components such as concrete ties and fasteners to fail. If the component failure is caused by a sudden fracture due to the infrequent occurrence of a high load exceeding the design strength, then the increase in low-probability high loads on curves may be quite important and should be given considerable weight in establishing performance specifications. However, if the failure is caused by cumulative fatigue damage, then the mean load cycles may be more important than the low-probability high loads. In either case, the differences between track loading on curves and tangent track are minimized by operating trains as close to the balance speed as possible to equalize vertical rail loads and minimize lateral forces.

The importance of track lateral loads on tie bending moments has also been a question of interest. High lateral forces from flanging create an overturning moment on the rail, and some percentage of this is reacted at each tie. The moment on the rail seat from a high lateral force will

TABLE 4-13. COMPARISON OF AVERAGE TRACK COMPONENT LOADS FOR ALL TRAFFIC ON TANGENT AND CURVE TRACK WITH 24-IN. TIE SPACING

	Tangent Track, (Site 1)	Curve Track (High Rail) (Site 2)
1. Vertical W/R Load (P)		
Avg. Mean, kips	16.8	14.7
Avg. S.D., kips (% mean)	8.0 (47)	8.2 (56)
Avg. 0.1% load, kips	41.6	40.1
2. Rail Seat Vertical Load (Q)		
Avg. Mean, kips	6.6	9.09*
Avg. S.D., kips (% mean)	4.1 (62)	5.88 (65)
Mean Ratio, Q/P	0.39	0.62
Avg. 0.1% load, kips	19.3	27.3
3. Rail Seat Moment		
Avg. Mean, in.-kips	0.5	2.6*
Avg. S.D., in.-kips	3.9	5.97
Avg. 0.1% load, in.-kips	12.6, -11.6	21.1, -16
4. Tie Rail Seat Bending Moment (M_{rs})		
Avg Mean, in.-kips	15.5	17.1
Avg. S.D., in.-kips (% mean)	8.8 (57)	10.5 (0.62)
Mean Ratio, M_{rs}/P	0.923	1.16
Avg. 0.1% Load, in.-kips	40.0	49.6
5. Tie Center Bending Moment, M_c		
Avg. Mean, in.-kips	8.9	9.46
Avg. S.D., in.-kips (% mean)	6.4 (72)	10.9 (115)
Avg. 0.1% load, in.-kips	29, -11	43, -24

Note: Average 0.1% load levels predicted from average mean and S.D. assuming normal probability distribution, i.e., 0.1% Load = Mean \pm 3.1 (SD)

(*) Average based on data for only two instrumented tie plates.

TABLE 4-14. COMPARISON OF EXTRAPOLATED STATISTICS FOR AVERAGE TIE BENDING MOMENTS IN TANGENT AND CURVED TRACK

Percent Level Exceeded	Normal Variable, Z (1)	Average Tie Bending Moment, in.-kips			
		Rail Seat		Rail Seat	
		Tangent	Curve	Tangent	Curve
50	0	15.5	17.1	+8.9	+9.46
1.0	2.33	36.0	41.5	+24, -6	+35, -16
0.1	3.1	40.0	49.6	+29, -11	+43, -24
0.01	3.75	48.5	56.5	+33, -15	+50, -31
0.001	4.3	53.3	62.3	+36, -19	+56, -37
10 ⁻⁴	4.75	57.3	66.9	+39, -22	+61, -42
10 ⁻⁵	5.22	61.4	71.9	+42, -25	+66, -47

Note:

1. $Z = (X - \bar{X}) / (S.D.)$.

increase the positive bending moment (compression at the tie bottom) in the end of the tie outside the rail seat region. However, the bending moment immediately under the rail will be reduced.

The quantitative effect of these rail seat moments on the tie bending moments has not been evaluated in detail. However, the mean rail seat moments are quite low compared to the mean tie bending moments at the rail seat for both tangent and curved track. Rail seat moments equal to 50 percent of the tie bending moment do occur at the 0.1 percent load level, but these infrequent occurrences of high loads do not necessarily occur simultaneously. In fact, some of the highest lateral loads and rail seat moments are caused by the hunting of light cars, where the low vertical loads cause relatively low tie bending moments. Joint probability statistics are needed to show the quantitative relationship between the simultaneous occurrence of high rail seat moments and vertical loads. However, it is expected that lateral rail loads are most important for the performance of rail fasteners and of secondary importance for tie loads.

4.7.5 Comparison with Test Data from Kansas Test Track

The Kansas Test Track (KTT) included three sections of RT-7 concrete ties and a wood tie control section on identical roadbed (10-inch ballast depth). Instrumentation in these sections included the same load cell ties used in the FEC tests to measure vertical rail seat loads and tie/ballast pressures and strain gaged ties (SGT) to measure the bending moments. The three concrete tie sections were constructed with tie spacings of 30 inches (Section 1), 27 inches (Section 2) and 24 inches (Section 3), while the wood tie control (Section 9) used the standard Santa Fe tie spacing of 19-1/2 inches.

Periodic trips were made by staff of the Portland Cement Association (PCA) to record track response data at different traffic intervals during the abbreviated life of the KTT. Data from three to five trains were recorded for each of many sets of track instrumentation, and track response for locomotives has been used by PCA to summarize the KTT performance. A limited sample of those data is presented herein and compared with the FEC data for locomotives at all speeds.

Figure 4-34 shows the effect of tie spacing on vertical rail seat loads. The KTT data from Trip 3 (January, 1975) are used for comparison. Data from earlier trips showed somewhat lower rail seat loads during track consolidation. The KTT data are the mean locomotive loads on the two rail seats on one load cell tie in each section. The FEC data show the range and the average of the mean loads from locomotives for the five instrumented tie plates in each section.

Data from the KTT and the FEC are similar for the 24-inch tie spacing, where a direct comparison can be made. The large tie-to-tie variation measured at the FEC shows the need for instrumenting several ties in order to average these spatial variations. The expected trend of an increasing percentage of the wheel load being transmitted to each tie as tie spacing is increasing is evident. But data scatter makes it difficult to judge the validity of the design guidelines from the current AREA specifications for concrete ties. It appears that the load cell tie used for the 27-inch tie spacing data at KTT was partially "hung" so that the rail seat loads were unusually low. The question of whether increasing tie spacing to 30 inches

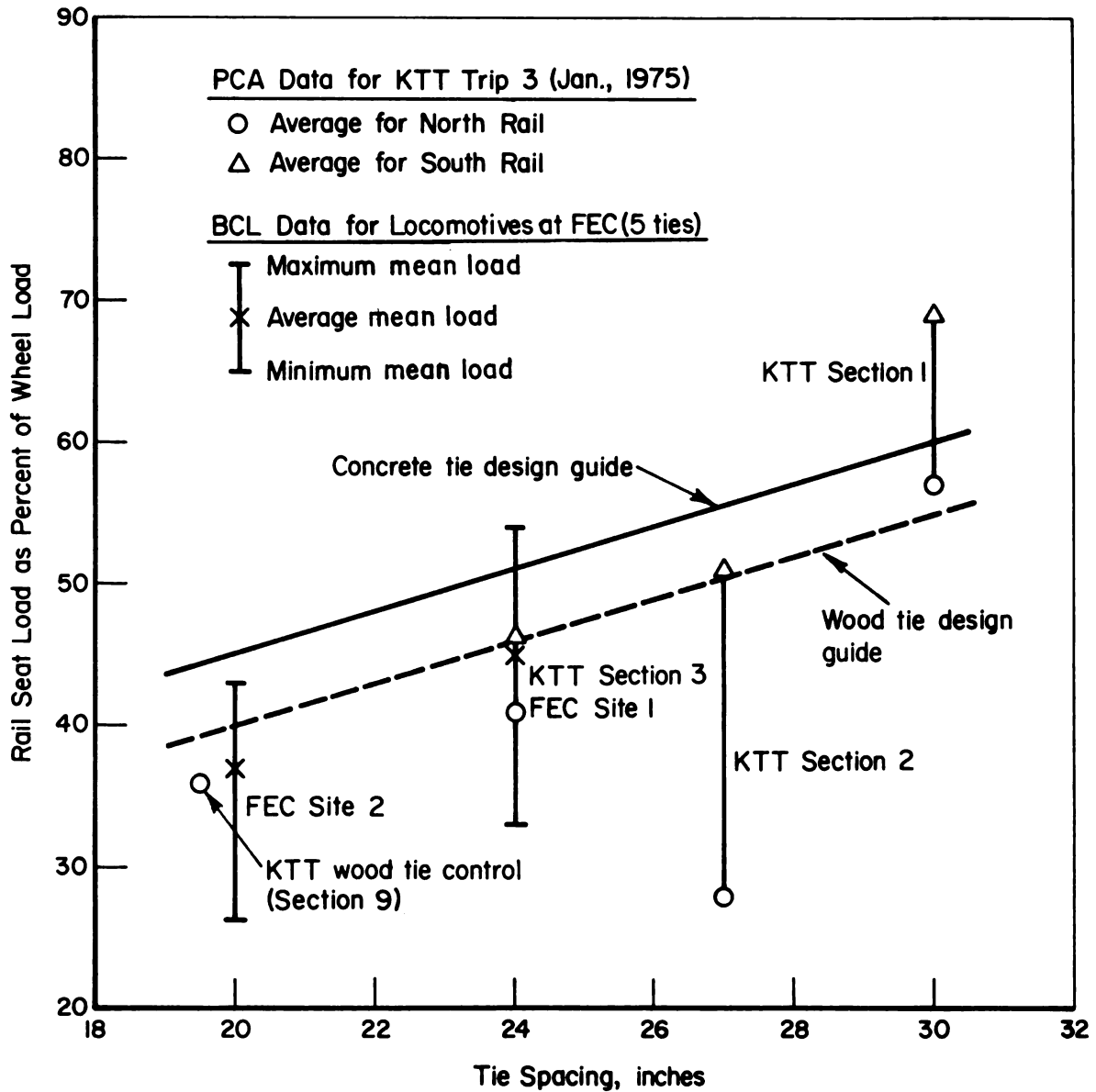


FIGURE 4-34. EFFECT OF TIE SPACING ON MEAN RAIL SEAT LOADS FOR LOCOMOTIVES

may produce higher tie loads than expected needs further evaluation if this large tie spacing is to be used for new track construction.

Figure 4-35 compares FEC and KTT data for tie bending moments at the rail seat. Mean rail seat bending moments for locomotives at all tie spacings are less than 30 percent of the design guides for static flexural strength. The effect of tie spacing is difficult to evaluate because of the large tie-to-tie variations. Maximum rail seat bending moments measured on the FEC track were about 80 inch-kips (0.1 percent exceedance). An extrapolation of vehicle load statistics for all cars showed that a bending moment exceeding 120 inch-kips would not be expected during a 50 year life with annual traffic up to 60 MGT. The data from KTT verify this range of tie bending moments. However, it has been reported [4-2] that 100 percent of the concrete ties in the KTT incurred flexural cracking in the rail seat region during 6 months of traffic. A review of KTT data taken from the different measurement trips does not show large variations from the Trip 3 data or trends which indicate that significantly higher bending moments occurred at some other time.

The center bending moments shown in Figure 4-36 indicate the loads measured at the FEC and the KTT are quite low. While only negative bending is reported for the KTT, positive bending at the tie center produced larger moments on the FEC ties. Bending moments measured by the C&O-B&O Railroad at Noble, Illinois for newly constructed concrete tie track with 27-inch spacing also indicated that the majority of strain measurements showed the top surface of the tie center to be in compression rather than tension. Maximum positive bending moments were in the range of 10 to 30 inch-kips and negative moments went to 50 inch-kips. These ranges agree with the FEC data listed in Table 4-7 for track with 20 and 24-inch tie spacing.

Data reported by PCA from periodic measurements during the first year of traffic (\approx 30 MGT) on the Santa Fe concrete tie test section at Streator, Illinois show maximum rail seat bending moments of 96 inch-kips and maximum negative bending at the tie center of 70 inch-kips. These maximum values were reportedly only 32 percent and 36 percent of the AREA flexural strength requirements for rail seat and tie center, respectively. The ranges of bending moments measured on four ties at Streator are shown in Figures 4-35 and 4-36 for comparison. The maximum moments are somewhat higher than those measured on the FEC or the KTT, but they are still well below the flexural strength requirements.

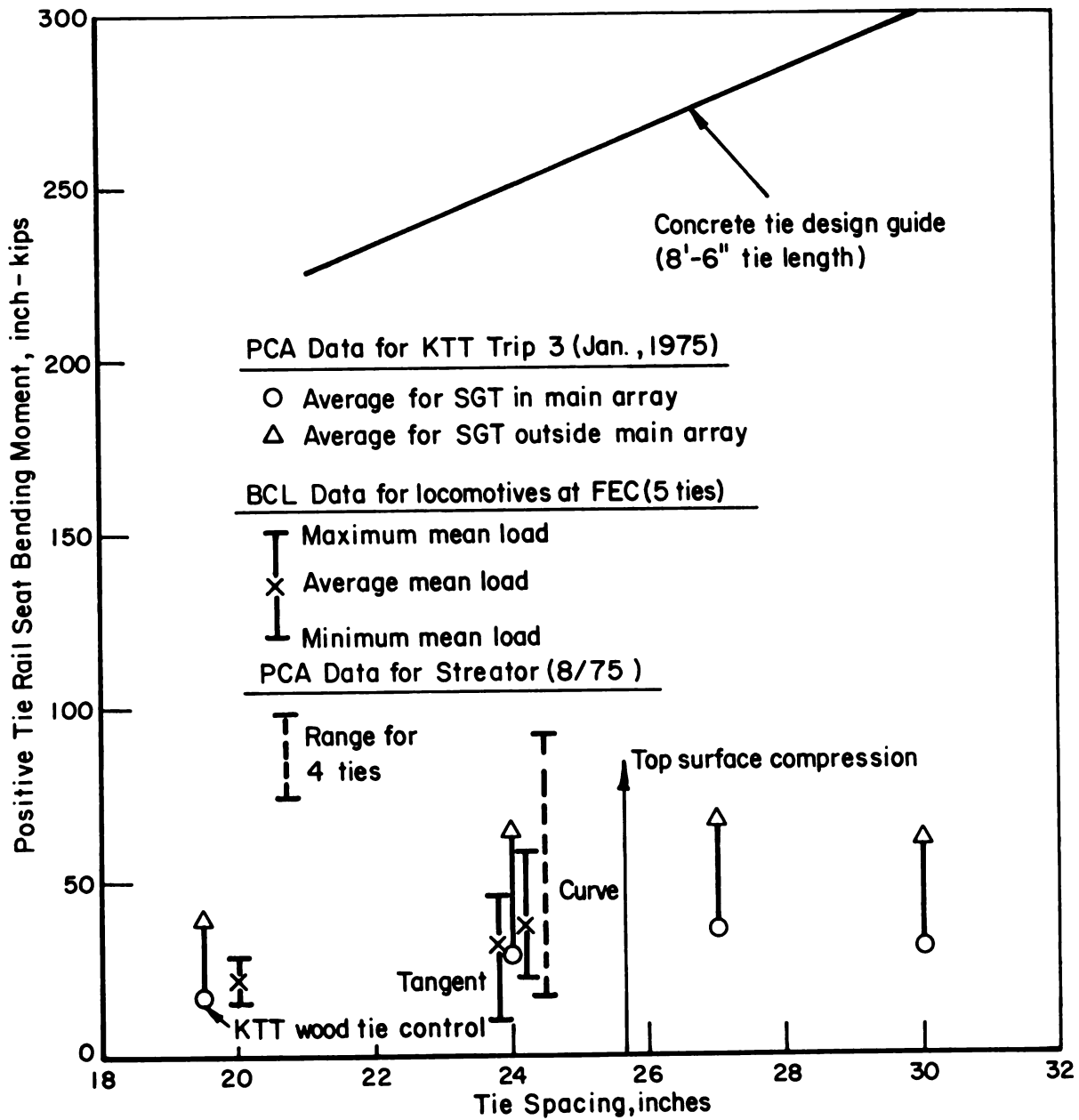


FIGURE 4-35. EFFECT OF TIE SPACING ON MEAN TIE RAIL SEAT BENDING MOMENTS

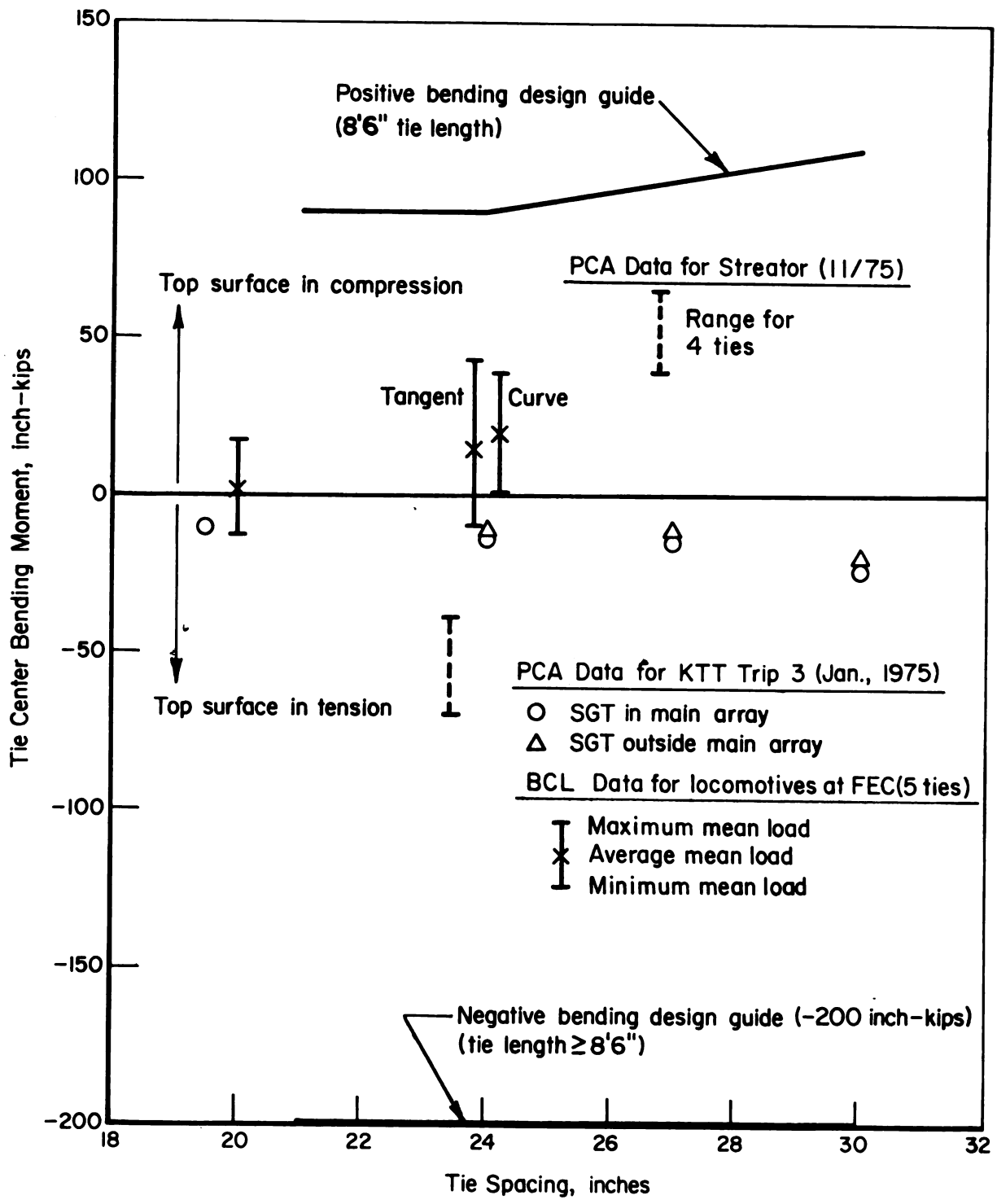


FIGURE 4-36. EFFECT OF TIE SPACING ON MEAN TIE CENTER BENDING MOMENTS

4.7.6 Summary of Results

The major results and conclusions based on the analysis of statistical data in Section 4.7 are summarized as follows:

a. Vertical track loads at the two tangent track test sites showed that the highest loads occurred in the low-speed range (30-40 mph). However, no significant vehicle dynamics effects were evident on this smooth track. The observed variations in track loads in the different speed ranges were caused by train operations, i.e., trains with heavy cars went slower than those with light cars, rather than a true speed effect from vehicle dynamic excitation. This weight/speed bias from operations might be eliminated by recording data for several weeks, but this is a much longer period than was required to obtain sufficient data for most other requirements.

b. Locomotive as a class caused the highest average vertical track loads on the FEC, but the maximum loads (0.1 percent exceedance) are about equal for locomotives and heavy cars. The greater number of heavy cars means that the low-probability maximum loads will occur much more often from heavy cars than locomotives. Previous evaluations of track load data were based on the assumption that loads from locomotives were the major contributors to concrete tie damage.

c. Vertical wheel/rail load measurements measured at several different locations at each test site were nearly identical, so spatial variations within each site can be neglected. Maximum vertical loads of 50 kips at the 0.1 percent probability level were recorded on the high rail at the curve site. The average standard deviation of vertical wheel/rail loads was about 50 percent of the average mean load of about 16 kips for freight traffic at the test sites.

d. The overall load statistics for lateral wheel/rail loads were nearly identical for the tangent and curved track sites. Mean lateral loads were quite low, less than 2 kips. However, spatial variations were considerable and more measurement locations are recommended for any future tests where it is important to define the average lateral loads for each site.

e. Vertical rail seat loads showed a large tie-to-tie variation at each site. Mean loads varied by as much as 3:1 as a result of several ties

developing considerable free play at the tie/ballast interface. However, maximum mean and maximum 0.1 percent rail seat loads of 11.3 and 31 kips, respectively, were considerably below the 52.6-kip rail seat load recommended in current concrete tie specifications for 24-inch tie spacing.

f. Measurements of rail seat moment on both tangent and curved track show that the mean peak moment was very small. This is a desirable condition for minimizing cutting and wear of rail pads. The maximum rail seat moments at the curve site were higher than those on tangent track, as expected.

g. Measurements of bending moments in the rail seat and center regions of several concrete ties at each test site showed large tie-to-tie variations in ballast support condition. Light cars frequently caused negative bending moments (tension in the top surface) at both the tie center and the rail seat, indicating a center bound condition. Heavy cars on the same ties would change the bending moment in the rail seat region to positive (tension in the bottom surface), and the center bending moment was frequently quite independent of car weight. This indicates a nonlinear support condition whereby the distribution of reaction loads along the tie bottom changes with load. For example, a tie with voids under each end would develop negative bending at both the center and rail seats with light loads. However, increased wheel loads could cause the tie to bear more fully on the ballast. This would shift the reaction loads toward the tie end and cause positive bending at the rail seat with very little change in the bending moment at the tie center.

The highest 0.1 percent tie bending moment measured in the rail seat region was 78 inch-kips, and this was in the curve at Site 3. Extrapolating the low-probability statistics by assuming a normal (Gaussian) distribution shows that bending moments exceeding 120 inch-kips would not be expected during a 50-year tie life with annual traffic up to 60 MGT. This is less than 50 percent of the rail seat bending moment requirements in current specifications for concrete ties. However, the possibility of higher moments that might be caused by severe wheel flat impacts needs further investigation.

h. Maximum bending moments of -56 and +67 inch-kips (0.1 percent level) were measured at the tie center. Negative bending moments at the tie center have the greatest importance because bending cracks in the tie center region usually start at the top surface. These maximum measured bending

moments were well below the currently specified strength of -200 and +90 inch-kips for ties at 24-inch spacing.

i. Measurements of dynamic force variations in several rail fastener bolts showed that maximum force variations (0.1 percent level) were less than 20 percent of the static preload and that the highest force variations occurred on the gage bolt. This is a relatively large force variation, and it would be increased considerably if a softer rail pad were used with the rigid rail clips used by the FEC.

j. Lateral deflections of the rails and ties under traffic were quite small at all of the test sections. Maximum lateral deflections at the 0.1 percent probability level were 45 mils for the rail relative to the tie and 30 mils for the absolute motion of the tie.

k. The effect of reducing tie spacing from 24 inches (Site 1) to 20 inches (Site 2) was evaluated by comparing average rail seat loads and tie bending moments for the several instrumented ties at each site to include the large spatial variations. The 16 percent reduction in tie spacing reduced vertical rail seat loads by about 9 percent and reduced tie mean and maximum rail seat bending moments by 36 percent and 12 percent, respectively, for the average traffic at the test sites. Data for only heavy cars indicate that changes in tie spacing may cause much greater than expected changes in tie bending moments due to the load dependent behavior of the tie support condition. How this would affect track loads where the average wheel load is much higher than normal, e.g., unit trains of 100-ton cars, needs further verification.

l. Train operations on curved track cause differential vertical loads on the low and high rails for speeds which are different from the curve balance speed. Maximum average tie bending moments (0.1 percent exceedance) were 25 percent higher at the rail seat and 50 percent higher at the tie center than they were on tangent track even though the mean bending moments were nearly identical. The importance of this increase in the low-probability maximum loads on curved track depends on the failure mode for concrete ties. Failures due to infrequent occurrences of loads exceeding the design strength would make this increase in loads on curves very important. However, failures due to cumulative fatigue damage are more dependent on the mean load cycles.

In either case, the increase in vertical loads on curves can be minimized by operating close to the balance speed.

m. The highest lateral forces at the curve site were produced by heavy cars and locomotives. Lateral forces from light cars operating in the 50-60-mph range were lower on the curve than on tangent track, which indicates that flange contact on curves probably eliminates hunting. A comparison of the overall statistical data for the curve and tangent track sites shows no major differences in the lateral loads. Also, lateral track loads seem to be most important with regard to rail wear and the performance of rail fasteners and less important as a contributor to tie cracking.

n. A comparison of rail seat load and tie bending moment data from the FEC measurement program with similar data from other sections of concrete tie track shows general agreement. Tie loads from revenue traffic are considerably lower than current flexural strength requirements even for probabilistic predictions of maximum loads for a 50-year tie life. It appears that tie cracking is initiated in service at loads substantially below the static load required to create a structural crack. A structural crack is one which extends from the tie surface in tension to the outermost level of the prestressing tendons (this is the failure criterion used for current flexural tests of concrete ties). It is conjectured that small cracks can be initiated in prestressed concrete ties at relatively low loads; and that once initiated, the cracks can continue to propagate from repeated cycling until they grow sufficiently large to be detected visually. Crack initiation may be a fatigue process where the total stress at the tie surface remains in compression due to the prestress, or it may be caused by the total stress at the outer surface exceeding the tensile strength of the material. This would indicate that the prestress at that location is insufficient for the applied load even though the load may be less than 50 percent of the flexural strength requirements. It is very difficult to determine at what load a small crack is initiated in a prestressed concrete tie, and this has not been a part of tie tests. An experiment where the surface of a new tie is instrumented sufficiently to detect crack initiation during static loading is needed to determine if the initiation load is substantially less than that required to propagate a crack to the prestress strands. An evaluation of tie performance for fatigue loading at load amplitudes which represent realistic service conditions is also recommended.

Recommendations regarding the identification of a crack initiation mechanism presuppose that any type of structural cracking of concrete ties constitutes a failure. This has been the criterion used to progressively increase the flexural strength requirements in current specifications. The justification cited for this is that a crack which reaches the prestress strands will cause local degradation around the strands during repeated loading under traffic and will ultimately cause a loss in bond and a rupture of the tie. It appears that this failure mode is regarded as more important than strand corrosion or structural damage from freeze-thaw cycling of a cracked tie. The long-term performance of ties which have structural cracks has not been verified by service experience. The installation of cracked RT-7 ties from the KTT in FAST provides an opportunity to monitor their degradation rate for accelerated loading. The effect of freeze-thaw cycles should be minimal for the short test duration of FAST.

4.8 TRACK DYNAMIC RESPONSE

Time histories generated during the data acquisition process showed considerable vibration within various portions of the track structure. This vibration was especially pronounced from the excitation of wheel flats due to the higher frequencies associated with these impacts. Data from the FEC indicate that about 10 percent of the car wheels have flats of sufficient size to excite noticeable vibration, but a much smaller portion of these would cause loads which exceed the normal load for a heavy car.

Figure 4-37 shows a typical recording of load data for several cars passing one tie location at the curved site (Site 3). The increased vibration caused by a few cars with wheel flats is quite noticeable. Figure 4-38 shows two sections of the Figure 4-37 recording in greater detail. Load data for a locomotive is shown in Figure 4-38a to demonstrate the tie response to heavy cars with no apparent wheel flats. Figure 4-38b shows that the response to light cars having wheel flats is clearly more severe, especially at the tie center. The damping of the track structure is quite low for this case, and it is difficult to distinguish the load pulses from individual wheels from the general vibration.

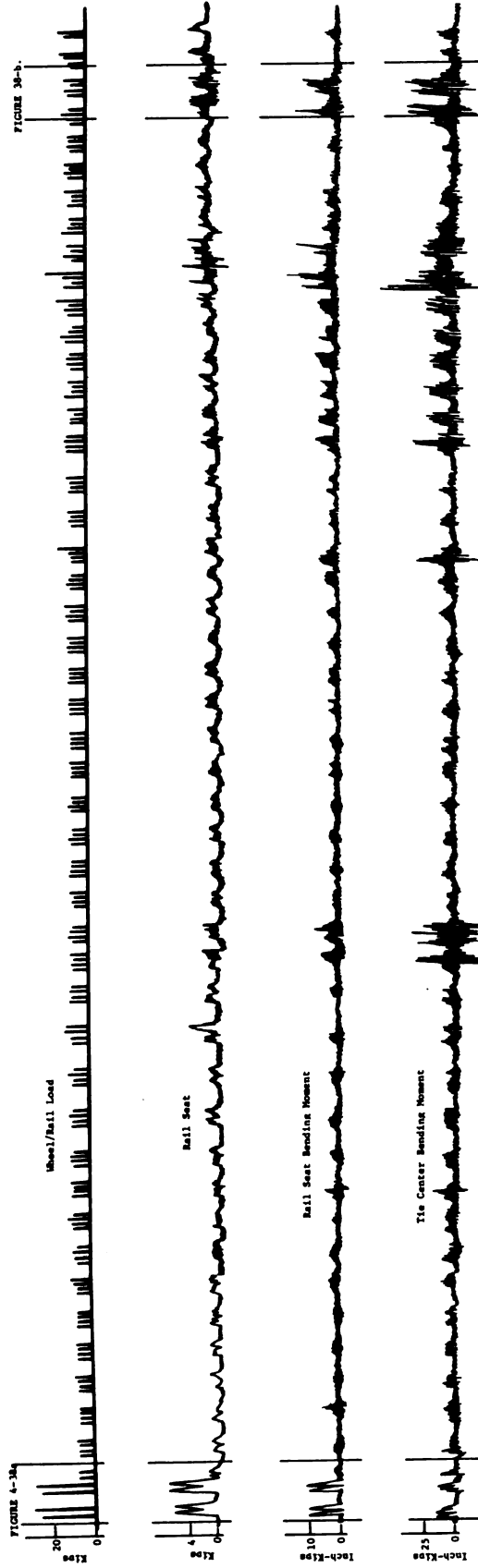


FIGURE 4-37. TYPICAL RECORDING OF TIE LOADS FOR SEVERAL CARS

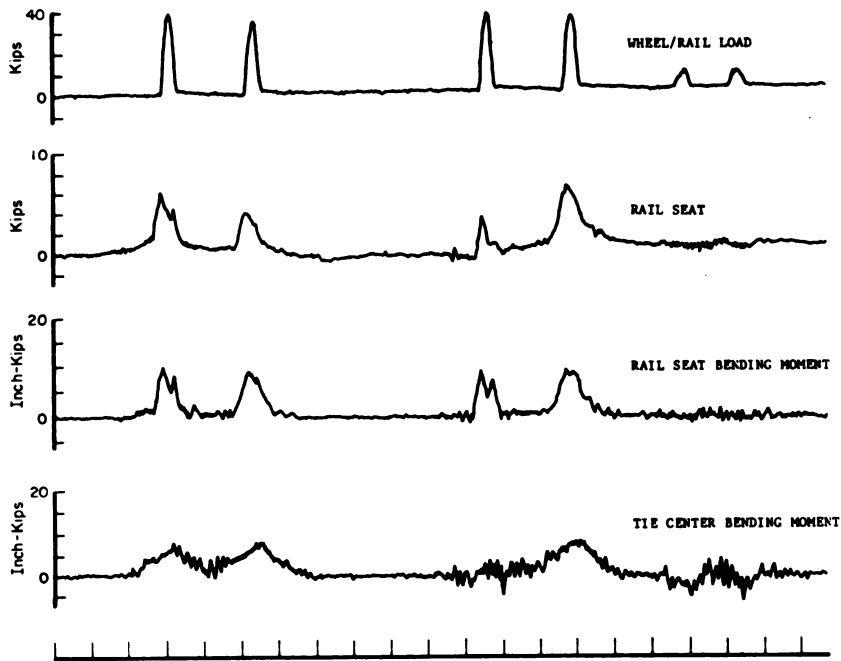


FIGURE 4-38a. TIME HISTORY OF TIE RESPONSE TO LOCOMOTIVE

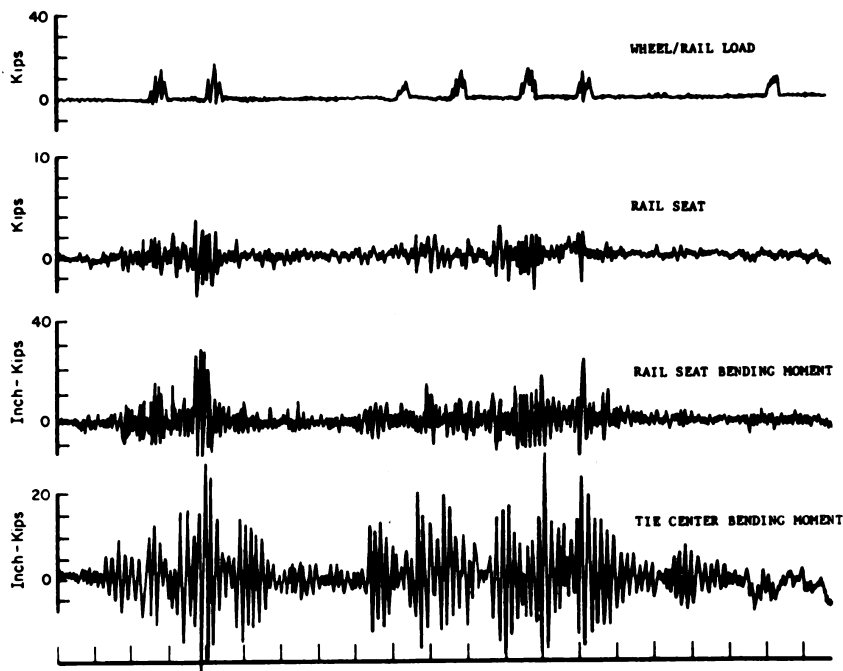


FIGURE 4-38b. TIME HISTORY OF TIE RESPONSE TO LIGHT CAR WITH WHEEL FLATS

4.8.1 Frequency Analysis of Tie Vibration

Spectrum analysis of several bending moment records indicates two primary modes of tie oscillation. Tie center bending moments show a marked resonance between 80 and 100 Hz, with an average of about 90 Hz. Figure 4-39 shows a typical spectrum using the time history for light cars with wheel flats shown in Figure 4-38b.

Rail seat bending moment, and all other parameters monitored adjacent to the rail seat, show a broader resonance ranging between 110 and 160 Hz, with an average at about 140 Hz. Figure 4-40 shows the spectrum of the rail seat bending moment record in Figure 4-38b. For comparison, Figure 4-41 shows a "quiet" spectrum for relatively smooth wheels. The dominant frequency components are at the wheel pass and truck pass frequencies. Wheels passing at 50 to 60 mph have a spectral line around 12 Hz, and the truck center spacing produces spectra below 5 Hz at these same speeds. By comparison, the bending moment spectra in Figures 4-39 and 4-40 are 5 to 10 times greater (14 to 20 dB) at their respective resonances than at the wheel-pass frequencies. The time history in Figure 4-38b confirms that there is essentially no visible wheel-pass fundamental frequency for the passage of a lightly loaded flat wheel.

A cursory analysis of the spectral data for bending moments of ties suggests that the 90 Hz and 140 Hz peaks represent two different modes of tie vibration. A high bending moment at the tie center relative to the rail seat region suggests a free-free beam model where the fundamental frequency is approximated by

$$f = \frac{(4.73)^2}{2\pi l^2} \left(\frac{EI}{m} \right)^{1/2} \quad (4-2)$$

The parameters for the RCCC tie are

$$l = 102 \text{ in.}$$

$$EI_{\text{avg}} = 900 \times 10^6 \text{ lb-in.}^2 \text{ for entire tie}$$

$$m = 575 \text{ lb}/102 \text{ in.} = 5.637 \text{ lb/in.}$$

The estimated frequency for this fundamental mode is 85 Hz, which is surprisingly close to the 90 Hz average frequency observed in the response spectra.

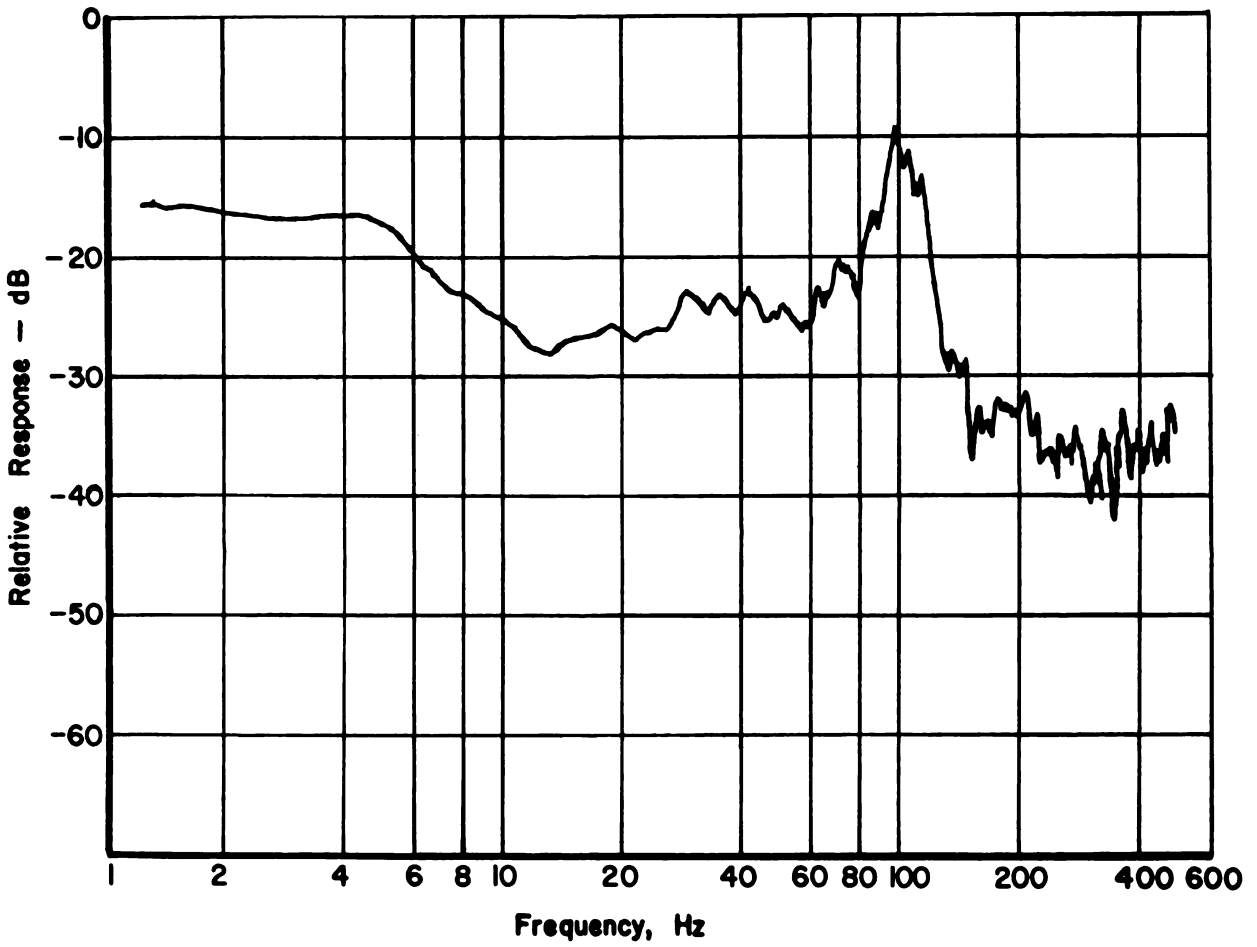


FIGURE 4-39. TIE CENTER BENDING SPECTRAL RESPONSE FOR LIGHT CAR WITH WHEEL FLATS

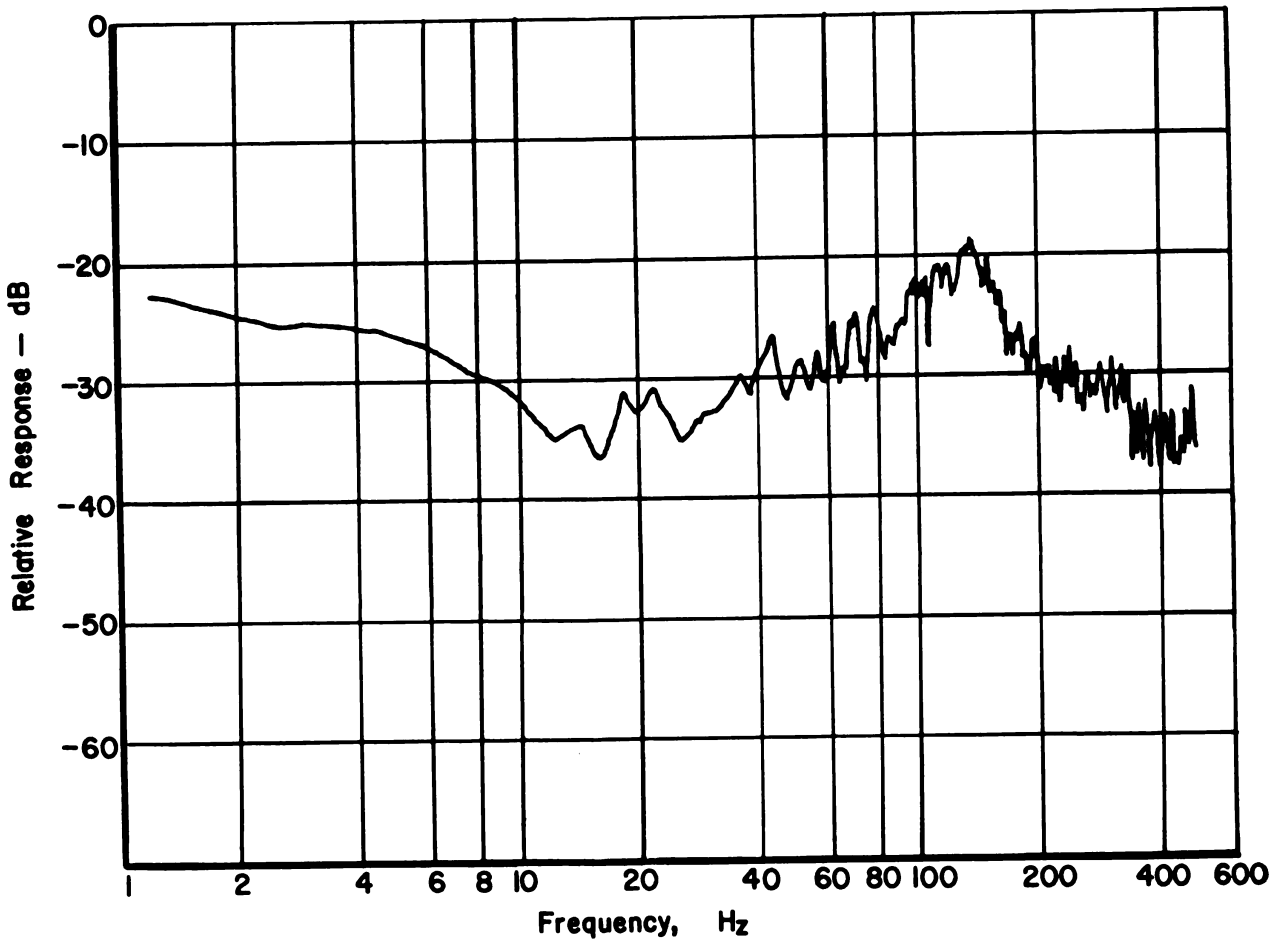


FIGURE 4-40. TIE RAIL SEAT BENDING MOMENT SPECTRAL RESPONSE FOR LIGHT CAR WITH WHEEL FLATS

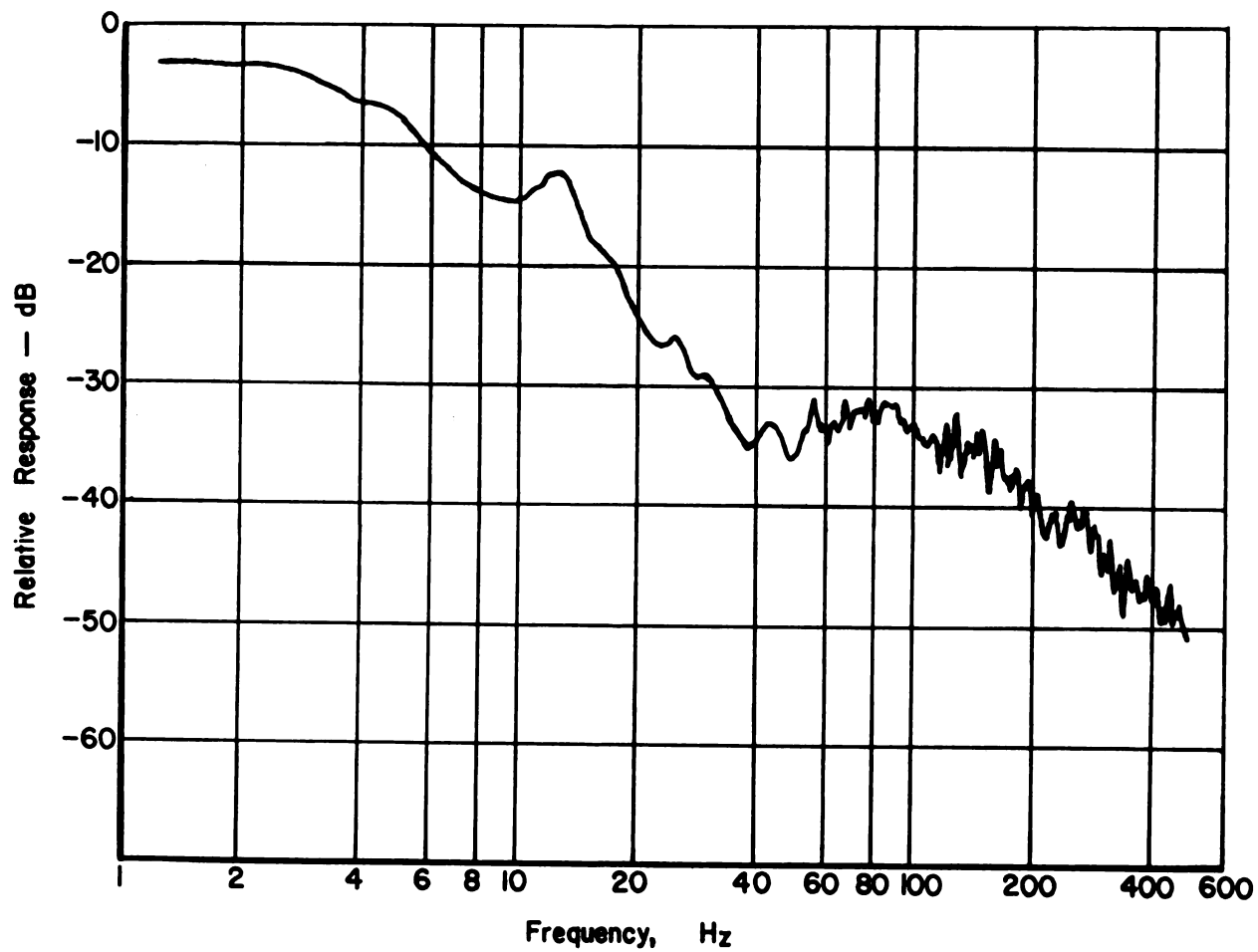


FIGURE 4-41. TIE RAIL SEAT BENDING MOMENT SPECTRAL RESPONSE FOR HEAVY CAR WITH SMOOTH WHEELS

Flat wheels clearly produce a relatively large vibratory response of the rails and ties on concrete tie track. Wheel flats on light cars can produce tie bending moments which exceed those for heavy car wheels which are in good condition. Fortunately, however, the increase in dynamic loads from wheel flats on heavy cars are not nearly as severe as those from light cars. This limits the increase in total maximum load.

This load-dependent effect on track response appears consistent with previous observations that the tie support can be very local for light cars and change to that of a relatively uniform support under heavy cars. This increased contact with the ballast reduces tie dynamic response. This is probably due to the increase in radiation damping through the ballast and an increase in effective stiffness.

The effect of wheel flats on the low-probability, high bending moments to which ties are subjected requires some additional investigation. The sampling rate of 125 Hz used for the statistical data analysis was not adequate to determine peak values from vibration in the range of 90 to 140 Hz. This vibratory response under light wheels was clearly responsible for some of the unexpected negative rail seat loads, negative tie bending moments at the rail seat, and positive bending moments at the tie center.

4.8.2 Rail and Tie Acceleration

Measurements of rail and tie acceleration under revenue traffic were made at each test site. The difference in the frequency spectra of the rail and tie acceleration gives a measure of the load attenuation provided by the rail fastener/pad assembly. Spectral analysis of the two signals generally showed identical response at frequencies below about 500 Hz, indicating that no appreciable low-frequency attenuation occurred from the rail-fastener assembly.

Figure 4-42 is a short time history that has been low-pass filtered at five different bandwidths to show the relative dynamic response. Due to the high response to flat wheels it was necessary to scale and accelerometer channels to ± 100 g for the rail and ± 30 g for the tie. The predicted tie acceleration generated by following the track deflection profile as an ideal wheel pass was less than 1 g (see Section 3.6). The resolution of the data at the 1 g level was not sufficient to be used to validate this analysis model. Figure 4-43 shows a typical spectrum for tie acceleration response

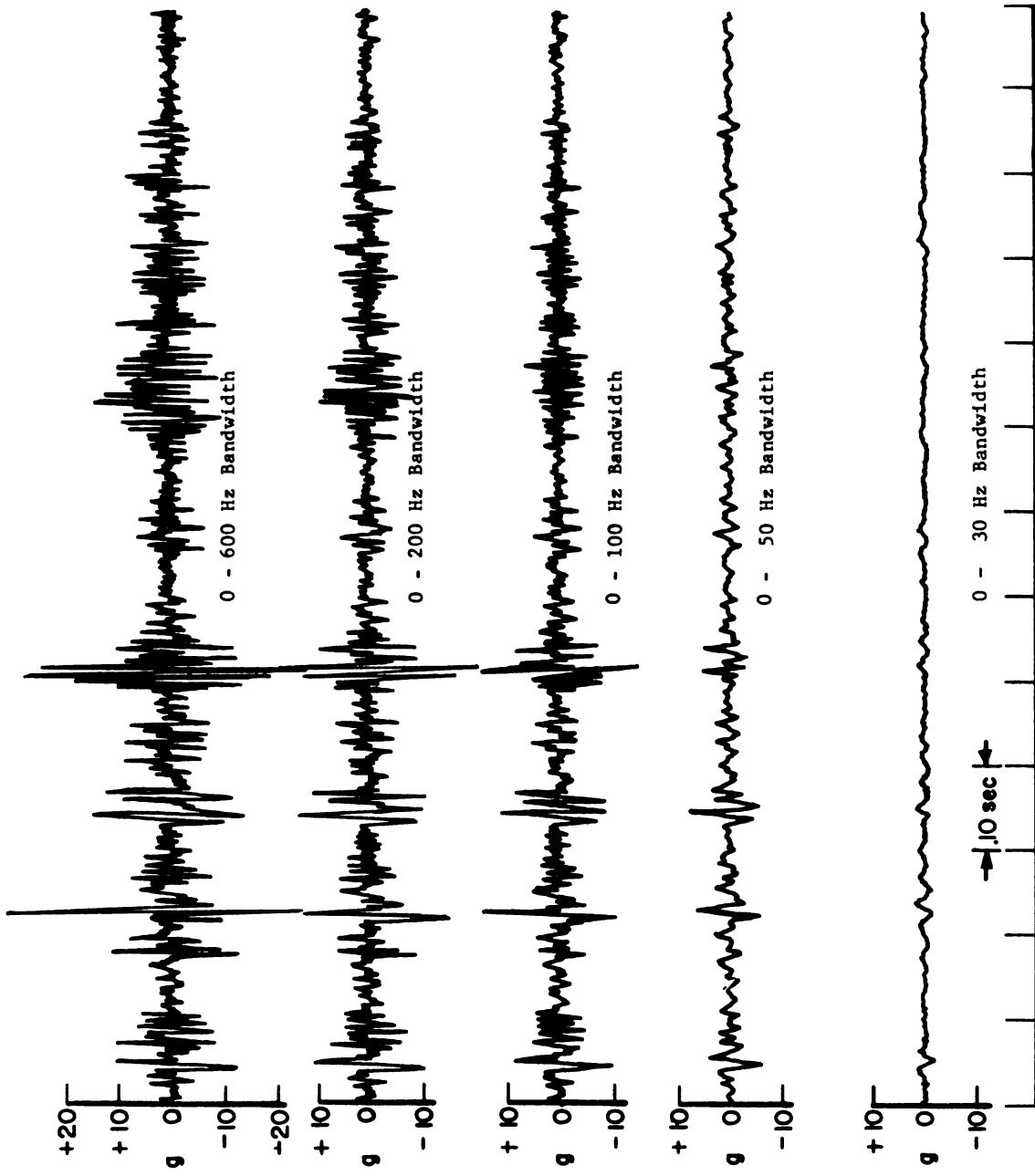


FIGURE 4-42. TYPICAL TIE ACCELERATION RESPONSE

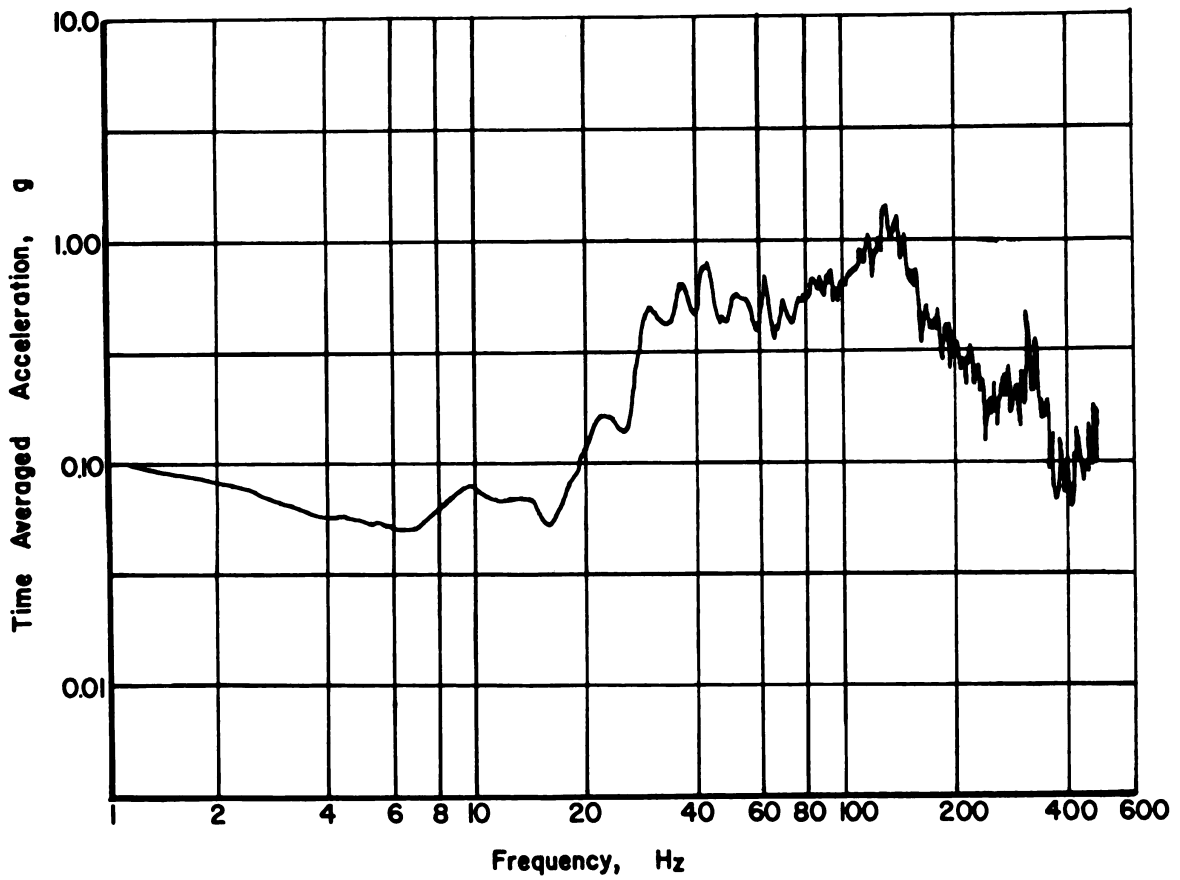


FIGURE 4-43. TYPICAL TIE ACCELERATION SPECTRAL RESPONSE UNDER LIGHT FLAT WHEELS

which confirm that most of the energy is above 30 Hz.

4.8.3 Rail Corrugation

Data recorded during testing at the curved site (Site 3) indicated that there were vibrations occurring in the 30-40-Hz frequency range which had not been observed at the previous sites. An examination of the rail surface revealed a corrugation pattern on the top of the rail head on the high rail with a wavelength approximately equal to the 24-inch tie spacing. This corrugation would produce vibration in the 30-40 Hz range for train speeds of 40 to 55 mph. Figure 4-44 is a photograph using a telephoto lens to enhance the appearance of the corrugation. The corrugation peak was always over the tie. The peak-to-peak amplitudes were generally less than about 0.015 in. The corrugation pattern was visible throughout most of the curve, but it was not observed on the adjacent tangent track. It appears that the stiffness variation encountered between the center of the tie and the mid span between ties on this high modulus track may be sufficient to initiate this type of corrugation.

4.8.4 Track Vertical Natural Frequency

An apparent fundamental natural frequency of the track structure was observed in several data channels. Figure 4-45 shows a time history of vertical rail seat load for two locomotives traversing the main array at different speeds. The tie experiences a complete unloading within the normal influence zone due to the dynamic response of the track system. A spectrum analysis of several data channels with varying train speeds indicates that this natural frequency was in the range of 40 to 50 Hz.

5. EVALUATION OF TRACK ANALYSIS MODEL

The MULTA track analysis model was selected to predict track response to train loads and to evaluate a wide range of track design parameters. This section of the report presents a comparison of measurements and predictions of

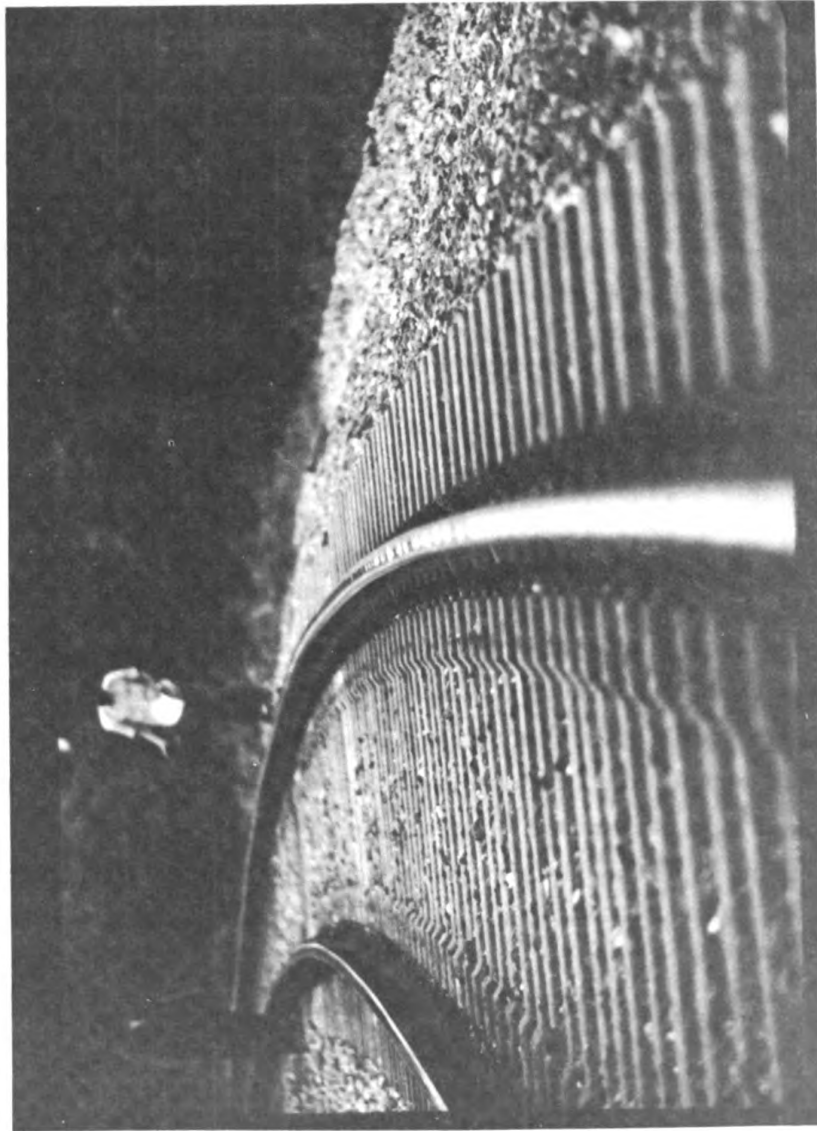


FIGURE 4-44. RAIL CORRUGATIONS AT CURVE

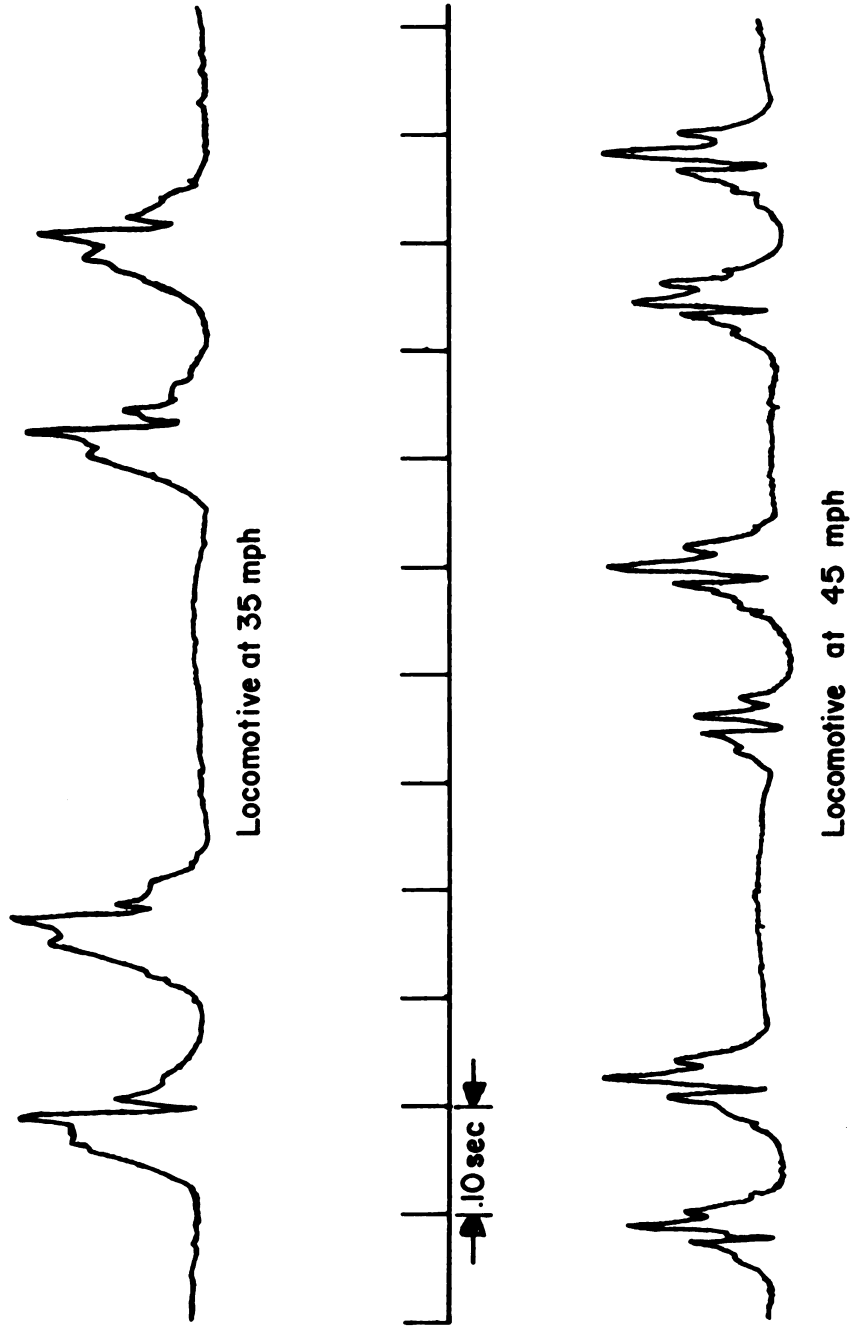


FIGURE 4-45. RAIL SEAT LOAD DYNAMIC RESPONSE AT SITE 1

rail-seat loads, tie bending moments, and tie/ballast pressures to determine the validity of using this track analysis model as a substitute for extensive measurement programs to evaluate many different variations of track construction.

5.1 COMPARISON OF MEASURED AND PREDICTED LOADS

5.1.1 Effect of Track Modulus on Rail Seat Loads

Data on vertical rail-seat loads from a slow roll-by of the work train were used to determine the track modulus, U . The effect of tie-to-tie variations in the main array was minimized by averaging the maximum rail seat load for a known wheel load during a slow traverse of the work train. The average ratio of rail seat load to wheel load (Q/P) was used with the theoretical relationship from the beam-on-elastic-foundation formulation to determine an experimental track modulus.

Figure 5-1 shows the effect of tie-to-tie variations for all five instrumented tie plates at Sites 1 and 2. The results in Figure 5-1 show considerable tie-to-tie variation. They also show that the instrumented tie plate on ties 57 and 30 measured rail seat loads higher than the wheel load-- a physically unacceptable conclusion. Since the same tie plate was used on both ties, it was apparent that it had been operating incorrectly and these data were eliminated. One of the load cells did fail later in the test program.

Table 5-1 lists maximum measured vertical rail seat to wheel load ratio in percent. These data show a considerable load dependent effect as well as large tie-to-tie variations. The average rail seat load for heavy cars on track with 20-inch tie spacing was 12.5 percent lower than that for 24-inch tie spacing. A 16 percent reduction would normally be expected based on conventional guides for track design. However, individual ties in both sections carried as much as 65 percent of the heavy car wheel load and as much as 76 percent of the light car wheel load.

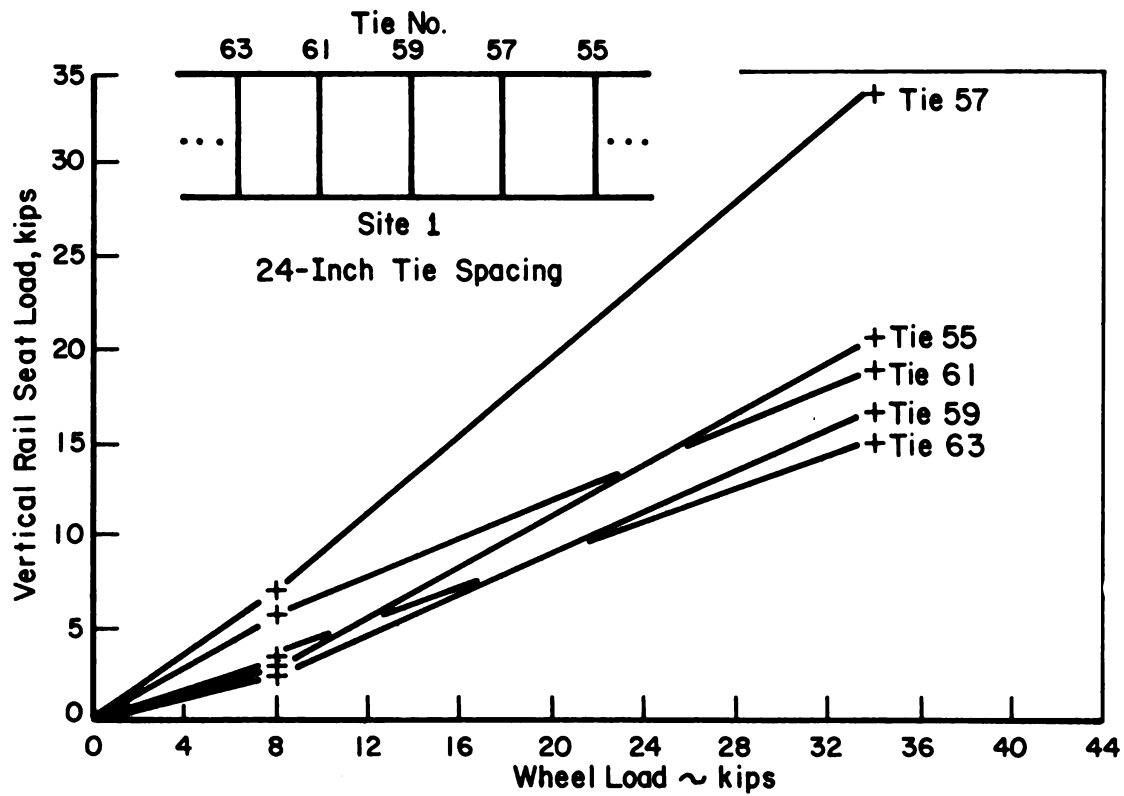


FIGURE 5-1a. MAXIMUM VERTICAL RAIL-SEAT LOAD AT SITE 1

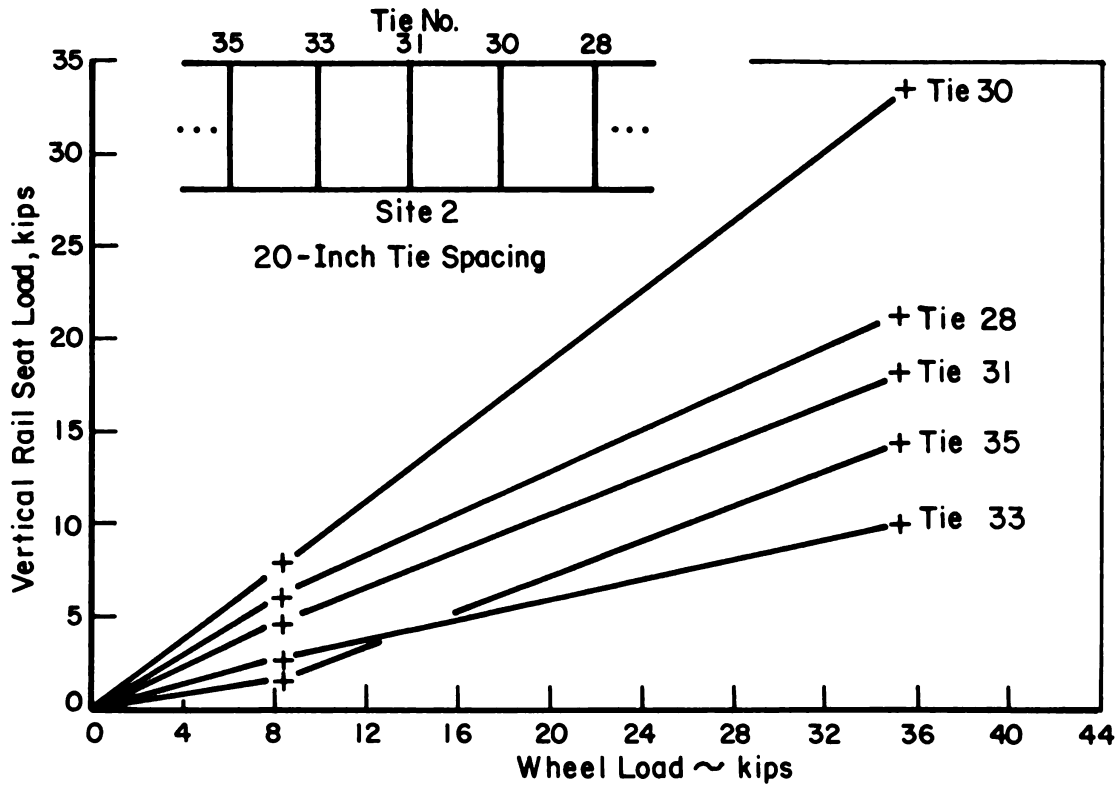


FIGURE 5-1b. MAXIMUM VERTICAL RAIL-SEAT LOAD AT SITE 2

TABLE 5-1. MAXIMUM MEASURED RAIL-SEAT TO WHEEL-LOAD RATIO (Q/P) IN PERCENT (%)

	Tie Number					Average
	1	2	3	4	5	
I. Tangent Track, 24-inch tie spacing (Site 1)						
a. Light Car	43	71	31	-	33	44.5
b. Heavy Car	47	58	53	-	65	55.8
II. Tangent Track, 20-inch tie spacing (Site 2)						
a. Light Car	22	38	64	-	76	50
b. Heavy Car	44	31	56	-	64	48.8

Figure 5-2 shows a comparison of measured and predicted rail seat loads for light and heavy car wheels centered in the main array of Site 2. Since the readings from ties 57 and 30 were eliminated, a symmetrical tie plate load distribution was assumed. The model parameters corresponding to a track modulus of 30.4 ksi per rail (final values from Table 4-1) were used for the predictions. It is evident from the load distribution shape that the actual track was stiffer than this.

As discussed in Section 4.3.1, it was hoped that data from the initial and final load cycles of the plate-bearing load-deflection tests would provide a bound to the estimate for the roadbed parameters. However, the comparison in Figure 5-2 shows that the plate-bearing test data are not providing a reliable prediction of roadbed stiffness even though the values for subgrade and ballast modulus appear reasonable when compared to the WES subgrade measurements and to typical values for ballast.

Since the FEC roadbed is stiffer than that predicted using the plate bearing data, the following procedure was adopted in an attempt to synthesize the model parameters that determine roadbed stiffness and track modulus. The ratio of ballast to subgrade modulus determined from the plate-bearing tests was retained, and the actual ballast (E_1) and subgrade (E_2) modulus values

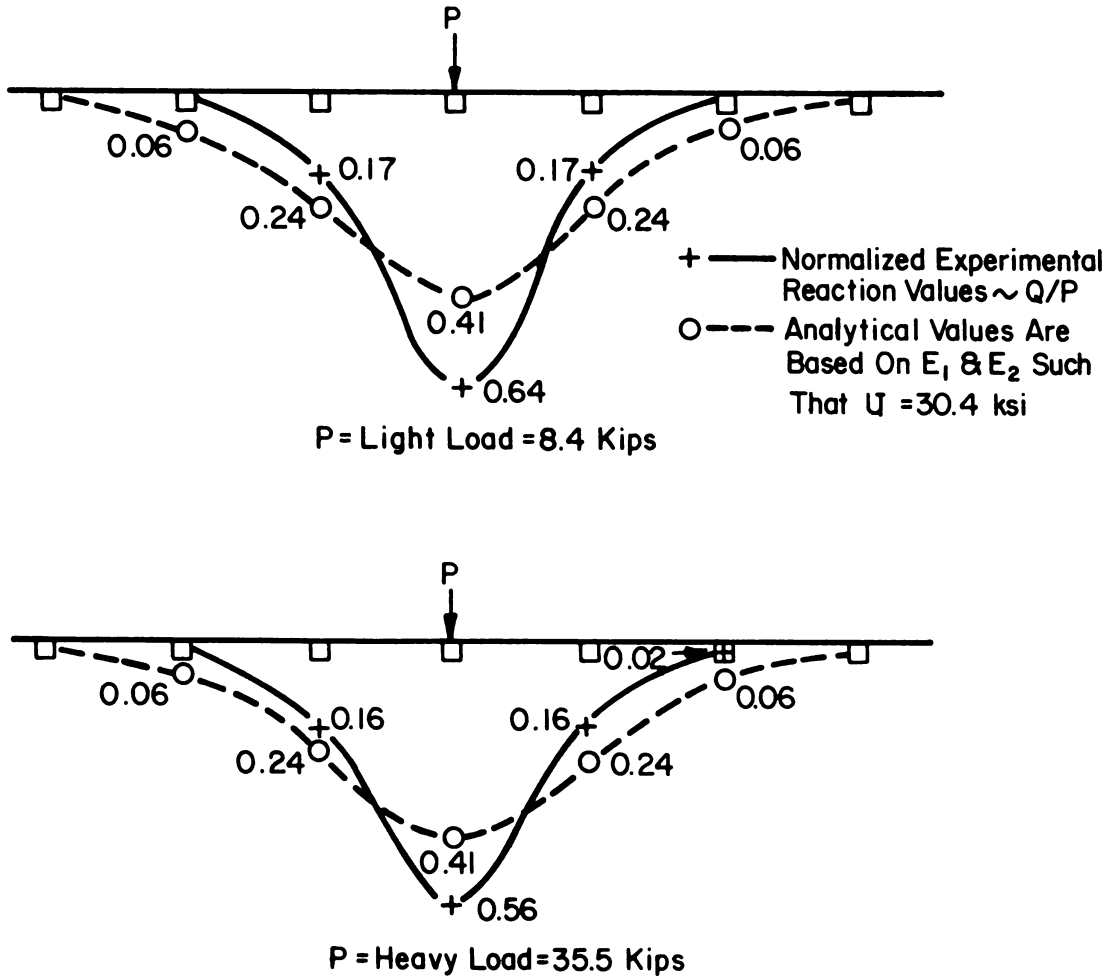


FIGURE 5-2. COMPARISON OF EXPERIMENTAL AND ANALYTICAL RAIL SEAT LOADS FOR SITE 2 (Tangent track with 20-inch tie spacing)

were increased so that the maximum predicted rail seat load equals the average maximum experimental rail seat load for the heavy car. The heavy car was chosen to reduce the effect of any nonlinearities. This procedure was used to adjust E_1 and E_2 values so that the maximum predicted vertical rail seat load was within 1.2 percent of the average experimental data for the 20-inch tie spacing (Site 2) and within 1.6 percent for the 24-inch tie spacing (Site 1). The adjusted values of foundation properties were

$$E_1 = 60 \text{ ksi and } E_2 = 35.65 \text{ ksi, with } \nu_1 \text{ and } \nu_2 \text{ equal to } 0.4.$$

Figures 5-3 and 5-4 compare measured and predicted rail seat loads with a heavy car wheel centered in the main array of the track for the 24-inch and 20-inch tie spacings, respectively. The average maximum experimental rail seat load was 18.9 kips for an applied load $P = 33.9$ kips in the 24-inch tie spacing ($Q/P = 55.8$ percent). This gives a track modulus of $U = 47.6$ ksi. With the same adjusted values of E_1 and E_2 , the maximum predicted rail seat load was 18.6 kips, and the predicted track modulus was 44.7 ksi. The lower predicted modulus is apparent from the comparison of the rail-seat load distribution shapes shown in Figure 5-3.

The average maximum experimental rail-seat load at Site 2 was 17.4 kips for an applied load $P = 35.5$ kips. This gives a track modulus $U = 58.2$ ksi. With the adjusted values of E_1 and E_2 , the maximum predicted rail-seat load was 17.2 kips, and the predicted track modulus was 55.4 ksi. Here again the lower predicted modulus is obvious from the comparison of experimental and analytical values shown in Figure 5-4.

These comparisons show that the actual track structure is at least as stiff as the predicted value with the adjusted modulus values of E_1 and E_2 . The tie/ballast pressure distribution data in the following section also support this conclusion.

5.1.2 Tie/Ballast Pressure Distribution

Tie bending moments at the rail seat and bending and torsional moments at the tie center have been identified as the major causes of concrete tie failures. The distribution of the support reaction between the

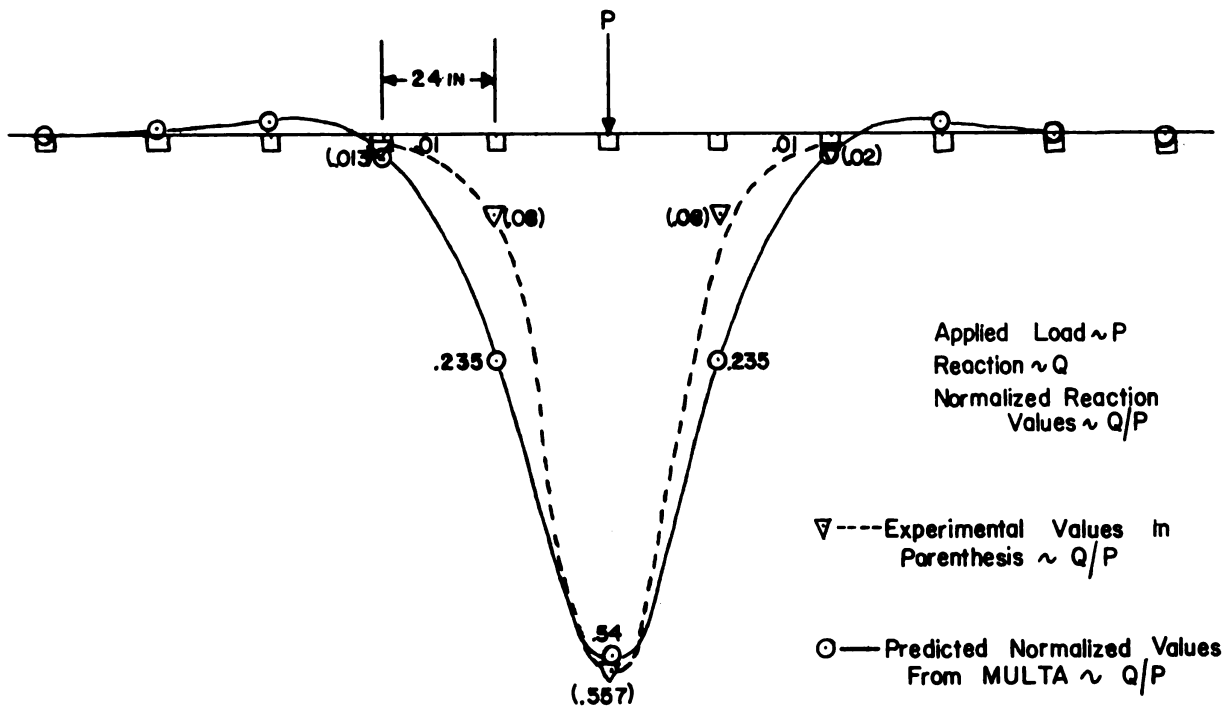


FIGURE 5-3. COMPARISON OF MEASURED AND PREDICTED VERTICAL RAIL SEAT LOADS AT SITE 1

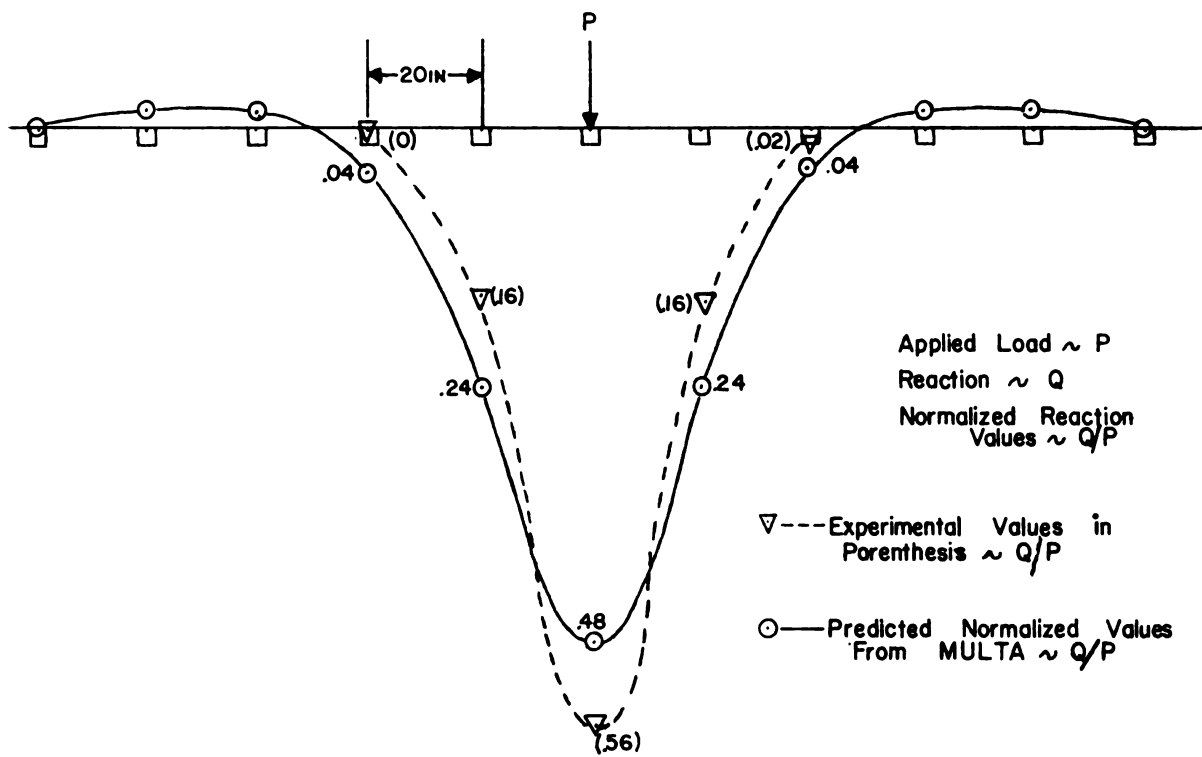


FIGURE 5-4. COMPARISON OF MEASURED AND PREDICTED VERTICAL RAIL SEAT LOADS AT SITE 2

tie and ballast is the principal unknown factor in validating the bending moments predicted by analytical models. Therefore, measurements of tie/ballast pressure distribution along the length of the tie were needed to validate fully the analytical prediction of bending moments at the tie rail seat and at the center.

Two load-cell ties were installed at Site 1 to measure the tie/ballast pressure distribution. The position and identification of each of these ties were as follows: LCT-18 (CT-1) was on the north side of the main array, and LCT-100 (CT-4) was on the south side of the many array, as shown in Figure 4-2. A third load-cell tie was installed in the curve track at Site 3. Recordings of the ballast pressure distribution under the tie for a few selected train passes were used to determine the shape of this distribution and to correlate the maximum pressure with the maximum rail seat loads.

The vertical tie/ballast pressures along the length of LCT-18 (CT-1) for heavy, medium, and light cars are shown in Figure 5-5. These pressure profiles indicate that this particular tie was noticeably center-bound for light car loads. That is, the tie center bears almost the entire load while the outer ends of the tie are carrying almost no load. As the magnitude of the load is increased, the peak pressures moved outward from the tie center toward the rail seat regions. The experimental data show that the peak pressure shift from the tie center to the rail seat region reaches a maximum on the gage side of the rail seat. Pressures up to about 40 psi were measured in the rail seat region for normal heavy cars. Maximum pressures as high as about 90 psi were observed from wheel flat impacts.

Predicted results from the MULTA program for the medium car weight are shown for comparison in Figure 5-5. The MULTA program assumes a uniform elastic support for the roadbed. The resulting tie-ballast pressure distribution is a maximum under the applied load (rail seat), and reaches a minimum at the tie center. The maximum predicted pressure of 33 psi is within 14 percent of the measured data for the medium load despite the center binding effect for this tie.

The only detectable malfunction for LCT-18 during the test program was that the end pressure cell (No. 10) didn't work. The experimental data in Figure 5-5 were graphically integrated, and vertical equilibrium was satisfied to within 4 percent of the total applied load. It can be concluded

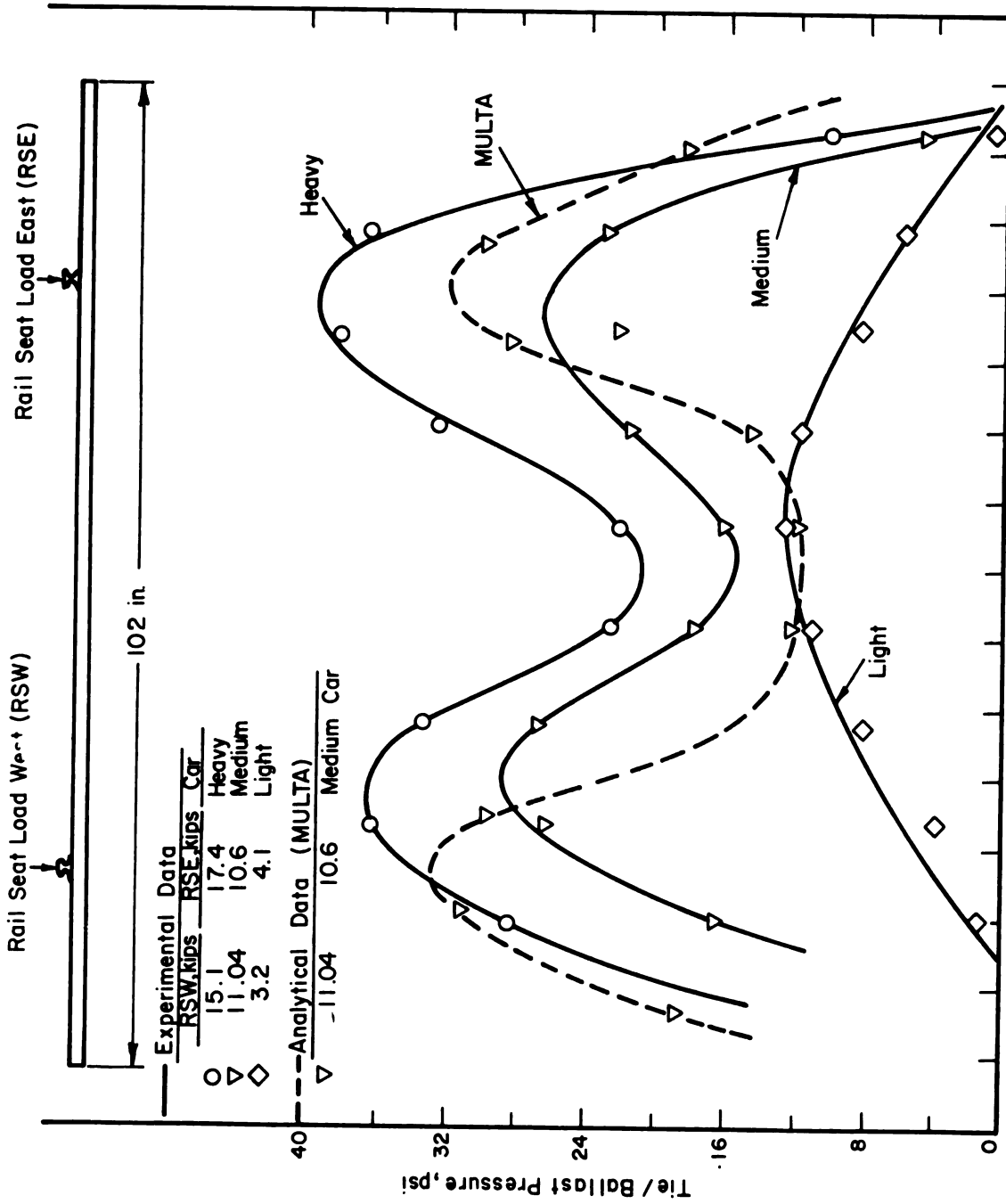


FIGURE 5-5. TIE/BALLAST PRESSURE DATA FROM LCT-18 AT SITE 1

that the pressure and rail-seat load cells from LCT-18 did operate satisfactorily. The load-dependent centerbinding effect was evident from the data, and it has a significant effect on the tie/ballast pressure distribution.

The experimental data shown in Figure 5-5 were normalized and replotted in Figure 5-6 so that peak pressures per unit rail seat loads can be easily determined. The MULTA results show that the ratio of peak pressure to applied rail seat load is approximately 3.0 psi/kip, and that the normalized peak pressure occurs under the rail seat region. The experimental results show that the ratio of peak pressure to applied rail seat load had an approximate maximum value of 3.2 psi/kip at the tie center for center binding under light loads and a maximum value of 2.5 psi/kip at the rail seat region for heavy loads.

Data from LCT-100 (CT-4) at Site 1 are shown in Figures 5-7 and 5-8. The results from the MULTA analysis are also shown for comparison. Since the results from the MULTA program guarantee system equilibrium, the comparison shows that either the pressure load cells or the rail seat load cells, or both, were not operating correctly. Integration of the pressure distribution from the measured data showed that the total load on the tie bottom was 50 percent higher than the total rail seat loads. Considering the experimental results in Figure 5-6, it might be argued that the high pressures were caused by the ballast under the rail seats being well consolidated and behaving like "hard" springs. However, this cannot be the case since vertical equilibrium still must be satisfied regardless of the nonlinearities in the roadbed system. It was therefore concluded that the experimental data from LCT-100 were inaccurate. The normalized pressure curve in Figure 5-7 supports this conclusion.

The experimental data from the load cell tie in the curved track section (Site 3) are shown in Figure 5-9 and 5-10. This tie is identified as LCT-0 (CT-2). Tie-ballast pressure distributions along the length of the tie for light, medium, and heavy wheel loads are shown in Figure 5-9. An integration of the pressure distributions showed that vertical equilibrium was satisfied to within 3 percent of the respective applied loads. This load cell tie was apparently operating effectively.

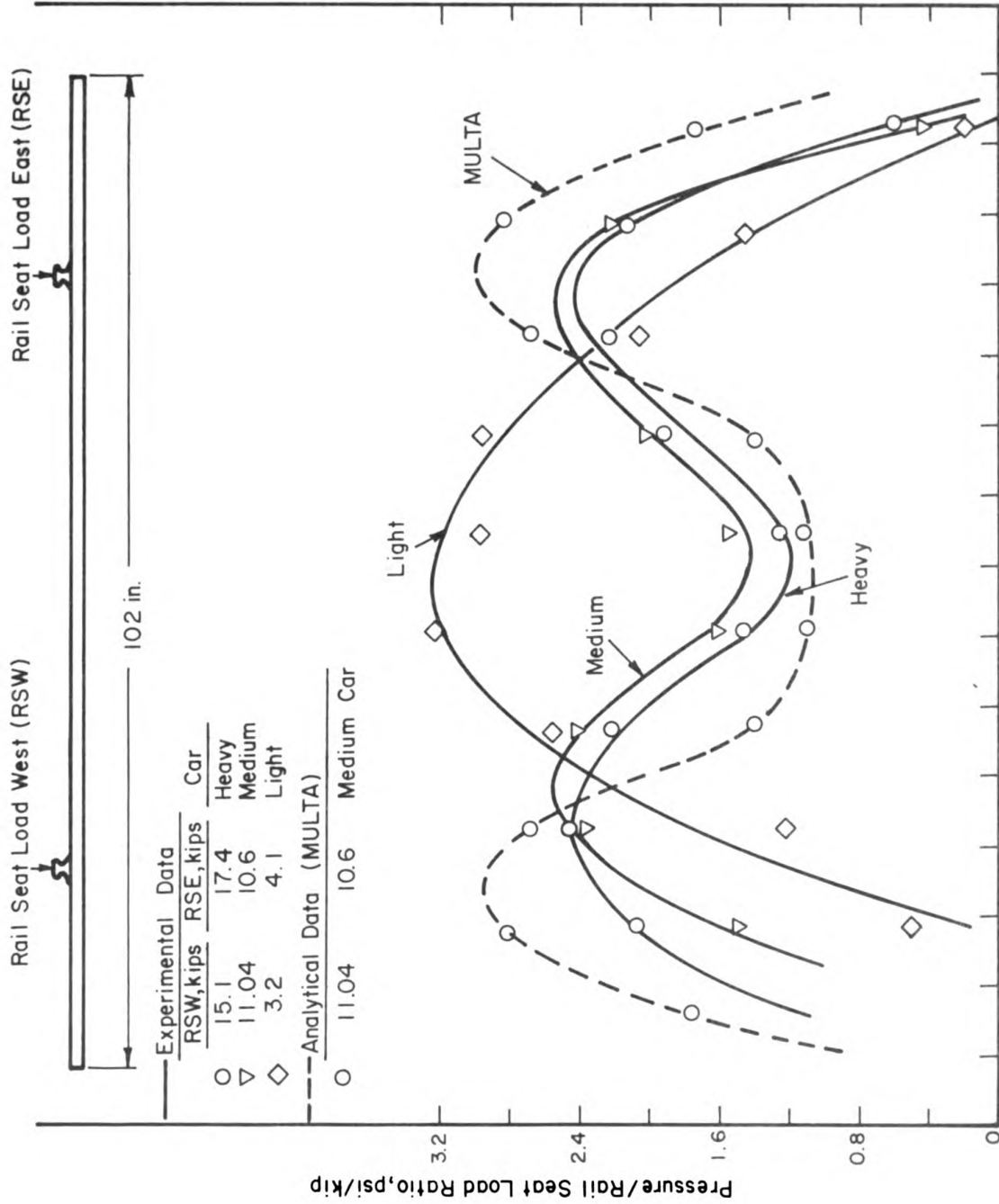


FIGURE 5-6. BALLAST/TIE VERTICAL PRESSURE NORMALIZED TO RESPECTIVE RAIL SEAT REACTION, LCT-18 AT SITE 1

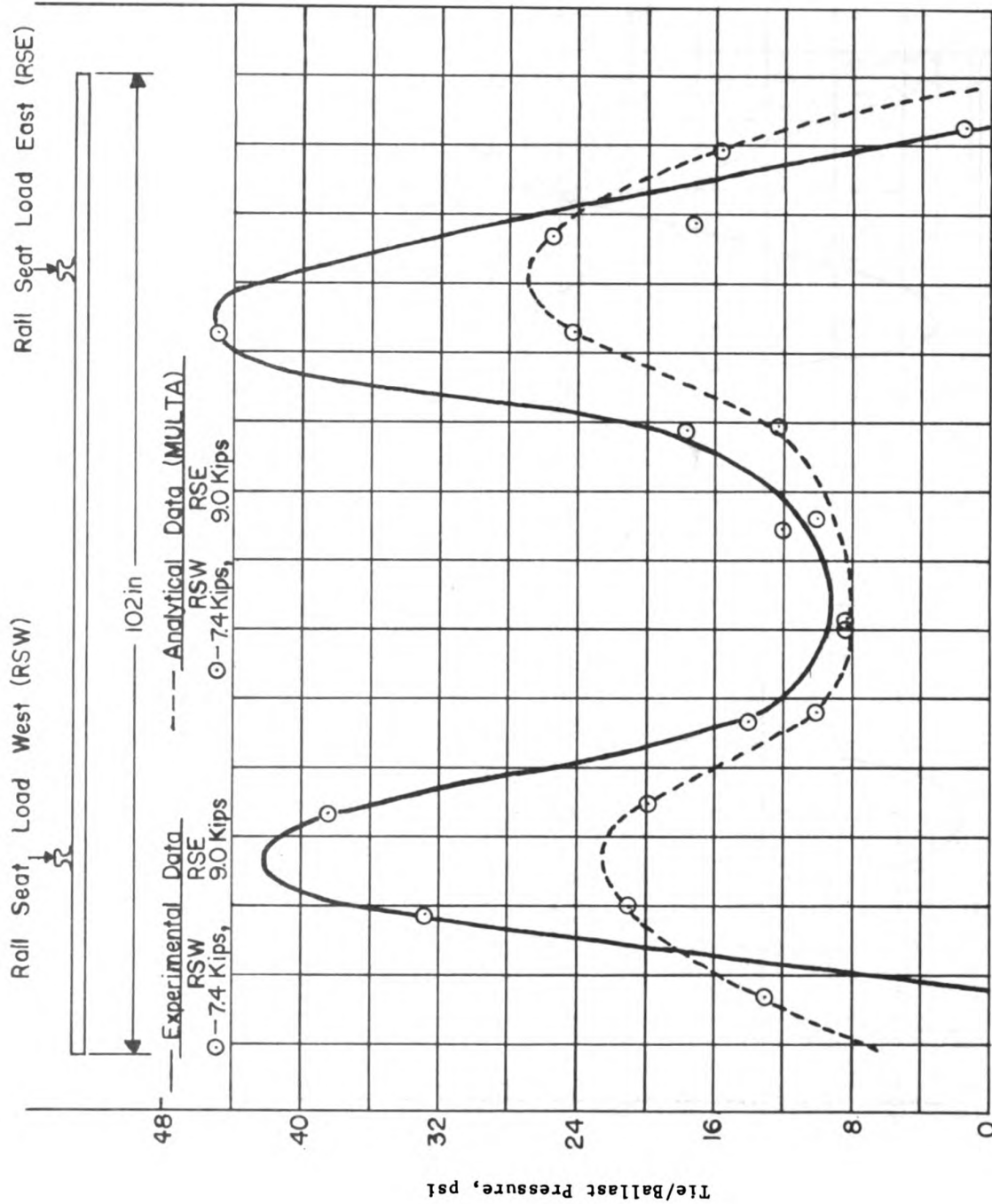


FIGURE 5-7. TIE/BALLAST PRESSURE DATA FROM LCT-100 at SITE 1

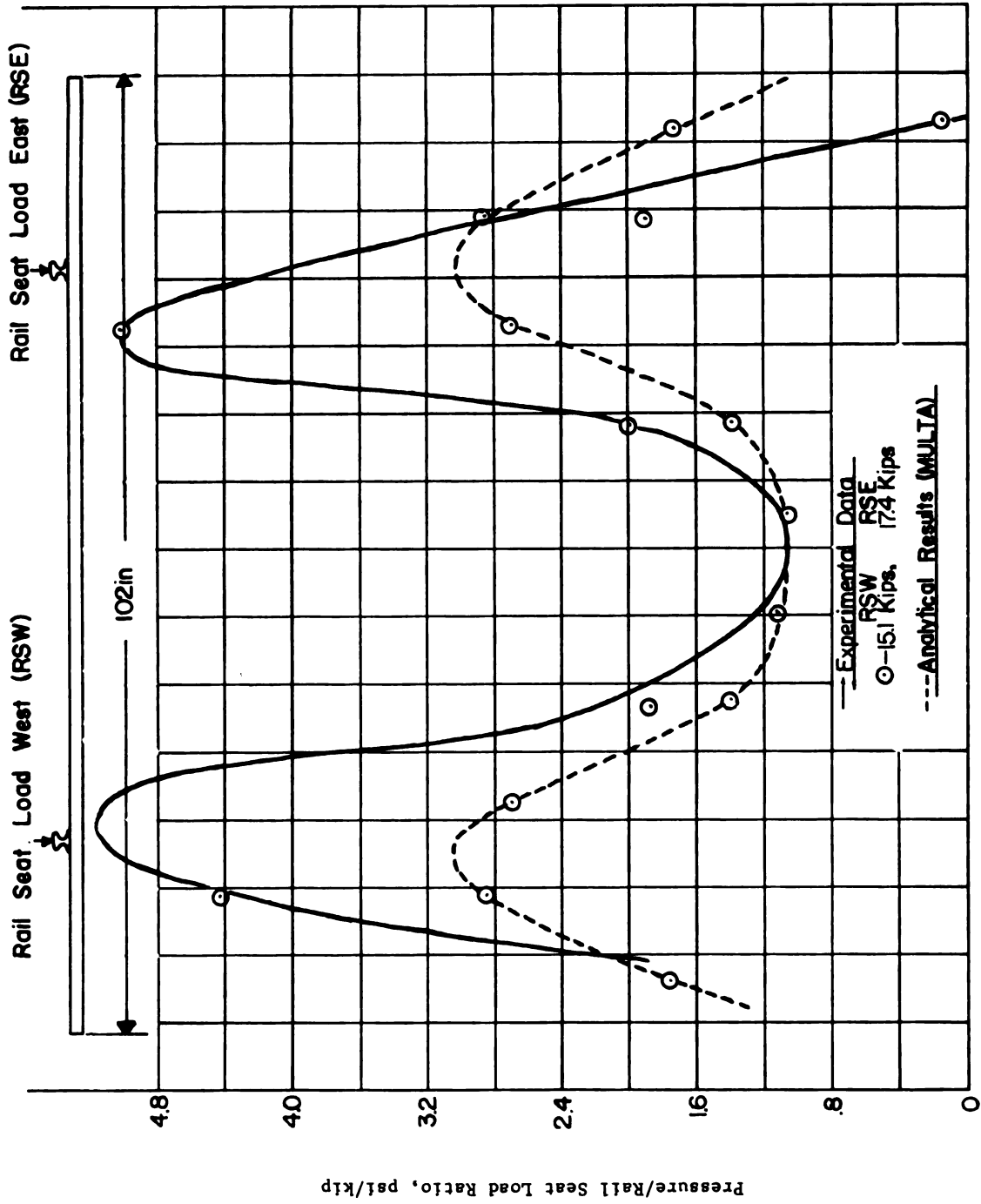


FIGURE 5-8. BALLAST/TIE VERTICAL PRESSURE NORMALIZED TO RESPECTIVE RAIL SEAT REACTION, LCT-100 at SITE 1

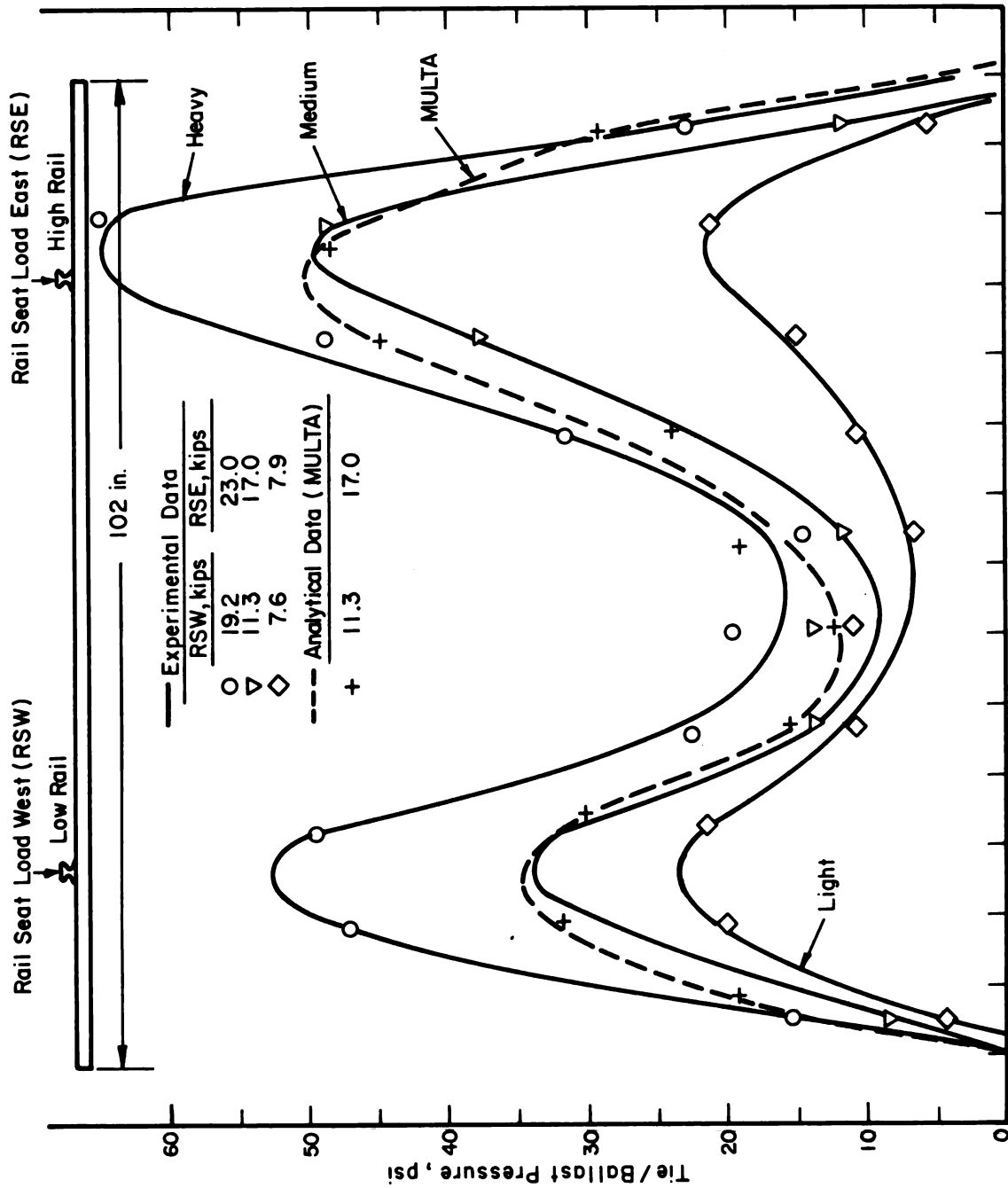


FIGURE 5-9. TIE/BALLAST VERTICAL PRESSURE, LCT - 0 DATA AT SITE 3

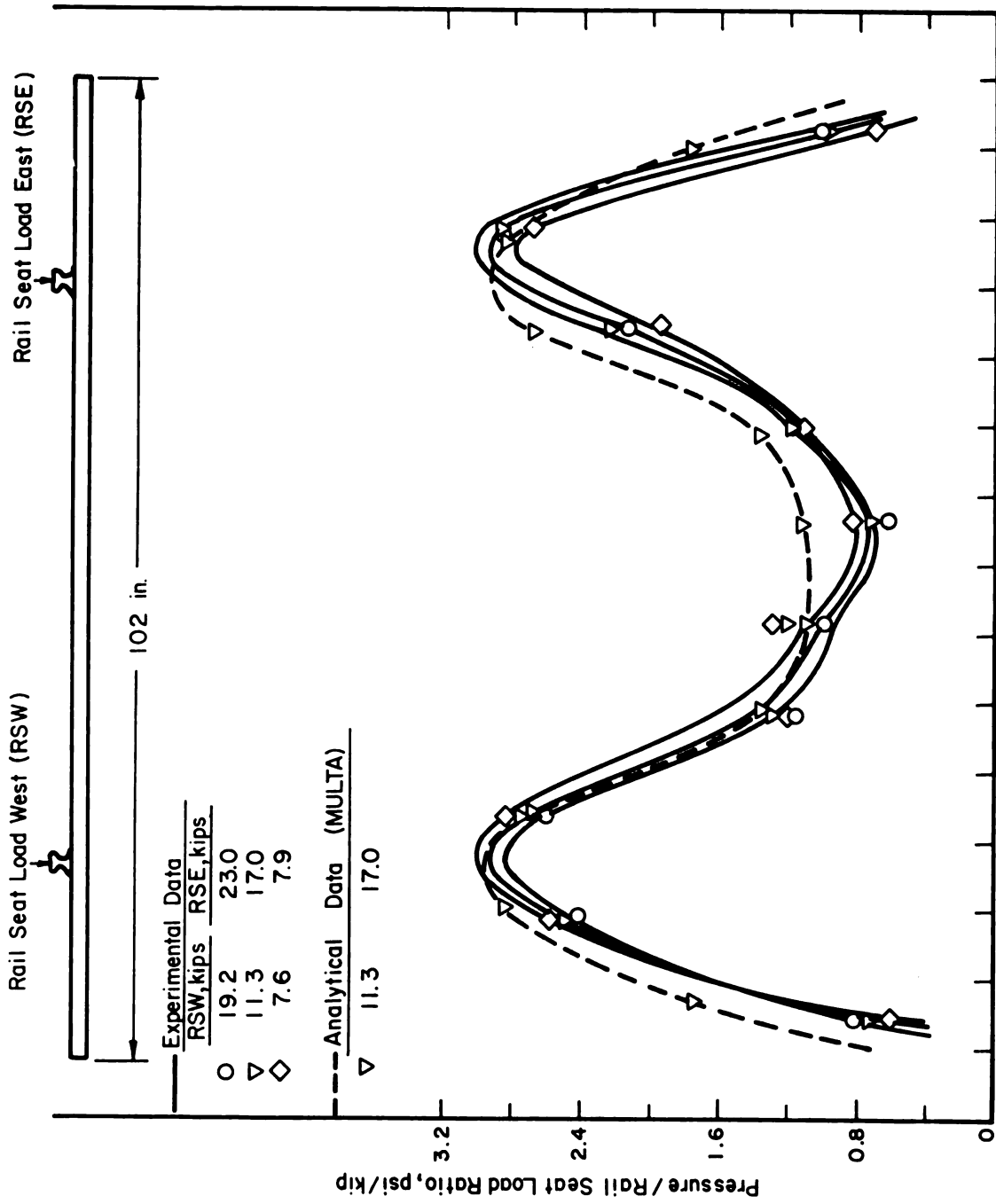


FIGURE 5-10. BALLAST/TIE VERTICAL PRESSURE NORMALIZED TO RESPECTIVE RAIL SEAT REACTION, LCT-0 DATA AT SITE 3

The results from the MULTA program shown in Figure 5-9 for medium wheel loads show good agreement with the experimental data. Maximum pressures are predicted within 5 percent, and the shape of the pressure distribution is very similar. It is also evident that the vertical load is considerably greater on the high rail.

The normalized pressure distributions for the three cases of light, medium, and heavy wheel loads are shown in Figure 5-10. The small variation shows that the support reactions for this tie behaved in a very linear manner, and that the uniform elastic foundation used in the MULTA program gave very good predictions for the pressure distributions for all wheel loads.

The results from the analytical model can also be used to predict bending moments for the rail seat and tie center. The pressure distributions for the medium wheel load shown in Figure 5-9 were used to calculate the shear and bending moment distributions along the tie length that are shown in Figures 5-11 and 5-12. Since the analytical and experimental pressures were in good agreement, the predicted bending moments should be equally accurate. Thus it is concluded that the MULTA model is capable of predicting rail seat and tie center bending moments that are typical of service loads except when ties have a very serious center binding condition. However, the data from LCT-18, which did have severe center binding for light wheel loads, were even in reasonably good agreement with predicted results for heavy wheel loads.

5.1.3 Track Displacement Predictions

Results from the MULTA program were used to determine how the track displacement compares to that for a Winkler foundation. The data shown in Figure 5-13 show that predicted displacements are distributed over a greater length of track than the tie load distribution. The difference in the displacement shape predicted by MULTA and the tie load distribution indicates that the rail is not behaving like a beam on a Winkler type foundation. The two distributions would be identical for a Winkler foundation.

The same conclusions regarding the displacement being distributed over a greater distance than the tie loads is evident in the data from Site 2

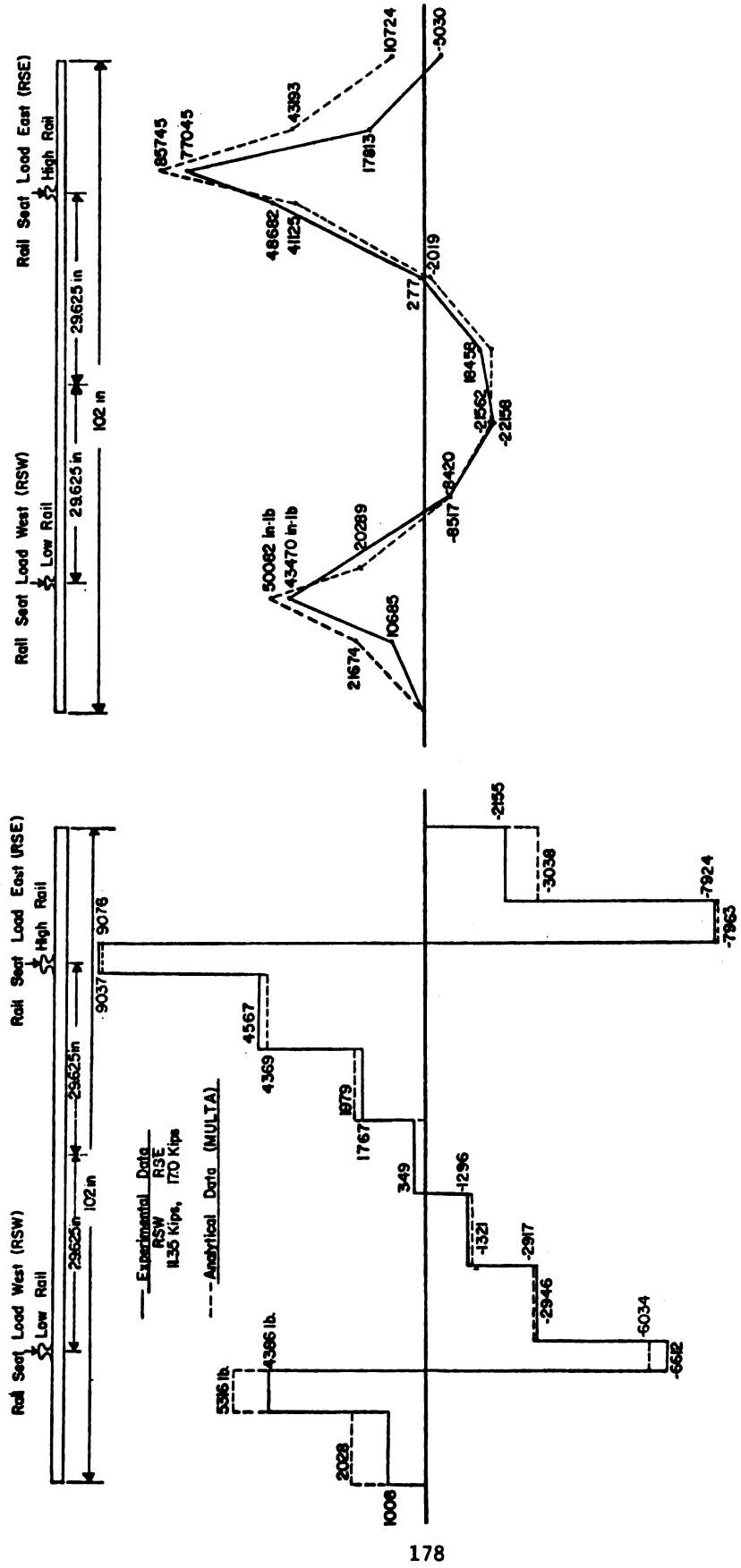


FIGURE 5-11. TIE SHEAR FORCE, LCT-0 DATA (SITE 3)

FIGURE 5-12. TIE BENDING MOMENT, LCT-0 DATA (SITE 3)

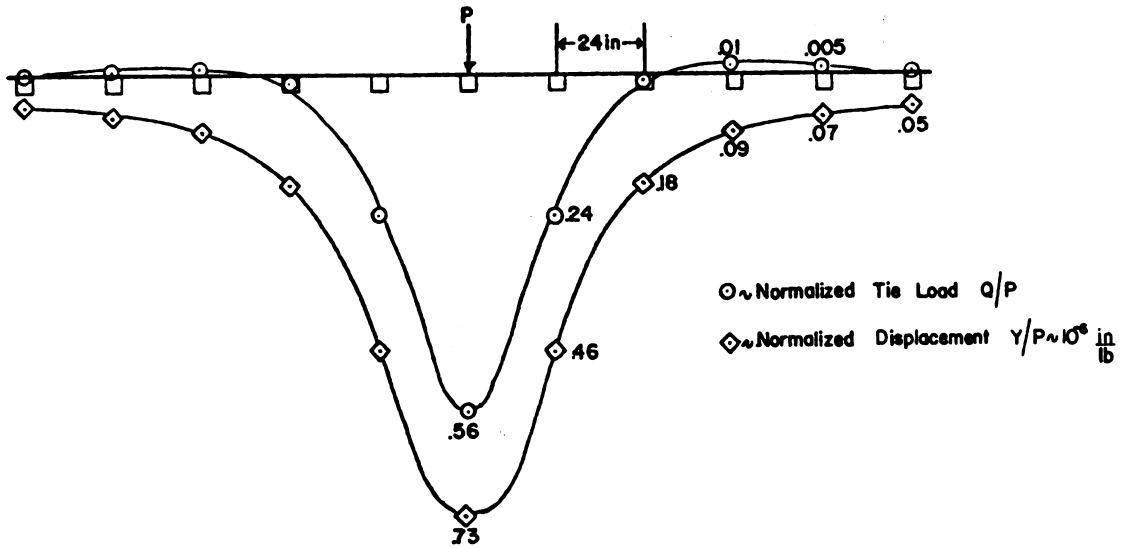


FIGURE 16. PREDICTED TIE LOAD AND DISPLACEMENT DISTRIBUTION (SITE 1)

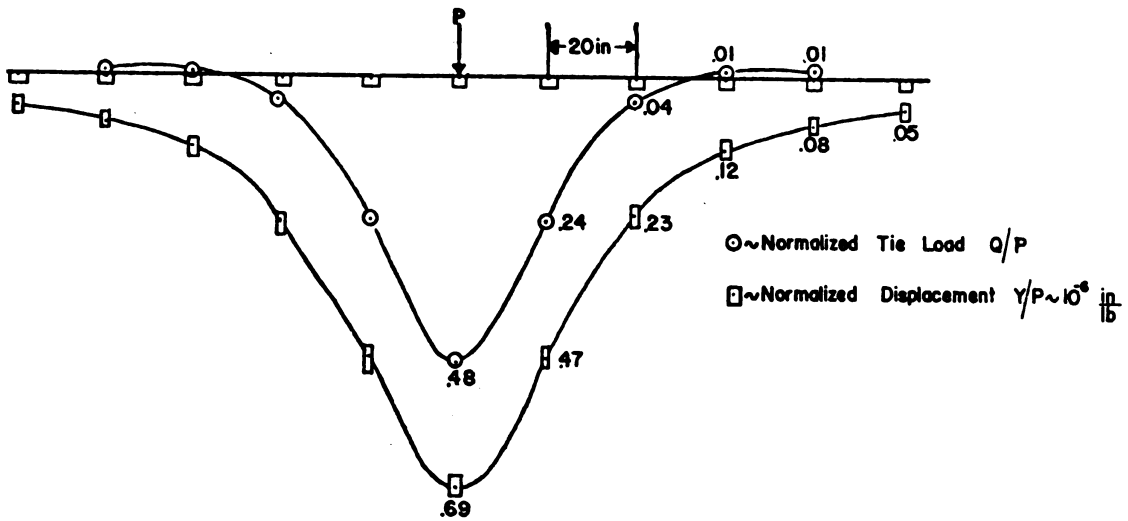


FIGURE 5-14. PREDICTED TIE LOAD AND DISPLACEMENT DISTRIBUTIONS (SITE 2)

(20-inch tie spacing). Comparison of Figures 5-13 and 5-14 show the influence of tie spacing on tie load and displacement. The predicted peak tie load and displacement values are reduced by 14 percent and 15 percent, respectively, when the tie spacing is reduced 16 percent from 24 to 20 inches.

Vertical rail displacements were measured at two locations at each test site. These vertical displacements were measured at the middle tie of the main array and at a tie about 35 feet outside the main array. Since only two locations were instrumented at each test site for vertical displacement data, it was difficult (in view of the local variations previously discussed) to characterize the track structure with experimental displacement values. However, some comparisons can be made with the results from the model.

Table 5-2 shows a comparison between measured track displacement values and values predicted from the model. In Table 5-2, ΔY = differential displacement for heavy and light wheel loads. This differential load, ΔP , was 24,750 pounds.

These experimental values show the variation in displacement values from site to site. In view of this variation, it is believed that more values of displacement (per test site) are required so that average maximum displacement values could be used to better predict track modulus. However, the alternative approach of averaging data from five instrumented tie plates gave good results.

5.1.4 Track Modulus Measurements

It was originally planned that rail bending strains measured under heavy and light loads similar to the displacement values would provide a check on the track modulus determined from the displacement data. However, the lack of a sufficient number of strain gages (i.e., at many positions along the length of the rail) prevents the sort of averaging process that subsequently was determined essential to minimize local variations. Difference (heavy load minus light load) stress and displacement values and corresponding track moduli are listed in Table 5-3.

**TABLE 5-2. COMPARISON OF MEASURED AND PREDICTED
TRACK DISPLACEMENTS**

Site Description	Measured Values $\Delta Y \sim \text{in.}$	Predicted Values $\Delta Y \sim \text{in.}$
I. Tangent Site		
24-inch Tie Spacing (Site 1)		
Main Array	0.015	0.018
Outside Main Array	0.0135	0.018
II. Tangent Site		
20-inch Tie Spacing (Site 2)		
Main Array	0.029	0.017
Outside Main Array	0.008	0.017
III. Curved Site		
25-inch Tie Spacing		
Main Array	0.034	0.018
Outside Main Array	0.044	0.018

TABLE 5-3. MEASURED VALUES OF TRACK MODULUS

Site Description	Δ Stress, (Psi)	Δ Disp. (in.)	Measured Track Modulus	
			Disp. ⁽¹⁾ (lb/in./in.)	Strain ⁽²⁾ (lb/in./in.)
I. Tangent Site, 24-inch Tie Spacing Main Array	4575	0.015	39,100	45,900
		Outside Main Array	0.0135	41,000
II. Tangent Site, 20-inch Tie Spacing Main Array	3850	0.029	18,300	87,000
		Outside Main Array	0.008	82,000

- (1) Calculated track modulus using rail differential displacement for light and heavy wheel loads.
- (2) Calculated track modulus using differential rail bending strains for light and heavy loads.

The values of track modulus shown in Table 5-3 indicate that the track structure is quite stiff. However, the data in Table 5-3 are for one or two discrete points along a rail at a particular test site, and they do not represent any sort of averaged values. As such, they should not be considered as truly representative of the overall track modulus.

Table 5-4 gives a summary of the track modulus values that were implicitly or explicitly generated from the test data. This summary directly compares the predicted and experimental modulus values discussed previously in other sections.

5.1.5 Track Response for Light and Heavy Cars

Figure 5-15 shows the track response for a slow roll-by of the work train at Site 1. The work train consist was one empty and one loaded 100-ton hopper car with a 4-axle locomotive. The first three channel outputs show vertical rail seat loads and the last four channels show bending stresses at the rail head and rail base.

The vertical tie plate load traces show the load-dependent behavior of track stiffness. For the high wheel loads, each axle produces a discrete load pulse and the maximum load from each axle is virtually unaffected by the load from adjacent axles. This absence of coupling from adjacent axles is only found on track where the modulus is quite high. However, the tie plate loads do show considerable coupling with the light wheel loads, which is indicative of an initially softer track foundation.

The recordings of bending stress in the rail base are quite typical. However, the bending stresses in the rail head shown in Figure 5-15 do display an interesting stress reversal phenomenon. This reversal effect can best be modeled and explained by considering the head of the rail as a separate beam acting on an elastic foundation consisting of the rail web. This local response is superimposed with the overall bending of the rail, which produces tension in the rail base and compression in the rail head as the wheel passes over a given location. Local bending of the rail head appears like a beam with its neutral axis somewhere between the top of the rail head and the fillet such that the fibers at the fillet are in tension immediately under the wheel. This produces the stress reversal over a very short length as shown in Figure 5-15.

TABLE 5-4. SUMMARY OF TRACK MODULUS VALUES

Site Description	Measured Track Modulus ~ ksi			Predicted Track Modulus ~ ksi		
	Displacement (1)	Strain (2)	Average Tie (3) Plate Loads		Foundation Parameters from Plate Bearing Tests (4)	Adjusted Values of E_1 and E_2 (5)
			Light	Heavy		
I. Tangent Site 24-inch Tie Spacing Main Array	39.1	45.9	18.9	47.6	15.2 - 25.5	44.7
Outside Main Array	41				15.2 - 25.5	
II. Tangent Site 20-inch Tie Spacing Main Array	18.3	87	62.6	58.2	10.5 - 30.4	55.4
Outside Main Array	82				10.5 - 30.4	

- (1) Calculated track modulus using rail displacement for light and heavy wheel loads.
- (2) Calculated track modulus using rail bending strains for light and heavy wheel loads.
- (3) Based on average maximum tie plate loads on 4 ties, light load \approx 8 kips, heavy load \approx 34 kips.
- (4) Range for initial to final values for model parameters based on predicted maximum tie plate load. (See Table 4.1)
- (5) E_1 = ballast modulus and E_2 = subgrade modulus, adjusted so that maximum predicted rail seat load equals average maximum experimental rail-seat load at Site 1.

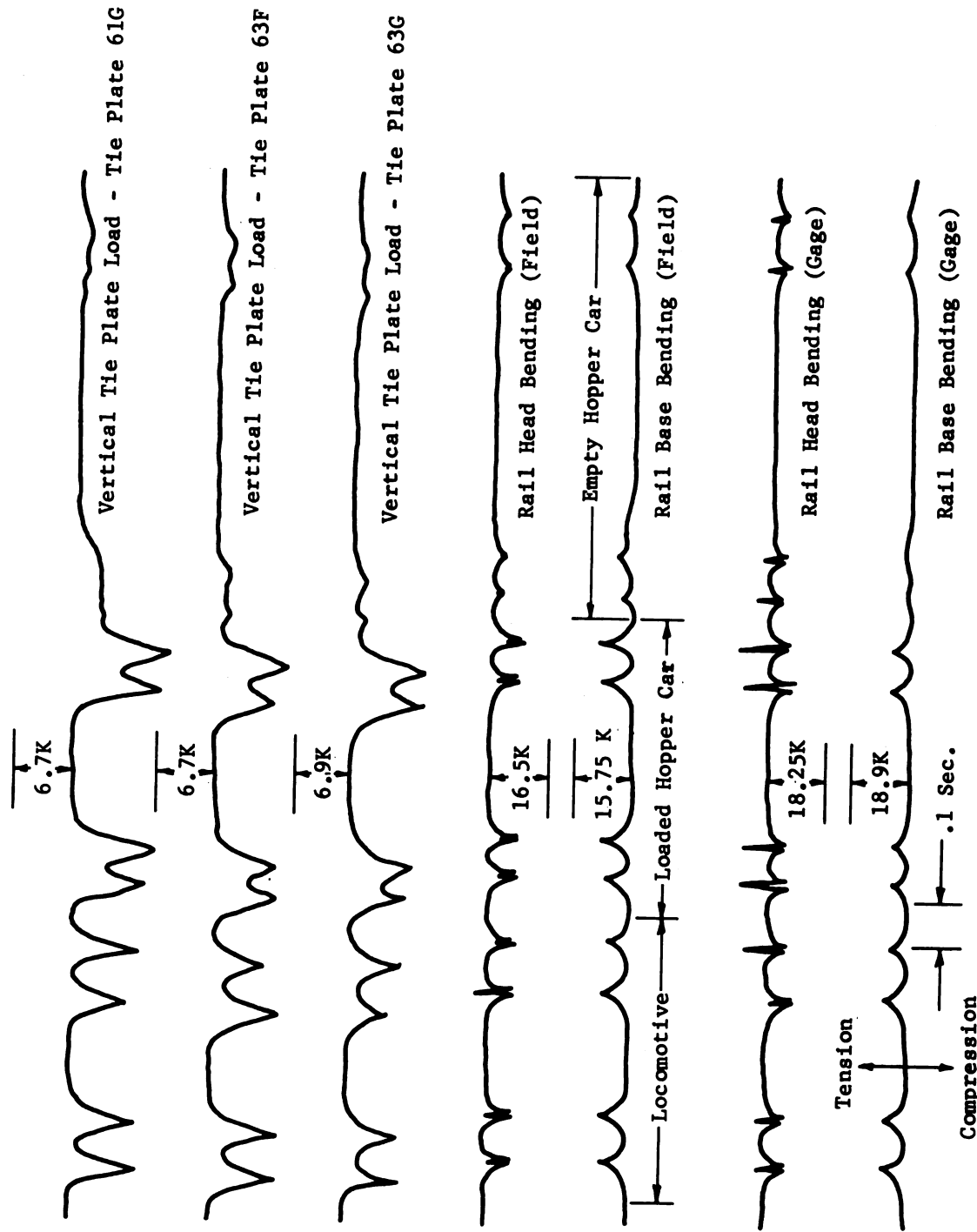


FIGURE 5-15. TRACK RESPONSE FOR SLOW RAIL BY OF WORK TRAIN AT SITE 1

Results from the MULTA program are shown in Figure 5-16, where the vertical tie-plate loads from two successive wheel loads have been superimposed. The results from the MULTA program are generally consistent with the observed results for heavy wheel loads where the influence from adjacent wheels on this stiff track is negligible.

5.2 SUMMARY OF RESULTS AND CONCLUSIONS

The comparison of predicted and measured track response parameters in the previous section shows that the MULTA track analysis program is capable of making good predictions of tie loads and tie/ballast pressures. The inclusion of tie bending has been shown to be quite important in predicting ballast pressures. The program can also be used to predict rail bending stresses and tie bending moments.

No experimental data on stresses in the ballast and subgrade below the tie were measured for comparison. However, the good agreement with the predicted ballast pressures immediately under the tie gave confidence that pressures predicted elsewhere in the roadbed will be sufficiently accurate for track design evaluations. Predictions of soil behavior are limited by the assumptions of linear elasticity in the MULTA model, so inelastic behavior of highly loaded soils could not be predicted accurately.

The major difficulty in using MULTA, or any other track analysis program, is in the accurate modeling of the ballast and subgrade. The elastic continuum used in the MULTA model does show that the transfer of shear in the roadbed produces appreciable tie-to-tie coupling in displacements. This effect is also observed in track response measurements but it is not included in conventional beam-on-elastic-foundation models. However, the real difficulty is in establishing the material properties for a layered model of the ballast and subgrade that match the overall track modulus measurements. The plate bearing tests on the ballast and subgrade and independent vibroseismic measurements of subgrade properties did not give sufficiently accurate predictions of the track modulus for predicting track loads with heavy wheel loads even though pressures in excess of maximum pressures under traffic were used for the plate bearing tests. This difficulty cannot be explained at this time. However, it is hoped that current research on the use of plate bearing tests to evaluate ballast compaction being carried out by Dr. Ernest Sel

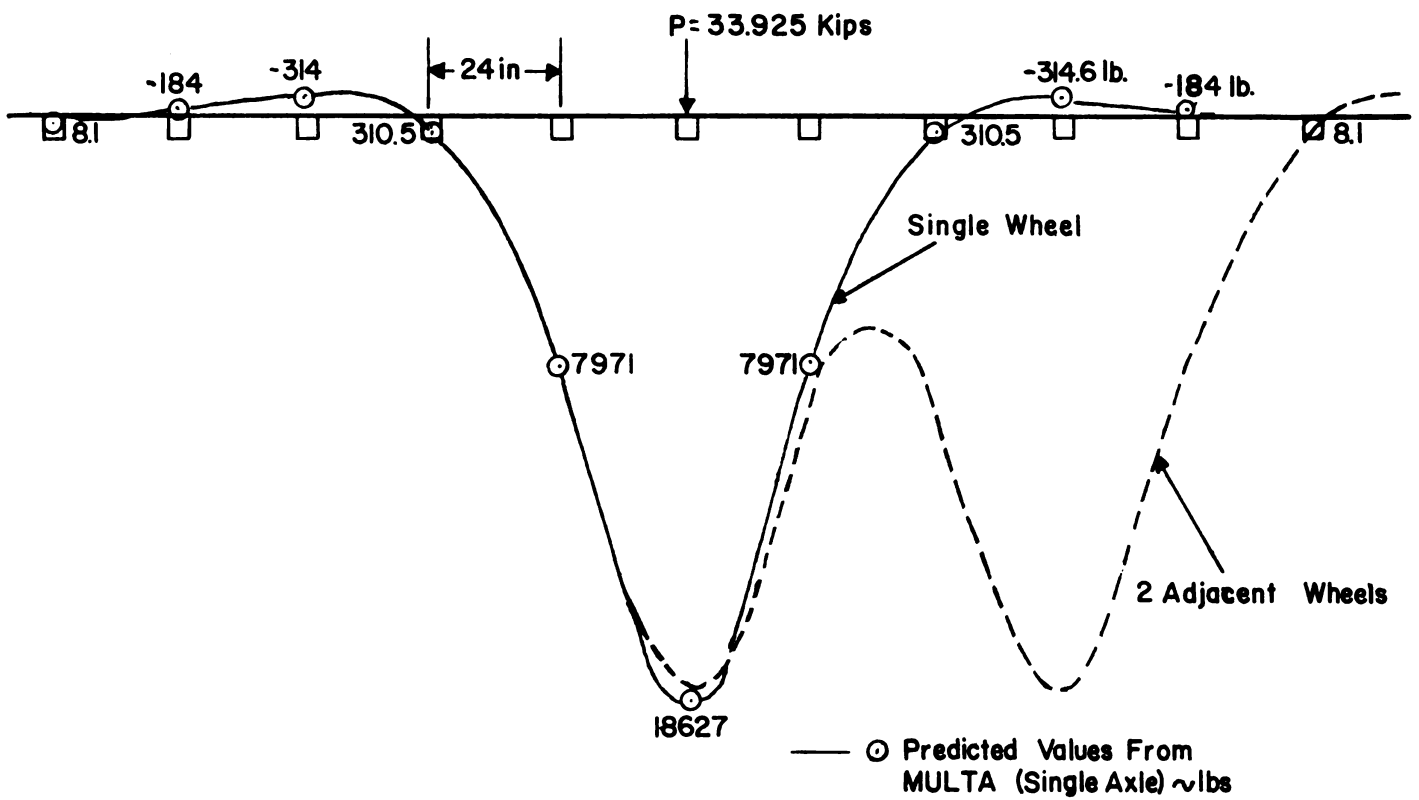


FIGURE 5-16. INFLUENCE OF ADJACENT AXLE ON TIE PLATE REACTIONS AT SITE 1

on a concurrent DOT/TSC project will help to resolve this question. In the meantime, it is recommended that the ballast and subgrade properties be adjusted to match experimental measurements of track modulus under heavy wheel loads using representative soil data for the relative ballast/soil stiffness. Predictions of tie loads, track deflections, and roadbed pressures will not be greatly influenced by changes in the relative ballast and soil stiffnesses as long as the track modulus is matched. Inaccurate estimates of these parameters will have the greatest effect on predicting relative deflections in the ballast and subgrade layers.

APPENDIX A

REVIEW OF TRACK ANALYSIS MODELS

Introduction

An important part of this project for improving synthetic cross tie/fastener assemblies is the prediction of detailed stress and deflection distribution for the rail, fastener, tie, ballast, and subgrade. These predictions can then be used to evaluate track structure deterioration. To this end, many different mathematical models have been reviewed. In general, these analysis techniques fall into one of four categories: algebraic expressions for ballast and subgrade pressures, finite element models, exact solutions to differential equations, and lumped parameter models.

Algebraic expressions for ballast and subgrade pressures are usually obtained from the theory of elasticity. The most significant problems with this approach are the simplistic assumptions about boundary conditions and material properties which are necessary to develop closed-form solutions. Some investigators have introduced correction factors to account for the inconsistency between theory and experiment. While this method will provide good results for many conditions, it will not provide realistic answers for non-uniform roadbed conditions such as soft spots in the ballast or subgrade.

Algebraic Equations for Ballast and Subgrade Pressures and Deflections

Talbot's Equation

The empirical model developed by Talbot [A-1] can be used to predict the vertical pressure, P , at a depth, h , and at a horizontal distance, x , from the line of action of the load. It is assumed that the ballast and subgrade material is a homogeneous, noncohesive granular substance. The applied

vertical pressure is a constant over the tie length, which is considered to be a rigid element. The normal flexibility of a tie causes variations in the tie/ballast pressure along the tie bottom. The vertical pressure as given by Talbot is

$$P = \frac{KP_0 \exp(-K^2 x^2)}{\sqrt{\pi}} \quad (A-1)$$

where

P_0 is the applied vertical pressure and

K is an experimentally determined parameter that depends on h . Inputs to this model include the vertical (static) load and effective tie dimensions to calculate the applied vertical pressure. The parameter K must be determined experimentally. Manual superposition can be used to account for the effects of multiple ties.

Several other empirical pressure equations are available and a comparison of pressure predictions from some of these empirical equations and measured data are shown in [A-2]. The pressure values determined by the empirical equations are frequently higher than measured pressures. Thus, predictions from the empirical equations give a conservative estimate of the pressures in the track substructure.

Pyramid of Stress Model

The pyramid of stress model [A-2] is an attempt to account for spreading of the stress distribution with depth. Vertical pressure and deflection are uniform at every depth, while material outside the pyramid is not stressed at all. There are no horizontal stress components. The area at the top of this truncated pyramid is determined by the tie bearing area, while the area at the bottom is determined by the angle of internal friction and the depth of the ballast and subgrade, Figure A-1. This model does calculate pressures, and it also gives an effective stiffness of the ballast and subgrade under the tie. This stiffness can be combined in series with the pad and tie stiffnesses to give a total rail support stiffness at each tie. Since the ballast and subgrade are two different materials, a more sophisticated model can be derived by assuming a ballast pyramid on top of a subgrade pyramid [A-2].

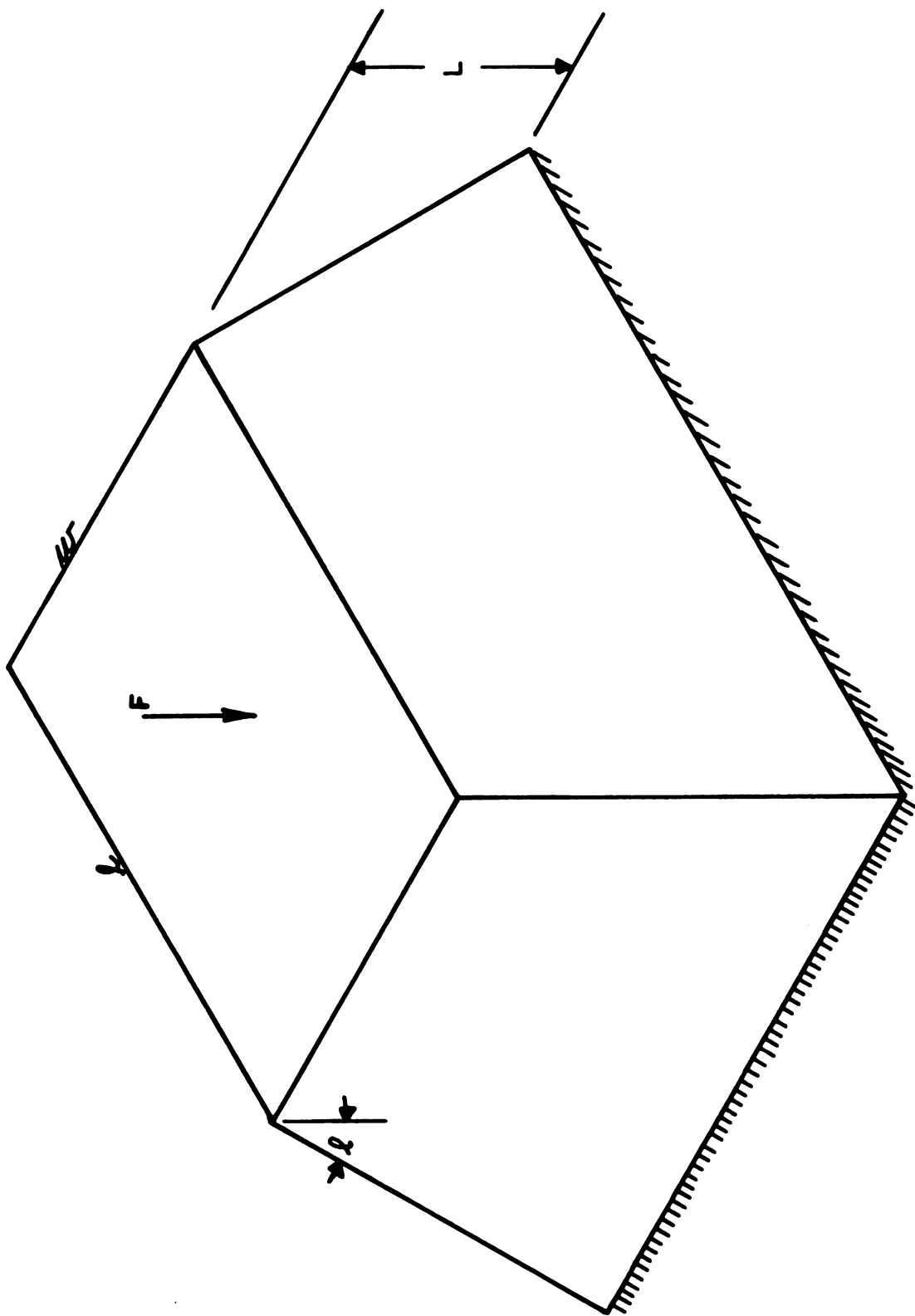


FIGURE A-1. PYRAMID MODEL

The equation for stiffness in the pyramid model is found by considering the soil as a rod of length L in the shape of a truncated pyramid with a compressive force, F , acting on its top.

The equation for the compressive deflection, $d\delta$, of a rod of length dh is

$$d\delta = \frac{F}{E} \frac{dh}{A(h)}. \quad (A-2)$$

Expressing $A(h)$ in terms of W , L , C , and h , and integrating Equation (A-2) will lead to the effective stiffness of the pyramid.

$$K = \frac{E C (l-w)}{\ln \left[\frac{l(CL+w)}{W(CL+l)} \right]}, \quad (A-3)$$

where

E is Young's modulus

$C = 2 \tan \alpha$

α = angle of internal friction.

In the derivation of Equation (A-3), Young's modulus for the soil, the angle of internal friction and the force acting on the top of the pyramid are assumed constant with depth. These assumptions are discussed in [A-2].

Boussinesq's Equation

A vertical external force Q acts normal to the surface of a semi-infinite solid producing a state of stress which has circular symmetry about a vertical line through the point of application, Figure A-2. The soil is considered to be homogeneous and isotropic.

The stresses at N as determined by Boussinesq [A-3] are:

$$\sigma_z = \frac{3Q}{2\pi Z^2} \cos^5 \psi + Z\gamma \quad (A-4)$$

$$\sigma_r = \frac{Q}{2\pi Z^2} \left[3 \cos^3 \psi \sin^2 \psi - (1 - 2\mu) \frac{\cos^2 \psi}{1 + \cos \psi} \right] + \frac{\mu \gamma Z}{1 - \mu} \quad (A-5)$$

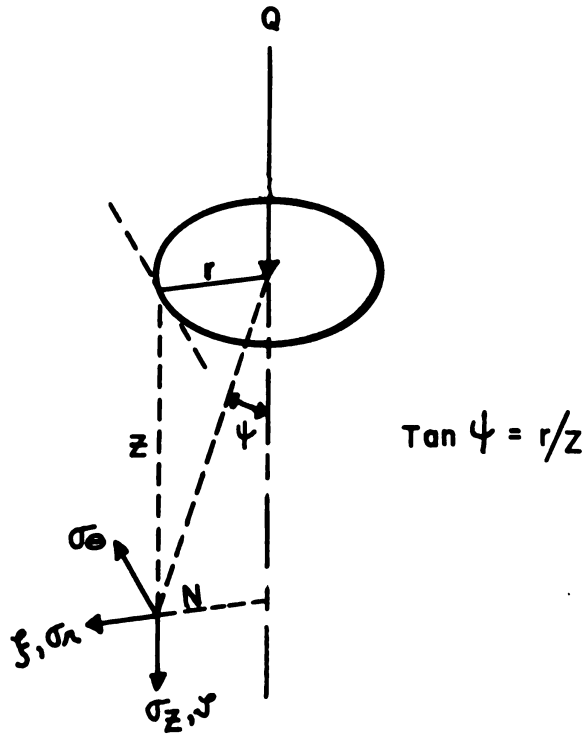


FIGURE A-2, STRESSES AND DISPLACEMENTS AT POINT N DUE TO LOAD Q

$$\sigma_{\theta} = \frac{-Q}{2\pi Z^2} (1 - 2\mu) \left[\cos^3 \psi - \frac{\cos^2 \psi}{1 + \cos \psi} \right] + \frac{\mu \gamma Z}{1 - \mu} \quad (\text{A-6})$$

$$\tau_{rZ} = \frac{3Q}{2\pi Z^2} [\cos^4 \psi \sin \psi] \quad (\text{A-7})$$

The deformations at N are:

$$\zeta = \frac{Q}{2\pi r} \frac{1 + \mu}{E} [2(1 - \mu) + \cos^2 \psi] \sin \psi \quad (\text{A-8})$$

$$\xi = \frac{Q}{2\pi r} \frac{1 + \mu}{E} [-(1 - 2\mu) + \cos \psi + \cos^2 \psi] \sin \psi \tan \frac{\psi}{2}, \quad (\text{A-9})$$

where μ = Poisson's ratio
 E = Young's modulus
 γ = weight density.

These equations are applicable for the case when Q is a concentrated load, but a discontinuity occurs in the stresses and displacements at the surface directly under the load. These equations must be integrated over an area to represent the case of a uniformly distributed load on the elastic half space. These integrated expressions can be found in reference [A-4].

Westergaard's Equation

A concentrated vertical force Q acts normal to the surface of semi-infinite, laterally restrained solid. Deformations in the horizontal direction are prevented without interfering with deformations in the vertical direction. Cylindrical coordinates are used in the problem formulation. Since the Westergaard formulation is a subset of the Boussinesq equations, stress calculations are also discontinuous under the load.

Using the notation of Figure A-2, Westergaard's solution gives the following expression for the vertical stress [A-3].

$$\sigma_z = \frac{Q}{z^2} \frac{c}{2\pi} \left[\frac{1}{c^2 + (r/z)^2} \right]^{3/2} + z\gamma \quad (\text{A-10})$$

where

$$c = \left[\frac{1-2\mu}{2(1+\mu)} \right]^{1/2}$$

μ = Poisson's ratio

γ = specific density.

The computer program [A-14] using Westergaard's formulation calculates surface stresses in the x and y directions in addition to the vertical stress σ_z . Displacements are currently not calculated in the computer program but expressions for the displacements could be included in the program if desired.

Cerruti's Equations

If a force, Q , is acting tangential to a point on the surface of a semi-infinite homogeneous, isotropic material in the X direction, Figure A-3, the deformations in the solid at point N are [A-5]:

$$u = \frac{Q}{4\pi\mu} \left[\frac{\lambda + 3\mu}{r(\lambda + \mu)} + \frac{x^2}{r^3} \right] - \frac{Q}{2\pi r(\lambda + \mu)} + \frac{Q}{4\pi(\lambda + \mu)} \left[\frac{1}{z+r} - \frac{x^2}{r(z+r)^2} \right] \quad (\text{A-11})$$

$$v = \frac{Q}{4\pi\mu} \frac{xy}{r^3} - \frac{Q}{4\pi(\lambda + \mu)} \cdot \frac{xy}{r(z+r)^2} \quad (\text{A-12})$$

$$w = \frac{Q}{4\pi\mu} \frac{xz}{r^3} + \frac{Qx}{4\pi(\lambda + \mu)r(z+r)} \quad (\text{A-13})$$

where $\mu = \frac{E}{2(1+\nu)}$

$$\lambda = \frac{E\nu}{(1+\nu)(1-2\nu)}$$

E = Young's modulus

ν = Poisson's ratio

u = x-displacement

v = y-displacement

w = z-displacement

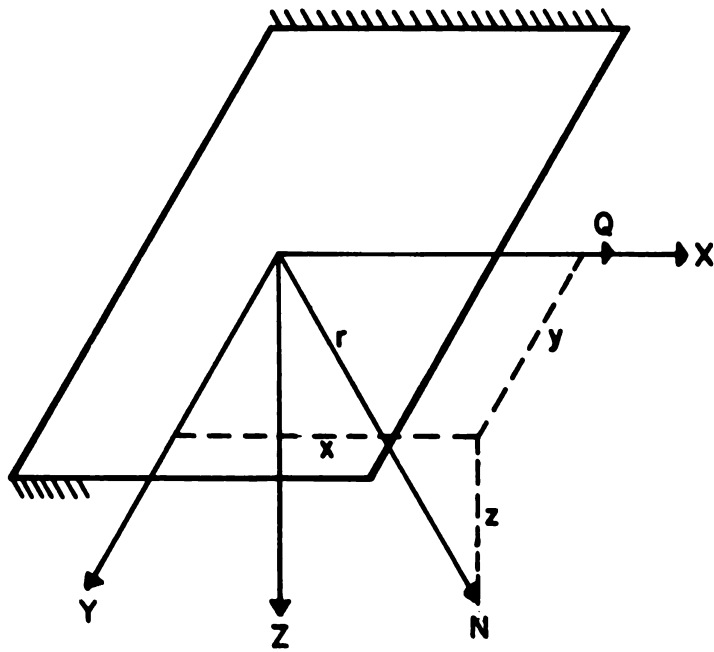


FIGURE A-3. DISPLACEMENTS IN A SEMI-INFINITE SOLID DUE TO A HORIZONTAL LOAD Q

Cerruti's model assumes that the boundary is free of traction forces. Although no specific expressions for stresses appear in [A-5], the computer program [A-14] using Cerruti's model calculates stresses and strains in the x, y and z directions.

Burmister's Multilayer Elastic System

Burmister's theory [A-6] is based on a multi-layered system. Each layer has a finite thickness with infinite dimensions in the horizontal directions. The last layer represents an infinite thickness. As many as seven layers can be used in current computer models. The layers are homogeneous, isotropic, and obey Hooke's law. A uniform pressure over a circular load bearing area acts in the vertical downward direction. Expressions for stress and displacement at a depth below the load are obtained by using a stress function which is written in terms of Bessel and exponential functions. Two separate solutions are given depending on the boundary condition. Case 1 assumes that the layers are continuously in contact with shearing resistance fully active between them. In Case 2, the layers are in continuous contact but with a frictionless interface. The reader is referred to Reference [A-6] for the stress and deflection equations for Burmister's model.

The principal disadvantages of the Burmister model are: (a) infinite horizontal dimensions (b) the foundation must be composed of layers of homogeneous, isotropic and linearly elastic material and (c) no lateral loads can be applied.

JNR Model

The Japanese National Railways [A-17] have used the following equation to obtain subgrade pressure, P_s , in psi.

$$P_s = \frac{50 P_b}{10 + h^{1.35}} \quad (A-14)$$

where h is the depth of the ballast in centimeters and P_b is the pressure under the tie in psi.

Love Equation

An application of Boussinesq's theory [A-18] provides the following expression for subgrade pressure due to a uniformly loaded circle with an area equal to the effective tie bearing area under one rail seat.

$$P_s = P_b \left\{ 1 - \left[\frac{1}{1+(r/h)^2} \right]^{3/2} \right\} \quad (A-15)$$

where r is the radius of the uniformly loaded circle.

The results of the JNR and Love equations are compared with measured data in reference [A-2].

Salem and Hay

Two equations developed by Salem and Hay [A-7] include correction factors C and K to relate test results to theoretical predictions. A theoretical equation based on ideal conditions was first developed and then multiplied by a correction factor based on experimental data which include the effect of tie bending on the tie/ballast pressure distribution.

It was concluded in the Salem and Hay study that:

a) The depth of ballast needed to get a fairly uniform pressure on the subgrade equals the tie spacing minus three inches. The vertical pressure at this depth should be less than the allowable bearing capacity of the subgrade to prevent subgrade deformation.

b) The magnitude of the vertical pressure below the centerline of a tie is always smaller than that given by Talbot for the same unit pressure applied.

Weissmann's Model

Weissmann [A-8] presents a model of a slab supported by a soil foundation that includes an equivalent mass, a viscous dashpot, and a linear spring. The mass accounts for some of the soil vibrating in phase with the slab. The equivalent parameters from [A-8] are listed below.

$$M_E = M_A \left[1 + \frac{0.2A_f^{1/2} \rho_{\text{soil}} G}{(1-\mu) t \rho_{\text{slab}} G_{\text{seis}}} \right] \quad (\text{A-16})$$

$$C_E = \frac{A_f \rho_{\text{soil}}^{1/2} G}{(1-\mu) G_{\text{seis}}^{1/2}} \quad (\text{A-17})$$

$$K_E = \frac{2.26GA_f^{1/2}}{(1-\mu)} \quad (\text{A-18})$$

where

A_f = base area of foundation (tie)

G = shear modulus of elasticity for soil

G_{seis} = seismic shear modulus of elasticity for soil

M_A = total mass of component (tie and rail)

t = slab thickness (tie)

ρ_{slab} = slab density

ρ_{soil} = soil density

μ = Poisson's ratio for soil

Some recommended soil properties, also from [A-8] are listed below.

	$G(\text{psf})$	$G_{\text{seis}}(\text{psf})$	μ
Rocks	$>15 \times 10^5$	$>30 \times 10^5$	0.33
Gravel, sand	6 to 15×10^5	12 to 30×10^5	0.35

Using the results of equations (A-16), (A-17), and (A-18), a single degree-of-freedom dynamic model can be established from which a compliance and phase angle can be obtained as a function of the forcing frequency. The vertical deflection can be estimated using equation (A-18).

Finite Element Models

Finite element models are another approach for representing track structures. In general, these models not only analyze the ballast and subgrade, but also include the tie, pad, fastener, and rail. Another distinct advantage in using finite elements is the ability to vary the

properties of each element, so that the analysis is no longer that of an ideal system. The main disadvantage with any finite element method of analysis is the high cost of making a computer run and formulating all of the input data.

2-D Finite Element Model - Lundgren

The objective of this model is to analyze the factors entering into the track modulus and to develop a systematic numerical procedure for determining track response under load. A computer solution by methods of matrix structural analysis is given for a track structure under static vertical loads [A-11]. A two-dimensional finite element method as shown in Figure A-4 gives deflections, strains, stresses, moments, and track modulus. The soil is assumed to be small square plate elements; the ties are represented by a spring or springs; the rail is a continuous beam resting on the tie springs. Separate springs for fastener pads can be included in the tie effective stiffness.

This model can accept randomly assigned soil properties. The solution is modified to take into account the inability of the soil to take high tensile loading and high shear stresses. A new stiffness matrix is formulated when shear or tensile failure occurs. This provides an iterative solution for nonlinear soil behavior under high loads.

The boundary conditions are chosen such that the surface boundary is free to move vertically while the lower boundary is fixed. The model will accept any boundary condition on the sides. The rail end may be fixed or free in the vertical direction with a zero or full moment restraint. The weight of the ballast/subgrade material and the weight of the rail, fastener, and a portion of the tie are applied at grid points to reduce upward deflections of the rail. Uplift forces on the ties which exceed the rail weight are removed during the iteration procedure to simulate the free uplift of unrestrained rail.

No provision for incorporating lateral or longitudinal loads is provided in the simulation.

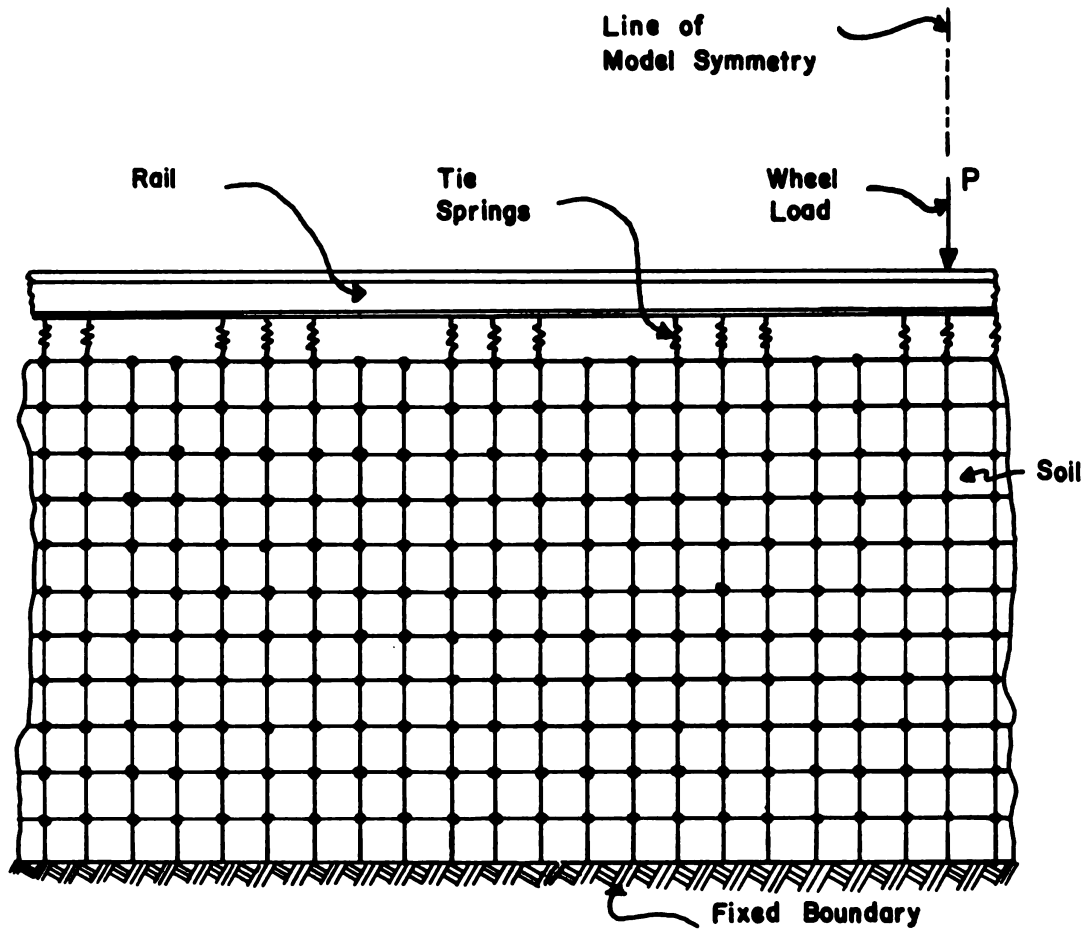


FIGURE A-4. FINITE ELEMENT MODEL OF TRACK STRUCTURE SECTION

Finite Element Model by Kilmartin

This 3-D finite element program [A-12] models the rail-tie structure accurately, but does not include detailed modeling of the ballast. Rail segments between ties are represented as prismatic beams, and the cross ties are finite sections of a uniform beam on a continuous elastic foundation. A variable number of static vertical loads can be placed on the rail at any point. Grid points occur at the intersections of each tie and rail. If a load is placed between ties, an imaginary tie is used.

The program will accept variable properties for the tie, right rail, and left rail. Rail joints may be optionally placed at the cross tie-rail intersections. Joint stiffness is scaled from 0 to 1 compared to CWR. Vertical and lateral deflections and 3 rotations are calculated at each grid point. The analysis does not consider including rail pad stiffnesses, fasteners, or variable ballast modulus.

An iteration procedure is used to eliminate upward tie deflections. This is accomplished by selecting a second foundation modulus for ties with an upward deflection and recomputing a solution.

Finite Element Model - Robnett (ILLI-TRACK)

This two stage finite element approach was used by the authors to model the track structure, since they believe a three dimensional solution would be cost prohibitive [A-10]. A longitudinal analysis is followed by a transverse analysis in the two stage analysis scheme. This is an extension of the Lundgren model [A-11].

The longitudinal analysis considers point loads (corresponding to wheel loads), acting on a single rail supported by the tie-ballast-subgrade system. Figure A-5 shows a typical finite element mesh used for the longitudinal analysis. The rail-tie subsystem is represented as a continuous beam supported on tie springs. Rectangular planar plate elements are used to represent the ballast, the subballast and the subgrade. The width of the elements is increased with depth using a "pseudo" plane strain technique.

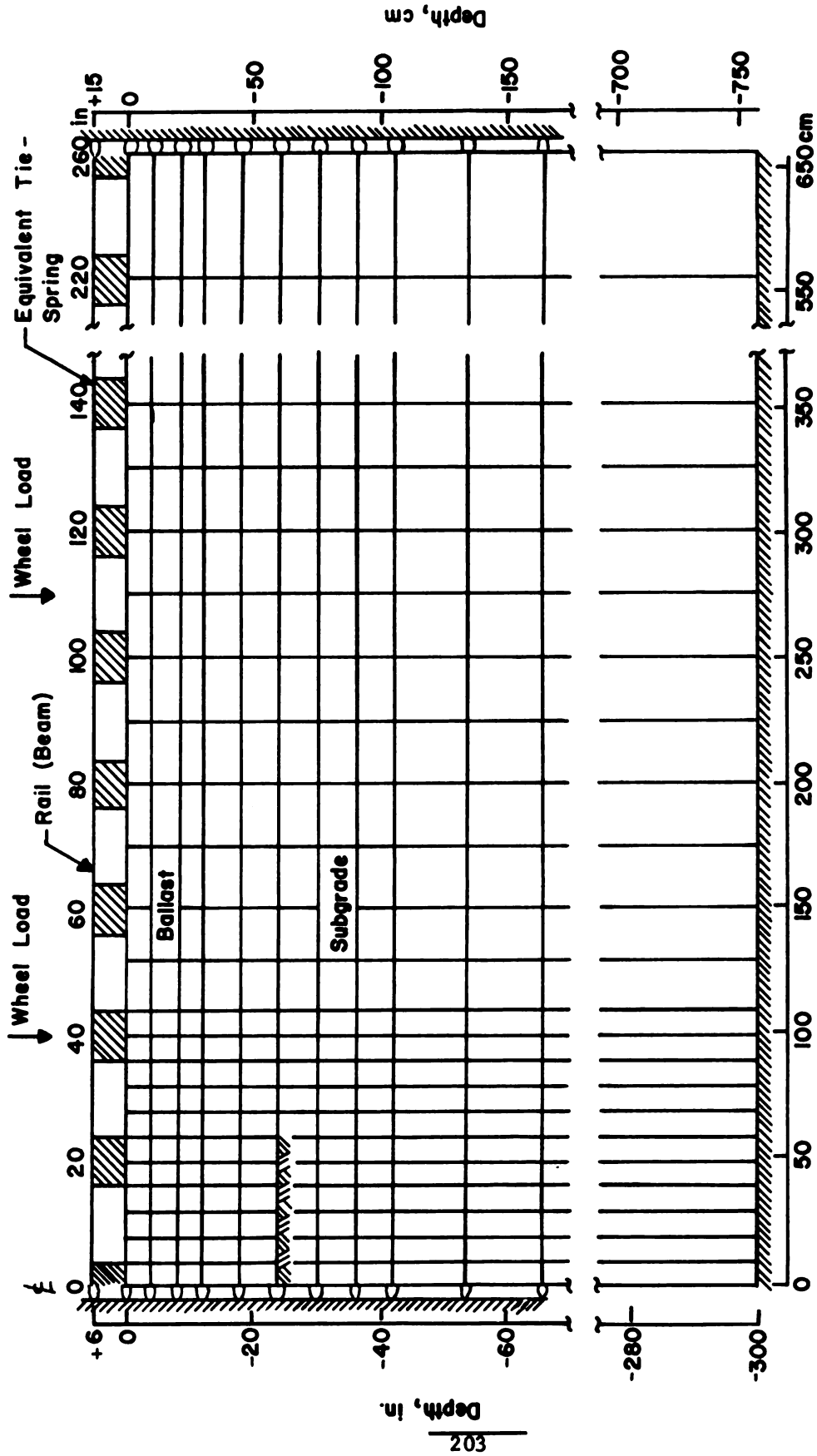


FIGURE A-5. A TYPICAL FINITE ELEMENT MESH USED FOR LONGITUDINAL ANALYSIS

This allows a three-dimensional representation of the loading to be simulated with a two dimensional model. The displacement components are assumed to vary linearly over each element.

In the longitudinal analysis, a symmetrical loading is assumed and only half of the system is modeled. Grid points along a vertical boundary representing the centerline of the track are restrained from horizontal movement as are grid points along the other vertical boundary at a distance of 260 inches. Grid points along the bottom boundary at a distance of 300 inches below the surface and those on the vertical boundaries are fixed, see Figure A-6.

The transverse analysis uses the output from the longitudinal analysis as input. Either the maximum reaction or the maximum deflection at a tie obtained from the longitudinal analysis is used as input at a tie which rests on the ballast-subgrade system.

The pseudo plane strain state mentioned above is used to obtain a realistic stress distribution with depth. The angle of distribution, which accounts for an increase in element size with depth, is constant. An incremental load technique is used in developing the final stress distribution. This allows the use of stress dependent material properties. After the last load increment is applied, a single iteration is performed to obtain the stress state which is compatible with total load. During the incremental loading, failure criteria for the ballast and subgrade are checked and material properties are adjusted accordingly.

Although the ILLI-TRACK model includes a detailed, non-linear model of the track roadbed, the use of two pseudo plane-strain models instead of a 3-dimensional model has some important disadvantages. The assumption of an effective tie bearing area at the beginning gives questionable results and eliminates any evaluation of the important effects of tie bending on the tie/ballast pressure distribution. The generation of depressed areas (gaps) in the ballast under the rail seat region leading to center bound ties is a major mode of track degradation requiring non-linearities. However, this cannot be evaluated using a two-dimensional model.

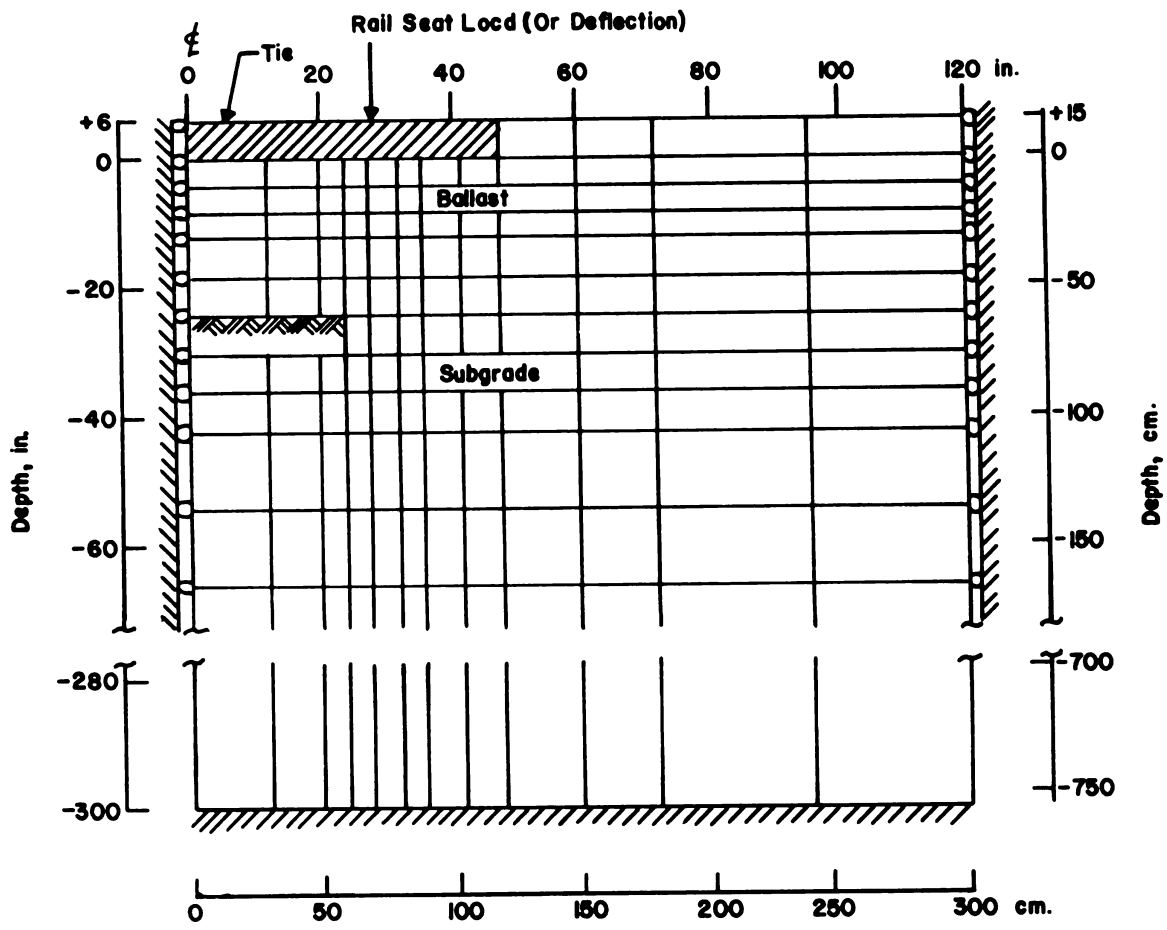


FIGURE A-6. A TYPICAL FINITE ELEMENT MESH USED FOR TRANSVERSE ANALYSIS

3-D Finite Element Model (Queen's University)

The Queen's University model [A-9] is a 3-dimensional step-by-step non-linear elastic finite element track model. The rail is represented by simple beam elements with vertical displacement and rotation in the beam direction. Ties can be either simple beam elements or 3-dimensional brick elements selected to match realistic local variations in tie bending rigidity. The ballast, sub-ballast and subgrade are brick elements which utilize a bicubic spline function to represent non-linear, stress-dependent variations in Young's modulus. The program can be modified to allow separation of the tie from the ballast in order to simulate the development of rutting under repetitive loads.

The Queen's model is the most comprehensive track model under development. The principal disadvantage is the high cost for modeling and computer time and the difficulty in getting realistic data for the ballast and subgrade properties. This model is still under development and will require extensive validation before the high cost can be justified for its use.

Finite Element - BCL

A single rail is divided into n grid points with a variable distance between each grid point. Associated with each grid point is a vertical spring (tie) a torsional spring (fastener), a beam flexural stiffness (EI), and a vertical static load. Any of the above quantities can vary from grid point to grid point. An investigation of ineffective ties or fasteners, rail joints, and multiple wheel loads can be handled in the vertical plane only.

The solution is obtained by writing equilibrium equations at each grid point in the form of a matrix equation. The unknown deflections, slopes, moments and shears of the rail at each grid point are calculated. Outputs also include tie vertical and torsional restraint loads.

Lateral Rail-Tie-Foundation Model - AAR

A static finite element model [A-14] of the rail-tie-foundation lateral reaction due to multiple wheel loads has been formulated and somewhat validated with experiments. This 2-dimensional model (lateral and longitudinal translations and rotation about the vertical axes) is represented by 1-dimensional finite elements. A beam is used to represent a single rail supported by springs at the tie locations. These springs, which may be nonlinear, simulate the total lateral stiffness of the tie, fastener, and ballast. A rotational stiffness about the vertical axis at the tie is provided by the fastener.

This analysis is capable of handling rail irregularities such as rail joints, nonlinear foundation support, missing ties and off-loading. A rail joint is simulated by inputting joint bar properties at the desired location. The nonlinear characteristics of the fastener and ballast - subgrade are incorporated into the program by a multi-linear stiffness. Missing ties can be represented by reduced tie and fastener stiffness. Forces or displacements in the lateral, longitudinal, and rotational direction can be applied at all node points. The other forces or displacement are the unknowns.

Outputs of the finite element program include lateral and longitudinal rail-tie-reactions, and rotational rail-fastener reactions about the vertical axis. In addition, member axial and shear forces, bending moment, and deflection of the rail are given.

The model has been partially verified with test data of lateral rail deflections obtained in the mid 30's. The effect of rail joints, missing ties, and nonlinear ballast characteristics have not been determined experimentally, so the accuracy has not been verified for these effects.

Parameter studies using the model for track which has vertical loads have shown small changes in rail lateral deflection and bending moment due to fastener and rail stiffness. But a significant reduction in deflection and bending moment is obtained for increased lateral tie-foundation stiffness.

Vertical Rail-Tie-Foundation - AAR

The basic two-dimensional finite element model used here is just like that of the previous model. The track is represented by a beam on springs which may be linear or nonlinear. Each spring represents the rail-tie reaction at each tie. Thus this is a two-dimensional model with one-dimensional finite elements.

The inputs to this model are the vertical stiffness of the springs (includes the tie, fastener, ballast and subgrade), moment of inertia and Young's modulus of the rails, and the vertical loads representing wheel loads.

The outputs from this model are the vertical deflections of the rail, moments, shears and bending stresses in the rails, foundation pressures, and rail-tie loads.

The basic disadvantages with this and the previous model are a) each model assumes that the foundation is like a dense fluid which neglects shear coupling in the roadbed, and b) the model cannot simulate off-loading conditions on staggered joints in the rail since the model uses only one rail. This is also a serious limitation for accurately modeling the "frame" effects for lateral resistance.

3-Dimensional Track Model by Member Representation - AAR

This model [A-14] is a 3-dimensional track model representing the rails, fasteners, ties and ballast-subgrade by 1-dimensional structural members and springs, see Figure A-7. Rails and ties are represented by beams and the ballast-subgrade is represented by springs. Each fastener group can be separated into fastener components with each component being represented by a structural element or spring. Multiple loads, off-loading, staggered joints, ineffective ties, and fasteners can be modeled. Rail joints are simulated by a beam equivalent to a joint bar.

Predictions of this model include rail and tie bending moments and deflections, fastener deflections, and the loading environment for the ties, fasteners, and ballast-subgrade.

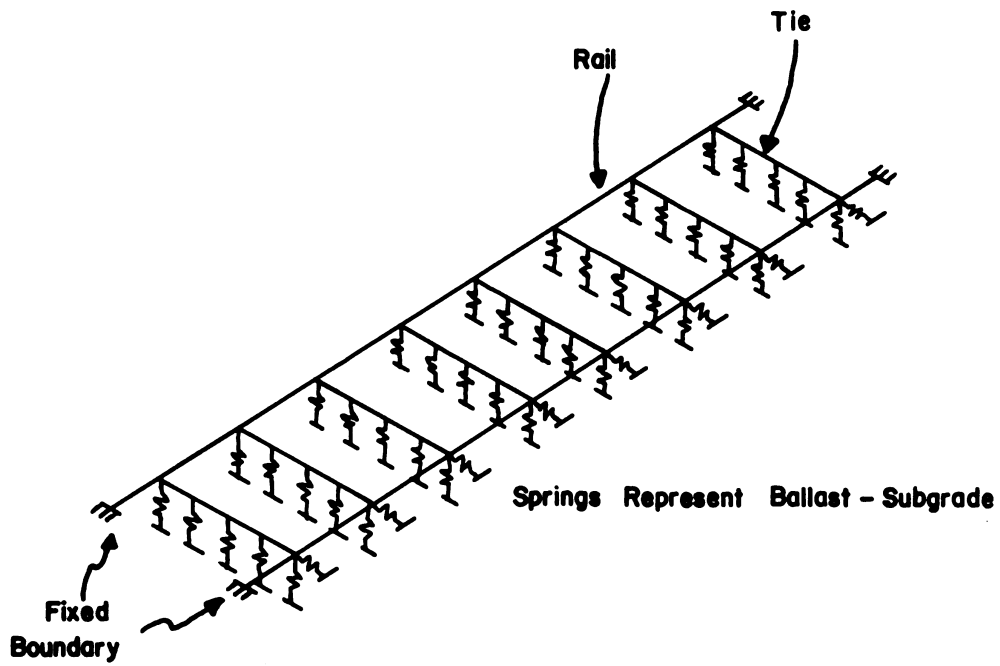


FIGURE A-7. THREE DIMENSIONAL FINITE ELEMENT TRACK MODEL BY MEMBER REPRESENTATION

A comparison of predicted vertical rail deflection with test data obtained some 60 years ago shows good agreement for a large vertical track load (25,000 lb) but poor correlation for a light load (5,000 lb). Lateral deflections are also verified by test data developed in the 1930's. Many other possible cases have not been validated because of a lack of experimental data.

A general purpose 3-dimensional structural analysis program (SAP-IV) [A-15] is used to solve this problem. It should be noted that SAP-IV is a linear structural analysis program in its original form. The nonlinear behavior of fasteners etc., can be modeled with NONSAP.

Rail-Fastener Model - AAR

The three-dimensional track model noted in the previous paragraph can have various levels of detail. Each fastener group can be further separated into fastener components, each component being represented by a structural element or spring. This then becomes the Rail-Fastener Model whereupon this 3-dimensional finite element model [A-14] predicts rail fastener loads and rotations about three axes given the vertical and lateral wheel loads, fastener rotational stiffnesses, ballast-subgrade stiffness, and material properties of the rail and tie. The claim that any type of fastener can be modeled is made in the documentation, but modeling fasteners with beam elements is quite difficult.

Three-Dimensional Elasticity Analysis - Herrmann

Herrmann has developed a 3-dimensional finite element computer program which analyzes a periodically loaded prismatic solid [A-16]. The basic assumptions of the prismatic body is that it is infinite in length with constant cross sectional and Fourier series material properties in the longitudinal direction. The loading is represented by a Fourier series. Isolated loads can be analyzed by point loads sufficiently separated as to prevent interaction. Temperature strains and body forces in three orthogonal directions (periodic in the longitudinal direction) are also included. All body forces and temperature effects may be a function of position in the cross section. Boundary conditions (stress and displacement) are also described

by periodic functions. The periodicity of all functions is handled by determining the first N coefficients of the Fourier series.

Two-dimensional finite elements-quadrilateral and/or triangular shaped-are used to describe the cross section of the prism. Although the materials are considered perfectly elastic, each finite element may have different material properties.

The inputs to the computer program include the finite element representation of the cross section of the ballast, Fourier coefficients of body forces, boundary conditions, a temperature term, and the material properties (Young's modulus and Poisson's ratio) for every element in a cross-section. The outputs, which can be given at any cross section, are three orthogonal linear displacements at each node point, the six components of strain and three normal components of stress at each element's c.g.

Several limitations are immediately obvious. Since the analysis is linear, ballast failure cannot be modeled. Because all loads are periodically spaced, the individual load on each tie due to multiple wheel loads must be determined in terms of Fourier coefficients as an input to the program. Thirdly, since all loads are periodic, a longitudinal loading will result in zero displacements at half period points which means the elastic body is not really infinitely long. Rail joints and missing ties can be investigated by determining the periodic loading on the ties due to the track irregularity. This complex loading would be represented by a Fourier series of many terms.

Continuous Solutions

The third approach to modeling a track structure is by using the solution of a differential equation describing a loaded continuous system. The method is applicable to both the rail and to the finite length beam (tie) as individual units.

Beam on an Elastic Foundation (Vertical) - BCL

The basic equation for the vertical deflection y of a rail having flexural rigidity EI supported continuously by an elastic foundation and loaded by a point load P at the origin is

$$EI \frac{d^4 y}{dx^4} + Uy = P\delta(x) \quad (A-19)$$

where U is the track modulus for a Winkler foundation defined as the load per inch of rail length required to depress the foundation one inch.

The solution of the above equation for a single point load results in the well known relation for rail deflection $y(x)$ and rail bending moment $M(x)$

$$y(x) = (P/K_r) e^{-\beta x} (\cos\beta x + \sin\beta x) \quad (A-20)$$

$$M(x) = (P/4\beta) e^{-\beta x} (\cos\beta x + \sin\beta x) \quad (A-21)$$

where $\beta = (U/4EI)^{1/4}$, $K_r = 2U/\beta$, and where K_r represents the track stiffness, or spring rate (lb/in), for a vertical point load applied to the rail head.

In this model the modulus can include pad stiffness, a ballast stiffness, and a soil stiffness. The ballast is represented by the pyramid stress model. In order to utilize the beam on elastic foundation solution, all individual stiffnesses along the length of the rail are identical. The program will accept four equal wheel loads to calculate the track structure response in the vicinity of two trucks.

Output includes the rail deflection and moment at several points, the pressure at the base of the tie and ballast, subgrade pressure, and the rail bending stress.

This model has the usual restrictions from assumptions of equal tie spacing, homogeneous isotropic ballast, equal pad stiffness, no joints in the rail, a foundation modulus which acts in tension, and a uniform deflection and pressure distribution in the ballast. However, it is useful and efficient for track design parametric studies.

Tie on an Elastic Foundation - BCL

To obtain tie deflections, the configuration of an infinite beam on a uniform elastic foundation is first formulated with two wheel loads separated by an effective gage, Figure A-8.

The governing differential equation is

$$EI \frac{d^4 w}{dx^4} + Kw = q_0 + [\delta(c) + \delta(l-c)] \quad (A-22)$$

where

E = Young's Modulus of the tie, psi

I = Bending moment of inertia of tie, in.⁴

$\delta(\text{arg})$ = Dirac delta function = 1 if arg = 0
= 0 if arg \neq 0

q_0 = rail seat load, lb

l = tie length, in.

c = distance from tie end to rail load, in.

K = foundation modulus of ballast, lb/in./in.

From this solution, the moments and shears which exist at the free ends of the tie are calculated. Then the infinite beam problem is solved with the negative of the moments and shears found above as boundary conditions and applied at the free ends of the tie. By superimposing the two solutions with the opposite reactions at ends of a tie along with the solution of the infinite-length beam, the solution for a finite-length tie on an elastic foundation is derived. From this solution, displacements, slopes, moments and shears across the tie can be found. A disadvantage of this closed-form solution is that variations in tie or support characteristics along the tie length cannot be included.

Detailed expressions for $w(x)$ and $M(x)$, tie moment, are given in [A-2] as a superposition of the three solutions discussed above. As in the case of the rail on an elastic foundation, this solution will allow upward deflections; but because of the length of the tie, such deflections are not likely. In this problem, the foundation modulus does represent a continuous roadbed and is given by

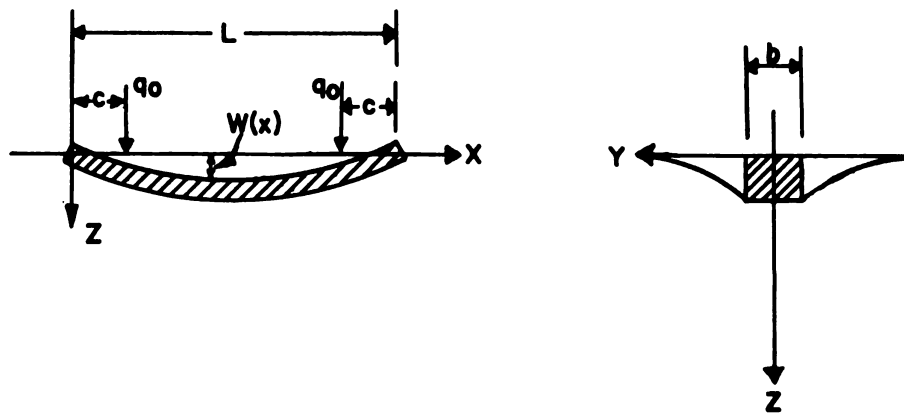


FIGURE A-8. ILLUSTRATION OF A TIE ON AN ELASTIC FOUNDATION

$$K = \frac{\pi E}{2 (1 - \mu^2) \ln (l/b)} \quad (A-23)$$

where

μ = Poisson's ratio

b = tie width, in.

Then the ballast pressure under the tie is given by

$$\sigma_z = \frac{2k}{\pi b} w(x) \left[1 - \left(\frac{2y}{b}\right)^2 \right]^{-1/2} \quad (A-24)$$

where

y = lateral distance along width of tie from load application, in.

Lumped Parameter Method

The fourth type of analysis used to obtain track response is the lumped parameter method. This technique involves representing each element of the track as a rigid body connected by springs and dashpots. This results in a system of ordinary differential equations which can be solved in the time or frequency domain.

Lumped Parameter Dynamic Track Response - BCL

A simple model which considers the response of the wheel and the track structure is shown in Figure A-9.

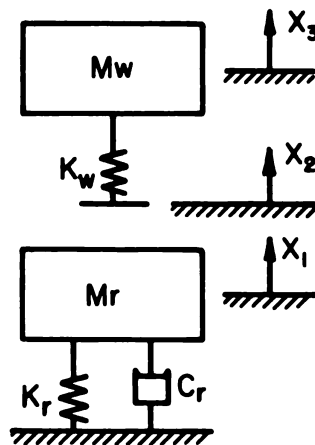


FIGURE A-9. WHEEL-TRACK STRUCTURE LUMPED PARAMETER MODE

The equations of motion for the system shown in Figure [A-9] are:

$$M_w \ddot{X}_3 + K_w (X_3 - X_2) = 0. \quad (A-25)$$

$$M_r \ddot{X}_1 + C_r \dot{X}_1 + K_r X_1 + K_w (X_2 - X_3) = 0. \quad (A-26)$$

$$X_2 = X_1 + N(t), \quad (A-27)$$

where

M_w = effective wheel mass

M_r = effective track mass

K_w = wheel stiffness

K_r = track structure stiffness

C_r = track structure damping

$N(t)$ = time function of track irregularities.

The track structure stiffness is found from the beam on an elastic foundation solution

$$K_r = \frac{2U}{\beta} \quad (A-28)$$

where

U = the foundation modulus, lb/in./in.

$\beta = [U/4EI]^{1/4}$

E = Young's modulus of the rail

I = rail bending moment of inertia

If the input, $N(t)$, is a high frequency disturbance and there is a soft primary suspension, the truck and car body mass can be ignored. On the other hand, for a low frequency input or a stiff primary suspension, the mass of the truck must be included in the term M_w and additional degrees of freedom are needed for the secondary suspension and car body.

The variable $N(t)$ can represent any transient, periodic, or random track geometry irregularity. If the input is transient, a numerical integration solution will give W/R forces, and track structure deflection as a

function of time. Impact factors can be generated from this analysis. For periodic or random signals, a frequency domain solution will provide frequency response or P.S.D. information on W/R forces and track structure deflection. Mean square values of track deflection can be found from integrating the P.S.D.

This simple model can be extended by adding a second wheel to the system. If the wheels are close (less than 10 ft), the track response will be coupled. In this case, Equation (A-26) is modified to

$$M_r \ddot{X}_1 + C_r \dot{X}_1 + K_r X_1 + K_w (X_2 - X_3) - \alpha(x) [C_r \dot{Y}_1 + K_r Y_1] = 0. \quad (A-29)$$

The equations for the second wheel-track structure are:

$$M_r \ddot{Y}_1 + C_r \dot{Y}_1 + K_r Y_1 + K_w (Y_2 - Y_3) - \alpha(x) [C_r \dot{X}_1 + K_r X_1] = 0. \quad (A-30)$$

$$M_w \ddot{Y}_3 + K_w (Y_3 - Y_2) = 0. \quad (A-31)$$

$$Y_2 = Y_1 + N (t + x/v) \quad (A-32)$$

where

x = the wheel separation distance

v = vehicle velocity

$$\alpha(x) = e^{-\beta x} (\cos \beta x + \sin \beta x) \quad , \quad x \geq 0$$

The term $\alpha(x)$ comes from the solution of the rail on an elastic foundation, and is based on static deflection due to a static load.

Half Car Model - BCL

This model, Figure A-10, was used to evaluate the dynamic interaction of a typical truck with various track structures [A-2]. It includes the vertical degree of freedom of one half of the car body, a bolster, a truck frame, two wheels on the same axle, 2 rail masses, and 2 ties. A roll degree of freedom of the truck frame is also specified for a total of 10 degrees of freedom. Suspension systems representing the secondary suspension, a shock pad between the bolster and truck frame, primary suspensions, wheel stiffnesses, rail pad and rail stiffness, and ballast

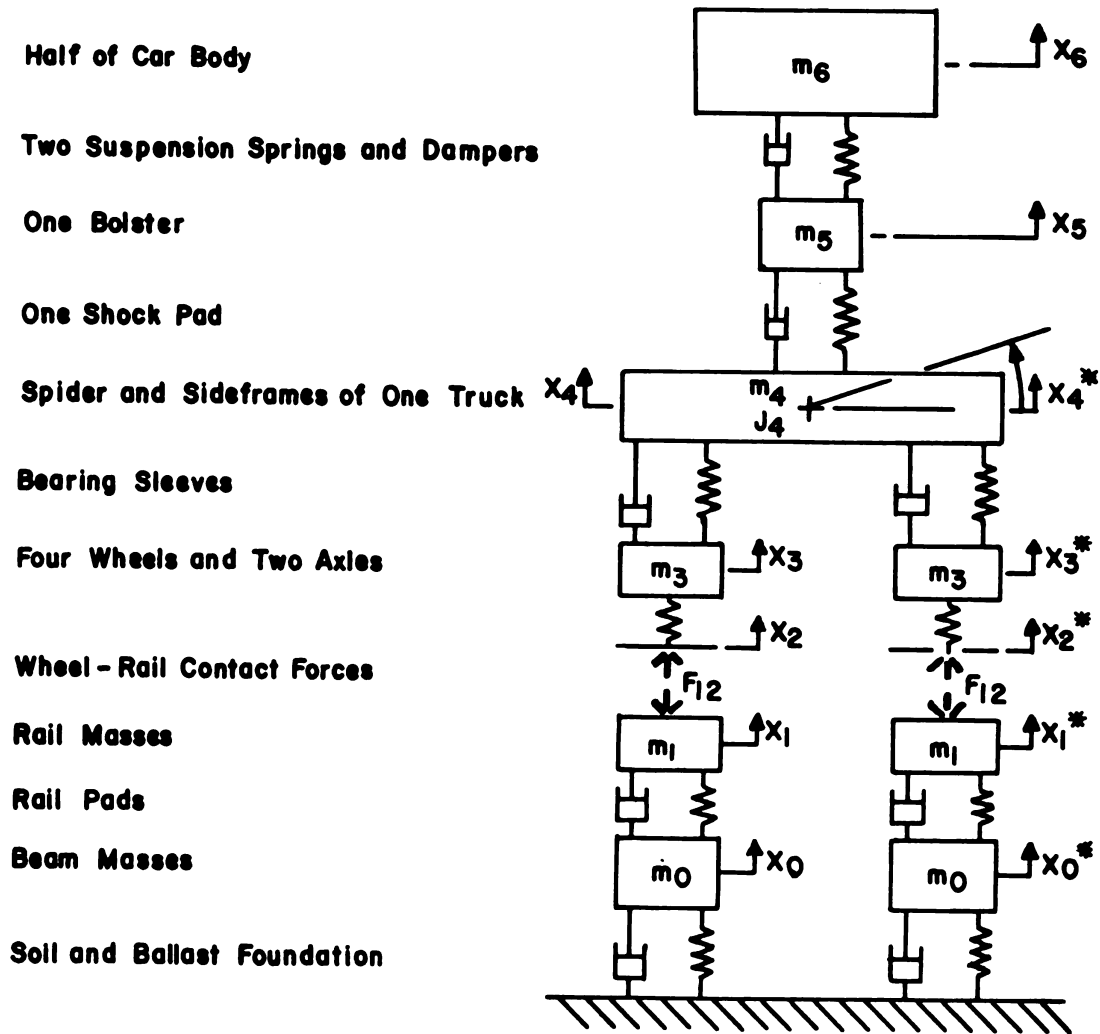
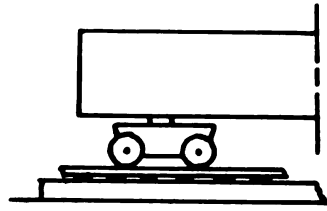


FIGURE A-10. LUMPED PARAMETER MODEL REPRESENTING PORTION OF CAR AND TRACK STRUCTURE ASSOCIATED WITH ONE TRUCK

stiffness can be used to represent several types of nonlinear stiffnesses and damping. Zero wheel/rail forces at wheel lift were also programmed into the model which has been used to predict rock and roll motions. Rail joints have been used as primary disturbance functions for this hybrid computer simulation.

This model has also been used to determine track component loads for variations in tie and rail mass, and pad, rail and ballast stiffness. Since the track portion of this model is rather general, the masses and springs can be adjusted to model conventional tie-ballast track or track constructed from concrete slab or twin longitudinal beams.

Dynalist

Dynalist II [A-13] is a general computer code which will generate dynamic characteristics (eigenproblem) of subsystems of rail vehicles (e.g., a truck), and then combine subsystems with a constraint matrix, to generate dynamic characteristics of the total system. Each individual subsystem may have up to 25 D.O.F. with a maximum of 50 D.O.F. for the total system. Nonrigid structural components may be incorporated by modal representation of the problem is generated.

The user then has the option of inputting sinusoidal or random excitation at selected points on the system. Output in the form of acceleration, velocity, or displacement response at selected locations on the vehicle is given versus frequency. Mean square values are computed by integrating the response P.S.D.

The program permits the user to generate his own equations of motion by inputting mass, damping and stiffness matrices. Track structure could be inputted in this way. Additionally, the program will automatically generate coefficient matrices for a truck (6 D.O.F.) or a complete car (14 D.O.F.) in the lateral plane.

APPENDIX B

TRACK ANALYSIS BENCHMARK PROBLEMS

Introduction

This appendix includes a review of the assumptions and limitations of the Burmister multi-layer elastic model and the Hermann prismatic solid analysis (PSA) finite element model for representing track roadbeds. Several benchmark problems have been selected and solved to evaluate these differences and to demonstrate the application of these models for track structure analyses.

Burmister Multi-Layer Analysis

The Burmister analysis assumes that the roadbed is infinite in extent in the horizontal plane and in the vertical (subgrade) direction. Because of the axial symmetry inherent in the point load case, cylindrical coordinates are used in the Burmister formulation and in the subsequent solution procedure. Thus, the resulting stress and displacement components are in a cylindrical coordinate system as shown in Figure B-1.

The axial symmetry associated with the Burmister simulation produces displacement and stress information at a point q whose coordinates are r and y relative to the load L . The value of stress at a given point $q(r,y)$ is independent of angle θ . For track analysis it is necessary to determine the (r,y) coordinates of each point whose stress/displacement influence coefficients are needed as input to the loads combination program. Appropriate transformations for the displacement vector and stress tensor are used to transform from cylindrical coordinates to the cartesian coordinate system employed in the loads/combination code for the track structure. This output data is written on tape for later use in the loads/combination program.

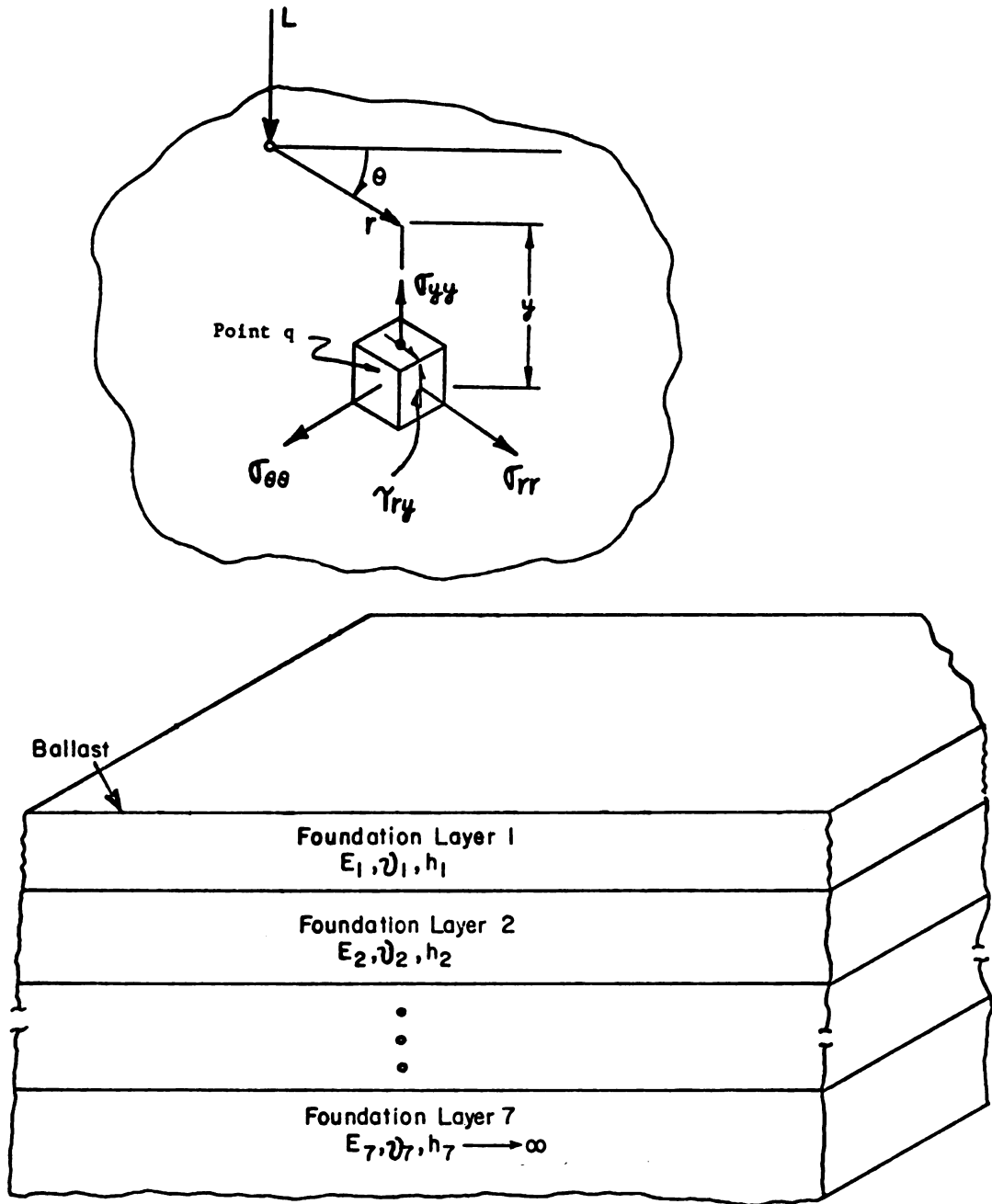


FIGURE B-1. GEOMETRY AND COORDINATE SYSTEM FOR BURMISTER MULTI-LAYER ROADBED MODEL

Hermann PSA Analysis

Figure B-2 shows the general geometrical formulation associated with the PSA roadbed model. The coordinate system is rectangular cartesian and the resulting stress and displacement components are in this cartesian system. The input data for the loads combination program includes stress and displacement influence coefficients along the tie (x-direction), throughout the foundation (y-direction) and in the longitudinal direction (-z). This generates a rectangular grid of points whose surface displacement pattern is completely defined by the vertical displacement of each node. As many stress values can be generated as there are finite elements in the model. However, one usually picks only those elements that illustrate the most interesting stresses for a given track system geometry and loading condition.

Comparison of Burmister and PSA Roadbed Models for Single Tie Loading

The roadbed loading from a single tie was selected in order to compare the Burmister and PSA models. Figure B-3 shows the PSA model which included a ballast depth of 12 inches and a subgrade depth of 18 inches. It was recognized that this subgrade depth is inadequate for simulating real track, but this choice was used to reduce the size of the model for comparison purposes.

The Burmister simulation can include as many as seven different layers of roadbed materials. The last layer is always assumed to be of infinite depth. For comparison with the PSA solution, the first layer was made 12 inches thick with $E_1 = 37,500$ psi, the second layer was 18 inches thick with $E_2 = 10,000$ psi. The value of the subgrade (third) layer modulus (E_3) was varied to determine its effect on the total deflections. The applied load was simulated by five (for the half tie) equal loading segments representing a uniform load distribution on the roadbed. The only role that the tie plays in this analysis is to determine the number and size of the load segments.

The specific variable monitored was the vertical displacement of

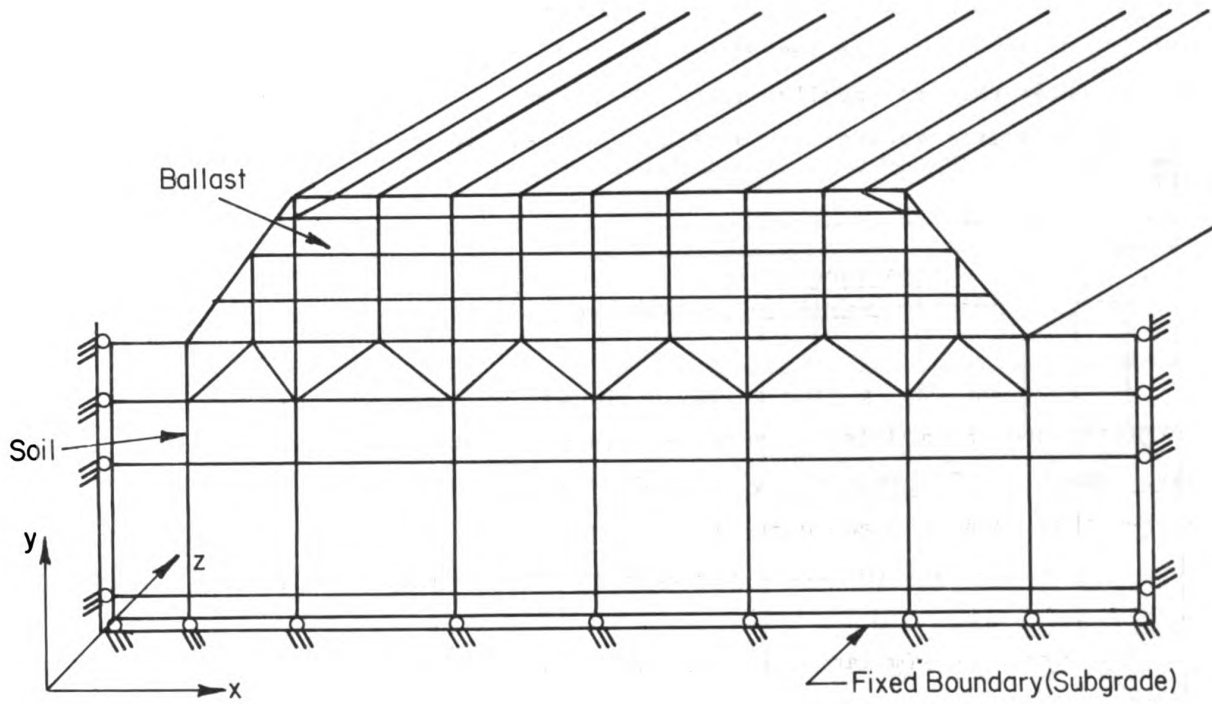


FIGURE B-2. GEOMETRY AND COORDINATE SYSTEM FOR HERMANN
PSA ROADBED MODEL

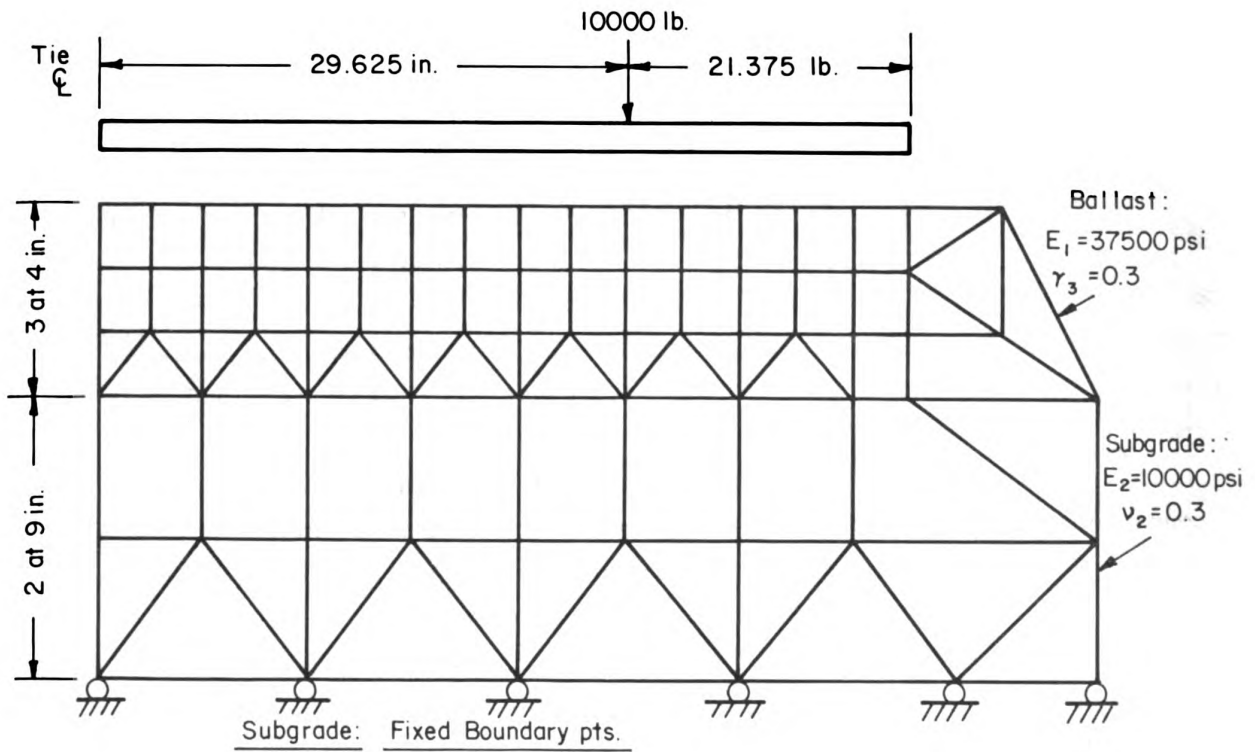


FIGURE B-3. FINITE ELEMENT MODEL USED IN PSA ANALYSIS

the foundation directly under the rail seat center. Figure B-4 shows the sensitivity of this displacement to the modulus of the bottom layer in the Burmister model. The displacement predicted by the PSA code is equal to the displacement calculated by the Burmister code if the subgrade modulus (E_3) is equal to or greater than 10^7 psi. Consequently, the PSA model with only 18 inches of subgrade does not realistically simulate the deflection of actual track which has infinite depth. The fact that the state of stress in the foundation is (for practical purposes) independent of E_3 will be established shortly.

The purpose of this investigation was to compare results obtained using the two mathematical models and not necessarily to determine which model best approximates the true physical situation. Indeed, the Burmister simulation probably approximates the true situation more realistically than the PSA model since the earth below the track is really not rigidly supported as indicated in Figure B-2. This fact is mentioned because of the computation time requirements for the two solutions. Using the Burmister code for the single tie case and two layers of material beneath the surface requires approximately 40 seconds computational time for each load segment under the tie. This is increased to approximately 70 seconds per load segment for 3 layers.

The total computational time for the PSA code was approximately 700 seconds for 5 load segments. Thus, we compare the 2-layer Burmister solution time of 200 seconds or the 3-layer solution time of 350 seconds for 5 segments to the PSA solution time of 700 seconds. Also, preparing the input data for a multi-tie configuration using the Burmister code usually requires a few (no more than 3) hours while preparing and checking the data for the PSA code requires a minimum of one day.

Effect of Tie Load Segment Geometry

The Burmister solution gives some rather unexpected results depending on how the tie loads are distributed on the roadbed, and these effects are not well documented on the literature. In the Burmister model the total load

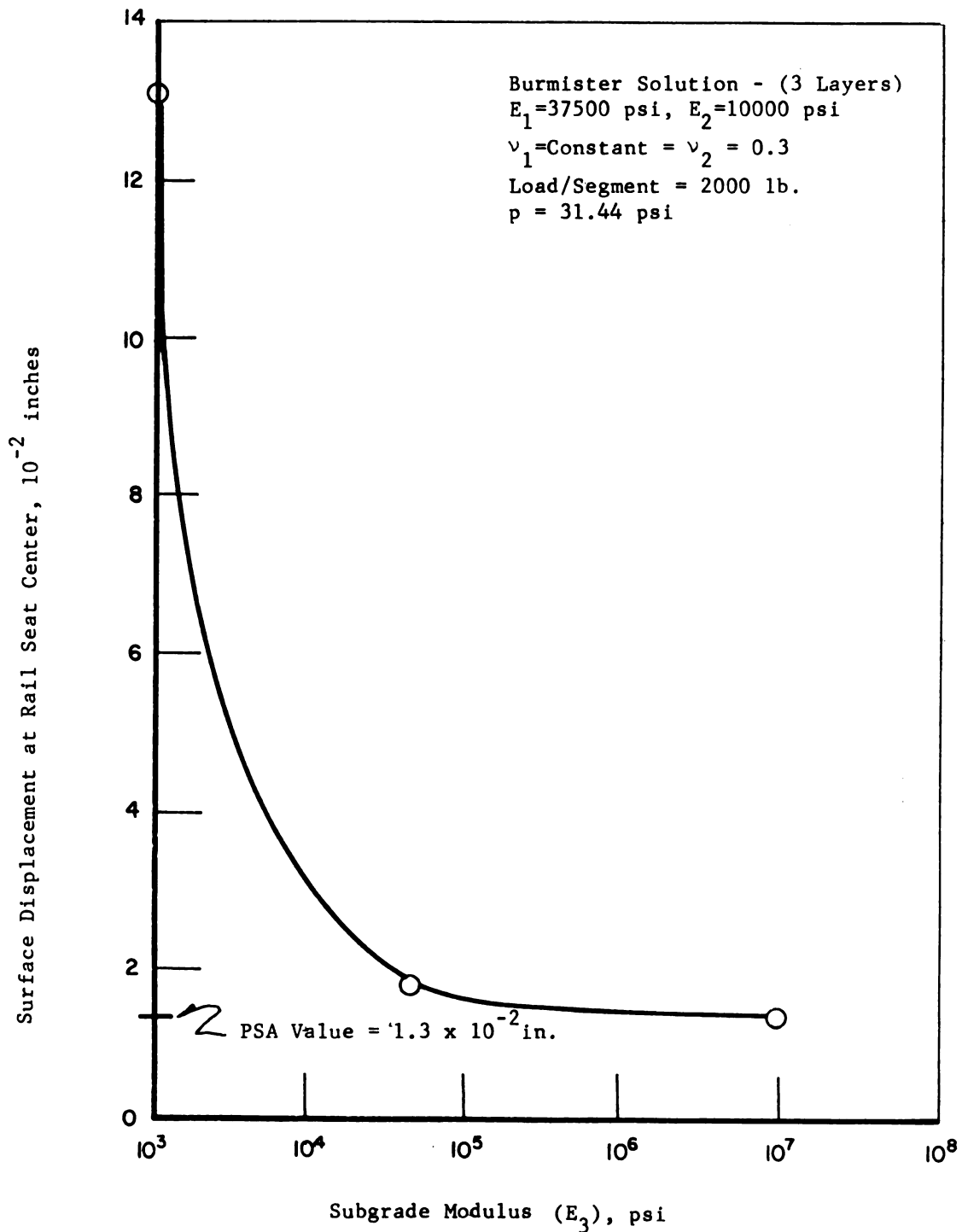


FIGURE B-4. DISPLACEMENT AT RAIL SEAT
 Vs. SUBGRADE MODULUS

is divided into a number of equal circular load segments along the tie length, and the number of load segments plays an important role in obtaining accurate results. The distributed load from the tie can be interpreted as a series of uniformly loaded squares (or rectangles). The procedures for accurately simulating a square (or rectangular) loaded area on an elastic half space have been documented.

Galín [B-1] suggested that in simulating a uniformly loaded square on an elastic half space, a circular load such that the areas of the circle and square are equal yields best results. If the uniformly loaded segment is of rectangular shape, the circular load with equal area still gives the best compromise. However, Galín shows that the accuracy degenerates rapidly outside the region where the circle and rectangle overlap. This problem can be minimized by having load segments that are rectangular with length to width ratios near unity. Therefore, the number of circular segments in the Burmister formulation should be selected so that each circular area equals the area of a nearly square rectangle.

As an example, consider a tie with length L and width C . Let the values of L and C be such that we can divide the total load into 10 nearly square segments. The area of each circle is $\pi r^2 = C \cdot L / 10$. This "r" is the load radius referred to in the Burmister program. For a given total tie load W , the segment load is $w = W / 10$, and the segment pressure $p = w / \pi r^2$.

For a given tie geometry, the resulting equivalent circular load segments may overlap, gap, or just touch. Several analyses were performed to evaluate the effect of these variations in loading geometry.

The Burmister solution is a classical elasticity solution that employs Bessel functions and exponential functions with positive and negative arguments for the stress function. The stress behavior in an elastic half space beneath a single applied load is shown in Figure B-5 for $w = 1,000$ lb and $r = 5.1$ inches such that $p = 12.24$ psi. The effect of the load circle approximation for a rectangular load is visible in the pressure reduction at the edges of the load circle.

For the case of a tie that is 102 in. long and 8 inches wide loaded with 10,000 lb., the effect of all the load segments must be superimposed. If the 102 in. tie is divided into 10 segments for distributing the load on the

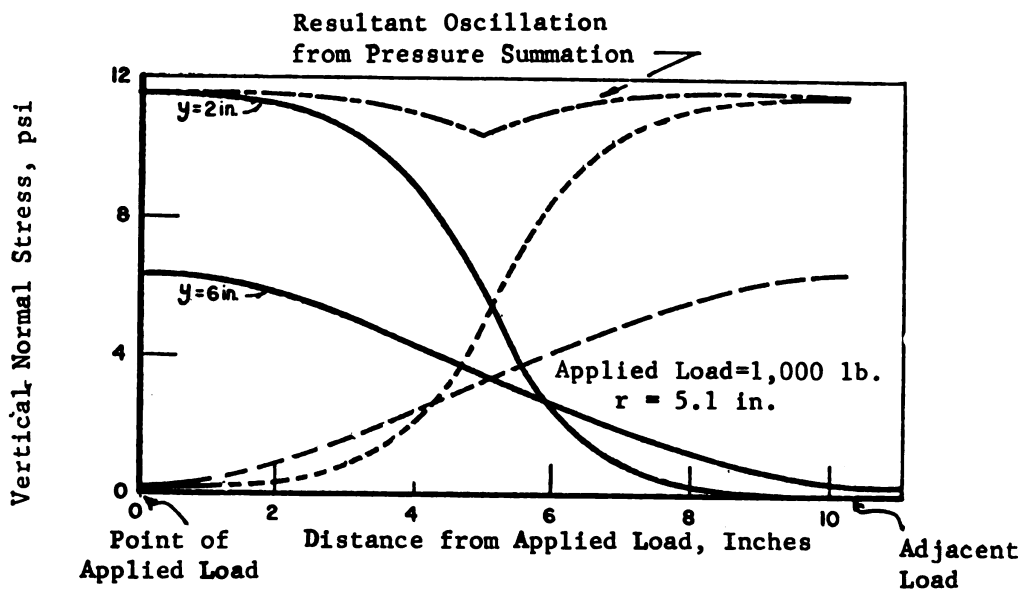


FIGURE B-5. PRESSURE DISTRIBUTION FOR ADJACENT LOAD SEGMENTS AND EFFECT OF SUPERPOSITION

ballast, we have a series of 10 equal load circles that are each 10.2 inches apart. This is the case of "just touching" load circles. Because of symmetry, the model is a half tie with 5 equal circular load segments. The resulting vertical normal stresses σ_{yy} at $y = 2$ in. and $y = 6$ in. below the surface are shown in Figure B-6. The amplitude of oscillation which results from superimposing the pressures from two adjacent load segments is relatively small at a depth of 2 inches below the surface.

The effect of gapped and overlapping circular loads was established by using the same total load divided into 10 equal circular load segments centered 10.2 inches apart along the length of the tie. Four cases considered were:

Case 1. Slightly overlapping load circles, $r = 5.41$ in., $p = 21.79$ psi.

Case 2. Overlapping load circles, $r = 6.0$ in., $p = 17.68$ psi.

Case 3. Just touching load circles, $r = 5.10$ in., $p = 24.48$ psi.

Case 4. Gapped load circles, $r = 2.25$ in., $p = 125.75$ psi.

Figure B-7 shows vertical stress intensity for three of the four cases. Case 4 results are not shown because those stress values exceeded the scale. As can be seen from Figure B-7, the stresses reach a maximum value under the centerline of each load segment when $r = 5.10$ in. This is also the case for $r = 2.25$ in. (Case 4). However when the load circles overlap ($r > 5.1$ in.), the peak stresses occur between centerline of the load segments. This gives an unrealistically high prediction of roadbed stresses. The data from circular loaded areas used to approximate tie loading must be used with caution. Only those pressure predictions immediately under the center of each load segment are accurate. Pressures at intermediate points should be ignored.

Figure B-8 shows similar effects on roadbed displacement. The case for $r = 5.1$ in. (case of just touching load circles) appears to be the load radius for which no oscillation occurs. The two overlapping load circle cases, $r = 5.4$ inches and $r = 6.0$ inches, show an increase in oscillation as the amount of overlap increases. The peak displacement for the cases $r = 5.4$ in. and $r = 6.0$ in. occur between centerlines of the load segments. This same peaking was consistently evident in the stresses σ_{yy} at $y = 2$ in. The case of a gapped load circle ($r = 2.25$ in.) is not shown here for scaling reasons, but the peak displacements for the gapped load circles occurred under the load segment centerline.

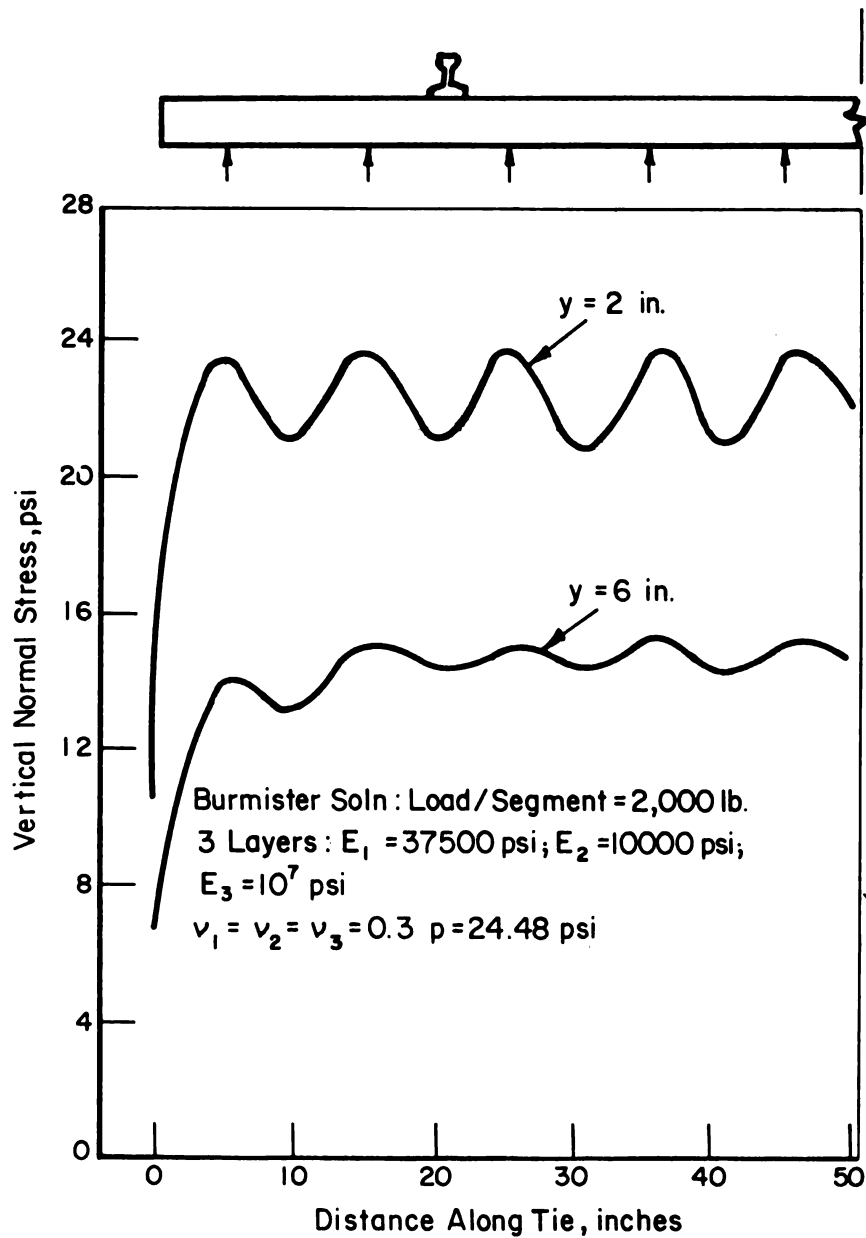


FIGURE B-6. PRESSURE DISTRIBUTION ALONG TIE BOTTOM FOR UNIFORM ROADBED LOAD DISTRIBUTION

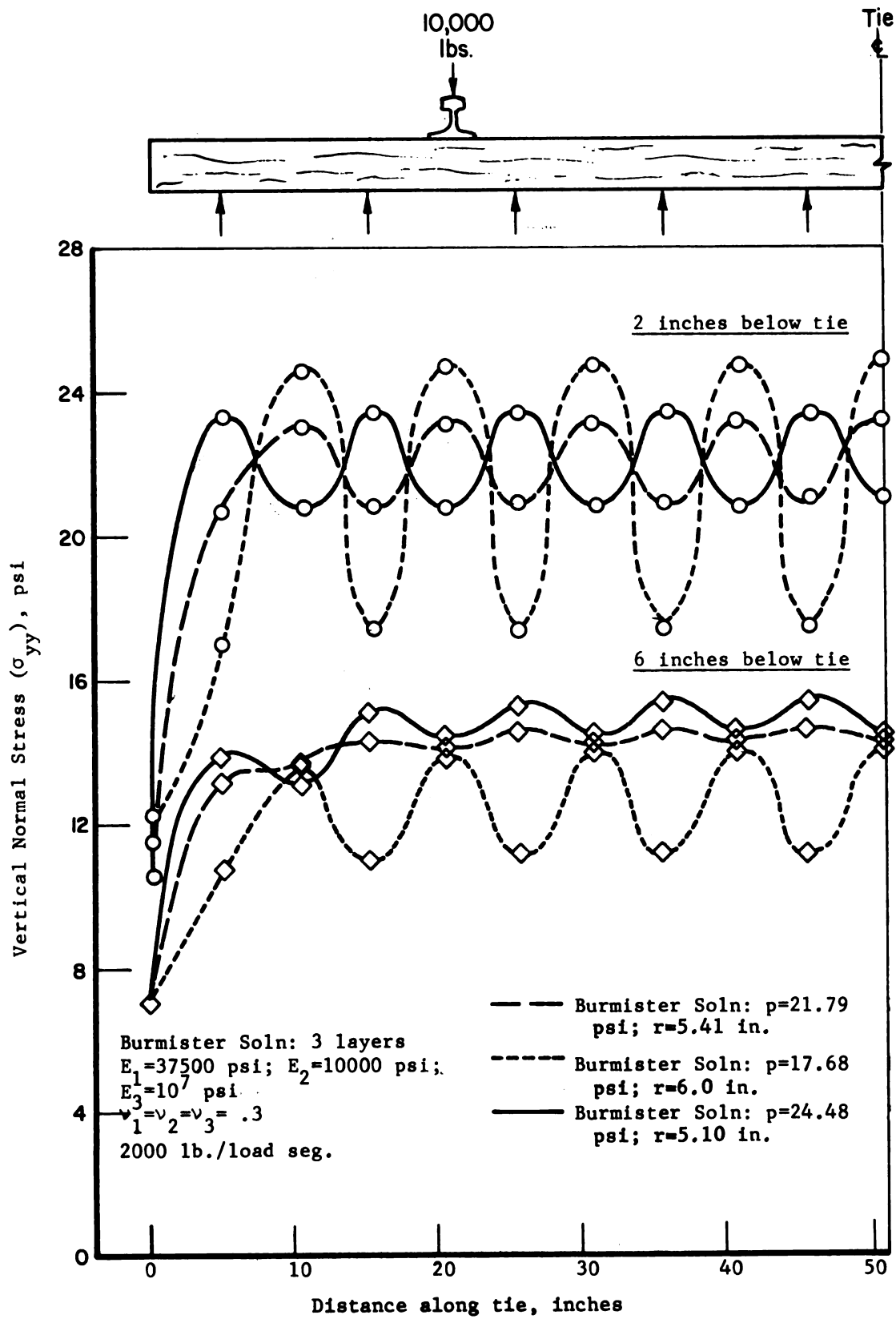


FIGURE B-7. EFFECT OF LOAD CIRCLE RADIUS ON FOUNDATION STRESSES

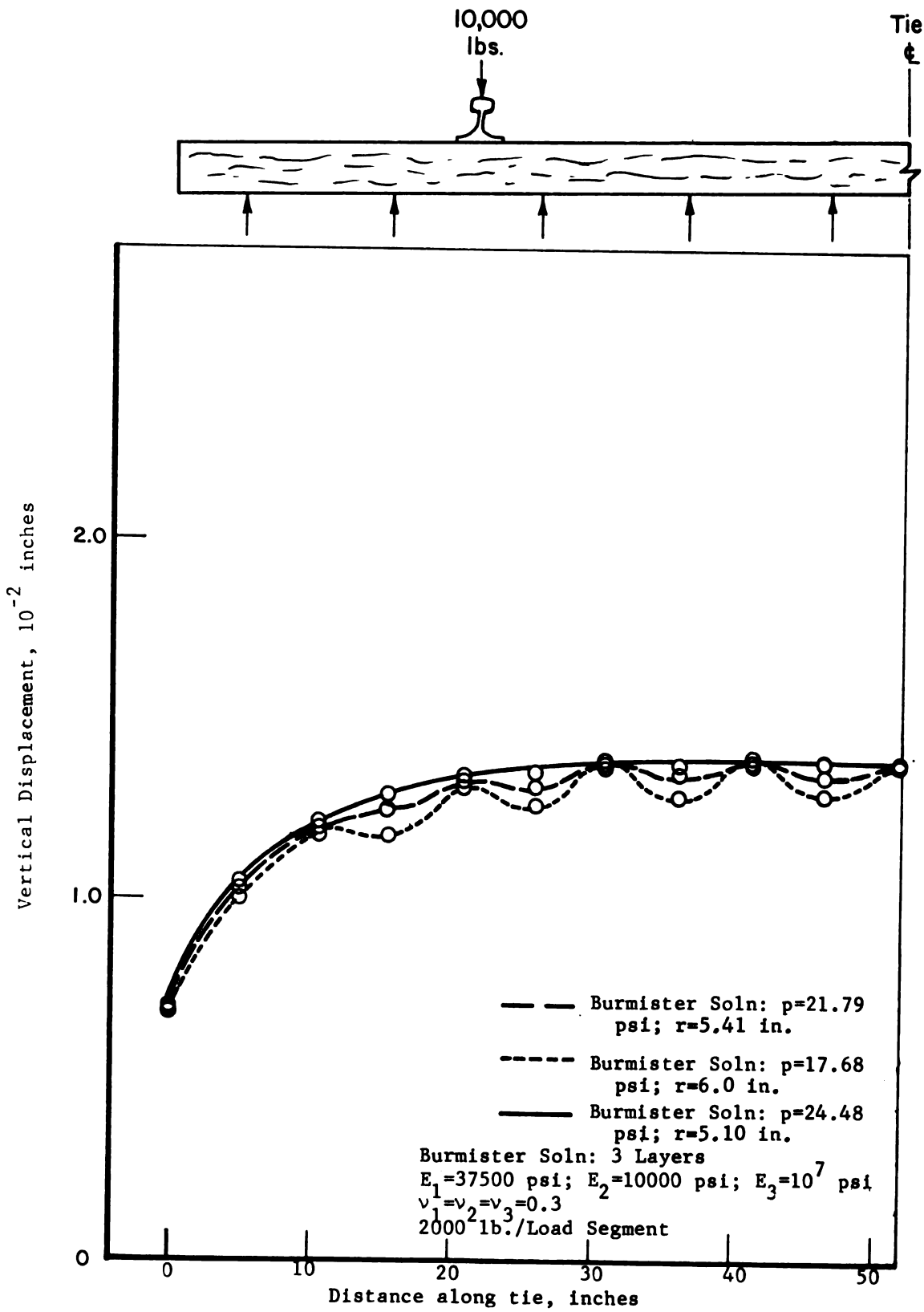


FIGURE B-8. EFFECT OF LOAD CIRCLE RADIUS ON FOUNDATION DISPLACEMENT (at Tie-Ballast Interface)

The misinterpretation of the Burmister displacement predictions is not only possible, but quite probable, if only a few points are monitored. Figure B-8 shows that if only the peak values were determined, one might erroneously conclude that displacement was independent of the applied pressure. However, the displacements under the center of each load segment give a more accurate analysis and show that increasing the pressure for a constant total load does increase the displacement, as expected.

Knowing the behavior of the Burmister stress and displacement predictions, the track structure can be modeled so that the stress and displacement influence functions needed as input to the loads combination program can be predicted accurately. It is recommended that the following guidelines be used in formulating a track model:

- a. Choose a sufficient number of load segments for the tie so the load segment aspect ratio is near unity. Use this number of circular load segments in the Burmister simulation.
- b. Select the load circle radius so the area of the circular load segment is equal to the area of the nearly square load segment.
- c. Pick those values of stress and displacement directly under the centerline of the load segments for information used in the loads combination program. These values represent the best approximation to the stress/displacement behavior in the foundation.

Comparison of Burmister and PSA Solutions for Roadbed Pressure

The values of vertical stress intensity were calculated at several stations along the length of a single tie and at various depths through the foundation using both PSA and Burmister computer codes. The PSA model chosen for the foundation for this single tie case is illustrated in Figure B-3. The model for the Burmister code is similar except for infinite horizontal dimensions and a third layer of $E_3 = 10^7$ psi to simulate the PSA rigid boundary. The justification for using this value of E_3 was discussed

previously. The Burmister and PSA stress predictions shown in Figure B-9 for this single tie case show that the stresses from the two methods of solution are generally in good agreement. Only those stresses directly under the center of the load segments are plotted for the Burmister solution to eliminate the oscillation between segments.

Figure B-9 also shows that the stresses are relatively insensitive to the number of layers or the modulus of the bottom layer.

Effect of Ballast Geometry

An evaluation of ballast cross-sectional geometry effects was made using the PSA model for comparison with the multi-layer analysis. The model used was the configuration shown in Figure B-3. Two ballast shoulder widths and 2 subgrade depths were evaluated. The ballast shoulder end slope was kept at a constant value of 2:1, which is typical of ballast profiles. The ballast shoulder width was varied from 6 inches to 24 inches and the subgrade depth was varied from 18 to 30 inches.

The results of varying the ballast shoulder width and subgrade depth are shown in Figures B-10 and B-11. Reducing the shoulder width by a factor of 4 (from 24 inches to 6 inches) only slightly affected those stress values near the end of the tie. Increasing the soil depth by 67 percent (from 18 inches to 30 inches) did not affect the stress predictions, see Figure B-10. It can be concluded that finite shoulder width and soil depth variations have little effect on the stress predictions.

Figure B-11 shows the effect of ballast/subgrade geometry on the displacement predictions. As expected, ballast shoulder width variations have little effect on the displacement while extending the depth of the soil has a significant effect on the displacements. The Burmister solution for $r = 5.41$ inches (slightly overlapping load circles) and a rigid third layer is superposed on Figures B-10 and B-11 for comparison.

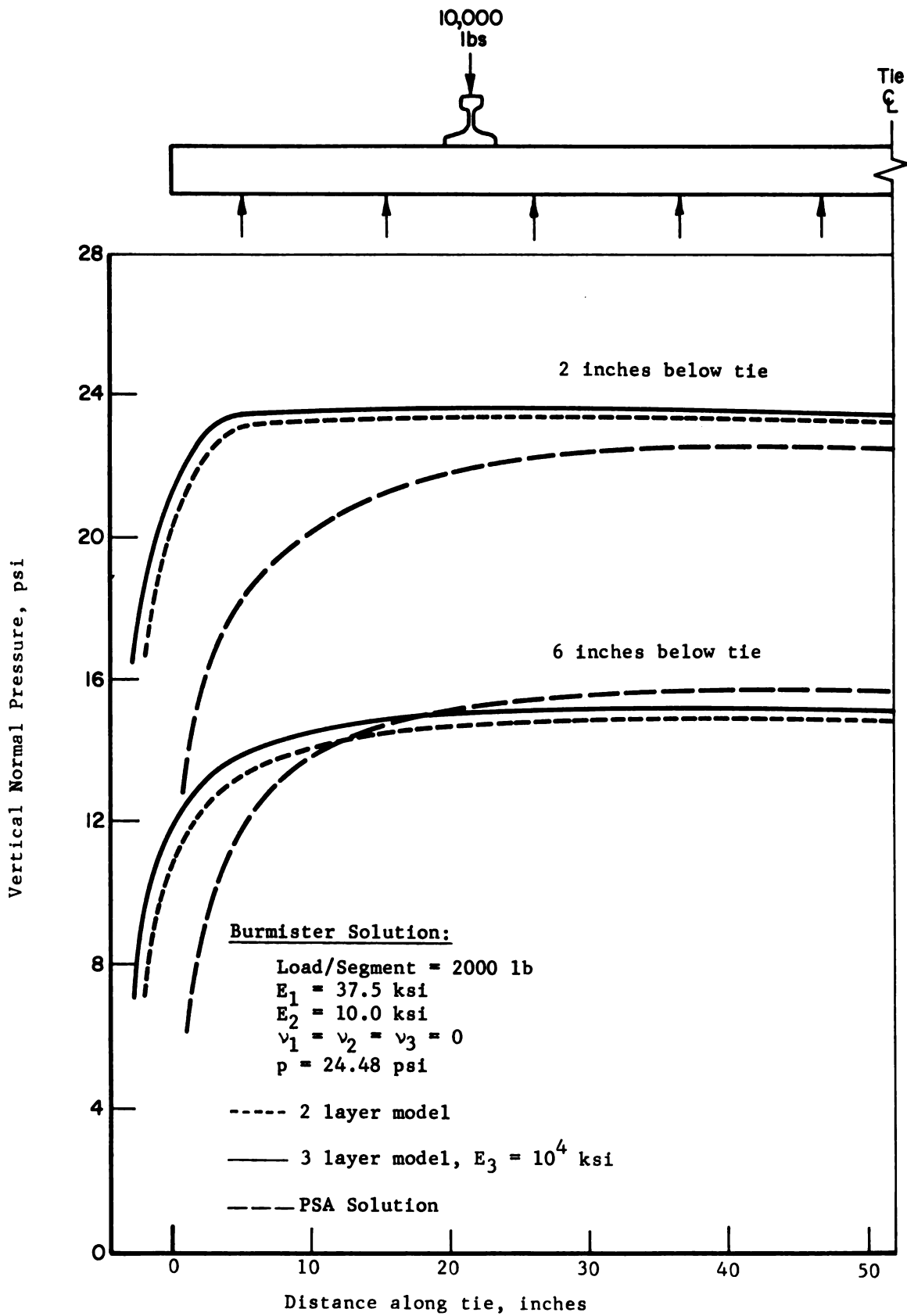


FIGURE B-9. COMPARISON OF BURMISTER AND PSA ROADBED PRESSURE PREDICTIONS

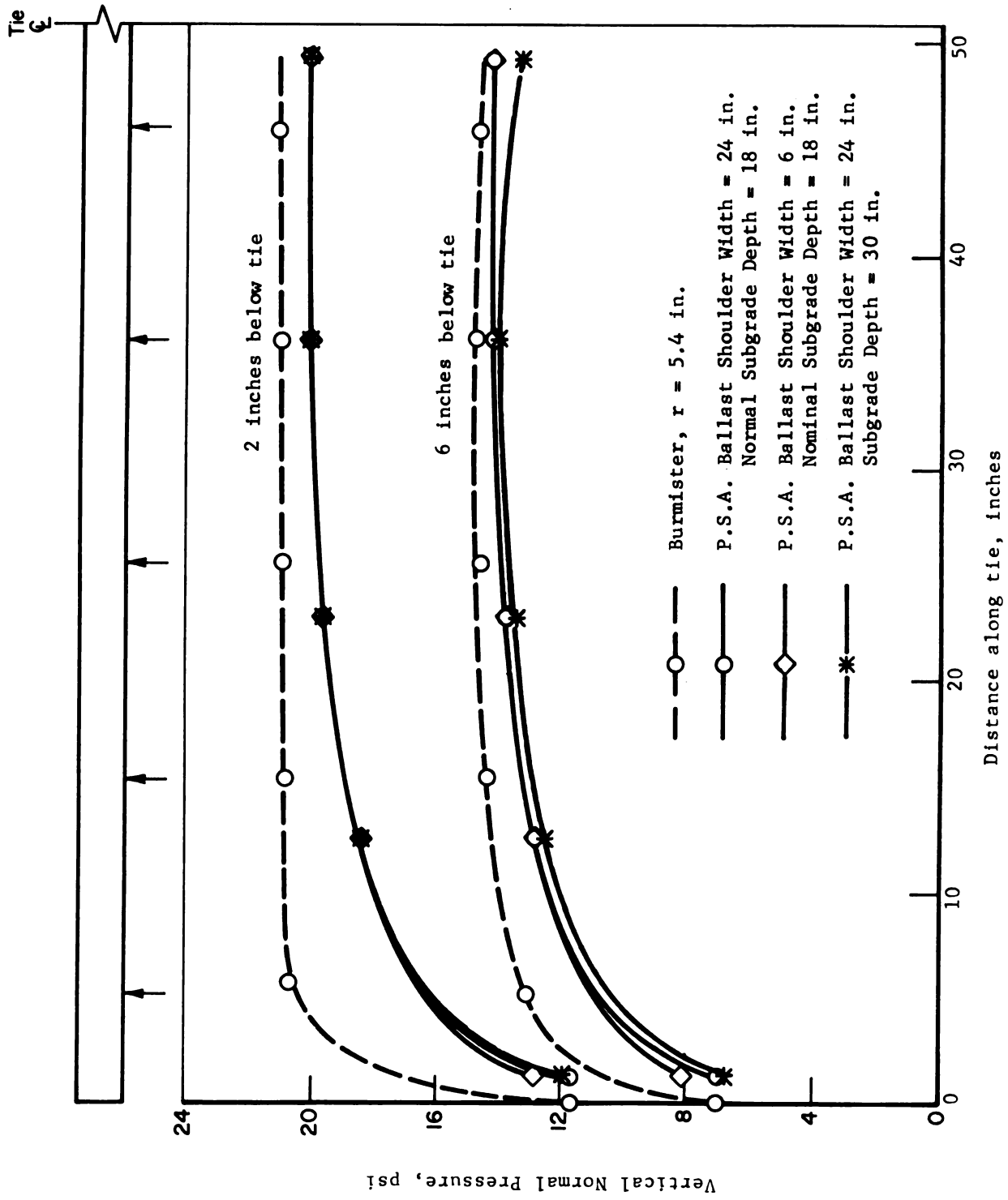


FIGURE B-10. COMPARISON OF BURMISTER AND PSA ROADBED PRESSURE PREDICTIONS

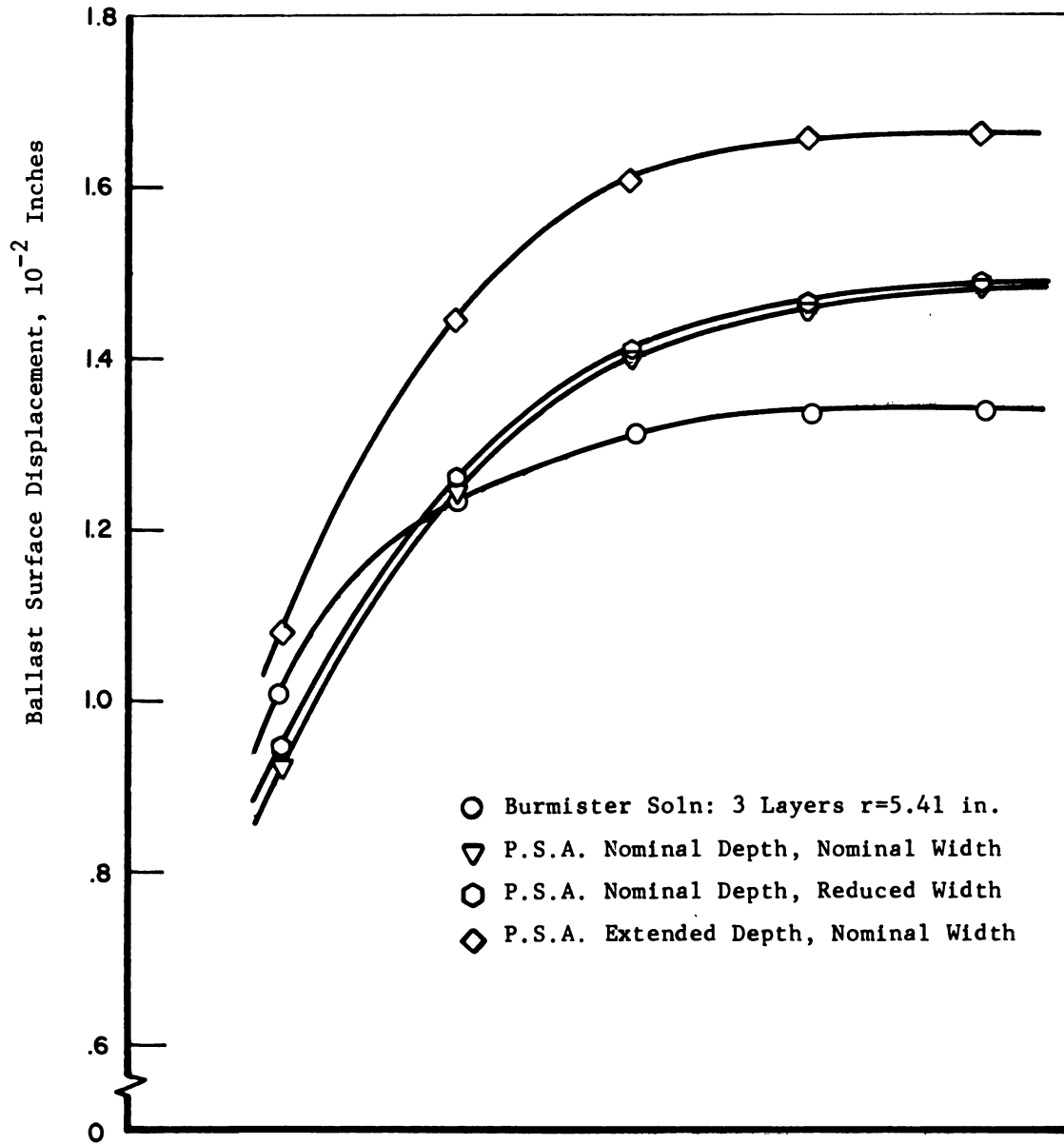
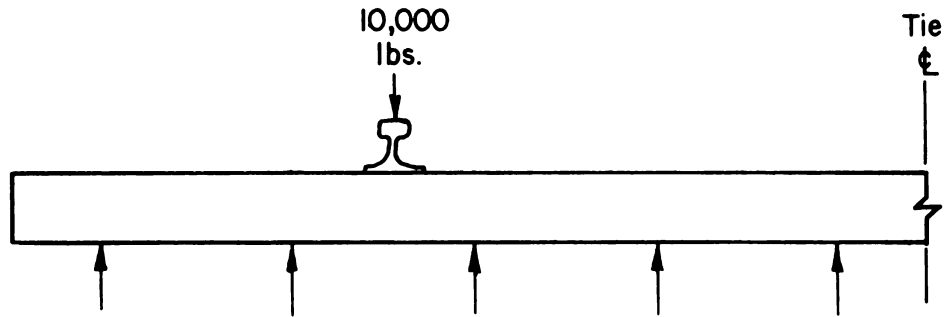


FIGURE B-11. EFFECT OF BALLAST/SUBGRADE GEOMETRY ON DISPLACEMENT OF BALLAST SURFACE UNDER A TIE

Effect of Tie Bending

The effect of tie bending on ballast-tie reactions, displacements and foundation stresses was evaluated using a single tie case. Results of the load combination program using influence functions from the PSA analysis and from the Burmister analysis were compared. The basic input from the foundation analysis to the load combination program are the displacement and stress influence functions. The displacement influence function is made up of a series of displacement shapes of the foundation surface node points from a unit load applied at each foundation surface load segment. The stress influence function is made up of a series of stress vectors, each one being the stress response at selected points in the foundation due to a unit load applied at each foundation surface load segment.

The loads/composition program is a matrix equation solver that couples the reactions for the rails and ties with the influence functions for the roadbed. The loads/composition program was modified by BCL to properly handle the Burmister influence functions. Figure B-12 compares results from using roadbed influence functions for a single wood tie from the Burmister and PSA codes as input to the loads program. In general, there is good agreement between the two methods for roadbed stresses, and the inclusion of tie bending is quite noticeable in the pressure distribution under the tie.

The effect of tie and rail bending on ballast reactions, foundation stresses, and rail/tie displacements was evaluated using a track section with 3 ties. Wood ties and steel rails with the properties listed below were used.

	<u>Tie</u>	<u>Rail</u>
Size	7"x9"x102"	132 lb/yd
Young's Modulus (E), psi	1.83×10^6	28.9×10^6
Area (A), in. ²	63	12.95
Area Moment (I), in. ⁴	275.25	89

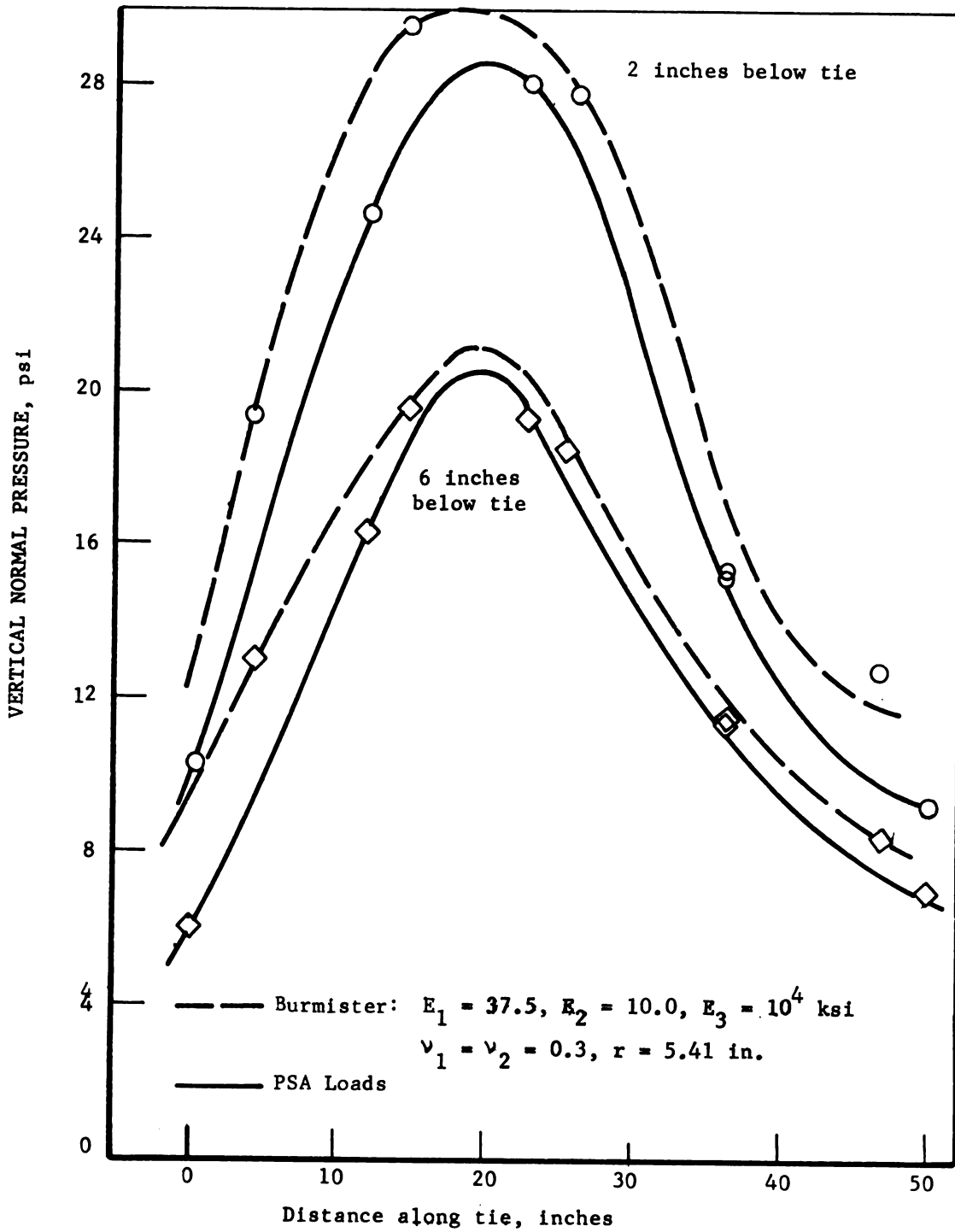


FIGURE B-12. EVALUATION OF TIE BENDING EFFECTS

The 10,000 lb -wheel loads were symmetrically placed on the rails over the center tie. The ballast-tie reaction values from both codes are shown in Figure B-13. The shapes of the force distributions compare favorably with the exception that at the end of the tie and at the tie centerline the Burmister load predictions are somewhat higher than the PSA loads predictions.

Figures B-14 and B-15 show the comparison of stress contours in the roadbed at depths of 2 in. and 6 in., respectively. The stresses calculated from the Burmister loads program are slightly higher at the ends and centers of the ties, which is consistent with the deflection functions.

Figures B-16 and B-17 show the results for an evaluation of tie bending stiffness (wood versus concrete). The wood ties for this analysis were the same as those used previously. The simulated concrete tie had the same bearing area as the wood tie and an average value of bending stiffness of $EI = 1.58 \times 10^9 \text{ lb-in.}^2$.

This is approximately 50 percent higher than the measured stiffness of the FEC concrete tie. Figure B-16 shows a comparison of tie-ballast reactions and rail-tie displacements for concrete and wood ties. The effect of the concrete tie is to move the peak reaction toward the end of the tie and lower the tie-rail displacement. This is not totally unexpected since the concrete tie is more than 3 times as stiff as the wood tie. That is, the stiffer the tie, the more the response should resemble that of a rigid plate on an elastic half space. This is also evident from the stresses shown and compared in Figure B-17. The stresses at the ends of the concrete tie should increase relative to the stresses at the ends of the more flexible wood ties. Also the general smoothing of the stresses toward the center of the concrete tie is consistent with classical analyses and earlier studies.

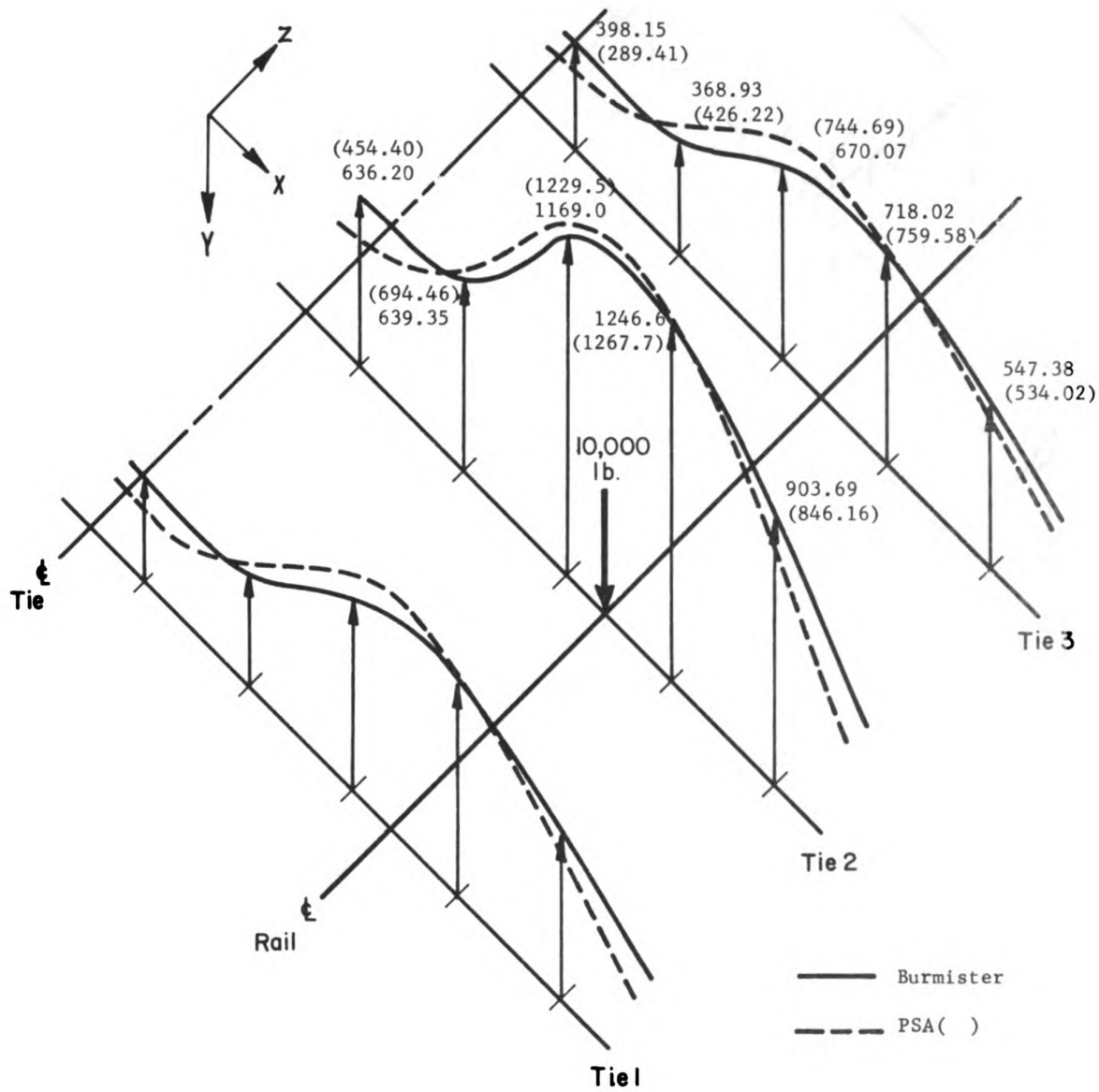


FIGURE B-13. COMPARISON OF BALLAST-TIE REACTIONS(LBS) FOR WOOD TIE TRACK STRUCTURE

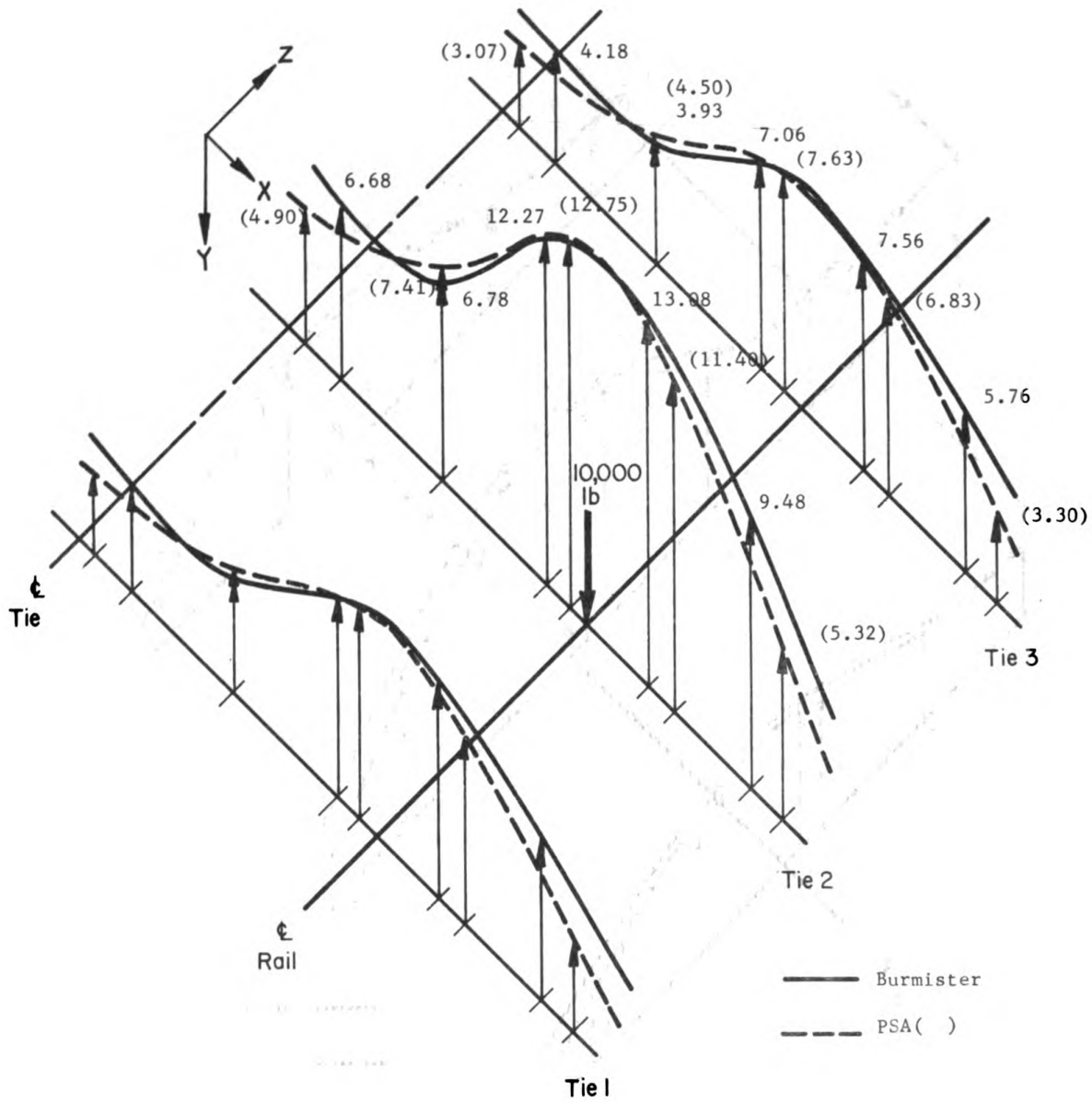


FIGURE B-14. COMPARISON OF BALLAST STRESSES (PSI)
 2 INCHES BELOW TIE FOR WOOD TIE
 TRACK STRUCTURE

Generated for Ricardo Jose Quiros Orozco (University of Illinois at Urbana-Champaign) on 2018-07-23 00:57 GMT / http://hdl.handle.net/2027/mdp.39015040727094
 Public Domain, Google-digitized / http://www.hathitrust.org/access_use#pd-google

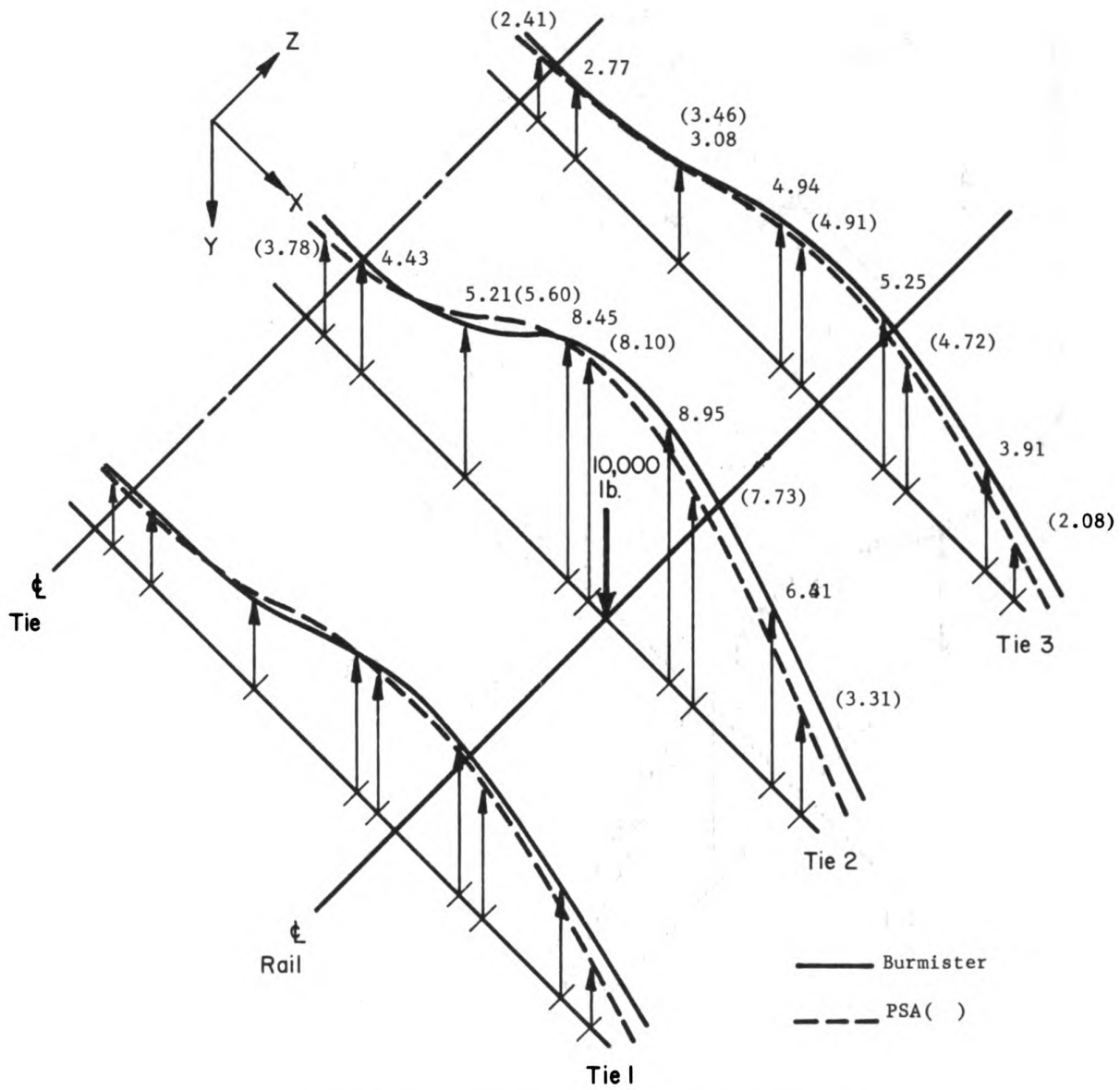


FIGURE B-15. COMPARISON OF BALLAST STRESSES (PSI) 6 INCHES BELOW TIE FOR WOOD TIE TRACK STRUCTURE

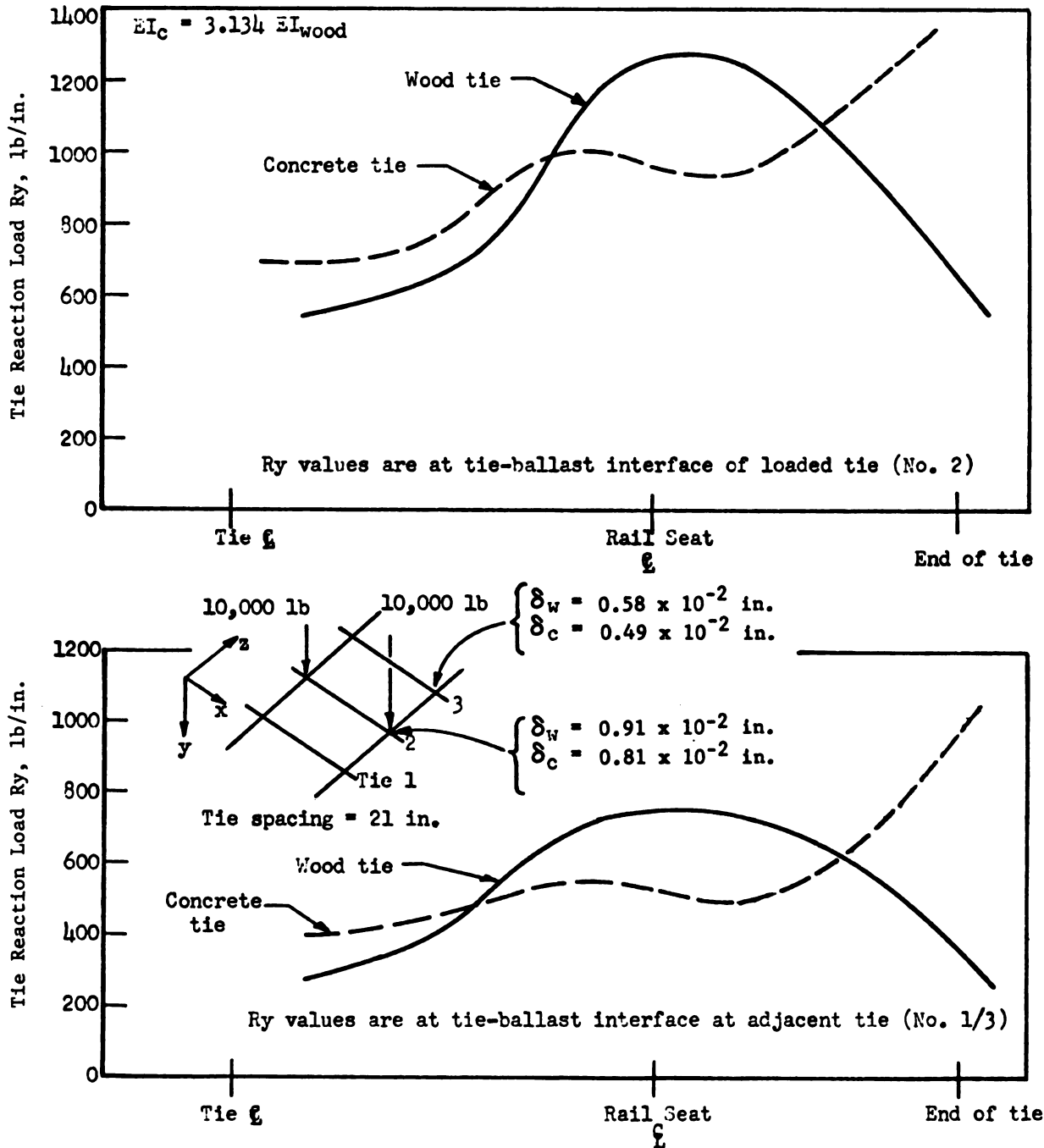


FIGURE B-16. TIE-BALLAST REACTIONS FOR WOOD AND CONCRETE TIES

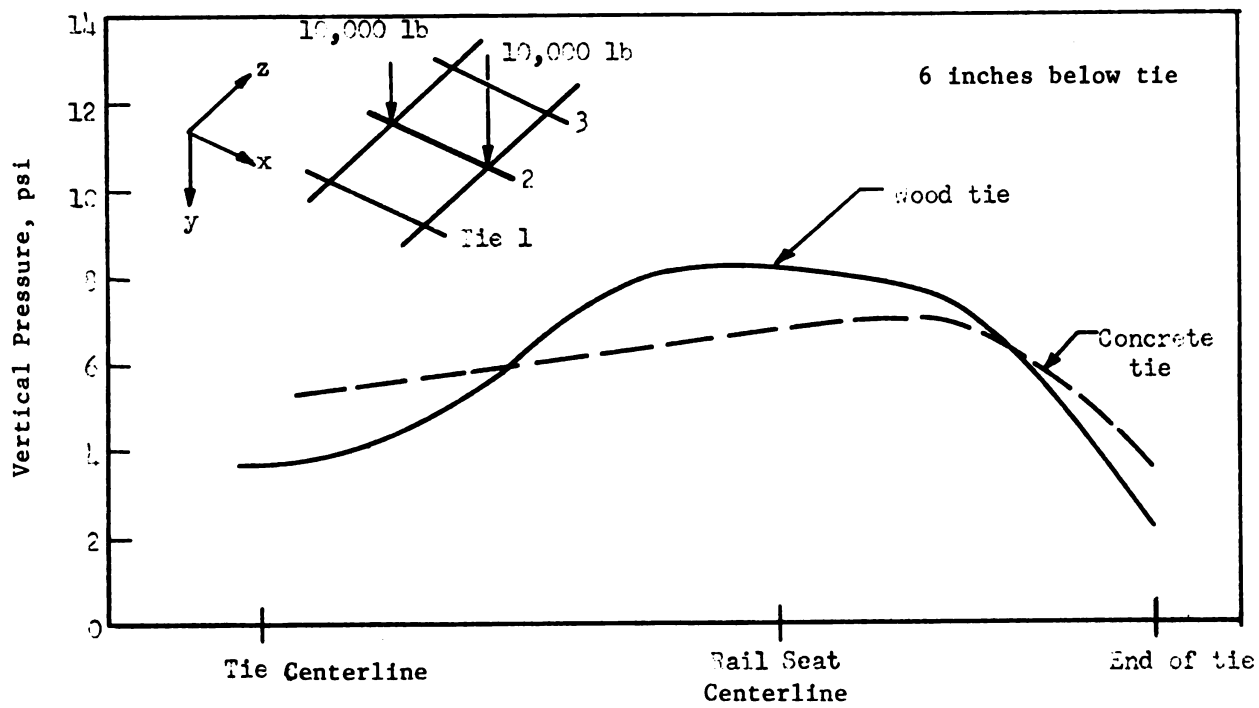
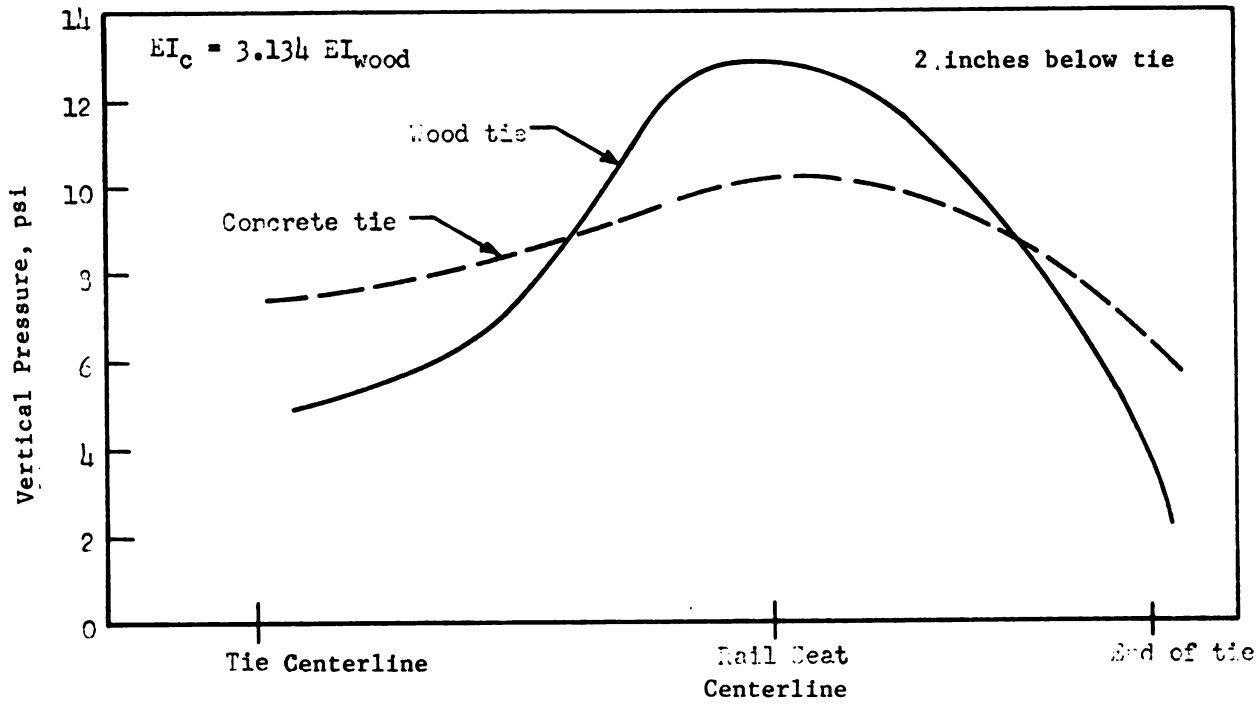


FIGURE B-17. BALLAST PRESSURE UNDER CENTER TIE

APPENDIX C

CALIBRATION OF INSTRUMENTED TIE PLATES

Introduction

The objectives of the tests reported herein were to calibrate the instrumented tie plates and measure the stiffness characteristics of both the standard and instrumented tie plate and rail fastener assembly used for the FEC concrete ties.

Technical Discussion

Laboratory tests were performed to establish the characteristic stiffness properties of a standard rail fastener assembly consisting of a True Temper Cliploc fastener and a 1/8-inch-thick polyethylene rail pad. Tests were also performed on the instrumented tie plate assembly shown in Figure C-1 to determine the change in stiffness of this assembly relative to the standard fastener. Figure C-2 shows the test configuration with the tie-plate installed on a concrete tie. Vertical and lateral loads were applied to a short section of 132-lb rail. Dial gauges were installed on diagonally opposite corners of the rail seat to average out any uneven compliance in the rail pad. Figure C-3 shows the vertical load-deflection curves for the standard and instrumented assemblies. The standard rail fastener showed a vertical stiffness of 7.27×10^6 lb/in. compared to the instrumented tie plate and fastener stiffness of 2×10^6 lb/in. However, considering only the fastener stiffness, an instrumented track section would have a track modulus of $U = 83,300$ psi for 24-inch tie spacing and 100,000 psi for 20-inch tie spacing. This is much higher than normal track modulus measurements, so the effect of fastener stiffness should be minor. The increased compliance of the instrumented assembly may be attributed to the reduced loading area on the rail pad, the deflection of the load cells and load washers, some increase in deflection of the bolts and rail clips and local deformation of the rail base.

Lateral stiffness data for several different vertical loads are shown in Figure C-4. The lateral performance of both fastener configurations were compromised by the inherent characteristic of the rail to slip laterally under the rail clips. The 1:4 slope of the top of the rail base wedges the field side clip and unloads the gage side clip. To alleviate this problem (which

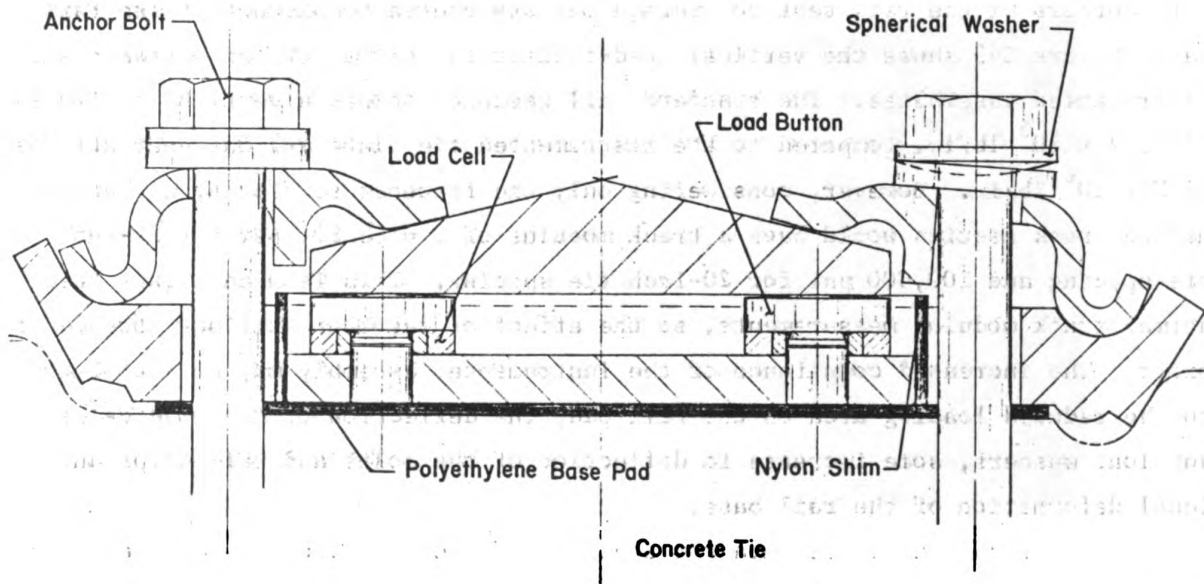
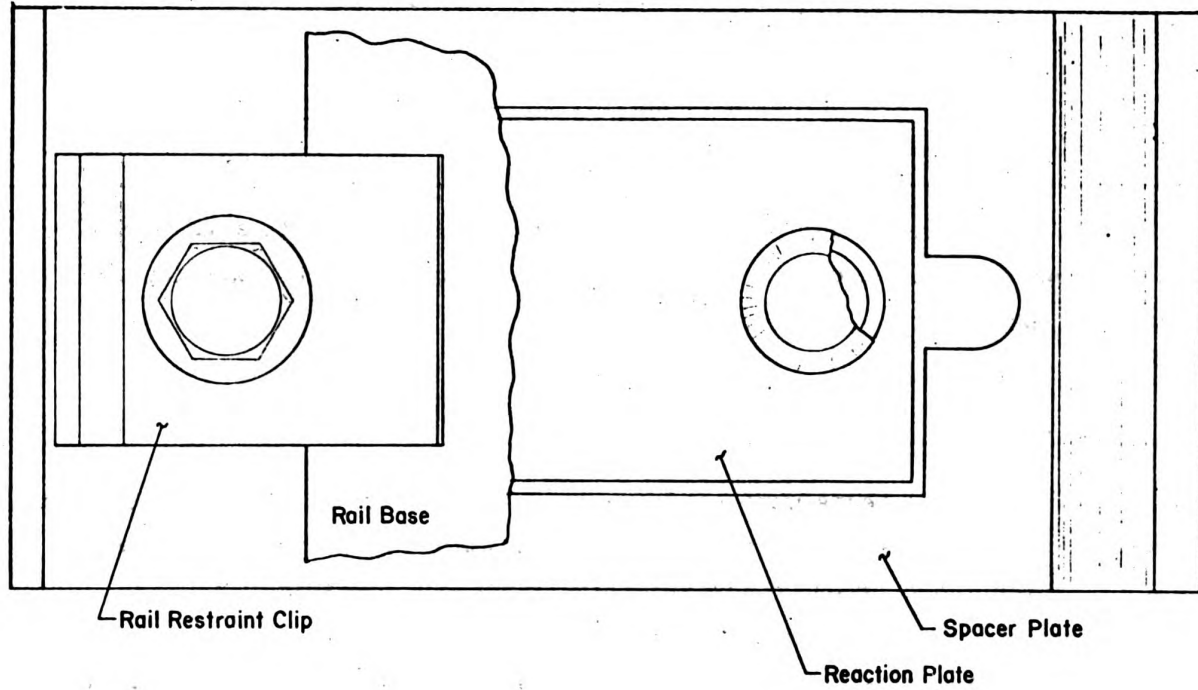


FIGURE C-1. INSTRUMENTED TIE PLATE ASSEMBLY

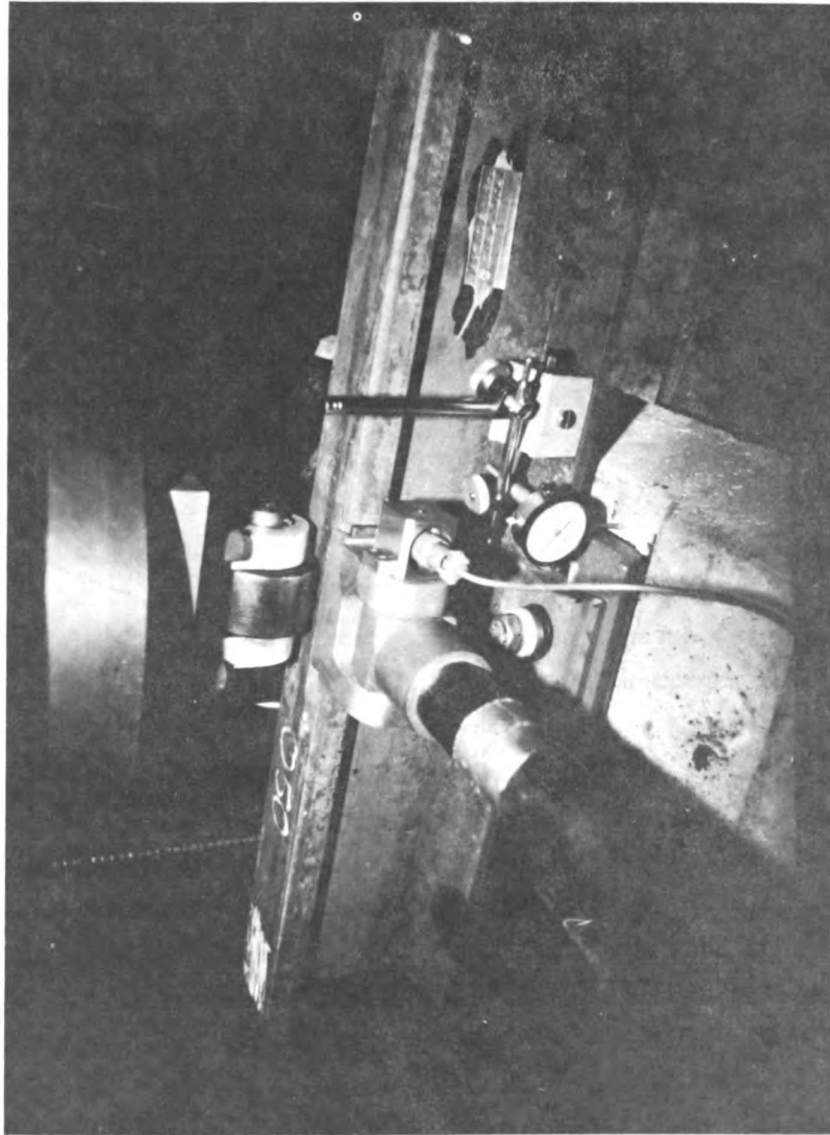


FIGURE C-2. INSTRUMENTED TIE PLATE TEST CONFIGURATION

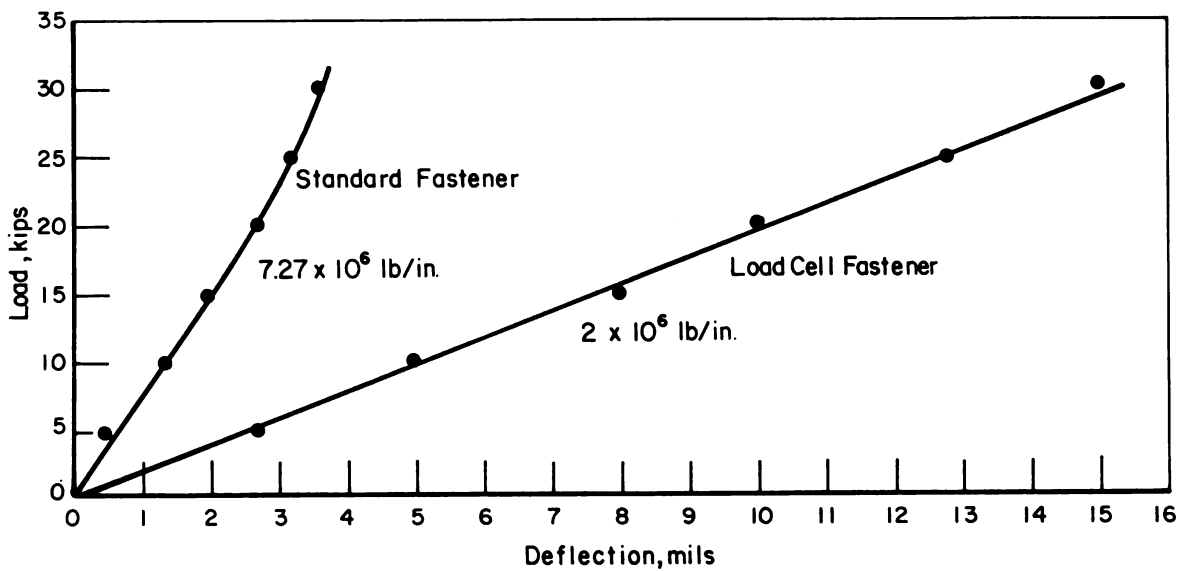


FIGURE C-3. VERTICAL STIFFNESS CURVE FOR RAIL FASTENER ASSEMBLIES

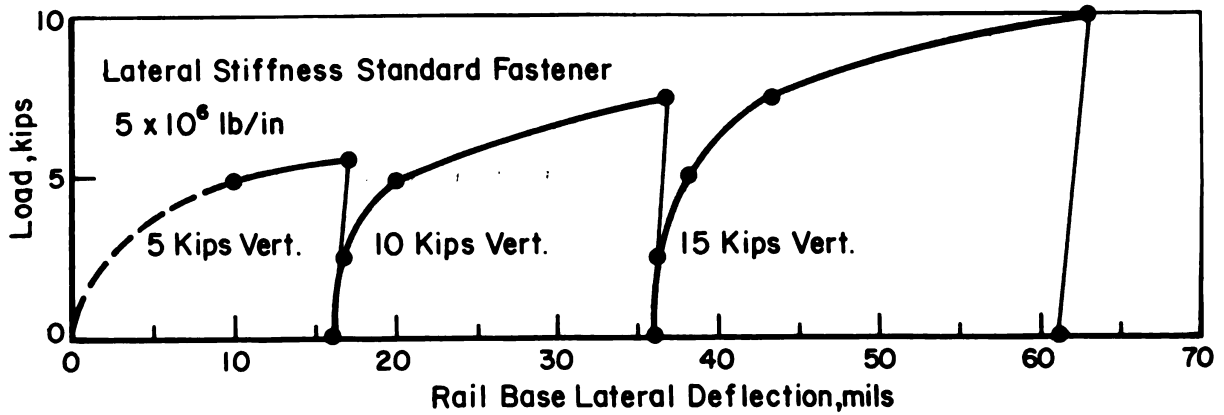
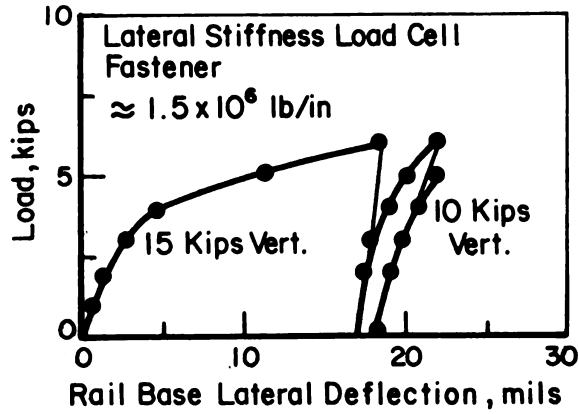


FIGURE C-4. LATERAL STIFFNESS CURVES FOR RAIL FASTENER ASSEMBLIES

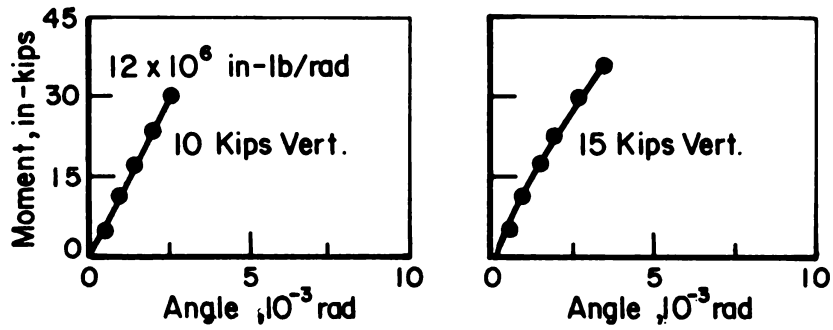
also occurs in the field) the rail would have to be loaded laterally to values greater than the maximum expected loads and then the gauge side clip should be retorqued. The rotational stiffnesses shown in Figure C-5 have similar reactions to lateral slip.

Figure C-6 is a plot of the change in output of the four load cells as a function of vertical load applied at the rail head. Two of the load cells measure reactions at the rail base and the other two measure the changes in fastener preload. A complete force balance cannot be determined with the load cells installed due to the manner in which part of the fastener bolt load is transferred through the rail clip into the concrete. However, the ratio of load applied to the rail (total rail seat load) to the total load measured at the rail base by the load cells represents a factor to be applied to the measured output of the "tie plates" during the test program. This ratio was measured as 1.18 compared to 1.14 based on an analytical estimate of the fastener stiffness.

Calibration of the individual load cells was performed using a standard hydraulic test machine and a reference load cell. The sensitivities were measured through the data acquisition system amplifiers with a 100-ft extension data cable to duplicate field test conditions. The sensitivity of individual load cells showed variations requiring that individual calibration factors be used for each cell. Table C-1 summarizes these load cell calibrations based on their sensitivities at 20 kips. Figure C-7 is a typical sensitivity curve for the response characteristics of these transducers.

Post test calibrations of the surviving load cells revealed a shift in sensitivities for several load cells that was large enough to effect the results of the test program. An evaluation of the changes suggests that wear occurring at the load cell interfaces is causing these shifts in sensitivity. To minimize the effect of this change, the average of the pre- and post-test calibrations was used to establish final calibration factors for the tie plate data.

Load Cell Fastener



Standard Fastener

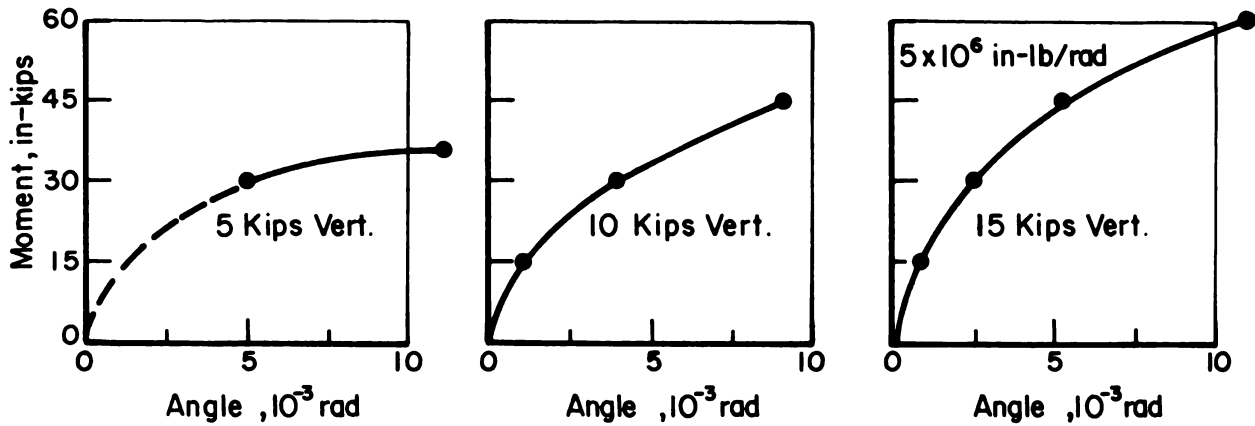


FIGURE C-5. ROTATIONAL STIFFNESS CURVES FOR RAIL FASTENER ASSEMBLIES

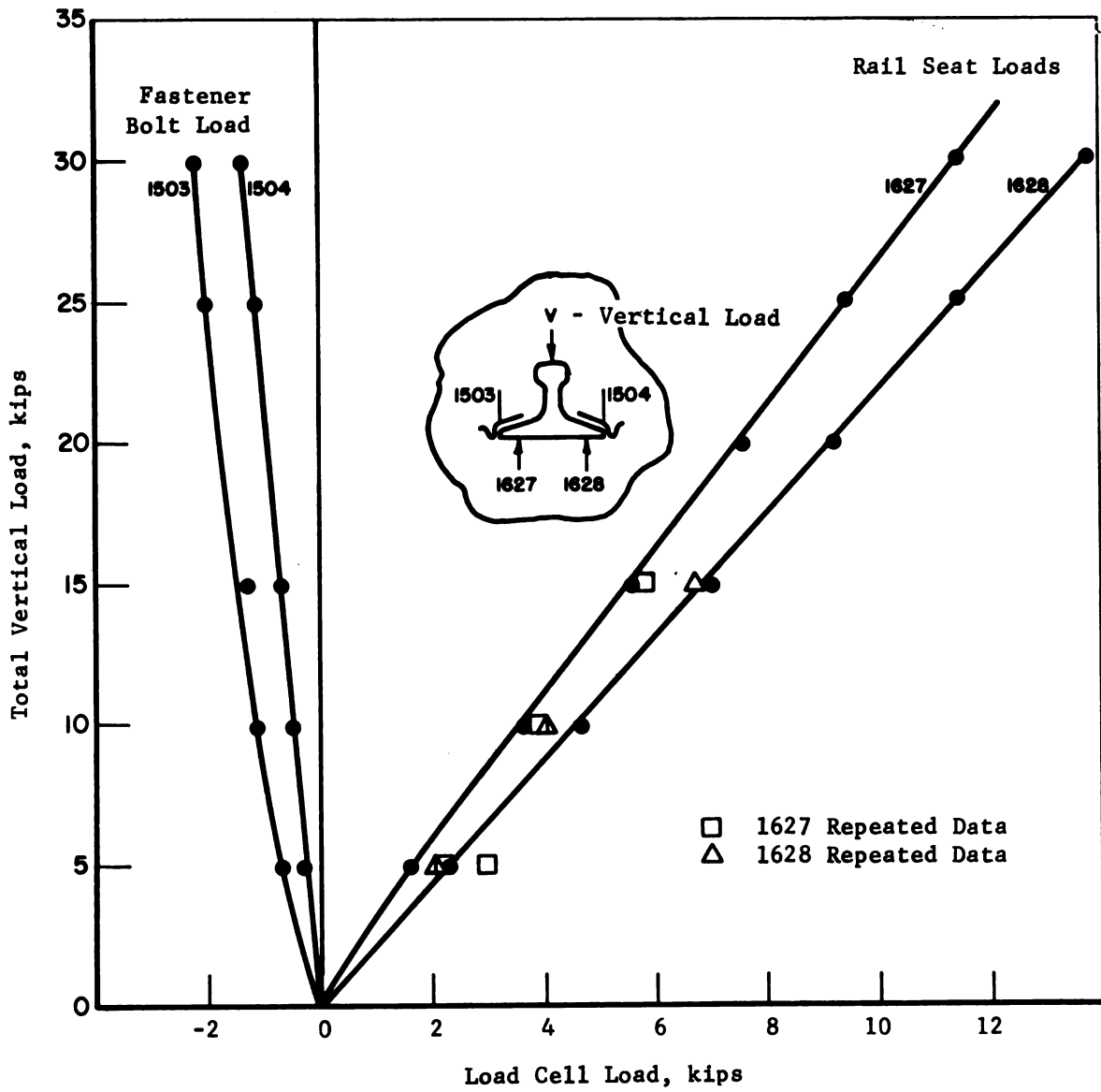


FIGURE C-6. LOAD DISTRIBUTION IN RAIL SEAT LOAD CELLS AND FASTENER BOLT LOAD CELLS

TABLE C-1. LOAD CELL CALIBRATION SUMMARY

Cell	Orig. Cal. (20 kips)	Post Cal (20 kips)	Avg.	Δ	Factor $\frac{1.18}{\Delta}$
1479	2.37 mv/v	3.09 mv/v	2.73	1.30	0.91
1480	1.42	1.60	1.51	1.13	1.04
1482	1.44	Failed	(1.79)*		(0.95)
1485	3.06	3.31	3.19	1.08	1.09
1625	2.16	2.54	2.35	1.18	1.00
1626	2.16	Failed	(2.68)*		(0.95)
1627	2.22	3.12	2.67	1.41	0.84
1628	2.22	Failed	(2.75)*		(0.95)
1629	2.16	2.30	2.23	1.06	1.11
1630	2.12	3.24	2.68	1.53	0.77
1631	2.15	2.41	2.28	1.12	1.05
1632	2.16	2.91	2.54	1.35	0.87

$$\bar{X} (\Delta) = 1.24 \pm 0.16$$

* Determined from mean values of surviving load cells

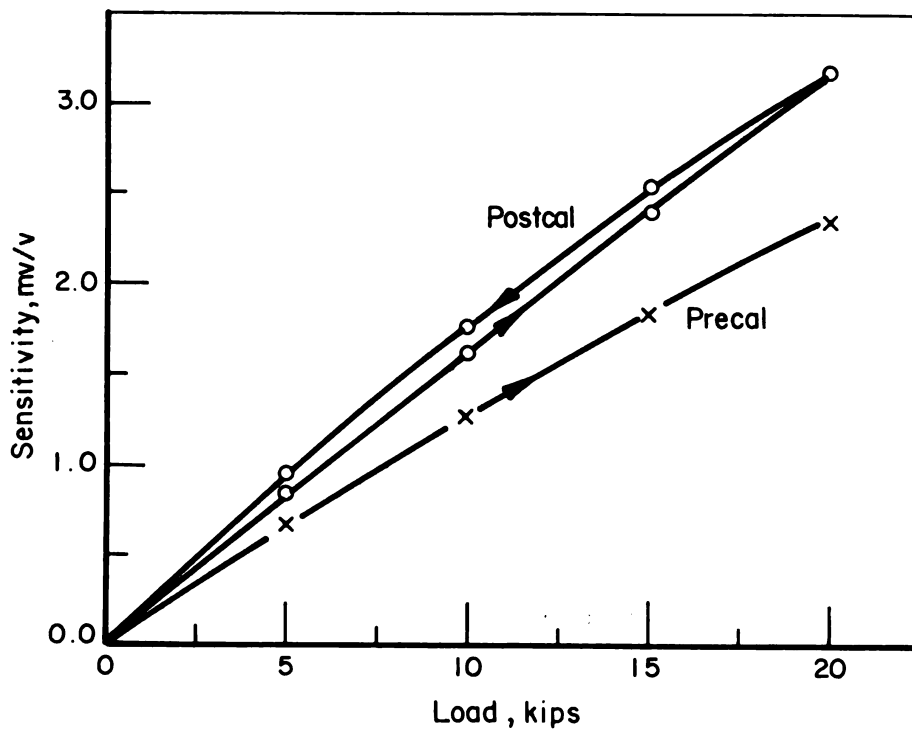


FIGURE C-7. TYPICAL LOAD CELL RESPONSE CURVE (NO. 1479)

APPENDIX D

CALIBRATION OF FRA/PCA LOAD CELL TIES

Introduction

The objective of the test reported herein was to measure the sensitivities of the repaired load cell ties in preparation for their installation at the FEC test site.

Technical Discussion

The FRA/PCA load cell ties (LCT) were designed and built by the Portland Cement Association (PCA) and were initially installed in the Kansas Test Track (KTT). During the time they were installed in the KTT they suffered damage from water and mud seepage. An examination of the simulated concrete ties at BCL resulted in the selection of three for repair and refurbishment. Water damage to the gages on the fourth tie (CT-3) was excessive, so repairs were discontinued.

The load cell ties which simulate a concrete tie are a steel channel section that has been reinforced to the bending stiffness of the RT-7 tie. This channel section is the upper portion of the tie and it rests on 40 spools on which the gaging is done to measure tie/ballast pressure. Twelve additional spools support the two rail base plates for measuring vertical tie plate load. Each spool has two longitudinal and two transverse strain gages. Sets of four adjacent spools on the bottom side (and the six spools supporting each rail base) are wired into individual bridges. All wiring is routed along the length of the tie between the rows of spools and terminated in "old style" MS connectors. The entire underside of the tie, including spools, wiring and connectors, was coated with a heavy layer of beeswax. A bottom cover was mounted on each set of four spools to provide the reaction face for that region of the tie bottom.

Calibration

After the three load cell ties were repaired they were each installed in a hydraulic test machine. The two rail seat load cells and the ten ballast pressure load cells on each tie were subjected to a load cycling to check for

any zero shifts or hysteresis. This would indicate any remaining defective strain gage installations. After each cell was cycled, a calibration was performed using a standard null-balance strain indicator.

Table D-1 summarizes the sensitivities of each ballast pressure load cell for a 10 kip change in load. The mean sensitivity is 233.5 $\mu\text{v/v/10 kips}$ and the standard deviation is 2.8 $\mu\text{v/v/10 kips}$, or about ± 1 percent. The area of each load face is 118.25 in.² yielding a mean pressure sensitivity of 2.76 $\mu\text{v/v/psi}$. This mean value of sensitivity will be used for all of the load cell tie pressure cells because the cell-to-cell variation is so small.

TABLE D-1. SUMMARY OF BALLAST PRESSURE LOAD CELL SENSITIVITIES ($\mu\text{v/v/10 kips}$)

Load Cell	Tie CT1	Tie CT2	Tie CT4
1	229	230	231
2	235	228	233
3	238	233	230
4	236	238	234
5	236	235	236
6	230	233	237
7	235	236	234
8	233	230	235
9	233	230	236
10	234	239	231

Mean value = 233.5. Standard deviation = 2.8.

The rail seat load cells were loaded to 36,000 lb, and Table D-2 summarizes their sensitivities. The mean sensitivity is 103 $\mu\text{v/v/10 kips}$ and the standard deviation is 2.5 $\mu\text{v/v/10 kips}$. This mean value of sensitivity will be used for all of the rail seat load measurements. Figure D-1 shows the relative location of the load sensitive sections. Figure D-2 illustrates a sample sensitivity curve for a rail seat and a soffit load cell.

TABLE D-2. SUMMARY OF RAIL SEAT LOAD CELL SENSITIVITIES ($\mu\text{v}/\text{v}/10$ kips)

Load Cell	CT1	CT2	CT4
11	102	106	102
12	104	103	98.3

Mean value sensitivity = 103. Standard deviation = 2.5 \approx 2.4 percent.

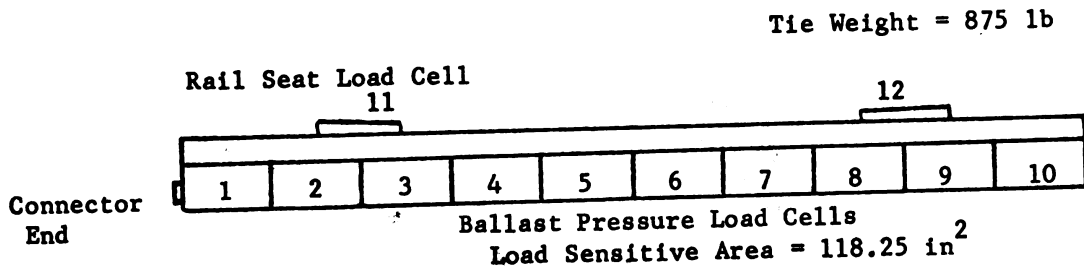


FIGURE D-1. RELATIVE LOCATION OF LOAD SENSITIVE SECTIONS

Wiring Diagrams

The circuit diagrams shown in Figure D-3 for the soffit and rail seat load cells illustrate rather elaborate bridge configurations. Because individual calibrations of single load spools is not practical, it is important that these spools and the gage installations on them, be as consistent as possible to minimize variations of sensitivity with load location.

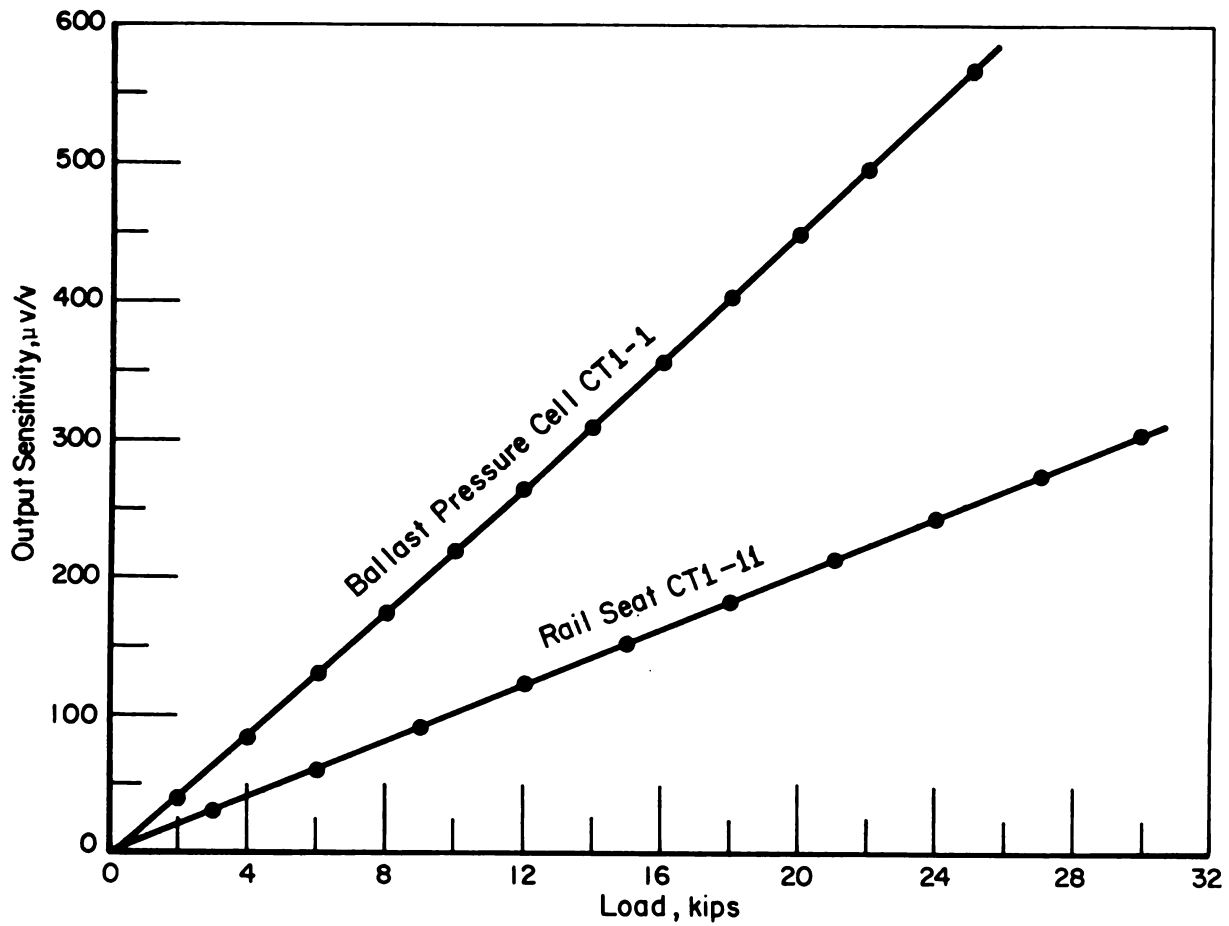
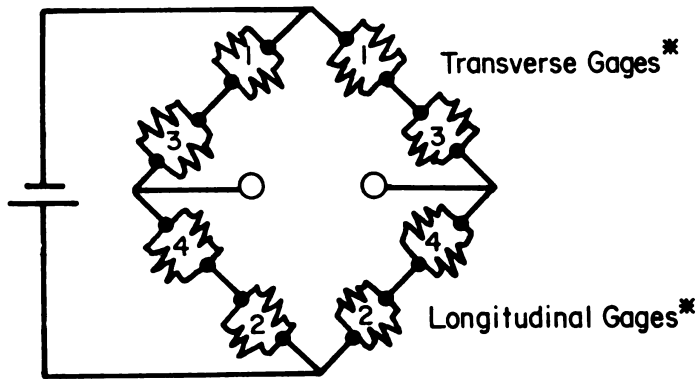
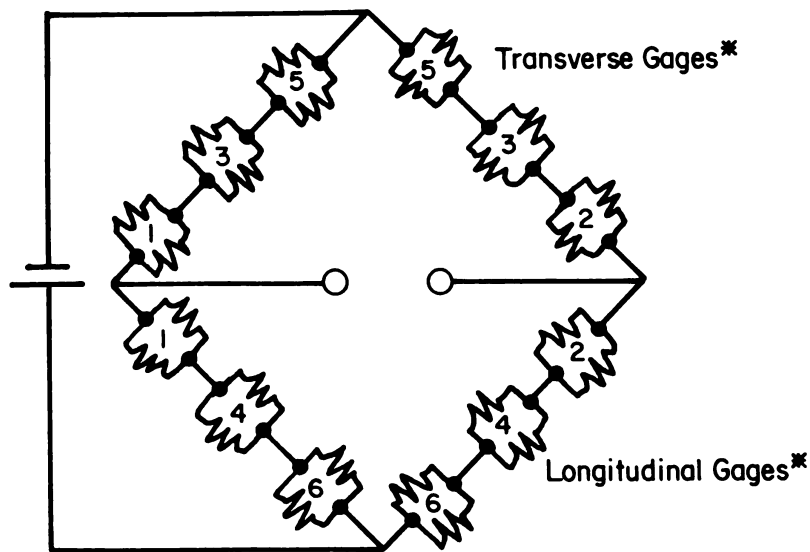


FIGURE D-2. TYPICAL SENSITIVITIES FOR BALLAST PRESSURE AND RAIL SEAT LOAD CELLS



Ballast Pressure Load Cell Schematic (4 spools)



Rail Seat Load Cell Schematic (6 spools)

* 2 Longitudinal and 2 Transverse Gages per Spool

FIGURE D-3. BALLAST PRESSURE AND RAIL SEAT LOAD CELL SCHEMATICS

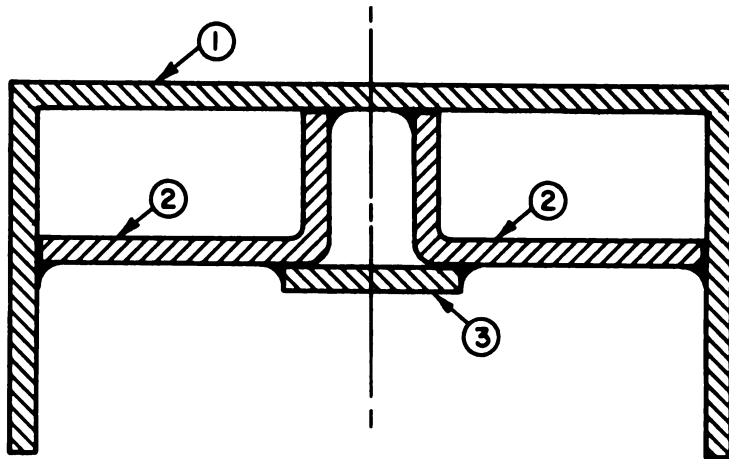
Comparison of the Bending Stiffness of the
FRA/PCA Load Cell Tie and the RCCC Tie

The stiffness curves furnished by PCA for the load cell and RT-7 ties were established strictly by theoretical calculations based on the gross cross sectional properties of each of the ties. A modulus of 5×10^6 psi was used by PCA in the stiffness calculations for the RT-7 concrete tie. This assumes an ultimate comprehensive strength of approximately 7500 psi for the concrete.

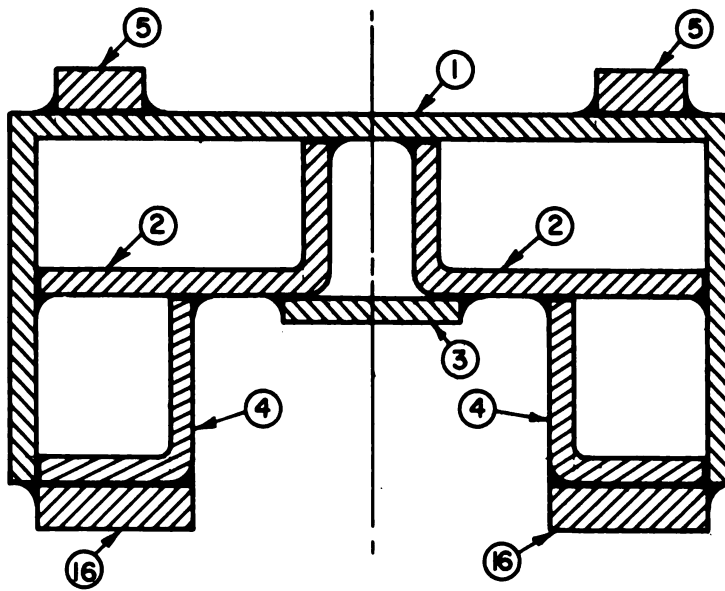
In order to generate the stiffness required to approximate that of the RT-7 tie, additional channel sections and plates were added to the basic load cell tie in the vicinity of the rail seat section. These additional elements were welded to the basic structure as shown in Figure D-4. It was assumed by PCA that these welds were fully effective in shear so that the modified cross section is fully effective in bending.

Based strictly on theoretical calculations, Figure D-5 shows that the LCT and RT-7 stiffness curves have similar values at all stations along the tie length except for the stations just to the right and left of the rail seat. The stiffness of the RT-7 tie is somewhat higher at these stations. Figure D-5 also shows the calculated stiffness for the concrete tie furnished by the Railway Concrete Crosstie Corporation (RCCC), which is the tie used on the Florida East Coast Railroad (FEC). The stiffness properties of the three ties agree well at their middle, but the RCCC tie is significantly less stiff at the rail seat section. Note also that the RCCC tie is 8'-6" long, whereas the RT-7 and the load cell ties are 9'-0" long.

In order to perform comparable load measurements using the RCCC and load cell ties, it is desirable that stiffness properties in critical areas (such as the middle and rail seat) be comparable. If the theoretical calculations are accepted as giving accurate stiffness values, it would be necessary to remove some of the material that was added to the original load cell tie so that both tie stiffnesses agree. This could be accomplished easily by removing items 16 and reducing the size of items 5, see Figure D-4. However, it was decided to check the theoretical calculations with data obtained from load-deflection tests on the load cell and RCCC ties before making any modifications to the load cell ties.



Tie Center Region



Rail Seat Region

FIGURE D-4. LOAD CELL TIE CROSS SECTION

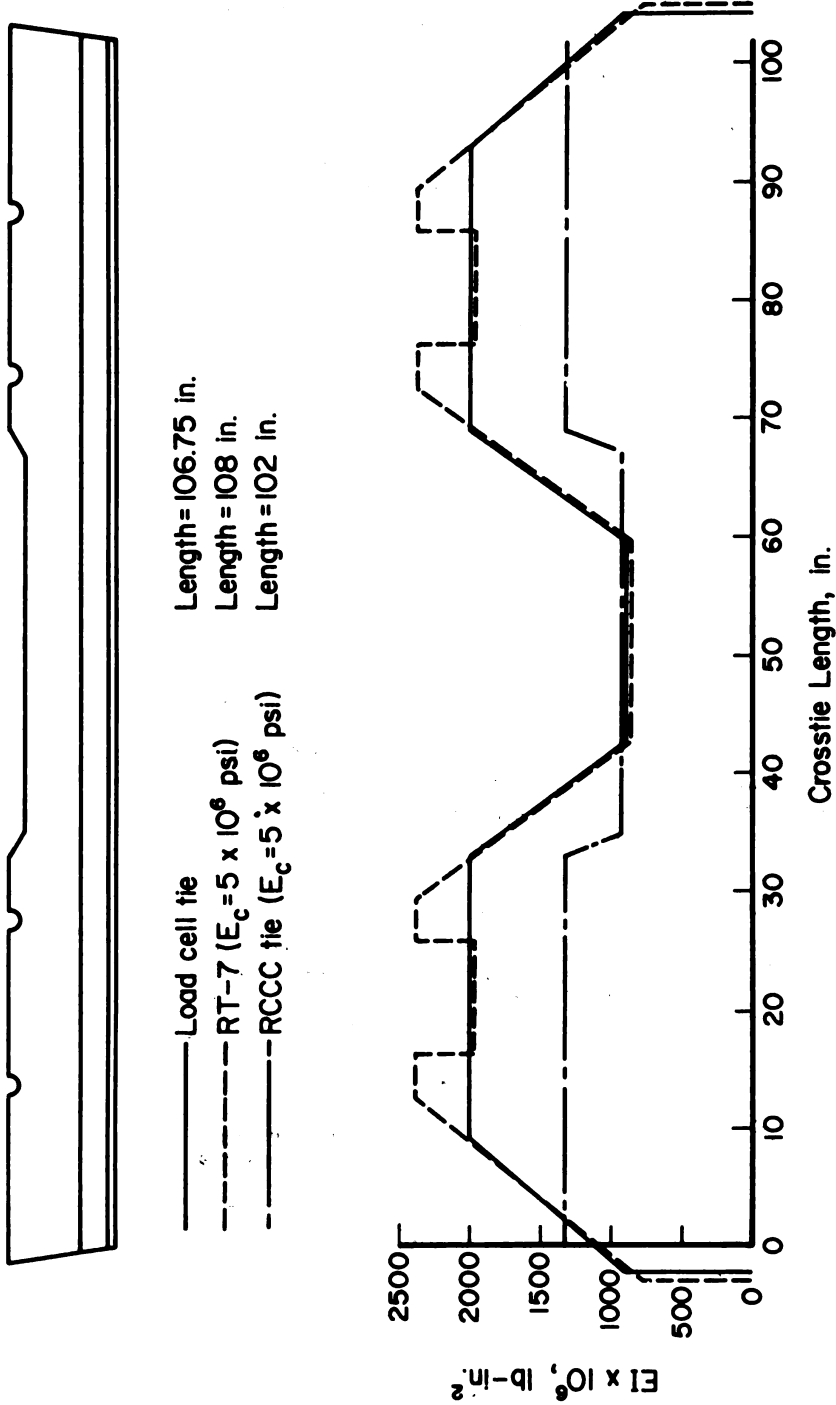


FIGURE D-5. COMPARISON OF BENDING STIFFNESS OF LOAD CELL AND CONCRETE TIES

PCA had made load-deflection tests on the RT-7 concrete tie and its load cell counterpart. The type of loading, supports and deflections from this test are illustrated in Figure D-6. The results of this test do not establish the fact that specific stations along the length of the tie are similar in stiffness, but the results do show that the average stiffness properties of the RT-7 and load cell ties agree reasonably well at low load levels. PCA believes that the theoretical calculations are sufficiently validated by these experimental results.

Three separate loading configurations were used by BCL on the RCCC and load cell ties. These are shown schematically in Figure D-7. It was hoped that the experimental results from each of the three loading configurations would yield data that would verify the stiffness properties at the critical points of each of the ties. The results of these three loading tests are shown in Figures D-8, D-9, and D-10.

The EI values in Table D-3 were calculated from the last tests for each tie. However, these tests yielded somewhat inconclusive results. Table D-3 shows inconsistency in the stiffness properties from section to section for the two ties that were tested. Consider the theoretical calculations illustrated in Figure D-5. The load cell and RCCC ties have similar values in the center section based on an assumed modulus of 5×10^6 psi for concrete and (as mentioned before) differ considerably in the rail seat sections. It therefore seems reasonable to expect the data from the test performed as indicated in Figure D-7 to show the average value of stiffness for the load cell tie to be higher than that of the RCCC tie if the theoretical calculations are at all descriptive of the actual stiffnesses. But this was not the case. Some later discussion of this will point out that this behavior is not totally unreasonable.

The experimental stiffness value for the center section of the load cell tie looks respectable compared with the theoretical calculations. The measured value is approximately 6 percent lower than the theoretical value. This difference may be due to shear deformation. The value determined from the experimental test for the RCCC ties is very low compared with the theoretical prediction at the center section. This measured value includes shear effects. It is pointed out that to measure stiffness values in prestressed or reinforced concrete beams is quite difficult. If theoretical stiffness calculations are based strictly on gross cross sectional properties and an assumed

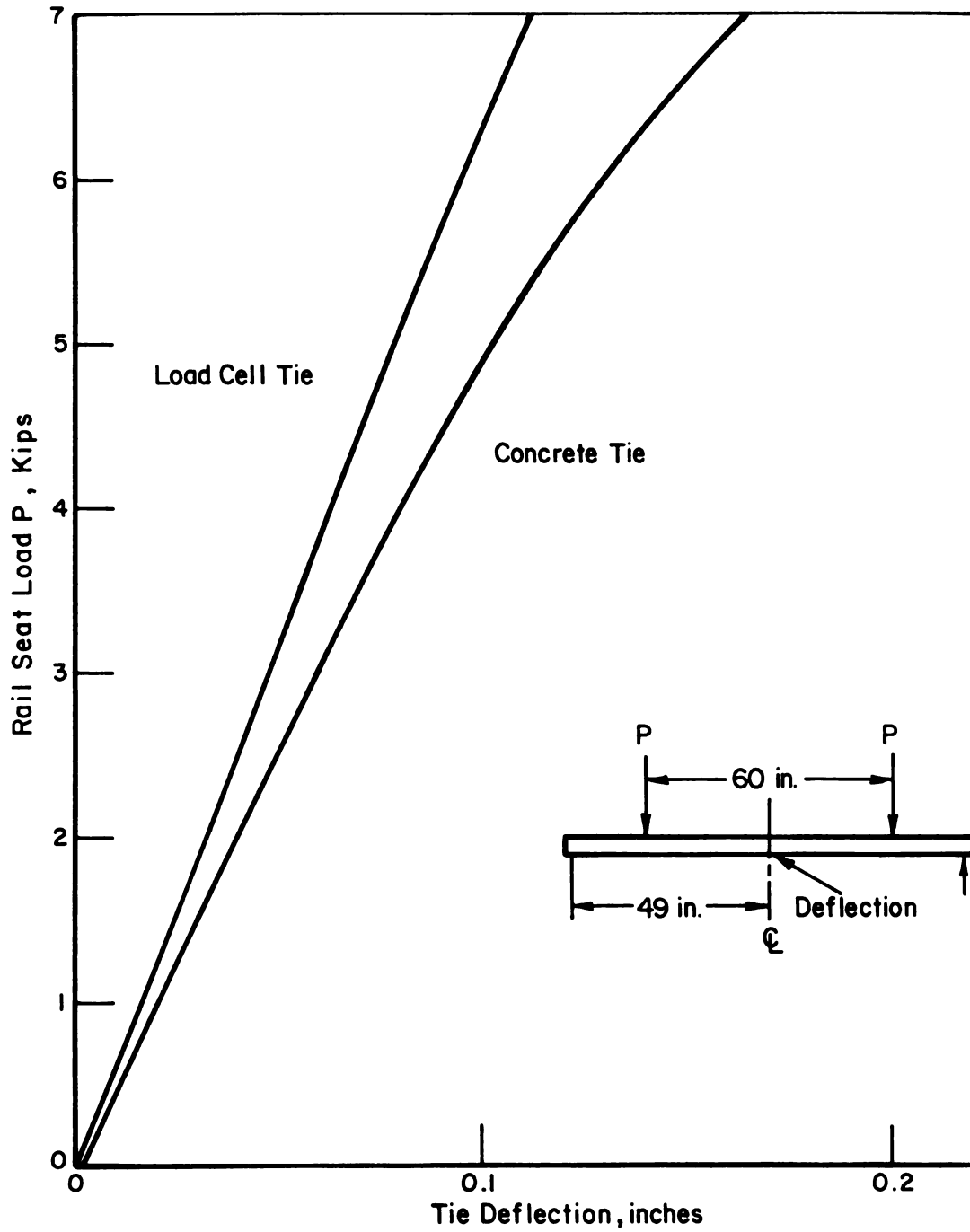
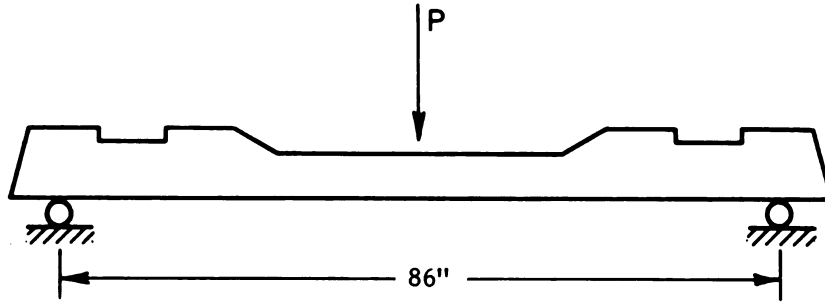
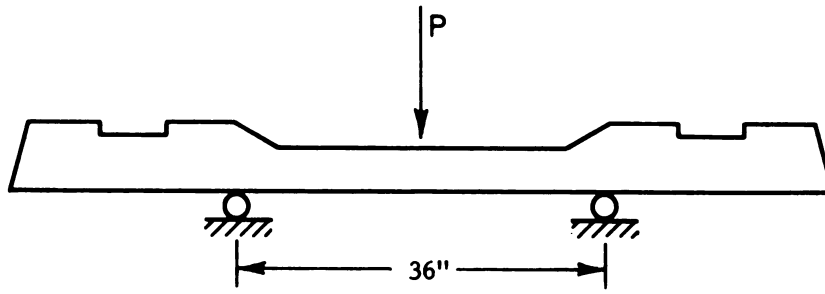


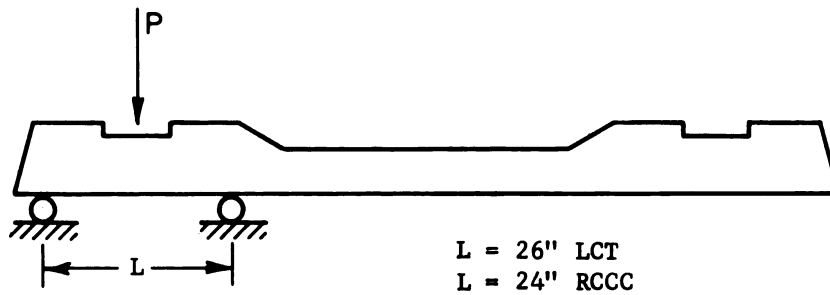
FIGURE D-6. LOAD-DISPLACEMENT VALUES FOR LOAD CELL AND RT-7 CONCRETE TIES (Tests Conducted by PCA)



Entire Span



Center Section



Rail Seat Region

FIGURE D-7. LOADING CONFIGURATIONS USED TO MEASURE TIE BENDING RIGIDITY

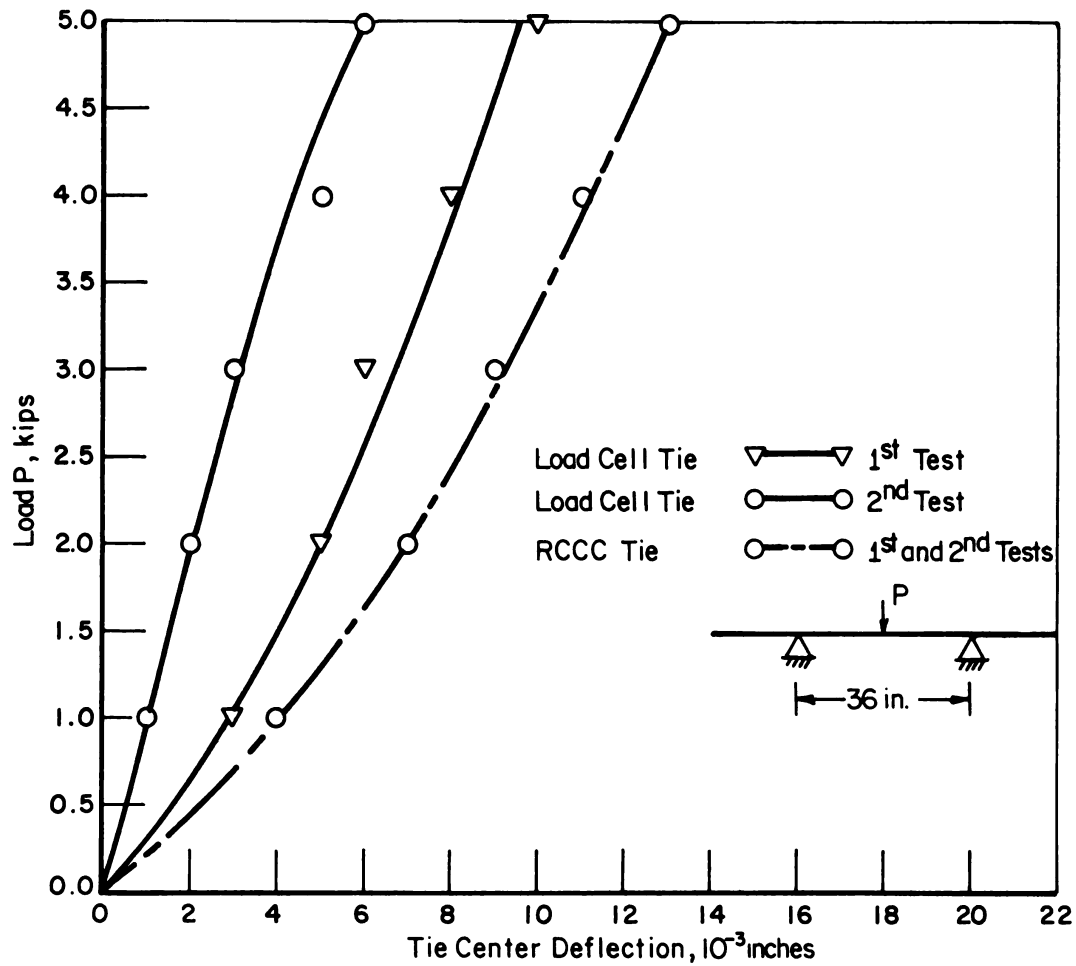


FIGURE D-8. LOAD TESTS ON TIE CENTER SECTION

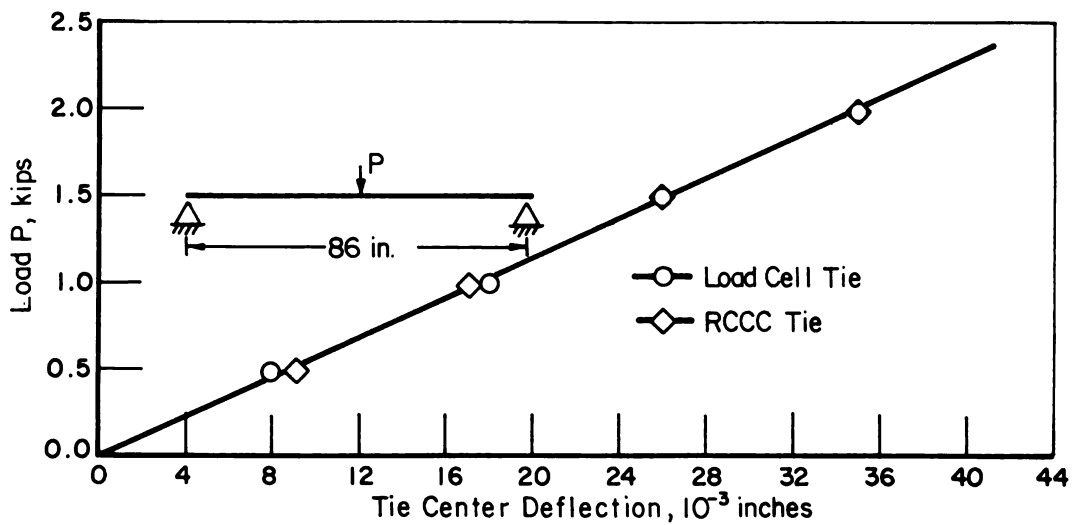


FIGURE D-9. LOAD TESTS ON TOTAL TIE SPAN

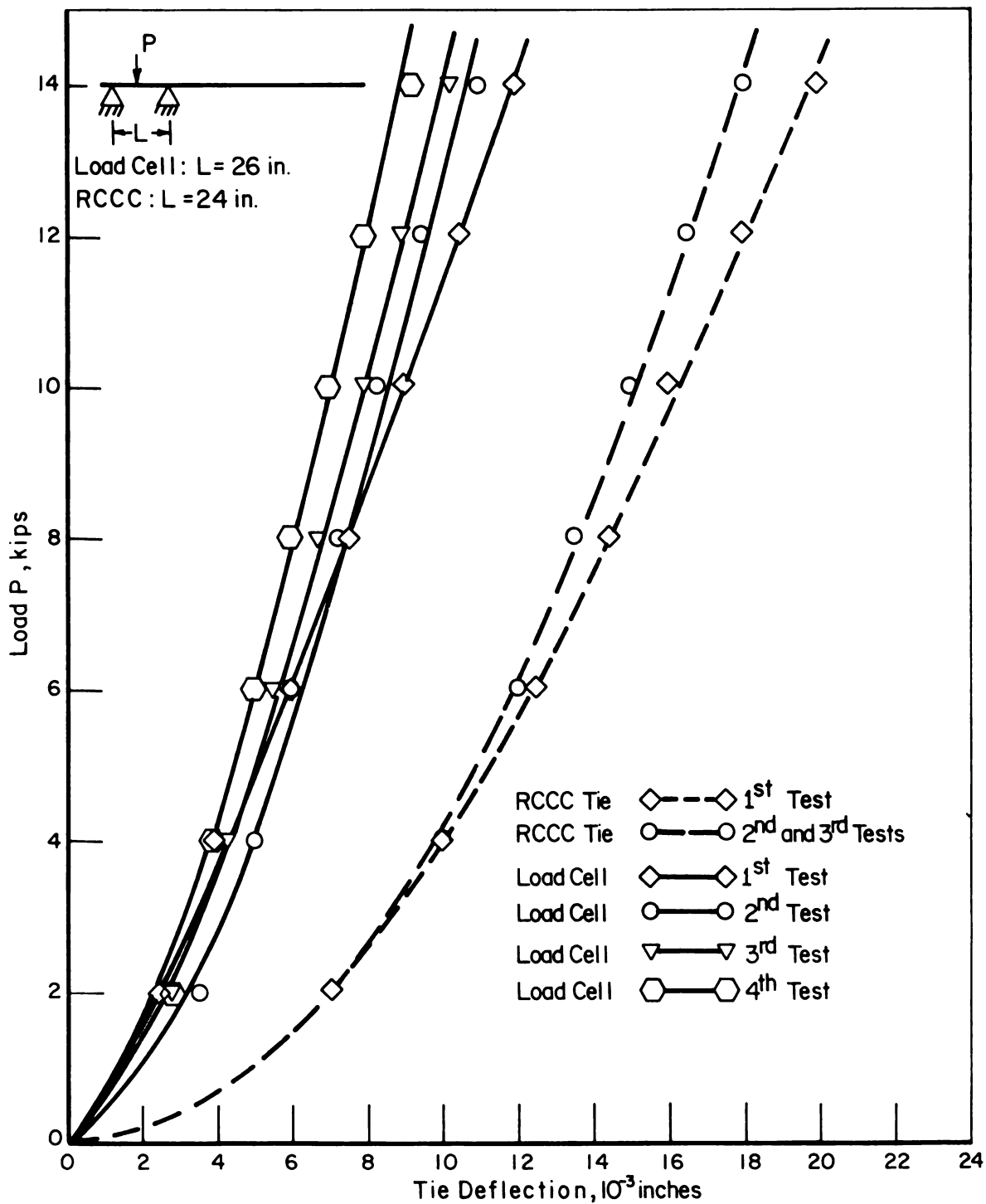


FIGURE D-10. LOAD TESTS ON TIE RAIL SEAT REGION

constant modulus E_c , these calculated values can vary considerably from the measured values depending on the extent of cracking and variations in material properties of the specimen. It is not uncommon to have ratios of calculated stiffness to measured stiffness as high as 3.4 and as low as 2 for reinforced concrete beams [D-1, D-2], but cracking should not have this effect on a beam that is effectively prestressed. From Table D-3, the theoretical stiffness for the RCCC concrete tie at the center section is slightly less than two times the measured value.

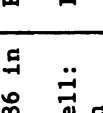

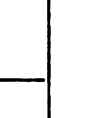
But this does not explain why the stiffness value derived from the load-deflection measurements for the load cell tie at the rail seat are unreasonably lower than the theoretical predictions. The two more obvious reasons why this dilemma exists may be due to: a) shear deformation and b) the elements added to the basic load cell tie may not be fully effective in resisting bending.

a) Obtaining an exact value for shape factor which reflects the actual shear profile in a cross section for the load cell tie is tedious but not difficult. This should account for the amount of shear deformation that is present at the rail seat section. To get a lower bound for this shear deformation (and to avoid the tedious algebra) we consider the load cell tie as having a solid cross section with limiting dimensions the same as the actual load cell cross section. This gives a value for rail seat bending stiffness of

$$EI = \frac{P}{\delta} \cdot \frac{L^3}{48} \left[1 + 3.9 \frac{h^2}{L^2} \right] = 929.91 \times 10^6 \text{ lb-in}^2$$

which is low by more than a factor of 2. That is, if we consider the load cell tie at the rail seat to be a beam with solid cross section with $h \approx 6.3$ in. and $L = 24$ in. the increase in deformation due to shear is about 20%.

TABLE D-3. SUMMARY OF TIE STIFFNESS DATA

Loading Configuration	Purpose of Configuration	Supported Length, L	Predicted EI from Measured Data	Theoretical EI (From Figure 2)
	Generate Average EI for Entire Span	RCCC: 86 in Load Cell: 86 in	RCCC: $764.5 \times 10^6 \text{ lb-in}^2$ Load Cell: $764.5 \times 10^6 \text{ lb-in}^2$	Not Calculated
	Generate EI for Center Section	RCCC: 36 in Load Cell: 36 in	* $477.02 \times 10^6 \text{ lb-in}^2$ $837.86 \times 10^6 \text{ lb-in}^2$	$917.98 \times 10^6 \text{ lb-in}^2$ $892.6 \times 10^6 \text{ lb-in}^2$
	Generate EI for Rail Seat Section	RCCC: 26 in Load Cell: 24 in	* $515.286 \times 10^6 \text{ lb-in}^2$ $732.33 \times 10^6 \text{ lb-in}^2$ *($929.91 \times 10^6 \text{ lb-in}^2$)	$1320.59 \times 10^6 \text{ lb-in}^2$ $2035.8 \times 10^6 \text{ lb-in}^2$

* Includes shear deformation

b) Another factor that would reduce the stiffness at the rail seat section (or at any other segment) is if the constituent elements of the cross section are not sufficiently secured to each other so that they act as a unit. This is an extremely difficult factor with which to associate a numerical value. However, suppose we consider the contents of Table D-3 and make the following observations about the load cell tie. Further suppose that we use the shear effect as calculated above for the rail seat section. We then have the calculated and measured values approximately agreeing at the midlength section. The overall values agree but are somewhat lower than even the calculated values at the tie middle. The measured value at the rail seat is less than half the predicted value. The actual rail seat section value is less stiff than the predicted value because we hypothesize that the added elements are not fully effective in resisting bending. If none of the added elements were sufficiently secured to the basic elements, this would give a lower bound to the stiffness of 903.6×10^6 lb-in², without including any shear effects. Thus, it may well be that the "beefed up" section in the vicinity of the rail seat is not fully effective in resisting bending for the load cell tie.

Conclusions and Recommendations

The overall, or average, stiffness for the entire span for both RCCC and load cell ties have similar values. This is probably due to the fact that most of the bending in the ties occurs between the rail seat sections. If this were not the case, the significant difference in sectional properties of the ties at the rail seat sections would be more obvious in the stiffness measurements for the entire span.

It is virtually impossible to reach any positive conclusions about measured stiffness values at specific stations along the tie length. Many factors influence the measured stiffness predictions for the concrete tie. This is particularly true at the rail seat and midlength stations. Since no universally accepted method is available for determining this type of stiffness measurement in concrete beams, we can make no positive conclusion about the stiffness values at these stations from our load-deflection tests.

The stiffness properties of the load cell tie at specific stations along its length are also difficult to predict accurately from the test data.

The unknown contributors here are amount of shear deformation present and effectiveness of added material in resisting bending. The first of these is calculable, but the second is quite difficult (maybe impossible from a practical viewpoint) to determine.

For the foregoing reasons it was recommended that the load cell ties should not be changed from their present configuration for use in the track measurement program on the FEC Railroad. The differences in apparent stiffness values at critical points along the tie length can be accounted for with appropriate numerical factors, if indeed this difference is considered significant to the overall testing procedure.

APPENDIX E

CALIBRATION OF STRAIN GAGED CONCRETE TIES

Introduction

The objectives of the tests reported herein were to determine the sensitivity of strain gage circuits for measuring bending moments and torsional moments on FEC concrete ties. This includes an evaluation of the effect of tie cracks and the location of the applied loads.

Technical Discussion

Strain Gage Circuits. A series of laboratory tests were performed at BCL using two new FEC concrete ties to calibrate the bonded strain gage bending and torsional circuits to be installed on-site in Florida. Two circuit configurations were used: a beam bending circuit used under the rail seats and at the tie center, and a torsion circuit applied at the tie center. Figure E-1 shows the layout of the rail seat strain gages. Figure E-2 shows the layout for the tie center bending gages and the tie torsion gages. Figure E-3 shows the bridge configurations and corresponding gage numbers for all circuits on one tie.

Four active arm bridges were used at each location to maximize sensitivity to bending or torsion and minimize the effect of axial loads and out-of-plane bending, and the maximize rejection of externally induced noise (the test site in Florida was adjacent to a 400,000 watt Loran transmitter).

Strain Gage Installation. Of the several strain gage installation techniques that were evaluated in the preliminary tests, a bonded foil strain gage with a 2-in. gage length was selected to span the concrete aggregate of up to 0.6 in. This gage was premounted on 0.003-in.-thick stainless steel shim to reduce the time required for field installation. Other gages evaluated were 1-in. foil gages, either bonded directly to the concrete or to shim stock of aluminum or stainless steel foil, and weldable gages. Weldable strain gages were considered due to their integral lead

design, but their higher initial cost offset any fabrication advantages. Several types of epoxy were tested with the primary criteria for epoxy performance being a combination of high moisture resistance, fast setup time, and relatively low creep. The epoxy was to be used in two separate applications. The first application was as a preliminary sealer and void filling material to prepare the surface of the concrete. The second application was to bond the gage subassemblies to the tie surface. The final adhesive selected for both applications was the strain gage epoxy AE-10 primarily because of its superior wetting characteristics as well as its moisture resistance after setup. Its slow curing time in the laboratory proved to be no problem in the field due to the high temperatures encountered in Florida in June. In fact, the pot life was too short when ambient temperatures exceeded 80 F and chilling was required to provide sufficient pot life during gage installation.

Templates were constructed to facilitate rapid and repeatable layout of each of the tie circuits. Specially constructed clamping fixtures were also designed to retain the newly bonded gages in position until the adhesive began to cure. These templates and fixtures were used to install the gage assemblies on the calibration ties in the laboratory to assure as much repeatability as practical between the lab test ties and the field installed ties.

After a gage was bonded to the tie by the heat-curing process, the clamping fixture was removed and the gage resistance was checked. The gage was then coated with M-Coat BT-2 nitrile rubber, allowed to dry, and covered with an M-Coat FB-2 butyl sheet and M-Coat FN-2 neoprene sheet.

Terminal blocks were installed on the sides of the concrete ties with epoxy type AE-10. Terminal blocks used for wiring the bending gages were placed on the north side of the tie, and torsion gages were wired to the terminal block placed on the south side of the tie.

Gage Wiring. The procedure for wiring the strain gages was reduced to a simple memory pattern of the color-coded lead wires in the following order: red, white, green, black. The top row of terminal screws is used to wire the gages, starting with the east side of the block and using only the first four terminals.

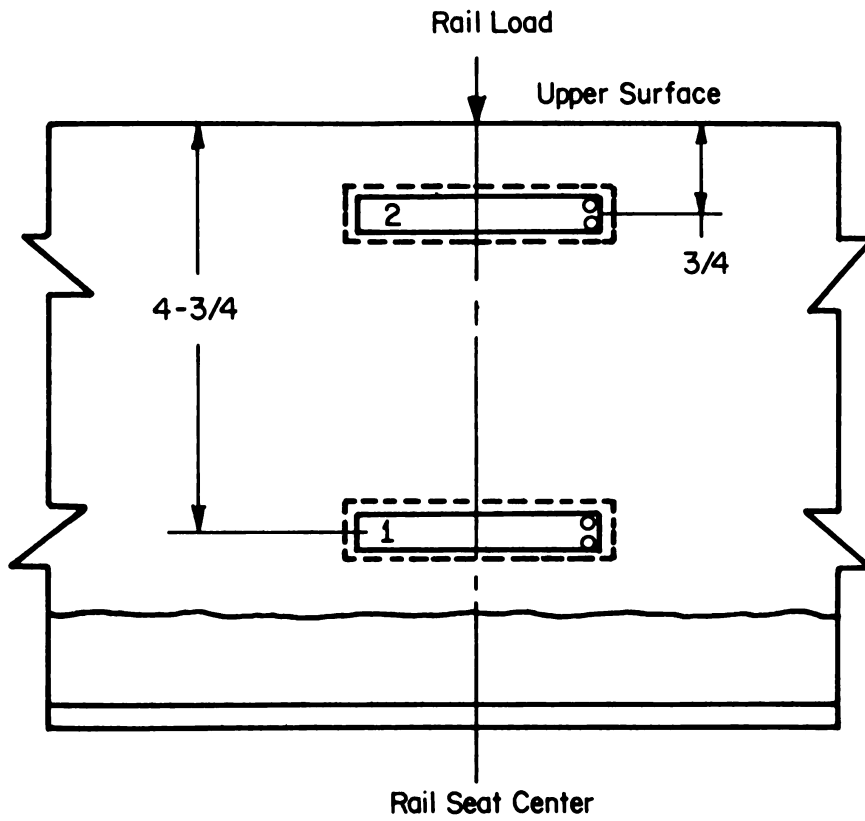


FIGURE E-1. RAIL SEAT GAGE LOCATIONS AND ORIENTATION

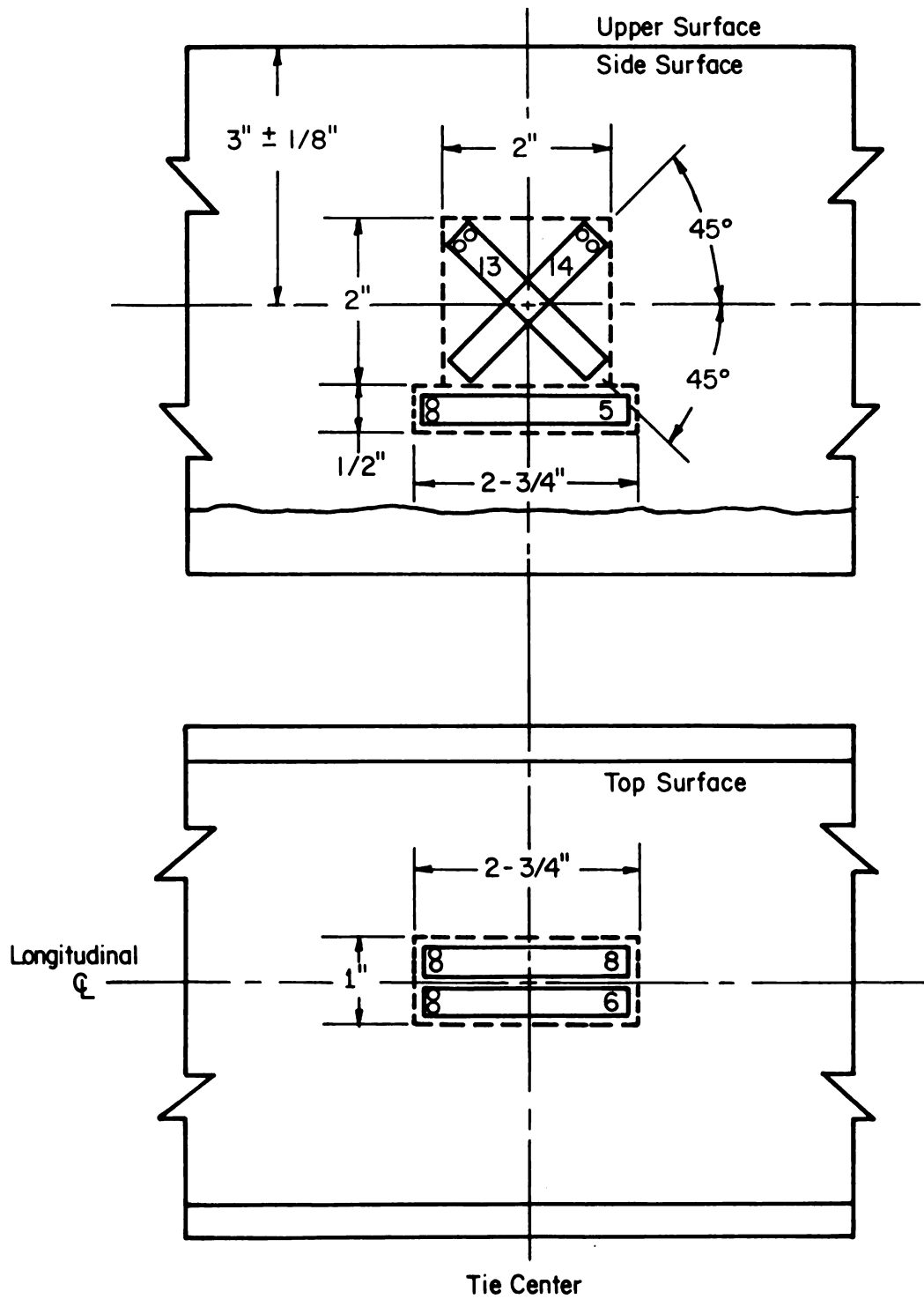


FIGURE E-2. MID-TIE GAGE LOCATION AND ORIENTATION

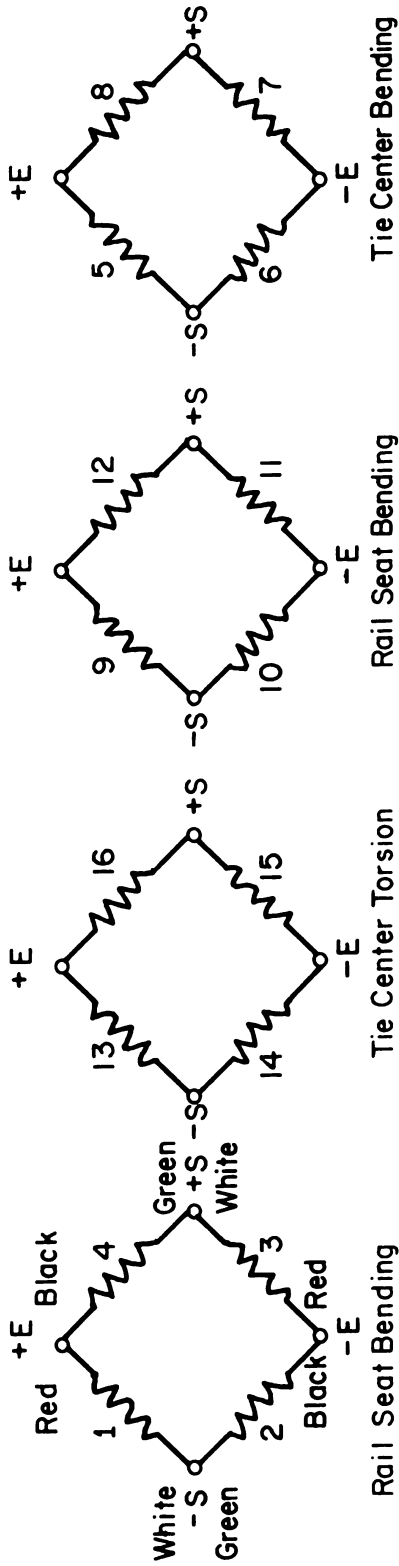
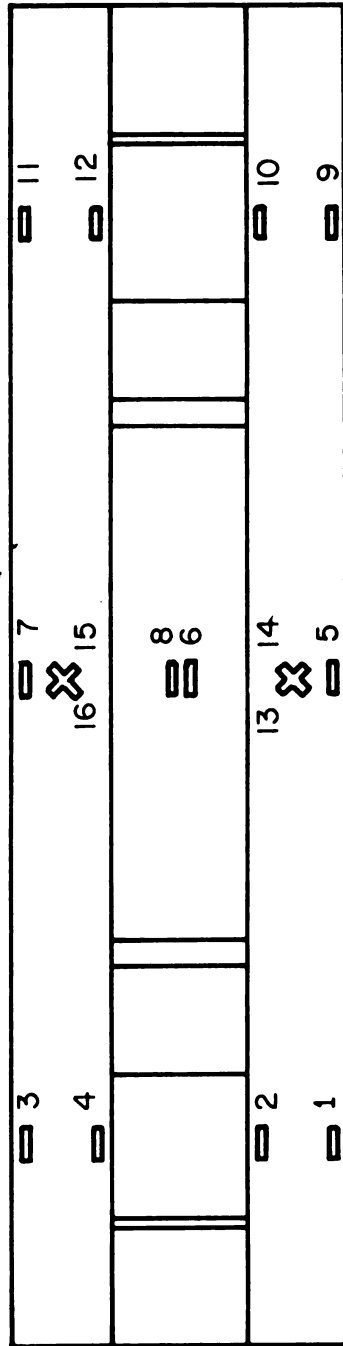


FIGURE E-3. SCHEMATICS FOR ALL TIE CIRCUITS

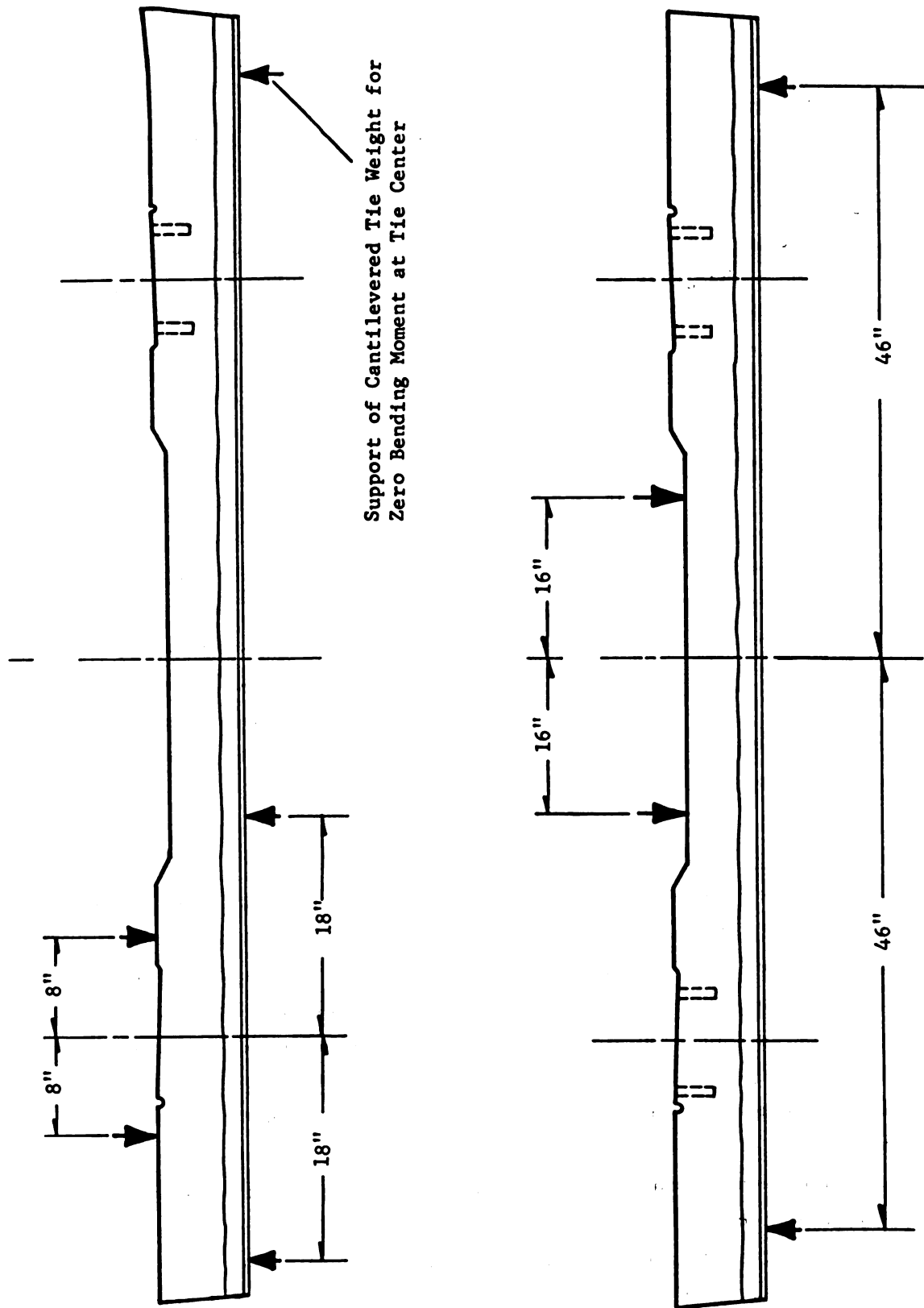
The gages located on the north side of the tie were always wired first. The wiring diagram on Figure E-3 shows the color code followed. The terminal +E is the initial terminal used for wiring, with the wiring being completed in a counter-clockwise manner according to the diagram for gages 1-4.

A layer of duct tape was applied to the tie surface under the lead wires from the gages to the terminal blocks. RTV was applied at the connection of all lead wires to the gages, and on all lead wires attached to the sides of the ties for protection against damage. The lead wires were then covered with two layers of duct tape for added protection against moisture and damage.

Upon completion of the gage wiring, connector cables were wired to the terminal blocks. The cables had five wires to be connected to the five terminal screws on the bottom row of the terminal block. Beginning with the far east terminal screw, the wires were individually connected in the following color-coded order: red, white, black, green, shield. A jumper was attached between the black lead and the shield to establish the reference point for the amplifier guard circuit. The cables were then attached to the sides of the tie with duct tape. In all cases, cables were laid in the direction of the access road adjacent to the track for hook-up to the instrument van.

Tie Calibration. Two loading techniques were used to calibrate the rail seat bending and tie center bending circuits in the laboratory. The first technique was to support the tie at the maximum possible separation distance centered about the gage circuit. The input load was applied through two points which were also well outside the gaged region. This provides a constant bending moment between the loading points and minimizes the effect of local stress gradients from the loading points. Figure E-4 illustrates this layout along with the dimensions used for the rail seat and the tie center tests.

The second loading technique followed the guidelines in the preliminary AREA concrete tie specification. This requires the placement of the input load directly on supports spaced 6 in. apart using two rubber blocks. For the rail seat tests, the lower supports were placed at a distance of 14 in. from the center line of the rail seat using the relations shown in Figure E-5.



Support of Cantilevered Tie Weight for
Zero Bending Moment at Tie Center

FIGURE E-4. RAIL SEAT AND TIE CENTER LOADING POINTS FOR MINIMUM LOCAL STRESS GRADIENTS

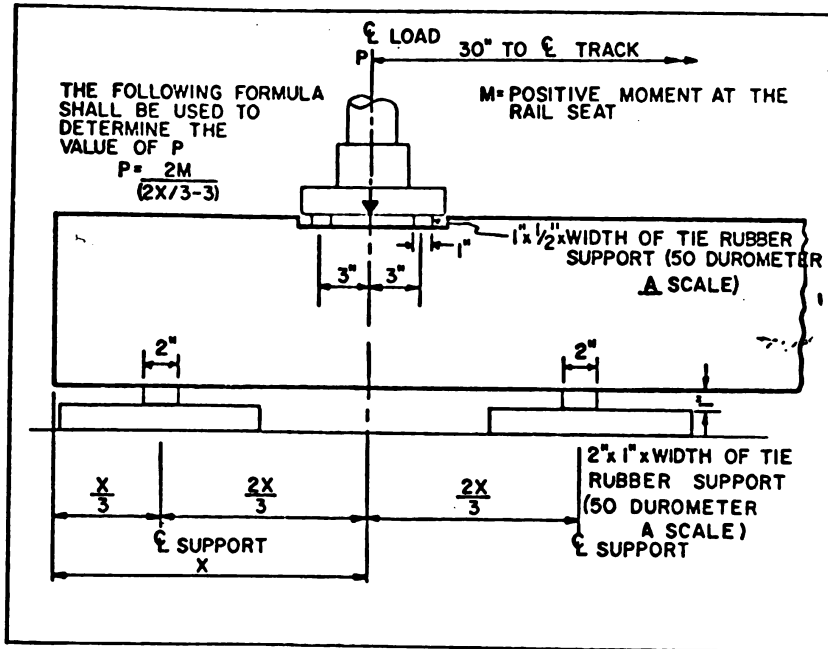


FIGURE E-5. AREA RAIL SEAT BENDING MOMENT TEST

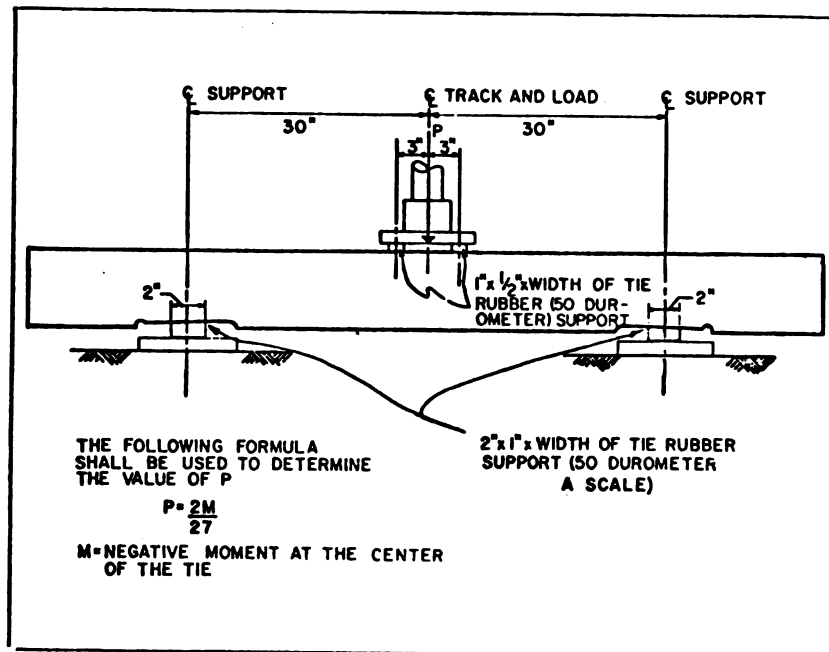


FIGURE E-6. AREA TIE CENTER BENDING MOMENT TEST

The tie center tests require the reaction loads to pass through the rail seats as shown in Figure E-6. The only deviation from this approach was the substitution of a specially contoured piece of hardwood between the tie bottom and the rubber support to match the concave shape of the bottom of the RCCC concrete tie used on the FEC railroad.

During preliminary tests to evaluate gage installation techniques, effects of cracks in the concrete were identified. A crack directly underneath the sensitive region of a strain gage caused a significant increase in output sensitivity when the input load exceeded the prestress limit. If the crack appeared outside the gaged region there was a minor change in the circuit sensitivity below the prestress limit and a gradual reduction of sensitivity above the prestress limit due to a change in the effective section modulus and stress relieving of the surface regions on either side of the crack.

The calibration tests were performed on each of the three circuits on each tie up to safe (uncracked) load limits prior to repeating the sequence to the breaking point of each section of the tie. Crack locations were then identified and cracked tie calibrations were performed. Finding the crack required careful examination of large areas of the tie with a 10 power glass and a strong light. Wetting the surface of the concrete helped confirm the crack location and length. Because of the prestress it was necessary to examine the ties for cracks under full load.

Figure E-7 illustrates a typical load-failure curve and a subsequent sensitivity plot after cracking. Figure E-7 shows that the tie cracked with a center bending moment of about 105,000 in.-lb as indicated by the sudden change in circuit sensitivity. Repeated loading of the cracked tie shows that the output of the bending bridge is linear and nearly the same as that for the uncracked tie as long as the bending moment does not exceed about 60,000 in.-lb. The concrete appears to have considerable tensile strength.

Tie torsion was produced by clamping one end of the tie in a fixed configuration and attaching a moment arm to the rail fastener bolts at the opposite end of the tie. Bending strains were minimized by adjusting a vertical support at the free end of the tie while monitoring the bending strain circuit at the tie center for zero bending moment. Figure E-8 shows the 50-in. moment

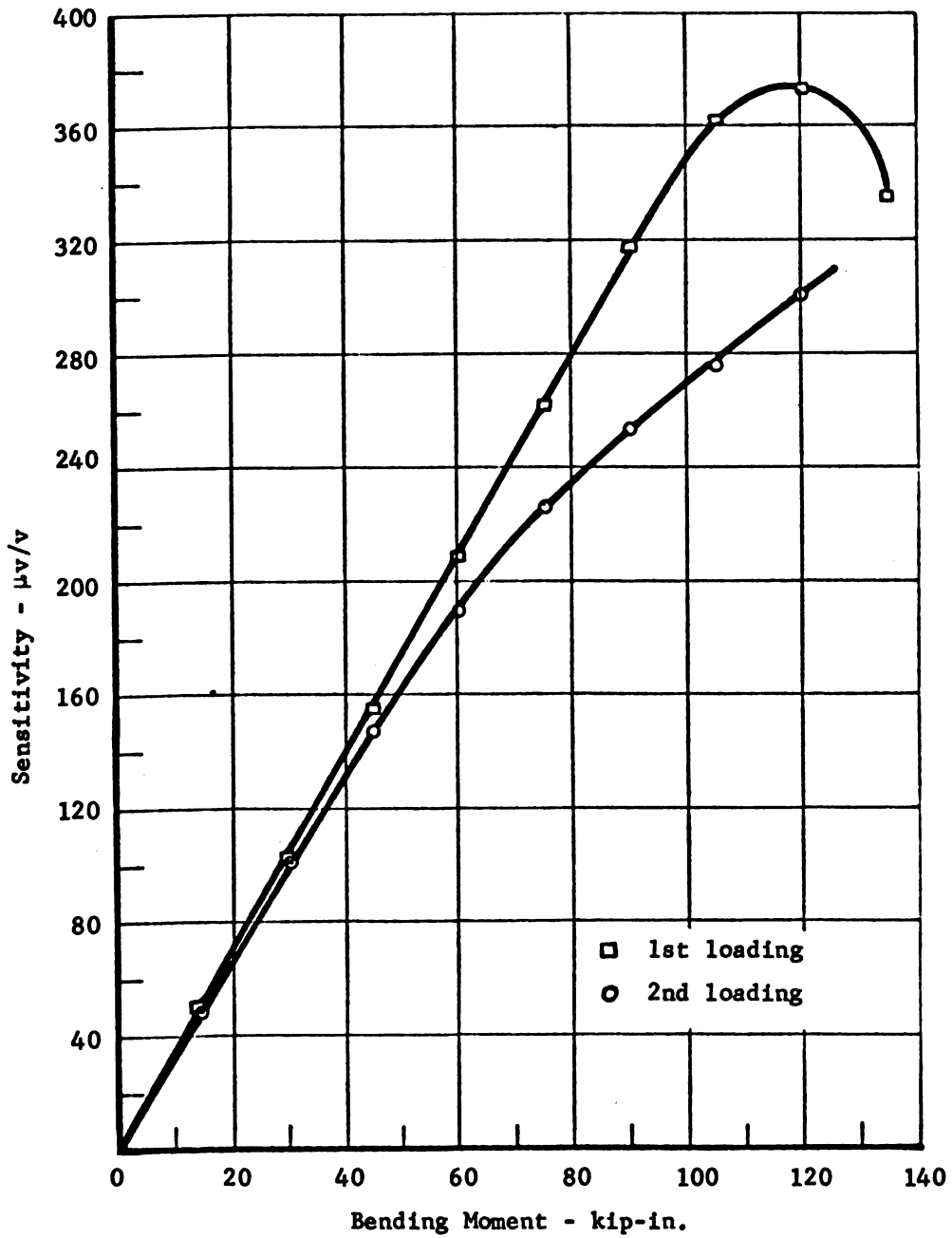


FIGURE E-7. TIE CENTER BENDING CIRCUIT REACTION AT CRACKED TIE

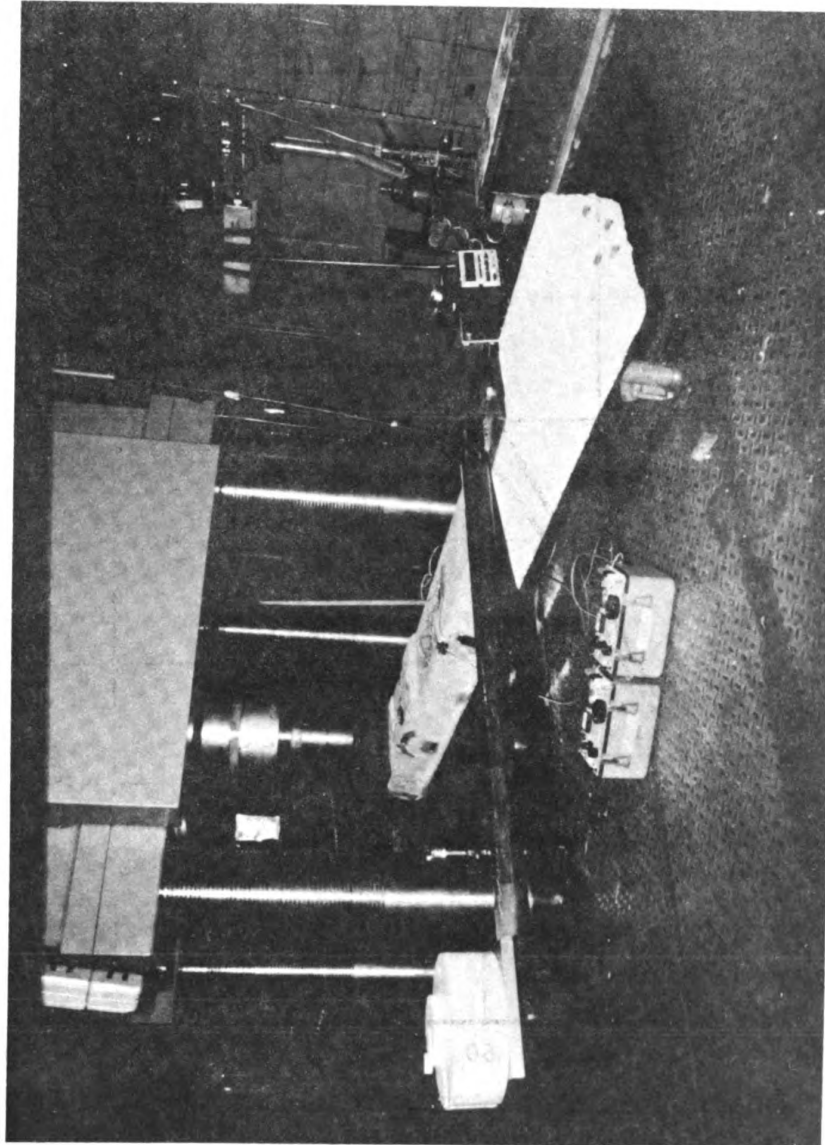


FIGURE E-8. TORSION TEST CONFIGURATION

arm and static weight used for the torsion test. Although a full active bridge was used to measure torsion at the tie center, the normal strains induced are extremely low. Sensitivity for this circuit proved to be only 32 $\mu\text{v/v}$ per 10,000 in.-lb torsion, which was estimated to be close to the torsional failure load. This is only one percent of a typical sensitivity for a normal transducer.

A variety of special measurements were made to compare minor changes in loading application points to evaluate stress concentrations caused by surface irregularities, and to calibrate half bridge performance in anticipation of partially failed circuits installed in the field. Of major interest to the results of the FEC test program, however, is the importance of local stress concentrations caused by the load input at the rail seat influencing the rail seat bending circuit. Figure E-9 shows the sensitivities achieved by each of the two loading techniques used during the calibration of the rail seats and tie center. This effect was not a factor in the calibration of the tie center bending, as shown in the lower graph in Figure E-9, due to the large separation of the gaged regions from the point of load application. After comparing the similarity between the AREA load technique and the actual field environment, the sensitivity generated by the AREA calibration procedure was selected for use in the analysis of the FEC rail seat data. Applying the rail seat load through a rail section and rail pad would give a more realistic loading, but the actual bending moment at the gage location can not be calculated with sufficient accuracy for calibration purposes.

Numbers produced during the analysis of the FEC field data using the calibration factor chosen here probably represent a lower bound to the magnitudes of tie bending moment. A reduction in stress concentration from the rail seat loading and the presence of small cracks outside the gaged region would both tend to desensitize the rail seat bending moment circuit. Therefore, this would cause the measured data to underestimate the actual bending moment at the rail seat. The measured failure load for rail seat bending moment was about 150,000 in.-lb as indicated by the change in slope of the gage output versus bending moment curve. The load required for visual detection of a crack, which is the AREA failure criteria, would be considerably higher. The output sensitivity of the rail seat bending circuit remained constant for bending moments up to 75,000 in.-lb on both cracked and uncracked ties.

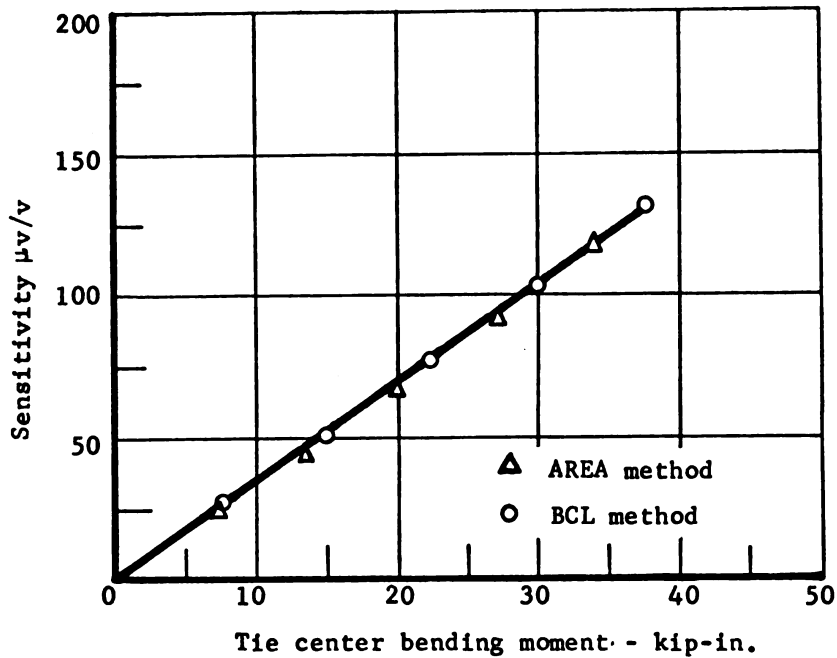
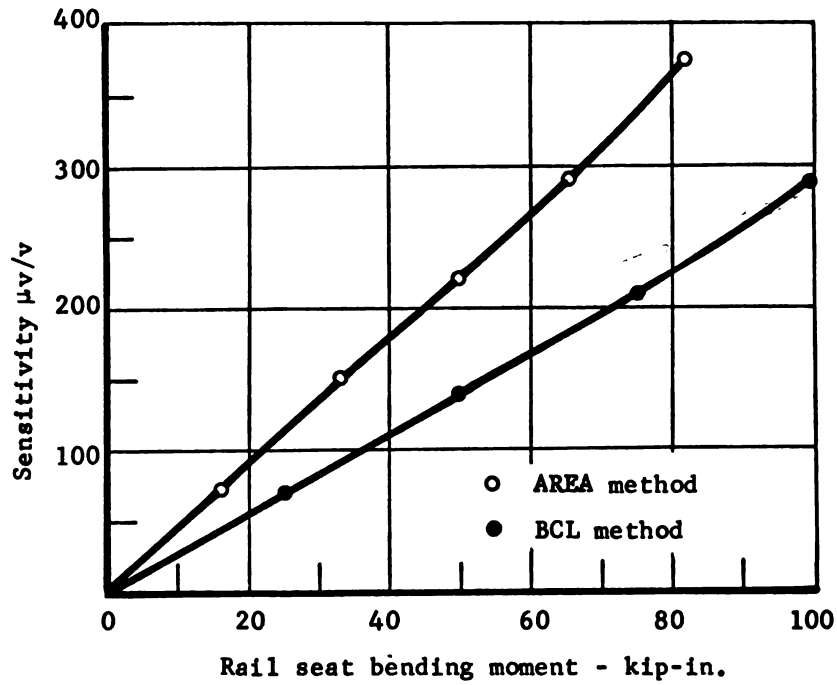


FIGURE E-9. EFFECT OF LOADING TECHNIQUE ON RAIL SEAT AND TIE CENTER BENDING CIRCUIT RESPONSE

APPENDIX F

SUBGRADE SIEVE ANALYSIS AND
MOISTURE DENSITY DATA

Table F-1 lists the sieve analysis data for the tangent track test sites having 24-inch tie spacing (Site 1) and 20-inch tie spacing (Site 2). There were considerably more limestone ballast particles in the subgrade sample taken from Site 1.

Figures F-1 and F-2 show the moisture/density relationships (Proctor curve) for the samples from the two test sites. The data reported in this appendix were obtained by the Pittsburgh Testing Laboratory office in West Palm Beach, Florida.

TABLE F-1. SIEVE ANALYSIS DATA

Sieve Size	Percent Passing	
	Site 1 ⁽¹⁾	Site 2 ⁽²⁾
1-1/2"	100	
1"	94	
3/4"	88	
1/2"	77	
3/8"	71	
No. 4	59	100
No. 10	51	100
No. 20	46	97
No. 40	39	69
No. 80	20	22
No. 260	13	1.7

(1) Brown sand with limerock.

(2) Tan sand with traces of limerock.

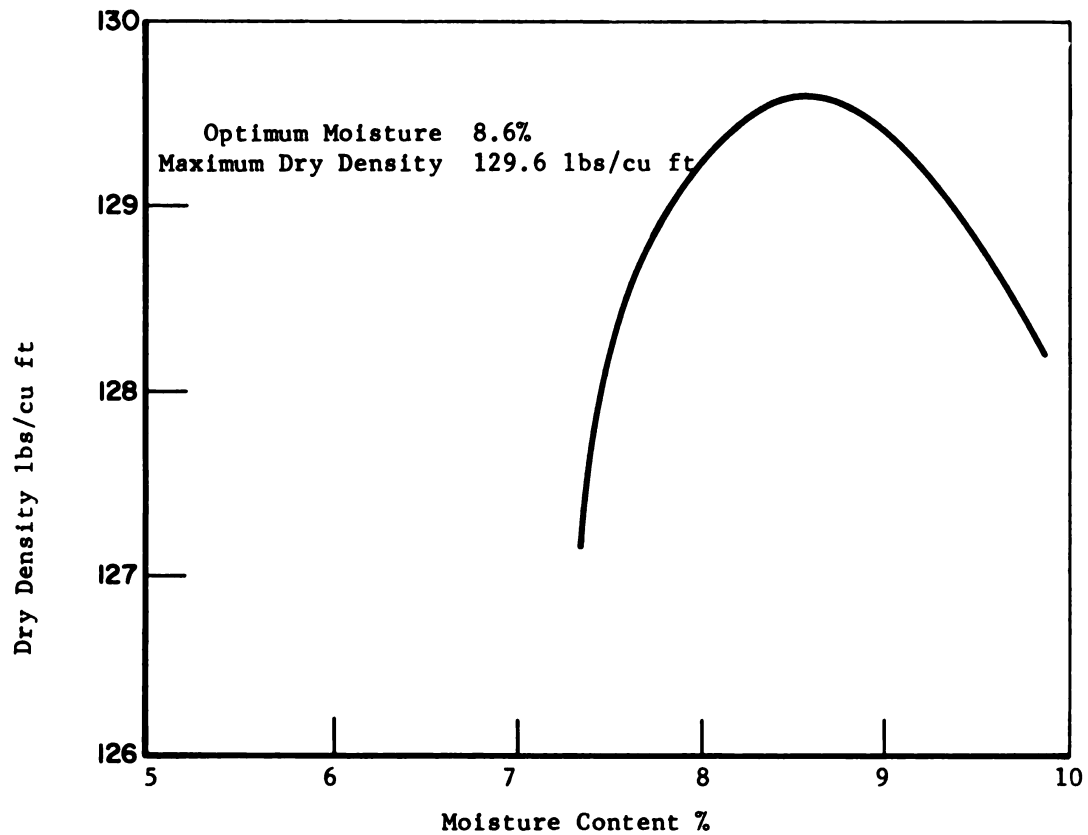


FIGURE F-1. MOISTURE-DENSITY CURVE FOR SITE 1
SUBGRADE MATERIAL [AASHO T-180C (Replacement)
test procedure]

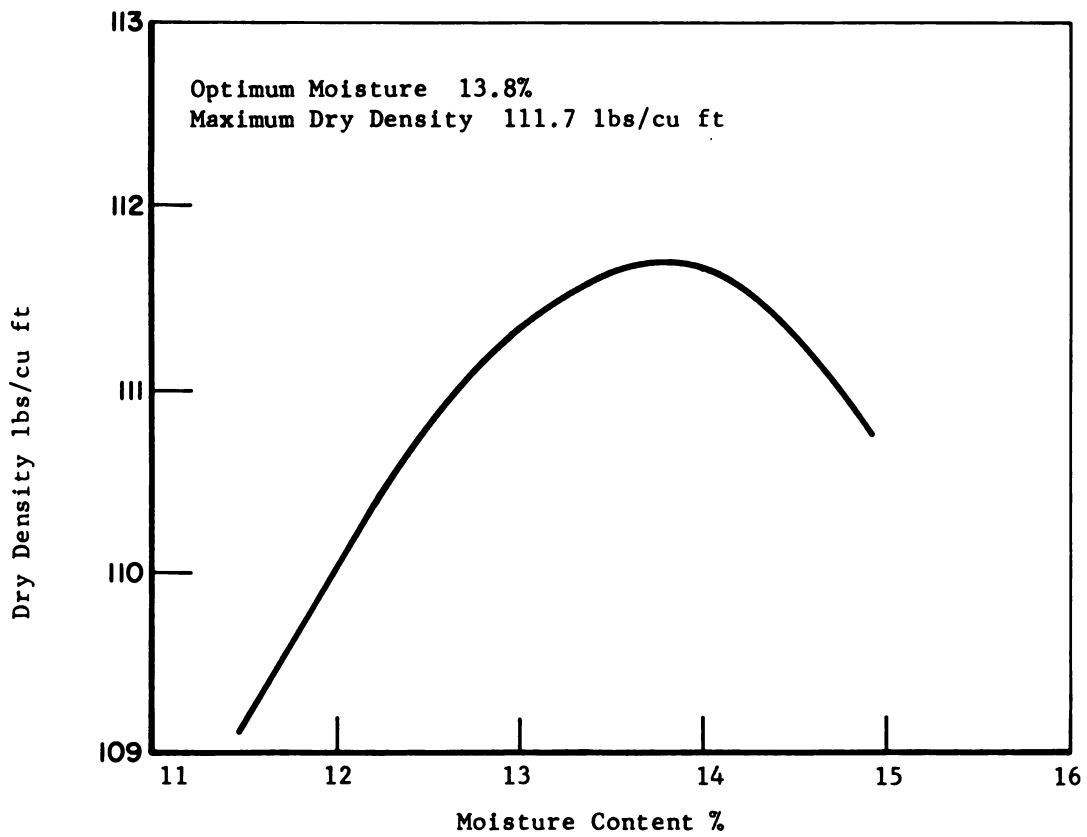


FIGURE F-2. MOISTURE DENSITY CURVE FOR SITE 2 SUBGRADE MATERIAL (AASHTO T-180A test procedure)

APPENDIX G

VIBROSEISMIC SURVEY DATA OBTAINED BY THE USAE WATERWAYS EXPERIMENT STATION (WES)

Purpose and Scope

The purpose of the investigation was to determine, by vibroseismic methods, the elastic properties of the foundation soil at the Florida East Coast railroad test sites. This report summarizes the WES test procedures used in the field investigation, and cites references which may be used to obtain a detailed understanding of the data reduction and analysis techniques. Final results of this study are presented in plots which show the variation in shear modulus (G), and Young's modulus (E), as a function of depth in the subgrade.

Test Methods and Computations

The vibroseismic survey was conducted in two phases: surface refraction seismic and vibratory tests. Each type of tests was designed to reveal specific information relative to soil conditions and elastic properties of the embankment.

Refraction Seismic Tests

The refraction seismic tests were conducted using a SIE Model P-19 seismograph. Resolution time using this recording unit is about 0.5 msec when the oscillograph is operated at a speed of 50 ips or more. A 16-lb sledgehammer provided the seismic energy source. Twelve vertical, velocity-type geophones were placed in a straight line along the surface of the embankment at 2 and 5-ft intervals, which ensured that detailed data were obtained from the embankment and subgrade materials. A steel plate, placed on the ground surface at one end of the seismic line, was struck with the sledgehammer, and a recording of the motion registered

by each geophone was obtained. The plate was moved to the opposite end of the seismic line and was again struck with the sledgehammer, and another recording was taken. When this procedure had been accomplished, the result was two seismic traverses (forward and reverse) that were either 22 or 55 ft in length.

Information obtained from surface refraction seismic tests consists basically of the time required for a compression wave to travel from a seismic source (sledgehammer) to the points of measurement (geophones). Data are plotted in graphic form as travel time from the seismic source to each geophone versus the respective distances of the geophones from the source. The inverse slope of the lines drawn to connect the plotted points indicates the velocity of the compression wave through each subsurface medium encountered. A change in the slope of the line shows that the wave has passed through an interface between two subsurface layers having different velocities, and the second inverse slope of the line indicates the velocity of the second material encountered. The depth at which the first interface occurs below the surface can be calculated from the following equation:

$$D_1 = \frac{X_1}{2} \sqrt{\frac{v_{c2} - v_{c1}}{v_{c2} + v_{c1}}} \quad (G-1)$$

where:

- D_1 = depth from surface to first interface, L
- X_1 = distance from seismic source to point at which first change in slope occurs, L
- v_{c1} = compression-wave velocity in first layer, LT^{-1}
- v_{c2} = compression-wave velocity in second layer, LT^{-1}

It should be noted that, in most cases, data from the forward and reverse profiles along a seismic line indicate different velocities for a particular soil layer. This difference in velocities is caused by a dip of the soil layer, and the velocities determined are apparent. However, the true velocity of the soil layer can be determined using the following equation:

$$v_t = \frac{2v_u v_d}{v_u + v_d} \quad (G-2)$$

where:

v_t = true velocity of a soil layer, LT^{-1}

v_u = apparent velocity of a soil layer along the up-dip profile,
 LT^{-1}

v_d = apparent velocity of a soil layer along the down-dip profile,
 LT^{-1}

Vibratory Tests

The vibratory tests were conducted utilizing a 50-lb electro-magnetic vibrator as the seismic wave source. This vibrator and associated instrumentation is described in detail in WES Miscellaneous Paper (MP) No. 4-691, Determination of Soil Shear Moduli at Depths by In Situ Vibratory Techniques, dated December 1964 and in A Procedure for Determining Elastic Moduli of In Situ Soils by Dynamic Techniques, an excerpt from the Proceedings, International Symposium on Wave Propagation and Dynamic Properties of Earth Materials, 1967.

Vibration tests consisted basically of determining the length of surface (Rayleigh) waves generated by vibrators at controlled frequencies. From this, the wave velocity can be computed as follows:

$$v = \lambda f \quad (G-3)$$

where:

v = wave velocity, LT^{-1}

λ = wavelength, L

f = frequency of the vibrator, cycles T^{-1}

Computation of Poisson's Ratio and Elastic Modulus

Wave velocity is dependent upon the ratio of the elasticity of the medium to its mass density ρ and the wave type. The relation of shear modulus G and shear-wave velocity v_s is as follows:

$$G = v_s^2 \rho \quad (G-4)$$

where:

- G = shear modulus of soil, FL⁻²
- v_s = shear-wave velocity, LT⁻¹
- ρ = mass density of soil, γ/g, GL⁻⁴ T²
- γ_m = wet unit weight of soil, FL⁻³
- g = acceleration due to gravity, LT⁻²

Shear-wave velocity and surface-wave velocity are related by Poisson's ratio. For homogeneous media and Poisson's ratio ranging between 0.2 and 0.5, the difference in velocities is less than 9 percent. Therefore, for practical purposes, shear waves can be considered to have the same velocity as surface waves. Thus, shear-wave velocities can be determined by the vibratory tests described, and shear moduli can be calculated by the use of the above equation.

With the assumption that compression-wave velocity and shear-wave velocity were determined for comparable materials, Poisson's ratio can be calculated from the ratio of velocities v_r:

$$v_r = \frac{v_c}{v_s} \quad (G-5)$$

Poisson's ratio ν is then:

$$\nu = \frac{v_r^2 - 2}{2(v_r^2 - 1)} \quad (G-6)$$

The compression modulus E (Young's modulus) can be determined by:

$$E = 2(1 + \nu)G \quad (G-7)$$

Based on WES experience, it appears that variations in E and G correlate best with conventional exploration methods when it is assumed that the depth for the computed value of E and G is one-half the length of the surface wave. Therefore, the computed values of E and G are considered to be the elastic moduli at these depths.

Field Investigation

During the period 24-27 July, a two-man WES field party conducted vibroseismic tests at three railroad track test sites on the FEC railroad. Topography in the locale consists of gently rolling sand dunes which are typically covered with stands of pine trees and/or palmetto thickets and marsh

grasses. Locations of the vibroseismic lines at each test site are shown in Table G-1.

Data Analysis and Results

Additional documentation of the WES vibroseismic method for determining insitu elastic moduli may be obtained from J. R. Curro, Jr., Vibroseismic Survey, Railroad Test Embankment, Aikman, Kansas, and Miscellaneous Paper S-72-36, U. S. Army Engineer Waterways Experiment Station, CE, Vicksburg, MS, June 1972. As stated, the vibroseismic method is based on measurements of the compression (P-wave) and shear (S-wave) velocities in the foundation material(s). Thus, refraction seismic measurements were made at each site to determine P-wave velocities in the soil material as well as the depths to interfaces between layers having different velocities. Refraction seismic results are shown in Figures G-1 through G-4. Vibratory measurements were made at discrete frequencies to determine S-wave velocities as a function of depth in the subgrade. A composite plot of shear wave velocity versus depth for Sites 1, 2, and 3 is shown in Figure G-5.

These data were used, according to procedures outlined in the references listed, to derive the plots of elastic moduli versus depth shown in Figures G-6, G-7, and G-8. Table G-1 summarizes these data together with other pertinent information used in the derivations. The densities shown in Table G-1 were estimated, based on previous work with similar materials, since no density measurements were made. The previous work is documented in Investigation of Foundations for Launch Facilities for Space Vehicles, Cape Canaveral, Florida, Miscellaneous Paper S-4-576, May 1963.

It is important to note that the moduli values presented herein are interpreted as being lower bound approximations of roadbed response since one can safely assume that the materials beneath the track have been compacted by repeated train loadings, particularly in the upper foot or two. Consequently, those materials should exhibit a slightly stiffer response than that measured beside the track. Unfortunately testing beneath the track structure was not possible.

Figures G-5, G-6, and G-7 contain WES recommended curves and approximate averages for the site-dependent variation in elastic moduli with

TABLE G-1. RESULTS OF VIBROSEISMIC SURVEY

Per Unit Weight γ_m , pcf	Seismic Tests			Vibration Tests			Wave Velocity v_s , fps	Modulus, 10^3 psi Shear G	Poisson's Ratio, ν	Vibroseismic Location				
	Wave Velocity v_c , fps	Depth d_s , ft	Frequency f_s , ft	Length λ_s , ft	Depth d_v , ft	Wave Velocity v_s , fps								
100	3300 1120	6.7+ 1.4-6.7	25 30 40 50 70 80	14.4 11.0 8.6 6.4 4.6 4.5	7.2 5.5 4.3 3.2 2.3 2.25	360 330 345 320 320 360	0.49 0.45 0.45 0.46 0.46 0.44	2.8 2.3 2.6 2.2 2.2 2.8	8.4 6.8 7.4 6.4 6.4 8.1	<p>Test east of siding, 5 ft from track-Cross ties 24 in. apart-Test section on straight array-53 ft N of Battelle main array-Geophone spacing 2 ft-Ballast size 1 in. - 2-1/2 in. Vibroseismic Location</p>				
											100 150 200 250 300 350	3.6 2.0 1.4 1.3 1.2 0.8	1.8 1.0 0.7 0.6 0.5 0.4	360 300 280 320 350 270
	100	1140	2.5+	35 40 50 70 80	12.3 10.0 8.2 5.7 5.1	6.2 5.0 4.1 2.9 2.6	430 450 410 400 410	0.42 0.40 0.43 0.43 0.43	4.0 4.4 3.6 3.5 3.6		11.2 12.2 10.6 10.0 10.6	<p>Test section 1 mile south of test section 1-Cross ties 20 in. apart-1st geophone 33 ft N of Battelle main array-5 ft from rail. Vibroseismic Location</p>		
													100 150 200 250 350 400	2.6 1.8 1.4 1.0 0.8
		100	1240	1.6+	25 35 40 50 70 80	20.0 12.6 10.7 8.0 6.3 5.9	10.0 6.3 5.4 4.0 3.2 2.9	500 444 428 400 444 470	0.40 0.43 0.43 0.44 0.43 0.42		5.4 4.3 3.9 3.5 4.2 4.8		15.1 12.3 11.5 10.0 12.3 13.3	<p>Curve track, with slope east to west-Railroad ties spaced 24 in.-Test on east side of rail, spacing of geophones 2 ft-1st geophone 10 ft N of Battelle main array-Test conducted 5 ft from rails. Vibroseismic Location</p>

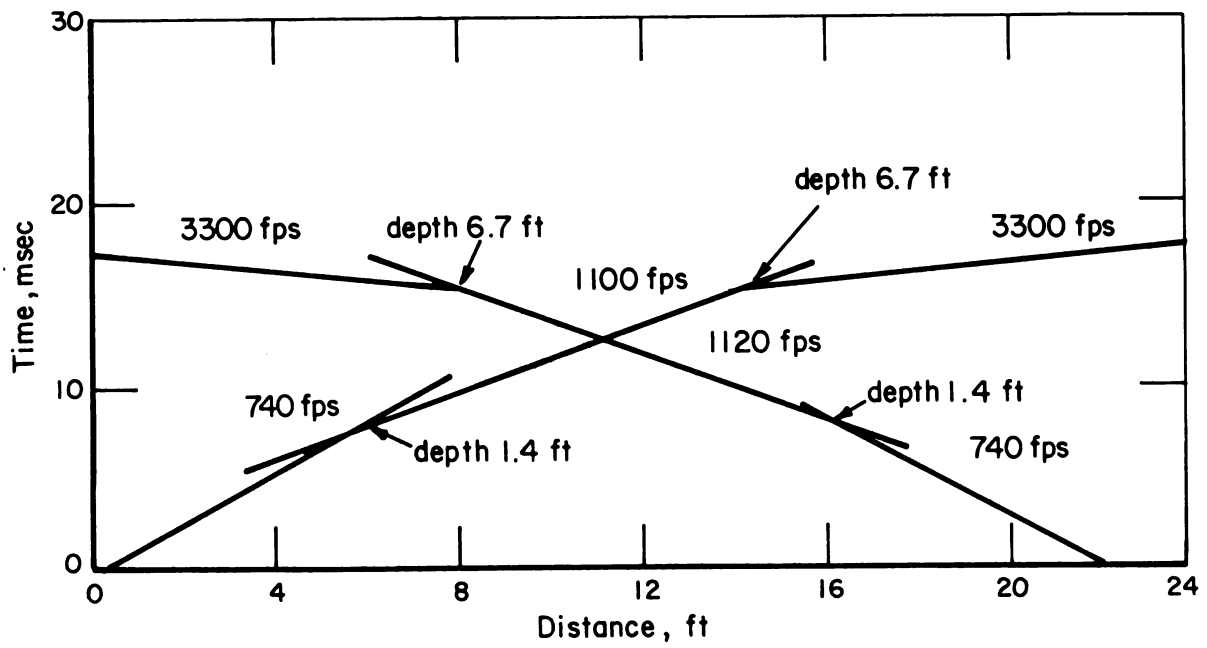


FIGURE G-1. REFRACTION SEISMIC DATA FOR SITE 1

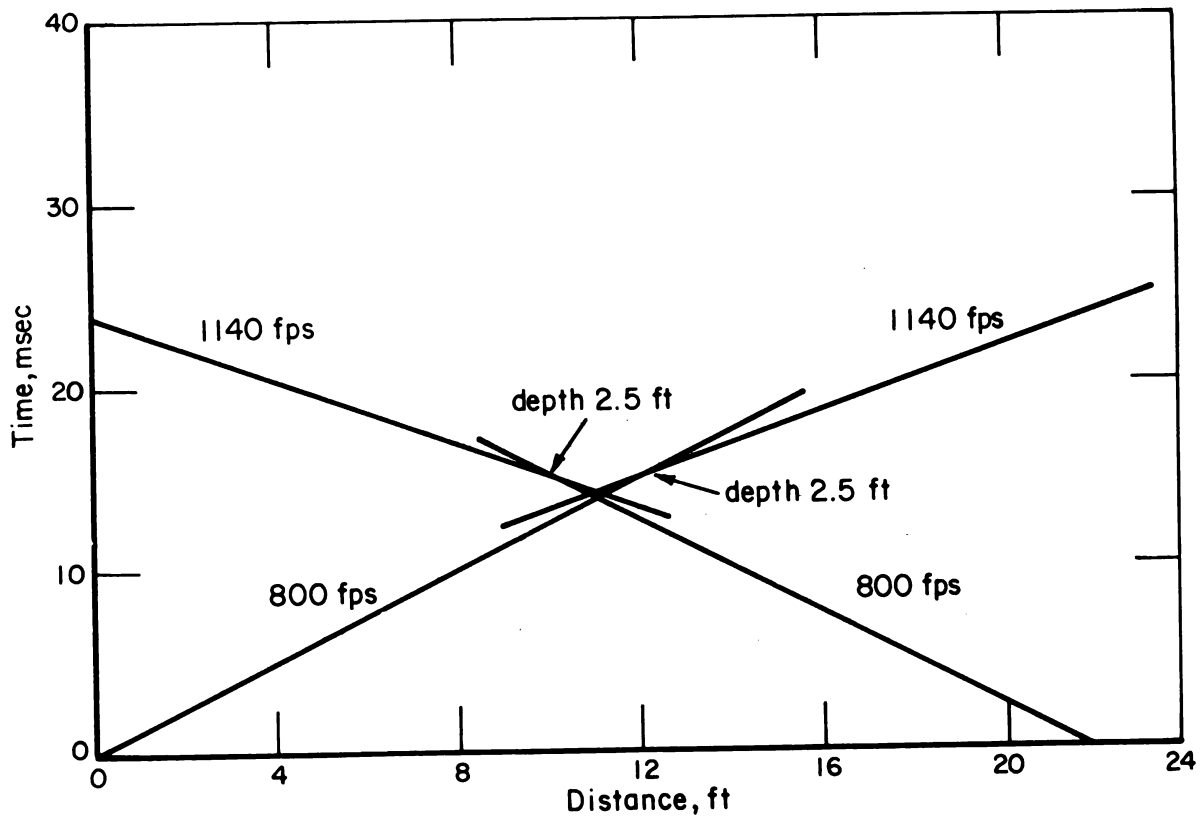


FIGURE G-2. REFRACTION SEISMIC DATA FOR SITE 2

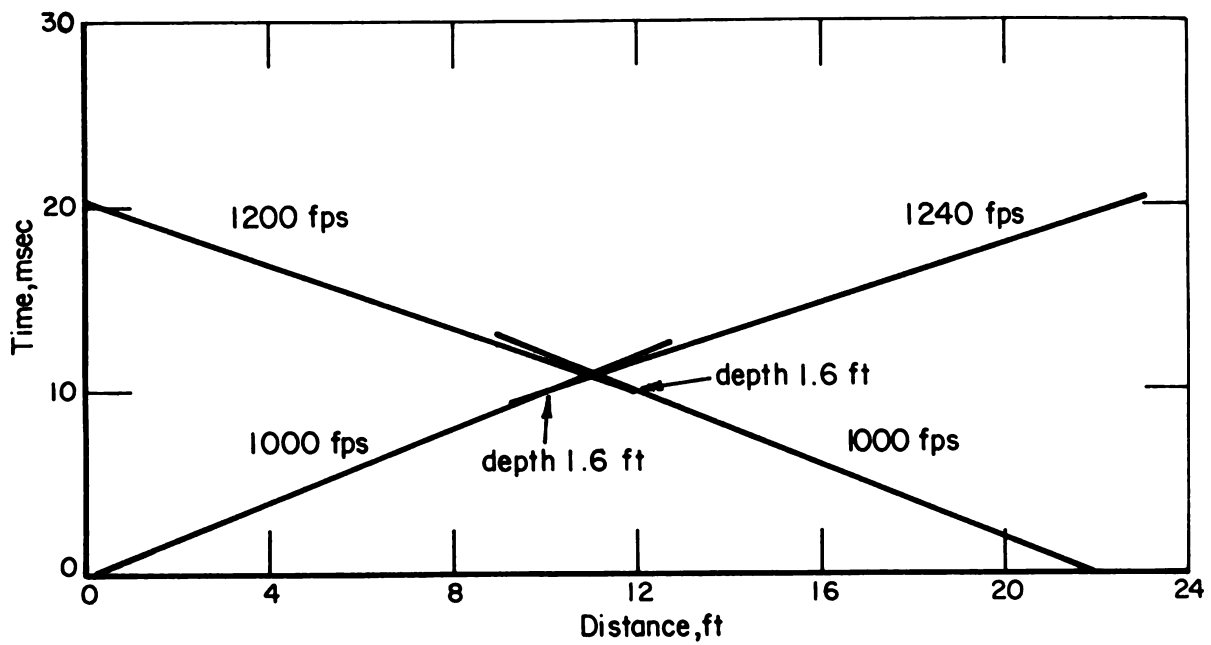


FIGURE G-3. REFRACTION SEISMIC DATA FOR SITE 3

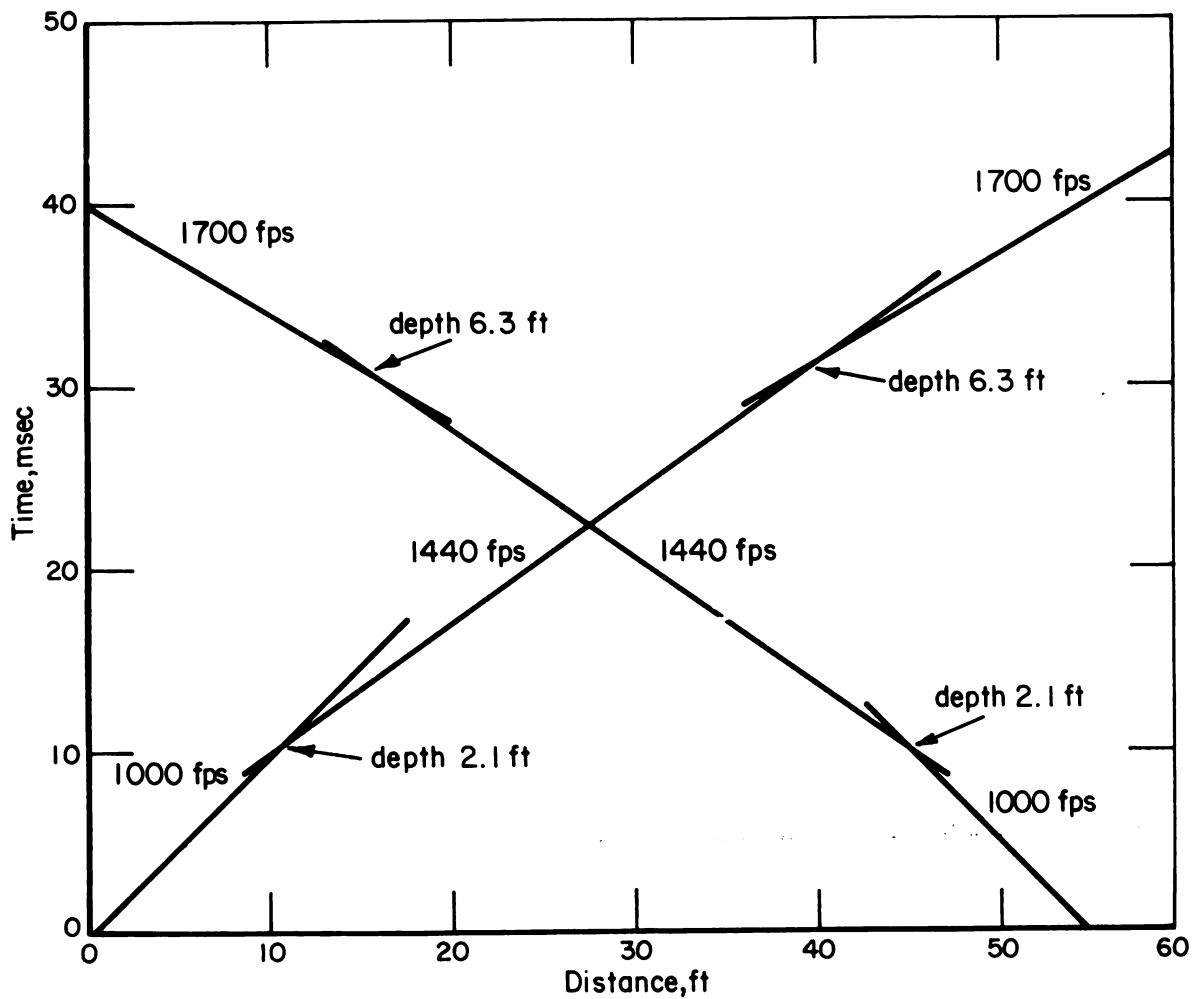


FIGURE G-4. REFRACTION SEISMIC DATA FOR SITE 3 WITH 5-FT GEOPHONE SPACING

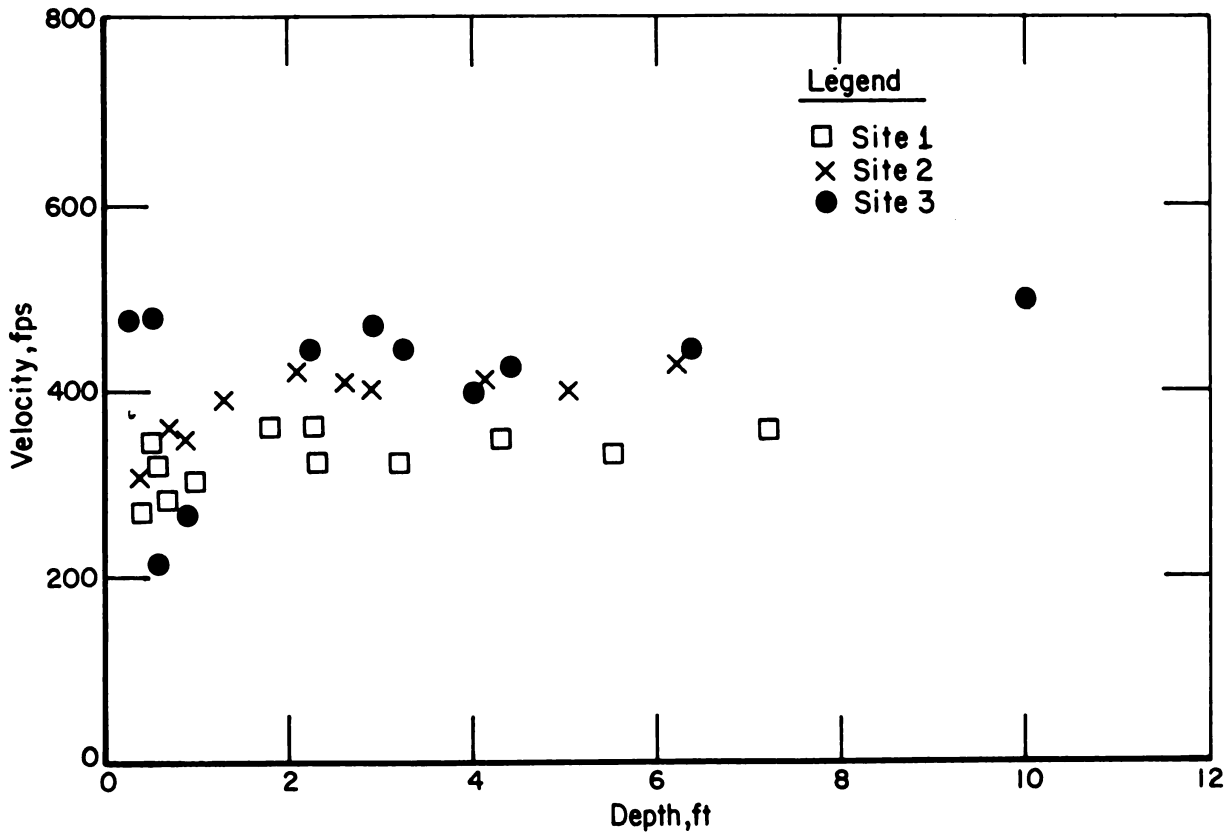


FIGURE G-5. SUMMARY OF SHEAR WAVE VELOCITY VERSUS DEPTH DATA

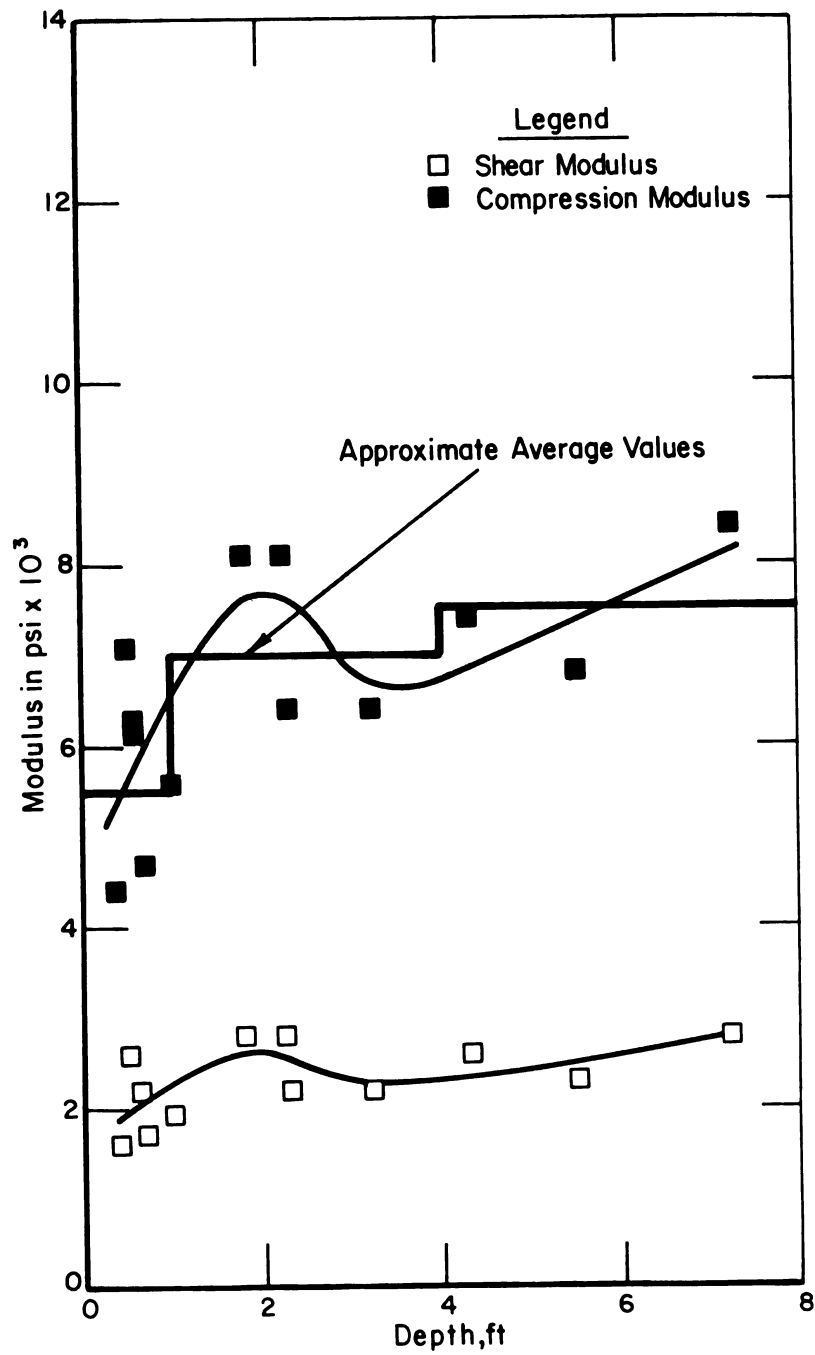


FIGURE G-6. ELASTIC MODULI VERSUS DEPTH FOR SITE 1

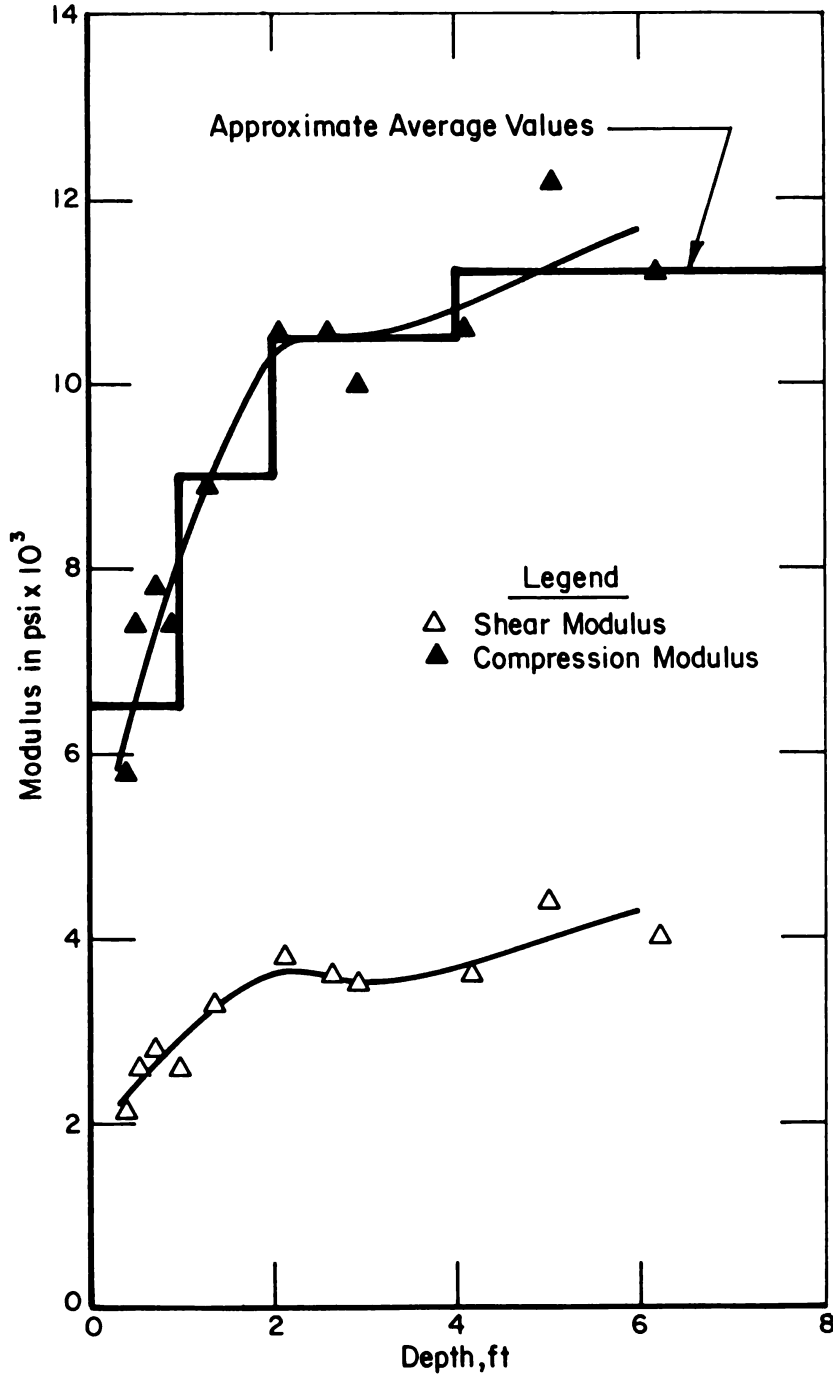


FIGURE G-7. ELASTIC MODULI VERSUS DEPTH FOR SITE 2

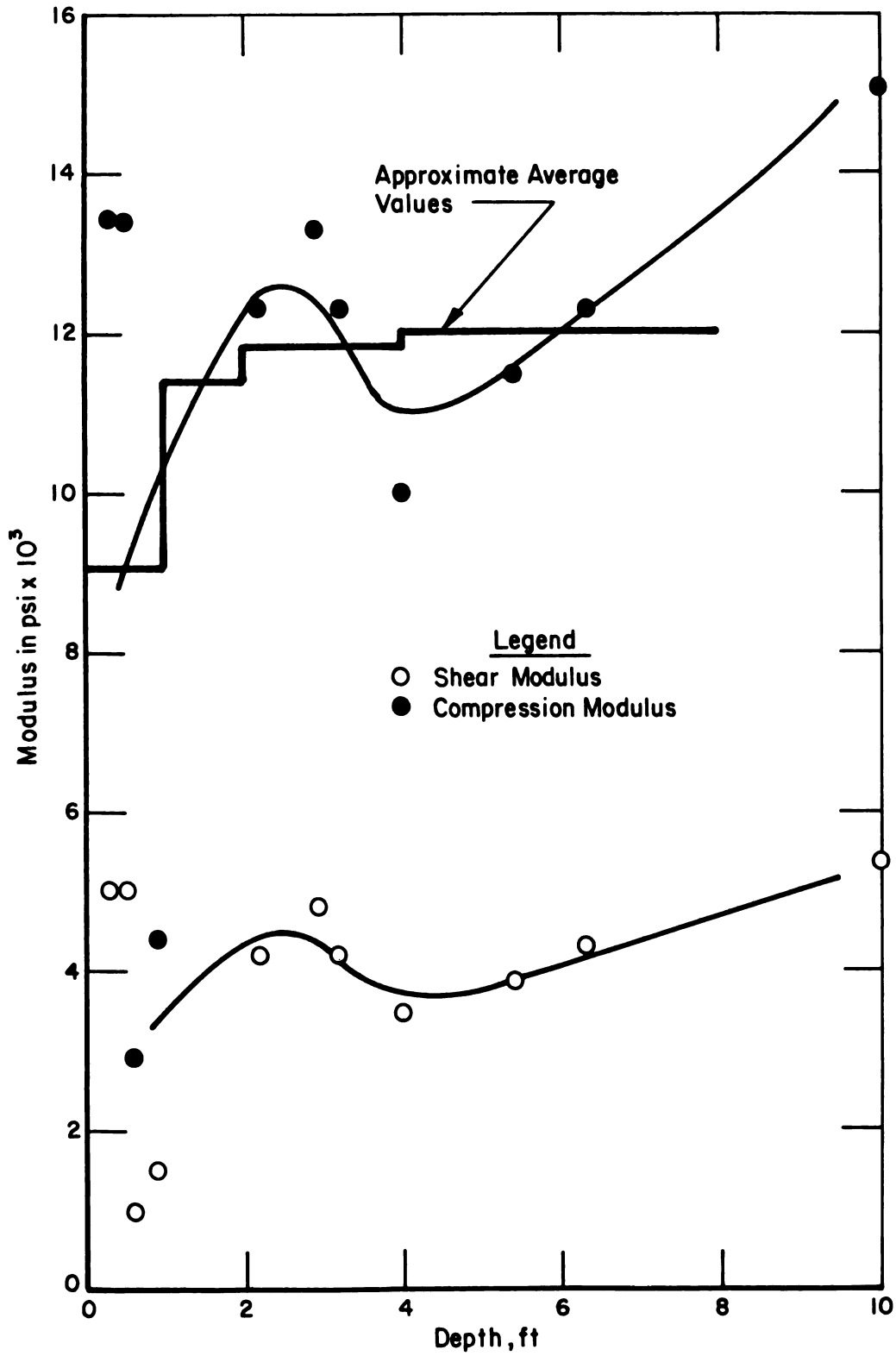


FIGURE G-8. ELASTIC MODULI VERSUS DEPTH AT SITE 3

depth. The curves indicate a significant variation in subgrade response between sites, with Site 3 having the highest modulus subgrade materials. All sites exhibit a similar characteristic, i.e., a zone of greater stiffness at depths of 2 (Sites 1 and 2) to 4 (Site 3) feet. This response is probably caused by traffic-induced densification of materials beneath the roadbed and/or the imbedment of ballast material during earlier periods of service.

Finally, a short refraction seismic line was run on the ballast materials at site 3. Results of this test are presented in Figure G-9, which indicates that the average P-wave velocity in the ballast at this location is about 820 fps. These data suggest that the preferred travel path of P-waves was through the higher velocity subgrade materials rather than through the ballast. Hence, we conclude that the close proximity of the ballast to the seismic line had no adverse effect on refraction seismic measurements of P-wave velocity in the subgrade.

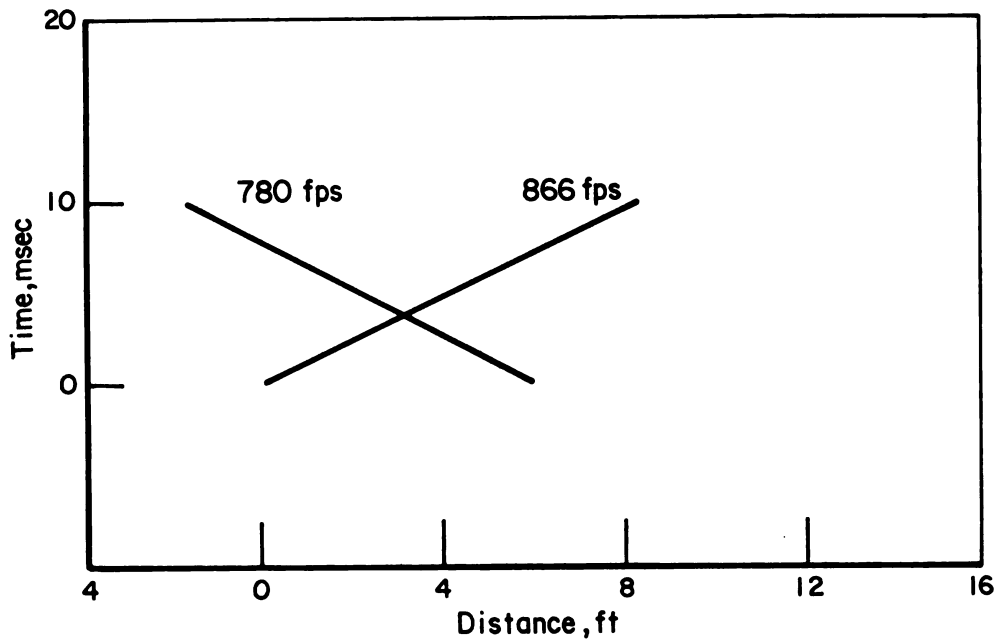


FIGURE G-9. REFRACTION SEISMIC DATA FROM BALLAST AT SITE 3

APPENDIX H

STATISTICAL ANALYSIS OF TRACK LOAD DATA

The tables at the end of this appendix summarize all of the statistical data for mean values and standard deviations for each speed and car weight subcategory of the track load data base. The content of these tables is identified in the following sections.

Data Key. A 6-digit identification number is used for each data category. The format for this key number is shown below with the possible combinations for numerical indices.

[A]	[B]	[C]	[D]	[E]
Summation Index	Site No.	Vehicle Category	Speed Category	Channel No.
1 = No Summation	1 = Site 1	0 = All cars	0 = All speeds	(01-42)
2 = Summation on vehicle and/or speed categories with 0 in C or D	2 = Site 2 3 = Site 3	1 = Locomotives 2 = Light cars 3 = Heavy Cars	3 = 30-40 mph 4 = 40-50 mph 5 = 50-60 mph	

For example, the key of 111301 designates data for measurement channel No. 01 at Site 1 for locomotives in the 30-40 mph speed range. The key of 210001 gives the measurement channel No. 01 summation data for all cars and all speeds (all traffic) at Site 1. Battelle's interactive graphics program can be used to plot individual curves for the probability density and distribution functions for any selected key numbers listed in the tables. It is also possible to combine any of the categories at one site to give an average for several measurement channels. Tables H-1, H-2, and H-3 list the locations and descriptions of each measurement channel used at the three track test sites shown in Figure H-1.

Axle Count. The column labeled AXLES in Tables H-4, H-5, and H-6 gives the total number N of data points (one peak value for each axle) in the specified category.

Mean Load. The column labeled MEAN gives the mean value estimate \bar{p} of all peak load data p_i in that category using the equation

$$\bar{p} = \frac{1}{N} \sum_{i=1}^N p_i \quad (\text{H-1})$$

Standard Deviation. The standard deviation (STD DEV) σ is calculated for each category from

$$\sigma^2 = \frac{1}{(N-1)} \sum_{i=1}^N (p_i - \bar{p})^2 \quad (\text{H-2})$$

Confidence Limits. Confidence limits (percent) are calculated for the mean value estimates based on an assumed normal distribution for the sampling distribution of mean values. The true mean value \bar{p}_t is expected to be within a tolerance band of the estimated mean value as given by

$$\bar{p}_t = \bar{p} \pm \frac{\sigma t_{n;\alpha/2}}{\sqrt{N}} \quad , \quad (\text{H-3})$$

where $t_{n;\alpha/2}$ is the student t probability distribution function which is readily available in statistical tables. The confidence statement for the range, or tolerance band, given by Equation (H-3) is that the true mean value \bar{p}_t will be in the specified range with a confidence level of 100 (1 - α) percent. Confidence limits in percent are listed for tolerance bands of ± 10 percent CONF (10) and ± 20 percent CONF (20) of the mean value.

Tolerance Bands. The columns labeled TOL (95) and TOL (90) give the mean value tolerance bands as a \pm percent of mean value for confidence limits of 95 and 90 percent, respectively. Data having large standard deviations and mean values close to zero typically show the lowest confidence levels and the largest tolerance bands.

TABLE H-1. MEASUREMENT CHANNEL IDENTIFICATION FOR SITE 1
(Tangent track with 24-inch tie spacing)

Channel Number	Measurement Description (Units)	Site 1 Location
01	Vertical W/R Load (kips)	0E
03	" " "	27E
06	" " "	58E
10	" " "	86E
15	Tie Center Bending Moment (inch-kips)	2
16	Tie Rail Seat Bending Moment "	2E
17	Tie Center Bending Moment "	59
18	Tie Rail Seat Bending Moment "	59E
19	Lateral W/R Load (kips)	59E
20	Vertical W/R Load "	59E
21	Rail Seat Vertical Load (kips)	59E
22	Rail Seat Moment (inch-kips)	59E
23	Rail Seat Vertical Load (kips)	61E
24	Rail Seat Moment (inch-kips)	61E
25	Rail Seat Vertical Load (kips)	63E
26	Rail Seat Moment (inch-kips)	63E
27	Lateral Rail/Tie Displacement (mils)	59E
28	Lateral Tie Displacement (mils)	59E
29	Tie Center Bending Moment (inch-kips)	29
30	Tie Rail Seat Bending Moment "	29E
31	Tie Center Bending Moment "	57
32	Tie Rail Seat Bending Moment "	57E
33	Tie Center Torsion Moment "	85
34	Tie Center Bending Moment "	85
35	Tie Rail Seat Bending Moment "	85E
36	Rail Seat Vertical Load (kips)	55E
37	Rail Seat Moment (inch-kips)	55E
38	Rail Seat Vertical Load (kips)	57E
39	Rail Seat Moment (inch-kips)	57E
40	Lateral W/R Load (kips)	29E
42	Fastener Bolt Force (gage side-kips)	29E

E - East Rail
W - West Rail

TABLE H-2. MEASUREMENT CHANNEL IDENTIFICATION FOR SITE 2
(Tangent track with 20-inch tie spacing)

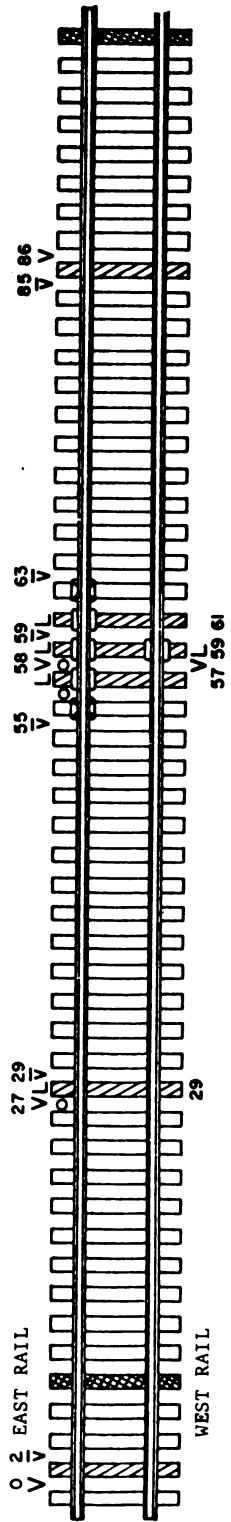
Channel Number	Measurement Description (Units)	Site 2 Location
01	Vertical W/R Load (kips)	97E
03	" " " "	65E
06	" " " "	31E
10	" " " "	1E
15	Rail Seat Vertical Load (kips)	28E
16	Rail Seat Moment (inch-kips)	28E
17	Rail Seat Vertical Load (kips)	30E
18	Rail Seat Moment (inch-kips)	30E
19	Tie Center Torsion Moment "	1
20	Tie Center Bending Moment "	1
21	Tie Rail Seat Bending Moment (inch-kips)	1E
22	Tie Center Bending Moment "	97
23	Tie Rail Seat Bending Moment "	97E
24	Lateral W/R Load (kips)	1E
25	Tie Center Bending Moment (inch-kips)	30
26	Tie Rail Seat Bending Moment "	30E
27	Fastener Bolt Force (gage side-kips)	1E
28	Fastener Bolt Force (field side-kips)	1E
29	Rail Seat Vertical Load (kips)	31E
30	Rail Seat Moment (inch-kips)	31E
31	Rail Seat Vertical Load (kips)	33E
32	Rail Seat Moment (inch-kips)	33E
33	Rail Seat Vertical Load (kips)	35E
34	Rail Seat Moment (inch-kips)	35E
35	Tie Center Bending Moment "	31
36	Tie Rail Seat Bending Moment (inch-kips)	31E
37	Lateral W/R Load (kips)	31E
38	Vertical W/R Load "	31W
39	Tie Center Bending Moment (inch-kips)	65
40	Tie Rail Seat Bending Moment "	65E
41	Lateral Rail/Tie Displacement (mils)	31E
42	Lateral Tie Displacement (mils)	31E

E - East Rail
W - West Rail

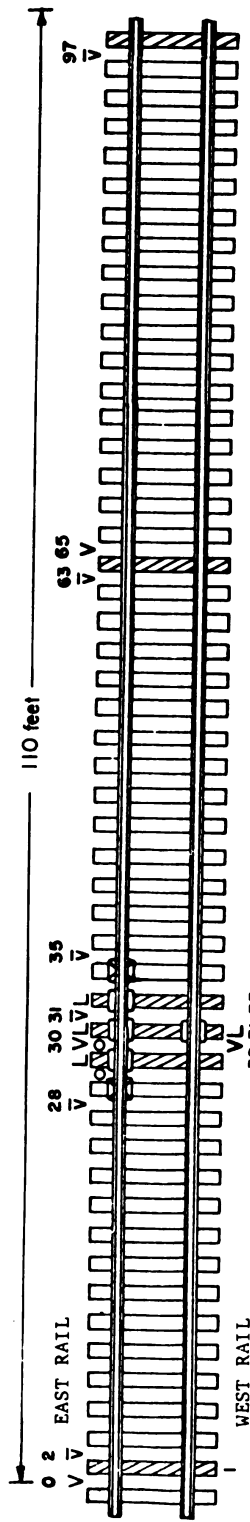
TABLE H-3. MEASUREMENT CHANNEL IDENTIFICATION FOR SITE 3
(Curve track with 24-inch tie spacing)

Channel Number	Measurement Description (Units)	Site 3 Location
01	Vertical W/R Load (kips)	96E
03	" " " "	70E
06	" " " "	44E
10	" " " "	18E
15	Rail Seat Vertical Load (kips)	41E
16	Rail Seat Moment (inch-kips)	41E
17	Lateral W/R Load (kips)	18E
20	Tie Rail Seat Bending Moment (inch-kips)	18E
21	Tie Center Bending Moment "	18
22	Tie Center Torsion Moment "	18
23	Tie Rail Seat Bending Moment "	43E
24	Tie Rail Seat Bending Moment "	69E
25	Tie Center Bending Moment "	69
26	Tie Center Bending Moment "	43
28	Fastener Bolt Force (Gage side-kips)	18E
29	Vertical W/R Load (kips)	44W
30	Tie Center Bending Moment (inch-kips)	45
31	Lateral W/R Force (kips)	45E
32	Tie Center Bending Moment (inch-kips)	47
33	Tie Rail Seat Bending Moment "	45E
34	Tie Rail Seat Bending Moment "	47E
37	Rail Seat Vertical Load (kips)	47E
38	Rail Seat Moment (inch-kips)	47E
39	Rail Seat Vertical Load (kips)	49E
40	Rail Seat Moment (inch-kips)	49E
41	Lateral Rail/Tie Displacement (mils)	45E
42	Lateral Tie Displacement (mils)	45E

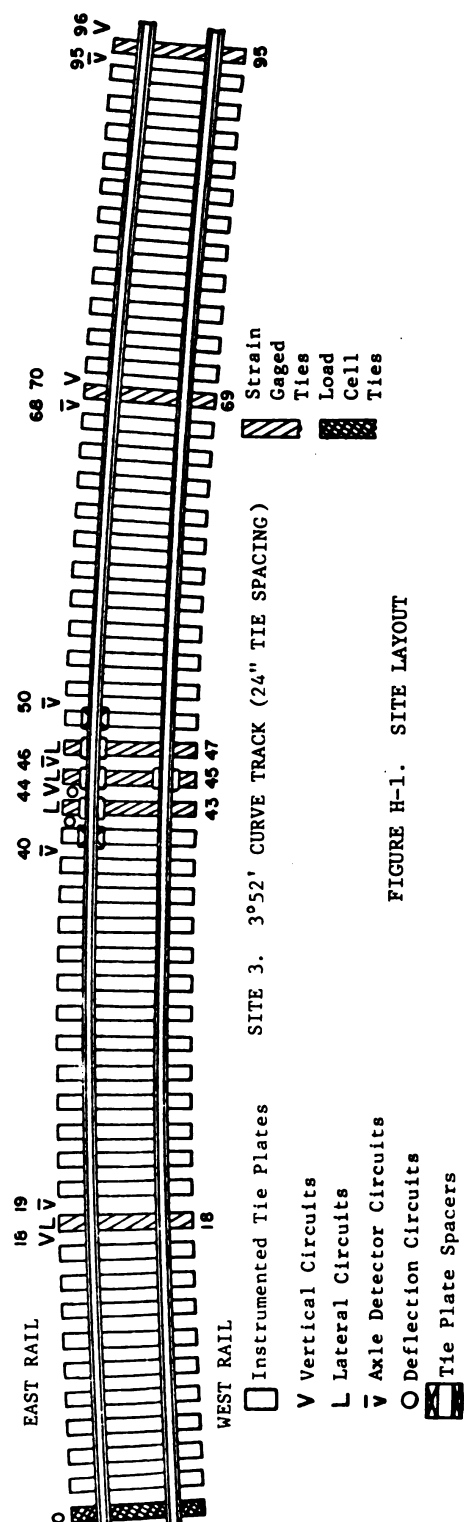
E - East Rail (High rail on curve)
W - West Rail (Low rail on curve)



SITE 1. TANGENT TRACK (24" TIE SPACING)



SITE 2. TANGENT TRACK (20" TIE SPACING)



SITE 3. 3°52' CURVE TRACK (24" TIE SPACING)

FIGURE H-1. SITE LAYOUT

TABLE B-4. SITE 1 STATISTICAL DATA SUMMARY

KEY	AXLES	MEAN	STD. DEV.	CONF.(101)	CONF.(201)	YOL(1951)	YOL(1981)
111301	12.	.328E+02	.318E+01	99.6	100.0	6.1	5.8
111401	20.	.344E+02	.344E+01	100.0	100.0	2.6	2.1
111501	72.	.341E+02	.301E+01	100.0	100.0	2.1	1.7
112301	28.	.113E+02	.148E+01	90.8	99.8	11.8	9.8
112401	724.	.937E+01	.232E+01	100.0	100.0	1.6	1.3
112501	658.	.110E+02	.117E+01	100.0	100.0	2.2	1.9
113301	408.	.276E+02	.522E+01	100.0	100.0	1.9	1.6
113401	244.	.172E+02	.561E+01	100.0	100.0	4.1	3.4
113501	1116.	.208E+02	.532E+01	100.0	100.0	1.6	1.3
111303	12.	.324E+02	.324E+01	97.6	100.0	6.9	6.9
111403	20.	.340E+02	.340E+01	100.0	100.0	3.8	3.1
111503	72.	.351E+02	.369E+01	100.0	100.0	2.5	2.1
112303	28.	.118E+02	.357E+01	88.5	99.7	12.6	10.5
112403	724.	.936E+01	.217E+01	100.0	100.0	1.7	1.4
112503	658.	.117E+02	.336E+01	100.0	100.0	2.2	1.8
113303	408.	.270E+02	.571E+01	100.0	100.0	2.1	1.7
113403	244.	.178E+02	.563E+01	100.0	100.0	4.0	3.4
113503	1116.	.214E+02	.549E+01	100.0	100.0	1.5	1.3
111306	12.	.353E+02	.396E+01	99.0	100.0	7.1	5.8
111406	20.	.372E+02	.349E+01	100.0	100.0	4.4	3.6
111506	72.	.354E+02	.399E+01	100.0	100.0	2.2	2.2
112306	28.	.118E+02	.318E+01	94.0	99.9	10.5	8.7
112406	724.	.108E+02	.271E+01	100.0	100.0	1.9	1.6
112506	658.	.117E+02	.316E+01	190.0	100.0	1.7	1.7
113306	408.	.246E+02	.546E+01	100.0	100.0	2.0	1.7
113406	244.	.206E+02	.606E+01	100.0	100.0	3.8	3.2
113506	1116.	.213E+02	.595E+01	100.0	100.0	1.6	1.4
111310	12.	.303E+02	.242E+01	99.9	100.0	5.1	4.2
111410	20.	.334E+02	.284E+01	100.0	100.0	4.0	3.3
111510	72.	.332E+02	.286E+01	100.0	100.0	2.0	1.7
112310	28.	.118E+02	.399E+01	84.5	99.3	14.0	11.6
112410	724.	.936E+01	.222E+01	100.0	100.0	1.7	1.5
112510	658.	.109E+02	.326E+01	100.0	100.0	2.3	1.9
113310	408.	.264E+02	.522E+01	100.0	100.0	1.9	1.6
113410	244.	.165E+02	.604E+01	100.0	100.0	4.5	3.8
113510	1116.	.194E+02	.527E+01	100.0	100.0	1.6	1.3
111315	12.	-.419E+01	.130E+02	8.6	17.1	198.7	162.1
111415	20.	-.120E+01	.151E+02	2.8	5.6	588.2	486.0
111515	72.	-.125E+02	.646E+01	89.5	99.8	12.1	10.1
112315	28.	.947E+01	.641E+01	53.2	84.8	27.9	23.1
112415	724.	.808E+01	.809E+01	99.2	100.0	7.3	6.1
112515	658.	.257E+01	.741E+01	61.2	90.9	23.2	19.5
113315	408.	-.869E+01	.767E+01	97.7	100.0	8.6	7.2
113415	244.	.544E+01	.114E+02	54.6	86.5	26.3	22.0
113515	1116.	-.522E+01	.608E+01	99.6	100.0	6.8	5.7
111316	12.	.147E+02	.562E+01	72.6	95.8	19.1	15.6
111416	20.	.221E+02	.442E+01	94.5	99.9	10.2	8.4
111516	72.	.227E+02	.477E+01	100.0	100.0	4.9	4.1
112316	28.	.269E+01	.420E+01	26.3	49.7	60.5	50.2
112416	724.	.223E+01	.437E+01	83.0	94.4	14.3	12.0
112516	658.	.571E+00	.563E+01	20.5	39.8	75.4	63.2
113316	408.	.116E+02	.604E+01	100.0	100.0	5.0	4.2
113416	244.	.594E+01	.943E+01	67.3	94.9	20.1	16.0
113516	1116.	.655E+01	.677E+01	97.3	100.0	8.7	7.3
111317	12.	.223E+02	.449E+01	88.0	99.4	12.8	10.5

TABLE H-4. SITE 1 STATISTICAL DATA SUMMARY (CONTINUED)

KEY	AXLES	MEAN	STD. DEV.	CONF.(101)	CONF.(201)	TOL(1951)	TOL(1901)
111417	20.	.256E+02	.713E+01	.17.5	99.5	13.0	10.8
111517	72.	.192E+02	.427E+01	100.0	100.0	5.2	5.4
112317	28.	.245E+02	.350E+01	99.9	100.0	5.5	4.6
112417	724.	.245E+02	.599E+01	100.0	100.0	1.6	1.3
112517	65A.	.211E+02	.579E+01	100.0	100.0	2.1	1.8
113317	40A.	.179E+02	.382E+01	100.0	100.0	2.1	1.7
113417	244.	.261E+02	.597E+01	100.0	100.0	2.9	2.4
113517	1116.	.184E+02	.334E+01	100.0	100.0	1.1	.9
11311A	12.	.344E+02	.441E+01	.97.9	100.0	8.1	6.6
11141A	20.	.351E+02	.833E+01	91.9	99.8	11.4	9.4
11151B	72.	.339E+02	.672E+01	100.0	100.0	4.7	3.9
11231A	28.	.599E+01	.823E+01	29.7	55.2	53.3	44.2
11241A	724.	.960E+01	.515E+01	100.0	100.0	3.9	3.3
11251A	65A.	.873E+01	.652E+01	99.9	100.0	5.7	4.8
11331B	40A.	.232E+02	.545E+01	100.0	100.0	2.3	1.9
11341A	244.	.164E+02	.869E+01	99.7	100.0	6.5	5.5
11351E	1116.	.175E+02	.716E+01	100.0	100.0	2.4	2.0
111319	12.	.168E+01	.340E+01	13.2	26.1	128.9	105.2
111419	20.	.108E+01	.432E+01	8.8	17.4	187.6	155.0
111519	72.	.114E+01	.411E+01	18.5	36.0	84.8	70.9
112319	28.	.537E+00	.200E+01	11.2	22.2	144.4	119.9
112419	724.	.435E+00	.219E+01	41.1	72.0	36.3	30.5
112519	65A.	.846E+00	.250E+01	63.2	93.0	21.6	18.2
113319	40A.	.273E+01	.468E+01	70.4	95.2	16.6	13.9
113419	244.	.138E+01	.371E+01	43.9	75.4	33.8	28.4
113519	1116.	.635E+00	.253E+01	60.1	90.8	23.3	19.5
111320	12.	.303E+02	.342E+01	98.9	100.0	7.2	5.8
111420	20.	.282E+02	.368E+01	99.7	100.0	6.0	5.0
111520	72.	.295E+02	.409E+01	100.0	100.0	3.3	2.7
112320	28.	.921E+01	.276E+01	91.1	99.8	11.6	9.7
112420	724.	.791E+01	.229E+01	100.0	100.0	2.1	1.8
112520	65A.	.959E+01	.297E+01	100.0	100.0	2.4	2.0
113320	40A.	.250E+02	.559E+01	100.0	100.0	2.2	1.8
113420	244.	.164E+02	.622E+01	100.0	100.0	4.8	4.0
113520	1116.	.190E+02	.483E+01	100.0	100.0	1.6	1.3
111321	12.	.145E+02	.225E+01	95.2	99.9	9.9	8.1
111421	20.	.156E+02	.322E+01	95.7	100.0	9.7	8.0
111521	72.	.151E+02	.240E+01	100.0	100.0	4.4	3.6
112321	28.	.255E+01	.197E+01	50.0	91.9	30.0	24.9
112421	724.	.295E+01	.166E+01	100.0	100.0	4.1	3.5
112521	65A.	.317E+01	.238E+01	99.9	100.0	5.8	4.8
113321	40A.	.104E+02	.284E+01	100.0	100.0	2.7	2.2
113421	244.	.634E+01	.407E+01	99.4	100.0	8.1	6.8
113521	1116.	.800E+01	.349E+01	100.0	100.0	2.6	2.1
111322	12.	-.270E+01	.596E+01	12.2	24.1	140.2	114.4
111422	20.	-.871E+00	.600E+01	5.1	18.2	323.0	266.8
111522	72.	-.975E+00	.511E+01	13.1	25.8	120.8	100.9
112322	28.	.429E-01	.252E+01	.7	1.4	2279.9	1892.6
112422	724.	.149E+00	.359E+01	9.9	17.7	175.4	147.4
112522	65A.	.356E-01	.414E+01	1.8	3.5	890.4	746.9
113322	40A.	-.622E+01	.460E+01	99.3	100.0	7.2	6.0
113422	244.	-.345E+01	.451E+01	76.4	94.3	16.5	13.8
113522	1116.	.159E+00	.420E+01	10.1	20.0	155.1	130.2
111323	12.	.109E+02	.515E+01	96.7	99.5	8.5	6.3
111423	20.	.136E+02	.174E+01	99.8	100.0	6.0	4.9

TABLE B-4. SITE 1 STATISTICAL DATA SUMMARY (CONTINUED)

KEY	AXLES	MEAN	STD_DEV	CONF(10%)	CONF(20%)	10L(95%)	10L(90%)
11523	64	-105E+02	-397E+01	96.1	100.0	9.5	7.9
11523	12	-235E+01	-139E+01	43.0	73.3	37.6	30.7
11243	724	-102E+01	-103E+01	99.2	100.0	7.4	6.2
11523	510	-164E+01	-147E+01	94.5	100.0	6.9	5.8
11323	32	-434E+01	-90AF+00	94.9	100.0	7.6	6.3
11323	244	-451E+01	-3AF+01	93.4	100.0	10.7	8.9
11523	1632	-564E+01	-300E+01	100.0	100.0	3.2	2.7
11324	4	-341E-12	-337E+01	.0	.0
11424	20	-300E+00	-402E+01	2.6	5.3	626.9	517.9
11524	64	-703E+00	-517E+01	8.6	17.1	143.8	153.6
11324	12	-110E+01	-175E+01	16.9	32.9	100.9	82.3
11244	724	-105E+01	-222E+01	79.5	98.9	15.5	13.0
11524	510	-236E+00	-372E+01	11.4	22.6	137.0	114.9
11324	32	-A63E+00	-1AE+01	20.2	39.3	7A.6	65.3
11424	244	-5A1E+00	-269E+01	30.7	57.0	49.9	41.8
11524	1032	-113E+01	-400E+01	63.6	93.1	21.6	18.1
11425	20	-156E+02	-14AF+01	99.4	100.0	6.6	5.4
11525	72	-16AE+02	-152E+01	100.0	100.0	4.6	3.8
11325	28	-422E+01	-21AE+01	100.0	100.0	1.0	2.5
11425	724	-443E+01	-314E+01	51.6	83.3	28.9	24.0
11525	654	-471E+01	-195E+01	100.0	100.0	1.7	1.5
11325	404	-115E+02	-267E+01	100.0	100.0	2.9	2.4
11425	244	-81AE+01	-301E+01	100.0	100.0	2.3	1.9
11525	1116	-966E+01	-316E+01	130.0	100.0	4.6	3.9
11426	12	-565E+01	-425E+01	34.6	62.4	47.7	39.0
11526	20	-390E+01	-424E+01	31.5	56.0	50.8	42.0
11526	72	-A9AE+01	-633E+01	76.7	9A.1	16.6	13.8
11246	28	-394E+01	-172E+01	76.4	97.8	16.9	14.1
11426	724	-389E+01	-137E+01	100.0	100.0	2.6	2.2
11526	654	-476E+01	-31AE+01	100.0	100.0	5.1	4.3
11326	404	-334E+01	-246E+01	49.2	70.0	7.2	6.0
11426	244	-612E+01	-18E+01	99.9	100.0	5.8	4.8
11526	1116	-608E+01	-325E+01	100.0	100.0	3.1	2.6
11427	12	-134E+02	-927E+01	37.2	66.1	44.0	35.9
11527	12	-209E+02	-122E+02	53.5	73.9	37.1	30.3
11427	48	-100E+01	-10AE+02	39.1	59.2	39.1	32.6
11527	28	-357E+01	-772E+01	19.2	37.2	43.8	39.6
11247	352	-647E+01	-854E+01	44.4	99.5	13.8	11.6
11527	454	-281E+01	-87AE+01	50.5	A2.7	29.8	24.2
11327	404	-164E+02	-714E+01	100.0	100.0	4.2	3.6
11427	224	-101E+02	-133E+02	74.1	97.6	17.3	14.5
11527	640	-798E+01	-610E+01	100.0	100.0	5.1	4.2
11328	12	-163E+01	-514E+01	42.7	73.0	37.4	30.9
11428	12	-13AE+01	-61E+01	6.1	12.1	282.2	230.3
11528	56	-A90E+01	-534E+01	7A.3	9A.4	16.1	13.4
11328	28	-630E+01	-421E+01	56.4	87.5	25.9	21.5
11428	352	-190E+01	-720E+01	37.9	67.7	39.8	33.3
11528	546	-803E+01	-76AE+01	9A.5	100.0	6.0	6.7
11328	404	-993E+01	-2A9E+01	105.0	100.0	2.8	2.4
11428	224	-644E+01	-677E+01	67.3	94.9	20.1	16.8
11528	732	-156E+01	-45AE+01	100.0	100.0	3.9	3.3
11429	12	-52E+01	-707E+00	97.2	100.0	6.6	7.0
11429	20	-492E+01	-194E+01	72.9	96.5	1A.5	15.2
11529	72	-3A0E+01	-242E+01	91.2	99.0	15.0	1.5

TABLE N-4. SITE 1 STATISTICAL DATA SUMMARY (CONTINUED)

KEY	AXLES	MEAN	STD DEV	CONF(10%)	CONF(20%)	TOL(95%)	TOL(98%)
112329	28.	.167E+01	.185E+01	36.1	65.2	43.0	35.7
112429	724.	.161E+01	.137E+01	99.8	100.0	6.2	5.2
112529	658.	.148E+01	.174E+01	96.0	100.0	9.2	7.8
113329	408.	.475E+01	.133E+01	100.0	100.0	2.7	2.3
113429	244.	.311E+01	.154E+01	99.8	100.0	6.2	5.2
113529	1116.	.269E+01	.215E+01	100.0	100.0	4.7	3.9
111330	12.	.735E+01	.902E+01	21.7	41.6	78.0	63.6
111430	72.	.345E+01	.124E+02	10.9	21.7	150.2	124.1
111530	20.	.136E+02	.541E+01	96.4	100.0	9.4	7.8
112330	28.	-.114E+00	.535E+01	.9	1.4	1815.7	1507.3
112430	724.	-.923E-01	.645E+01	3.1	6.1	510.6	420.3
112530	658.	.510E+01	.440E+01	99.7	100.0	6.6	5.5
113330	408.	.103E+02	.520E+01	100.0	100.0	4.9	4.1
113430	244.	.193E+01	.497E+01	26.4	49.9	58.5	49.0
113530	1116.	.836E+01	.295E+01	100.0	100.0	2.1	1.7
111331	12.	.192E+02	.560E+01	73.9	96.3	18.6	15.2
111431	20.	.226E+02	.451E+01	75.0	97.2	17.6	14.6
111531	52.	.159E+02	.366E+01	99.7	100.0	6.4	5.3
112331	28.	.195E+02	.619E+01	49.2	99.7	12.3	10.2
112431	724.	.207E+02	.644E+01	100.0	100.0	2.3	2.0
112531	470.	.162E+02	.427E+01	100.0	100.0	2.4	2.0
113331	408.	.145E+02	.400E+01	100.0	100.0	2.6	2.2
113431	244.	.207E+02	.765E+01	100.0	100.0	4.7	3.9
113531	936.	.147E+02	.230E+01	100.0	100.0	1.0	0.8
111332	12.	.466E+02	.645E+01	96.8	100.0	9.0	7.3
111432	20.	.531E+02	.521E+01	100.0	100.0	4.6	3.8
111532	68.	.446E+02	.441E+01	100.0	100.0	2.6	2.2
112332	28.	.255E+02	.848E+01	45.9	99.5	13.5	11.2
112432	724.	.266E+02	.574E+01	100.0	100.0	1.6	1.3
112532	642.	.230E+02	.594E+01	100.0	100.0	2.0	1.7
113332	408.	.421E+02	.424E+01	100.0	100.0	1.0	0.8
113432	244.	.366E+02	.940E+01	100.0	100.0	3.2	2.7
113532	1060.	.330E+02	.605E+01	100.0	100.0	1.1	0.9
111333	12.	-.159E+02	.170E+01	99.2	100.0	6.8	5.5
111433	20.	-.160E+02	.230E+01	99.4	100.0	6.7	5.6
111533	72.	-.153E+02	.250E+01	100.0	100.0	3.4	3.2
112333	28.	-.530E+01	.236E+01	75.5	97.5	17.3	14.3
112433	724.	.405E+01	.216E+01	100.0	100.0	3.9	3.3
112533	658.	-.503E+01	.231E+01	100.0	100.0	3.0	3.0
113333	408.	-.156E+02	.299E+01	100.0	100.0	1.9	1.6
113433	244.	-.984E+01	.347E+01	100.0	100.0	4.4	3.7
113533	1116.	-.211E+01	.274E+01	100.0	100.0	1.7	1.4
111334	12.	.500E-01	.140E+02	.1	.2	17800.7	14924.4
111434	20.	.612E+01	.150E+02	14.2	28.2	114.4	94.5
111534	72.	-.573E+01	.779E+01	46.6	74.4	31.9	26.7
112334	28.	.101E+02	.645E+01	55.6	86.0	26.4	21.9
112434	724.	.101E+02	.754E+01	100.0	100.0	5.5	4.6
112534	658.	.446E+01	.675E+01	90.9	99.9	11.6	9.7
113334	408.	-.347E+01	.749E+01	67.8	95.2	19.8	16.6
113434	244.	.907E+01	.115E+02	78.0	94.5	16.0	13.4
113534	1116.	.240E+01	.495E+01	94.1	100.0	10.4	8.7
111335	12.	.417E+02	.535E+01	97.9	100.0	8.2	6.7
111435	20.	.477E+02	.753E+01	98.9	100.0	7.4	6.1
111535	72.	.426E+02	.514E+01	100.0	100.0	2.9	2.4
112335	28.	.130E+02	.450E+01	57.4	46.4	25.3	21.0

TABLE R-4. SITE 1 STATISTICAL DATA SUMMARY (CONTINUED)

KEY	AXLES	MEAN	STD.DEV	CONF(10%)	CONF(20%)	TOL(95%)	TOL(90%)
112435	724.	.118E+02	.664E+01	100.0	100.0	2.9	2.4
112535	650.	.116E+02	.542E+01	100.0	100.0	3.6	3.0
113335	408.	.360E+02	.943E+01	100.0	100.0	2.3	1.9
113435	244.	.238E+02	.107E+02	99.9	100.0	5.0	4.9
113535	1116.	.239E+02	.048E+01	100.0	100.0	2.1	1.7
113136	12.	.161E+02	.158E+01	99.7	100.0	5.9	4.8
111436	20.	.184E+02	.203E+01	99.9	100.0	5.1	4.2
111536	64.	.183E+02	.254E+01	100.0	100.0	3.5	2.9
112336	28.	.511E+01	.277E+01	66.2	93.8	21.1	17.5
112436	724.	.477E+01	.177E+01	100.0	100.0	3.0	2.5
112536	510.	.540E+01	.210E+01	100.0	100.0	3.4	2.8
113336	408.	.144E+02	.339E+01	100.0	100.0	2.3	1.9
113436	244.	.932E+01	.345E+01	100.0	100.0	4.7	3.9
113536	1032.	.104E+02	.325E+01	100.0	100.0	1.9	1.6
111337	12.	.519E+01	.547E+01	25.1	47.2	67.5	55.1
111437	20.	.125E+01	.614E+01	7.4	14.7	222.0	184.0
111537	64.	.281E+01	.928E+01	21.2	41.1	71.6	61.5
112337	28.	-.643E+00	.278E+01	9.7	19.2	157.5	139.1
112437	724.	-.152E+00	.327E+01	9.9	19.7	157.3	131.9
112537	510.	-.324E+00	.474E+01	12.3	24.4	126.5	106.1
113337	408.	-.193E+01	.367E+01	70.9	96.5	18.6	15.6
113437	244.	-.551E+00	.315E+01	21.5	41.5	72.1	60.4
113537	1032.	-.206E+01	.420E+01	97.1	100.0	9.0	7.5
111338	12.	.299E+02	.611E+00	109.0	100.0	1.7	1.4
111438	20.	.298E+02	.118E+01	100.0	100.0	1.9	1.5
111538	72.	.295E+02	.177E+01	100.0	100.0	1.4	1.2
112338	28.	.113E+02	.431E+01	82.5	99.0	14.7	12.2
112438	724.	.109E+02	.264E+01	100.0	100.0	1.8	1.5
112538	658.	.109E+02	.410E+01	100.0	100.0	2.9	2.4
113338	408.	.274E+02	.397E+01	100.0	100.0	1.4	1.2
113438	244.	.184E+02	.543E+01	100.0	100.0	4.0	3.3
113538	1116.	.210E+02	.530E+01	100.0	100.0	1.5	1.2
111339	12.	-.118E+02	.536E+01	50.8	61.7	30.9	25.2
111439	20.	-.145E+02	.129E+02	43.1	74.0	36.1	29.8
111539	72.	-.991E+01	.121E+02	51.1	83.0	28.7	24.0
112339	28.	.161E+01	.445E+01	15.0	29.5	107.3	89.1
112439	724.	.161E+01	.343E+01	79.3	98.8	15.5	13.0
112539	658.	.154E+01	.594E+01	50.2	82.5	28.9	24.3
113339	408.	-.132E+02	.889E+01	99.7	100.0	6.5	5.5
113439	244.	-.384E+01	.782E+01	55.6	87.3	25.7	21.5
113539	1116.	-.598E+01	.809E+01	98.6	100.0	7.9	6.7
111340	12.	.450E+00	.230E+01	5.3	10.5	325.2	265.3
111440	20.	.162E+00	.356E+01	1.6	3.2	1024.1	846.1
111540	72.	.615E+00	.312E+01	13.2	26.3	118.4	99.8
112340	28.	.928E+00	.106E+01	35.4	63.9	44.2	36.7
112440	724.	.114E+01	.152E+01	95.7	100.0	9.7	8.1
112540	658.	.198E+01	.180E+01	99.5	100.0	5.9	5.9
113340	408.	.189E+01	.137E+01	99.4	100.0	7.1	5.9
113440	244.	.237E+01	.181E+01	95.8	100.0	9.6	8.1
113540	1116.	-.190E+01	.155E+01	100.0	100.0	4.8	4.0
111542	72.	-.113E+00	.161E+00	13.5	26.4	134.6	107.8
112542	56.	.771E-01	.203E+00	22.2	42.7	70.6	58.9
113542	236.	.153E+00	.145E+00	84.2	99.9	12.2	10.2

TABLE H-4. SITE 1 STATISTICAL DATA SUMMARY (CONTINUED)

KEY	AXLES	MEAN	STD DEV	CONF(101)	CONF(281)	TOL(951)	TOL(981)
21001	322.	.169E+02	.800E+01	100.0	100.0	1.6	1.4
21001	488.	.262E+02	.645E+01	100.0	100.0	2.3	1.9
21001	988.	.118E+02	.501F+01	100.0	100.0	3.1	2.6
21001	1886.	.173E+02	.712E+01	100.0	100.0	1.9	1.6
21101	104.	.340E+02	.288E+01	100.0	100.0	1.6	1.4
21201	1410.	.102E+02	.249F+01	100.0	100.0	1.5	1.2
21301	1768.	.213E+02	.628E+01	100.0	100.0	1.4	1.2
21003	3282.	.175E+02	.922E+01	100.0	100.0	1.6	1.3
21003	488.	.262E+02	.666F+01	100.0	100.0	2.4	2.0
21003	988.	.119E+02	.595E+01	100.0	100.0	3.1	2.6
21003	1886.	.104E+02	.736E+01	100.0	100.0	1.8	1.5
21103	104.	.346E+02	.371E+01	100.0	100.0	2.1	1.7
21203	1410.	.105E+02	.305F+01	100.0	100.0	1.5	1.3
21303	1768.	.221E+02	.628E+01	100.0	100.0	1.3	1.1
21006	3282.	.191E+02	.449E+01	100.0	100.0	1.6	1.3
21006	488.	.276E+02	.706E+01	100.0	100.0	2.4	2.0
21006	988.	.133E+02	.661F+01	100.0	100.0	3.1	2.6
21006	1886.	.104E+02	.763E+01	100.0	100.0	1.9	1.6
21106	104.	.357E+02	.396F+01	100.0	100.0	2.2	1.8
21206	1410.	.110E+02	.301E+01	100.0	100.0	1.4	1.2
21306	1768.	.228E+02	.671F+01	100.0	100.0	1.4	1.2
21010	3282.	.166E+02	.763F+01	100.0	100.0	1.6	1.4
21010	488.	.255E+02	.635E+01	100.0	100.0	2.3	1.9
21010	988.	.117E+02	.575E+01	100.0	100.0	3.1	2.6
21110	104.	.329E+02	.701E+01	100.0	100.0	1.9	1.6
21210	1410.	.101E+02	.297F+01	100.0	100.0	1.8	1.5
21310	1768.	.209E+02	.269E+01	100.0	100.0	1.5	1.3
21015	3282.	.372E+00	.622F+01	100.0	100.0	1.4	1.2
21015	488.	.746E+01	.100E+02	16.9	33.0	92.1	77.3
21015	988.	.723E+01	.898E+01	92.0	99.9	11.2	9.4
21015	1886.	.273E+01	.935F+01	88.5	100.0	8.1	6.8
21115	104.	.938E+01	.795F+01	85.9	99.7	13.3	11.2
21215	1410.	.522E+01	.407E+02	62.6	92.3	22.2	18.6
21315	1768.	.552E+01	.840F+01	98.6	100.0	7.9	6.7
21016	3282.	.854E+01	.654E+01	97.5	100.0	8.4	7.4
21016	488.	.477E+01	.767E+01	100.0	100.0	5.5	4.6
21016	988.	.113E+02	.643F+01	100.0	100.0	5.3	4.4
21016	1886.	.355E+01	.679F+01	89.9	99.9	12.0	10.8
21016	1886.	.384E+01	.761E+01	97.0	100.0	9.0	7.6
21106	104.	.221E+02	.505F+01	100.0	100.0	4.4	3.7
21206	1410.	.146E+01	.506E+01	72.3	97.0	18.0	15.1
21306	1768.	.638E+01	.763E+01	100.0	100.0	5.6	4.7
21017	3282.	.210E+02	.561E+01	100.0	100.0	.9	.8
21017	488.	.144E+02	.819E+01	100.0	100.0	2.1	1.8
21017	988.	.252F+02	.660E+01	100.0	100.0	1.4	1.2
21017	1886.	.194E+02	.859E+01	100.0	100.0	1.1	.9
21107	104.	.207E+02	.559E+01	100.0	100.0	5.2	4.4
21207	1410.	.231E+02	.587E+01	100.0	100.0	1.3	1.1
21307	1768.	.193E+02	.876E+01	100.0	100.0	1.1	1.0
21014	3282.	.151E+02	.897E+01	100.0	100.0	2.0	1.7
21014	488.	.224E+02	.729F+01	100.0	100.0	3.0	2.5
21014	988.	.110E+02	.761E+01	100.0	100.0	4.1	3.4
21014	1886.	.150E+02	.891E+01	100.0	100.0	2.7	2.3
21104	104.	.342E+02	.641E+01	100.0	100.0	3.9	3.3
21204	1410.	.913E+01	.593F+01	100.0	100.0	3.4	2.8

TABLE R-4. SITE 1 STATISTICAL DATA SUMMARY (CONTINUED)

KEY	AXLES	MEAN	STD DEV	CONF (10%)	CONF (20%)	TOL (95%)	TOL (90%)
213018	1768	.187E+02	.747E+01	100.0	100.0	1.9	1.6
210019	3282	.976E+00	.304E+01	93.4	100.0	10.7	9.0
210119	448	.256E+01	.453E+01	76.9	98.3	16.4	13.8
210419	988	.273E+01	.685E+00	57.0	88.5	24.9	20.9
210519	1846	.746E+00	.260E+01	78.2	98.6	15.9	13.4
211019	104	.119E+01	.408E+01	23.3	44.6	66.8	55.9
212019	1410	.649E+00	.234E+01	70.3	96.2	18.9	15.8
213019	1768	.122E+01	.341E+01	86.8	99.7	13.0	10.9
210020	3282	.151E+02	.758E+01	100.0	100.0	1.7	1.4
210320	448	.241E+02	.666E+01	100.0	100.0	2.6	2.1
210420	988	.104E+02	.579E+01	100.0	100.0	3.5	2.9
210520	1846	.154E+02	.646E+01	100.0	100.0	1.9	1.6
211020	104	.293E+02	.398E+01	100.0	100.0	2.6	2.2
212020	1410	.872E+01	.276E+01	100.0	100.0	1.7	1.4
213020	1768	.194E+02	.607E+01	100.0	100.0	1.5	1.2
210021	3282	.627E+01	.430E+01	100.0	100.0	2.3	2.0
210321	448	.100E+02	.345E+01	100.0	100.0	3.2	2.7
210421	988	.804E+01	.335E+01	100.0	100.0	5.2	4.3
210521	1846	.656E+01	.423E+01	100.0	100.0	2.9	2.5
211021	104	.151E+02	.285E+01	100.0	100.0	3.7	3.1
212021	1410	.304E+01	.204E+01	100.0	100.0	3.5	2.9
213021	1768	.833E+01	.366E+01	100.0	100.0	2.1	1.7
210022	3282	-.973E+00	.471E+01	76.3	98.2	16.6	13.9
210322	448	-.574E+01	.881E+01	98.8	7.8	10.0	6.5
210422	988	-.762E+00	.420E+01	43.1	74.6	34.4	28.9
210522	1846	.709E+01	.422E+01	5.8	11.5	271.9	228.0
211022	104	-.115E+01	.536E+01	17.3	33.9	90.3	75.6
212022	1410	.940E+01	.384E+01	7.3	14.6	213.3	178.9
213022	1768	-.181E+01	.511E+01	86.4	99.7	11.0	9.2
210023	2642	.365E+01	.348E+01	100.0	100.0	3.6	3.0
210323	448	.839E+01	.238E+01	79.3	98.6	15.7	13.1
210423	988	.214E+01	.307E+01	97.1	100.0	9.0	7.5
210523	1846	.662E+01	.340E+01	100.0	100.0	3.6	3.0
211023	104	.112E+02	.373E+01	99.4	100.0	7.1	5.9
212023	1410	.137E+01	.130E+01	100.0	100.0	5.3	4.4
213023	1768	.540E+01	.317E+01	100.0	100.0	3.2	2.7
210024	2642	-.776E+00	.347E+01	74.9	97.8	17.1	14.3
210324	448	-.850E+00	.203E+01	22.7	43.5	69.5	58.0
210424	988	-.929E+00	.240E+01	77.5	98.5	16.2	13.6
210524	1846	-.681E+00	.402E+01	50.2	82.5	28.9	24.3
211024	104	-.443E+00	.488E+01	6.8	13.5	233.4	195.2
212024	1410	-.522E+00	.299E+01	46.2	78.1	31.9	26.8
213024	1768	-.104E+01	.375E+01	68.4	95.5	19.6	16.4
210025	3282	.781E+01	.398E+01	100.0	100.0	1.7	1.5
210325	448	.111E+02	.325E+01	100.0	100.0	2.7	2.3
210425	988	.584E+01	.279E+01	100.0	100.0	3.1	2.6
210525	1846	.819E+01	.399E+01	100.0	100.0	2.2	1.9
211025	104	.163E+02	.218E+01	100.0	100.0	2.6	2.2
212025	1410	.456E+01	.151E+01	100.0	100.0	1.7	1.5
213025	1768	.980E+01	.320E+01	100.0	100.0	1.5	1.3
210026	3282	.488E+01	.309E+01	100.0	100.0	2.2	1.8
210326	448	.344E+01	.252E+01	99.6	100.0	6.8	5.7
210426	988	.395E+01	.162E+01	100.0	100.0	2.6	2.1
210526	1846	.573E+01	.351E+01	100.0	100.0	2.8	2.4
211026	104	.762E+01	.614E+01	79.2	98.7	15.7	13.1

TABLE E-4. SITE 1 STATISTICAL DATA SUMMARY (CONTINUED)

KEY	AXLES	MEAN	STD. DEV.	CNF(10t)	CNF(20t)	TOL(95t)	TOL(90t)
210206	1410.	.430E+01	.243E+01	100.0	100.0	3.0	2.5
21026	1768.	.518E+01	.315E+01	100.0	100.0	2.0	2.4
210027	241A.	-.645E+01	.930E+01	100.0	100.0	4.4	3.7
210327	44A.	-.155E+02	.76AF+01	100.0	100.0	4.0	4.0
210427	58A.	-.816E+01	.110E+02	92.0	100.0	10.9	9.2
210527	139Z.	-.624E+01	.76AF+01	99.9	100.0	6.4	5.4
211027	72.	-.110E+02	.118E+02	57.0	45.3	15.1	21.0
212027	A3A.	-.434E+01	.663E+01	64.8	99.6	23.7	11.5
213027	151Z.	-.106E+02	.464E+01	100.0	100.0	4.1	3.5
21002A	2370.	-.666E+01	.707E+01	100.0	100.0	4.3	3.6
21032A	44A.	-.967E+01	.320E+01	100.0	100.0	3.1	2.6
21042A	59A.	-.524E+00	.766E+01	13.3	26.2	117.5	98.6
21052A	133A.	-.635E+01	.604E+01	100.0	100.0	3.9	3.3
21102A	A0.	-.732E+01	.655E+01	6A.C	95.1	19.9	16.6
21202A	926.	-.420E+01	.835E+01	85.2	99.6	13.5	11.4
21302A	136A.	-.924E+01	.206E+01	100.0	100.0	2.4	2.4
210029	324Z.	-.253E+01	.206E+01	100.0	100.0	3.2	2.6
210329	44A.	.457E+01	.155E+01	100.0	100.0	2.8	2.6
210429	98A.	-.204E+01	.162E+01	100.0	100.0	4.9	4.2
210529	1746.	-.229E+01	.212E+01	100.0	100.0	4.2	3.6
211029	104.	.618E+01	.227E+01	93.0	100.0	10.6	8.9
212029	1410.	.153E+01	.157E+01	100.0	100.0	5.3	4.5
213029	176A.	.322E+01	.208E+01	100.0	100.0	3.0	2.5
210030	324Z.	.561E+01	.653E+01	100.0	100.0	4.0	3.3
210130	44A.	.954E+01	.592E+01	99.9	100.0	5.8	4.8
210430	98A.	.444E+00	.738E+01	16.5	32.2	94.4	79.2
210530	1846.	.740E+01	.415E+01	100.0	100.0	2.6	2.1
211030	104.	.110E+02	.865E+01	A0.0	98.9	15.3	12.4
212030	1410.	.233E+01	.614E+01	84.6	99.6	13.8	11.5
213030	176A.	.791E+01	.540E+01	100.0	100.0	3.2	2.7
210031	269A.	.171E+02	.561E+01	100.0	100.0	1.2	1.0
210331	44A.	.153E+02	.444E+01	100.0	100.0	2.7	2.2
210431	98A.	.207E+02	.495E+01	100.0	100.0	2.1	1.8
210531	1458.	.152E+02	.320E+01	100.0	100.0	1.1	.9
211031	A4.	.174E+02	.616E+01	99.1	100.0	7.4	6.2
212031	122Z.	.1A9E+02	.623E+01	100.0	100.0	1.0	1.5
213031	158A.	.157E+02	.455E+01	100.0	100.0	1.4	1.2
210032	3206.	.314E+02	.905E+01	100.0	100.0	1.0	.8
210332	44A.	.412E+02	.626E+01	100.0	100.0	1.4	1.2
210432	98A.	.296E+02	.474E+01	100.0	100.0	1.0	1.5
210532	1770.	.298E+02	.821E+01	100.0	100.0	1.3	1.1
211032	130.	.464E+02	.613E+01	100.0	100.0	2.6	2.2
212032	139A.	.249E+02	.619E+01	100.0	100.0	1.3	1.1
213032	171Z.	.357E+02	.733E+01	100.0	100.0	1.0	.8
210033	328Z.	-.945E+01	.473E+01	100.0	100.0	1.9	1.6
210333	44A.	-.150E+02	.345E+01	100.0	100.0	2.4	2.0
210433	98A.	-.573E+01	.347E+01	100.0	100.0	4.2	3.5
210533	1446.	-.832E+01	.373E+01	100.0	100.0	2.0	1.7
211033	104.	-.155E+02	.241E+01	100.0	100.0	3.0	2.5
212033	1410.	-.453E+01	.229E+01	100.0	100.0	2.6	2.2
213033	176A.	-.112E+02	.341E+01	100.0	100.0	1.0	1.3
210034	324Z.	.426E+01	.644E+01	99.6	100.0	6.8	5.7
210334	44A.	-.249E+01	.474E+01	51.6	43.0	28.0	23.5
210434	98A.	.975E+01	.491E+01	99.9	100.0	5.7	4.8
210534	1746.	.386E+01	.618E+01	96.9	100.0	9.1	7.6

TABLE E-4. SITE 1 STATISTICAL DATA SUMMARY (CONTINUED)

KEY	AXLES	MEAN	STD DEV	GMF(100)	GMF(200)	TOL(95%)	TOL(100%)
211034	104	-.270E+01	.114F+02	19.6	38.1	79.5	66.6
212034	1410	.746E+01	.799F+01	120.0	100.0	5.4	4.5
213034	1760	.212E+01	.796F+01	73.8	97.5	17.5	14.7
213035	3282	.207E+02	.118F+02	100.0	100.0	1.9	1.6
210335	448	.347E+02	.161F+02	100.0	100.0	2.7	2.3
210435	998	.154E+02	.953F+01	100.0	100.0	3.9	3.2
210535	1846	.202E+02	.104E+02	100.0	100.0	2.4	2.0
211035	196	.435E+02	.509F+01	100.0	100.0	2.7	2.3
212035	1410	.117E+02	.512F+01	100.0	100.0	2.3	1.9
213035	1760	.266E+02	.102F+02	100.0	100.0	1.8	1.5
210036	3042	.875E+01	.476E+01	100.0	100.0	1.9	1.6
210036	448	.139E+02	.403E+01	100.0	100.0	2.7	2.3
210436	998	.581E+01	.366F+01	100.0	100.0	3.9	3.3
210536	1606	.912E+01	.415E+01	100.0	100.0	2.2	1.9
211036	96	.181E+02	.245E+01	100.0	100.0	2.7	2.3
212036	1262	.475E+01	.202E+01	100.0	100.0	2.3	2.0
213036	1688	.112E+02	.388F+01	100.0	100.0	1.6	1.4
210037	3042	-.121F+01	.435F+01	97.4	99.8	12.6	10.7
210337	448	-.165E+01	.396E+01	63.4	92.9	21.7	18.2
210437	998	.121E+02	.344E+01	.1	.2	17175.5	14410.0
210537	1606	-.187E+01	.444E+01	86.9	99.7	13.0	10.9
211037	96	.279E+01	.765E+01	27.8	52.3	55.6	46.5
212037	1262	-.590F+01	.393E+01	4.2	8.5	368.1	308.8
213037	1688	-.230E+01	.402E+01	98.1	100.0	8.6	7.0
210038	3282	.174E+02	.774E+01	100.0	100.0	1.5	1.3
210338	448	.264E+02	.556E+01	100.0	100.0	2.0	1.6
210438	998	.129F+02	.557F+01	100.0	100.0	2.7	2.3
210538	1846	.177E+02	.717F+01	100.0	100.0	1.8	1.6
211038	104	.296E+02	.159F+01	100.0	100.0	1.0	.9
212038	1410	.107E+02	.344F+01	100.0	100.0	1.7	1.4
213038	1768	.221F+02	.593F+01	100.0	100.0	1.3	1.0
210039	3282	-.367E+01	.881E+01	98.2	100.0	8.3	7.0
210339	448	-.123E+02	.933F+01	99.4	100.0	7.1	5.9
210439	998	-.601F+01	.600E+01	2.5	5.0	623.3	522.9
210539	1646	-.344E+01	.852F+01	91.7	99.9	11.3	9.5
211039	104	-.109E+02	.115E+02	66.5	94.4	20.5	17.1
212039	1410	.160E+01	.481E+01	78.8	98.7	15.7	13.2
213039	1768	-.736E+01	.888F+01	99.9	100.0	5.6	4.7
210040	3282	.173E+01	.172E+01	100.0	100.0	3.4	2.9
210340	448	.179E+01	.142E+01	99.2	100.0	7.4	6.2
210440	998	.143E+01	.175E+01	98.9	100.0	7.7	6.4
210540	1846	.189F+01	.175E+01	100.0	100.0	4.3	3.6
211040	104	.512E+00	.313E+01	13.2	26.0	119.1	99.6
212040	1410	.153E+01	.170E+01	99.9	100.0	5.8	4.9
213040	1768	.196E+01	.156E+01	100.0	100.0	3.7	3.1
210042	300	.131E+00	.166F+00	82.7	99.3	14.6	12.1
210342	236	.153E+00	.145E+00	89.2	99.9	12.2	10.2
210442	236	.153E+00	.145E+00	89.2	99.9	12.2	10.2
210542	300	.131E+00	.166E+00	82.7	99.3	14.4	12.1
211042	8	-.113E+00	.181F+00	13.5	26.4	134.6	107.8
212042	56	.771E+01	.203E+00	22.2	42.7	70.6	58.9
213042	236	.153E+00	.145E+00	89.2	99.9	12.2	10.2

TABLE B-5. SITE 2 STATISTICAL DATA SUMMARY

KEY	AXLES	MEAN	SID. DEV.	CONF(10.0)	CONF(21.1)	CONF(95.1)	CONF(99.1)
12131	24	304E+02	270E+01	100.0	100.0	3.7	3.1
121401	12	337E+02	261E+01	99.9	100.0	4.9	4.0
121501	28	314E+02	261E+01	100.0	100.0	3.2	2.7
122001	44	904E+01	209E+01	100.0	100.0	2.1	1.4
12201	44	973E+01	210E+01	100.0	100.0	2.0	1.7
12201	44	977E+01	210E+01	100.0	100.0	3.1	2.6
12301	44	233E+02	503E+01	100.0	100.0	2.3	1.9
123401	196	178E+02	306E+01	100.0	100.0	2.4	2.0
123501	212	255E+02	400E+01	100.0	100.0	4.7	3.9
121303	24	306E+02	244E+01	100.0	100.0	3.4	2.8
121403	12	316E+02	135E+01	100.0	100.0	2.7	2.2
121503	28	313E+02	244E+01	100.0	100.0	2.5	2.1
12203	44	917E+01	201E+01	100.0	100.0	2.0	1.7
12203	44	823E+01	186E+01	100.0	100.0	2.1	1.8
122503	44	988E+01	278E+01	100.0	100.0	2.8	2.3
121406	12	232E+02	604E+01	100.0	100.0	2.4	2.0
121506	28	300E+02	297E+01	100.0	100.0	3.7	3.1
12206	44	965E+01	197E+01	100.0	100.0	1.9	1.6
12206	44	853E+01	203E+01	100.0	100.0	2.2	1.9
12206	44	918E+01	313E+01	100.0	100.0	3.3	2.8
12306	44	239E+02	601E+01	100.0	100.0	2.3	2.0
12306	44	175E+02	320E+01	100.0	100.0	2.6	2.2
12306	212	229E+02	742E+01	100.0	100.0	4.4	3.7
121310	24	298E+02	229E+01	100.0	100.0	3.3	2.7
121410	12	317E+02	314E+01	99.5	100.0	6.3	5.1
121510	28	298E+02	237E+01	100.0	100.0	3.1	2.6
12210	44	888E+01	220E+01	100.0	100.0	2.3	1.9
12210	44	781E+01	202E+01	100.0	100.0	2.4	2.0
122510	44	914E+01	282E+01	100.0	100.0	3.0	2.5
12310	44	233E+02	566E+01	100.0	100.0	2.3	2.0
12310	196	170E+02	332E+01	100.0	100.0	2.8	2.3
12310	212	241E+02	850E+01	100.0	100.0	4.8	4.0
121315	16	213E+02	170E+01	100.0	100.0	4.3	3.5
121415	12	203E+02	165E+01	99.9	100.0	5.2	4.2
121515	24	211E+02	244E+01	100.0	100.0	4.9	4.0
12215	44	556E+01	184E+01	100.0	100.0	3.0	2.6
12215	44	456E+01	179E+01	100.0	100.0	3.7	3.1
122515	366	827E+01	266E+01	100.0	100.0	5.0	4.2
12315	144	113E+02	352E+01	100.0	100.0	5.1	4.3
12315	196	117E+02	276E+01	100.0	100.0	3.3	2.8
12315	36	119E+02	306E+01	100.0	100.0	5.2	4.4
121316	16	109E+01	878E+01	3.9	7.8	130.1	153.7
121416	12	147E+02	116E+02	33.0	60.0	50.3	41.0
121516	24	272E+01	215E+01	14.9	28.1	104.4	90.2
12216	44	443E+01	327E+01	93.6	100.0	6.8	5.7
12216	44	656E+01	825E+01	100.0	100.0	3.2	2.7
122516	396	644E+01	283E+01	100.0	100.0	4.8	4.0
12316	144	862E+01	687E+01	87.5	99.8	12.4	10.7
12316	196	942E+01	538E+01	98.9	100.0	7.7	6.5
123516	36	372E+01	558E+01	40.5	80.6	30.4	25.4
121317	16	270E+02	243E+01	100.0	100.0	4.6	3.9

TABLE H-5. SITE 2 STATISTICAL DATA SUMMARY (CONTINUED)

KEY	AXLES	MEAN	STD_DEV	CONF(10.0)	CONF(23.0)	CONF(95.0)	CONF(99.0)
121417	12.	.266E+02	.229E+01	99.8	100.0	100.0	5.5
121517	28.	.266E+02	.153E+01	100.0	100.0	100.0	1.7
122317	456.	.732E+01	.190E+01	100.0	100.0	100.0	2.4
122417	444.	.674E+01	.224E+01	100.0	100.0	100.0	3.2
122517	404.	.827E+01	.262E+01	100.0	100.0	100.0	3.1
123317	144.	.152E+02	.443E+01	100.0	100.0	100.0	4.8
123417	196.	.148E+02	.321E+01	100.0	100.0	100.0	2.6
123517	212.	.209E+02	.609E+01	100.0	100.0	100.0	3.3
121318	16.	-.139E+02	.906E+01	45.2	76.2	34.7	28.5
121418	12.	-.111E+02	.145E+02	20.4	39.3	83.1	47.8
121518	28.	-.108E+02	.965E+01	74.0	97.1	17.9	14.8
123318	456.	-.392E+01	.314E+01	99.1	100.0	100.0	6.1
123418	444.	-.465E+01	.301E+01	99.9	100.0	100.0	5.1
123518	404.	-.275E+01	.454E+01	77.2	98.4	16.3	13.7
123318	144.	-.978E+01	.590E+01	90.9	99.9	11.6	9.7
123418	196.	-.105E+02	.520E+01	98.2	100.0	8.3	7.0
123518	212.	-.141E+02	.877E+01	98.0	100.0	8.4	7.1
121319	24.	-.865E+01	.930E+00	100.0	100.0	100.0	4.8
121419	12.	-.883E+01	.120E+01	97.3	100.0	6.6	7.0
121519	28.	-.829E+01	.695E+00	100.0	100.0	3.3	2.7
123319	464.	-.323E+01	.782E+00	100.0	100.0	2.2	1.9
123419	444.	-.322E+01	.801E+00	100.0	100.0	2.3	1.9
123519	404.	-.392E+01	.111E+01	100.0	100.0	2.8	2.3
123320	448.	-.659E+01	.140E+01	103.0	100.0	2.0	1.6
123420	196.	-.697E+01	.926E+00	100.0	100.0	2.2	2.2
123520	212.	-.650E+01	.202E+01	100.0	100.0	4.2	3.5
121420	12.	-.539E+01	.930E+01	22.0	42.3	73.1	60.5
121520	28.	-.109E+02	.203E+01	91.0	98.7	11.8	9.7
123320	464.	-.319E+01	.679E+01	19.5	37.7	82.4	68.4
123420	444.	-.361E+01	.461E+01	80.8	98.8	11.6	8.8
123520	404.	-.242E+01	.385E+01	81.4	99.2	14.8	12.4
122521	404.	-.343E+01	.577E+01	78.4	98.6	15.9	13.3
123320	448.	-.976E+01	.634E+01	99.9	100.0	6.0	5.1
123420	196.	-.526E+01	.133E+01	100.0	100.0	3.6	3.0
123520	212.	-.545E+01	.917E+01	61.3	91.5	22.8	19.1
121321	24.	-.207E+02	.474E+01	95.7	100.0	8.7	8.0
121421	12.	.235E+02	.322E+01	97.2	100.0	6.7	7.1
121521	24.	.255E+02	.440E+01	99.1	100.0	7.3	6.0
123221	464.	.500E+01	.173E+01	100.0	100.0	2.6	2.2
123421	444.	.419E+01	.355E+01	98.7	100.0	7.9	6.6
123521	396.	.801E+01	.334E+01	100.0	100.0	4.1	3.5
123321	448.	.128E+02	.332E+01	103.0	100.0	2.4	2.0
123421	196.	.119E+02	.299E+01	103.0	100.0	3.5	3.0
123521	96.	.149E+02	.277E+01	100.0	100.0	3.8	3.2
121322	24.	-.143E+02	.943E+01	52.5	84.1	28.5	23.6
121422	12.	-.195E+02	.176E+01	99.7	100.0	5.7	4.7
121522	28.	-.122E+02	.390E+01	89.0	99.7	12.4	10.3
123322	464.	.736E+00	.694E+01	18.1	35.2	86.1	72.2
123422	444.	-.443E+01	.757E+01	78.2	98.6	15.9	13.4
123522	404.	-.265E+01	.983E+01	41.1	72.0	36.4	30.5
123322	448.	-.153E+02	.617E+01	100.0	100.0	3.8	3.2
123422	196.	-.123E+02	.314E+01	100.0	100.0	3.6	3.0
123522	212.	-.111E+02	.102E+02	88.3	99.8	12.5	10.5
121323	24.	-.276E+02	.661E+01	94.8	100.0	10.1	8.4
121423	12.	.228E+02	.363E+01	94.8	99.9	10.1	8.2

TABLE H-5. SITE 2 STATISTICAL DATA SUMMARY (CONTINUED)

KEY	AVLES	MEAN	STD DEV	CONF(10.0)	CONF(20.0)	TOL(95.0)	TOL(99.0)
121923	28.	.282E+02	.652E+01	97.0	100.0	9.0	7.4
121923	46.	.596E+01	.679E+01	106.0	106.0	6.4	7.4
122823	44.	.172E+01	.588E+01	48.1	78.7	37.3	31.3
122823	40.	.698E+01	.921E+01	72.2	92.0	18.1	15.2
123323	48.	.154E+02	.766E+01	100.0	100.0	4.6	3.9
123423	196.	.226E+01	.471E+01	96.4	100.0	9.1	7.7
123523	212.	.150E+02	.138E+02	88.5	99.8	12.4	10.4
123523	24.	.133E+01	.213E+01	21.8	43.9	73.9	61.2
121424	12.	.605E+01	.368E+01	46.9	77.7	34.1	27.8
121524	28.	.378E+01	.658E+01	33.4	61.0	42.0	39.0
122324	46.	.101E+01	.803E+00	93.6	100.0	6.8	5.7
122824	44.	.163E+01	.112E+01	93.8	100.0	6.4	5.4
122824	40.	.125E+01	.133E+01	94.0	100.0	10.4	8.7
123224	48.	.217E+01	.127E+01	100.0	100.0	5.4	4.6
123424	196.	.320E+01	.158E+01	99.5	100.0	7.0	5.8
123524	212.	.625E+01	.309E+01	95.4	100.0	9.8	8.2
121425	24.	.163E+02	.741E+01	76.1	97.6	17.1	14.2
121525	12.	.127E+02	.229E+01	85.6	99.1	14.0	11.4
121525	28.	.191E+02	.283E+01	99.9	100.0	5.8	4.8
122325	46.	.145E+02	.376E+01	100.0	100.0	2.4	2.0
122825	44.	.105E+02	.251E+01	100.0	100.0	1.9	1.9
122825	40.	.134E+02	.695E+01	100.0	100.0	3.6	3.0
123325	48.	.133E+02	.258E+01	100.0	100.0	1.8	1.5
123425	196.	.122E+02	.504E+01	98.9	100.0	5.8	4.9
123525	212.	.173E+02	.373E+01	100.0	100.0	4.5	3.8
121426	4.	.261E+02	.205E+01	91.5	98.5	12.5	9.3
121526	8.	.117E+02	.984E+01	25.4	47.8	70.1	56.2
121826	8.	.159E+02	.127E+02	26.6	48.8	66.8	53.5
122826	88.	.929E+01	.165E+01	100.0	100.0	3.8	3.2
122826	392.	.254E+01	.244E+01	94.0	100.0	9.5	8.0
123326	20.	.724E+01	.604E+01	40.2	70.3	39.0	32.2
123326	104.	.156E+02	.653E+01	99.9	100.0	5.6	4.7
123826	144.	.126E+02	.697E+01	90.8	100.0	9.1	7.6
123926	156.	.800E+01	.625E+01	68.0	95.2	19.8	16.6
121427	8.	.150E+01	.397E+01	9.2	16.3	221.2	177.2
121427	12.	.308E+01	.300E+01	26.4	49.7	63.5	51.4
121527	28.	.540E+01	.164E+00	18.2	35.3	89.9	74.3
122827	268.	.108E+03	.341E+01	100.0	100.0	3.8	3.2
122827	44.	.105E+00	.441E+01	100.0	100.0	3.9	3.3
122827	200.	.112E+00	.408E+01	100.0	100.0	4.3	3.6
123327	132.	.668E+01	.663E+01	75.2	97.8	17.0	14.3
123427	188.	.217E+01	.341E+01	62.7	92.4	22.1	18.5
123527	204.	.297E+01	.743E+01	43.1	74.5	34.5	28.9
121428	24.	.125E+01	.248E+00	97.9	100.0	6.4	5.9
121828	12.	.153E+01	.169E+00	99.1	100.0	7.8	5.7
121828	28.	.148E+01	.329E+00	97.5	100.0	8.6	7.2
122828	46.	.609E+00	.153E+00	100.0	100.0	3.4	2.9
122828	40.	.352E+00	.183E+00	100.0	100.0	4.9	4.1
122828	40.	.536E+00	.249E+00	100.0	100.0	4.5	3.8
123328	48.	.112E+01	.258E+00	100.0	100.0	2.1	1.8
123828	196.	.692E+00	.197E+00	100.0	100.0	3.1	2.6
123928	212.	.134E+01	.181E+00	100.0	100.0	4.2	3.5
121429	24.	.125E+02	.135E+01	103.0	100.0	4.6	3.8
121429	12.	.126E+02	.136E+01	99.2	100.0	6.9	5.6
121529	28.	.132E+02	.152E+01	100.0	100.0	4.5	3.7

TABLE B-5. SITE 2 GEOMETRICAL MEAN QUANTILES (CONTINUED)

KEY	ANLES	MEAN	STD DEV	CONF(49.1)	CONF(83.1)	CONF(95.1)	CONF(99.1)
122329	464.	.303E+01	.103E+01	100.0	100.0	2.4	2.0
122429	444.	.350E+01	.904E+00	100.0	100.0	2.4	2.0
122529	484.	.411E+01	.102E+01	100.0	100.0	2.4	2.0
123229	448.	.971E+01	.263E+01	100.0	100.0	2.5	2.1
123429	196.	.650E+01	.129E+01	100.0	100.0	2.6	2.3
123529	212.	.902E+01	.336E+01	100.0	100.0	2.6	2.2
121330	24.	.573E+01	.45E+01	45.2	76.5	33.9	28.1
121430	12.	.650E+00	.504E+01	3.5	7.8	492.7	462.8
121530	28.	.111E+02	.635E+01	64.7	93.1	21.7	18.8
122330	464.	.314E+00	.164E+01	76.9	98.3	16.4	13.7
122430	444.	.200E+01	.224E+01	94.0	100.0	10.4	8.7
122530	484.	.397E+01	.229E+01	99.8	100.0	5.6	4.7
123330	448.	.627E+01	.428E+01	99.8	100.0	6.3	5.3
123430	196.	.163E+01	.224E+01	68.9	95.6	19.4	16.3
123530	212.	.495E+01	.650E+01	72.1	96.9	18.2	15.2
121331	24.	.796E+01	.974E+00	99.9	100.0	5.2	4.3
121431	12.	.334E+01	.107E+01	97.9	100.0	8.2	6.7
121531	28.	.817E+01	.762E+00	100.0	100.0	3.6	3.0
122331	464.	.164E+01	.711E+00	100.0	100.0	4.0	3.3
122431	444.	.112E+01	.823E+00	99.6	100.0	6.9	5.8
122531	484.	.189E+01	.109E+01	99.9	100.0	5.7	4.8
123331	448.	.604E+01	.210E+01	100.0	100.0	3.2	2.7
123431	196.	.350E+01	.112E+01	100.0	100.0	4.5	3.8
123531	212.	.598E+01	.320E+01	98.8	100.0	6.8	5.5
121332	24.	.505E+01	.325E+01	61.3	90.9	23.5	19.4
121432	12.	.645E+01	.326E+01	43.3	60.2	32.1	26.2
121532	28.	.409E+01	.249E+01	60.7	90.6	23.6	19.6
122332	464.	.257E+01	.108E+01	100.0	100.0	3.9	3.2
122432	444.	.263E+01	.141E+01	100.0	100.0	5.0	4.2
122532	484.	.277E+01	.178E+01	99.8	100.0	6.3	5.3
123332	448.	.420E+01	.185E+01	100.0	100.0	4.1	3.4
123432	196.	.298E+01	.164E+01	98.6	100.0	7.9	6.6
123532	212.	.503E+01	.358E+01	95.1	100.0	9.5	8.0
121333	24.	.131E+02	.131E+01	100.0	100.0	4.2	3.5
121433	12.	.134E+02	.125E+01	99.6	100.0	6.0	4.9
121533	28.	.137E+02	.141E+01	100.0	100.0	4.0	3.3
122333	464.	.324E+01	.105E+01	100.0	100.0	3.0	2.5
122433	444.	.331E+01	.974E+00	100.0	100.0	2.7	2.3
122533	484.	.349E+01	.180E+01	100.0	100.0	5.3	4.4
123333	448.	.103E+02	.294E+01	100.0	100.0	2.7	2.2
123433	196.	.670E+01	.147E+01	100.0	100.0	3.1	2.6
123533	212.	.954E+01	.398E+01	99.9	100.0	5.6	4.7
121334	24.	.625E+01	.461E+01	59.1	89.4	24.6	20.4
121434	12.	.740E+01	.372E+01	49.5	80.5	31.9	26.0
121534	28.	.696E+01	.424E+01	63.4	90.4	23.8	19.8
122334	464.	.345E+01	.134E+01	100.0	100.0	3.5	3.0
122434	444.	.344E+01	.124E+01	100.0	100.0	3.3	2.8
122534	484.	.259E+01	.280E+01	93.6	100.0	10.6	8.8
123334	448.	.742E+01	.329E+01	100.0	100.0	4.1	3.5
123434	196.	.437E+01	.249E+01	98.5	100.0	8.0	6.7
123534	212.	.635E+01	.427E+01	96.6	100.0	9.1	7.6
121335	24.	.157E+02	.669E+01	73.7	96.8	18.0	14.9
121435	12.	.965E+01	.167E+01	92.9	99.8	11.0	9.0
121535	28.	.165E+02	.387E+01	96.8	100.0	9.1	7.5
122335	464.	.155E+02	.346E+01	103.0	100.0	2.0	1.7

TABLE B-3. SITE 2 STATISTICAL DATA SUMMARY (CONTINUED)

KEY	AWLES	MEAN	SID DEV	COMET(2011)	COMET(2011)	COMET(2011)	COMET(2011)
122435	448.	.962E+01	.324E+01	100.0	100.0	3.1	2.6
122436	408.	.135E+02	.337E+01	100.0	100.0	2.4	2.8
122335	448.	.826E+01	.565E+01	99.8	100.0	6.4	5.3
123435	196.	.103E+02	.110E+01	103.0	100.0	1.6	1.4
123535	212.	.186E+02	.653E+01	103.0	100.0	4.2	3.5
121336	288.	.290E+02	.352E+01	98.9	100.0	5.2	4.3
121436	12.	.287E+02	.391E+01	97.3	100.0	8.7	7.1
121536	28.	.312E+02	.295E+01	103.0	100.0	3.7	3.0
122336	468.	.116E+02	.298E+01	100.0	100.0	2.3	2.0
122436	448.	.982E+01	.230E+01	100.0	100.0	2.2	1.8
122536	408.	.119E+02	.271E+01	100.0	100.0	2.2	1.9
123336	448.	.230E+02	.567E+01	100.0	100.0	2.3	1.9
123436	196.	.168E+02	.332E+01	100.0	100.0	2.8	2.3
123536	212.	.285E+02	.866E+01	100.0	100.0	5.0	4.2
121337	288.	-.239E+01	.190E+01	45.6	76.9	33.6	27.8
121437	12.	-.525E+00	.257E+01	5.5	11.0	310.9	253.7
121537	28.	-.219E+01	.208E+01	41.6	72.3	37.0	30.7
122337	468.	.521E+00	.786E+00	85.1	98.6	13.6	11.4
122437	448.	-.451E+00	.922E+00	69.7	96.0	19.1	16.0
122537	408.	-.718E+00	.129E+01	73.4	97.4	17.6	14.8
123337	448.	-.216E+01	.130E+01	100.0	100.0	5.6	4.7
123437	196.	-.431E+00	.155E+01	36.5	65.7	41.5	34.4
123537	212.	-.158E+01	.164E+01	84.0	99.5	14.0	11.7
121338	288.	.329E+02	.420E+01	98.9	100.0	5.4	4.5
121438	12.	.332E+02	.277E+01	99.8	100.0	5.3	4.3
121538	28.	.302E+02	.232E+01	100.0	100.0	3.0	2.5
122338	468.	.103E+02	.234E+01	100.0	100.0	2.1	1.7
122438	448.	.835E+01	.274E+01	100.0	100.0	3.1	2.6
122538	408.	.912E+01	.309E+01	100.0	100.0	3.3	2.8
123338	448.	.252E+02	.637E+01	103.0	100.0	2.3	2.0
123438	196.	.189E+02	.374E+01	100.0	100.0	2.8	2.3
123538	212.	.235E+02	.762E+01	100.0	100.0	4.4	3.7
121439	12.	-.165E+01	.113E+02	5.7	11.3	288.1	238.7
121539	28.	-.893E+01	.943E+00	99.3	100.0	6.7	5.5
121539	28.	.356E+00	.701E+01	2.3	4.6	704.4	584.7
122339	468.	.359E+01	.582E+01	80.7	98.1	15.1	12.6
122439	448.	.299E+01	.487E+01	80.2	99.0	15.2	12.8
122539	408.	.229E+01	.845E+01	41.4	72.4	36.1	30.3
123339	448.	-.758E+01	.593E+01	99.3	100.0	7.3	6.1
123439	196.	-.394E+01	.321E+01	91.3	99.9	11.5	9.6
123539	212.	-.439E+01	.881E+01	53.1	85.2	27.2	22.8
121340	288.	.185E+02	.317E+01	98.1	100.0	7.2	6.0
121440	12.	.149E+02	.160E+01	99.2	100.0	6.8	5.6
121540	28.	.182E+02	.331E+01	97.9	100.0	8.3	6.9
122340	468.	.417E+01	.370E+01	98.4	100.0	8.1	6.8
122440	448.	.318E+01	.354E+01	94.1	100.0	10.4	8.7
122540	408.	.406E+01	.497E+01	89.9	99.9	12.0	10.0
123340	448.	.115E+02	.459E+01	100.0	100.0	3.7	3.1
123440	196.	.633E+01	.294E+01	99.7	100.0	6.5	5.5
123540	212.	.108E+02	.628E+01	98.7	100.0	7.9	6.6
121341	288.	.155E+03	0.	100.0	100.0	0.0	0.0
121441	12.	.155E+03	0.	100.0	100.0	0.0	0.0
121541	28.	.155E+03	0.	100.0	100.0	0.0	0.0
122341	468.	.155E+03	0.	100.0	100.0	0.0	0.0
122441	448.	.155E+03	0.	100.0	100.0	0.0	0.0

TABLE B-5. SITE 2 STATISTICAL DATA SUMMARY (CONTINUED)

KEY	APLES	MEAN	STD_DEV	CONF(10)	CONF(20)	CONF(90)
122541	406.	.155E+03	0.	100.0	100.0	101.0
123341	448.	.155E+03	0.	100.0	100.0	101.0
123441	196.	.155E+03	0.	100.0	100.0	100.0
123541	212.	.155E+03	0.	100.0	100.0	100.0
121342	24.	.155E+03	0.	100.0	100.0	100.0
121442	12.	.155E+03	0.	100.0	100.0	100.0
121542	28.	.155E+03	0.	100.0	100.0	100.0
123342	464.	.155E+03	0.	100.0	100.0	100.0
122442	444.	.155E+03	0.	100.0	100.0	100.0
122542	406.	.155E+03	0.	100.0	100.0	100.0
123342	448.	.155E+03	0.	100.0	100.0	100.0
123442	196.	.155E+03	0.	100.0	100.0	100.0
123542	212.	.155E+03	0.	100.0	100.0	100.0

TABLE 3. STATE STATISTICAL DATA SUMMARY (CONTINUED)

YEAR	MAKES	MEAS	STD_DEV	CONFIDENCE	CONFIDENCE	TOTALS	CONFIDENCE
220700	2782	.157E+02	.032E+01	100.0	100.0	2.3	1.9
220701	976	.164E+02	.057E+01	100.0	100.0	3.3	2.8
220702	552	.126E+02	.052E+01	100.0	100.0	3.2	2.7
220703	644	.168E+02	.075E+01	100.0	100.0	4.7	3.9
220704	64	.031E+02	.028E+01	100.0	100.0	2.3	1.9
220705	1312	.056E+02	.025E+01	100.0	100.0	1.4	1.2
220706	856	.026E+02	.063E+01	100.0	100.0	2.0	1.7
220707	232	.144E+02	.079E+01	100.0	100.0	2.3	1.8
220708	936	.164E+02	.053E+01	100.0	100.0	3.3	2.8
220709	652	.110E+02	.050E+01	100.0	100.0	3.5	3.0
220710	644	.150E+02	.021E+01	100.0	100.0	4.2	3.6
220711	154	.031E+02	.021E+01	100.0	100.0	1.7	1.4
220712	1312	.097E+02	.233E+01	100.0	100.0	1.4	1.2
220713	856	.214E+02	.641E+01	100.0	100.0	2.0	1.7
220714	232	.147E+02	.613E+01	100.0	100.0	2.3	1.9
220715	336	.170E+02	.051E+01	100.0	100.0	3.2	2.7
220716	652	.115E+02	.050E+01	100.0	100.0	3.6	3.0
220717	644	.146E+02	.072E+01	100.0	100.0	4.6	3.9
220718	64	.030E+02	.255E+01	100.0	100.0	2.1	1.8
220719	1312	.091E+02	.245E+01	100.0	100.0	1.5	1.2
220720	856	.222E+02	.644E+01	100.0	100.0	2.0	1.6
220721	232	.144E+02	.041E+01	100.0	100.0	2.4	2.0
220722	336	.163E+02	.063E+01	100.0	100.0	3.4	2.8
220723	652	.118E+02	.066E+01	100.0	100.0	3.9	3.3
220724	64	.030E+02	.255E+01	100.0	100.0	2.1	1.8
220725	1312	.091E+02	.245E+01	100.0	100.0	1.5	1.2
220726	856	.222E+02	.644E+01	100.0	100.0	2.0	1.6
220727	232	.144E+02	.041E+01	100.0	100.0	2.4	2.0
220728	336	.163E+02	.063E+01	100.0	100.0	3.4	2.8
220729	652	.118E+02	.066E+01	100.0	100.0	3.9	3.3
220730	64	.030E+02	.255E+01	100.0	100.0	2.1	1.8
220731	1312	.091E+02	.245E+01	100.0	100.0	1.5	1.2
220732	856	.222E+02	.644E+01	100.0	100.0	2.0	1.6
220733	1784	.071E+02	.439E+01	100.0	100.0	2.8	2.4
220734	616	.230E+02	.466E+01	100.0	100.0	4.4	3.7
220735	652	.070E+02	.429E+01	100.0	100.0	4.7	3.9
220736	316	.725E+01	.484E+01	99.9	100.0	5.8	4.8
220737	52	.210E+02	.211E+01	100.0	100.0	2.6	2.3
220738	1296	.051E+02	.215E+01	100.0	100.0	2.3	1.9
220739	436	.116E+02	.311E+01	100.0	100.0	2.5	2.1
220740	1784	.620E+01	.456E+01	100.0	100.0	3.4	2.9
220741	616	.037E+02	.499E+01	99.2	100.0	7.3	6.2
220742	652	.076E+02	.421E+01	100.0	100.0	4.2	3.5
220743	516	.033E+02	.391E+01	99.8	100.0	6.4	5.4
220744	1296	.050E+02	.103E+02	27.1	51.1	57.6	48.1
220745	436	.059E+02	.296E+01	100.0	100.0	2.9	2.4
220746	616	.081E+02	.642E+01	93.2	100.0	7.4	6.2
220747	1912	.109E+02	.642E+01	100.0	100.0	2.7	2.2
220748	616	.096E+02	.514E+01	100.0	100.0	4.2	3.5
220749	652	.092E+02	.505E+01	100.0	100.0	4.1	3.4
220750	644	.133E+02	.787E+01	100.0	100.0	4.6	3.8
220751	56	.277E+02	.219E+01	100.0	100.0	2.1	1.8
220752	1304	.074E+02	.235E+01	100.0	100.0	1.7	1.4
220753	552	.172E+02	.562E+01	103.0	100.0	2.7	2.3
220754	1912	.064E+02	.671E+01	100.0	100.0	4.7	3.9
220755	616	.055E+02	.536E+01	99.0	100.0	7.6	6.4
220756	652	.065E+02	.540E+01	99.8	100.0	6.4	5.3
220757	644	.071E+02	.699E+01	96.3	100.0	9.4	7.9
220758	56	.158E+02	.108E+02	72.1	98.7	18.3	15.3
220759	1304	.038E+02	.370E+01	100.0	100.0	5.3	4.4

TABLE B-5. SITE 2 STATISTICAL DATA SUMMARY (CONTINUED)

KEY	VALUES	MEAN	STD DEV	CONF(90%)	CONF(95%)	CONF(99%)	FOUR SIG
223018	552.	-.117E+02	.769E+01	100.0	100.0	100.0	5.5
223019	2232.	-.464E+01	-.195E+01	100.0	100.0	100.0	1.7
223031	936.	-.498E+01	.209E+01	100.0	100.0	100.0	2.7
226419	652.	-.385E+01	.135E+01	100.0	100.0	100.0	2.7
220519	644.	-.496E+01	.202E+01	100.0	100.0	100.0	3.2
221019	644.	-.835E+01	.945E+00	100.0	100.0	100.0	2.1
223019	1312.	-.344E+01	.960E+00	100.0	100.0	100.0	1.5
223019	856.	-.623E+01	.164E+01	100.0	100.0	100.0	1.5
223020	2232.	-.220E+01	.757E+01	83.1	99.4	14.2	12.0
220320	936.	-.302E+01	.870E+01	71.2	96.6	18.8	15.8
220420	652.	-.343E+01	.366E+01	92.3	100.0	8.2	6.9
226520	644.	-.218E+00	-.817E+01	5.4	10.4	289.8	243.1
221020	64.	-.546E+01	.782E+01	42.1	73.1	35.8	29.9
222020	1312.	-.151E+01	.548E+01	68.3	95.5	19.6	16.4
223020	856.	-.766E+01	.685E+01	99.9	100.0	6.0	5.0
220021	2104.	-.889E+01	.527E+01	100.0	100.0	2.5	2.1
220321	936.	.962E+01	.466E+01	100.0	100.0	3.1	2.6
220421	652.	.687E+01	.540E+01	99.9	100.0	6.8	5.1
220521	516.	.101E+02	.543E+01	100.0	100.0	4.7	3.9
221021	60.	-.232E+02	.684E+01	100.0	100.0	5.4	4.5
222021	1304.	.599E+01	.333E+01	100.0	100.0	3.0	2.5
223021	740.	.128E+02	.327E+01	100.0	100.0	1.8	1.5
220022	2232.	-.676E+01	.971E+01	99.9	100.0	6.0	5.0
220322	936.	-.719E+01	.103E+02	96.2	100.0	0.2	7.7
220422	652.	-.708E+01	.761E+01	98.2	100.0	8.3	6.9
220522	644.	-.581E+01	.106E+02	83.5	99.4	14.1	11.8
221022	64.	-.142E+02	.591E+01	89.6	99.8	12.1	10.1
222022	1312.	-.205E+01	.842E+01	62.3	92.3	22.2	18.6
223022	856.	-.134E+02	.718E+01	100.0	100.0	3.6	3.0
220023	2232.	-.829E+01	.100E+02	100.0	100.0	5.1	4.2
220423	652.	.105E+02	.865E+01	100.0	100.0	5.3	4.4
220523	644.	.377E+01	.723E+01	81.7	99.2	14.7	12.4
221023	644.	.929E+01	.125E+02	94.1	100.0	10.4	8.7
222023	1312.	.270E+02	.545E+01	99.9	100.0	6.0	5.0
223023	856.	.387E+01	.725E+01	94.6	100.0	10.2	8.5
220024	2232.	-.134E+02	.971E+01	100.0	100.0	6.8	6.1
220424	652.	.200E+01	.191E+01	100.0	100.0	4.0	3.3
220524	644.	.161E+01	.124E+01	100.0	100.0	4.8	4.1
221024	64.	.220E+01	.167E+01	99.9	100.0	5.8	4.9
222024	1312.	.235E+01	.268E+01	97.3	100.0	8.8	7.4
223024	856.	.343E+01	.420E+01	48.5	61.5	30.5	25.5
220025	2232.	.132E+01	.112E+01	100.0	100.0	4.6	3.8
220425	652.	.292E+01	.213E+01	100.0	100.0	4.9	4.1
220525	644.	.140E+02	.449E+01	100.0	100.0	1.4	1.2
221025	64.	.115E+02	.352E+01	100.0	100.0	1.6	1.3
222025	1312.	.149E+02	.356E+01	100.0	100.0	2.5	2.1
223025	856.	.176E+02	.555E+01	100.0	100.0	2.9	2.4
220026	2232.	.128E+02	.418E+01	100.0	100.0	7.0	6.6
220426	652.	.141E+02	.661E+01	100.0	100.0	1.8	1.5
220526	644.	.704E+01	.690E+01	99.8	100.0	6.3	5.3
221026	196.	.130E+02	.505E+01	100.0	100.0	5.5	4.6
222026	544.	.534E+01	.623E+01	95.4	100.0	9.8	8.2
223026	184.	.571E+01	.701E+01	72.9	97.2	17.0	15.0
221026	20.	.162E+02	.115E+02	46.7	78.0	33.0	27.3

TABLE B-5. SITE 2 STATISTICAL DATA SUMMARY (CONTINUED)

KEY	AKLES	MEAN	STD DEV	CONF(10.0)	CONF(20.0)	CONF(95.0)	TOL(10.0)
222026	500.	.392E+01	.369E+01	98.2	100.0	100.0	6.9
223026	404.	.104E+02	.760E+01	99.4	100.0	100.0	7.1
220027	1564.	.795E-01	.610E-01	100.0	100.0	100.0	3.2
220327	408.	.865E-01	.490E-01	100.0	100.0	100.0	5.5
220427	652.	.773E-01	.578E-01	99.9	100.0	100.0	4.8
220527	604.	.265E-01	.211E-01	98.2	100.0	100.0	6.9
220027	46.	.210E-01	.954E-01	12.3	24.2	130.1	100.4
222027	932.	.108E+00	.808E-01	100.0	100.0	100.0	2.0
223027	532.	.310E-01	.563E-01	73.5	98.9	15.0	13.0
220028	2232.	.723E+00	.444E+00	100.0	100.0	100.0	2.1
220328	936.	.771E+00	.618E+00	100.0	100.0	100.0	2.9
220428	652.	.536E+00	.338E+00	100.0	100.0	100.0	4.1
220528	652.	.843E+00	.510E+00	103.0	100.0	100.0	3.9
221028	64.	.140E+00	.300E+00	100.0	100.0	100.0	4.5
222028	1312.	.429E+00	.211E+00	100.0	100.0	100.0	2.2
223028	856.	.112E+01	.334E+00	100.0	100.0	100.0	1.7
220029	2232.	.600E+01	.332E+01	100.0	100.0	100.0	1.9
220329	936.	.687E+01	.362E+01	100.0	100.0	100.0	2.8
220429	652.	.462E+01	.201E+01	106.0	100.0	100.0	3.3
220529	644.	.512E+01	.345E+01	100.0	100.0	100.0	3.7
221029	64.	.128E+02	.147E+01	100.0	100.0	100.0	2.9
222029	1312.	.384E+01	.101E+01	100.0	100.0	100.0	1.4
223029	856.	.883E+01	.290E+01	100.0	100.0	100.0	1.9
220030	2232.	.337E+01	.604E+01	103.0	100.0	100.0	4.2
220330	936.	.360E+01	.822E+01	99.1	100.0	100.0	6.3
220430	652.	.184E+01	.235E+01	95.4	100.0	100.0	8.2
220530	644.	.450E+01	.460E+01	98.8	100.0	100.0	6.5
221030	64.	.691E+01	.709E+01	56.7	86.0	25.3	21.2
222030	1312.	.222E+01	.241E+01	99.9	100.0	100.0	4.9
223030	856.	.416E+01	.497E+01	99.6	100.0	100.0	5.8
220031	2232.	.313E+01	.264E+01	100.0	100.0	100.0	2.9
220331	936.	.391E+01	.274E+01	100.0	100.0	100.0	3.4
220431	652.	.197E+01	.168E+01	99.7	100.0	100.0	5.5
220531	644.	.338E+01	.285E+01	99.7	100.0	100.0	5.5
221031	64.	.812E+01	.919E+00	100.0	100.0	100.0	2.4
222031	1312.	.154E+01	.937E+00	100.0	100.0	100.0	2.8
223031	856.	.534E+01	.249E+01	100.0	100.0	100.0	2.6
220032	2232.	.323E+01	.210E+01	100.0	100.0	100.0	2.2
220332	936.	.343E+01	.182E+01	100.0	100.0	100.0	2.9
220432	652.	.280E+01	.163E+01	100.0	100.0	100.0	3.8
220532	644.	.357E+01	.273E+01	99.9	100.0	100.0	5.0
221032	64.	.419E+01	.311E+01	81.4	98.8	15.0	12.5
222032	1312.	.265E+01	.144E+01	100.0	100.0	100.0	2.5
223032	856.	.413E+01	.245E+01	100.0	100.0	100.0	3.3
220033	2232.	.590E+01	.369E+01	100.0	100.0	100.0	2.7
220333	936.	.685E+01	.421E+01	100.0	100.0	100.0	3.3
220433	652.	.652E+01	.228E+01	100.0	100.0	100.0	3.3
220533	644.	.593E+01	.426E+01	100.0	100.0	100.0	4.7
221033	64.	.134E+02	.137E+01	100.0	100.0	100.0	2.1
222033	1312.	.334E+01	.335E+01	100.0	100.0	100.0	1.8
223033	856.	.926E+01	.331E+01	100.0	100.0	100.0	2.0
220034	2232.	.456E+01	.324E+01	100.0	100.0	100.0	2.5
220334	936.	.547E+01	.327E+01	100.0	100.0	100.0	3.2
220434	652.	.379E+01	.189E+01	100.0	100.0	100.0	3.2
220534	644.	.401E+01	.369E+01	99.1	100.0	100.0	6.3

TABLE B-5. SITE 2 STATISTICAL DATA SUMMARY (CONTINUED)

KEY	AXLES	MEAN	SID DEV	CONF(10.1)	CONF(20.1)	CONF(50.1)	CONF(90.1)
221034	64.	.755E+01	.483E+01	82.1	99.2	101.9	101.9
222034	1312.	.310E+01	.193E+01	139.3	100.0	100.0	100.0
223034	856.	.646E+01	.362E+01	100.0	100.0	100.0	100.0
220035	2232.	.120E+02	.90E+01	100.0	100.0	100.0	100.0
220335	936.	.120E+02	.595E+01	100.0	100.0	100.0	100.0
220435	682.	.482E+01	.27E+01	100.0	100.0	100.0	100.0
220535	644.	.140E+02	.388E+01	100.0	100.0	100.0	100.0
221035	64.	.149E+02	.51E+01	96.6	100.0	100.0	100.0
222035	1312.	.129E+02	.417E+01	100.0	100.0	100.0	100.0
223035	856.	.103E+02	.538E+01	100.0	100.0	100.0	100.0
220036	2232.	.156E+02	.750E+01	100.0	100.0	100.0	100.0
220336	936.	.175E+02	.73E+01	100.0	100.0	100.0	100.0
220436	652.	.123E+02	.459E+01	100.0	100.0	100.0	100.0
220536	644.	.169E+02	.863E+01	100.0	100.0	100.0	100.0
221036	64.	.299E+02	.357E+01	100.0	100.0	100.0	100.0
222036	1312.	.112E+02	.262E+01	100.0	100.0	100.0	100.0
223036	956.	.221E+02	.68E+01	100.0	100.0	100.0	100.0
220037	2232.	.101E+01	.141E+01	98.8	100.0	100.0	100.0
220337	936.	.135E+01	.137E+01	99.7	100.0	100.0	100.0
220437	652.	.465E+03	.115E+01	69.6	96.0	19.1	16.0
220537	644.	.107E+01	.153E+01	92.3	100.0	100.0	100.0
221037	64.	.195E+01	.223E+01	51.3	83.3	28.6	23.9
222037	1312.	.558E+00	.101E+01	95.4	100.0	100.0	100.0
223037	856.	.164E+01	.457E+01	99.8	100.0	100.0	100.0
220038	2232.	.153E+02	.87E+01	100.0	100.0	100.0	100.0
220338	936.	.100E+02	.906E+01	100.0	100.0	100.0	100.0
220438	652.	.120E+02	.640E+01	100.0	100.0	100.0	100.0
220538	644.	.140E+02	.900E+01	100.0	100.0	100.0	100.0
221038	64.	.318E+02	.350E+01	100.0	100.0	100.0	100.0
222038	1312.	.923E+01	.285E+01	102.0	100.0	100.0	100.0
223038	856.	.233E+02	.672E+01	100.0	100.0	100.0	100.0
220039	2232.	.591E+00	.790E+01	27.6	52.0	55.5	46.6
220339	936.	.109E+01	.823E+01	51.8	86.0	27.9	23.4
220439	652.	.603E+00	.557E+01	24.6	46.9	62.7	52.6
220539	644.	.83E-02	.907E+01	.2	.4	8365.6	7017.6
221039	64.	.212E+01	.898E+01	14.9	28.3	105.9	88.4
222039	1312.	.298E+01	.654E+01	90.1	99.9	11.9	10.0
223039	856.	.595E+01	.655E+01	99.2	100.0	7.4	6.2
220040	2232.	.664E+01	.501E+01	160.0	160.0	3.6	3.0
220340	936.	.807E+01	.577E+01	100.0	100.0	4.6	3.8
220440	652.	.435E+01	.392E+01	99.5	100.0	6.9	5.8
220540	644.	.688E+01	.688E+01	99.1	100.0	7.5	6.3
221040	64.	.177E+02	.358E+01	100.0	100.0	5.0	4.2
222040	1312.	.36E+01	.411E+01	99.3	100.0	5.9	4.9
223040	856.	.102E+02	.521E+01	100.0	100.0	3.4	2.9
220041	2232.	.155E+03	0.	100.0	100.0	0.0	0.0
220341	936.	.155E+03	0.	100.0	100.0	0.0	0.0
220441	652.	.155E+03	0.	100.0	100.0	0.0	0.0
220541	644.	.155E+03	0.	100.0	100.0	0.0	0.0
221041	64.	.155E+03	0.	100.0	100.0	0.0	0.0
222041	1312.	.155E+03	0.	100.0	100.0	0.0	0.0
223041	856.	.155E+03	0.	100.0	100.0	0.0	0.0
220042	2232.	.155E+03	0.	100.0	100.0	0.0	0.0
220342	936.	.155E+03	0.	100.0	100.0	0.0	0.0
220442	652.	.155E+03	0.	100.0	100.0	0.0	0.0

TABLE H-3. SITE 2 STATISTICAL DATA SUMMARY (CONTINUED)

KEY	AVL ES	MEAN	STD DEV	CONF(10.1)	CONF(25.1)	TOL(95.1)	TOL(99.1)
220542	544.	.155E+03	0.	100.0	100.0	0.0	0.0
221042	64.	.155E+03	0.	100.0	100.0	0.0	0.0
222042	1312.	.155E+03	0.	100.0	100.0	0.0	0.0
223042	856.	.155E+03	0.	100.0	100.0	0.0	0.0

TABLE H-6. SITE 3 STATISTICAL DATA SUMMARY

KEY	AXLES	MEAN	STD. DEV.	CONF.(100)	CONF.(200)	IGL(1951)	IGL(1981)
131301	16.	.250E+02	.219E+01	100.0	100.0	4.7	3.6
131401	32.	.279E+02	.245E+01	100.0	100.0	3.2	2.7
131501	48.	.325E+02	.370E+01	100.0	100.0	3.5	2.9
132301	68.	.787E+01	.151E+01	100.0	100.0	2.1	1.7
132401	568.	.739E+01	.238E+01	100.0	100.0	2.7	2.2
132510	516.	.184E+02	.242E+01	100.0	100.0	2.8	1.7
133301	144.	.190E+02	.333E+01	100.0	100.0	3.4	2.9
133401	276.	.177E+02	.508E+01	100.0	100.0	3.4	2.8
133501	476.	.201E+02	.591E+01	100.0	100.0	2.6	2.2
131303	16.	.291E+02	.102E+01	100.0	100.0	3.3	2.7
131403	36.	.311E+02	.234E+01	100.0	100.0	2.5	2.1
131503	52.	.350E+02	.359E+01	100.0	100.0	2.7	2.3
132307	408.	.812E+01	.256E+01	100.0	100.0	2.7	2.3
132403	516.	.899E+01	.274E+01	100.0	100.0	2.6	2.2
132503	528.	.111E+02	.276E+01	100.0	100.0	2.1	1.8
133303	144.	.280E+02	.425E+01	100.0	100.0	3.8	2.9
133403	328.	.184E+02	.594E+01	100.0	100.0	3.1	2.6
133503	628.	.237E+02	.774E+01	100.0	100.0	2.4	2.0
131304	16.	.290E+02	.140E+01	100.0	100.0	2.6	2.2
131406	40.	.327E+02	.232E+01	100.0	100.0	2.3	1.9
131506	52.	.359E+02	.243E+01	100.0	100.0	1.9	1.6
132306	408.	.841E+01	.157E+01	100.0	100.0	1.8	1.5
132406	592.	.897E+01	.276E+01	100.0	100.0	2.5	2.1
132506	576.	.116E+02	.277E+01	100.0	100.0	2.8	1.7
133306	144.	.216E+02	.400E+01	100.0	100.0	3.7	3.1
133406	472.	.195E+02	.520E+01	100.0	100.0	2.5	2.1
133506	628.	.253E+02	.794E+01	100.0	100.0	2.3	2.0
131310	16.	.256E+02	.171E+01	100.0	100.0	3.5	2.9
131410	48.	.286E+02	.257E+01	100.0	100.0	2.9	2.4
131510	52.	.347E+02	.330E+01	100.0	100.0	2.6	2.2
132310	408.	.640E+01	.161E+01	100.0	100.0	2.4	2.1
132410	592.	.866E+01	.292E+01	100.0	100.0	2.8	1.7
132510	528.	.915E+01	.302E+01	100.0	100.0	2.8	2.4
133310	144.	.106E+02	.379E+01	100.0	100.0	3.4	2.8
133410	432.	.170E+02	.430E+01	100.0	100.0	2.4	2.0
133510	628.	.223E+02	.634E+01	100.0	100.0	2.2	1.9
131315	12.	.269E+02	.163E+01	100.0	100.0	3.9	3.1
131415	32.	.291E+02	.692E+00	100.0	100.0	.8	.7
131515	20.	.302E+02	.316E+00	100.0	100.0	.5	.4
132312	408.	.861E+01	.208E+01	100.0	100.0	2.3	2.0
132412	588.	.112E+02	.280E+01	100.0	100.0	2.8	1.6
132512	356.	.135E+02	.294E+01	100.0	100.0	2.3	1.9
133312	68.	.199E+02	.360E+01	100.0	100.0	4.4	3.7
133412	336.	.208E+02	.371E+01	100.0	100.0	1.8	1.5
133512	96.	.278E+02	.371E+01	100.0	100.0	2.7	2.3
131316	12.	-.115E+01	.101E+02	7.1	6.2	525.5	423.2
131416	32.	-.063E+00	.110E+02	3.5	7.0	461.4	383.6
131516	20.	.297E+01	.102E+02	10.2	28.2	161.4	133.4
132316	408.	.254E+01	.213E+01	97.2	100.0	7.9	7.5
132416	588.	-.134E-01	.330E+01	.9	4.6	280.3	180.3
132516	356.	.148E+00	.454E+01	4.9	9.8	318.7	267.3
133316	68.	.341E+01	.742E+01	29.4	54.9	52.6	44.8
133416	336.	.440E+01	.601E+01	65.0	99.6	13.6	11.4
133516	96.	.591E+01	.133E+02	42.5	73.6	32.3	29.5
131317	16.	-.097E+00	.351E+01	8.0	15.9	280.8	171.7

TABLE B-6. SITE 3 STATISTICAL DATA SUMMARY (CONTINUED)

KEY	AXLES	MEAN	STD. DEV.	CONF(100)	CONF(200)	YOL(95)	YOL(90)
131417	40.	.504E+00	.494E+01	5.1	10.2	314.0	261.5
131417	44.	.566E+01	.397E+01	65.2	93.5	21.3	17.7
132317	498.	.202E+00	.202E+01	41.0	41.0	73.0	61.2
132417	592.	.211E+00	.164E+01	99.4	100.0	14.4	12.0
132517	436.	.234E+01	.170E+01	99.6	100.0	6.8	5.7
132617	144.	-.544E+00	.400E+01	13.0	25.7	120.3	100.7
132717	432.	.141E+01	.356E+01	61.5	91.7	22.6	19.0
132817	572.	.344E+01	.393E+01	96.3	100.0	9.4	7.9
131320	16.	.969E+01	.404E+01	57.4	47.7	26.1	21.4
131420	40.	.105E+02	.663E+01	67.6	94.7	20.2	16.9
131520	52.	.225E+02	.669E+01	90.1	100.0	8.3	6.9
132320	408.	.116E+01	.552E+01	33.7	61.7	45.0	37.0
132420	592.	.372E+01	.753E+01	1.0	1.9	1635.7	1372.0
132520	528.	-.221E+01	.705E+01	52.6	64.7	27.4	23.0
133320	144.	.250E+01	.614E+01	37.4	67.0	40.5	33.9
133420	432.	.117E+00	.813E+01	2.4	4.0	659.0	552.7
133520	628.	.459E+01	.104E+02	71.2	96.6	18.5	15.5
131321	16.	.119E+02	.827E+01	51.7	82.9	29.7	24.4
131421	40.	.112E+02	.122E+02	43.5	74.7	34.9	29.1
131521	52.	.850E+01	.143E+02	33.0	60.5	46.0	39.1
132321	408.	-.174E+01	.797E+01	34.0	62.1	44.7	37.5
132421	592.	-.304E+00	.104E+02	5.7	11.3	275.6	231.2
132521	598.	-.637E+01	.105E+02	63.7	99.5	14.1	11.0
133321	144.	.111E+02	.901E+01	85.7	99.6	13.4	11.2
133421	432.	.264E+01	.116E+02	35.6	64.7	42.3	35.5
133521	628.	-.228E+01	.138E+02	32.1	59.3	47.4	39.7
131422	16.	.814E+01	.148E+01	95.5	99.9	9.7	8.0
131522	40.	.995E+01	.202E+01	99.7	100.0	6.5	5.4
132322	52.	.694E+01	.304E+01	96.2	100.0	9.4	7.9
132422	408.	.171E+01	.144E+01	92.4	100.0	8.1	6.8
132522	592.	.177E+01	.236E+01	93.2	99.8	10.7	9.0
133322	528.	.180E+01	.267E+01	87.9	99.8	12.7	10.6
133422	144.	.557E+01	.216E+01	99.8	100.0	6.4	5.3
133522	432.	.402E+01	.290E+01	99.6	100.0	6.8	5.7
131323	628.	.524E+01	.324E+01	100.0	100.0	4.8	4.0
131423	16.	.249E+02	.133E+01	99.1	100.0	7.1	5.9
131523	40.	.201E+02	.342E+01	100.0	100.0	3.9	3.2
132323	52.	.309E+02	.503E+01	100.0	100.0	3.6	3.0
132423	408.	.272E+01	.434E+01	79.4	98.6	15.5	13.0
132523	592.	.336E+01	.623E+01	60.9	95.1	15.0	12.6
133323	528.	.683E+01	.624E+01	99.9	100.0	6.1	5.1
133423	144.	.177E+02	.424E+01	100.8	100.0	4.0	3.3
133523	432.	.149E+02	.681E+01	100.0	100.0	4.3	3.6
131324	628.	.214E+02	.804E+01	100.0	100.0	3.1	2.6
131424	16.	.278E+02	.554E+01	93.7	99.9	10.6	8.7
131524	40.	.296E+02	.362E+01	100.0	100.0	3.9	3.3
132324	52.	.304E+02	.610E+01	100.0	100.0	4.4	3.7
132424	408.	.179E+01	.522E+01	51.1	83.4	28.4	23.8
132524	592.	.457E+01	.618E+01	92.8	100.0	10.9	9.2
133324	528.	.699E+01	.651E+01	94.6	100.0	8.0	6.7
133424	144.	.165E+02	.308E+01	100.0	100.0	3.9	3.3
133524	432.	.122E+02	.702E+01	100.0	100.0	5.5	4.6
131325	628.	.194E+02	.106E+02	100.0	100.0	4.1	3.4
131425	16.	.127E+01	.113E+02	3.5	7.0	480.6	395.3
131525	40.	-.221E+01	.104E+02	10.4	20.6	154.1	128.3

TABLE H-6. SITE 3 STATISTICAL DATA SUMMARY (CONTINUED)

KEY	AXLES	MEAN	STD. DEV.	CONF.(10%)	CONF.(20%)	TOL(95%)	TOL(90%)
131525	52.	.300E+01	.136E+02	12.6	24.9	126.1	105.2
132325	40.8	-.450E+00	.811E+01	11.7	23.8	132.8	112.2
132425	59.2	.447E+02	.109E+02	8.0	15.8	196.5	164.8
132525	52.8	.535E+01	.118E+02	70.1	98.2	18.9	15.9
133225	14.4	.105E+01	.113E+02	8.8	17.5	170.2	149.3
133425	432.	-.329E+01	.725E+01	65.1	93.9	21.0	17.6
133525	62.8	-.308E+00	.102E+02	6.0	12.0	260.0	218.1
131326	16.	.280E+02	.625E+01	90.7	99.7	11.9	9.8
131426	40.	.267E+02	.104E+02	68.9	95.8	12.4	10.3
131526	52.	.332E+02	.856E+01	99.3	100.0	7.2	6.0
132326	40.8	.121E+01	.956E+01	20.2	39.1	76.9	64.5
132426	59.2	.402E+01	.121E+02	5.8	8.5	24.2	20.3
132526	52.8	.980E+01	.116E+02	94.7	100.0	10.1	8.5
133226	14.4	.221E+02	.579E+01	100.0	100.0	4.3	3.6
133426	432.	.118E+02	.127E+02	-4.6	100.0	10.2	8.5
133526	62.8	.143E+02	.164E+02	97.1	100.0	9.0	7.5
131328	12.	-.500E-02	.524E+00	3	5	6657.4	5432.1
131428	12.	-.260E+00	.531E+00	13.2	25.9	129.7	105.8
131528	36.	.285E+00	.704E+00	19.0	37.0	83.6	69.6
132328	40.0	.362E+00	.333E+00	97.0	100.0	9.0	7.6
132428	16.4	.156E+00	.219E+00	63.9	93.1	21.6	18.1
132528	4.24	.538E-01	.907E+00	21.4	41.3	72.2	60.6
133228	100.	-.223E+00	.531E+00	32.5	59.8	47.2	39.5
133428	60.	.210E+00	.418E+00	30.1	56.0	51.4	43.0
131529	420.	.157E+00	.566E+00	45.1	76.9	32.8	27.5
131329	16.	.359E+02	.293E+01	100.0	100.0	4.4	3.6
131429	40.	.349E+02	.385E+01	100.0	100.0	3.5	2.9
131529	52.	.305E+02	.399E+01	100.0	100.0	3.6	3.0
132329	40.8	.880E+01	.211E+01	100.0	100.0	2.3	2.0
132429	59.2	.102E+02	.244E+01	100.0	100.0	1.9	1.6
132529	52.8	.877E+01	.287E+01	100.0	100.0	2.8	2.3
133229	14.4	.261E+02	.576E+01	100.0	100.0	5.5	4.6
133429	432.	.211E+02	.557E+01	100.0	100.0	2.5	2.1
131529	62.8	.200E+02	.627E+01	100.0	100.0	2.5	2.1
131330	16.	.192E+02	.699E+01	71.1	95.6	19.4	16.0
131430	40.	.167E+02	.871E+01	76.8	98.0	16.6	13.9
131530	52.	.216E+02	.887E+01	91.4	93.9	11.5	9.6
132330	40.8	.451E+01	.788E+01	75.2	97.9	17.0	14.2
132430	59.2	.700E+01	.932E+01	93.2	100.0	10.8	9.0
132530	52.8	.972E+01	.753E+01	99.7	100.0	6.6	5.6
133230	14.4	.165E+02	.545E+01	100.0	100.0	5.4	4.5
133430	432.	.965E+01	.694E+01	99.6	100.0	6.8	5.7
131530	62.8	.112E+02	.970E+01	59.6	100.0	6.8	5.7
131331	16.	.457E+01	.217E+01	59.2	80.4	25.6	21.0
131431	40.	.198E+01	.472E+01	20.8	40.1	76.3	63.5
131531	52.	.107E+01	.430E+01	14.1	27.8	112.4	93.8
132331	40.8	.540E+00	.115E+01	64.1	93.3	21.4	17.9
132431	59.2	.992E-01	.117E+01	16.3	32.0	55.3	50.0
132531	52.8	-.251E+00	.175E+01	34.5	62.8	44.0	36.9
133231	14.4	.336E+00	.325E+01	9.9	19.6	159.1	133.3
133431	432.	-.118E+01	.292E+01	60.0	90.7	23.3	19.6
131531	62.8	-.262E+01	.332E+01	95.2	100.0	9.9	8.3
131332	16.	.382E+02	.552E+01	98.6	100.0	7.7	6.3
131432	40.	.365E+02	.495E+01	100.0	100.0	4.3	3.6
131532	52.	.407E+02	.591E+01	101.0	101.0	4.0	3.4

TABLE N-3 STATISTICAL DATA SUMMARY (CONTINUED)

KEY	AXLES	MEAN	STD. DEV.	CONE (1981)	CONE (2011)	IOL (1981)	IOL (2011)
132332	408.	.187E+02	.653E+01	100.0	100.0	3.4	2.8
132432	592.	.224E+02	.806E+01	100.0	100.0	2.9	2.4
132532	528.	.268E+02	.538E+01	100.0	100.0	1.7	1.4
132632	144.	.242E+02	.508E+01	100.0	100.0	2.4	2.8
132732	432.	.387E+02	.424E+01	100.0	100.0	1.3	1.1
132832	624.	.345E+02	.515E+01	100.0	100.0	1.2	1.8
132932	16.	.187E+02	.253E+01	99.0	100.0	7.2	5.9
133032	48.	.188E+02	.333E+01	100.0	100.0	5.2	4.3
133132	52.	.261E+02	.472E+01	100.0	100.0	5.1	4.2
133232	480.	.288E+02	.422E+01	95.2	100.0	15.9	12.5
133332	592.	.377E+01	.474E+01	93.7	100.0	10.5	8.8
133432	528.	.417E+01	.476E+01	95.5	100.0	9.8	8.2
133532	144.	.184E+02	.371E+01	99.9	100.0	5.9	4.9
133632	432.	.138E+02	.512E+01	99.8	100.0	9.8	5.7
133732	624.	.715E+01	.713E+01	100.0	100.0	4.3	3.6
133832	16.	.549E+02	.259E+01	100.0	100.0	2.5	2.1
133932	40.	.580E+02	.332E+01	100.0	100.0	1.9	1.6
134032	52.	.625E+02	.435E+01	100.0	100.0	2.8	1.8
134132	408.	.231E+02	.542E+01	100.0	100.0	2.3	1.9
134232	592.	.275E+02	.676E+01	100.0	100.0	2.0	1.7
134332	528.	.357E+02	.565E+01	100.0	100.0	1.4	1.2
134432	144.	.478E+02	.475E+01	100.0	100.0	1.5	1.3
134532	432.	.436E+02	.647E+01	100.0	100.0	1.4	1.2
134632	624.	.529E+02	.917E+01	100.0	100.0	1.4	1.1
134732	16.	.450E+02	.154E+01	99.7	100.0	6.0	4.9
134832	48.	.437E+02	.178E+01	100.0	100.0	3.5	2.9
134932	52.	.178E+02	.212E+01	100.0	100.0	2.8	2.8
135032	480.	.315E+01	.433E+01	100.0	100.0	3.7	4.8
135132	592.	.219E+01	.222E+01	98.3	100.0	6.2	6.9
135232	528.	.450E+01	.456E+01	100.0	100.0	3.2	2.6
135332	144.	.108E+02	.241E+01	100.0	100.0	4.8	3.3
135432	432.	.947E+01	.373E+01	100.0	100.0	3.3	2.8
135532	624.	.116E+02	.458E+01	100.0	100.0	3.1	2.6
131338	16.	.652E+01	.854E+01	23.6	45.8	69.7	57.4
131438	40.	.915E+01	.736E+01	56.4	67.7	26.7	21.4
131538	52.	.133E+02	.738E+01	82.0	92.1	15.8	12.3
132338	408.	.234E+01	.365E+01	60.0	98.9	15.3	12.9
132438	592.	-.446E-01	.464E+01	1.8	3.7	84.0	71.3
132538	528.	.540E+01	.258E+01	100.0	100.0	4.1	3.4
132638	144.	.567E+01	.565E+01	76.9	98.3	16.4	13.8
132738	432.	.850E+01	.572E+01	99.9	100.0	5.8	4.9
132838	624.	.127E+02	.844E+01	100.0	100.0	5.4	4.6
131339	16.	.213E+02	.314E+01	98.4	100.0	7.6	6.4
131439	36.	.234E+02	.202E+01	100.0	100.0	2.9	2.4
131539	44.	.252E+02	.277E+01	100.0	100.0	2.9	2.4
132339	408.	.485E+01	.475E+01	100.0	100.0	3.5	2.9
132439	516.	.663E+01	.206E+01	100.0	100.0	2.7	2.3
132539	520.	.867E+01	.244E+01	100.0	100.0	2.4	2.0
132639	144.	.170E+02	.352E+01	100.0	100.0	3.0	2.5
132739	328.	.147E+02	.435E+01	100.0	100.0	3.2	2.7
132839	412.	.193E+02	.444E+01	100.0	100.0	2.4	2.0
131340	16.	-.840E+01	.974E+01	26.5	49.9	61.0	58.8
131440	36.	-.423E+01	.579E+01	37.6	61.3	46.3	38.5
131540	44.	.955E+01	.693E+01	74.3	115.5	212.5	183.8
132340	408.	-.878E+00	.226E+01	56.8	88.3	25.8	21.8

TABLE H-6. SITE 3 STATISTICAL DATA SUMMARY (CONTINUED)

KEY	AXLES	MEAN	STD DEV	CONF(10:)	CONF(20:)	YOL(95:)	TOL(98:)
132440	516.	-.102E+01	.279E+01	59.4	98.3	23.6	19.8
132540	520.	-.447E+00	.227E+01	27.7	52.2	55.4	56.5
132740	144.	-.245E+01	.614E+01	36.7	66.0	41.3	34.6
132840	328.	-.244E+01	.502E+01	62.0	92.0	22.5	18.9
133540	412.	.425E+00	.622E+01	10.4	20.5	150.9	126.5
131351	16.	-.121E+02	.112E+02	32.7	55.7	49.5	40.7
131841	40.	-.738E+00	.130E+02	2.8	5.7	563.5	469.2
131541	52.	-.963E+01	.146E+02	36.4	65.4	52.2	35.2
132341	400.	-.102E+01	.586E+01	29.3	54.9	52.2	43.8
132441	592.	-.283E+01	.735E+01	67.1	94.9	20.1	16.8
132541	528.	.184E+01	.120E+02	27.5	51.9	55.0	46.8
132341	144.	-.799E+01	.112E+02	60.7	91.1	23.1	19.3
132441	432.	.158E+01	.717E+01	34.0	62.0	44.7	37.5
131541	628.	.125E+02	.512E+02	44.1	75.7	33.6	28.2
131342	16.	.500E+00	.520E+01	3.0	6.0	553.8	458.5
131442	40.	-.325E+01	.672E+01	23.9	45.5	66.2	53.1
131542	52.	-.492E+01	.645E+01	41.3	72.1	36.7	30.6
132342	402.	-.223E+00	.523E+01	7.5	14.9	209.0	175.2
132442	592.	.126E+01	.872E+01	27.5	51.8	55.0	46.8
132542	528.	-.537E+01	.930E+01	81.5	99.2	14.8	12.3
133342	144.	.215E+01	.624E+01	31.9	50.9	47.9	40.1
133442	432.	-.438E+01	.545E+01	92.3	100.8	11.1	9.3
133542	628.	-.117E+02	.569E+01	180.0	100.0	3.0	3.2

TABLE B-6. SITE 3 STATISTICAL DATA SUMMARY (CONTINUED)

KEY	AXLES	MEAN	SID DEV	CONF(100)	CCNE(28.1)	ICL(95.1)	ICL(98.1)
270001	2472	.131E+02	.725E+01	100.0	100.0	2.2	1.0
270001	568	.106E+02	.619E+01	100.0	100.0	4.0	4.0
270401	868	.114E+02	.665E+01	100.0	100.0	3.9	3.3
273001	1035	.150E+02	.773E+01	100.0	100.0	2.8	2.4
273001	97	.295E+02	.435E+01	100.0	100.0	3.1	2.6
273001	1414	.876E+01	.267E+01	100.0	100.0	1.6	1.4
273001	896	.192E+02	.533E+01	100.0	100.0	1.9	1.6
273001	2656	.155E+02	.850E+01	100.0	100.0	2.1	1.8
280307	568	.117E+02	.661E+01	100.0	100.0	4.6	3.9
280403	810	.134E+02	.684E+01	100.0	100.0	3.4	2.9
280507	1204	.187E+02	.910E+01	100.0	100.0	2.7	2.3
281007	104	.331E+01	.755E+01	100.0	100.0	2.3	2.0
282003	1452	.951E+01	.295E+01	100.0	100.0	1.6	1.3
283003	1100	.217E+02	.686E+01	100.0	100.0	1.9	1.6
283006	2840	.162E+02	.945E+01	100.0	100.0	2.0	1.7
283006	568	.124E+02	.655E+01	100.0	100.0	4.7	3.9
283006	1064	.141E+02	.742E+01	100.0	100.0	3.2	2.7
283006	1208	.196E+02	.944E+01	100.0	100.0	2.7	2.3
283006	108	.378E+02	.318E+01	100.0	100.0	1.8	1.5
283006	1528	.972E+01	.245E+01	100.0	100.0	1.5	1.2
283006	1204	.227E+02	.733E+01	100.0	100.0	1.7	1.5
280010	2840	.141E+02	.821E+01	100.0	100.0	2.1	1.8
2830210	568	.106E+02	.678E+01	100.0	100.0	5.2	4.4
2830410	1064	.125E+02	.624E+01	100.0	100.0	3.0	2.5
2830510	1208	.174E+02	.917E+01	100.0	100.0	3.0	2.5
281010	104	.311E+02	.454E+01	100.0	100.0	2.8	2.3
282010	1528	.800E+01	.256E+01	100.0	100.0	1.6	1.3
283010	1204	.202E+02	.614E+01	100.0	100.0	1.7	1.4
280015	1956	.147E+02	.663E+01	100.0	100.0	2.0	1.7
2830315	434	.196E+02	.523E+01	100.0	100.0	6.4	3.7
280415	1000	.155E+02	.617E+01	100.0	100.0	2.5	2.1
280515	472	.171E+02	.703E+01	100.0	100.0	3.7	3.1
281015	64	.295E+02	.155E+01	100.0	100.0	1.3	1.1
282015	1340	.110E+02	.318E+01	100.0	100.0	1.5	1.3
283015	562	.219E+02	.459E+01	100.0	100.0	1.8	1.5
280016	1956	.180E+01	.546E+01	85.4	95.6	13.5	11.3
280316	444	.240E+01	.741E+01	83.5	99.4	14.1	11.9
280416	1000	.167E+01	.519E+01	67.4	95.0	20.0	16.8
280516	472	.144E+01	.685E+01	35.2	63.8	43.1	36.1
281016	64	.281E+00	.104E+02	1.7	3.3	956.3	799.0
282016	1340	.739E+00	.356E+01	55.3	87.1	25.8	21.7
283016	552	.454E+01	.715E+01	86.4	95.7	13.2	11.0
280017	2644	.165E+01	.318E+01	99.3	100.0	7.3	6.1
280117	568	.294E+01	.274E+01	2.0	4.1	767.0	643.4
280417	1064	.110E+01	.266E+01	82.3	99.3	14.5	12.2
280517	1052	.308E+01	.329E+01	99.8	100.0	6.5	5.4
281017	100	.256E+01	.517E+01	37.8	67.5	40.1	33.6
282017	1436	.117E+01	.195E+01	97.6	100.0	8.7	7.3
283017	1148	.217E+01	.395E+01	97.5	100.0	10.6	8.9
280020	2840	.153E+01	.891E+01	67.9	93.2	21.4	18.0
280320	568	.170E+01	.557E+01	53.3	85.4	27.0	22.7
280420	1064	.462E+00	.400E+01	14.9	29.4	104.1	87.4
280520	1208	.298E+01	.107E+02	56.3	86.0	25.2	21.2
281020	108	.162E+02	.834E+01	24.0	100.0	10.4	8.7
282020	1574	-.456E+00	.693E+01	20.3	39.3	76.2	63.9

TABLE B-6. SITE 3 STATISTICAL DATA SUMMARY (CONTINUED)

KEY	AXLES	MEAN	STP DEV	CONF(10%)	CONF(20%)	TOL(95%)	TOL(98%)
233020	1204.	.873E+01	.967E+01	157.3	193.0	210.0	16.0
233021	2840.	-.164E+00	.121E+02	22.4	18.0	69.0	57.0
233021	564.	.199E+01	.102E+02	85.6	84.5	42.4	35.6
233021	1464.	.132E+01	.113E+02	29.7	153.4	51.5	43.2
233021	1204.	-.361E+01	.169E+02	16.9	194.8	28.2	16.9
233021	1104.	.105E+02	.130E+02	59.5	191.2	28.7	19.9
233021	1528.	-.278E+01	.102E+02	71.4	195.7	18.4	15.4
233022	1204.	.108E+01	.133E+02	22.1	142.5	78.0	58.0
233022	2840.	.377E+01	.326E+01	100.0	100.0	3.6	3.0
233022	568.	.290E+01	.251E+01	59.4	100.0	6.0	6.0
233022	1064.	.301E+01	.312E+01	59.8	100.0	6.3	5.2
233022	1204.	.351E+01	.355E+01	100.0	100.0	5.2	4.8
233022	1104.	.921E+01	.859E+01	100.0	100.0	5.4	4.5
233022	1528.	.174E+01	.222E+01	159.0	100.0	6.4	5.4
233022	1204.	.646E+01	.306E+01	100.0	100.0	3.8	3.0
233022	2840.	.120E+02	.108E+02	100.0	100.0	3.3	2.0
233023	1564.	.714E+01	.833E+01	95.8	100.0	9.6	6.1
233023	1054.	.699E+01	.931E+01	199.8	100.0	5.8	5.2
233023	1204.	.170E+02	.111E+02	100.0	100.0	3.7	3.1
233023	1104.	.328E+02	.222E+01	100.0	100.0	4.3	3.6
233023	1528.	.502E+01	.642E+01	199.8	100.0	6.3	5.3
233023	1204.	.199E+02	.841E+01	100.0	100.0	2.1	2.5
233024	2840.	.108E+02	.107E+02	100.0	100.0	3.6	3.1
233024	1564.	.625E+01	.884E+01	90.7	199.9	11.7	9.0
233024	1084.	.860E+01	.851E+01	159.9	100.0	6.0	5.0
233024	1204.	.149E+02	.117E+02	100.0	100.0	3.7	3.0
233024	1104.	.335E+02	.202E+01	100.0	100.0	4.0	3.3
233024	1528.	.167E+01	.639E+01	199.6	100.0	6.9	5.8
233024	1204.	.165E+02	.924E+01	100.0	100.0	5.2	2.6
233025	2840.	.519E+00	.109E+02	20.7	140.1	78.6	62.6
233025	564.	-.123E+00	.916E+01	12.5	51.1	616.3	516.0
233025	1064.	-.117E+01	.975E+01	30.9	56.6	50.1	42.4
233025	1208.	.231E+01	.114E+02	51.7	85.9	28.0	23.5
233025	1104.	.317E+00	.125E+02	15.4	10.8	291.7	244.2
233025	1528.	.186E+01	.209E+02	49.7	81.9	29.3	23.0
233025	1204.	-.122E+01	.956E+01	34.1	62.3	44.4	37.3
233026	2840.	.101E+02	.143E+02	100.0	100.0	3.2	1.4
233026	568.	.726E+01	.130E+02	81.6	93.2	18.6	12.4
233026	1064.	.803E+01	.134E+02	95.0	100.0	10.0	8.4
233026	1208.	.132E+02	.150E+02	99.8	100.0	6.4	5.4
233026	1108.	.300E+02	.950E+01	99.9	100.0	6.0	5.1
233026	1528.	.527E+01	.110E+02	91.0	99.3	13.3	9.4
233026	1204.	.143E+02	.146E+02	99.9	100.0	5.7	4.8
233028	1528.	.154E+00	.461E+00	83.2	149.4	11.9	11.9
233028	1512.	.239E+00	.451E+00	77.0	91.3	16.3	13.7
233028	1564.	.149E+03	.319E+00	52.6	88.7	27.5	23.0
233028	840.	.112E+00	.691E+00	50.3	82.5	28.9	24.2
233028	1160.	.110E+00	.676E+00	10.7	21.2	148.0	123.6
233028	984.	.196E+00	.180E+00	85.5	93.9	13.1	10.2
233028	580.	.964E+01	.565E+00	37.1	60.0	48.9	38.6
233029	2840.	.153E+02	.846E+01	100.0	100.0	2.0	1.7
233029	1564.	.145E+02	.145E+02	99.9	100.0	3.9	3.0
233029	1064.	.156E+02	.768E+01	100.0	100.0	3.0	2.5
233029	1204.	.155E+02	.805E+01	100.0	100.0	2.9	2.5
233029	104.	.329E+02	.444E+01	100.0	100.0	2.6	2.2

TABLE B-6. SITE 3 STATISTICAL DATA SUMMARY (CONTINUED)

KEY	AXLES	MEAN	STD DEV	CONF (18.1)	CONF (20.1)	CONF (95.1)	TOT (198.1)
232029	1526.	.924E+01	.261E+01	100.0	100.0	1.4	1.2
233029	1204.	.214E+02	.697E+01	100.0	100.0	1.8	1.5
230030	2040.	.944E+01	.905E+01	100.0	100.0	3.5	3.0
230330	558.	.790E+01	.918E+01	96.1	100.0	9.5	8.0
230430	1064.	.844E+01	.847E+01	99.8	100.0	6.2	5.2
230530	1204.	.110E+02	.905E+01	100.0	100.0	4.7	3.9
231030	108.	.894E+02	.844E+01	97.6	100.0	8.7	7.3
232030	1526.	.728E+01	.869E+01	99.9	100.0	5.9	5.0
233030	1204.	.113E+02	.861E+01	100.0	100.0	4.3	3.6
230031	2040.	-.619E+00	.271E+01	77.6	95.5	16.1	13.5
230331	568.	.601E+00	.207E+01	51.1	83.3	20.4	23.0
230431	1064.	-.350E+00	.238E+01	36.9	66.4	40.8	34.2
230531	1204.	-.143E+01	.258E+01	90.4	95.9	11.8	9.9
231031	108.	.197E+01	.477E+01	35.0	63.5	43.6	36.5
232031	1526.	.950E+01	.126E+01	33.5	44.9	65.7	55.1
233031	1204.	-.175E+01	.333E+01	93.2	100.0	10.7	9.0
230032	2040.	.279E+02	.849E+01	100.0	100.0	1.1	.9
230332	558.	.572E+02	.914E+01	100.0	100.0	3.4	2.8
230432	1064.	.267E+02	.803E+01	100.0	100.0	1.8	1.5
230532	1204.	.314E+02	.677E+01	100.0	100.0	1.2	1.0
231032	108.	.308E+02	.584E+01	100.0	100.0	2.9	2.4
232032	1526.	.230E+02	.752E+01	100.0	100.0	1.6	1.4
233032	1204.	.331E+02	.515E+01	100.0	100.0	.9	.7
230033	2040.	.732E+01	.725E+01	100.0	100.0	3.6	3.1
230333	568.	.527E+01	.578E+01	96.9	100.0	9.1	7.6
230433	1064.	.571E+01	.592E+01	99.9	100.0	6.1	5.1
230533	1204.	.972E+01	.824E+01	100.0	100.0	4.8	4.0
231033	108.	.222E+02	.531E+01	100.0	100.0	4.6	3.8
232033	1578.	.760E+01	.676E+01	99.7	100.0	6.5	5.5
233033	1204.	.106E+02	.571E+01	100.0	100.0	3.6	3.0
230034	2040.	.384E+02	.132E+02	100.0	100.0	1.3	1.1
230334	558.	.301E+02	.123E+02	100.0	100.0	3.4	2.8
230434	1064.	.351E+02	.110E+02	100.0	100.0	1.9	1.6
230534	1204.	.653E+02	.120E+02	100.0	100.0	1.5	1.3
23034	108.	.590E+02	.312E+01	100.0	100.0	1.7	1.4
23034	1526.	.289E+02	.775E+01	100.0	100.0	1.3	1.1
23034	1204.	.496E+02	.881E+01	100.0	100.0	1.0	.9
23037	2040.	.689E+01	.514E+01	100.0	100.0	2.7	2.3
23047	568.	.522E+01	.395E+01	99.9	100.0	6.1	5.1
23047	1064.	.366E+01	.477E+01	100.0	100.0	5.2	4.4
230537	1204.	.870E+01	.529E+01	100.0	100.0	3.4	2.9
231037	108.	.166E+02	.226E+01	100.0	100.0	2.6	2.2
232037	1526.	.324E+01	.211E+01	100.0	100.0	3.3	2.7
233037	1204.	.107E+02	.808E+01	100.0	100.0	2.2	1.8
230038	2040.	.613E+01	.738E+01	100.0	100.0	4.4	3.7
230338	568.	.330E+01	.472E+01	99.4	99.9	11.8	9.9
230438	1064.	.377E+01	.660E+01	93.7	100.0	10.5	8.8
230538	1204.	.954E+01	.762E+01	100.0	100.0	4.5	3.8
231038	108.	.108E+02	.793E+01	84.3	95.5	13.9	11.6
232038	1526.	.247E+01	.446E+01	97.0	100.0	9.0	7.6
233038	1204.	.104E+02	.782E+01	100.0	100.0	4.3	3.6
230039	2040.	.113E+02	.652E+01	100.0	100.0	2.3	2.0
230339	568.	.838E+01	.610E+01	99.9	100.0	6.0	5.0
230439	1064.	.103E+02	.563E+01	100.0	100.0	3.6	3.0
230539	1204.	.139E+02	.677E+01	100.0	100.0	3.1	2.6

TABLE B-6. SITE 3 STATISTICAL DATA SUMMARY (CONTINUED)

KEY	AXLES	MFAN	STD DEV	C/NF(191)	C/NF(195)	TOL(190)
231039	96.	.73RE+02	.277E+01	100.0	100.0	2.4
232039	144.	.606E+01	.262E+01	100.0	100.0	2.0
233039	88.	.172E+02	.485E+01	100.0	100.0	1.7
230040	242.	-.965E+00	.456E+01	70.2	96.3	1.9
230740	508.	-.149E+01	.421E+01	60.0	90.7	18.0
230440	440.	-.160E+01	.401E+01	78.6	98.7	23.3
230540	976.	-.154E-01	.503E+01	0	1.5	15.0
231040	96.	-.255E+01	.791E+01	24.7	47.1	2054.9
232040	144.	-.774E+00	.265E+01	72.5	97.1	62.0
233040	88.	-.110E+01	.616E+01	40.6	71.3	18.0
230041	284.	.195E+01	.271E+02	29.0	55.6	36.8
230741	568.	-.310E+01	.826E+01	62.8	92.6	51.2
230441	1064.	-.962E+00	.782E+01	31.2	57.7	22.0
230541	1208.	.604E+01	.400E+02	45.0	76.0	48.9
231041	108.	-.669E+01	.143E+02	37.2	66.6	32.0
232041	1528.	-.734E+00	.855E+01	25.0	47.6	40.8
233041	1204.	.612E+01	.358E+02	40.7	71.5	61.5
230042	280.	-.414E+01	.867E+01	90.9	100.0	36.7
230742	568.	.304E+00	.559E+01	13.0	25.7	7.7
230442	1064.	-.144E+01	.820E+01	43.4	74.9	119.9
230542	1708.	-.865E+01	.810E+01	100.0	100.0	34.2
231042	108.	-.350E+01	.666E+01	41.4	72.3	5.3
232042	1528.	-.143E+01	.867E+01	48.1	80.3	36.3
233042	1204.	-.764E+01	.752E+01	100.0	100.0	30.4
						5.6
						4.7

APPENDIX I

REPORT OF INVENTIONS

This report includes the development and evaluation of track structure analysis models using measured rail and tie load data. A careful review of the work performed under this contract indicates that no new inventions, discoveries, or improvements of inventions were made.

REFERENCES

- 3-1. Proceedings of the American Railway Engineering Association, 77 (655) Chicago, Illinois, Nov. - Dec., 1975, pp 193-236.
- 3-2. Proceedings of the American Railway Engineering Association, Bulletin 660, Chicago, Illinois, Nov. - Dec., 1976, pp 133-137.
- 3-3. Prause, R. H., and Harrison, H. D., "Data Analysis and Instrumentation Requirements for Evaluating Rail Joints and Rail Fasteners in Urban Track", Report No. UTMA-MA-06-0025-75-B prepared for U.S. Department of Transportation by Battelle-Columbus Laboratories, February 1975.
- 3-4. Track Safety Standards, Federal Railroad Administration, Reprinted from Railway Track and Structures, February 1973, containing modifications as published in the Federal Register on January 5 and January 15, 1973.
- 3-5. Prause, R. H., Meacham, H. C., et al., "Assessment of Design Tools and Criteria for Urban Rail Track Structures", Vol. I, At-Grade Tie-Ballast Track, Report No. UMTA-MA-06-0025-74-3, prepared for U.S. Department of Transportation by Battelle-Columbus Laboratories, April 1974, PB'233016/5.
- 3-6. Proceedings of the American Railway Engineering Association, Bulletin 645, Chicago, Illinois, pp 176-187.
- 3-7. Howell, R. P., Kendall, R. A., et al., "Northeast Corridor High-Speed Rail Passenger Service Improvement Study, Task 3 - Track and Structures Standards Development", Report No. FRA-ONECD-75-3 prepared for U.S. Department of Transportation by DC/STV, September 1975, pp 33-41.
- 3-8. Lundgren, J. R., Martin, G. C., and Hay, W. W., "A Simulation Model of Ballast Support and the Modulus of Track Elasticity", University of Illinois, Urbana, Illinois, September 1970, pp 15-16.
- 3-9. "Capability of Fasteners to Resist Rail Overturning", Report No. ER-77, Engineering Research Division, AAR Research Center, November, 1967.
- 3-10. Proceedings of the American Railway Engineering Association, Bulletin 645, Chicago, Illinois, P. 181.
- 3-11. Srinivasan, M., "Modern Permanent Way", Somaiga Publications, Bombay, India, 1969, pp 134-136.
- 3-12. Schramm, G., "Permanent Way Technique and Permanent Way Economy", Trans. by H. Lange, 1961, Otto Elsner Verlagsgesellschaft, Darmstadt, Germany.

REFERENCES (Continued)

- 3-13. Clarke, C. W., "Track Loading Fundamentals", Part 7, Railway Gazette, 106 (1957), London, England, pp 479.
- 3-14. Howell, R. P., Kendall, R. A., et al., "Northeast Corridor High-Speed Rail Passenger Service Improvement Study, Task 3 - Track and Structures Standards Development", Report No. FRA-ONECD-75-3 prepared for U.S. Department of Transportation by DC/STV, September, 1975, p. 29-32.
- 3-15. Eisenmann, J., "Germans Gain a Better Understanding of Track Structure", Railway Gazette International, August, 1972, pp 305-308.
- 3-16. Birman, F., "Track Parameters, Static and Dynamic", Proceedings of the Institute of Mechanical Engineers, Vol. 180, Pt. 3 F, Paper 5, 1965-66, pp 73-85.
- 3-17. Ahlbeck, D., et al., "Evaluation of Analytical and Experimental Methodology for the Characterization of Wheel/Rail Loads", Report No. FRA-OR&D-76-276 prepared by Battelle's Columbus Laboratories for U.S. Department of Transportation, November, 1976.
- 3-18. Proceedings of the American Railway Engineering Association, Volume 53, 1952, pp 423-448.
- 3-19. Satoh, V., and Toyoda, M., "Deformation of Railway Track Under High-Speed Train--Measurements on the Test-Run Section of the New Tokaido Line", Quarterly Report RTRI, Vol. 7, No. 2, 1966, pp 20-23.
- 3-20. Jenkins, H. H., Stephenson, J. E., Clayton, G. A., and Lyon, D., "The Effect of Track and Vehicle Parameters on Wheel/Rail Vertical Dynamic Forces", Railway Engineering Journal, January, 1974, pp 2-16.
- 3-21. Tayabji, S., and Thompson, M., "Track Support Systems Parameter Study", Report No. FRA-OR&D-76-256 prepared for U.S. Department of Transportation by University of Illinois, Urbana, Illinois, July, 1976.
- 3-22. Knutson, R., Thompson, M., Mullin, T., and Tayabji, S., "Materials Evaluation Study - Ballast and Foundation Materials Research Program, Report No. FRA-OR&D-77-02, prepared for U.S. Department of Transportation by University of Illinois, Urbana, Illinois, January, 1977.
- 3-23. Raymond, G. P., Gaskin, P. N., and Svec, O., "Selection and Performance of Railroad Ballast", paper presented at Symposium on Railroad Track Mechanics, Princeton University, April, 1975.

REFERENCES (Continued)

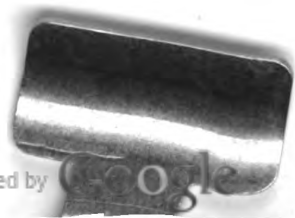
- 4-1. Prause, R. H., Harrison, H. D., and Arnlund, R. C., "Measurement Plan for the Characterization of the Load Environment for Cross Ties and Fasteners", Report No. FRA/ORD-77/03 prepared for U. S. Department of Transportation by Battelle-Columbus Laboratories, April, 1977.
- 4-2. Hanson, N. W., Ball, C. G., and Weber, J. W., "Kansas Test Track Instrumentation", Draft report prepared for U. S. Department of Transportation by Portland Cement Association, July, 1976, p. 25.
- A-1. Talbot, A. N., et al, "Second Progress Report of the Special Committee on Stresses in Track", AREA, Vol. 21, 1920, pp 645-814.
- A-2. Prause, R. H., et al, "Assessment of Design Tools and Criteria for Urban Rail Track Structures", Vol. I. At-Grade Tie Ballast Track, Report No. UMTA-MA-06-0025-74-3, prepared by Battelle-Columbus Laboratories, July, 1974, PB 233016/5.
- A-3. Terzaghi, K., Theoretical Soil Mechanics, John Wiley & Sons, Inc., New York, 11th Printing, 1963.
- A-4. Meacham, H. C., et al, "Assessment of Design Tools and Criteria for Urban Rail Track Structures", Vol. II. At-Grade Slab Track, Report No. UMTA-MA-06-0025-74-4, prepared by Battelle-Columbus Laboratories, July, 1974, PB 233017.
- A-5. Love, A.E.H., "A Treatise on the Mathematical Theory of Elasticity", Fourth Edition, New York Dover Publications, 1944.
- A-6. Burmister, D. M., "The General Theory of Stresses and Displacements in Layered Systems", Journal of Applied Physics, Vol. 15, February, 1945.
- A-7. Salem, M. T. and Hay, W. W., "Vertical Pressure Distribution in the Ballast Section and on the Subgrade Beneath Statically Loaded Ties", Civil Engineering Studies, Transportation Series No. 1, University of Illinois, July, 1966.
- A-8. Poppitz, J. V., "Simplified Dynamics of Hardened Buried Buildings", Shock and Vibration Bulletin, August, 1968, Bulletin 38, Part 2.
- A-9. Svec, O. J., et al, "Analytical and Experimental Investigation of a Rail Track Structure", Dept. of Civil Engineering, Queens University, Kingston, Canada, presented at the Second Symposium: Applications of Solid Mechanics, June 17, 1974.
- A-10. Robnett, Q. L., et al, "Ballast and Foundation Materials Research Program - Development of A Structural Model and Materials Evaluation Procedures", Dept. of Civil Eng., University of Illinois, May, 1975.

REFERENCES (Continued)

- A-11. Lundgren, J. R., et al, "A Simulation Model of Ballast Support and the Modulus of Track Elasticity", Dept. of Civil Eng., University of Illinois, Sept., 1970.
- A-12. Kilmartin, M. D., "A Numerical Discrete Element Analysis of Railroad Track", Masters Thesis, Tufts University, November, 1972.
- A-13. Hasselman, T. K., "DynaIist II, A Computer Program for Stability and Dynamic Response Analysis of Rail Vehicle Systems", Vol. 1 - Technical Report, Vol. 2, -User's Manual, Contract No. DOT-TSC-760, October, 1974.
- A-14. Track Structures Research Program, Interim Report, Contract No. DOT-FR-30038, Association of American Railroads, Technical Center, April, 1974 (unpublished).
- A-15. Bathe, K. J., et al., "SAP-IV: A Structural Analysis Program for Static and Dynamic Response of Linear Systems", Univ. of Calif., Berkeley, 1973.
- A-16. Herrmann, L. R., User's Manual for PSA (Three-Dimensional Elasticity Analysis of Periodically Loaded Prismatic Solids), Univ. of California, Davis, Calif., November, 1968.
- B-1. Galin, L. A., "Contact Problems in the Theory of Elasticity", Translated by H. Moss, edited by I. N. Sneddon, North Carolina State University, Raleigh, N. C., October, 1961.
- D-1. Wang, C., and Salmon, C. G., Reinforced Concrete Design, International Textbook Company, Scranton, Pennsylvania, 1969.
- D-2. Eppes, B. G., "Comparison of Measured and Calculated Stiffnesses for Beams Reinforced in Tension Only", ACI Journal Proceedings, Vol. 56, October, 1959.



Digitized by



Original from
UNIVERSITY OF MICHIGAN



U.S. DEPARTMENT OF TRANSPORTATION
FEDERAL RAILROAD ADMINISTRATION
Washington, D.C. 20590

Official Business

PENALTY FOR PRIVATE USE, \$300

POSTAGE AND FEES PAID
FEDERAL RAILROAD
ADMINISTRATION
DQT 516

